Investigating the characteristics and functions of extracellular vesicles from umbilical cord mesenchymal stem cells

by

Mairead Hyland

A thesis submitted for the degree:

DOCTOR OF PHILOSOPHY

December 2021

University of Keele

Abstract

Rheumatoid Arthritis (RA) is a chronic autoimmune disease which is characterised by a loss of immune tolerance, and an infiltration of immune cells into joints causing inflammation. Current pharmaceutical treatments for RA have adverse side effects and many patients do not respond favourably to them. Human umbilical cord mesenchymal stem cells (UCMSCs) present a promising alternative therapeutic due to their innate anti-inflammatory properties. Evidence from *in vitro* and *in vivo* studies of autoimmune diseases show that UCMSCs exert strong immunosuppressive effects. The therapeutic mechanism of action has been attributed to paracrine signalling, by which nanosized acellular particles called 'extracellular vesicles' (EVs) are one of the essential components. As UCMSC-mediated immunosuppression involves the use of EVs, and there are some safety concerns associated with MSC transplants, the anti-inflammatory properties of their EVs were explored with the aim to see if they too were capable of immunosuppression.

In this thesis, UCMSCs were sourced from previous work looking at large scale cell expansion in the Quantum® bioreactor. UCMSCs were characterised and analysed based on their growth, morphology, and surface marker production before isolating EVs. Bone Marrow derived MSCs were also characterised and served as an MSC control. UCMSCs proliferated well in culture, had a spindle-like morphology, and produced cell surface markers in line with the International Society for Cell Therapy (ISCT) criteria for MSCs. The growth of UCMSCs in hypoxic and pro-inflammatory environments has been associated with a stronger anti-inflammatory response. Therefore, UCMSCs were cultured in normoxia (21% O_2), hypoxia (5% O_2) and 'primed' with pro-inflammatory cytokines in both normoxia and hypoxia. The aim was to see if their EVs, like the cells, had enhanced anti-inflammatory properties. Analysis of the EV protein cargo identified an increase in proteins associated with chemotaxis (MCP2, MCP4

CCL3, CCL11) in the pro-inflammatory primed EVs from both normoxic and hypoxic conditions. There was also an increased expression of the anti-inflammatory proteins MMP-10 in the normoxic/primed EVs, and LIF and TRAIL in the hypoxic/primed EVs. Normoxic, hypoxic and normoxic/primed EVs were analysed through RNA sequencing. RNA sequencing of UCMSC-EVs had not been carried out before on hypoxic and normoxic/pro-inflammatory primed EVs and it identified differentially expressed miRNAs with potential anti-inflammatory properties (miR-139-5p, miR-140-5p, miR-214-5p) in the normoxic/primed EVs only. Findings also showed that the upregulated miRNAs had a low expression and were associated with cancer pathways.

These normoxic and normoxic/primed UCMSC-EVs were used in functional *in vitro* studies and co-cultured with individual cultures of peripheral blood mononuclear cells (PBMCs) from healthy donors, and with Jurkat lymphoblastic T-cells. The co-culturing of UCMSC-EVs with Jurkat cells is the first of its kind and results revealed that the pro-inflammatory primed EVs reduced the production of the inflammatory cytokine IL-17A in Jurkat cells as assessed via flow cytometry. Furthermore, the normoxic/primed EVs increased the production of the anti-inflammatory protein FoxP3 in PBMCs. Neither normoxic nor normoxic/primed EVs exerted a pro-inflammatory effect on PBMCs and Jurkat cells. Instead, the findings point towards potential anti-inflammatory properties of normoxic/primed UCMSC-EVs, but further work is needed to establish their suitability for treating RA.

Acknowledgements

I would like to extend a sincere thank you to Dr. Oksana Kehoe for her valuable support and guidance throughout the last three and a half years. I would like to acknowledge the help and supportive feedback of my co-supervisors Dr. Claire Mennan and Dr. Emma Wilson and my advisor Dr. Karina Wright who were always on hand to lend some advice and steer me in the right direction.

It has been a pleasure and a lot of fun to work at the Robert Jones and Agnes Hunt Orthopaedic Hospital, and for this, I would like to acknowledge all the postdocs and PhD students there, who have made it a very memorable journey for me. I will especially miss the lunch time chats! I would like to thank Miss Becky Davies. Together we made up 'Team Rheumatology', and it's been a joy to work alongside you and have your support. I'll miss the laughs, EV puns and Six Nations discussions.

I would like to extend a thank you to Dr. Aled Clayton and Dr. Dan Tonge both of which offered their help with my project. Your input and expertise are very much appreciated.

I'm incredibly grateful to have my partner Jack by my side. You have been with me since the start and have been a pillar of support through the joys and struggles of PhD life. You are the kindest and most patient person I know. I promise to come out of the little study now! Finally, I would like to recognise the incredible support of my parents. Although across the water, you have been with me all the way and the daily phone calls were the perfect break I needed. I really appreciate all that you have done for me and can't thank you enough.

Table of Contents

List of Figures

List of Tables

Supplementary Tables and Figures

Abbreviations

ACPA: Anti-citrullinated Protein Antibody

Ago2: Argonaute 2

AIA: Antigen Induced Arthritis

Anti-CCP: anti-Cyclic Citrullinated Peptide

ATMSC: Adipose Tissue Mesenchymal Stem Cell

BCA: Bicinchoninic Acid

bFGF: basic Fibroblast Growth Factor

BMMSC: Bone Marrow Mesenchymal Stem Cell

BSA: Bovine Serum Albumin

CCL: Chemokine Ligand

CCR: C-C chemokine Receptor

CDAI: Clinical Disease Activity Index

cDNA: complementary DNA

CFU: Colony Forming Unit

CIA: Collagen Induced Arthritis

CM: Conditioned Media

CMO: Cell Mask Orange

COX: Cyclooxygenase

CRP: C-reactive protein

Ct: Cycle threshold

CXCL/R: Chemokine (CXC motif) ligand/ receptor

DAS28: Disease Activity Score 28

DAVID: Database for Annotation, Visualization and Integrated Discovery

DMARD: Disease Modifying Anti-Rheumatic Drug

DNA: Deoxyribonucleic acid

DPBS: Dulbecco's Phosphate-buffered Saline

DTH: Delayed-Type Hypersensitivity

EAE: Experimental Autoimmune Encephalomyelitis

EAU: Experimental Autoimmune Uveoretinitis

EDTA: Ethylenediaminetetraacetic acid

ELISA: Enzyme-linked Immunosorbent Assay

ESCRT: Endosomal Sorting Complex Required for Transport

ESR: Erythrocyte Sedimentation Rate

EV: Extracellular Vesicles

FBS: Fetal Bovine Serum

FC: Fold Change

FDR: False Discovery Rate

FGF: Fibroblast Growth Factor

FSC-A: Forward Scatter Area

GM-CSF: Granulocyte Macrophage Colony-stimulating Factor

GO: Gene Ontology

GvHD: Graft versus Host Disease

H&E: Haematoxylin and Eosin

HGF: Hepatocyte Growth Factor

HIF: Hypoxia Inducible Factor

HLA: Human Leukocyte Antigen

HSA: Homo sapiens

HUCPVC: Human Umbilical Cord Perivascular Cells

HUVEC: Human Umbilical Vein Endothelial Cells

IBMX: 3-Isobutyl-1-methylxanthine

ICAM: Intercellular Adhesion Molecules

ICCS: Intracellular Cytokine Staining

IDO: indoleamine 2,3-dioxygenase

IFN-γ: Interferon gamma

IL: Interleukin

ILV: Intraluminal Vesicle

ISCT: International Society for Cellular Therapy

ISEV: International Society of Extracellular Vesicle

JIA: Juvenile Idiopathic Arthritis

KEGG: Kyoto Encyclopaedia of Genes and Genomes

LIF: Leukaemia Inhibitory Factor

lncRNA: long noncoding RNAs

LOD: Limit of Detection

LPS: Lipopolysaccharide

MA: Minus-Average

MCAM: Melanoma Cell Adhesion Molecule

MCSP: Melanoma Chondroitin Sulphate Proteoglycan

miRNA: microRNA

MMP: Matrix metalloproteinase

MP: microparticles

mRNA: messengerRNA

MSC: Mesenchymal Stem Cell

mtDNA: mitochondrial DNA

MVB: Multivesicular Body

NEAA: Non-essential Amino Acids

NGS: Next Generation Sequencing

NICE: National Institute for Health and Clinical Excellence

NK: Natural Killer

NLRP3: Nod-like Receptor Pyrin Domain-containing P protein 3

NPX: Normalized Protein Expression

NSAID – Non-steroidal Anti-inflammatory Drugs

NTA: Nanoparticle Tracking Analysis

OA: Osteoarthritis

P/S: Penicillin/Streptomycin

PAD: Peptidylarginine deiminase

PBMC: Peripheral Blood Mononuclear Cell

PBS: Phosphate Buffered Saline

PCA: Principal Component Analysis

PCR: Polymerase Chain Reaction

PDGF: Platelet-derived Growth Factor

PDT: Population Doubling Time

PEA: Proximity based Extension Assay

PGE2: Prostaglandin E2

PMA: phorbol 12-myristate 13-acetate

PMSF: Phenylmethylsulfonyl fluoride

qPCR: quantitative Polymerase Chain Reaction/ real time PCR

RA: Rheumatoid Arthritis

RF: Rheumatoid Factor

RIN: RNA Integrity Number

RIPA: Radioimmunoprecipitation assay

RJAH: Robert Jones and Agnes Hunt Orthopaedic Hospital

RISC: RNA-induced Silencing Complex

RNA: Ribonucleic acid

RT: Reverse Transcription

RT-qPCR: Quantitative reverse transcription PCR

SD: Standard Deviation

SDAI: Simplified Disease Activity Index

SE: Shared Epitope

SLE: Systemic Lupus Erythematosus

snoRNA: small nucleolar RNA

SSC-A: Side Scatter Area

T1D: Type 1 Diabetes

TBST: Tris-buffered Saline with Tween

TEM: Transmission Electron Microscopy

Tfh: T follicular helper

TNF: Tumour Necrosis Factor

TRAF1: TNF Receptor Associated Factor 1

Tregs: regulatory T-cells

tRNA: transfer RNA

TSDR: Treg cell-specific demethylated region

UCB-MSC: Umbilical Cord Blood Mesenchymal Stem Cell

UCMSC: Umbilical Cord Mesenchymal Stem Cell

VCAM: Vascular Cell Adhesion Protein

VEGF: Vascular Endothelial Growth Factor

WJMSCs: Wharton's Jelly Mesenchymal Stem Cells

Presented Work

1. Poster Presentation

Event: Research Day, Robert Jones and Agnes Hunt Orthopaedic Hospital, Oswestry.

Date: 27th April 2018

Title: Mesenchymal stem-cell derived extracellular vesicles as therapeutic agents in Juvenile Idiopathic Arthritis.

Authors: Hyland M, Mennan C, Wright K, Wilson E, Kehoe O.

2. Poster Presentation

Event: ISTM PGR Symposium, Wade Theatre at the North Staffordshire Medical Institute (NSMI), Hartshill Road, Stoke-on-Trent

Date: 15th May 2018

Title: Mesenchymal stem-cell derived extracellular vesicles as therapeutic agents in Juvenile Idiopathic Arthritis.

Authors: Hyland M, Mennan C, Wright K, Wilson E, Kehoe O.

3. Poster Presentation and Published Abstract

Event: Tissue and Cell Engineering Society 2018 Conference, Chancellor's Building, Keele University, Keele, Staffordshire

Date: 2-4th July 2018

Title: Mesenchymal stem-cell derived extracellular vesicles as therapeutic agents in Juvenile Idiopathic Arthritis.

Authors: Hyland M, Mennan C, Wright K, Wilson E, Kehoe O.

Journal: European Cells and Materials (eCM)

4. Oral Presentation

Event: Orthopaedic Institute Research Panel meeting, Robert Jones and Agnes Hunt Orthopaedic Hospital, Oswestry.

Date: 1st October 2018

Title: Proposal to analyse the miRNA content of Extracellular Vesicles released from Umbilical Cord Mesenchymal Stem Cells

Authors: Hyland M & Kehoe O.

5. Poster Presentation

Event: Mercia Stem Cell Alliance 2018 Conference, University of Birmingham

Date: 6-7th December 2018

Title: The immunomodulatory potential of Extracellular Vesicles derived from Umbilical Cord Mesenchymal Stem Cells

Authors: Hyland M, Mennan C, Wright K, Wilson E, Kehoe O.

6. Poster Presentation

Event: UK-EV Conference, University of Sheffield

Date: 11th December 2018

Title: Analysis of Extracellular Vesicles Derived from Umbilical Cord Mesenchymal Stem Cells

Authors: Hyland M, Mennan C, Wright K, Wilson E, Clayton A, Kehoe O.

7. Oral Presentation

Event: Research Day, Robert Jones and Agnes Hunt Orthopaedic Hospital, Oswestry.

Date: 26th April 2019

Title: Characterisation of Extracellular Vesicles released from Umbilical Cord Mesenchymal Stem Cells grown in different culture conditions

Authors: Hyland M, Mennan C, Wright K, Wilson E, Clayton A, Kehoe O.

8. Oral Presentation

Event: ISTM PGR Symposium, North Staffordshire Medical Institute (NSMI), Hartshill Road, Stoke-on-Trent

Date: 23rd May 2019

Title: Characterisation of Extracellular Vesicles from Umbilical Cord Mesenchymal Stem Cells

Authors: Hyland M, Mennan C, Wright K, Wilson E, Clayton A, Kehoe O.

9. Oral Presentation

Event: Rheumatology Group Annual Business Meeting, Robert Jones and Agnes Hunt Orthopaedic Hospital, Oswestry

Date: 19th June 2019

Title: Can Extracellular Vesicles from Umbilical Cord Mesenchymal Stem Cells dampen the immune response in patients with RA?

Authors: Hyland M, Mennan C, Wright K, Wilson E, Clayton A, Kehoe O.

10. Abstract Submission

Event: British Society for Immunology Conference, University of Liverpool

Date: 2-5th December 2019

Title: Anti-inflammatory Potential of Extracellular Vesicles from Umbilical Cord Mesenchymal Stem Cells

Authors: Hyland M, Mennan C, Wilson E, Clayton A, Kehoe O.

11. Oral Presentation

Event: UK-EV Conference, Francis Crick Institute, London

Date: 9-10th December 2019

Title: Proteomic Profile of Extracellular Vesicles from Umbilical Cord Mesenchymal Stem Cells

Authors: Hyland M, Mennan C, Wilson E, Clayton A, Kehoe O.

12. Poster Presentation

Event: Mercia Stem Cell Alliance 2019 Conference, University of Chester

Date: 16-17th December 2019

Title: Umbilical Cord Mesenchymal Stem Cells cultured in pro-inflammatory conditions release EVs with an altered protein profile

Authors: Hyland M, Mennan C, Wilson E, Clayton A, Kehoe O.

13. Oral Presentation

Event: International Society of Extracellular Vesicles 2020 Conference, Philadelphia, online

Date: 20-24th May 2020

Title: Changes in extracellular vesicle protein cargo after pro-inflammatory priming of umbilical cord mesenchymal stem cells.

Authors: Hyland M, Mennan C, Wilson E, Clayton A, Tonge D, Kehoe O.

14. Abstract Submission

Event: Tissue Engineering and Regenerative Medicine International Society (TERMIS) European Chapter Meeting 2020, Manchester Central Conference Centre

Date: 26-29th May 2020

Title: Alteration of Extracellular Vesicle Cargo after Pro-inflammatory Priming of Umbilical Cord Mesenchymal Stem Cells.

Authors: Hyland M, Mennan C, Wilson E, Clayton A, Kehoe O.

15. Oral Presentation

Event: UKEV-GSEV Autumn Meeting 2020, 2nd & 3rd September 2020, Saarland University, online

Date: 2nd-3rd September 2020

Title: Analysis of Extracellular Vesicle Cargo from Umbilical Cord Mesenchymal Stem Cells.

Authors: Hyland M, Mennan C, Wilson E, Clayton A, Tonge D, Kehoe O.

16. Oral Presentation

Event: 5th Annual ILAS Keele Postgraduate Conference, Keele Hall Ballroom, University of Keele

Date: 23rd November 2020

Title: An investigation into the therapeutic properties of umbilical cord mesenchymal stem cell derived extracellular vesicles

Authors: Hyland M, Mennan C, Wilson E, Clayton A, Kehoe O.

17. Oral Presentation

Event: Orthopaedic Institute Annual Meeting

Date: 2nd December 2020

Title: Regulatory T-cell derived extracellular vesicles in patients with rheumatoid arthritis: a cell-free modality for suppression of inflammation.

Authors: Hyland M, & Kehoe O.

18. Abstract Submission

Event: 12th Annual Congress on Autoimmunity

Date: 28th May-1st June 2021

Title: Molecular profile of extracellular vesicles from umbilical cord mesenchymal stem cells

Authors: Mairead Hyland, Claire Mennan, Daniel Tonge, Emma Wilson, Aled Clayton, Oksana Kehoe

Outcome: Accepted Oral Presentation

19. Abstract Submission

Event: 6th World Congress of the Tissue Engineering and Regenerative Medicine International Society (TERMIS 2021)

Date: 15 November – 19 November 2021

Title: An investigation into the miRNA cargo of extracellular vesicles from umbilical cord mesenchymal stem cells

Authors: Mairead Hyland, Claire Mennan, Daniel Tonge, Emma Wilson, Aled Clayton, Oksana Kehoe

Publications

Hyland, M., Mennan, C., Wilson, E., Clayton, A., & Kehoe, O. (2020). Pro-Inflammatory Priming of Umbilical Cord Mesenchymal Stromal Cells Alters the Protein Cargo of Their Extracellular Vesicles. *Cells*, *9*(3), 726. https://doi.org/10.3390/cells9030726

Jones, F. K., Stefan, A., Kay, A. G., Hyland, M., Morgan, R., Forsyth, N. R., Pisconti, A. & Kehoe, O. (2020). Syndecan-3 regulates MSC adhesion, ERK and AKT signalling in vitro, and its deletion enhances MSC efficacy in a model of inflammatory arthritis in vivo. *Scientific Reports*, 10, 20487.

Hyland, M., Mennan, C., Wilson, E., Clayton, A. & Kehoe, O. (2020). Alteration of Extracellular Vesicle Cargo after Pro-inflammatory Priming of Umbilical Cord Mesenchymal Stem Cells. *eCM Periodical Collection 1; TERMIS EU*, 104.

In review:

Kay, A. G., Treadwell, K., Roach, P., Morgan, R., Lodge, R., Hyland, M., Piccinini, A. M., Forsyth, N. R., Kehoe, O. (2020). Mesenchymal stem cell-derived extracellular vesicles reduce disease severity and immune responses in inflammatory arthritis. Research Square, DOI:10.21203/rs.3.rs-70181/v1

Awards

- Awarded £7200 funding towards carrying out Next Generation Sequencing (2018).
- Received travel grant to the value of £100 towards UK-EV conference travel (2019).
- Awarded £450 travel bursary by Keele Postgraduates Association (2020).
- Awarded £300 from Tissue Cell and Engineering Society to present my work at an international conference (2020).
- Awarded $500 scholarship from the International Society of Extracellular Vesicles (2020).
- 3rd place in 3-minutes thesis competition at Keele Postgraduate Symposium (2020).
- Awarded £45,723 from the Orthopaedic Institute Ltd for postdoctoral research.

Chapter 1: Introduction

1.1 Rheumatoid Arthritis

1.1.1 Overview and epidemiology of RA

Rheumatoid arthritis (RA) is a chronic, inflammatory autoimmune disease characterised by joint inflammation, erosion of bone and cartilage, the presence of autoantibodies and citrullinated proteins, and other systemic conditions such as cardiovascular, pulmonary and musculoskeletal disorders [1,2]. There is a breakdown in immune tolerance which results in an invasion of immune cells into joints [3,4]. This triggers a cascade of processes that leads to cartilage damage, endothelial cell activation, synovial cell hyperplasia and eventually bone erosion [3,4] **(Figure 1).** RA can be divided into two categories: 'seropositive' and 'seronegative', with seropositive RA denoting the presence of autoantibodies such as Rheumatoid Factors and anti-citrullinated protein antibodies (ACPA) [5]. These autoantibodies can be present in the serum years before an RA diagnosis, in a period that has been described as 'Preclinical RA' [5]. Patients with seropositive RA generally have a more severe disease progression than those with seronegative RA [6].

It is estimated that approximately $4.3x10^5$ people are living with rheumatoid arthritis in the UK [7]. It affects adults of any age but its peak of onset is between 40-60 years old [7]. Epidemiological studies of RA are limited, but there appears to be a geographical variance with the highest prevalence in Australasia (0.46%), Western Europe (0.44%) and North America (0.44%) and the lowest levels in Asia and North Africa (0.16%) [8]. Both genetic and environmental factors contribute to the prevalence of RA in a population. For example, researchers have found a strong link between RA and the 'shared epitope' (SE) of the human leukocyte antigen (HLA) [5]. More than 80% of RA patients carry the HLA-DRB1 alleles which are associated with greater disease severity such as cartilage destruction [9] and the

production of ACPAs [10]. Different subtypes of the SE vary amongst ethnic groups which may account for differences in prevalence stated above. Additionally, polymorphisms to the gene CYP17 often found in a Chinese population is associated with a reduced risk of RA. Environmental factors such as a high BMI [11,12], a high incidence of tobacco smoking [2,13,14] and exposure to pollutants [15–17] are all associated with greater risk of developing RA. As these environmental factors differ between populations, this may account for some geographical variances in the prevalence of RA.

The global prevalence of RA is 0.24% and is two times higher in females compared to males [8]. The difference between females and males may be explained by the link between RA and female reproductive hormones, menopause, or polycystic ovary syndrome. Specifically, studies have shown that menopause, polycystic ovary syndrome, endometriosis, and hormone replacement therapy all present a greater risk of developing RA [18,19]

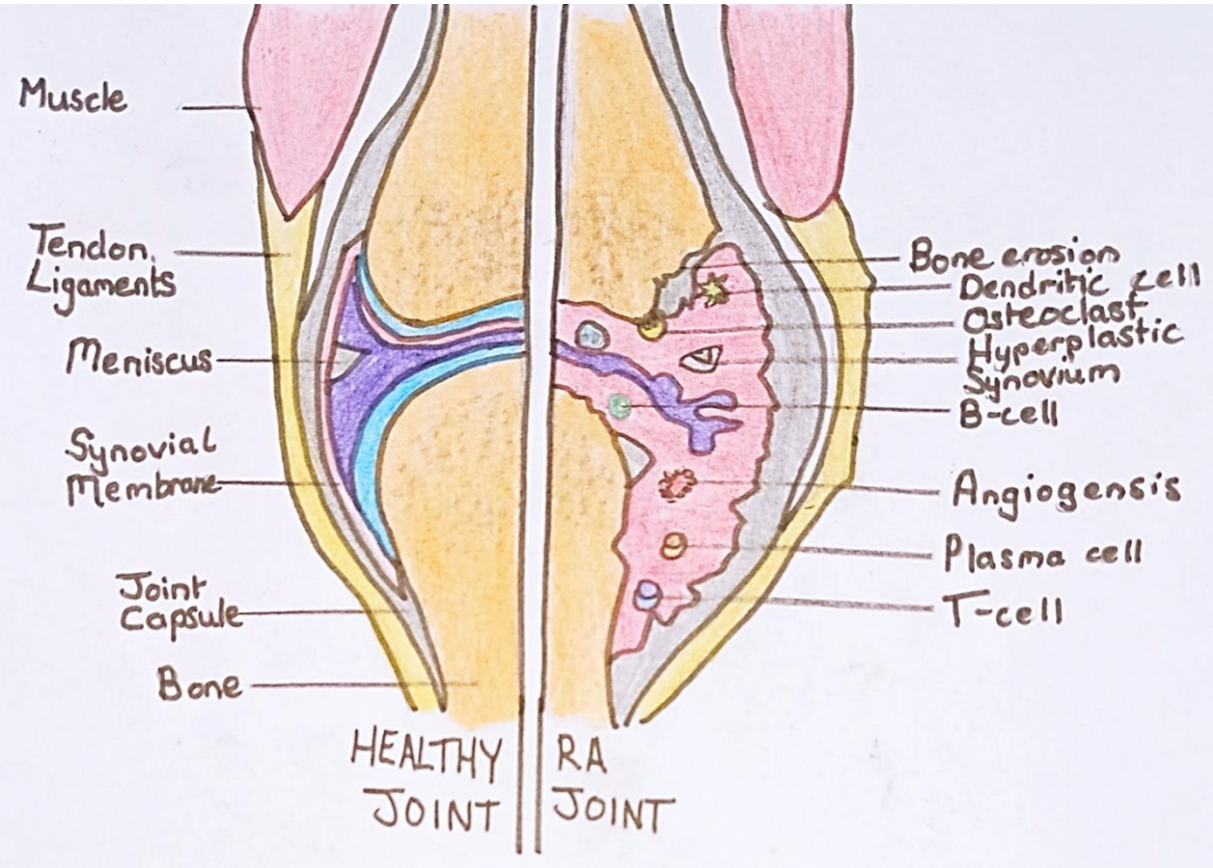

Figure 1: Comparison of healthy vs RA joint

Visual representation of a healthy knee joint (left) compared to a knee joint affected by RA (right). Morphological changes in the RA knee include an infiltration of immune cells, inflammation of the synovial lining, formation of new blood vessels (angiogenesis) and erosion of bone and cartilage. Image adapted from Wollbold et al. [20].

1.1.2 Genetic link to RA

A lot of research has gone into establishing a cause of RA but, at present, no one definitive cause has been discovered. Instead, it is known that there is an interplay of different genetic, environmental and autoimmune factors that trigger the onset of RA, a term that Kurko et al. [21] described as the "Bermuda triangle" due to the mystery and challenge of unravelling how these factors interact. When looking purely at the genetic link to RA, researchers have found a strong link between RA and the 'shared epitope' (SE) of the human leukocyte antigen (HLA)

[5]. More than 80% of RA patients carry the HLA-DRB1 alleles which are associated with greater disease severity such as cartilage destruction [9] and the production of ACPAs [10].

After the HLA-DRB1 gene, a polymorphism to the gene PTPN22 has shown the second strongest association with RA [21], as this modification leads to T-cells being easily activated by antigen stimulation [22]. The next strongest genetic association to RA is the TNF receptor associated factor 1 (TRAF1) gene which is linked to the development of ACPA positive RA [21]. Variants to other genes which control inflammatory pathways, such as IL23R [23], CTLA4 [24], STAT4 [25], and IL-6 [26], are also associated with a higher risk of developing RA.

Genetic factors may also determine how patients with RA respond to medication. This is an area of research termed 'pharmacogenetics' and studies have shown that patients carrying one or two copies of the *FCGR3A*-158 V allele respond more favourably to rituximab [27]. Additionally, there is a decreased effectiveness of methotrexate when given to patients with a polymorphism of the gene IL1RN [28]. Pharmacogenetic research has highlighted the need to develop biomarkers associated with disease outcomes so that patients can be given the most therapeutic treatments tailored to their genome and symptoms [21].

1.1.3 Environmental link to RA

Some environmental factors have been known to trigger the onset of Rheumatoid Arthritis. **Figure 2** summarises the risk factors and development of RA. Environmental risk factors include, but are not limited to: a high BMI [11,12], silica/pollutant exposure [15–17], bacteria in the microbiome such as *Porphyromonas gingivalis* [29], and tobacco smoking [2,5,13,14,30]. Connections have also been made to the female sex hormones and RA,

specifically the development of natural menopause before the age of 44 is associated with seronegative RA only [18]. Additionally, Merlino et al. [19] identified polycystic ovary syndrome as a risk factor for RA in a cohort study of 158 women with RA [31]. These connections help to explain the higher prevalence of RA in females compared to males.

Table 1 displays a summary of the risk and protective factors in RA as discussed in this review. Out of all the genetic and environmental links to RA, the strongest associations include the 'shared epitope' of the HLA allele, smoking, female gender and family history of the disease [5]. However, there may be other genetic and environmental factors yet to be discovered that trigger the disease.

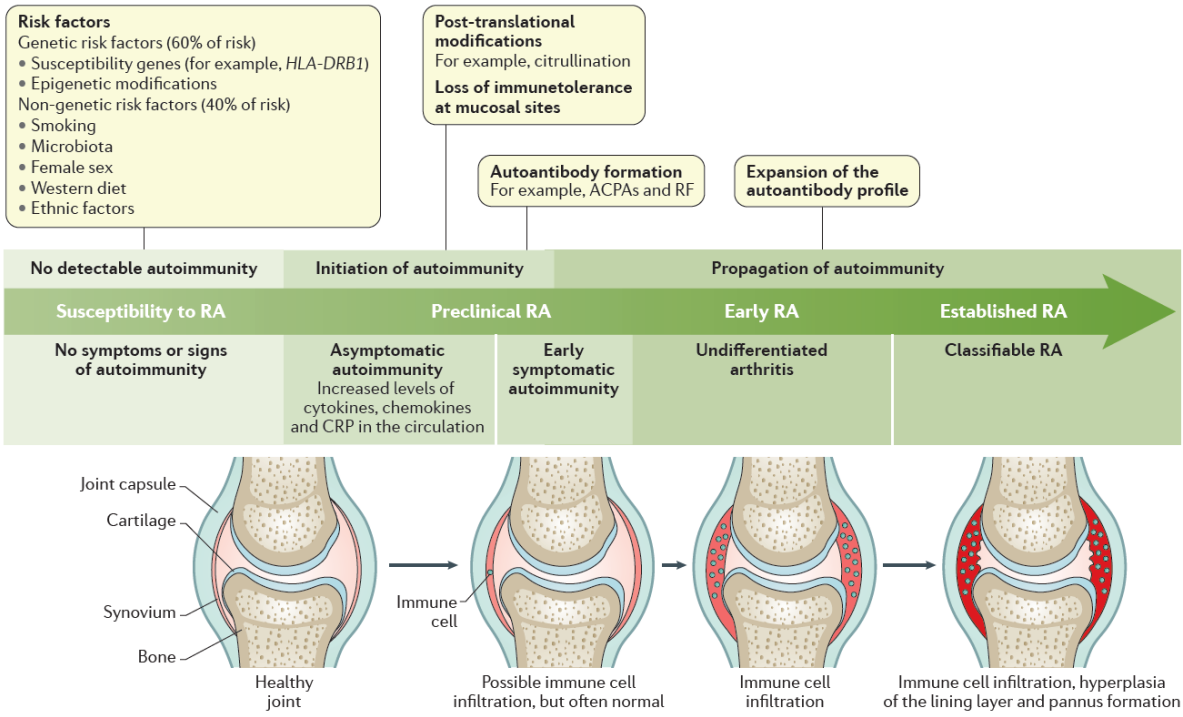

Figure 2: Diagram of the progression of RA

Schematic diagram showing the risk factors involved in developing RA and the progression of RA from a healthy joint to an established diseased joint. Image taken from Smolen et al. [2].

Table 1: Summary of risk and protective factors in RA

Risk Factors	Protective Factors
• Female sex	• HLA DRB*1301 allele
• Rheumatoid factor	• Hormone replacement therapy
• ACPAs	• Oral contraceptive pill
• Genes: HLA-DRB1, PTPN22, TRAF1	• Healthy diet
• Genes which control IL23R, CTLA4, STAT4, and IL-6 pathways	• Omega-3 fatty acids
• Family history	
• Smoking	
• Silica and pollutant exposure	
• Obesity	
• Presence of porphyromonas gingivalis bacteria	
• Postmenopausal women and early menopausal women	

1.1.4 Immunobiology of RA

RA is a heterogeneous disease and patients present with a diverse range of signs and symptoms which often overlap with other conditions such as psoriatic arthritis, peripheral spondylarthritis, metabolic diseases and osteoarthritis, making it challenging to diagnose and treat [2]. However, there are some hallmark signs of RA such as joint swelling, damage to bone and cartilage on adjacent joints [2], pannus formation, a high C-reactive protein (CRP) and erythrocyte sedimentation rate (ESR) level, and positivity for Rheumatoid factor (RF) and ACPAs [32]. Blood test, joint scans and a physical examination all contribute towards establishing a diagnosis of RA.

RA is described as a failure of the immune system to maintain self-tolerance [33]. In a normal functioning immune system, innate immune cells such as mast cells, neutrophils, natural killer (NK) cells, macrophages, and dendritic cells become activated in recognition of a foreign substance such bacteria or viruses [34]. When further help is required to fight an infection,

macrophages and dendritic cells travel to lymphoid tissues and present part of the processed pathogenic antigen (MHC molecules) to naïve CD4+ T-cells [34]. These cells, along with B-cells, are part of the adaptive immune response and they can differentiate into memory cells to provide the body with lasting immunological memory to the pathogen. The effector T-cells (a subset of activated CD4+ T-cells) release cytokines to activate B-cells and cytotoxic T-cells [34]. The role of the B-cells is to release antibodies to destroy the pathogen [35]. This explains how the innate and adaptive immune responses help to remove pathogens. However, in RA the innate immune response is not triggered by a foreign pathogen but rather a self-antigen such as a citrullinated protein [36], which is not harmful and has been mis-identified as a risk by the immune system. In RA, autoreactive B-cells also advance this process by mistaking self-antigens as 'foreign' and subsequently secrete autoantibodies targeting these self-antigens [33]. B-cell autoantibodies, such as RF and ACPAs, form part of a larger immune complex and trigger a cascade of immune responses that exacerbate RA pathology.

Other key participants involved in the pathogenesis of RA are CD4+ T-cells which have been activated by dendritic cells displaying part of the self-antigen [3,37]. The CD4+ T-cells prematurely develop into hyper-proliferative memory T-cells which in turn differentiate into pro-inflammatory Th1 and Th17 cells [37,38]. Th17 cells secrete IL-17, a potent cytokine that promotes synovitis, this leads to a porous synovial membrane and the infiltration of immune cells into the synovium [2,39]. The activated CD4+ T-cells play a strong role in the development of RA by secreting a range of pro-inflammatory cytokines (IL-2; IFN-γ) that activate other mononuclear cells, synovial fibroblasts, chondrocytes and osteoclasts which enhance disease pathogenesis [39]. They also stimulate non-effector T-cells which in turn secrete TNF-α and IL-1 [40]. Bone resorption in RA is also promoted by the secretion of RANKL by CD4+ T-cells which promotes osteoclast activity [40].

There is also erosion of cartilage in RA; this mainly promoted by the production of cartilage-degrading enzymes by neutrophils, synoviocytes and chondrocytes [39]. Fibroblast-like synoviocytes from the synovial membrane also contribute to joint swelling and extracellular matrix breakdown by producing a range of pro-inflammatory cytokines (IL-1, IL-6, TNF-α), matrix metalloproteinases (MMP-1, MMP-3, MMP-13), ADAMTS- 1, -4 and -5 (a disintegrin and metalloproteinase with thrombospondin motifs), prostaglandins and leukotrienes [2,41].

Other mechanisms also contribute to the pathology of RA, there is evidence that the innate immune system is constantly activated due to the sustained high levels of macrophage-associated cytokines (TNFα, IL-1, IL-6) [34]. These macrophages, along with other immune cells continually make their way through the permeable synovial membrane promoting the pro-inflammatory environment and sustaining joint swelling [2]. This sequence of events shows how the immune system can escalate in an uncontrolled fashion as the immune cells in the joint stimulate each other in a paracrine or autocrine way to maintain an activated immune response. The interplay between these immune cells in the development of RA is shown in **Figure 3.**

However, there are immune cells that aim to supresses the heightened immune response. $Foxp3^+$ regulatory T-cells (Treg cells) travel to the site of inflammation and play a role in supressing mainly Th1, Th2 and Th17 cells [33]. However, $Foxp3^+$ Treg cells have been found to be deficient in patients with RA and are more prone to apoptosis compared to healthy controls [1]. There is also a disturbance in the balance of Treg/Th17 cells in RA patients leading to a 5-fold increased production of IL-17 [1]. This evidence points towards a defect in Treg cells in patients with RA. Properly functioning immune suppressor cells are essential to maintain joint homeostasis and a lack of healthy functioning Tregs contributes to the survival

of pro-inflammatory immune cells. The complete involvement of immune cells and their communication pathways in RA is complex and still not fully understand. It is known that the balance between pro-inflammatory and anti-inflammatory cells is askew, favouring a pro-inflammatory environment [1]. Most medical treatments aim to suppress this activated immune response to restore joint homeostasis and reduce pain and swelling.

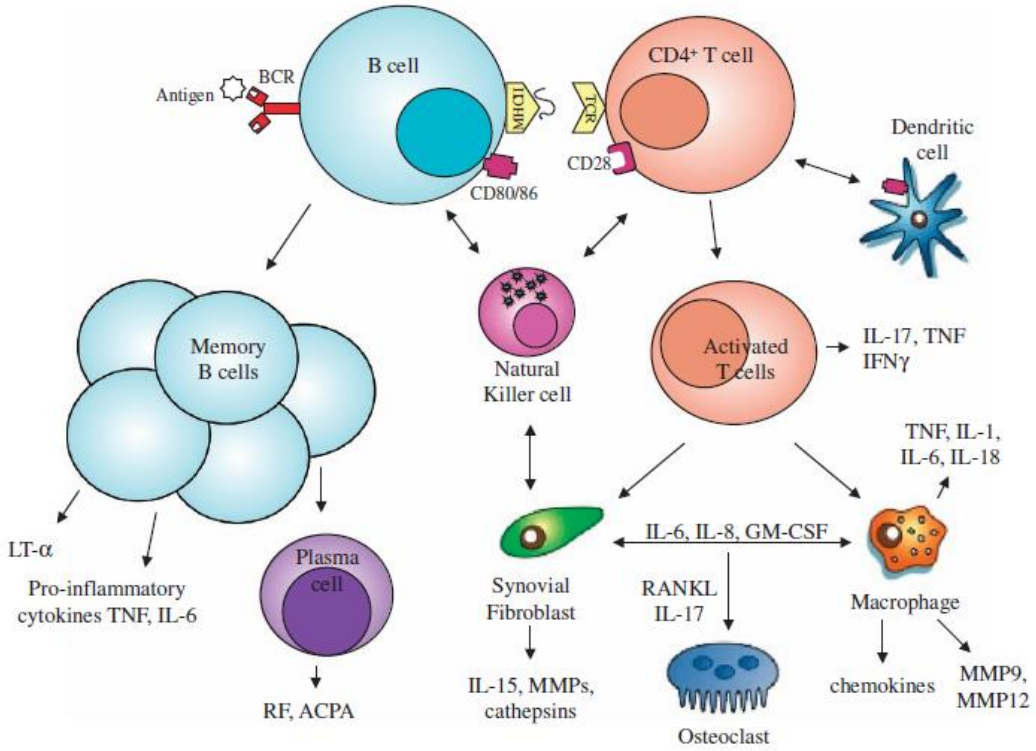

Figure 3: Diagram of cells and cytokines involved in RA

Schematic illustrating the interplay of innate and adaptive immune cells in RA. This diagram shows the activation, differentiation and pro-inflammatory cytokine secretion of immune cells which act to promote and maintain a pro-inflammatory environment in RA. Image taken from Chimenti et al. [10].

1.1.5 Pharmaceutical treatments

As there is no cure for RA, disease remission has become the main goal for RA patients. The aim when starting a treatment for RA is to achieve a 50% improvement in disease activity in 3 months [2]. RA severity is measured using the Disease Activity Score 28 (DAS28) assessment,

which is a measure of disease activity in RA, that looks at joint tenderness, joint swelling, patient reported assessment of disease activity, and the ESR count [42]. Other useful metrics to measure RA severity include the clinical disease activity index (CDAI) and the simplified disease activity index (SDAI) [2,42]. Pharmaceutical treatments include the use of Non-Biologic and Biologic Disease Modifying Anti-Rheumatic Drugs (DMARDs), Non-steroidal anti-inflammatory drugs (NSAIDs) and Glucocorticoids.

1.1.5.1 Non-biologic and biologic DMARDs

DMARDs are the most popular choice of drug for RA due to their ability to change the course of the disease [10,43]. Commonly administered DMARDs include methotrexate, sulfasalazine, and leflunomide. Of these DMARDs, methotrexate is the most commonly administered drug for RA and has been shown to slow down disease progression and reduce bone erosions and joint pain [10,42,43]. The above mentioned DMARDs are referred to as 'Non-Biologic DMARDs'. They have different molecular targets, but most work off inhibiting phosphoinositide 3-kinases, glycosidases, matrix metalloproteinases and cathepsin [44]. 'Biologic DMARDs', on the other hand, are highly specific and block T-cells, B-cells and pro-inflammatory cytokines such as TNF-α, IL-1 and IL-6 [44]. Examples of Biologic DMARDs and their targets are shown in **Table 2**. However, there are side effects to using Biologic DMARDs which include bacterial infections [45], fungal infections [46] and lymphoma [47]. While many RA patients respond well to DMARDs and Biologic Agents, there are a group of non-responders to these medications and alternative therapies are needed to treat these patients [10]. Additionally, there are some limitations to the use of DMARDs, for example, they lose their efficacy as the disease develops and they also carry an increased risk of serious infections, such as tuberculosis [2,42]. However, there are other options for non-responders of DMARDs. A new category of drugs, Janus kinase inhibitors, have emerged recent years which supress

Janus kinase enzymes of the JAK-STAT signalling pathway, a pathway which regulates the cytokines and growth factors involved in immunomodulation [48]. This provides another new and alternative treatment for RA, however these drugs are also associated with serious side effects [49].

1.1.5.2 Non-steroidal anti-inflammatory drugs (NSAIDs)

NSAIDs are used to relieve symptomatic pain and are often administered as a bridge therapy while RA patients await the therapeutic benefits of DMARDs [44]. NSAIDs, such as Naproxen or Celecoxib, work mainly by inhibiting cyclooxygenase (COX), an enzyme that breaks down cell membrane-derived arachidonic acid to form pro-inflammatory prostaglandins [43,44]. NSAIDs are purely used for pain relief and they do not have any effect on the disease, therefore, they are not used as a monotherapy for the treatment of RA [43,44]. Additionally, NSAIDs come with some serious side effects such as gastric ulceration, bleeding, nausea and nephrotoxicity, so a lot of research into NSAIDs has focused on trying to reduce these adverse effects [44].

1.1.5.3 Glucocorticoids

Similar to NSAIDs, glucocorticoids are often administered to RA patients to alleviate pain but are not recommended as a monotherapy [44]. Glucocorticoids are class of steroid hormones and they have strong anti-inflammatory and analgesic effects [43,44]. Low dose of glucocorticoids over a long period of time has been shown to reduce cartilage and bone erosion in RA patients [50]. But glucocorticoids also come with serious side effects which have been linked to most organs in the body [44]. Some side effects include osteoporosis, cataract, hypertension and peptic ulcers [43,44]. As a result, the National Institute for Health and

Clinical Excellence (NICE) recommends the use of other treatment options before considering the administration of glucocorticoids [43].

All the therapies mentioned show different levels of symptomatic relief for RA patients but many of these treatments produce severe side effects and require increasing high doses, as the disease progresses [43]. This shows that the treatments for RA are not completely without fault and further research on alternative therapies is required.

Table 2: Summary of some of the main drugs used to treat RA.

Type of Drug	Drug	Target
Non-Biological DMARD	Methotrexate	Reduces cytokine production, T-cell proliferation and diminishes polyamine levels in the joint [59].
	Sulfasalazine	Reduces T-cell proliferation and secretion of autoantibodies by B-cells
	Leflunomide	Reduces the release of pro-inflammatory cytokines
Biological DMARD	Infliximab	TNF-α
	Etanercept	TNF-α
	Adalimumab	TNF-α
	Certolizumab pegol	TNF-α
	Golimumab	TNF-α
	Anakinra	IL-1
	Tocilizumab	IL-6
	Abatacept	Binds to CD80/CD86 on antigen presenting cells and inhibits interaction with CD28 on T-cells which prevents their activation.
	Rituximab	Anti-CD20 monoclonal antibody-prevents B-cell activation
Non-steroidal anti-inflammatory drugs (NSAIDs)	Naproxen	COX-1 and COX-2 inhibitor
	Celecoxib	
	Ibuprofen	
Glucocorticoids	Prednisone	Suppression of macrophages, reduces the permeability of capillaries
	Hydrocortisone	
	Dexamethasone	

1.1.6 Conclusion

RA is a complex autoimmune disease, involving an interplay of innate and adaptive immune cells. It is characterised by joint inflammation, synovitis, bone erosion and pannus formation and, as a result, it can be a very debilitating disease [2]. Current treatments for RA, such as the use of DMARDs have been successful in bringing the disease into remission in a cohort of patients. However, not all patients respond well to current treatments, therefore, there is a need to develop alternative therapies to treat RA and bring immune responses under control.

1.2 Mesenchymal Stem Cells

1.2.1 Overview of mesenchymal stem cells

Mesenchymal Stem Cells (MSCs), also known as Multipotent Stromal Cells, are cells capable of differentiation into osteoblasts, adipocytes, and chondrocytes and can be characterised by their adherence to plastic in culture, the presence of CD105, CD73, CD90 and absence of markers CD45, CD34, CD14, CD11b, CD79a, CD19, and HLA-DR [51]. The first discovery of MSCs came in 1867, when the German pathologist Cohnheim found a population of fibroblast-like cells of non-hematopoietic origin in bone marrow [52,53] However, it took another 100 years before bone marrow cells were isolated and studied *in vitro* by Friedenstein et al. [53,54]. They discovered that these cells had the potential to form colonies and differentiate into fat, bone and cartilage in mice [53,54]. It wasn't until 1992 that the term 'mesenchymal stem cell' was coined after Caplan et al. [55] found that the multilineage differentiation potential and self-renewal properties of human MSCs was indicative of 'stemness' [53,54]. It is now known that MSCs can be obtained from bone marrow, adipose tissue, umbilical cord, amniotic membrane, placenta [56], endometrium [57], dental pulp [58] and synovial membrane [59].

Each source of MSCs shows different characteristics, but all have been found to contain some immunosuppressive effects. A general summary of the types of MSCs and their role in immune modulation is shown in **Figure 4.** One reason why MSCs have immunosuppressive effects may be attributed to their reduced expression of MHCII surface markers, meaning that they can evade immune responses when transplanted [60]. Bone marrow mesenchymal stem cells (BMMSCs) have long been considered the 'gold standard' for cellular immunosuppressive therapy, however, umbilical cord MSCs (UCMSCs) also possess many of the

immunosuppressive properties of BMMSCs and are worth exploring [61]. UCMSCs can be obtained from different areas such as Wharton's jelly, cord lining, and the perivascular region [62] however, studies carried out by Mennan et al. [63] found no significant difference in immunophenotype between the compartments of the umbilical cord. UCMSCs proliferate quicker than BMMSCs and they are easily obtained since the umbilical cords are considered to be 'medical waste'; this makes UCMSCs advantageous for use as a treatment [62]. BMMSCs display a higher migratory capacity [64] as well as stronger osteogenic and adipogenic differentiation capabilities [65], due to these differences, the target outcomes for treatment need to be considered when choosing a source of MSCs. This chapter focuses on immunomodulation by MSCs, by which both BMMSCs and UCMSCs show strong immunoregulatory effects.

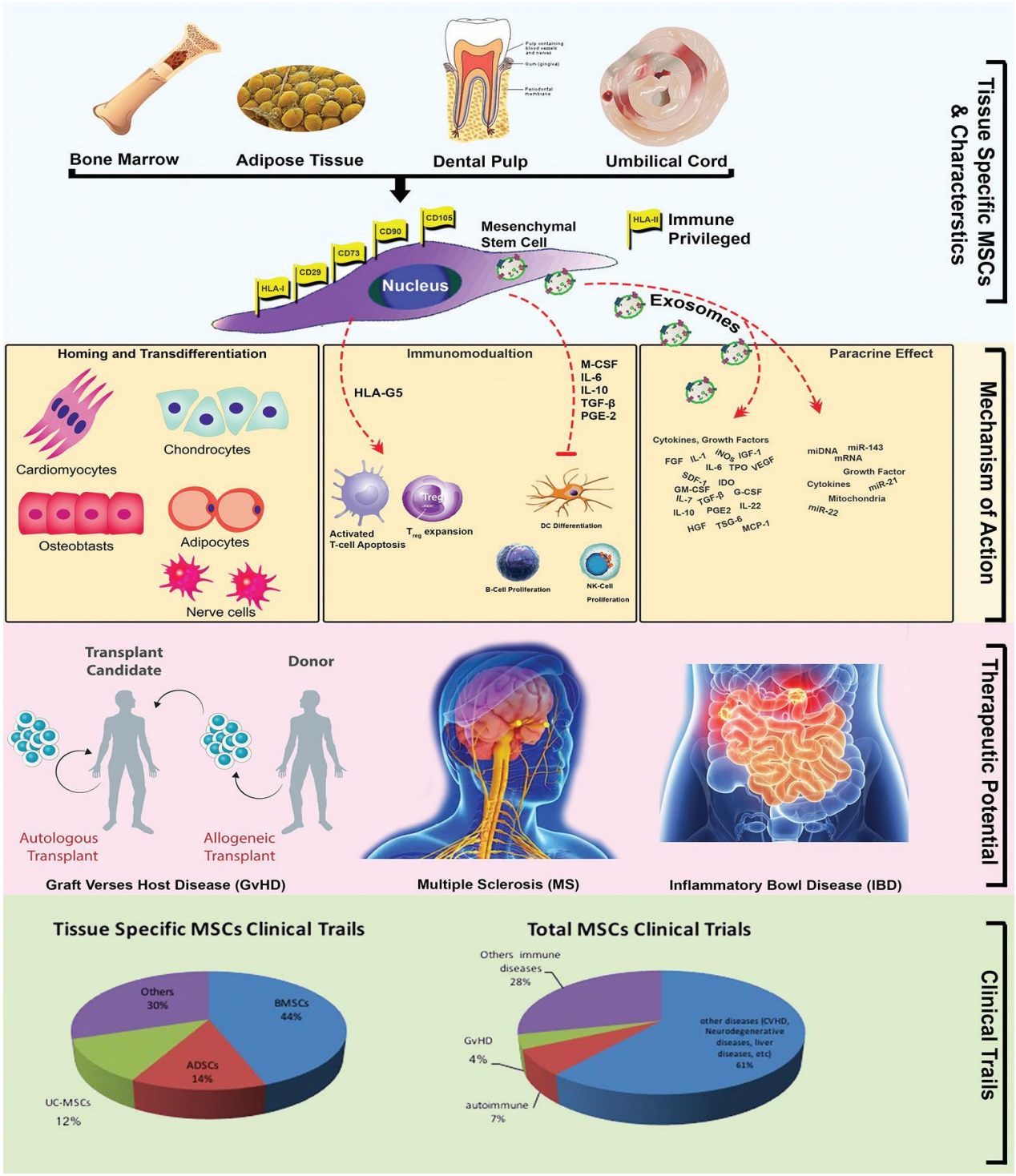

Figure 4: Overview of MSCs

Overview of the different sources of MSCs (bone marrow, adipose tissue, dental pulp, umbilical cord), their mechanisms of action (homing, differentiation, paracrine signalling), their therapeutic potential and their use in clinical trials. Image taken from Rawat et al. [66].

1.2.2 Immunomodulation by MSCs

MSCs exert their immunomodulatory effects via two mechanisms of action:

1. Cell-to-cell contact-dependent mechanism
2. Contact-independent mechanism (i.e. the secretion of soluble factors and extracellular vesicles) [67].

1.2.2.1 Cell-to-cell contact-dependent mechanism

A heavily studied area in MSC research explores if cell-to-cell contact is essential for MSCs to carry out optimal immunosuppressive effects. Luk et al. [68] compared the immunosuppressive effects of adipose tissue MSCs (ATMSCs) on B-cells in a direct co-culture and in a transwell culture system. They showed that the direct co-culture was needed for MSCs to increase the level of B-regs and IL-10; to reduce IgG production and to inhibit B-cell proliferation, as these effects were not seen in the transwell culture [68]. This study is supported by other research showing that contact dependent mechanisms aid MSCs to suppress Th17 function [69]; support T-cell and macrophage immune suppression [70] and differentiate dendritic cells into regulatory dendritic cells [71]. MSCs express integrins (α1 –α6, αV, β1 –β4), intercellular adhesion molecules (ICAM-1, ICAM-2), vascular cell adhesion protein (VCAM-1), CD72 and CD58 on their surface membranes which can modulate immune cells when in direct contact [72]. English et al. [73] showed that direct cell-to-cell contact between BMMSCs and CD4+ T-cells was required to induce FoxP3 and CD25 mRNA expression. However, direct cell-to-cell contact was not required between BMMSCs and peripheral blood mononuclear cells (PBMCs), highlighting that cell contact is not essential if there are other immune cells present [73]. These findings highlight a few ways that MSCs can suppress immune cells but many more immunosuppressive effects of MSCs have been discovered through their secretion of soluble factors [74,75].

1.2.2.2 Contact-independent mechanism

MSCs secrete many soluble factors which can affect the proliferation and polarisation of immune cells. Particularly research using *in vitro* co-culture experiments between BMMSCs and immune cells, found that BMMSCs exert immunosuppressive effects on myeloid and lymphoid cells via paracrine signalling and these signals can lead to altered cytokine expression (TNF-α, IFN-γ) and reduced proliferation in immune cells (T-cells, NK cells, dendritic cells, macrophages) [74,76]. BMMSCs have an ability to migrate to inflamed tissue where they can secrete cytokines such as TGF-β, hepatocyte growth factor (HGF) [76], and prostaglandin E2 (PGE2) [77] to reduce inflammation to maintain tissue homeostasis [78]. MSCs secrete PGE2 which reduces T-cell and NK cell release of IFN-γ [79–81]. PGE2 can also direct macrophage differentiation towards an IL-10 overexpressing phenotype, characteristic of M2 macrophages [77]. As M1 macrophages secrete pro-inflammatory cytokines which attract other immune cells to the site of damage, then a change toward the M2 phenotype represents an anti-inflammatory shift [82]. HLA-G6 secreted by UCMSCs has also been found to reduce NK cell activity [83]. Other evidence supporting a contact-independent mechanism of action was shown when BMMSCs inhibited dendritic cell differentiation and altered the cytokine secretion of other immune cells through the secretion of IL-6 [84]

In all, MSCs produce a range of soluble factors, many of which stimulate anti-inflammatory responses and aid in the regulation of the immune system. **Figure 5** displays the range of immunosuppressive effects by MSCs on innate and adaptive immune cells. In all, MSCs have wide ranging effects on innate and adaptive immunity which makes them an attractive source of cells for treatment of inflammatory conditions.

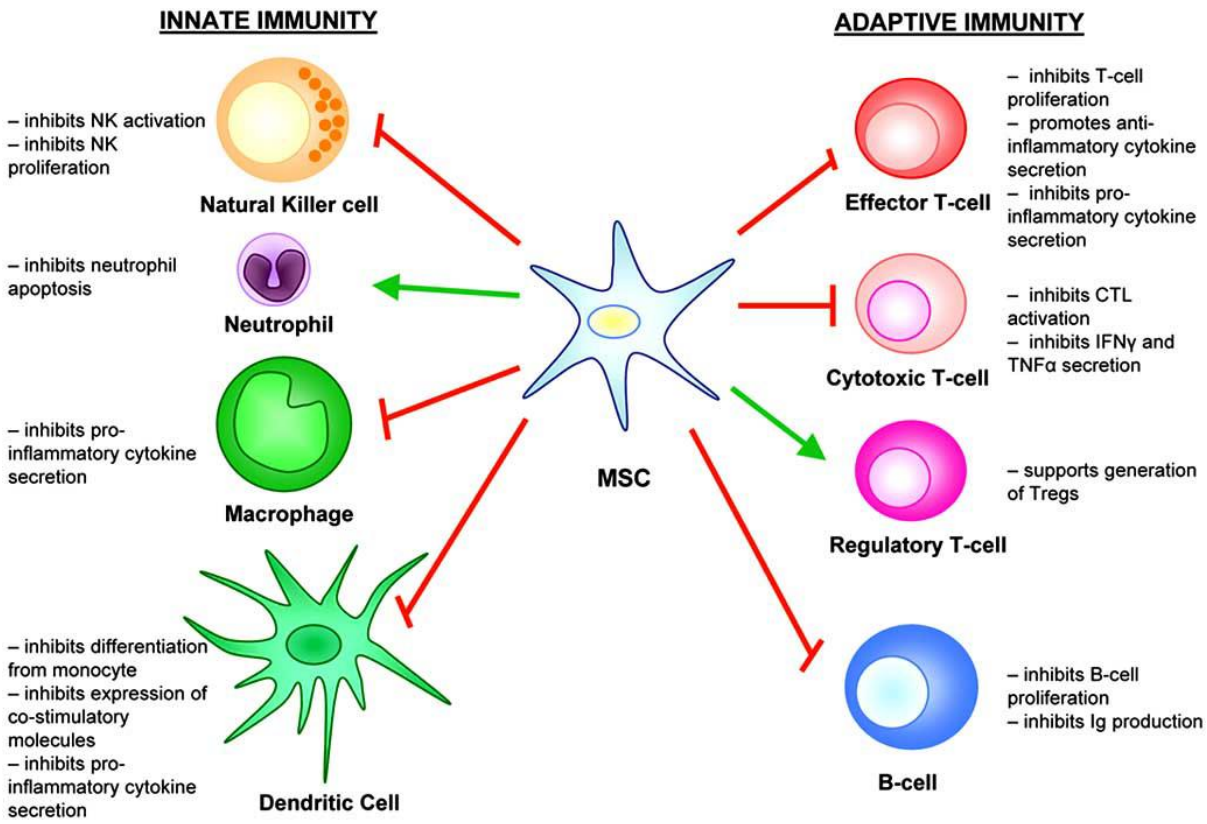

Figure 5: MSCs target innate and adaptive immune cells

Diagram displays the immunosuppressive functions of MSCs on innate and adaptive immune cells. Image taken from Newman et al. [85].

1.2.3 UCMSC interactions with T-cells

As T-cells are key contributors to RA disease pathogenesis, their interactions with UCMSCs are of interest to this thesis [37]. UCMSCs were able to increase the numbers of CD4+CD25highCD45RA+ Tregs, a subset of anti-inflammatory T-cells, in a co-culture set-up with PBMCs [86]. UCMSCs also shifted the environment towards and anti-inflammatory prolife with an upregulation of IL-10, TGF-β and PGE2 and a downregulation of IFN-γ [86]. They were found to reduce proliferation, cytotoxicity and IFN-γ expression in Vγ9Vδ2 T-cells [87]. These Vγ9Vδ2 T-cells aid in host defence, surveillance and immune response to infection

[87,88]. A high frequency of Vγ9Vδ2 T-cells has been found in RA patient blood and synovial fluid where they present antigens and secrete IFN-γ and IL-17 [37,89]. The inhibition of these cells by UCMSCs was independent of cell contact, strongly suggesting the therapeutic release of soluble factors by UCMSCs [87]. A separate study showed that UCMSCs are capable of reducing T-cell proliferation but only in the presence of monocytes [90]. There is also evidence to show that UCMSCs can supress T follicular helper (Tfh) cells [91]. There is a higher expression Tfh cells in RA and they provide antigens to B-cells which aid with the production of autoantibodies [92]. The high expression of Tfh cells in RA is also positively correlated with disease severity and the presence of anti-cyclic citrullinated peptide (anti-CCP) antibodies [91]. Liu et al. [91] showed that when PBMCs and naïve CD4+ T-cells were co-cultured with UCMSCs, the proliferation and differentiation of Tfh cells was reduced. To see if the same results were carried over into animal studies, the UCMSCs were injected into mice with collagen induced arthritis (CIA) and analysis showed a reduced number of Tfh, Th1 and Th17 cells in the spleen along with increased Treg cells [91]. There was also an improvement in hind limb swelling indicating that disease symptoms had improved. The secretion higher mRNA levels of indoleamine 2,3-dioxygenase (IDO), IL10 and HLA-G in UCMSCs was credited for these improvements [91].

In addition to Tfh cells, research by another group showed that UCMSCs can modulate Th1, Th2 and Treg cells. They cultured UCMSCs with T-cells from RA patients and found that UCMSCs supressed T-cell proliferation in both a direct and transwell culture set-up. The anti-inflammatory effects were mediated by the expression of PGE2, TGF-β1 and NO by MSCs and the downregulation of TNF-α by T-cells [93]. To corroborate these findings, a murine CIA model was used and the injection of UCMSCs successfully shifted the Th1/Th2 balance, increased Tregs, reduced pro-inflammatory cytokines (TNF-α, IL-6, MCP-1) and increased IL-

10 [93]. These findings were accompanied by an improvement in disease symptoms such as synovitis, bone degradation and pannus formation [93]. In all, UCMSCs hold similar immunosuppressive properties to BMMSCs in suppressing T- and B-cell function and both sources of stem cells hold promise for a potential treatment for autoimmune disease in the future.

1.2.4 Enhancing MSC immunosuppression

Researchers have discovered a way to promote MSCs immunosuppression by culturing them in the presence of pro-inflammatory cytokines (IFN-γ, TNF-α, IL-1β) [78,94,95]. Ren et al. [96] primed mouse BMMSCs with cytokine combinations of IFN-γ, with either TNF-α, IL-1α, or IL-1β and co-cultured them with immature T-cells. Interestingly, the immunosuppressive cytokines released by BMMSCs were only seen when they were pre-treated with pro-inflammatory cytokines, this shows that an inflammatory environment helps trigger MSC immunosuppression. Specifically, the pro-inflammatory primed BMMSCs secreted more IDO and inhibited the proliferation of T-cells. Similar findings were also true for UCMSCs, where exposure to pro-inflammatory cytokines increased the release of anti-inflammatory factors such as PGE2, TGF-β1, TSG-6, and IDO [97]. These factors are secreted at a higher level compared to BMMSCs, putting UCMSCs at the forefront for a potential cell therapy for immune suppression. These studies show that pro-inflammatory cytokines can enhance the immunosuppressive ability of MSCs ability through stimulating their production of anti-inflammatory cytokines. Future directions for MSC-based immune therapy may thereby involve priming MSCs with pro-inflammatory cytokines to enhance their activity. Positive results following pre-treatment with pro-inflammatory cytokines were found in animal models

of colitis [98] and myocardial ischemia [99]. The range of cytokines and growth factors released by MSCs after exposure to pro-inflammatory cytokines is displayed in **Figure 6.**

In addition to the pro-inflammatory priming of MSCs, hypoxic priming has also been used as a way to enhance MSC immunosuppression [100]. Hypoxic priming involves growing the MSCs in low oxygen environments to mimic their natural oxygen environment *in vivo* [101]. Indeed, research show that when rat BMMSCs are grown in hypoxic conditions, they have an increased expression of IDO and enhance Treg cell proliferation *in vitro* better than BMMSCs grown in normal oxygen conditions [100].

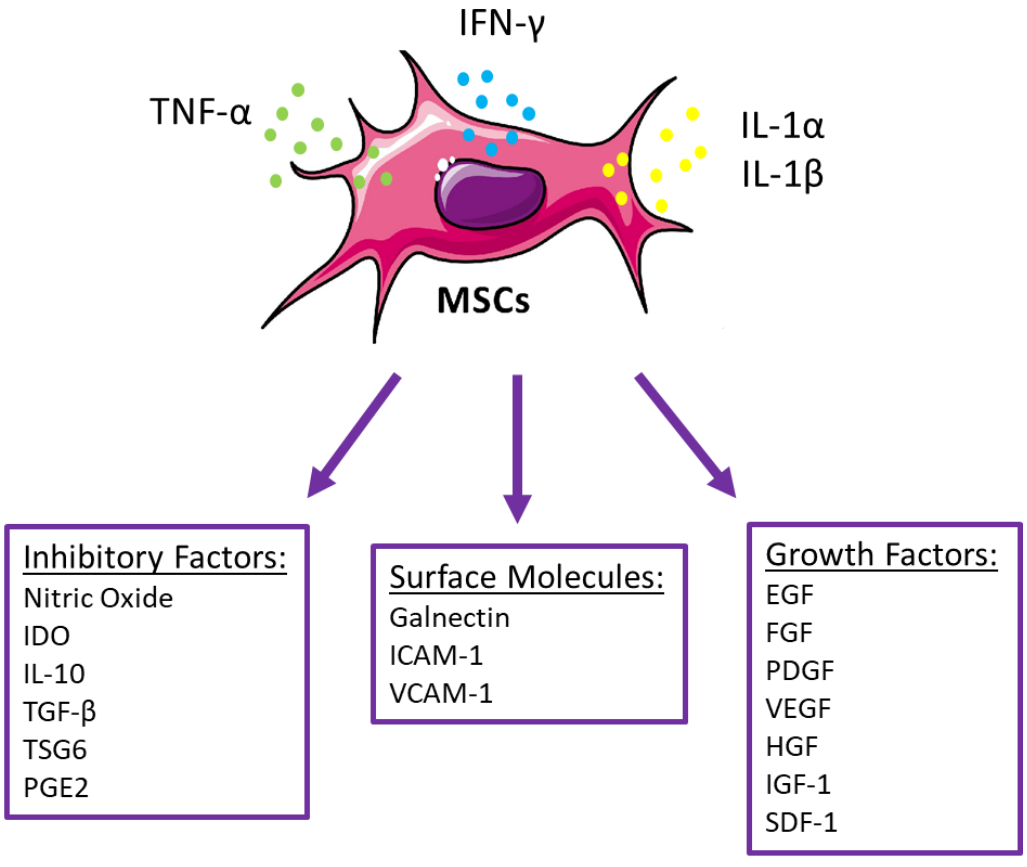

Figure 6: Secretion of soluble factors after inflammatory stimulation

When stimulated by pro-inflammatory cytokines IFN-γ (blue dots), TNF-α (green dots), IL-1α, IL-1β (yellow dots), MSCs have been found to secrete a range of inhibitory factors, surface molecules and growth factors (shown in purple boxes), which elicit a range of functional changes to immune cells. Image adapted from Shi et al. [78].

1.2.5 MSCs in animal studies of autoimmune disease

There is strong evidence of MSC immunosuppression *in vitro*, however, in order to better understand how MSCs interact with immune cells in a complex *in vivo* environment, animal studies are required. In an animal study of Systemic Lupus Erythematosus (SLE), a chronic autoimmune disease characterised by the presence of antibodies and autoreactive T and B-cells [102], mice had a reduced number of autoantibodies against double stranded DNA and nuclear cell proteins and also the reduction in pro-inflammatory cytokines (TNF-α, IFN-γ) in the UCMSC treated group compared to the control. Additionally, UCMSCs restored the CD4+/CD8+ ratio [102] which is important in cases of autoimmune disease where an imbalance of these cells promotes inflammation.

Similar results were seen for BMMSCs when they were used to treat mice with experimental autoimmune encephalomyelitis. BMMSCs, increased CD4+CD25+Foxp3+ Treg cells and reduced Th17 cells [103]. As Treg cells play a role in inhibiting autoreactive T-cells, this may explain the reduction in Th17 cells [74,103]. This study adds evidence to support the immunosuppressive effect of MSCs to modulate T-cell activity. As inflammation in RA is caused by an infiltration of T-cells through the synovial membrane, the ability of MSCs to change the T-cell phenotype to one that is less inflammatory could be therapeutically exploited as a treatment for RA.

In a further study that mimics the symptoms of RA using an Antigen Induced Arthritis (AIA) model, murine BMMSCs reduced joint swelling and TNF-α levels [104]. Intra-articular injections of BMMSCs led to reduced destruction of cartilage and the infiltration of leukocytes into the synovium, suggesting a reduction in inflammation [104]. However, a similar study

using a collagen-induced arthritis (CIA), a mouse model prototype of human RA, found that MSCs were ineffective in suppressing the immune system [105]. In this study, the MSCs were unable to inhibit CD4+ T-cells but instead enhanced Th1 activity. Further *in vitro* analysis found that the addition of TNF-α caused an increase in IL-6 and together these cytokines were able to overturn any immunosuppressive effects of MSCs on T-cell proliferation. As TNF-α and IL-6 are abundant in RA, this may explain why no improvement was seen using this model. In general, previous *in vitro* tests, have shown that an inflammatory environment can promote the immunosuppressive ability of MSCs [106]. However, the immunosuppressive ability of MSCs was not found in this study, which suggests that the severe inflammation induced by the CIA model reversed any immunosuppressive effects by the MSCs. This may mean that the use of MSCs may only be effective if TNF-α and IL-6 are blocked prior to MSC treatment in an animal model. Or perhaps, the dual use of drug and cellular therapy may together reduce the immune response in a CIA mouse model. However, this study did not use primary cells but rather murine immortalised MSCs, other studies that used primary MSCs found more positive outcomes when mice with CIA were injected with these MSCs. For example, Bouffi et al. [107] showed that MSCs reduced inflammation in CIA mice by increasing the secretion of PGE2 and by polarizing Th1/Th17 cells into Th2 cells. Additionally, Augello et al. [108] found that MSCs prevented bone and cartilage damage in CIA mice; they also found a reduced proliferation of T-cells and decreased level TNF-α indicating the immunosuppressive properties of MSCs in an RA model.

1.2.6 Clinical application of MSCs for the treatment of autoimmune disease

Figures from 2019 show that approximately 45% of clinical trials using MSCs are targeting immune related diseases, of which 69 out of 397 are focused on autoimmune conditions [66].

Both BMMSCs and UCMSCs have shown successful outcomes in trials to treat Crohn's disease, SLE, myocardial infarction and multiple sclerosis [83,109–112] but there are mixed findings for the treatment of RA [113].

In a phase 1 clinical trial aiming treat 4 RA patients with BMMSCs or UCMSCs, they found that the transplantation of both types of MSCs was safe but not effective as a long term treatment for RA [114]. Three out of four patients showed improvements in CRP, ESR and disease activity score (DAS28) after 6 months but these improvements were not sustained after this timepoint. One patient showed no clinical response to MSC treatment; however, a larger cohort is needed to determine the efficacy of this treatment.

UCMSCs have shown the most potential to reduce pro-inflammatory cytokines in RA. In a study of 172 patients with RA, half received DMARDs with UCMSCs and the other half received DMARDs only [115]. In the UCMSC treated group, there was a significant decrease in TNF-α, IL-6 and RF, accompanied by an increase in Treg cells. Improvements were also seen clinically by remission on the DAS28 and continuous infusions of UCMSCs maintained immune tolerance. Interestingly, there were no changes to CD3+, CD4+ and CD8+ T-cells which is contradictory to *in vitro* studies that found UCMSCs to reduce the proliferation of T-cells. The group that received DMARDs only did not show any improvements. Further evidence that UCMSCs could be potentially therapeutic came from a Phase I/II study of 64 RA patients who were treated with UCMSCs and DMARDs [116]. The efficacy of the treatment was confirmed by reduced ESR, CRP, RF and anti-CCP up to 3 years after treatment [116]. Additionally, improvements were also seen in the Health Index questionnaire and the DAS28 [116]. Similar to the previous studies, this study showed that UCMSCs may be a feasible and effective treatment for RA when combined with DMARDs.

Despite MSCs showing promise of the treatment of RA in clinical studies, their primary mechanism of action involves the secretion of soluble factors and extracellular vesicles [67,74,75]. It is therefore worthwhile researching EVs as the key contributors towards immune modulation. Additionally, using a full cellular transplant of MSCs as a treatment for RA is unnecessary due to the systemic nature of the disease. Localised diseases or injuries may benefit from MSC engraftment but, for RA, this is not the goal, therefore EVs are a more plausible and suitable therapeutic option to treat a widely systemic disease.

1.2.7 Considerations when using MSCs as a treatment

A number of considerations are required when preparing MSCs as a treatment. Firstly, the passage number of MSCs should be considered as this affects the cell's gene expression, phenotype and differentiation [117]. In studies of BMMSCs, average cell population doubling times fall after P6 and this is associated with a loss of genes associated with stemness, an irregular shape of MSCs, and a poor differentiation of MSCs into osteoblasts [118]. Additionally, the dose of MSCs is important for *in vivo* use; when MSC were co-cultured with $1x10^5$ lymphocytes, a high dose of MSCs ($1x10^4$ – $4x10^4$) was found to inhibit immune responses where a low dose ($1x10^1$ – $1x10^3$) was shown to increase immune cell proliferation [119]. There are a few potential risks to be considered when using MSCs as a clinical treatment, such as the biosafety of growth media for MSCs, the risk of abnormal tissue formation and the ability of cells to change phenotype *in vitro* [120]. Further challenges include trying to predict or control the differentiation of cells *in vivo* and there are a lot of regulatory restrictions associated with using cellular therapies [121].

1.2.8 Conditioned media as an alternative to cellular transplantation

Conditioned media (CM) from MSCs has been researched as an alternative to cellular therapy. The immunosuppressive functions of MSCs are often caused by soluble factors and extracellular vesicles, and the CM-MSC is thought to be rich in these immunosuppressive factors. Studies carried out in rats and mice demonstrated the anti-inflammatory properties of CM-MSCs in models of liver fibrosis [122], diabetic retinopathy [123], haemorrhagic shock induced lung injury [124], acute kidney injury [125], type 1 diabetes [126], osteoarthritis [127] and skin burns [128]. These positive outcomes were mainly due to the presence of anti-inflammatory soluble factors and EVs contained in the conditioned media. In a study of mice with AIA, Kay et al. [121] found promising results when there was a reduction in joint swelling, indicating that inflammation had reduced. Further analysis of the blood serum found that CM-MSC prevented TNF-α levels from rising and increased the expression of FoxP3, a transcriptional regulator for Treg development. This increase in FoxP3 may explain the increase in Treg cells in the spleen and this, coupled with a decrease in Th17, restored a balance of immune cells in the treated mice [121]. These results showed that CM-MSC can improve inflammation in an AIA mouse model, through reducing the pro-inflammatory cytokine TNF-α and restoring the FoxP3/Th17 balance.

The downfall of using conditioned media as a treatment approach is the researchers are blind sighted as to which specific EVs or soluble factors are responsible for the change in disease as conditioned media contains many different components.

1.2.9 Conclusion

Research has showed that MSCs can suppress immune responses using both contact dependent and independent mechanisms. Of interest to this study is the ability of MSCs to supress T-cells,

as these cells contribute to the pathogenesis of RA. Multiple studies using *in vitro*, animal, and clinical experiments show that MSCs can suppress Th1 and Th17 cells, promote Tregs and restore the Th1/Th2 balance. This makes MSCs a suitable therapeutic source to explore for the treatment of RA. Furthermore, this immunosuppression can be enhanced when the MSCs are primed with pro-inflammatory cytokines or hypoxia. The MSCs secrete EVs and soluble factors which has been heavily credited for their immunosuppressive abilities. Therefore, a more targeted approach involving the exploitation of immunosuppressive properties from MSC-EVs is gaining increasing interest in the scientific community.

1.3 Extracellular Vesicles

1.3.1 Overview of extracellular vesicles

Extracellular vesicles (EVs) are nanosized, membrane enclosed particles secreted by cells and they function as intercellular signalling molecules [129,130]. EVs are characterised based on their surface markers, size, cellular origin and content [74]. Their surface markers, protein and miRNA content are mainly determined by their cell of origin [74], which leads to wide variation in cytoplasmic content between EVs [131]. EVs contribute to paracrine signalling by transporting their cargo (mRNAs, miRNAs, proteins) to target cells [132]. EVs can interact with target cells via cell receptor binding; direct fusion with the plasma membrane of recipient cells; or endocytic internalisation [133]. After internalisation, EVs are hypothesized to deliver their intraluminal cargo to target cells, thereby altering recipient cell responses [134]. This way, EVs can influence the functions and phenotype of targeted cells [135]. MSC-EV mediated transfer of functional biomolecules into cells has led to the improvement in conditions such as cardiovascular disease, acute kidney injury, inflammatory arthritis and liver disease in animal models [136]. Since the discoveries that EVs have functional abilities and therapeutic properties, research on exosomes and EVs has grown substantially and continues to grow. This can be seen by an increase in the number of publications on exosomes and extracellular vesicles .**Figure *7*.**

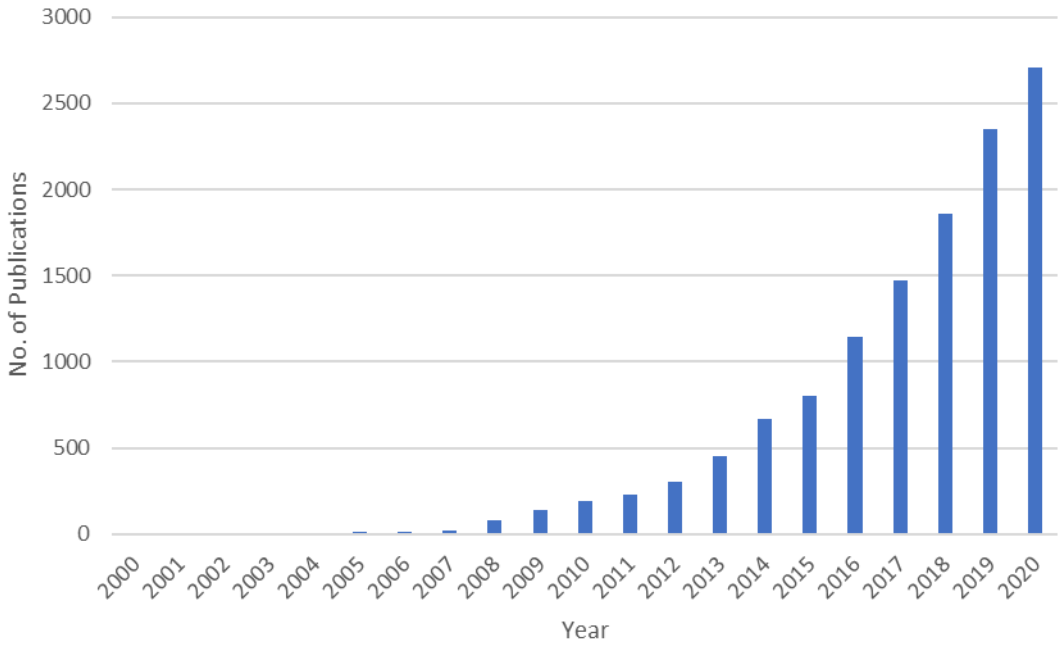

Figure 7: Increase in exosome publications

Bar chart displaying the number of publications related to 'exosome' or 'extracellular vesicle' research from 2000 to 2020. Data taken from PubMed searches.

1.3.2 Types of extracellular vesicles

There are four types of extracellular vesicles as displayed in **Figure *8*.**

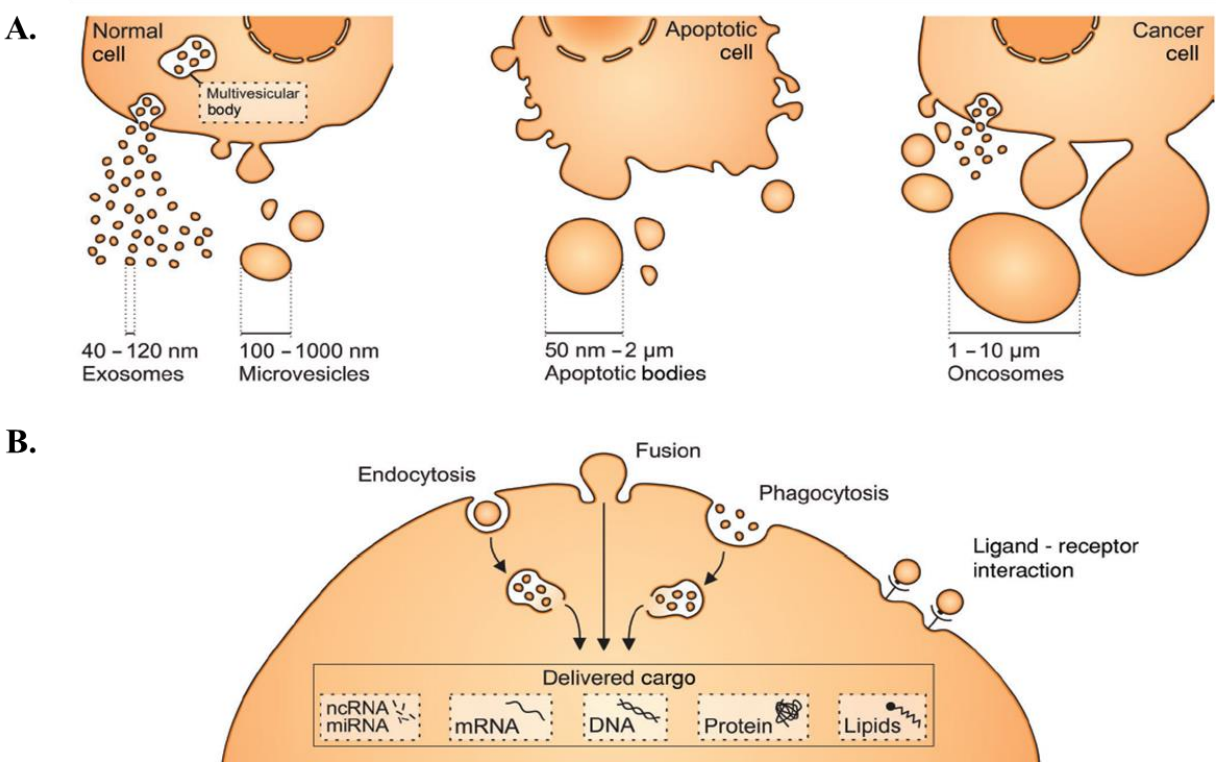

Figure 8: Type of EVs

A. *Visual representation of the size of exosomes, microvesicles, apoptotic bodies and oncosomes.* ***B.*** *These EVs interact with target cells by endocytosis, membrane fusion, phagocytosis or ligand-receptor interactions, and their cargo (miRNA, mRNA, DNA, protein, lipid) is delivered into the cell. Image taken from Zaborowski et al.* [129].

1.3.2.1 Exosomes

Exosomes are contained in intraluminal vesicles (ILV) within multivesicular bodies (MVB) in the cytosol and their content is released to the external environment via fusion of the MVB with the cell membrane [130] as shown in **Figure 9.** They range in size from 40-120nm [137] and contain a high concentration of glycoproteins and transmembrane proteins [129]. Some associated markers of exosomes include tetraspanins (e.g. CD63, CD81, CD9) [138], Tsg101, Alix, Hsc70 and Mfge8 [139]. Tsg101 plays a role in the secretion of EVs from cells [140] and it helps assemble ubiquitinated proteins into multivesicular bodies [141]. Alix is part of the ESCRT pathway and known to affect miRNA loading into EVs [142]. Hsc70 interacts with

TLRs of recipient cells and activates the NFKβ signalling pathway; it also aids with protein folding [143]. Finally, Mfge8 plays a role in EV secretion from cells [144], and in the EV complex it aids with binding to integrins on recipient cells [145]. Other exosome components include the phospholipid bilayer membrane which has a high rigidity due to the presence of sphingomyelin and desaturated lipids; this makes it more resistant to degradation compared to the cell plasma membrane [74,129,146]. This is important to prevent the degradation of exosomes in the extracellular matrix.

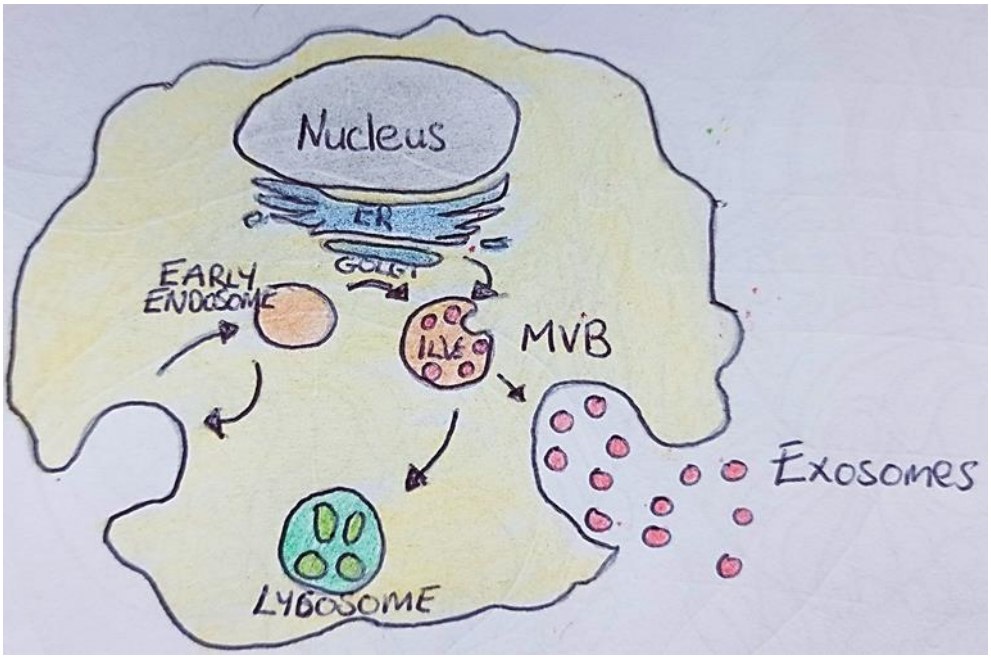

Figure 9: Diagram of exosome biogenesis

Image representing the secretion of exosomes from a cell. An early endosome buds from the plasma membrane and this leads to the formation of ILVs which eventually mature into a late endosome or MVBs. MVBs then travel to the cell membrane and fuse with it causing the release of ILVs (now termed exosomes) into the extracellular environment. Image adapted from Baglio et al. [147].

1.3.2.2 Microvesicles

Microvesicles, also known as shedding vesicles, contain cytoplasmic content such as soluble proteins and mRNA, but unlike exosomes they originate from direct budding from the plasma membrane [148]. Microvesicles are larger than exosomes, with sizes ranging from 100–1000nm [137], however, the biogenesis of EVs is more of a determining factor of its subtype than the size [139]. Microvesicles derived from MSCs express the surface markers CD29, CD73, CD44, and CD105, but these surface markers change depending on the cell of origin [74,135]. Microvesicles contain a higher abundance of proteins such as integrins (α4, α5) and glycoprotein Ib than exosomes which aid with cell adhesion [129,149].

1.3.2.3 Apoptotic bodies

Apoptotic bodies are released from dying cells [150] and they are the largest EVs ranging in size between 1μm–5μm [151] (shown in **Figure *10***). Therefore, under certain cases of cellular stress, these vesicles may be abundant in biofluid [129,137]. They bud from the plasma membrane and contain nuclear, cytosolic, and endoplasmic reticulum derived proteins [137]. They contain chromatin fragments and a reduced amount of glycoproteins [137]. They are eventually phagocytosed by macrophages in the extracellular environment [152].

1.3.2.1 Oncosomes

Malignant cells produce large vesicles (1–10μm) called oncosomes [129]. They originate from the plasma membrane of tumour cells and with increased shedding of oncomes there is a greater aggressiveness of cancer [153]. This is due to oncosomes containing signalling factors, bio-reactive molecules, miRNAs and metalloproteinases, which are involved in cancer signalling pathways and tumour progression [153].

A comparison between all four subtypes of EVs can be found in **Table 3.**

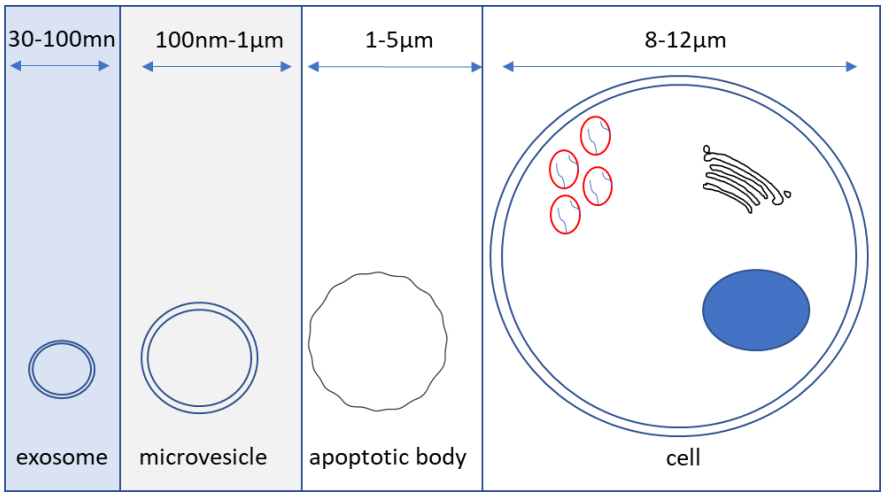

Figure 10: Size comparison of EVs

A picture representation of the size of exosomes, microvesicles, apoptotic bodies and cell as compared to one another. Size estimates taken from György et al. [151].

Table 3: Breakdown of EVs and their features

	Exosomes	Microvesicles	Apoptotic Bodies	Oncosomes
Size Range	40-120nm	100–1000nm	50 nm–2000nm	1000–10000nm
Mechanism of generation	Exocytosis of MVBs	Budding of the plasma membrane	Released as blebs from cells undergoing apoptosis	Released from plasma membrane of tumour cells
Composition	CD63, CD81, CD9, Tsg101, Alix, Hsc70, Mfge8, LAMP1	ARF6, Rho, Actin tubulin-β1 integrins, CD40 ligand, VAMP3, microRNA	Any cellular components, including DNA and rRNA	Tsg101, epidermal growth factor receptor VIII, mutant Ras family members, c-Met

nm-nanometre; Tsg-tumour susceptibility gene; Hsc-heat shock cognate, Mfge-Milk fat globule-EGF factor; LAMP-Lysosomal-associated membrane protein; ARF-ADP-ribosylation factor; VAMP-vesicle-associated membrane protein. Adapted from Burke et al. [132], *Minciacchi et al.* [153], *György et al.* [151] *and Buzas et al.* [154].

The term ‘extracellular vesicles’ (EVs) will be used from here on to describe both exosomes and microvesicles since both have molecular and functional similarities [155,156]. Additionally, there is no specific marker to distinguish exosomes from microvesicles and their sizes often overlap making it difficult to isolate a specific population of EVs [155,156].

1.3.3 Functional properties of MSC-EVs

1.3.3.1 The polarisation of immune cells by MSC-EVs

MSC-EVs have been shown to switch a pro-inflammatory immune environment into an anti-inflammatory environment. In order to figure out how they are capable of this suppressing immune function, researchers have studied the interactions between MSC-EVs and isolated immune cells. In terms of T-cells, the interaction between MSC-EVs and T-cells depends largely on the T-cell subset, as *in vitro* studies have shown that MSC-EVs can have an immunosuppressive role towards Th1 and Th17 cells, but an immunostimulatory role towards Th2 and Treg cells [157]. The polarising of T-cells into Th1 and Th2 effector cell types in response to MSC-EVs has been shown in numerous *in vitro* studies. For example, Chen et al. [157] found that MSC-EVs shifted Th1 cells into Th2 cells while also preventing the differentiation of Th1 cells down a Th17 lineage when MSC-EVs were co-cultured with PBMCs. Additionally, the ratio of Th17 to Treg cells changed to favour the immunomodulatory Tregs [157]. A reduction in TNF-α and IL-1β, and an increase in TGF-β in the co-culture media may explain how these T-cells were polarised towards an anti-inflammatory phenotype.

Not only have MSC-EVs shown potential to modulate T-cell activity, but they have also been shown to polarise M1 macrophages into an M2 phenotype. Lo Sicco et al. [82] studied the interactions between EVs from ATMSCs grown in normoxia (20% O_2) and hypoxia (1% O_2)

on macrophages [82]. They identified that the macrophages not treated with EVs had a stronger pro-inflammatory surface marker expression seen by higher expression of CD11b, CD40, and CD86, and an upregulation of the M2 markers Arg1 and Ym1 [82]. This shows that both normoxic and hypoxic EVs were altering the surface marker phenotype, indicative of a switch from an M1 to M2 phenotype. This is significant for immune modulation as M1 macrophages play a role in antigen presentation and activation of Th1 cells, whereas M2 macrophages have a more immunosuppressive role. These immunosuppressive findings were further confirmed by a reduction in IL-6 and an increase in IL-10 in a mouse model of skeletal muscle injury [82]. This *in vitro* and *in vivo* study showed evidence of macrophage polarisation to an anti-inflammatory phenotype which is mediated by the presence of MSC-EVs.

The polarisation of macrophages by MSC-EVs was also shown by another group. Ti et al. [158] treated MSC-EVs with lipopolysaccharide (LPS) and co-cultured them with a monocytic cell line. Through microarray analysis of macrophages there was an upregulation in Let7b. Let7b targets the TLR4 pathway which M1 macrophages use in generating a pro-inflammatory response [159]. The identification of this miRNA shows that EVs may use multiple mechanisms to polarise macrophages towards an anti-inflammatory phenotype. They also identified the surface marker CD163, a common M2 macrophage marker, in the co-culture. Furthermore, there was an increased expression of IL-10 and TGF-β and reduced presence of pro-inflammatory cytokines (IL-1, IL-6, TNF-α) [158], all indicative of an anti-inflammatory shift. These findings were supported further by a diabetic wound healing animal model in which LPS treated MSC-EVs decreased inflammation, promoted new blood vessel formation and reduced TLR4 expression to improve the wound healing [158].

All these studies show that EVs are altering the ratios of pro-inflammatory to anti-inflammatory immune cells in the blood. Analysis of an MSC-EV co-culture with PBMCs and monocytes shows that the EVs interact with many of the T-cell populations and macrophages, and collectively this can significantly reduce their ability to produce a pro-inflammatory immune response. These studies are important in evaluating if MSC-EVs can potentially be used as an anti-inflammatory therapy. The over-active immune response seen in many autoimmune conditions is complex and involves the interplay of many different innate and adaptive immune cells, so the finding that MSC-EVs can modulate many of these immune cell populations is promising for the potential formation of an EV therapy.

1.3.3.2 MSC-EVs alter the growth kinetics of immune cells

In addition to polarising T-cells, MSC-EVs have been shown to reduce T-cell proliferation. In a study of UCMSCs-EVs, they showed similar effects to their parent UCMSCs in inhibiting the proliferation of T-cells by 60% *in vitro* [160]. Blazquez et al. [161] found similar results for human ATMSC-EVs, where they reduced the proliferation of CD4+ and CD8+ T-cells, and decreased effector memory T-cells. In a study comparing UCMSCs, BMMSCs and their corresponding EVs, Pachler et al. [162] showed that EVs could effectively inhibit T-cell proliferation *in vivo*. However, this effect was dose dependent. In fact, EVs from ten times the amount of MSCs was required to achieve the same immunosuppressive effect as the cells [162]. These findings contradict a study by Conforti et al. [163] whom found increased doses of MSC-EVs ineffective at reducing T-cell proliferation.

Despite some results showing that MSC-EVs reduce the proliferation of T-cells, some researchers argue that the MSC-EVs are instead inducing their apoptosis. Chen et al. [157] found that MSC-EVs reduced the numbers of Th1 and Th17 cells through inducing apoptosis

rather than affecting cell proliferation. Mokarizadeh et al. [164] showed that MSC-EVs induced the apoptosis of T-cells and similarly, Del Fattore et al. [165] found that MSC-EVs induced apoptosis of CD3+ T-cells and CD4+ T-cells, whereas their parent MSCs inhibited CD3+ proliferation only with no change to apoptosis. In all, MSC-EVs have the potential to alter the growth kinetics of different T-cell populations, but whether this is via inducing their apoptosis or reducing their proliferation remains to be confirmed.

1.3.4 Which factors in the EV cargo are responsible for their therapeutic effect?

How EVs carry out their immunosuppressive functions is an area of great interest and many mechanisms of EV immunosuppression have been mentioned thus far, but this section provides an overview of some proteins and miRNAs that have shown immunosuppressive functions. From the exosome database 'ExoCarta', 938 proteins and >150 miRNAs have been identified in MSC-EVs [166]. These proteins and miRNAs are known to be functional and regulated by external stimuli in the environment [167]. Proteomic analysis of MSC-EVs found that many of the proteins regulate MSC self-renewal, differentiation, cell adhesion and migration [168,169]. Additionally, when comparing MSCs with MSC-EVs, some researchers identified proteins that were unique to EVs or expressed at a higher level than parent cells, indicating an enrichment in specific proteins in EVs [170,171]. These enriched proteins had roles in angiogenesis, immune regulation and cell adhesion and migration [170,171]. Common proteins found in MSC-EVs which stimulate Tregs and supress CD4+ T-cells and B-cells include TGF-β, PD-L1 and galectin-1 [164,172,173]. Mokarizadeh et al. [164] found that the expression of PD-L1 by MSC-EVs induced iTreg development, sustained the expression of FoxP3 and negatively regulated the activity of self-reactive T-cells in mice with experimental autoimmune encephalomyelitis (EAE) [174,175]. Studies of galectin-1 and TGF-β have shown that they can promote Treg proliferation and functioning [176–178]. Further analysis of MSC-EV cargo

shows the presence of chemoattractant proteins such as CXCL2, CXCL8, CXCL16 which may attract immune cells towards MSCs where they can carry out their immune protective roles [179]. The presence of anti-inflammatory proteins IL-10, HGF and LIF as well as angiogenic proteins VEGF in the MSC-EV cargo were also likely contributors to the immunosuppressive effects [179].

Additionally, miRNAs contained within the EV cargo are known to target multiple pathways. Specifically, MSC-EV miRNAs have been found to regulate stem cell differentiation (Let-7, miR-215) [180–183], immune responses (miR-155, miR-146, Let-7i) [184,185] and tumorigenesis (miR-192, miR-23b) [166,186,187]. As well as containing miRNAs, EVs also contained other messenger RNAs (mRNA), transfer RNAs (tRNA), long noncoding RNAs (lncRNAs), small nucleolar RNAs (snoRNAs) and mitochondrial DNA (mtDNA) [166]. Indeed, MSC-EVs are highly enriched in tRNA representing approximately 23-50% of small RNA in EV cargo, whereas miRNAs only represent approximately 2-5% of EV small RNAs [188]. However, although only a small fraction of EV-RNA is thought to consist of miRNAs, research has shown that it is functional and can silence gene targets in recipient cells [188]. Studies have shown that EV-miRNAs can suppress the translation of pro-inflammatory proteins in immune cells. Specifically, Di Trapani et al. [184] found miRNA-155 and miRNA-146, contained within the pro-inflammatory primed MSC-EV cargo, aided in reducing the proliferation of B- and NK- cells [184].

Even if EVs contain some therapeutic molecules, it is necessary that a pure population of EVs is isolated which is void of any contaminating factors which may override the therapeutic properties of EVs. This was highlighted in a study by Monguio-Tortajada et al. [160]. They co-cultured UCMSC-EVs with T-cells and found that the EVs did not promote a pro-inflammatory

cytokine response from T-cells, however non-EV components and conditioned media promoted the secretion of pro-inflammatory cytokines (IL-6, TGFβ1, IL-17A, IFN-γ) by T-cells. Additionally, non-EV and conditioned media cultures polarised T-cells down a pro-inflammatory Th17 lineage, but the pure EV population prevented this polarisation. As Th17 is a well-known inducer of inflammation in autoimmune disease [189], this is promising as the EV/T-cell co-culture did not contain the expression of the Th17 cells. This study shows that a pure population of the UCMSC-EVs is necessary and can prevent the further release of pro-inflammatory cytokines from T-cells [189].

In all, the mechanism of action between MSC-EVs and immune cells seem vast and very pleiotropic in nature. Therefore, the use of omics approaches, and gene knock-out studies has increased in the EV field in an aim to accurately characterise the EV protein and miRNA components that are responsible for change. Most research is pointing towards an immunosuppressive route for MSC-EVs which is positive for their potential application to ameliorate inflammation.

1.3.5 Comparison between MSCs and MSC-EVs in immune suppression

EVs exert a range of immunomodulatory effects similar to their parent MSCs, however there are cases where their mechanisms of action vary. Specifically, some studies have shown that MSC-EVs have different mechanisms of action towards suppressing T-cells than MSCs. Cosenza et al. [190] divided the EV population into the microparticle and exosome subgroups and found that neither group was able to change the proliferation of CD4+ and CD8+ T-cells but they were able to increase the Treg population, whereas the MSC group had the opposite effect; these cells were able to reduce the proliferation of CD4+ and CD8+ T-cells and they did

not affect Treg numbers. In findings similar to the Cosenza et al. [190] study, Del Fattore et al. [165] showed that MSC-EVs were able to increase Treg proliferation which skewed the Treg: T-effector cell ratio whereas MSCs alone had no effect on the Treg: T-effector cell ratio. Di Trapani et al. [184] also showed that MSC and MSC-EVs used different mechanisms to suppress PBMCs. They showed that MSCs mainly used the immunosuppressive enzyme IDO; which was undetected in MSC-EVs, instead they expressed PD-L1 which was responsible for their immunosuppressive effects. This study shows that MSCs and MSC-EVs have different mechanisms of action in suppressing immune responses.

In all, studies have shown MSC-EVs are capable of immune suppression [130]. However, whether this immunosuppressive effect is as strong as MSCs alone is of clinical importance. It has already been mentioned in **Section 1.3.3.2** that approximately ten times the amount EVs is needed to supress the proliferation of T-cells to the same degree as MSCs [162]. But this opens another question, are MSCs more immunosuppressive than MSC-EVs?

When trying to decipher which is more effective at suppressing immune cells – MSC or MSC-EVs, many groups have found that MSCs provide a more potent immunosuppressive ability in comparison to EVs [163,184]. Conforti et al. [163] showed that MSCs were superior to EVs in reducing T-cell proliferation, inhibiting plasma cell differentiation and lowering B-cell antibody production. In a co-culture assay between MSC and PBMCs, there were higher levels of IL-10 and TGF-β and lower levels of pro-inflammatory cytokines (granulocyte macrophage colony-stimulating factor (GM-CSF), IL-2, IFN-γ) compared to the co-cultures containing only MSC-EVs [163]. The only area that EVs had similar effect to MSCs was in inhibiting B-cell proliferation, but, in all MSCs had a stronger immunosuppressive ability [163]. Other groups have found MSC-EVs as capable as MSCs alone in inhibiting B-cells. Budoni et al. [191]

investigated the immunosuppressive effect of BMMSC-EVs compared to MSCs alone on B-cell activity *in vitro*. They found that MSC-EVs had a similar effect in inhibiting B-cell proliferation and differentiation compared to MSCs alone when used in high concentrations [191]. However, the immunosuppressive effect of MSCs was stronger than MSC-EVs in reducing the production of antibodies (IgM, IgG and IgA) by B-cells.

1.3.6 Can MSC-EV immunosuppression be enhanced?

Many studies have 'primed' or 'preconditioned' their MSCs with different pro-inflammatory agents to see if this elicits an anti-inflammatory response from the cells and generates EVs with a stronger immunosuppressive potential. However, in EV studies, findings are mixed whether this has a negligible or therapeutic effect. Monguió-Tortajada et al. [160] found no differences in T-cell proliferation and polarisation between IFN-γ primed and non-primed UCMSC-EVs. They subsequently recommend against priming of MSCs with IFN-γ before clinical use, as it did not have any effect on the immunomodulatory potential of UCMSCs, but instead increased the expression of HLA-DR, a ligand for the T-cell receptor [160]. Mokarizadeh et al. [164] found differing results when they primed their MSC-EVs with IL-1β. They found that the inhibition of splenic mononuclear cells and promotion of Foxp3+ Treg cells in mice with experimental autoimmune encephalomyelitis (EAE) was heighted in MSC-EVs primed with IL-1β. However, both the primed and rested EVs equally induced the apoptosis of T-cells [164]. Di Trapani et al. [184] co-cultured EVs with PBMCs and found that MSC-EVs had a stronger immunosuppressive ability when exposed to pro-inflammatory priming (TNF-α, IFN-γ). Interestingly, they found that the degree of EV-mediated suppression of immune cells was directly correlated with the degree of uptake of EVs by immune cells [184]. The increased uptake of primed MSC-EVs by immune cells is likely due to their increased expression of ICAM-1 compared to non-primed MSC-EVs [184]. Cosenza et al. [190] found that plasmablast

differentiation was inhibited in the presence of MSCs, microparticles and exosomes seen through a reduced production of IgG but found no difference in the EVs when the MSCs were primed beforehand with IFN-γ. This contradicts the findings by Di Trapani et al. which found an enhanced immunosuppressive role when EVs were primed [184].

In all, EVs show an immunosuppressive potential, but whether the priming of their parent cells generates a population of EVs with a heightened anti-inflammatory response needs to be addressed if EVs are to be biologically engineered as therapeutic agents.

1.3.7 Immunosuppression by MSC-EVs in animal studies

In order for EV research to develop to a clinical stage, it is important to see therapeutic immunosuppression in animal models of inflammation. Indeed, UCMSC-EVs have shown positive therapeutic effects in treating animal models of acute myocardial ischaemia [192], liver fibrosis [193], reducing bladder tumour growth [194] and preventing renal injury in a diabetic mouse model [195]. Additionally, in a study of two animal models of autoimmune disease: type 1 diabetes (T1D) and experimental autoimmune uveoretinitis (EAU), human BMMSC-EVs successfully prevented the onset of the diseases [196]. In the T1D model, there were fewer CD4+ cells in the pancreatic islets compared to the PBS-treated control, and in the EAU model, there was fewer infiltrating CD3+ T-cells in the retina, less structural damage and a reduction in pro-inflammatory cytokine transcripts compared to the control [196]. Further investigations were warranted to decipher how these MSC-EVs are carrying out immunosuppressive changes, so a co-culture experiment between MSC-EVs and a mixed lymphocyte population was set-up. Results from this showed that the EVs were able to supress several immune cells by reducing the levels of their activating cytokines. Namely, Th1

development was suppressed because the EVs reduced levels of IFN-γ, IL-12, p70, and TNF-α; and Th17 development was suppressed by a reduction in IL-6 and IL17 [196].

Cosenza et al. [190] looked at the anti-inflammatory potential of microparticles and exosomes in a mouse model of Delayed-Type Hypersensitivity (DTH) and Collagen-Induced Arthritis (CIA). Clinical improvements such as a reduction in paw swelling and global arthritis clinical score were seen in animals treated with exosomes but not microparticles (MPs). However, both groups showed a decrease in plasmablasts and an increase in the B-reg population. Analysis from mouse lymph nodes showed the exosomes were effective in reducing the pro-inflammatory cytokines IL-6 and IL-1β, whereas MPs only decreased IL-6. While both groups showed an anti-inflammatory potential, the exosomes demonstrated a stronger immunosuppressive role. In all, the positive effect of MPs and exosomes in the DTH and CIA models are promising as these models produce many similar symptoms to that of RA [197,198].

1.3.8 Therapeutic potential of MSC-EVs in human studies

There are few clinical trials using MSC-EVs to treat autoimmune diseases. BMMSC-EVs were used in a trial treating one patient with grade IV acute GvHD [199]. The EVs had been characterized prior to administration and they contained high concentrations of anti-inflammatory cytokines IL-10, TGF-β and HLA-G. Pro-inflammatory cytokines such as IL-1β, IL-6 and TNF-α were absent from the EV preparation. The treatment saw a reduction in PBMCs by 50%. There was also a reduction in IL-1β, TNF-α and IFN-γ [199]. Clinical symptoms of GvHD improved and remained stable four months after treatment. However, despite the findings indicating a therapeutic value for MSC-EVs, the trial involved one patient and significantly larger trials are required to prove its value as an immunosuppressive therapy.

Another study, treating a cohort of 40 patients (20 treated; 20 control) with chronic kidney disease, found therapeutic benefit using UCMSCs-EVs [200]. Results found that patients who received the EV treatment had improved urinary albumin creatinine ratio and decreased blood urea and serum creatinine which clinically indicate improved kidney function. EVs were effective in increasing TGF-β1 and IL-10 and decreasing TNF-α with no cytokine changes in the control group. Of interest to this review, is the clinical treatment of autoimmune diseases using MSC-EVs, by which more studies need to be published.

1.3.9 Advantages of EVs

It has been shown that UCMSCs are safe and well tolerated in clinical trials. Additionally, they have anti-inflammatory properties when combined with DMARDs for the treatment of RA. Then it must be asked ‘why study their EVs’? EVs offer a cell-free therapy solution which makes it easier to standardise treatments and assess changes [121]. They can be stored which makes it easier for clinical treatments and research suggests they have an immunosuppressive potential [135]. Additionally, the therapeutic benefit of MSCs is mainly attributed to their release of soluble factors and EVs [74], therefore further research is needed into the role of the secreted particles. For these reasons, MSC-EVs are an attractive alternative to using a cellular transplant but they warrant further research into their immunomodulatory properties. A summary of the advantages of using EVs is shown in **Table 4.**

Table 4: Advantages of using EVs

•Can be used as 'Off-the-shelf' therapy [66]
•Does not require cryopreservation in liquid nitrogen [66]
•Can be produced on a large scale [66]
•EV cargo can be modified to deliver specific effects [66,201]
•EVs are naturally found within the body so they are biocompatible when administered *in vivo* and retain structural and functional stability [201]
•EVs have a better safety profile than therapeutically administered cells and no toxicity or any side effects of EV administration are reported in published animal studies [201]

1.3.10 Challenges in EV research

For EVs to be a viable therapy in clinics, several obstacles need to be overcome.

Most labs grow MSCs in cell culture media containing Fetal Bovine Serum (FBS). FBS provides proteins and growth factors that support cell growth however, it also contains a large amount of bovine EVs with a similar morphology to human EVs [202,203], therefore, the collection of conditioned media from human MSCs would contain EVs of both bovine and human origin. This would lead to inaccurate results when trying to study the immunomodulatory potential of human MSC-EVs.

To address this problem, the FBS requires EV depletion before adding it to cell culture. The main advantage of EV depleting FBS is that it reduces the contamination of bovine EVs in the final EV preparation and it supports cell growth, albeit at a reduced rate of proliferation [203]. Another option is to serum starve cells however, there is a risk of cell apoptosis and this method induces a stress response from cells, shown by an increased level of reactive oxygen species

[203], which will affect the downstream analysis of EVs. Some labs used pre-made nutrient-enriched media which does not require the addition of serum. However, for trade purposes, the contents of this media are not disclosed by companies and therefore this may make it difficult fully understand cell behaviour. Finally, there is an option to purchase EV depleted FBS, however it is expensive, so research groups have developed protocols to deplete FBS of EVs.

Methods of FBS-EV depletion vary in terms speed and time. A summary of the methods used is found in **Table *5*.** Speeds ranging between 100,000xg and 120,000xg are generally accepted as being efficient for EV depletion [202,204]. Further variation is seen in the literature regarding the length of time to EV deplete the FBS. Shelke et al. [202] found that an 18 hour centrifugation at 120,000xg was effective at reducing RNA-containing FBS-EVs by 95%, whereas a 1.5 hour protocol is insufficient. They did not find any difference in the ultracentrifugation of neat FBS or FBS diluted with PBS at a 3:7 ratio [202]. Similarly, Eitan et al. [205] found that a 1 hour ultracentrifugation time was only effective in reducing EV concentration by 2.2-fold compared to a 7-fold decrease observed after 6 hours. However, whilst the longer spin depleted more EVs, there was also an increased depletion of other proteins contained in FBS indicating a reduced specificity of EV depletion [205]. Therefore, the greatest challenge is to identify the shortest length of time to optimally deplete the FBS of EVs whilst also retaining some of the larger proteins which support cell growth.

Table 5: Comparison of different methods of EV depleting FBS

Paper	FBS Viscosity	Speed	Time
Willms et al. [206]	Neat	110,000g	Overnight
Shelke et al. [202]	Neat	120,000g	18hours
Kornilov et al. [203]	Neat	121,896g	19hours
Greening et al. [207]	Neat	100,000g	18hours
Liao et al. [204]	1:4 (FBS: PBS)	110,000g	18hours
Aswad et al. [208]	20% FBS	100,000g	Overnight
Eitan et al. [205]	1:3 (FBS: DMEM)	2,000g for 10 minutes 10,000g for 40 minutes 120,000g for 1-6 hours	
Thery et al. [209]	20%FBS	100,000g	Overnight
Jeppesen et al. [210]	20%FBS	100,000g or 200,000g	16hours

Some other questions that remain to be answered in the EV field include:

- Is the cargo of EVs dependent on their biogenesis pathway? For example, are there certain proteins contained within exosomes that would be able to distinguish them from microvesicles? Answering this question may be able to identify different subtypes of EVs.
- Which source of MSCs produces the most immunosuppressive EVs?
- Is one EV subtype more efficacious than the other in reducing inflammation? For example, are exosomes more effective than microvesicles?
- What is the optimal method of isolation of EVs? At present researchers are using a wide range of EV isolation techniques such as ultracentrifugation, density gradient centrifugation, size exclusion chromatography, filtration, immunoaffinity capture, polymer-based precipitation [211]. The different techniques used by researchers leads to a wide variation in the final EV product in terms of size, purity, cargo, and surface marker expression. This can lead to different functional performance from EVs and makes it difficult for researchers to compare EVs from different studies. An example of how each isolation technique correlates with EV yield and purity is shown in **Figure**

11. Due to the variety of EV isolation methods available, researchers are introducing some isolation bias into their study based on the method they choose. This was demonstrated by Lobb et al. [212] who tested four different isolation methods on the same cancer cell line and found that precipitation based methods produce the least pure exosomes, repeated ultracentrifugation reduces particle yield, and density gradient purification contains particles with the most exosomal markers. There were also shortcomings identified in each method such as a high starting volume for ultracentrifugation and membrane blocking occurring with ultrafiltration [212].

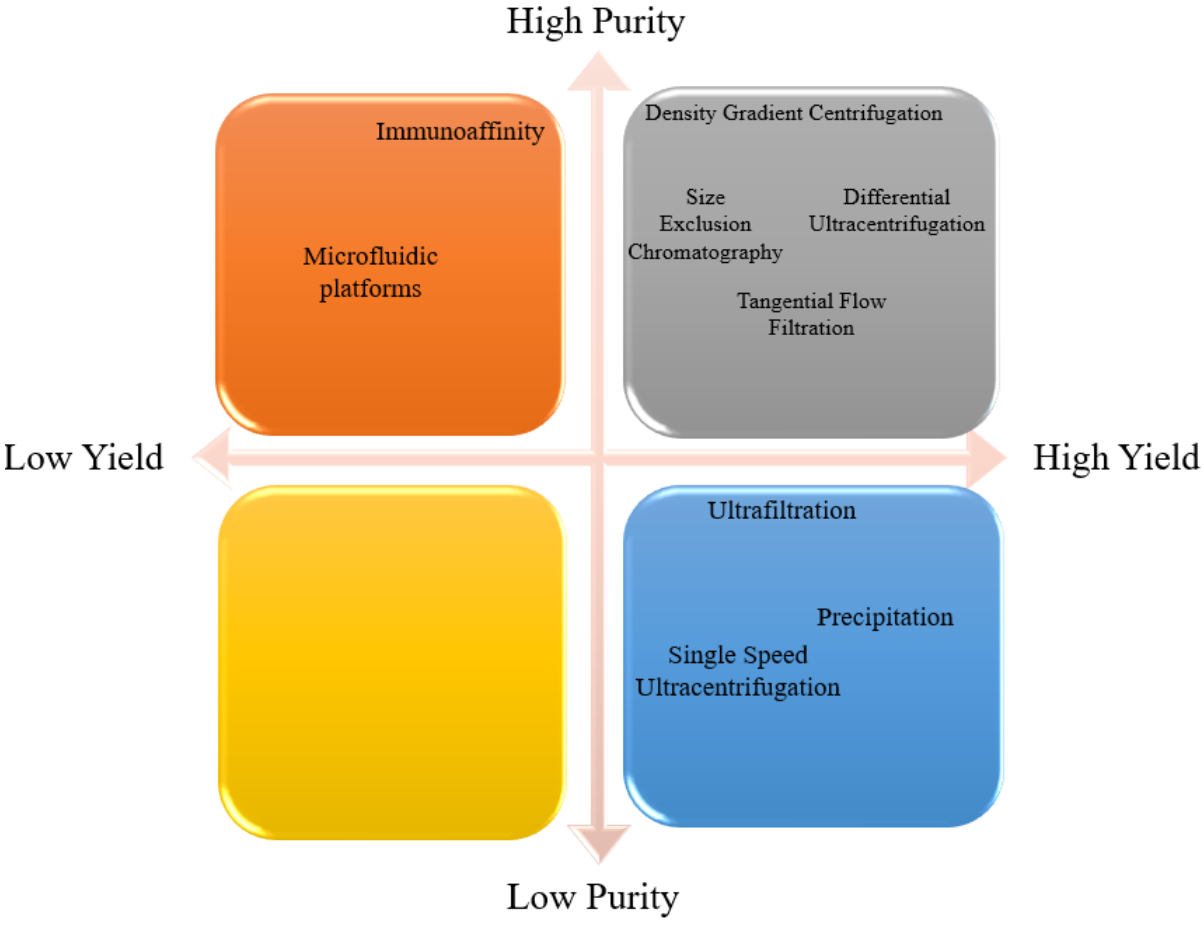

Figure 11: Purity and yield of different EV isolation methods

Figure represents the performance of different EV isolation methods in terms of yield and purity. The EV yield is presented on the x-axis and the EV purity is presented on the y-axis. Figure adapted from Fricke et al. [213].

1.3.11 Conclusion

MSC-EV mediated immunosuppression is a growing area in scientific research due to its potential to treat numerous autoimmune and inflammatory diseases. This chapter looked at one autoimmune disease, rheumatoid arthritis, and gained an understanding into the pathogenesis of this disease. This chapter also looked closely at the properties and immunosuppressive functions of MSCs and MSC-EVs. MSCs and MSC-EVs were critically explored as potential therapeutic products for the treatment of RA, and while research strongly shows that these cells and EVs can suppress immune responses, there are many questions remaining and lots of different avenues to explore before they can be employed for this purpose. This chapter thereby looked at some considerations required when using MSCs and some challenges that exist in EV research.

Overall, this chapter gave a detailed overview of RA, MSCs and MSC-EVs. It examined current research on MSCs and MSC-EVs as immune suppressors. It explored at some of the advantages and disadvantages of using MSCs and EVs, and finally, it highlighted some areas that are still unclear in the literature and need to be researched further.

1.4 Thesis Aims and Objectives

1.4.1 Rationale for the study

Recent research has shown the therapeutic, anti-inflammatory potential of MSC-EVs. However, there is a gap in the literature about which culture conditions produces a population of UCMSC-EVs with the strongest anti-inflammatory potential. Therefore, there is a need to firstly, research the immunomodulatory potential of UCMSC-EVs, and secondly, compare UCMSC-EVs from different culture environments to see which population can suppress immune responses. Normoxic, hypoxic and pro-inflammatory conditions are compared in this thesis. Throughout this thesis, 'normoxia' is defined as ambient atmospheric oxygen levels (i.e., 21% O_2), similar to atmospheric air, and 'hypoxia' is defined as low oxygen levels (i.e. 5% O_2). However, it is recognised that in other publications, 'hypoxia' is defined as a lack of oxygen to cells [214] and for UCMSCs, their 'normal' *in vivo* environment is 5% O_2, thereby the oxygen levels cannot be considered insufficient or lacking. But, for clarity throughout, this thesis adopts the term 'normoxia' to describe 21% O_2 and 'hypoxia' to describe 5% O_2.

1.4.2 Hypothesis

Clinical and animal research has shown that UCMSCs can ameliorate autoimmune diseases by suppressing pro-inflammatory immune responses [102,115,116]. Their immunosuppressive potential has largely been attributed to paracrine signalling. As EVs are involved in cell-to-cell communication via paracrine signalling, it is hypothesised that UCMSC-EVs possess many of the same immunomodulatory properties as their parent UCMSCs, i.e., they are anti-inflammatory and able to suppress immune responses. Additionally, the immunosuppressive potential is heightened by MSC preconditioning in hypoxia and with pro-inflammatory

priming. Therefore, the second hypothesis is the MSSC-EVs from hypoxic and pro-inflammatory primed UCMSCs show a stronger anti-inflammatory potential.

1.4.3 Aim of thesis

To examine the therapeutic properties of extracellular vesicles from umbilical cord mesenchymal stem cells for the treatment of rheumatoid arthritis.

1.4.4 Objectives:

1. To successfully isolate extracellular vesicles and characterise them based on their protein and miRNA content.
2. To compare extracellular vesicle characteristics and functioning from UCMSCs grown in four different conditions (normoxia, normoxia and pro-inflammatory primed, hypoxia, hypoxia and pro-inflammatory primed).
3. To investigate if UCMSC-EVs can polarise T-cells towards an anti-inflammatory phenotype.

Chapter 2: Materials and Methods

2.1 Materials

List of Reagents and Equipment Used			
Company	**Address**	**Chemicals Used**	**Cat No**
Abcam	Cambridge, UK	• H&E Staining Kit	• ab245880
Agar Scientific	Essex, UK	• Sonomatic Langford sonicator • Copper grids • Uranyl acetate	• N/A • G2002 • AGR1260A
Agilent Technologies	Waldbronn, Germany	• Agilent Bioanalyzer 2100 • RNA 6000 Pico kit • Agilent 4200 TapeStation • High Sensitivity RNA ScreenTape Assay	• G2939BA • 5067-1513 • G2991AA • 5067- 5579
AllCells	Alameda, CA, USA	• Bone marrow aspirate- 15ml	• ABM001
Atom Scientific	Cheshire, UK	• Toluidine Blue (1% aqueous)	• RRSP146-C
Baker Ruskinn	Bridgend, UK	• Invivo$_2$ hypoxic workstation • HypoxyCOOL™ media conditioning system	• N/A • N/A
BD Biosciences	Wokingham, UK	• Human BD Fc Block™ • CD105 APC • CD90 PE-CF594 • CD73 BV-421 • CD14 PerCP-Cy5.5 • CD45 PE-CF594 • CD34 APC • CD19 BV-421 • HLA-DR APC • CD106 APC • CD146 PE-CF594 • BD FACSDiva CS&T IVD Beads • FACSCanto II • FlowJo® software	• 564220 • 562408 • 562385 • 562430 • 562692 • 562279 • 555824 • 562440 • 559868 • 551147 • 564327 • 656047 • N/A • N/A
Beckman Coulter	High Wycombe, UK	• L8-M Ultracentrifuge • 10.4ml closed top polycarbonate tube • Fixed angle type 70.1Ti rotor	• N/A • 355603 • 342184
Bio-Rad	Oxford, UK Watford, UK	• CD81 monoclonal antibody • 4x Laemmli buffer • 4-15% TGX stain free gel • ChemiDoc MP Imaging System • Image Lab v. 6.0.1 software	• MCA1847 • 1610747 • 4568086 • N/A • N/A
BMG Labtech	Aylesbury, UK	• FLUROStar Omega plate reader • PHERAstar FS multi-mode plate reader	• N/A • N/A

Catalag Medsystems	Buckingham, UK	• AllCells bone marrow aspirate	• ABM001
Cell Signalling Technologies	London, UK	• Rab5a monoclonal antibody	• 30021200
eBioscience	Waltham, US	• mouse IgG2a • 1x Intracellular Fixation Buffer • Permeabilization Buffer (10X)	• 14-4724-85 • 88-8824-00 • 00-8333-56
Genta Medical	York, UK	• Isopropyl alcohol • Xylene	• IPA050 • XYL050
Gibco/Thermo Fisher/Life Technologies/Fisher Scientific	Warrington, UK Paisley, UK Rockford, USA Waltham, USA Loughborough, UK	• Pierce BCA protein assay kit • DMEM F12 • Fetal Bovine Serum (FBS) • Dulbecco's phosphate-buffered saline (DPBS) • Penicillin/Streptomycin (P/S) • Trypsin/EDTA • MEM Non-Essential Amino Acids Solution (100X) • poly-L-Lysine coated microscope slides • Gentamicin • TGF-β1 • CellMask Orange™ • Goat anti-mouse IgG-HRP • SuperSignal West Pico Chemiluminescent Substrate • Qubit® 2.0 instrument • Qubit™ RNA HS Assay Kit • Qubit™ RNA BR Assay Kit • Qubit® double-stranded DNA (high sensitivity) assay • IKA MS3 vortexer • PCR Sprint Thermal cycler • 0.2ml PCR tubes • Applied Biosystems QuantStudio 3 Real-Time PCR System • QuantStudio™ Design and Analysis Software v.1.5.1	• 23225 • 11320-033 • 10270 • 14190-144 • 15070063 • 25200072 • 12070346 • 5027988 • 15710064 • PHG9204 • 10093243 • 62-6520 • 34580 • Q32866 • Q32855 • Q10211 • Q32854 • 10492342 • HBSP02 • 11899221 • A28567 • N/A
Greiner Bio-One Ltd	Stonehouse, UK	• High-binding enzyme-linked immunosorbent assay (ELISA) strips	• 756071
Illumina Inc.	California, USA	• Illumina NovaSeq SP	• N/A
Kaivogen Oy	Turku, Finland	• Red assay buffer • Europium fluorescent intensifier	• 42-02 • 42-04
Koki Holdings Ltd	Tokyo, Japan	• 25PC polycarbonate thick-walled centrifuge tubes • Hitachi Himac Micro Ultracentrifuge CS150NX	• S309140A • N/A

Leica	Wetzlar, Germany	• Leica Diaplan microscope	• N/A
Life Science Solutions	MA, USA	• Olympus ix71 microscope	• N/A
Lonza	Basel, Switzerland	• Pen-Strep • Bone Marrow Aspirate	• DE17-603E • 1M-105
Malvern Instruments Ltd	Amesbury, UK	• NTA NS300 system	• N/A
Miltenyi Biotec	Woking, UK	• MACSPlex Exosome Kit (human) • T Cell TransAct™, human	• 130-108-813 • 130-111-160
New England BioLabs Inc.	Massachusetts, USA	• NEBNext® Multiplex Small RNA Library Prep Set	• E7300L
Nikon Instruments Inc.	Tokyo, Japan Melville, USA	• Nikon DS-Fi1 camera • Nikon Eclipse TS100 microscope	• N/A • N/A
OLink Bioscience	Upsalla, Sweden	• Proseek® Multiplex Inflammation Panel	• 91301
Peprotech	London, UK	• IFN-γ • IL-1β • TNF-α	• 300-02 • 200-01B • 300-01A
Perkin Elmer	Coventry, UK	• Goat anti-mouse IgG-biotinylated antibody • Europium conjugated streptavidin	• NEF823001EA • 1244-360
Qiagen	Manchester, UK	• miRNeasy micro kit • Proteinase K • miRCURY LNA RT Kit • miRCURY SYBR® Green PCR Kit	• 217084 • 19131 • 339340 • 339346
R&D Systems	Abingdon, UK	• BSA • CD9 monoclonal antibody	• DY995 • MAB1880
Sage Science	Beverly, US	• Pippin prep station	• N/A
Santa Cruz Biotechnology	Texas, US	• Alix monoclonal antibody • Hsp70 monoclonal antibody • Cytochrome C monoclonal antibody	• sc-53540 • sc-66048 • sc-13156
Sarstedt Ltd	Leicester, UK	• 0.22µm filter (Filtropur)	• 83.1826.001
Scientific Laboratory Supplies	Nottingham, UK	• 25PC Polycarbonate open top tubes	• S309140A
Sigma-Aldrich/Merck	Poole, UK Gillingham, UK	• Dexamethasone • β-Glycerophosphate • L-Ascorbic acid • IBMX (3-Isobutyl-1-methylxanthine) • Insulin-Transferrin-Selenium Media Supplement (100×) • Indomethacin • Naphthol AS-BI	• D4902 • G9891 • A4403 • I5789 • I3146 • I7378 • 3864

		• Fast Red ITR • Oil Red O • Paraffin wax • Toluidine Blue O • Crystal Violet • RIPA buffer • Bovine Serum Albumin • Deuterium Oxide • Sucrose • β-mercarptoethanol • Paraformaldehyde • cOmplete™ Protease Inhibitor Cocktail • Phenylmethylsulfonyl fluoride (PMSF) • RNaseA • Trypan blue • Brefeldin A • Fibronectin • Collagenase Type 1	• 201286 • O0625 • V001228 • T3260 • C0775 • R0278 • A1933 • 151882 • S0389 • M6250 • 158127 • 11697498001 • 10837091001 • R6513 • T8154 • B6542 • 10838039001 • SCR103
SIS systems	Birmingham, UK	• JOEL-JEM 1230 Transmission Electron Microscope • MegaView 3 Soft Imaging System	• N/A • N/A
Stem Cell Technologies	Cambridge, UK	• Lymphoprep™	• 07801
Terumo BCT	Colorado, USA	• Quantum® Cell Expansion System	• N/A

2.2 Methods

2.2.1 General Cell Culture

2.2.2 Isolation of MSCs from umbilical cord

Umbilical cords (n=4) were collected from the Robert Jones and Agnes Hunt Orthopaedic Hospital (RJAH) following natural delivery with ethical approval (National Research Ethics Service; 10/H10130/62). Patient demographic information are shown in **Table 6**. The isolation of MSCs from umbilical cord was not done as part of this work and is described in Mennan et al. [63].

Table 6: Demographic profile of the four umbilical cord donors

Figures obtained for BMI were obtained at the time of gestational booking (~week 8-11).

UCMSC	Age	BMI	Gender of newborn
Donor 1	35	19.2 (Healthy)	Male
Donor 2	23	25.4 (Overweight)	Male
Donor 3	24	23 (Healthy)	Female
Donor 4	28	24.4 (Healthy)	Male

2.2.3 Standard cell culture procedure

UCMSCs were passaged when they reached ~70-80% confluency. This was carried out by removing the spent culture medium and washing the cells in dPBS (pre-warmed to 37°C) to remove dead cells and residual FBS. The UCMSCs were then incubated in pre-warmed 0.05% trypsin/ 0.53 mM ethylenediaminetetraacetic acid (EDTA; Gibco, Warrington, UK) for 5 minutes at 37°C. UCMSCs were observed under a light microscope (Nikon Instruments Inc. Melville, USA) to ensure they had detached from the flask. To neutralise the trypsin activity, an equal volume of pre-

warmed complete media was added and the UCMSCs were centrifuged for 5 minutes at 700xg to pellet the cells. Following centrifugation, the supernatant was discarded, and the cell pellet gently re-suspended in 1ml of complete medium. The viability and number of cells were assessed using a trypan blue exclusion assay. This was performed by adding 10µl of trypan blue (Sigma, UK) to 10µl of cell suspension in a 0.5ml eppendorf tube. Ten microlitres of the suspension was pipetted under a glass coverslip on a haemocytometer, and the cells observed and counted under the microscope. Non-viable (dead cells) appear blue, while viable (live) cells do not take up the dye as they have intact cell membranes, so appear clear. Healthy cell cultures in the log-phase were expected to have > 95% viability.

2.2.4 Cell expansion of UCMSCs in normoxia

UCMSCs were first cultured on tissue culture plastic and then culture expanded in a Quantum® Cell Expansion System, shown in **Figure *12*** (Terumo BCT, Surrey, UK), and described in Mennan et al. [215]. UCMSCs were then grown under normoxic conditions (21% O_2; 5% CO_2) up to passage 8 and fed every 2-3 days with DMEM F12, 10% FBS, 1% P/S (Life Technologies, Warrington, UK).

Figure 12: Image of the Quantum® Cell Expansion System

UCMSCs were seeded into the Quantum® Cell Expansion System and grown in ~11,500 hollow fibre tubes. The computer-controlled system enables the flow of gases and media into the bioreactor. Waste

media is collected, and cell growth is monitored by glucose and lactate readings from the sample port [215,216]. *Image taken from https://www.terumobct.com/quantum.*

2.2.5 Cell expansion of UCMSCs in hypoxia

UCMSCs were also culture expanded in hypoxic conditions (5% O_2; 5% CO_2) in the Invivo$_2$ hypoxic workstation (Baker Ruskinn, Bridgend, UK) as shown in **Figure *13*.** UCMSCs were fed every 2-3 days with DMEM F12, 10% FBS, 1% P/S (Life Technologies, Warrington, UK). This media solution was the same as in normoxic conditions, but prior to feeding cells with media, the oxygen content of the DMEM F12 was lowered to approximately 5% as described below.

Figure 13: Image of Invivo$_2$ hypoxic workstation used for growing UCMSCs

The InvivO2 hypoxic workstation system was programmed to an oxygen level of 5% and a CO_2 level of 5%. All supplies were put into the system through the interlock side door (on the right of photo) and hands through the sleeve port. The system then equilibrized to the same gas concentration as the main chamber to ensure atmospheric gases were not altering the gas concentration that the cells were exposed to.

2.2.6 Degassing of media using HypoxyCOOL™ media conditioning system

Prior to culturing cells in hypoxia, the oxygen content of the media was reduced to 5% using the HypoxyCOOL™ media conditioning system (Baker Ruskinn, Bridgend, UK). This work was carried out at the Guy Hilton Research Centre. Briefly, vented caps were added to six 500ml bottles of DMEM, and these were loaded into the HypoxyCOOL™ which was programmed to 2% O_2 (or 5% O_2) for 3 hours at 4°C. The media was gently agitated in the machine to promote the gas exchange throughout the media. When the cycle had finished the vented caps were replaced with airtight caps and stored at 4°C until use. PBS was freeze/thawed to remove the dissolved oxygen in the solution before being used to wash cells.

2.2.7 Pro-inflammatory priming

In one experimental setting, UCMSCs were stimulated with pro-inflammatory cytokines (hereafter referred to as 'primed') for 48 hours in both normoxic and hypoxic conditions when they reached 80% confluence. They were treated with an inflammatory cocktail containing 5ng/ml TNF-α, 2.5ng/ml IFN-γ and 2.5ng/ml IL-1β (Peprotech, London, UK) added to DMEM F12, 10% EV depleted FBS, 1% P/S. The conditioned media of the primed cells was then collected for EV isolation. **Figure 14** outlines the experimental plan and culture conditions of UCMSCs.

2.2.8 Depletion of EVs from FBS

FBS is rich in EVs and steps must be taken to reduce the contamination of bovine EVs. Therefore, FBS was subject to a long ultracentrifugation to deplete FBS of EVs. The Depletion of EVs from FBS was carried out at the University of Keele. The EV depletion of FBS followed

a protocol by Shelke et al. [202]. Neat FBS was loaded into sterile 25PC polycarbonate thick-walled centrifuge tubes (Koki Holdings Co., Japan) and weighed to ensure that each tube was balance equally in the ultracentrifuge. The FBS was ultracentrifuged at 120,000g for 18 hours at 4ºC using a Hitachi Himac Micro Ultracentrifuge CS150NX (Koki Holdings Co., Japan). The FBS supernatant was removed, stopping ~3cm before the bottom of the tube to avoid the pellet. The FBS supernatant was subject to a 0.2µm syringe filter followed by a 0.1µm filtration and stored at -20ºC before use in cell culture.

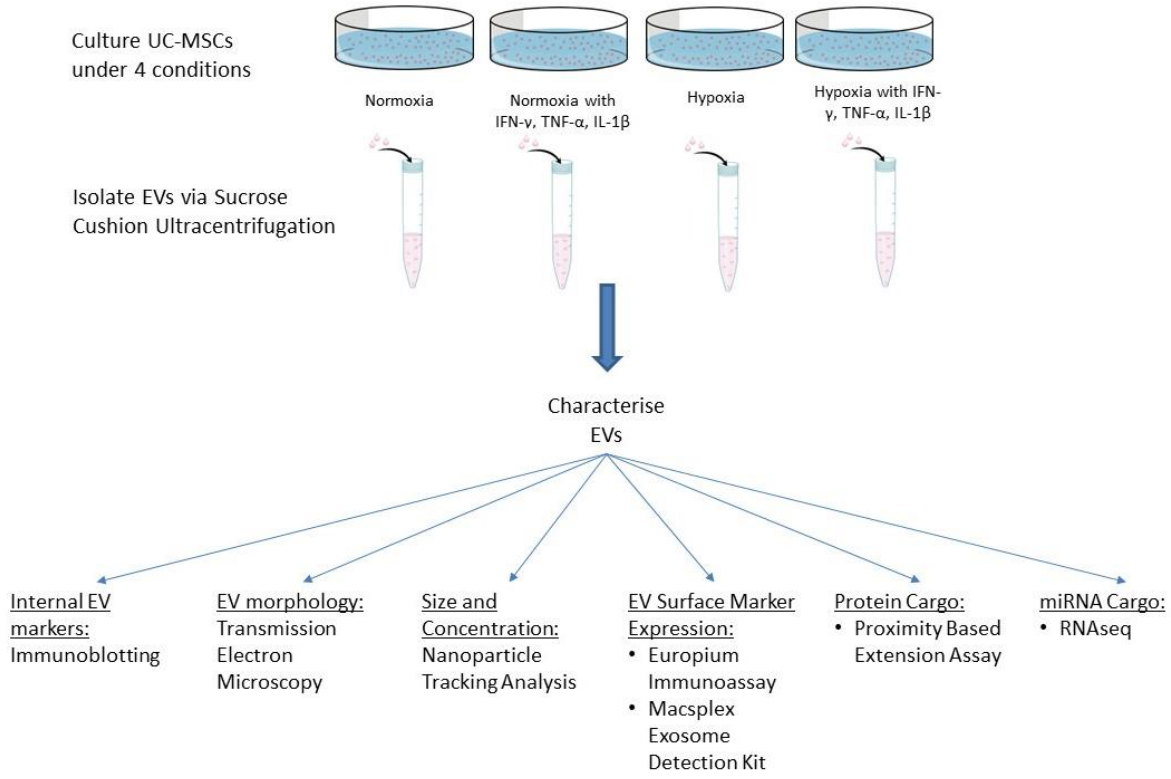

Figure 14: Schematic of study plan

Diagram displays the study design including culture conditions of UCMSCs, EV characterisation and cargo analysis experiments.

2.2.9 Isolation of MSCs from bone marrow

Human bone marrow aspirate (15ml) was ethically sourced from the Lonza Group Ltd (n=1) (Basel, Switzerland) and AllCells LLC (n=1) (CA, USA). Both aspirates originated from healthy young adults. Both companies collected the bone marrow in sodium heparin syringes from the iliac crest. MSCs isolated from the aspirate were initially cultured both in normoxic (21% O_2) and hypoxic (2% O_2) conditions.

2.2.10 Cell expansion of BMMSCs in normoxia

Bone marrow aspirates (n=2) was diluted 1:1 with Dulbecco's phosphate-buffered saline (DPBS) (Life Technologies, Warrington, UK) and layered over 10ml Lymphoprep™ (Stem Cell Technologies, Cambridge, UK). The aspirate was centrifuged at 900xg for 20 minutes and the buffy coat was extracted at the interface. The mononuclear cells were centrifuged at 750xg for 10 minutes and the pellet was resuspended in DMEM F12, 20% Fetal Bovine Serum (FBS), 1% Penicillin/Streptomycin (P/S) (Life Technologies, Warrington, UK). The cells were seeded at a density of $20x10^6$ in $75cm^2$ T-flasks and incubated at 37°C at 5% CO_2. The medium was changed every 2-3 days until passaging. When cells were confluent, the MSCs were passaged with Trypsin-EDTA (Life Technologies, Warrington, UK) and the FBS content of the media was reduced to 10%. Cells were seeded at a density of 5×10^3 cells/cm^2. Protocol adapted from Mennan et al. [217].

2.2.11 Cell expansion of BMMSCs in hypoxia

Fresh bone marrow aspirate was plated directly into $175cm^2$ tissue culture flasks, coated with 10ng/ml fibronectin diluted in sterile water, at a density of $10^5/cm^2$. Cells were cultured in an

InvivO$_2$ hypoxic workstation (Baker Ruskinn, Bridgend, UK) at 37^{o}C, 2% O_2 and 5% CO_2. The aspirate was seeded in DMEM F12 (30ml per flask), 10% FBS, 1% P/S, 1% L-Glutamine, 1% P/S and 1% non-essential amino acids (NEAA) (Life Technologies, Warrington, UK) for 14 days with half of the media changed after 7 days, protocol by Agrawal et al. [218]. At 14 days, the cells were washed with dPBS to remove non-adherent cells and the presence of fibroblastic colonies was identified. After 14 days, cells were cultured in DMEM F12, 10% FBS, 1% P/S (Life Technologies, Warrington, UK). When dense fibroblastic colonies were observed in the flask at the 21-day timepoint, the cells were passaged with Trypsin-EDTA and seeded into a new tissue culture flask at a density of 5×10^3 cells/cm^2 (Life Technologies, Warrington, UK).

2.2.12 Tri-lineage differentiation of BMMSCs

The BMMSCs (n=1) at passage 2-3 underwent trilineage differentiation to assess their osteogenic, adipogenic and chondrogenic potential differentiation.

2.2.12.1 Osteogenic differentiation

For osteogenic differentiation, BMMSCs were cultured in triplicate at a density of 1x10^4/cm^2 in a cell monolayer on a 24-well plate. Osteogenic media was added to BMMSCs containing DMEM F12, 10% FBS, 1% P/S, 10nM dexamethasone, 10mM β-glycerophosphate and 50µM ascorbic acid (Sigma-Aldrich, Poole, UK). BMMSCs grown in DMEM F12, 10% FBS and 1% P/S acted as a control. Fresh media was added to BMMSCs every 2-3 days for 21 days. To assess osteogenic differentiation cells were stained with alkaline phosphatase which is an early marker of osteoblast differentiation. BMMSCs were incubated in a solution of 0.2M Tris-HCL buffer pH 9.0, 0.5mg/mL Napthol AS-BI phosphate diluted in dimethyl formamide, 1mg/ml

Fast Red TR (Sigma-Aldrich, Poole, UK) and left at room temperature for 1 hour. Excess dye was removed with distilled H_2O. The presence of alkaline phosphatase was seen by red residue marks.

2.2.12.2 Adipogenic differentiation

For adipogenic differentiation, BMMSCs were cultured in triplicate at a density of $1x10^4/cm^2$ in a cell monolayer on a 24-well plate. BMMSCs were cultured in DMEM F12, 10% FBS, 1% P/S, 1% Insulin-Transferrin-Selenium, 0.5uM IBMX, 1µM dexamethasone and 100µM indomethacin (Sigma-Aldrich, Poole, UK). BMMSCs grown in DMEM F12, 10% FBS and 1% P/S acted as a control. Fresh media was added to BMMSCs every 2-3 days for 21 days. Oil Red O (Sigma-Aldrich, Poole, UK) was used to stain for lipids which are an indicator of adipogenic differentiation. BMMSCs were stained with 0.5% Oil Red O in isopropyl alcohol (Genta Medical, York, UK) and left at room temperature for 1 hour before the excess dye was removed with distilled H_2O. The presence of lipids was seen by red circular vacuoles. All images were captured using a Nikon Eclipse TS100 microscope (Nikon Instruments Inc., Melville, USA) or an Olympus ix71 microscope at 10x objective (Life Science Solutions, MA, USA).

2.2.12.3 Chondrogenic differentiation

Triplicate pellets of BMMSCs were used for chondrogenic differentiation, $5x10^5$ cells were suspended in 1ml DMEM F12 and centrifuged at 500xg for 5 minutes to pellet the cells. The pellets were then incubated overnight at 37ºC, 5% CO_2. The following day the pellet was fed with chondrogenic media containing DMEM F12, 2% FBS, 10µg/ml Gentamicin, 1% Insulin-Transferrin-Selenium, 0.1mM Ascorbic Acid, 10nm Dexamethasone and 10ng/ml TGF-β1

(Life Science Solutions, Paisley, UK). Cell pellets were fed every 2-3 days for 25 days. After this time period, cell pellets were fixed in 10% formalin overnight and then processed and sectioned in the histopathology department at RJAH. The process of wax-embedding the cells pellets firstly involved dehydrating them in 70% (v/v) isopropyl alcohol in phosphate buffered saline (PBS) (Gibco, Loughborough, UK), followed by two changes of 100% isopropyl alcohol. Cell pellets were then cleared in Xylene (Genta Medical, York, UK), before being embedded in a paraffin wax (Sigma-Aldrich, Poole, UK). Cell pellets were sectioned at a thickness of 5µm. The cut sections were incubated at 45°C in a water before being collected onto poly-L-Lysine coated microscope slides (ThermoFisher Scientific, Loughborough, UK). The slides were dried in an oven overnight at 37°C and then stained with haematoxylin and eosin (H&E) (Abcam, Cambridge, UK) and Toluidine Blue (1% Aqueous) (Sigma-Aldrich, Poole, UK). Slides were imaged using a Leica Diaplan microscope (Leica, Wetzlar, Germany) and a Nikon DS-Fi1 camera (Nikon, Tokyo, Japan).

2.3 Cell Characterisation

2.3.1 Growth kinetics

In order to determine the growth kinetics of the UCMSCs, Population Doubling Times (PDT) were calculated using the formula DT= T ln2/ln(Xe/Xb) where T is the incubation time, Xb is the cell number at the beginning of the incubation time and Xe is the cell number at the end of the incubation time [219,220].

2.3.2 Image analysis using ImageJ

Image analysis was carried out on normoxic UCMSCs (n=4) and hypoxic UCMSCs (n=4). Each donor was imaged using three different fields of view (x4, x10, x20 objective) and three images were captured on each field of view using a Nikon Eclipse TS100 microscope (Nikon Instruments Inc., Tokyo, Japan). These images were uploaded to ImageJ software (v. 1.53e) and converted to 8-bit images for analysis. The scale was set using the scale bars from the image as a reference point. A line was drawn around the perimeter of the MSCs and the centre filled in. The pixel density of the drawn boundary was then converted into surface area. Due to the heterogenous nature of MSCs, 50 cells were outlined and analysed per photo from the 4x objective. MSCs were determined based on a visible cell nucleus and cell boundary. The size of EVs was also measured on ImageJ after they were captured on a JOEL-JEM 1230 Transmission Electron Microscope (SIS systems, Birmingham, UK), described in **Section 2.7.1)**. A line was drawn across the diameter of the particle and calculated using a set scale from the reference bar. ImageJ analysis was carried out on normoxic EVs (n=2) and hypoxic EVs (n=2). One average 20 particles were measured per EV condition.

2.3.3 Flow cytometry

UCMSCs (n=4) were characterized using flow cytometry to confirm that cells were of a mesenchymal origin in accordance with The International Society for Cellular Therapy (ISCT) criteria. UCMSCs were harvested at passage 3-5 centrifuged at 500x*g* for 5 minutes and resuspended in PBS with 2% Bovine Serum Albumin (BSA) (Sigma-Aldrich, Poole, UK). Single-cell suspensions were incubated with Human BD Fc Block™ (BD Biosciences, Wokingham, UK) for 1 hour; after which time the receptor block was washed off via ultracentrifugation at 500xg for 5 min. The conjugated monoclonal antibodies against human surface antigens in 2% BSA were added to cell suspensions containing $3x10^5$ cells per tube. The cells with antibodies were incubated in the dark at 4°C for 30 minutes. The monoclonal antibodies used to identify human surface antigens on MSCs are displayed in **Table 7.** Control samples were stained with IgG controls. Flow cytometry was performed on a FACSCanto II (BD Biosciences, Wokingham, UK) and data analysed using FlowJo® software (FlowJo LLC, US).

Table 7: List of antibodies used to characterise UCMSCs

All antibodies were directly conjugated to a fluorochrome and used in a working concentration of 5µg/ml. All antibodies were purchased from BD Biosciences, Wokingham, UK.

Antibody	Conjugated Fluorochrome	Dilution	Isotype Control
CD105	APC	1:20	APC Mouse IgG1
CD90	PE-CF594	1:20	PE-CF594 Mouse IgG1
CD73	BV421	1:20	BV421 Mouse IgG1
CD14	PerCP-Cy5.5	1:20	PerCP-Cy5.5 Mouse IgG2b
CD45	PE-CF594	1:20	PE-CF594 Mouse IgG1
CD34	APC	1:5	APC Mouse IgG1
CD19	BV421	1:20	BV421 Mouse IgG1
CD106	APC	1:2.5	APC Mouse IgG1
CD146	PE-CF594	1:11	PE-CF594 Mouse IgG1
HLA-DR	APC	1:5	APC Mouse IgG2b
APC Mouse IgG1	APC	1:5	
PE-CF594 Mouse IgG1	PE-CF594	1:50	
BV421 Mouse IgG1	BV421	1:100	
PerCP-Cy5.5 Mouse IgG2b	PerCP-Cy5.5	1:5	
APC Mouse IgG2b	APC	1:5	

2.4 EV Characterisation

2.4.1 Isolation of EVs

At 80% confluence, cells were washed with PBS and DMEM F12 containing 10% EV depleted FBS was added and left for 48 hours. This media (conditioned media) was then collected and centrifuged at 300xg for 10 minutes to pellet cells. The CM supernatant was collected and spun at 2,000xg for 20 minutes to remove dead cells, followed by storage at -80^{o}C until EV isolation. EVs were isolated from the conditioned media via differential ultracentrifugation for western blotting and differential ultracentrifugation with a 30% sucrose cushion for all other experiments.

2.4.2 Differential ultracentrifugation

Figure 15A shows the process of EV isolation carried out on the conditioned media of UCMSCs. All conditioned media was stored at -80^{o}C prior to EV isolation. The media was stored for up to a maximum of 3 months and freeze-thawed once on the day of isolation. To isolate the EVs, the conditioned medium underwent differential ultracentrifugation using a fixed angle type 70.1Ti rotor, 10.4ml closed top polycarbonate tube and a L8-M Ultracentrifuge, *k*-factor 122.6 (Beckman Coulter, High Wycombe, UK), shown in **Figure 15B**. The CM was ultracentrifuged at10,000xg for 30 minutes to remove apoptotic cell debris. The supernatant was then passed through a 0.22µm filter (Sarstedt, Leicester, UK) and the filtered supernatant was then centrifuged at 100,000xg for 70 minutes to pellet EVs. All ultracentrifugation experiments were performed at 4^{o}C. The supernatant was completely removed and the EV pellets resuspended in DPBS and stored at -80^{o}C.

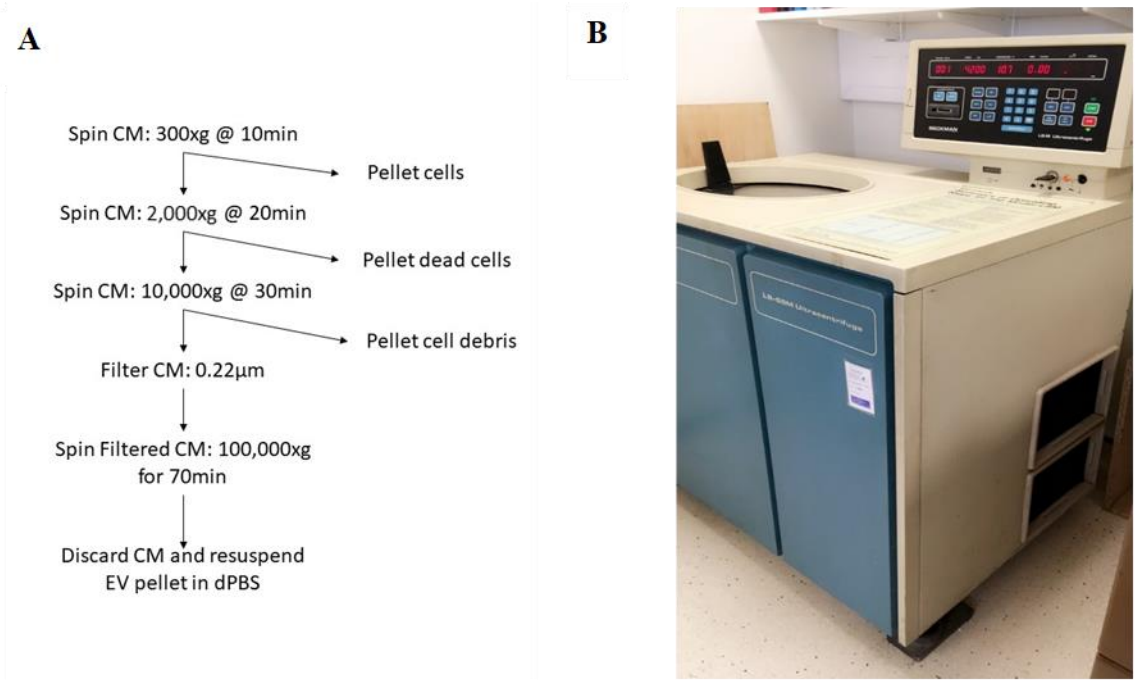

Figure 15: Differential ultracentrifugation protocol

A. *Flow chart of protocol used for isolation of EVs using differential ultracentrifugation.* ***B.*** *Machine used for ultracentrifugation of CM.*

2.4.3 Sucrose cushion isolation

To isolate the EVs, the conditioned medium underwent differential ultracentrifugation using a 30% sucrose/deuterium oxide (D_2O) (Sigma-Aldrich, Poole, UK) cushion, made up to a density of 1.210 g/cm^3 [209]. The conditioned media was first centrifuged at 2,000xg for 20 minutes to remove cell debris. The supernatant was then passed through a 0.22µm filter (Sarstedt, Leicester, UK), loaded onto a 30% sucrose cushion and then centrifuged at 100,000xg for 1hr 45 minutes on a SW28Ti rotor, 25PC Polycarbonate open top tubes (Scientific Laboratory Supplies, Nottingham, UK) and using a L8-M Ultracentrifuge; *k*-factor 296.8 (Beckman Coulter, High Wycombe, UK) **(Figure 16A).** Using a 21G needle and syringe, 3-4ml of EV suspension was collected at the interface between the sucrose cushion and conditioned media

(Figure 16B). DPBS was added to this suspension and it was centrifuged on a Type 70.1Ti fixed angle rotor at 100,000xg for 60 minutes to pellet pure EVs. All ultracentrifugation experiments were performed at 4^{oC} and EV pellets were stored at -80^{oC}.

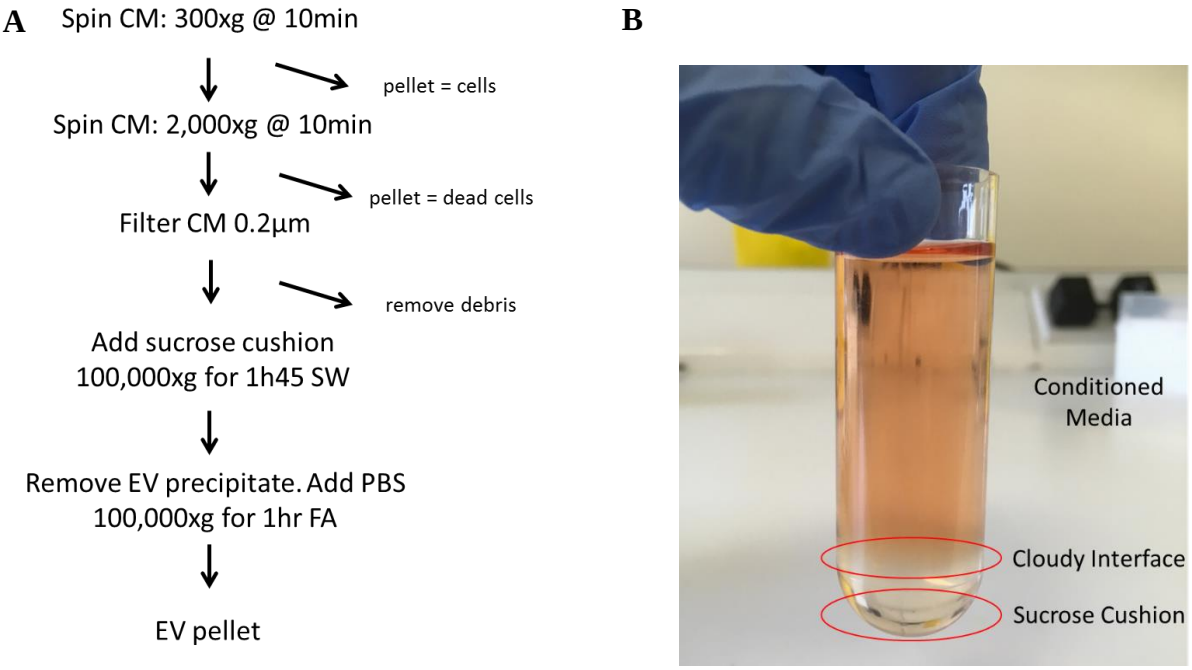

Figure 16: Sucrose cushion ultracentirfugation protocol

A. *Flow chart of protocol used for isolation of EVs using sucrose cushion ultracentrifugation.* ***B.*** *Image of conditioned media (pink) on a 30% sucrose cushion (clear) after ultracentrifugation. The cloudy interface between the conditioned media and the sucrose cushion contains the EVs.*

2.5 EV Concentration

2.5.1 BCA protein assay

Protein was extracted from EV samples by lysing samples with cold radioimmunoprecipitation assay (RIPA) buffer (150 mM NaCl, 1.0% IGEPAL®, 0.5% sodium deoxycholate, 0.1% SDS, 50 mM Tris) (Sigma-Aldrich, Poole, UK) for 30 minutes and sonicating the samples 3 times for 15 seconds using a Sonomatic Langford sonicator (Agar Scientific, Essex, UK). The protein concentration in the samples was then measured using the Pierce™ BCA Protein Assay Kit (Thermo Fisher Scientific, Waltham, MA, USA) **(Figure 17)**. A BCA assay was used to quantify protein expression in cells and EVs. This is a colorimetric assay that uses bicinchoninic acid (BCA). It is based on the reduction of Cu+2 to Cu+1 by protein when in an alkaline medium. This cuprous cation (Cu+1) is then detected by the bicinchoninic acid causing a colour change where a purple colour indicates the bonding of two BCA molecules with one cuprous cation. Briefly, a standard curve was made up by diluting BSA with PBS to make a working range of 20–2000 µg/ml. A blank well was included to analyse background noise. 25µl of the standards and 25µl of the samples are added to a 96-well plate and a working reagent containing BCA is added to each well. The plate is vortexed and incubated at 37ºC for 30 minutes. The plate is then read on a FLUROStar Omega plate reader (BMG Labtech, Aylesbury, UK) with spectrophotometer setting at 562nm. Colorimetric detection of the samples is then compared to the standard curve (known concentration) to quantify the concentration of total protein in EV and cellular samples.

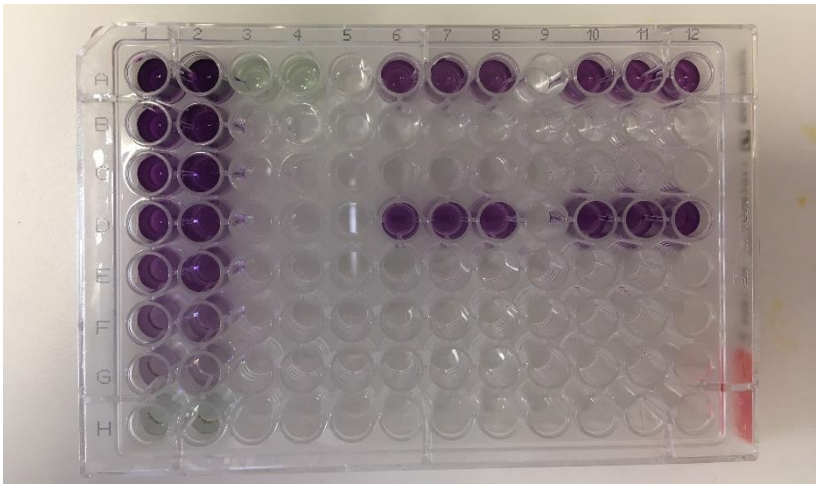

Figure 17: Image of BCA protein assay

Dilutions of BSA standards are present in column 1-4 and EV protein samples are present in 6-8 and 10-12 shown in dark purple. The plate is analysed on a FLUROStar Omega plate reader (BMG Labtech, Aylesbury, UK) and total protein is calculated by comparing the samples to the standard curve.

2.5.2 Nanoparticle tracking analysis

Nanoparticle tracking analysis (NTA) was used to measure EV particle size based on Brownian motion **(Figure 18A)**. Conditioned media (30ml) from approximately $2x10^6$ UCMSCs was subject to 30% sucrose cushion ultracentrifugation to isolate EVs. The EV pellet was resuspended in 50µl DPBS and frozen at -80^{o}C until NTA analysis. Isolated EV samples and conditioned media were diluted 1:50 in PBS and injected into the NTA NS300 system (**Figure 18B)** (Malvern Instruments Ltd, Amesbury, UK). Three videos of 60 seconds were taken of particles in motion under controlled fluid flow with a pump speed set to 50. Videos were then analysed with the NTA software to determine particle size.

To confirm that the particles seen through the NTA were EVs, a fluorescent dye CellMask Orange™ (CMO) (Thermo Fisher Scientific, Paisley, UK) was added to the EV suspension, which labels the plasma membrane of EVs. CMO in DMSO was added to a 10µl EV suspension isolated from hypoxic conditions, and diluted in PBS to give a final concentration of 5mg/ml. The CMO/EV suspension was mixed by gently pipetting and stored in the dark at room temperature for 15 minutes before being run on the NTA.

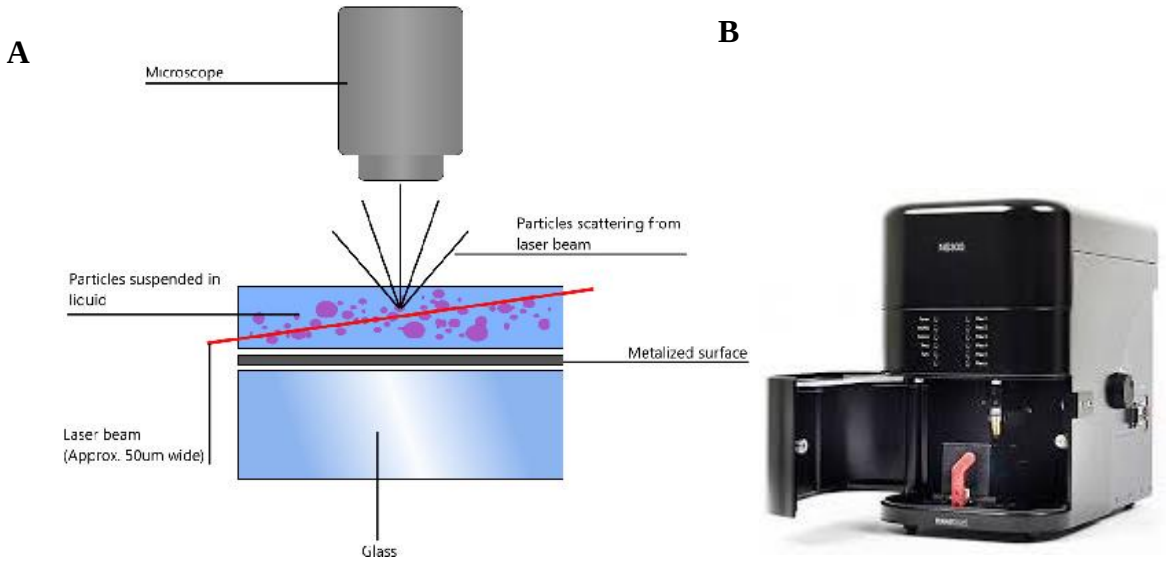

Figure 18: Images illustrating how the NTA measures the size and concentration of particles

A. *A laser beam is passed through particles in suspension which causes a scattering of light. This light scattered is focussed by the microscope onto the image sensor of the camera* [221]. *The NTA software tracks each particle in order to calculate the mean square displacement of particle movement, and together with data on temperature and liquid viscosity, particle size can be measured using the Stokes-Einstein equation* [221]. ***B.*** *Image of NS300 instrument used in the analysis of EVs. The NS300 instrument can detect nanoparticles from 0.01-1µm in diameter. Images taken from Malvern website (https://www.malvernpanalytical.com/).*

2.6 Expression of EV Markers

2.6.1 Flow cytometry of EVs

The characterisation of surface antigens on EVs was performed using the MACSPlex Exosome Kit (Miltenyi Biotec, Woking, UK) **(Figure 19)**. Approximately 8µg of EV protein was diluted to 120µl using MACSPlex Buffer. EVs were incubated in capture antibodies overnight according to the manufacturer's instructions, then washed with PBS and incubated with detection antibodies (CD9, CD63, CD81) for 1 hour according to the manufacturer's instructions and analysed using the FACSCanto II flow cytometer and FlowJo® software. In total, EVs were probed with antibodies against 37 exosomal protein epitopes and 2 isotype controls, detailed in **Table 8,** including common EV tetraspanin surface markers CD9, CD63 and CD81. The MACSPlex Exosome Kit uses mIgG1 and REA as a negative control to detect non-specific binding of the APC detection antibodies. The REA control is a REAfinity antibody which is recombinantly engineered whereby the F'ab portion of the antibodies has been sequenced and bound to human IgG1 Fc portion *in vitro*. Antibody conjugated bead populations are gated on the flow cytometer shown in **Figure 20.** Positive surface antigen expression is detected through fluorescent emission within the gated population.

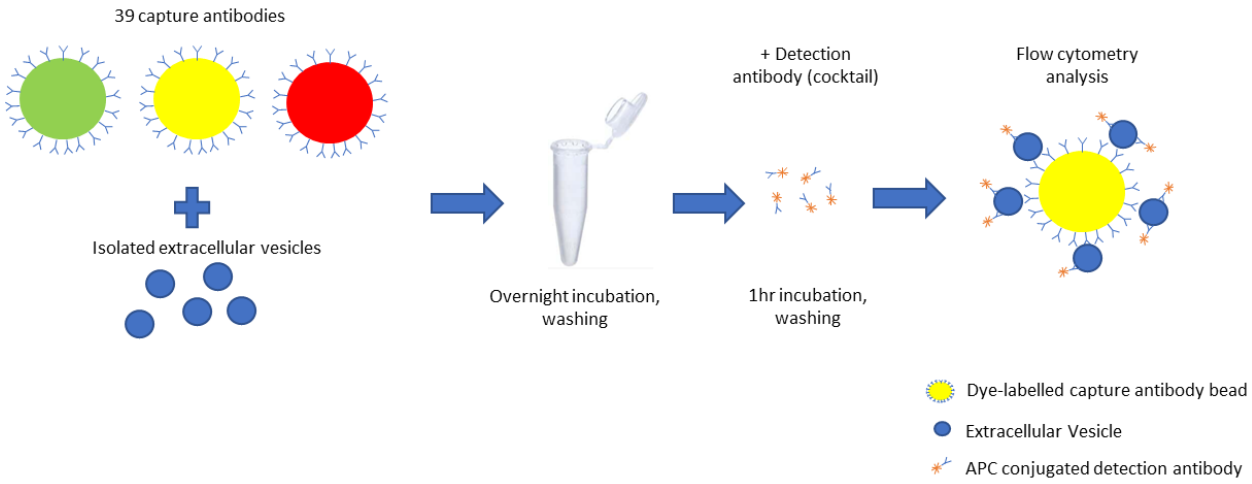

Figure 19: Schematic representation of the MACSPlex exosome detection kit.

EVs are first incubated with capture antibodies overnight. The following day, they are centrifuged, washed and incubated with a cocktail of detection antibodies containing CD9, CD63 and CD81; this creates a 'sandwich effect' with the EV in the middle. After 1 hour, they are ready to be analysed on the flow cytometer. Only antibodies which are bound to the EVs containing CD9, CD63 and CD81 are detected. Image adapted from http://www.miltenyibiotec.com

Table 8: Exosome surface markers

List of surface marker antibodies from the MACSPlex Exosome Detection kit (Miltenyi Biotec, Woking, UK). REA and mIgG1 isotype controls were used.

	Antibody	Isotype		Antibody	Isotype
1.	CD3	mIgG2a	**20.**	CD25	mIgG1
2.	CD4	mIgG2a	**21.**	CD49e	mIgG2b
3.	CD19	mIgG1	**22.**	ROR1	mIgG1κ
4.	CD8	mIgG2a	**23.**	CD209	mIgG1
5.	HLA-DRDPDQ	REA	**24**	CD9	mIgG1
6.	CD56	REA	**25.**	SSEA-4	REA
7.	CD105	mIgG1	**26.**	HLA-ABC	REA
8.	CD2	mIgG2b	**27.**	CD40	mIgG1κ
9.	CD1c	mIgG2a	**28.**	CD11c	mIgG2b
10.	CD63	mIgG1κ	**29.**	CD81	REA
11.	CD62P	REA	**30.**	MCSP	mIgG1
12.	CD146	mIgG1	**31.**	CD44	mIgG1
13.	CD41b	REA	**32.**	CD326	mIgG1
14.	CD42a	REA	**33.**	CD133/1	mIgG1κ
15.	CD24	mIgG1	**34.**	CD29	mIgG1κ
16.	CD86	mIgG1	**35.**	CD69	mIgG1κ
17.	CD142	mIgG1κ	**36.**	CD45	mIgG2a
18.	CD31	mIgG1	**37.**	CD14	mIgG2a
19.	CD20	mIgG1			

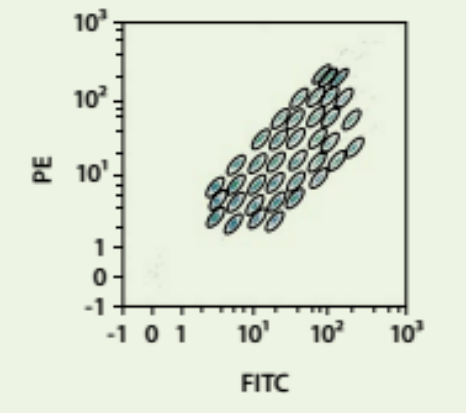

Figure 20: MACSPlex exosome detection kit - Gating of bead populations

Bead populations are gated on the flow cytometer and detection of a fluorescent signal within that gate indicates positivity for a specific protein. Image displays an example of the gates using the set-up beads on the FTIC vs PE channel. Image taken from https://www.miltenyibiotec.com/

2.6.2 Europium-based immunoassay

Characterisation of common EV surface markers CD9 and CD81 was carried out using a europium-based immunoassay. EVs were added to high-binding enzyme-linked immunosorbent assay (ELISA) strips (Greiner Bio-One Ltd, Stonehouse, UK) at a concentration of 10µg/ml and incubated overnight at 4^{o}C. The plate was washed three times with PBS and then blocked for 1hour 30minutes using 1% BSA (R&D Systems, Abingdon, UK). Primary antibodies (1µg/ml) were added against proteins CD9 (R&D systems, Abingdon, UK) and CD81 (Biorad, Oxford, UK) and 1µg/ml of mouse IgG2a (e-Bioscience, Waltham, US) was used as an isotype control. After washing, goat anti-mouse IgG-biotinylated antibody (Perkin Elmer, Coventry, UK), diluted 1:2500, was added and incubated for 45 minutes followed by europium conjugated streptavidin (1:1000; PerkinElmer, Coventry, UK) in red assay buffer (Kaivogen Oy, Turku, Finland) for 20 min. After washing three times, 100µl of europium fluorescent intensifier (Kaivogen Oy, Turku, Finland) was added, and time-resolved fluorescence was performed on a PHERAstar FS multi-mode plate reader (BMG Labtech,

Aylesbury, UK) set to detect excitation at a wavelength of 337nm and emission at a wavelength of 615nm.

2.6.3 Western blotting

Protein concentration was quantified by the Pierce BCA Protein Assay Kit (Thermo Fisher Scientific, Waltham, MA, USA). EV and cellular protein normalised to a concentration of 10µg was lysed with 4x Laemmli buffer (Bio-Rad, Watford, UK) with β-mercaptoethanol (Sigma-Aldrich, Poole, UK) and denatured by heating at 70^{o}C for 5 min. Samples were electrophoresed on a 4-15% TGX stain free gel (Bio-Rad, CA, USA) at 200 volts for 30-40 minutes. Samples were then blotted onto a nitrocellulose membrane using the wet transfer method overnight at 100 volts, as described in Inkabi et al. [222]. Membranes were then washed in Tris-buffered saline with 0.05% Tween (TTBS) and then blocked for 2 hours with 5% semi-skimmed milk in TTBS. The membranes were then washed again and then incubated with the following primary antibodies: 1µg/ml Alix (1:200 dilution), 1µg/ml Hsp70 (1:200 dilution), 1µg/ml Cytochrome C (1:200 dilution), 0.5µg/ml Tsg101 (1:100 dilution) (Santa Cruz Biotechnology, Texas, US) and Rab5a (1:1000 dilution, Cell Signalling Technology, London, UK) for 2 hours at RT. After three five-minute washes in TTBS, the membrane was probed with 1µg/ml goat anti-mouse IgG-HRP conjugated secondary antibody (1:1,000 in TBST, Life Technologies Limited, Paisley, UK) for 1 hour at room temperature and the wash step was repeated. SuperSignal West Pico Chemiluminescent Substrate working solution (Thermo Fisher Scientific, Waltham, MA, USA) was prepared by mixing equal parts by mixing equal parts of the stable peroxide solution and the luminol/enhancer solution following manufacturer's recommendation. 2ml working solution was added to the membrane and imaged with

ChemiDoc MP Imaging System (Bio-Rad, CA, USA) using Image Lab v. 6.0.1 software (Bio-Rad, CA, USA). Analysis of protein band intensity was carried out using ImageJ (v. 1.53e).

2.7 EV Morphology

2.7.1 Transmission electron microscopy

Images of EVs were obtained using Transmission Electron Microscopy (TEM) which was performed at the Central Electron Microscope unit at Keele University shown in **Figure 21.** Isolated EV pellets were fixed in 50µl of 4% paraformaldehyde (Sigma-Aldrich, Poole, UK) and stored at 4^{o}C for 1 week. EV samples (2µl) were dropped onto copper grids coated in 0.5% formvar in chloroform (Agar Scientific, Essex, UK) and left for 1 min. The grid was washed in a droplet of distilled H_2O for 1 minute and then dropped into uranyl acetate (2% in 70% ethanol) (Agar Scientific, Essex, UK) for 1 minute. Finally, the grid was placed into 70% ethanol for 1 minute and then left to air-dry for 1 hour. A JOEL-JEM 1230 Transmission Electron Microscope (SIS systems, Birmingham, UK) was used to visualise EVs at a voltage of 200-300kV and images were captured using a MegaView 3 Soft Imaging System (SIS systems, Birmingham, UK). Images were analysed on GIMP 2.10.12.

Figure 21: TEM image

Photo of a JOEL-JEM 1230 Transmission Electron Microscope used to image EVs.

2.8 EV Protein Cargo

2.8.1 Proximity based extension assay (PEA)

The protein profile of EVs was examined using a proximity extension assay to see if cell culture conditions altered selected proteins in the EV cargo. This assay analysed 92 inflammatory associated proteins to picogram level. This assay can detect some proteins as low as 0.01pg/ml and requires 1µl of EV sample. EVs were isolated from cells grown in four conditions: normoxic (n=4), hypoxic (n=4), normoxic/primed (n=4), hypoxic/primed (n=4). Isolated EVs were lysed with RIPA buffer (Merck, Poole, UK) and 1x protease inhibitor (Sigma-Aldrich,

Poole, UK). Protein concentration was analysed using a BCA protein kit (Thermo Fisher, Paisley, UK). Samples were normalised to a protein concentration of 0.5mg/ml and analysed by a sensitive proximity ligation assay. The Proseek® Multiplex Inflammation Panel was used (Olink Bioscience, Upsalla, Sweden) to detect the presence of 92 proteins **(Supplementary Table 1).** The assay uses two oligonucleotide-conjugated antibodies that bind to protein targets. Upon binding to the protein epitope, the paired oligonucleotide sequences are amplified through a quantitative real time PCR (qPCR) reaction. Data is then generated using normalized protein expression (NPX) values on a log2 scale whereby a higher NPX correlates with a higher protein expression. NPX values are relative quantification units aimed towards improving the interpretability of the results. NPX is calculated on a logarithmic scale which is related to the protein concentration. It is an arbitrary number; therefore, it does not tell the absolute concentration of the sample so different proteins should not be compared to each other. Only the same protein from different samples can be compared. Proteins containing NPX values >50% below the assays limit of detection (LOD) were excluded from analysis. For the data analysis, samples <LOD were substituted with LOD/$\sqrt{2}$. A picture diagram of the workflow is shown in **Figure 22.**

Quality control measures were implemented to control for factors such as background noise, unequal loading, signal saturation that can skew the results, and to confirm that the results came from accurate and true readings. Firstly, the samples were normalised so that equal concentrations of EV protein was added to the plate. Secondly, there were internal controls, external control, serial dilutions, sample randomisation across the plate.

One sample was serially diluted three times (neat; 1:10; 1:100) to control for the hook effect, which can happen if there is too much antigen present in the well compared to the antibody [223], leading to a falsely low readout.

The assay was spiked with four internal controls, this was divided up into two incubation controls, one extension control and one detection control. The two incubation controls are non-human antigens which monitor for variations throughout the running of the assay. The extension control involves DNA-tags which are conjugated to an antibody and, due to the proximity to each other, they always hybridise producing a constant signal. This control helps to monitor the extension and amplification and based on this data the sample signal can be adjusted. Finally, the detection control was a double stranded DNA that produces a known signal, this ensures that the amplicon is being detected by the machine. The signals for the detection control and incubation control are checked for each sample and compared with the NPX median value of all samples. If this NPX value deviates by ±0.3, then the sample fails the quality control. Likewise, if there is a significant deviation in the internal control or the detection control the plate is not reliable and will also fail quality control.

In addition to the plate controls already mentioned, there were also sample controls that were added to the plate. These consist of a triplicate of inter-plate controls with 92 DNA-tagged antibodies that hybridise and produce a high signal. The median of this signal can then be used to normalise the results of the samples. Included on the plate also was a negative control (RIPA buffer and 1x protease inhibitor (Sigma-Aldrich, Poole, UK) with no sample) to determine the background noise.

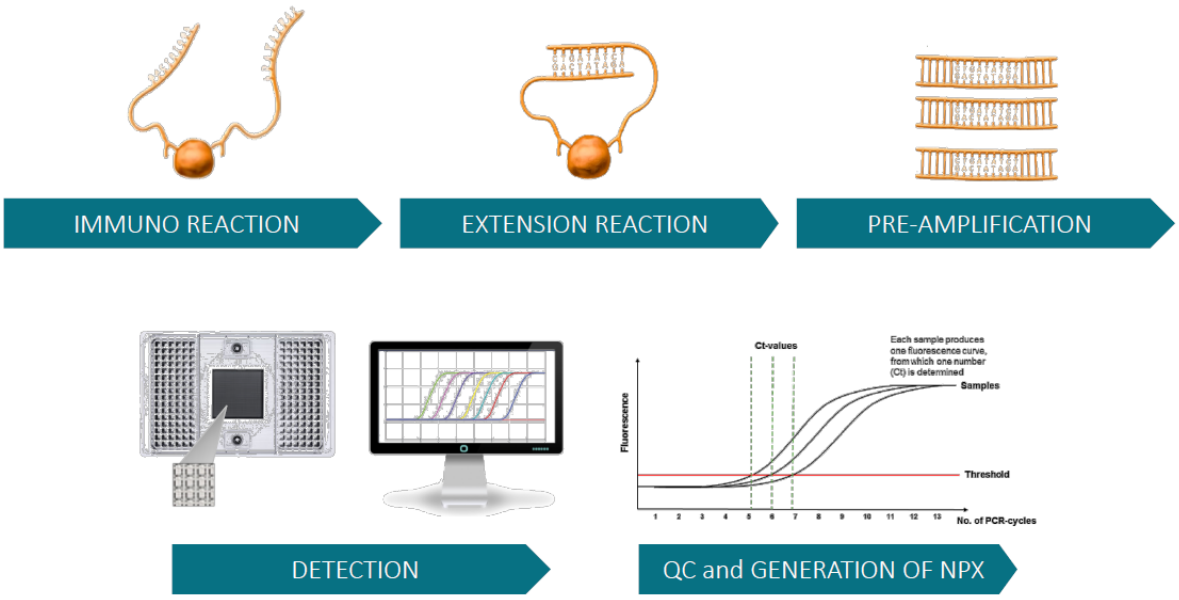

Figure 22: Workflow of the stages involved in PEA technology

EV proteins are incubated with PEA probes and the matched antibody pairs are linked to DNA sequences. These matched sequences are extended by DNA polymerase and amplified. A qPCR readout is then obtained and NPX values are obtained from the data. Image taken from https://www.olink.com/content/uploads/2019/02/Technical-Summary-Olink.pdf

2.8.2 Pathway analysis of differentially expressed proteins

To identify common pathways associated with the differentially expressed proteins, pathway analysis of was carried out using the Functional Annotation tool of Database for Annotation, Visualization and Integrated Discovery (DAVID) (v.6.8) [224,225]. Uniprot IDs for the proteins were submitted into the DAVID tool and GO: Biological Process analysis and Kyoto Encyclopaedia of Genes and Genomes (KEGG) pathway analysis were conducted. P-values ≤0.05 were statistically significant.

2.9 RNA Sequencing

2.9.1 Controlling for FBS contamination

EV isolation was carried out as described in **Section 2.4.3.** Media containing 10% EV depleted FBS was added to UCMSCs for 48 hours. This media was then collected and used for EV isolation as 'conditioned media'. As the 18-hour ultracentrifugation does not completely deplete 100% of EVs contained within the FBS, further steps were required to control for the possibility of FBS contamination. To control for this possibility, media containing 10% EV depleted FBS that had not been in contact with cells was subject to sucrose cushion ultracentrifugation, to isolate purely FBS-EVs. A similar volume of EV depleted media (~145ml) that had been added to the human EVs was used for FBS-EV isolation along with the same EV isolation method. RNA was extracted from the isolated FBS-EVs and used for RNA sequencing and RT-qPCR.

2.9.2 Removal of non-vesicular miRNA

In order to remove non-vesicular RNAs which may be circulating in the EV suspension or bound to Argonaute2 complex [226], the EV samples were treated with Proteinase K and RNase A [202]. The EV suspension was incubated in 0.05mg/ml Proteinase K (Qiagen, Manchester, UK) for 10 minutes at 37^{o}C to breakdown non-vesicular protein complexes. To inhibit Proteinase K activity, 5mM of phenylmethylsulfonyl fluoride (PMSF) (Sigma-Aldrich, Poole, UK) was added for 10 minutes at room temperature followed by 5 minutes incubation at 90^{o}C. RNase A (Sigma-Aldrich, Poole, UK) was then added to the samples, at a final concentration of 0.5 mg/ml, for 20 minutes at 37^{o}C to breakdown non-vesicular RNAs. RNA was then extracted as described in **Section 2.9.3.**

2.9.3 RNA isolation

Total ribonucleic acid (RNA) was extracted from UCMSCs and EVs using the miRNeasy micro kit (Qiagen, Manchester, UK). RNA was obtained from $3x10^5$ UCMSCs, cells were pelleted, washed in PBS and then lysed using 700µl QIAzol lysis buffer and stored at -80ºC until RNA extraction. For EV-RNA, a 100µl EV suspension in PBS was collected from the conditioned media from ~15×10^6 cells for NGS and 10×10^6 cells for qPCR. The EV pellet was then exposed to proteinase K and RNase A treatment to remove any protein/RNA complexes on the EV surface. More details on this treatment are provided in **Section 2.9.2.** 700µl QIAzol lysis buffer was then added to the EV suspension and stored at -80ºC. RNA extraction was carried out on cellular and EV samples using the Qiagen RNeasy® Micro kit in accordance with the manufacturer's standard instructions (Qiagen, Manchester, UK). RNA was eluted in 12µl of nuclease free water and stored at -80ºC until quality control steps.

2.9.4 Quality and quantity of RNA

The Quality and Quantity assessments of EV-RNA were carried out at the Centre for Genomic Research at the University of Liverpool for the NGS experiment. The quantity of RNA was determined using the Qubit RNA High Sensitivity™ Assay Kit and the Qubit™ RNA BR Assay Kit (Life Technologies, Waltham, MA, USA). The Qubit® working solution was prepared by diluting the Qubit® RNA BR Reagent 1:200 in Qubit® RNA BR Buffer. To make up the RNA standards, 10µl of the standards were added to 190µl of Qubit® working solution, vortexed for 2-3 seconds and left to stand at room temperature for 2 min. For the samples, 1µl of EV and cellular RNA was added to 199µl of the working solution and loaded into the Qubit® 2.0 instrument (Life Technologies, Waltham, MA, USA). Fluorometric readings of standards and samples were obtained and the quantity of RNA calculated.

The quality and integrity of the RNA was determined by electrophoresis on the Agilent Bioanalyzer 2100 using the RNA 6000 Pico kit (Agilent Technologies, Waldbronn, Germany) following the manufacturer's instructions. Briefly, 550µl of RNA 6000 Pico gel matrix was centrifuged in a spin filter for 10 minutes at 1500xg at stored at 4ºC. The RNA 6000 Pico dye was vortexed and 1µl was added to 65µl of filtered gel. The tube was centrifuged for 10 minutes at 13,000xg and the gel-dye (9µl) was loaded into a well on the RNA Pico chip and distributed along the chip using a syringe. To load the chip, 9µl of the RNA conditioning solution and 5µl of the RNA marker was loaded into the wells, followed by 1µl of sample into sample wells and 1µl RNA ladder into the ladder well. This chip was left stand for 60 seconds before being vortexed for 60 seconds at 2400 rpm IKA vortex mixer. Finally, the chip was loaded into the Agilent 2100 bioanalyzer.

For the qPCR experiment, the quality and quantity of EV-RNA was carried out inhouse at RJAH using the Agilent 4200 TapeStation (Agilent Technologies, Santa Clara, CA, USA). The quantity of cellular RNA was determined using the Agilent RNA ScreenTape Assay and the quantity of EV-RNA was determined using the High Sensitivity RNA ScreenTape Assay (Agilent Technologies, Santa Clara, CA, USA). For the Agilent RNA ScreenTape Assay, an electronic ladder was used, and the samples were prepared by adding 5µl RNA Sample Buffer to 1µl cellular RNA. For the High Sensitivity RNA ScreenTape Assay, the ladder was diluted in 10µl RNase free water and 2µl of this solution was added to 1µl sample buffer. The EV samples were prepared by adding 1µl High Sensitivity RNA Sample Buffer to 2µl EV-RNA. All samples were vortexed at 2000rpm for 1 minute on the IKA MS3 vortexer (Sigma-Aldrich, Poole, UK). The samples and ladder were then denatured at 72°C for 3 min, followed by cooling on ice for 2 min. The samples were spun down and loaded onto the Agilent 4200 TapeStation instrument.

After completion of electrophoresis on the Agilent 2100 Bioanalyzer and Agilent 4200 TapeStation, an RNA integrity number (RIN) and DV_{200} number was generated. The RIN number is useful to give an indication of intact ribosomal RNA in cellular samples. The number is calculated using the 18s and 28s peaks in the electropherogram and the lower the number, the more degradation in the sample. However, EV samples most often do not contain intact ribosomal subunits, so this is not an accurate measurement for the quality assessment of vesicular RNA [227]. Instead, the DV_{200} score was used to analyse RNA integrity in EV samples. The DV_{200} metric measures the size distribution of RNA, specifically, the percentage of RNA fragments >200 nucleotides [228]. This information is useful to know if EV samples are comprised of small RNAs.

2.9.5 Library preparation

The construction of small RNA libraries was carried out at the Centre for Genomic Research at the University of Liverpool with the NEBNext® Multiplex Small RNA Library Prep Set for Illumina (New England BioLabs Inc., Massachusetts, USA) followed by small RNA-Seq analysis on the Illumina NovaSeq SP (Illumina Inc., California, USA). Small RNA transcripts were first converted into cDNA libraries and quantified by Qubit® double-stranded DNA (high sensitivity) assay (Life Technologies, Waltham, MA, USA), followed by measurement using the Agilent 2100 (Agilent Technologies, Waldbronn, Germany). The final libraries were pooled together in equimolar concentration and size selected on Pippin prep station (Sage Science, Beverly, US) with a size selection range set between 130-160 bp. This was done to focus the sequencing on a specific size range of small RNAs while also including the expected miRNA peak at 147-149 bp. 1 normoxic cell sample and 3 EV samples (normoxic, hypoxic, normoxic/primed), each with 4 biological replicates were sequenced. 1 FBS-EV sample was sequenced to act as a control for potential contamination. Pooled libraries were loaded in the

flowcell for cluster formation and sequencing. Samples were sequenced to a depth of 40-100 million reads per sample. Initial file conversion and demultiplexing of sequencing data was carried out at the University of Liverpool. Briefly, the raw Fastq files was trimmed for the presence of Illumina adapter sequences using Cutadapt (version 1.2.1). The option -O 3 was used, so the 3' end of any reads which match the adapter sequence for 3 bp or more are trimmed. The reads were further trimmed using Sickle version 1.200 with a minimum window quality score of 20. Reads shorter than 15 bp after trimming were removed. University of Liverpool generated summary statistics using fastq-stats from EAUtils.

2.9.6 Sequencing data analysis

All further sequencing analysis was carried out at the University of Keele. Raw reads were extracted from the FASTQ files and trimmed of sequencing adapters using Trimmomatic; paired end reads were merged using the software 'PEAR'. The sequence length distribution and base calling accuracy were calculated using the phred quality score (Q score), with high phred scores of Q>30 were taken forward for analysis. Due to the large number of reads generated, only forward (R1) sequencing reads were utilised for this analysis. Absence of adapter contamination was confirmed using FASTQC. Reads were aligned to Human Genome build (hg38) using miRDEEP2 pipeline and collapsed for computational efficiency using Mapper.pl script. The prepared sequences were filtered and collapsed reads <18nt were removed to remove uninformative reads as these reads were unlikely to map to miRNA. To quantify miRNA reads and generate count files, the trimmed miRNA sequences were prepared by mapping entire contents of miRNA hairpin and mature sequences to the miRbase sequences using the Quantifier.pl script. A region 2nt upstream and 5nt downstream of the mature sequence was considered a "hit". All reads, including the bovine sample, were mapped to the

miRBase database of mature miRNAs for Homo sapiens (hsa). Although 1 bovine sample was used, the mapping of this sample to the human miRbase was important as the mapping output for hsa consists of 2,578 entries for mature miRNAs whereas the bovine database (bta) output only contains 783 entries for mature miRNAs [229]. The FBS-EV sample was also mapped to the bovine database to compare sequence conservation between human and bovine miRNAs. Collapsed reads mapped to miRbase were passed to DESeq2 (version 1.30.1, Harvard, MA, USA) for normalisation and statistical analysis. DESeq2 took the mean normalised counts and averaged them over all samples and conditions. P-values were created, and a p-value adjusted for multiple testing with the Benjamini-Hochberg procedure which controls false discovery rate (FDR) was also applied to the data set. The false discovery rate threshold was set to 10% and an adjusted p-values of <0.1 was considered statistically significant. A Log_2 fold change value was calculated comparing the miRNAs between samples. Differentially expressed miRNAs were visualised on a Minus-Average (MA) plot and a heatmap.

2.9.7 Pathway Enrichment Analysis and Target Prediction

To predict a common pathway of the differentially expressed miRNAs, the web-based analysis tool miRNet 2.0 was used (https://www.mirnet.ca/). This is a visualisation tool that constructs network-based connections of predicted gene targets from the inputted miRNAs. It integrates data from 11 different miRNA databases to aid in the functional analysis of differentially expressed genes [230,231]. Pathway Enrichment analysis for predicted gene targets was carried out using the Kyoto Encyclopaedia of Genes and Genomes (KEGG) database and the Gene Ontology (GO): Biological Process database on the differentially expressed miRNAs between the EV conditions. The hypergeometric test algorithm was applied to the data. A degree cut-off of 1.0 was selected for optimal visual exploration.

To establish if the differentially expressed miRNAs directly targeted secretome components, further gene target prediction analysis was applied using miRNet [230,231], miRDB [232,233] and TargetScan (v.7.2) [234]. Identification of gene targets from two out of the three web-based programs was considered as a potential miRNA-gene target. The list of positively identified gene targets was then cross checked with the identified secretome components to determine any direct relationships.

2.9.8 Validation of RNA sequencing data by RT-qPCR

Quantitative reverse transcription PCR (RT-qPCR) was carried out to validate the results of the RNA sequencing data. A diagram of the PCR study from the extraction through to the amplification is shown in **Figure *23,*** along with the process of sample normalisation at each step.

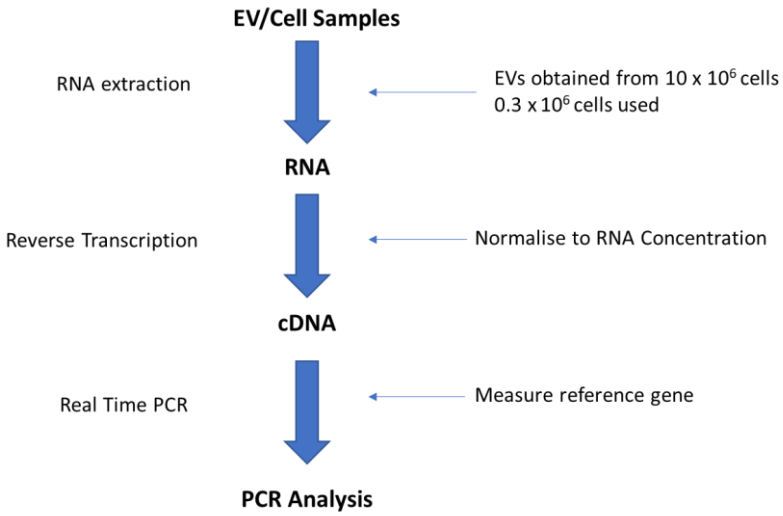

Figure 23: Stages involved in for PCR validation

Diagram details the process involved in generating PCR data, from RNA isolation through to reverse transcription and real time PCR. The righthand side of the diagram details to normalisation strategy employed at each stage of the process.

2.9.9 Reverse transcription PCR (RT-PCR)

Isolated RNA was reverse transcribed to create complementary DNA (cDNA). RT-PCR was carried out using the miRCURY LNA RT Kit (Qiagen, Manchester, UK). Samples were normalised to 64.6pg/µl with nuclease-free water, which concentration of the lowest RNA sample. The reverse transcription mix was prepared according to **Table 9.**

Table 9: List of reagents and volumes used to carry out Reverse Transcription

Reagent	Volume per Sample
5x miRCURY SYBR® Green RT Reaction Buffer	2µl
RNase-free water	4.5µl
10x miRCURY RT Enzyme Mix	1µl
UniSp6 RNA spike-in	0.5µl
Template RNA	5µl

Samples were loaded into the PCR Sprint Thermal cycler in thin walled 0.2mL PCR tubes (Thermo Fisher, Warrington, UK) and run according to the protocol in **Table 10.** cDNA was stored at -20^{o}C until it was used for real-time PCR.

Table 10: Temperature cycling protocol for reverse transcription

Step	Time	Temperature
Reverse Transcription	60 min	42^{o}C
Inactivation of Reaction	5min	95^{o}C
Storage	60min	4^{o}C

2.9.10 Real-time PCR (qPCR)

Real time PCR (qPCR) was carried out using the miRCURY SYBR® Green PCR Kit (Qiagen, Manchester, UK). cDNA was diluted 1:25 with nuclease free water prior to addition to the reaction mix. Reaction mix was prepared according to **Table 11.**

Table 11: Reaction mix for qPCR per sample

Reaction Mix	Volume
2x miRCURY SYBR® Green Master Mix	5µl
ROX Reference Dye	0.05µl
cDNA template	4µl
RNase-free water	1µl

The samples were vortexed and 10µl of sample/reaction mix was added to each well of a custom PCR plate which already contained the lyophilised primers shown in **Table 12.**

Table 12: List of miRNAs of interest and target sequences probed for in PCR reaction

Gene of Interest	Target Sequence
hsa-miR-221-3p	AGCUACAUUGUCUGCUGGGUUUC
hsa-miR-100-5p	AACCCGUAGAUCCGAACUUGUG
hsa-let-7f-1-3p	CUAUACAAUCUAUUGCCUUCCC
hsa-miR-139-5p	UCUACAGUGCACGUGUCUCCAGU
hsa-miR-214-5p	UGCCUGUCUACACUUGCUGUGC
hsa-miR-192-5p	CUGACCUAUGAAUUGACAGCC
hsa-miR-21-5p	UAGCUUAUCAGACUGAUGUUGA
hsa-let-7i-5p	UGAGGUAGUAGUUUGUGCUGUU
hsa-miR-146a-5p	UGAGAACUGAAUUCCAUGGGUU
hsa-miR-181a-5p	AACAUUCAACGCUGUCGGUGAGU
hsa-miR-155-5p	UUAAUGCUAAUCGUGAUAGGGGU
hsa-miR-24-3p	UGGCUCAGUUCAGCAGGAACAG

hsa-miR-10a-5p	UACCCUGUAGAUCCGAAUUUGUG
hsa-miR-215-5p	AUGACCUAUGAAUUGACAGAC
UniSp6	
UniSp3	

A ‘blank’ no template control containing nuclease free water was also included in each plate. The plate containing the sample, reaction mix, and primers was sealed, vortexed and centrifuged to collect the solution at the bottom of the well. The plate was held at room temperature for 5 minutes to wait for the primers to dissolve before the plate was loaded into the Applied Biosystems QuantStudio 3 Real-Time PCR System (Thermo Fisher, Warrington, UK). PCR cycling was carried out according to the protocol in **Table 13.** Data was analysed using QuantStudio™ Design and Analysis Software v.1.5.1 (Thermo Fisher, Warrington, UK). Relative gene expression was compared to the normalising genes miR-221-5p and calculated using the comparative delta Ct (cycle threshold) method.

Table 13: qPCR cycling protocol

Step	Time	Temperature
PCR initial heat activation	2 min	95ºC
2-step cycling • Denaturation • Combined annealing/extension	 10 seconds 60 seconds	 95ºC 56ºC
Number of cycles	40	
Melting Curve Analysis	15 seconds 60 seconds	95ºC 60ºC

2.10 Functional Experiments

2.10.1 Isolation, culture and characterisation of PBMCs

A 6ml vial of whole blood was obtained from healthy volunteers (n=6) in EDTA coated tubes. Blood was obtained from 5 females and 1 male, age range 26-64. Volunteers who were on immunosuppressive medication were excluded from the study. Blood was immediately processed to isolate peripheral blood mononuclear cells (PBMCs). This study was approved by the Robert Jones & Agnes Hunt Orthopaedic Hospital. Informed consent was obtained from the volunteers prior to blood collection. An example of the consent letter is provided in **Supplementary Figure 1.** PBMCs were separated from blood using gradient centrifugation over Lymphoprep™ (Stem Cell Technologies, Cambridge, UK). Whole blood was diluted in DPBS at a ratio of 1:1, this solution was then gently layered over Lymphoprep™ and centrifuged at 900xg for 20 minutes. The blood was separated into layers, shown in **Figure *24,*** and the white interphase of PBMCs was collected. PBMCs were resuspended in ice cold PBS and centrifuged at 500xg for 7 minutes. This washing step was repeated to remove platelets. PBMCs were counted and frozen at $20x10^6$ cells/ml in 90% FBS + 10% DMSO. After resurrection, PBMCs were cultured in RPMI-1640, 10% FBS, 1% P/S, 10ng/ml IL-2, at 37^{o}C, 5% CO_2.

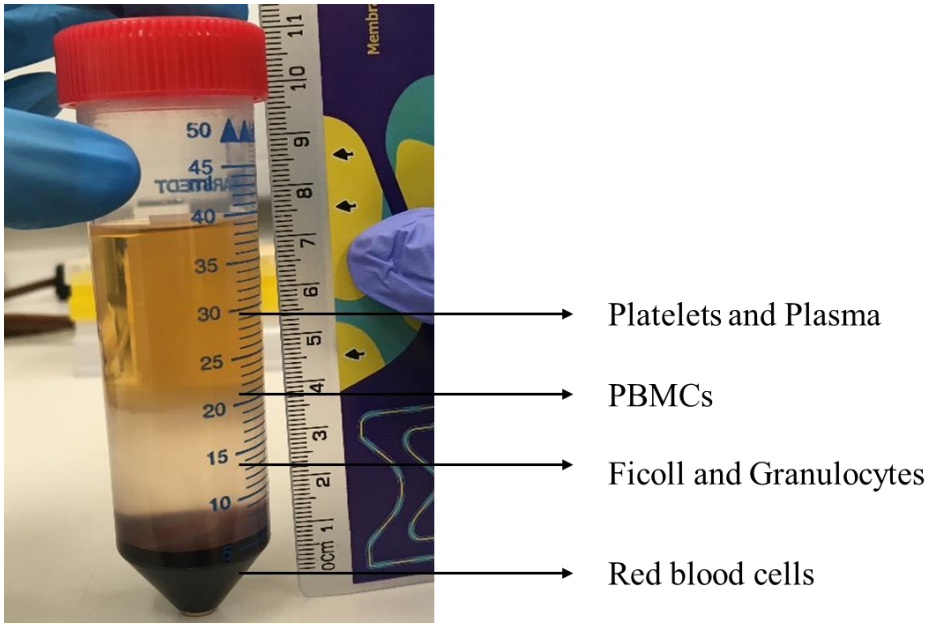

Figure 24: Separation of PBMCs from whole blood

Whole blood was diluted in PBS, layered over Ficoll and centrifuged. This resulted in the separation of layers into red blood cells, Lymphoprep™/granulocytes, PBMCs and platelets/plasma. The PBMCs were extracted from the white cloudy layer at the interface between the Ficoll/PBS and platelets/plasma.

2.10.2 Culture of Jurkat cells

Jurkat cells (Clone E61, ATCC® TIB152™), a T-lymphoblastoid suspension cell line, were kindly donated by the Guy Hilton Research Centre. Jurkat cells were seeded at a density of $5x10^5$ cells/ml in an upright $75cm^2$ flask. They were cultured in DMEM F12 with 10% FBS, 1% P/S and 1% NEAA and incubated at 37°C, 21% O_2, 5% CO_2. Fresh culture medium was replaced every 3 days. To maintain cell culture concentration under 1 x 10^6 cells/ml, cells were passaged every 5-6 days or when there was a visible increase in cell concentration seen under a light microscope. Jurkat cells were removed from the flask and centrifuged at 500xg for 5 minutes. The supernatant was discarded, and the cell pellet resuspended in 1 ml of fresh media. The cells were counted, and viability checked using trypan blue staining as described in **Section**

2.2.3. The cells were seeded in the appropriate volume of fresh media to get a concentration of $5x10^5$ cells/ml.

2.10.3 Activation of PBMCs/Jurkat cells

PBMCs/Jurkat cells were activated 48 hours prior to adding them to co-culture experiments. They were activated by adding a humanised CD3 and CD28 agonist (TransAct, Miltenyi Biotec) at a dilution of 1:100. IL-2 (10ng/ml) was added to the co-culture media of PBMCs. IL-2 was not added to Jurkat cells as it is not required to support cell growth. Activation was confirmed by the identification of surface marker CD25 by flow cytometry.

2.10.4 Co-culture experiments

All co-culture experiments were carried out in 6 well plates. A dose response experiment was firstly carried out with the co-cultures involving PBMCs (n=3) and normoxic EVs, whereby the EVs were added at 60µg: 2×10^6, 90µg: 2×10^6, and 120µg: 2×10^6 PBMCs cells. This was based on research by Ma et al. [235] who carried out a dose response experiment of 30µg, 60µg and 90µg EVs: 2×10^6 PBMCs and found 90µg EVs were most effective in increasing Treg cells; the Treg/Th17 ratio and the level of TGF-β. The dose response of PBMCs in co-culture with normoxic EVs was assessed by changes in their protein profile, analysed by flow cytometry which is described in **Section 2.10.5.**

In one experimental setting, 2×10^6 PBMCs (n=6) were co-cultured with 120µg EVs and $2x10^5$ MSCs separately to determine if the EVs or MSCs were able to change PBMC protein production. In another experimental setting, 2×10^6 Jurkat cells (n=1) were co-cultured with

120µg EVs and $2x10^5$ MSCs separately to determine if the EVs or MSCs could change the Jurkat protein production. 120µg EVs was obtained from approximately 24.3×10^6 ($\pm11.4\times10^6$) UCMSCs. MSCs were added to PBMCs and Jurkat cells at a ratio of 10:1 (PBMC/Jurkat: MSC) following a protocol by Kay et al. [121] and del Fattore et al. [165]. MSCs were allowed to adhere to plastic for 4 hours before addition of PBMCs/Jurkat cells to the co-culture. Both normoxic and normoxic/primed EVs and MSCs were used. Non-activated PBMCs/Jurkat cells only were used as a negative control and activated PBMCs/Jurkat cells only were used as a positive control.

2.10.5 Surface marker expression and intracellular cytokine staining (ICCS)

PBMCs (n=6) and Jurkat cells (n=1) were co-cultured in 6 well plates with both normoxic and normoxic/primed MSCs (10 PBMCs: 1 MSC) and normoxic and normoxic/primed EVs (120µg). After 3 days, $2x10^5$ PBMCs/Jurkat cells were harvested for immunophenotyping of surface markers or ICCS. Flow cytometry of PBMCs /Jurkat cell surface markers was carried out using the protocol described in **Section 2.3.3** and the antibodies listed in **Table 14.**

For ICCS, 10µg/ml Brefeldin A (Sigma-Aldrich, Poole, UK) was added to co-culture for 6 hours before harvesting for flow cytometry analysis. PBMCs/Jurkat cells were fixed in 1x Intracellular Fixation Buffer (eBioscience, Waltham, US) for 30 minutes at 4°C. Cells were centrifuged at 500xg for 5 minutes to removed fixative and the cell pellet was resuspended in 1x Permeabilization Buffer (eBioscience, Waltham, US). Human Fc Block™ (BD Biosciences, Wokingham, UK) was added at 0.5mg/ml for 10 minutes at room temperature before cells were washed in 1x Permeabilization Buffer. The cell pellet was resuspended in 2% BSA and

antibodies added. All experiments were carried out in triplicate and activated T-cells only acted as a control for the experiments.

Table 14: Antibodies used in the characterisation of PBMCs and Jurkat celdd

All antibodies were purchased from BD Biosciences, Wokingham, UK.

Antibody	Conjugated Fluorochrome	Dilution	Isotype control
CD3	APC	1:20	APC Mouse IgG1
CD4	PE	1:20	PE Mouse IgG1
CD127	BV421	1:50	BV421 Mouse IgG1
CD25	APC	1:50	APC Mouse IgG1
CD45	PE	1:20	PE Mouse IgG1
CD19	BV421	1:100	BV421 Mouse IgG1
HLA-DR	APC	1:5	APC Mouse IgG2b
IL-4	PE	1:20	PE Mouse IgG1
IL-17A	BV421	1:50	BV421 Mouse IgG1
IFN-y	PerCP-Cy5.5	1:20	PerCP-Cy5.5 Mouse IgG2b
FoxP3	PE	1:20	PE Mouse IgG1

2.11 Statistical analysis

All statistical analysis was performed on GraphPad Prism v.8 (GraphPad Software, San Diego, USA). A Shapiro Wilk test was used to confirm normal distribution. All analysis was carried out using paired Student's t-tests or 2-way ANOVA, except for the PEA assay and the MACSPlex Exosome Kit experiments whereby differential protein expression was identified using multiple t-tests with a false discovery rate of 5% to control for multiple comparisons. FDR-adjusted p-values (referred to as q-values) ≤ 0.05 were considered significant.

Chapter 3:

Characterisation of human MSCs

3.1 Introduction

This chapter examines the growth kinetics, morphology, and immune profile of UCMSCs. The characterisation of UCMSCs is an important part of this work when considering their EVs as a potential treatment for rheumatoid arthritis and an important pre-requisite step towards understanding EV function.

This chapter also looks at different culture conditions for UCMSCs, specifically cell growth in normoxia and hypoxia with and without pro-inflammatory cytokines. Research shows that the environment in which MSCs are cultured can alter their surface marker production, morphology, growth kinetics, secretome and functional properties [236]. Therefore, it is important to establish if different culture conditions affect UCMSC characteristics. This chapter analyses the growth, morphology, and surface marker production of donor matched UCMSC samples (n=4) in four conditions:

1. Normoxia (21% O_2)
2. Normoxia (21% O_2) primed with pro-inflammatory cytokines
3. Hypoxia (5% O_2)
4. Hypoxia (5% O_2) primed with pro-inflammatory cytokines

Pro-inflammatory cytokines used to prime the cells were IFN-γ, TNF-α and IL-1β.

Cell culture in normoxia (21% O_2) is the most commonly used method to expand cells [237]. However, cell culture at 21% O_2 is relatively toxic and does not resemble the *in vivo* environment. As a consequence, many researchers have moved towards the use of hypoxic cell culture conditions [238] as growth in hypoxia has been associated with enhanced therapeutic outcomes in MSCs [239–241]. When growing MSCs in hypoxia, it is important to tailor the

oxygen concentration to mimic the natural *in vivo* environment of the cells [242]. Neonatal derived tissues rarely exceed 5% *in vivo* [243], therefore, UCMSCs were cultured at 5% O_2. Growing cells in hypoxic conditions has also been associated with improved stem cell yield and colony forming units [244], prolonged lifespan [101] and enhanced osteogenesis [245]. In terms of immune suppression, research has shown that rat BMMSCs, grown in 5% O_2, release more IDO [100], which is a soluble factor known to suppress NK cells, CD4+ and CD8+T-cell proliferation [246]. They also have a greater ability to promote Treg proliferation compared to MSCs grown in normoxia [100]. Further immunomodulatory effects of hypoxia were found in porcine BMMSCs where there was a suppression of IL-8 and an increase of the anti-inflammatory factors GM-CSF and Interleukin 1 receptor antagonist compared to BMMSCs in normoxia [247]. Research has shown that culturing BMMSCs in hypoxia strongly promotes their immunosuppressive properties, whereas for UCMSCs cultured in hypoxia, a lot of the research details their enhanced proliferation [248], increased glucose consumption and increased production of specific growth factors (hypoxia-inducing factor-alpha, fibroblast growth factor-7, vascular endothelial growth factor receptor 2, stem cell factor receptor, insulin-like growth-factor-binding proteins 3 and 6) [249,250]. Hypoxia induces a large range of effects on MSCs; therefore, this chapter characterises the hypoxic UCMSCs, and their EVs will be analysed for immunomodulatory proteins and miRNAs in later chapters.

UCMSCs were also cultured in pro-inflammatory environments to ‘activate’ them and enhance their anti-inflammatory properties, as described in **Section 1.2.4** [243]. There is an increasing body of evidence showing that priming MSCs with pro-inflammatory cytokines stimulates the MSCs to release EVs and soluble factors with enhanced anti-inflammatory properties [251–254]. This priming approach results in an improved ability of MSCs and EVs to suppress T-cells and PBMCs [78,94–96,164,184,254]. For this reason, the pro-inflammatory priming of

MSCs was explored in this chapter. Indeed, research has shown that when MSCs are cultured in a combined hypoxic and pro-inflammatory environment, their immunosuppression is further enhanced as the IFN-γ upregulates cytokines with anti-inflammatory properties (e.g. IDO, PD-L1, HLA-G), and hypoxia promotes glucose consumption which increases lactate levels to suppress T-cells [255]. Therefore, UCMSCs will also be characterised from the dual hypoxic/primed condition.

As bone marrow derived MSCs are still considered to be the 'gold standard' to which other sources of MSC are compared [61], this chapter sought to use BMMSCs as a control to compare the characterisation of UCMSCs. Two bone marrow aspirates were sourced and MSCs were isolated. BMMSCs were characterised by assessing growth kinetics, cell morphology and surface marker production in normoxia and hypoxia. However, this was only done on one donors' BMMSCs. The second BM aspirate suffered a long delay in delivery which adversely affected cell viability and unfortunately the sample could not be used. BMMSCs were used as a control to confirm that UCMSCs had a similar MSC characteristics.

Aim:

The **aim** of this chapter is to characterise the UCMSCs by studying their growth kinetics, morphology, and cell surface markers compared to the 'gold standard' BMMSCs in normoxia and hypoxia.

Objectives:

1. Establish the growth kinetics of UCMSCs in normoxia and hypoxia, by calculating population doubling times.

2. Compare cell morphology between UCMSCs in normoxia, hypoxia and pro-inflammatory conditions.
3. Characterise the surface marker production of UCMSCs grown in normoxic, hypoxic and pro-inflammatory primed conditions. This will be achieved by analysing their surface marker production via flow cytometry.
4. Compare cell growth, morphology, and surface marker production of UCMSCs (n=4) to the BMMSC (n=1) control.

A diagram of the objectives is shown in the picture below **(Figure *25*).**

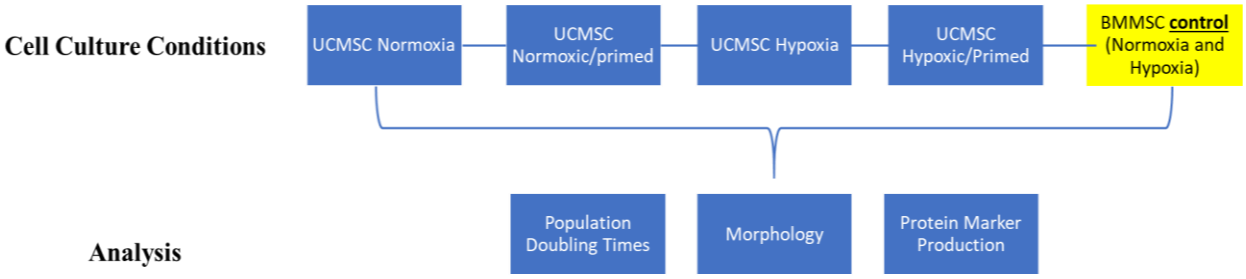

Figure 25: Diagram of the objectives of this chapter

UCMSCs will be grown in normoxia, hypoxia and with/without pro-inflammatory priming. The UCMSCs will then be analysed for their population doubling times, morphology, and protein marker production. Results will be compared to a BMMSC control grown in normoxia and hypoxia and also analysed in the same way for their population doubling times, morphology, and protein marker production.

3.2 Results

3.2.1 Population doubling time of UCMSCs

Population doubling times (PDT) were calculated as described in **Section 2.3.1**. UCMSCs were grown in complete media up to 80% confluence, then EV depleted FBS replaced normal FBS in the media for 48 hours, in order to collect the conditioned media for EV isolation **(Section 2.4.1)**. The average PDT for UCMSCs grown in normoxic conditions, from P3-8, was 2.82 days (± 0.2 SD) compared to 2.52 days (± 0.38 SD) for UCMSCs grown in hypoxic conditions. There were no statistical differences between the conditions **(Figure 26)**. Population doubling times were not calculated for UCMSC grown with pro-inflammatory cytokines as these cytokines were added for only 48 hours and UCMSCs were discarded thereafter. UCMSCs were grown up to passage 8, after this, the growth of cells slowed, and they were not used for further experiments.

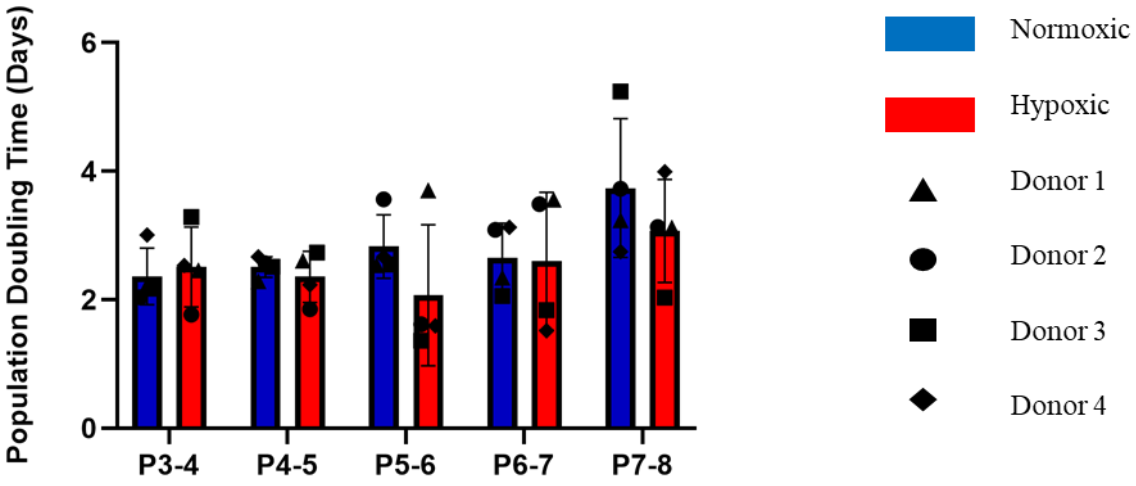

Figure 26: Population doubling times for UCMSCs

Bar chart represents the average population doubling times (y-axis) for UCMSCs (n=4) grown in normoxia (21% O_2; blue) and hypoxia (5% O_2; red). Individual donors are shown by the presence of different symbols. Cell counts were performed in triplicate at each passage from P3-8 (x-axis).

UCMSCs had an average PDT of 2.82 days in normoxia and 2.52 days in hypoxia. Data shown as the mean ± SD.

3.2.2 Comparison of UCMSCs in normoxic and hypoxic conditions

Images of UCMSCs were captured at P3 and P4 (**Figure 27A).** Image analysis was caried out using ImageJ software as described in **Section 2.3.2.** Images of the analysis carried out on the UCMSCs is shown in **Supplementary Figure 2.** UCMSCs in normoxia had a statistically larger surface area (61µm^2 ± 41SD) compared to UCMSCs in hypoxia (32µm^2 ± 21SD) ($p \leq 0.0001$) shown in **Figure 27B.** In both conditions, UCMSCs contained spindle shaped and had a consistent distribution in the flask, however the UCMSCs grown in normoxia contained a larger, flattened morphology. There were also some slight variations in morphology between UCMSC donors shown in **Supplementary Figure 3.** Donor 1 and Donor 2 UCMSCs appeared to cluster more together, Donor 3 UCMSCs had a heterogeneous population with a mix of round and spindle-like cells and Donor 4 UCMSCs were thinner and more elongated.

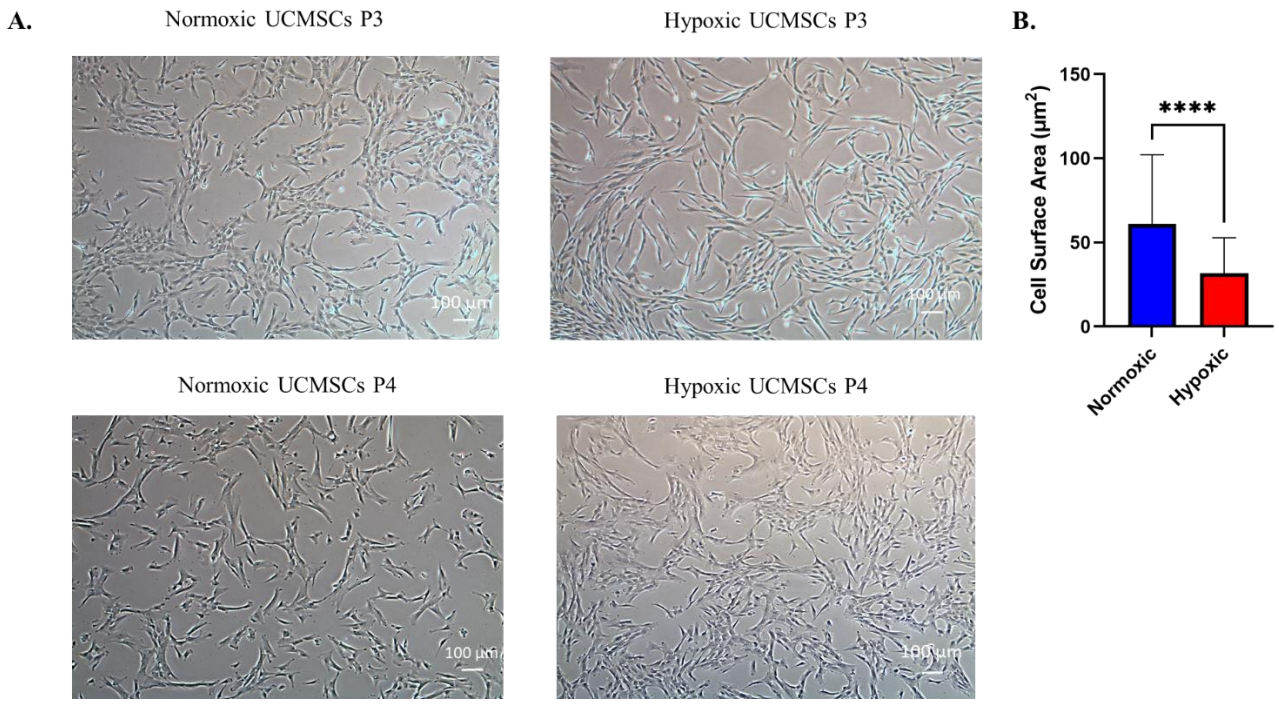

Figure 27: Pictures of UCMSCs in normoxic and hypoxic conditions

(A) *Images show UCMSCs in normoxic and hypoxic conditions at passage 3 and 4. UCMSCs had a similar morphology in both conditions. Images taken on Eclipse TS100 microscope at a 4x objective.* ***(B)*** *Bar chart displaying the cell surface area of normoxic (n=4) and hypoxic cells (n=4). The normoxic UCMSCs had a statistically larger surface area compared to the hypoxic UCMSCs. Data is shown as mean ± SD.*

3.2.3 Effect of pro-inflammatory priming on UCMSC morphology

Images of UCMSCs were taken before and after pro-inflammatory priming to assess any cell morphology changes. There were no obvious changes to cell morphology after priming other than a higher percentage confluence seen after the 48-hour incubation due to the normal growth rate of these cells **(Figure 28)**.

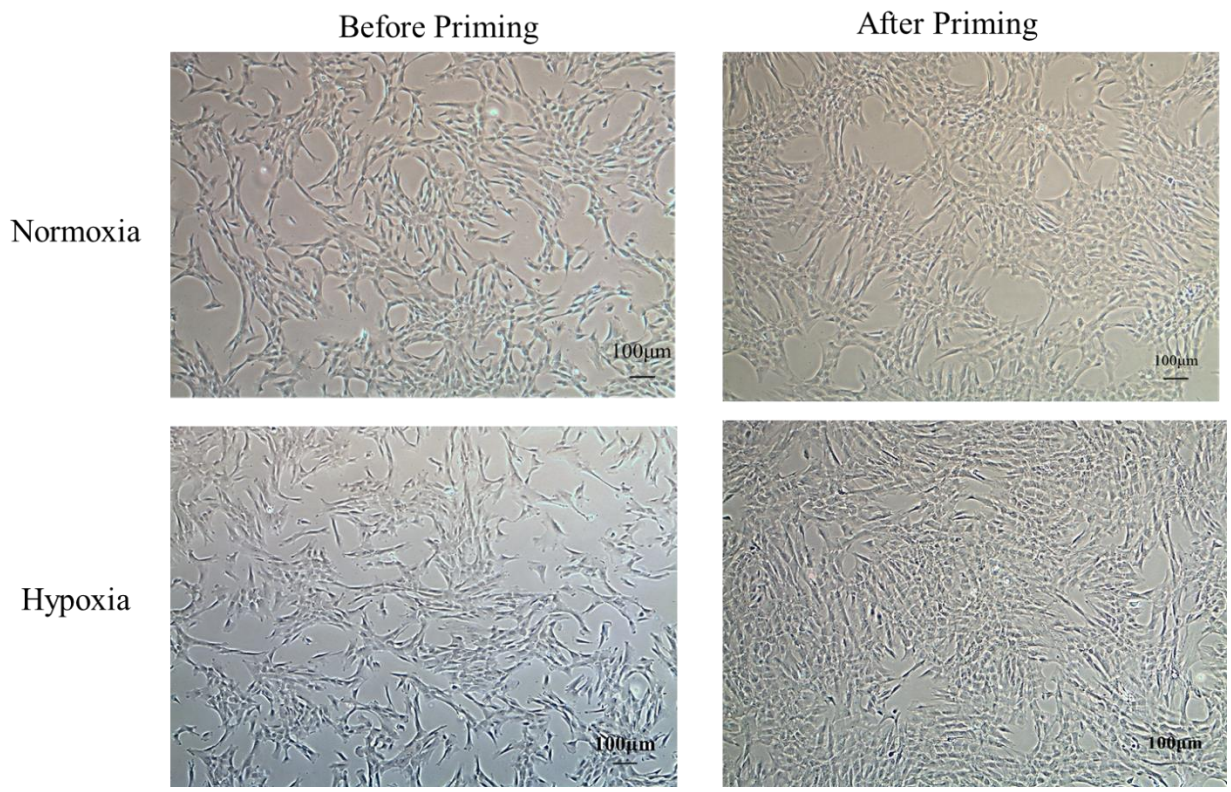

Figure 28: Images of UCMSCs

Images displaying UCMSCs at P6 grown in normoxia, hypoxia and primed with pro-inflammatory cytokines. For each flask of cells, three images were taken of three fields of view (x4, x10, x20 objective) Images shown here were taken under 4x objective on an Eclipse TS100 microscope.

3.2.4 Surface marker production on primed and non-primed UCMSCs

Part of the ISCT criteria for defining MSCs is that they must display the cell surface markers CD105, CD73, and CD90 (≥90%) and lack expression of CD45, CD34, CD14 or CD11b, CD79 or CD19, and HLA-DR (≤2%) [51]. For this reason, UCMSCs were analysed for their surface marker production via flow cytometry. Results showed that normoxic and hypoxic UCMSCs at P4-6 were ≥95% positive for CD105, CD73, and CD90, and lacked CD45, CD34, CD14, CD19 and HLA-DR (≤2%) **(Figure 29)**. They were also adherent to tissue culture plastic, and these results, together with their positive tri-lineage differentiation, show that the MSCs are in accordance with the ISCT guidelines [51]. There were no differences in MSC surface marker production between the normoxic and hypoxic UCMSCs. In addition to the characteristic MSC surface marker panel, CD106 was tested on all UCMSCs. There was a low production of CD106 in normoxic UCMSCs (0.8% ± 0.6) and hypoxic UCMSCs (0.5% ± 0.4).

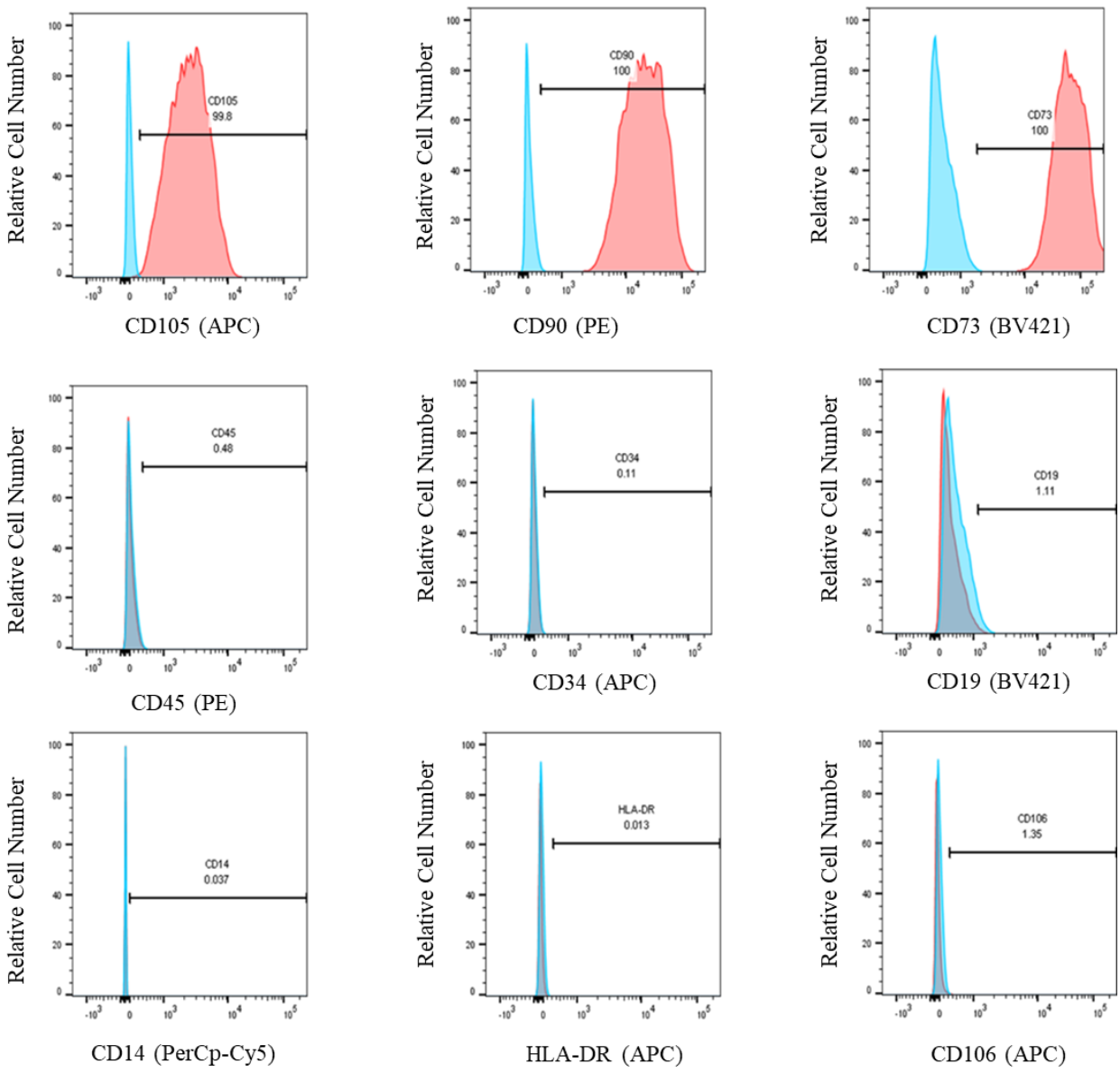

Figure 29: Surface marker production of normoxic UCMSCs

Representative single parameter histograms of UCMSCs from normoxic donor 1. Relative cell number is displayed on the y-axis and the surface marker on the x-axis. There was a positive production of CD105, CD90, CD73 (≥95%) and a negative production of CD14, CD45, CD34, CD19, HLA-DR (≤2%) shown by the red histograms. Isotype controls are shown in blue. There was a low production of CD106 (1.35%) from this donor.

The ISCT also recommends the characterisation of MSCs after they have been primed with pro-inflammatory cytokines such as TNF-α and IFN-γ. UCMSCs were analysed again via flow cytometry after 48-hour exposure to TNF-α, IL-1β and IFN-γ to detect any change in their markers. Results showed the primed UCMSCs still displayed the positive (CD105, CD90, CD73) and negative markers (CD45, CD34, CD19) in accordance with the ISCT criteria **(Figure 30).** The level of HLA-DR was initially low (<2%) in UCMSCs but this increased after pro-inflammatory priming (average production 34.9% ± 39.7 SD). HLA-DR production increased in all donors with the exception of donor 3 in normoxic/primed and hypoxic/primed conditions, and donor 4 in hypoxic/primed.

A similar trend was identified when the production levels of CD106 were assessed. There was a low level of CD106 (<2%) detected in all UCMSCs grown in normoxic and hypoxic conditions whereas its production increased upon pro-inflammatory priming of UCMSCs (average production 57.5% ± 45.3 SD). In all donors (n=4), CD106 increased in normoxic/primed and hypoxic/primed conditions, albeit there was a high donor variability in the percentage increase of CD106 despite the UCMSC samples being donor matched. This indicates that there is likely donor to donor variability in the characteristics of MSCs.

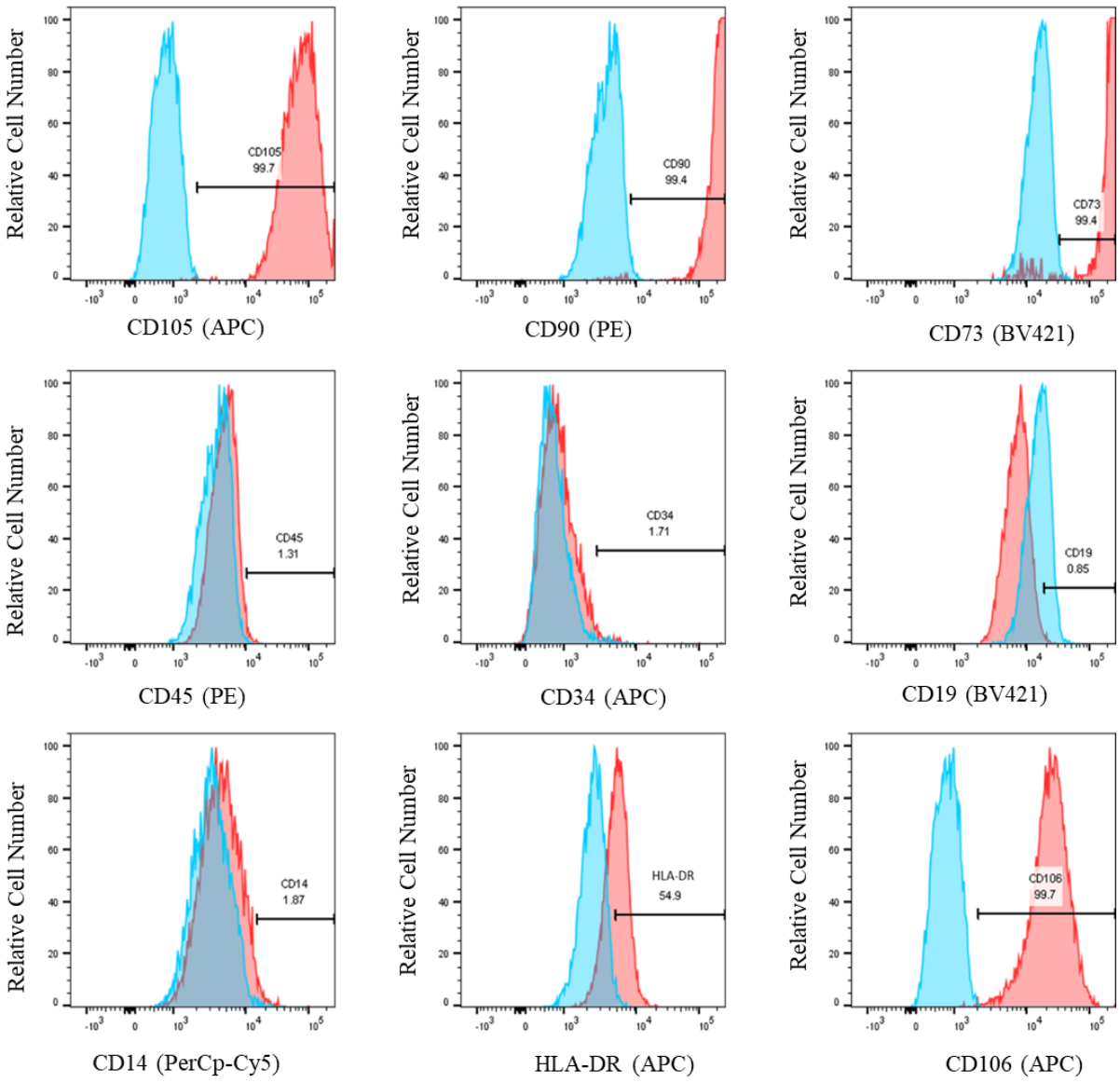

Figure 30: Surface marker production of normoxic/primed UCMSCs

Single parameter histograms of UCMSCs primed with TNF-α, IL-1β and IFN-γ for 48 hours. Relative cell number is displayed on the y-axis and the surface marker on the x-axis. Flow cytometry analysis after priming showed that they maintained their positive (CD105, CD90, CD73 (≥95%)) and negative (CD14, CD45, CD34, CD19 (≤2%)) surface marker production shown by the red histograms. Isotype controls are shown in blue. Histograms show the surface marker production profile for Donor 2 grown in normoxic/primed conditions. The production of HLA-DR was 54.9% and CD106 was 99.7% for this donor.

On comparison of the surface marker profile of UCMSCs grown in normoxia, hypoxia and with pro-inflammatory conditions, there were no differences between normoxia and hypoxia, and there was a statistically higher level of CD106 and HLA-DR in pro-inflammatory primed conditions shown in **Figure 31,** albeit not all primed UCMSC donors responded the same. Instead, there was considerable donor variability in response to priming with regards to HLA-DR and CD106 expression only. Donor 1 showed an increased production of HLA-DR and CD106 after pro-inflammatory priming but only in hypoxic conditions. Donor 2 showed an increased production of HLA-DR and CD106 after pro-inflammatory priming in both normoxic and hypoxic conditions. Donor 3 showed no increase in HLA-DR/CD106 in response to priming with the exception of CD106 in normoxic/primed conditions which increased from 0.19% to 22.2%. Lastly, Donor 4 showed an increased production of HLA-DR and CD106 after pro-inflammatory priming but only in normoxic conditions.

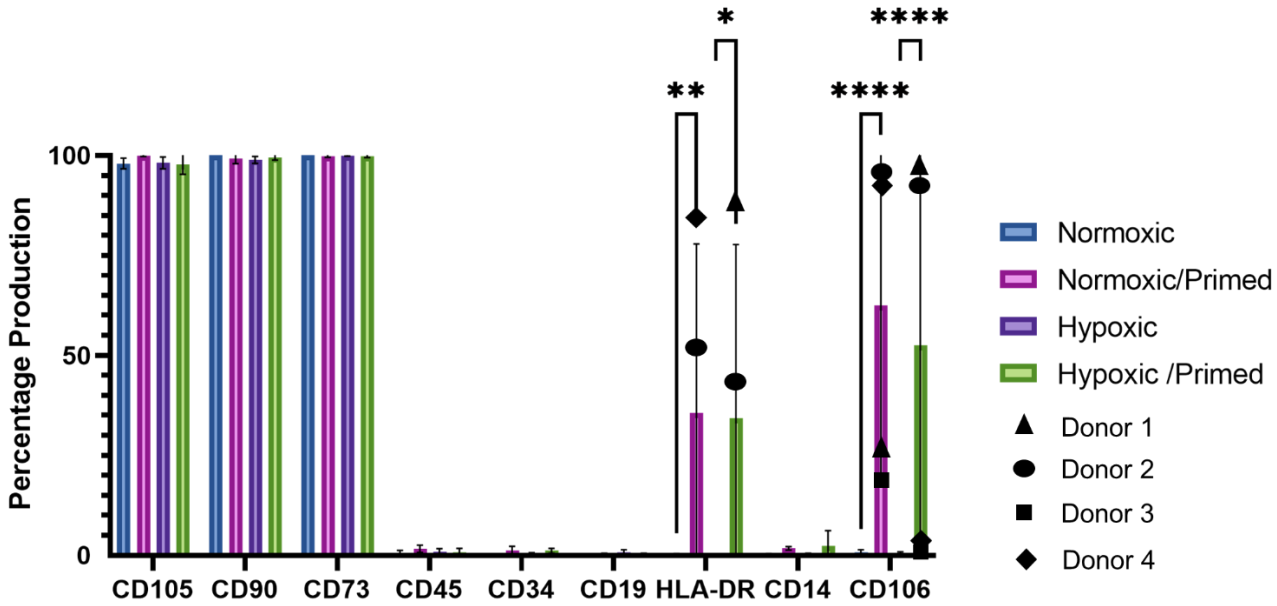

Figure 31: Comparison of surface marker production in normoxic, hypoxic and primed UCMSCs

The bar chart shows the percentage production (y-axis) of surface markers (x-axis) from UCMSCs grown in four different conditions. There were no differences in the production of CD105, CD90, CD73,

*CD45, CD34 and CD19 between normoxic, hypoxic, and primed UCMSCs (n=4). Collectively, the primed UCMSCs had a statistically higher production of HLA-DR and CD106 to normoxic and hypoxic UCMSCs. There was variance in the production of HLA-DR and CD106 seen by large error bars. The individual donor production of these markers is thereby denoted using symbols. *p≤ 0.05, **p ≤ 0.01, ****p≤ 0.0001.*

3.2.5 Comparison of UCMSCs to BMMSC control

Research shows that BMMSCs are strong immunomodulators and they are the most frequently used source of MSCs for clinical trials [256]. Therefore, it was important to assess how the characterised UCMSCs (n=4) compared to the BMMSCs (n=1) in terms of growth, morphology, and surface marker characteristics.

3.2.5.1 Growth of BMMSCs

Bone marrow aspirate (15ml) was collected with a total mononuclear cell count of 20.2 x 10^6 MNC/ml. This aspirate was split equally between normoxia and hypoxia (7.5ml each). After the first passage, the total yield of isolated BMMSCs was 1.1 x 10^6 for normoxic conditions and 16.8 x 10^6 for hypoxic conditions. The average PDT for BMMSCs (n=1) was calculated using three technical replicates. The average PDT of BMMSCs grown in normoxic conditions, from P1-5, was 6.1 ± 1.1 days compared to 5.1 ± 0.7 days for BMMSCs grown in hypoxic conditions. There were no statistical differences between the normoxic and hypoxic BMMSCs at each passage **(Figure *32*A)**. The population doubling times of UCMSCs and BMMSCs were compared. BMMSCs were grown from P1-5 and stopped thereafter due to slowed cell growth. UCMSCs were first expanded on tissue culture plastic and then seeded in the Quantum® cell expansion system where they underwent another passage. This means that the growth of UCMSCs on tissue culture plastic for this experiment started at P3 and continued to P8 due to the cells maintaining a consistent PDT up to this stage. As a result, the comparison of UCMSCs

and BMMSCs can only be made from P3-5, whereby UCMSCs had a statistically quicker PDT in normoxic conditions, and from P4-5 in hypoxic conditions, shown in **Figure *32*B**.

3.2.5.2 Morphology of BMMSCs

The morphology of BMMSCs grown in normoxic and hypoxic conditions was compared. There were also some notable differences between the conditions including a clustering of cells in normoxic BMMSCs compared to hypoxic BMMSCs and, in general, the normoxic BMMSCs had a flattened, spread morphology and the hypoxic BMMSCs had a spindle-like shape **(Figure *32*C)**. The normoxic and hypoxic UCMSCs (shown in **Figure 27**) showed a similar morphology to the BMMSCs, with the normoxic UCMSCs contained some larger, flattened cells and the hypoxic UCMSCs containing primarily long spindle-like shaped cells.

3.2.5.3 Surface marker production of BMMSCs

BMMSCs (n=1) at P3 were also analysed for MSC surface markers and, similar to UCMSCs, they had a surface marker profile consistent with UCMSCs in normoxia and hypoxia, but with the exception of CD14 which had a 4% (± 0.05 SD) production in normoxic BMMSCs **(Figure *32*D).**

3.2.5.4 Tri-lineage differentiation of BMMSCs

The ISCT stipulates that, as part of the characterisation of MSCs, they must be able to differentiate into osteoblasts, adipocytes, and chondroblasts [51]. Therefore, trilineage differentiation was carried out on BMMSCs. Previous tri-lineage differentiation had already been established for the UCMSCs used in this study, as described in Mennan et al. [63]. The BMMSCs (n=1) demonstrated signs of differentiation down all three lineages shown in **Supplementary Figure 4.** Osteoblast differentiation was seen by the presence of alkaline

phosphatase staining (ALP) in dark red after 21 days. Some ALP was found in the control cells but there was stronger staining in the cells treated with osteogenic media indicating the differentiation of BMMSCs down an osteoblast lineage. Adipogenic differentiation was seen by the presence of lipid vacuoles in the BMMSC culture which appeared red after staining with Oil Red O, indicating differentiation down an adipogenic lineage. Finally, at 28 days, a chondrogenic BMMSC pellet was fixed, sectioned, and stained with a H&E stain and toluidine blue. The cell nuclei and cytoplasm could be visualised after H&E staining and some glycosaminoglycan staining via toluidine blue, which is in keeping with research in our group and from others showing toluidine blue staining of chondrogenic pellets from MSCs [257].

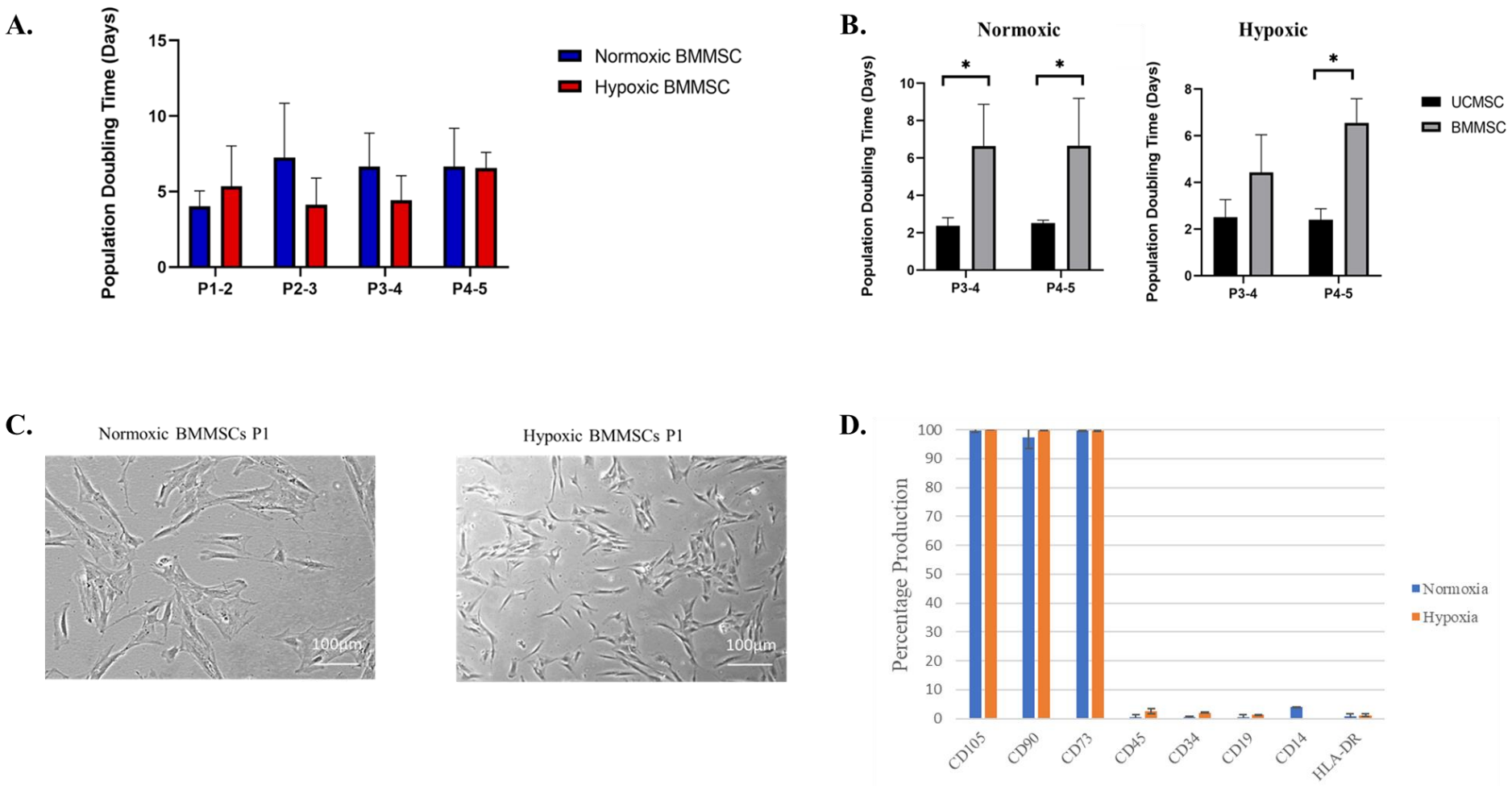

Figure 32: Growth, morphology, and surface marker production of BMMSCs

BMMSCs (n=1) were analysed for their growth, morphology, and surface marker production. ***(A)*** *Bar chart represents the average population doubling times (y-axis) for BMMSCs grown in normoxia (with 21% O_2) and hypoxia (with 2% O_2). Cell counts were performed in triplicate at each passage from P1-5 (x-*

*axis). **(B)** BMMSCs and UCMSCs were counted in triplicate and compared from P3-5. In normoxic conditions, UCMSCs had a statistically quicker PDT from P3-4 and P4-5 compared to BMMSCs. In hypoxic conditions, UCMSCs had a statistically quicker PDT from P4-5 compared to BMMSCs (*p<0.05). Population doubling time is presented on the y-axis and passage number on the x-axis. Data is shown as mean ± SD. **(C)** Normoxic BMMSCs appeared to cluster closely together in comparison to hypoxic BMMSCs which had a more spindle-like morphology. Images taken on Eclipse TS100 microscope at a 10x objective. **(D)** Bar chart represents the surface marker production of BMMSCs grown in normoxia and hypoxia. BMMSCs showed a positive production of CD105, CD90, CD73 and a negative production (≤2%) of CD45, CD34, CD19, CD14* and HLA-DR. *CD14 had a 4% (± 0.05 SD) production in normoxia.*

3.3 Discussion

The ISCT has established a minimal set of criteria for the characterisation of MSCs. The chapter aimed to fully characterise MSCs in adherence to these guidelines. Part of the ISCT criteria states that MSCs must be able to differentiate into osteoblasts, adipocytes, and chondroblasts [51]. The UCMSCs, used in this study, had previously undergone tri-lineage differentiation as detailed by Mennan et al. [63]. They displayed positive differentiation down osteogenic, adipogenic and chondrogenic lineages [63]. Therefore, the characterisation of UCMSCs (n=4) in this chapter was based on their population doubling times, morphology, and surface marker production. All UCMSCs were plastic adherent and positively displayed the surface markers CD105, CD90, CD73 (≥95%) and had a negative production (≤2%) of CD45, CD34, CD19, CD14 and HLA-DR in normoxic and hypoxic conditions. Thus, the UCMSCs were in accordance with the ISCT criteria for the identification of MSCs.

In this chapter, the UCMSCs were grown in normoxia, hypoxia and with and without pro-inflammatory cytokines as research has shown that different culture environments influence MSCs immunosuppressive properties [243]. UCMSCs showed a strong proliferative ability *in vitro* with mean population doubling times of approximately 2.82 days (± 0.2 SD) in normoxia and 2.52 days (± 0.38 SD) in hypoxia. This is in line with other studies that reported the population doubling times of UCMSCs to be 1.6 days [258], 3-4 days [259] and 1.5 days [260]. There were no differences identified between the growth kinetics of cells grown in normoxia and hypoxia. The lack of change in growth may be due to the way the cells were first isolated and expanded. The cells were isolated under normoxic (21%) conditions and cultured up to passage 2 in this environment. Exposure to hypoxia (5%) at an earlier stage may have been an influencing factor in their proliferation, as MSCs isolated in hypoxic conditions have been

found to have strong self-renewal abilities [261,262]. However, both conditions supported the growth of cells. In all, there are mixed results regarding the culturing of MSCs in hypoxia, with researchers reporting stimulatory effects [101,261,263], inhibitory effects [264] and no differences in cell proliferation between normoxic and hypoxic MSCs [265]. This may be attributable to the hypoxic cell culture methods that different groups use (e.g., many groups do not degas their media prior to use). In general, there is more research showing that hypoxia supports MSC growth better than normoxia. Specifically, hypoxic conditions appear to maintain the proliferation of BMMSCs over time rather than stimulate their growth, in comparison to normoxic conditions where MSCs slow down over time due to inhibitory signals [261]. Additionally, UCMSCs grown in 2.5% O_2 for 72 hours have increased proliferation compared to UCMSCs grown in normoxia [266]. The findings in this chapter show that both normoxia and hypoxia support the growth of UCMSCs to a similar extent up to P8.

An objective of this chapter was to compare cell morphology between UCMSCs cultured in normoxia, hypoxia and in pro-inflammatory conditions. Culturing the cells in different growth environments has previously been found to alter the cells morphology [253]. For example, Prasanna et al. [253] found that pro-inflammatory priming of BMMSCs with IFN-γ and TNF-α caused them to be larger, flattened and more irregular in shape, whereas there were no effects seen in Wharton's Jelly MSCs (WJMSCs). In this chapter, a quantitative analysis was carried out on the surface area of normoxic and hypoxic UCMSCs at P3 and P4. The normoxic UCMSCs had a statistically larger size compared to the hypoxic UCMSCs (**Figure 27**). The UCMSCs, in both conditions, contained spindle shaped cells and an even distribution in the flask, but the normoxic UCMSCs also contained larger, flattened cells and, in general, had a more mixed morphology, showing that the UCMSCs are responding differentially to their culture environment.

This chapter also compared the surface marker production of UCMSCs grown in normoxic, hypoxic and pro-inflammatory primed conditions. There was no change in the MSC surface marker production between UCMSCs grown normoxia and hypoxia. Other research groups have also found no differences in MSC surface marker production in cells cultured in normoxic and hypoxic conditions [264,265]. Both Nekanti et al. [267] and Widowati et al. [268] compared WJMSCs grown in normoxia and hypoxia (5% O_2) and there was no difference between the two populations up to P10 in the Nekanti et al. [267] study, and between early (P4) and late passages (P8) in the Widowati et al. [268] study.

Flow cytometry analysis of normoxic/primed UCMSCs revealed that HLA-DR had a statistically higher production in two out of four umbilical cord donors' primed cells. This explains the large error bars shown in **Figure 31** and highlights the heterogeneity of MSCs particularly in response to pro-inflammatory priming. HLA-DR is an MHC class II surface antigen, known to exist on antigen presenting cells and plays a role in displaying protein fragments to T-cells, thus facilitating activation [269]. Findings are mixed in the literature regarding the expression and production of HLA-DR on MSCs when exposed to pro-inflammatory priming. Some papers show that HLA-DR expression is reduced in MSCs that are grown in pro-inflammatory conditions [243,270,271], this finding supports the theory that MSCs are immunosuppressive as the downregulation of HLA-DR would reduce the likelihood of cells being rejected upon transplantation. Contradictory to this are studies that show that pro-inflammatory priming, particularly IFN-γ priming, leads to a greater production of HLA-DR [272–274]. As HLA-DR has been found to increase in MSCs after IFN-γ priming, some authors argue the HLA-DR should be considered informative data rather than a criterion of MSCs [275].

Interestingly, previous work by Mennan et al. [215], using the same UCMSCs and primed with IFN-γ only, showed that there was no increase in production of HLA-DR on UCMSCs. However, there were two variables to the culture of UCMSCs in this chapter. The first was the use a pro-inflammatory cocktail (TNF-α, IL-1β, IFN-γ) and research has shown that IFN-γ upregulates HLA-DR in MSCs [272–274]. Therefore, it is more likely to be the second variable, which was the culture of UCMSCs in EV depleted FBS compared to normal FBS in Mennan et al. [215]. Indeed, Romieu-Mourez et al. [274] showed that HLA-DR production is increased in MSCs primed with IFN-γ and this production is further increased when MSCs are cultured in high density and serum deprived environments. UCMSCs were cultured in EV depleted serum for 48 hours, this serum is largely depleted of FBS proteins, growth factors and enzymes and not just EVs. Therefore, it is likely that the reduced serum conditions contributed to the increase in production of HLA-DR in some UCMSC donors, although further work will be needed to understand the cause of this.

When these findings are considered in light of UCMSCs immunosuppressive ability, they raise slight concerns about the transplantation of UCMSCs as an allogenic therapy, as one of hallmarks of MSC-induced immunosuppression is its lack of expression of HLA-DR (along with T-cell co-stimulatory molecules CD80 and CD86), which means that they can evade immune responses [276]. However, as UCMSCs have already been used extensively in human clinical trials with no reported adverse events, therefore, it is obvious that they are well tolerated *in vivo* [115,116]. Even with the increase in production of HLA-DR, research has shown that MSCs are unable to stimulate T-cells without the presence of co-stimulatory molecules [119]. Van Megen et al. [272] showed that IFN-γ primed MSCs that expressed HLA-DR were unable to stimulate HLA-mismatched lymphocytes or increase the proliferation of CD4+ T-cells, whereas dendritic cells, with the same HLA class II mismatch as the MSCs, did stimulate CD4+

T-cell proliferation. This shows that the presence of HLA-DR alone is not enough to trigger an immune response.

The surface marker CD106, also known as vascular cell adhesion molecule 1 (VCAM-1) was also investigated in the UCMSC population. CD106 in this study showed an increased production in both normoxic/primed and hypoxic/primed conditions. CD106 is associated with immunomodulation and angiogenesis [277,278]. Research has previously identified a subpopulation of placental chorionic villi MSCs that express CD106 and these CD106+ MSCs were found to have more potent immunosuppressive properties [277]. Furthermore, CD106 has been found to be upregulated in UCMSCs, WJMSCs, ATMSCs and murine BMMSCs upon pro-inflammatory priming with IFN-γ [270,279–281] or TNF-α [282,283]. As IFN-γ and TNF-α upregulate the expression of adhesion receptors such as CD106 on endothelial cells and MSCs, this facilitates the recruitment of leukocytes to the site of injury and this is one theory as to how MSCs promote wound healing [282] and capillary tube formation [118,278]. The higher expression of CD106 on MSCs correlates with a greater immunosuppression [280]. This can be explained by MSCs upregulating CD106 which promotes T-cells adhesion, thus bringing T-cells into close proximity MSCs, where they can carry out their immunosuppressive functions [280]. Other studies support these findings showing that CD106+ MSCs reduce IFN-γ and TNF-α in Th1 cells and also reduce CD4+ T-cell polarisation into pro-inflammatory Th1 cells [277]. Further immunomodulatory abilities were seen by the higher expression of Tregs in co-cultures with CD106+ MSCs compared to CD106- MSCs [277]. These results may mean that pro-inflammatory primed UCMSCs in this chapter are more immunosuppressive than non-primed UCMSCs through the upregulation of CD106. But it is recognised that CD106 is just one marker of immune modulation and many more markers such as IDO and PGE2 may have significant changes between the primed and non-primed conditions.

This study showed that CD106 can be increased by a pro-inflammatory cocktail of IFN-γ, TNF-α and IL-1β, but there is great variability in CD106 production across the donors. This inconsistency has also been found in other studies where the protein production of CD106 on BMMSCs has ranged from 47-90% [284] and from 20.2-62.7% in another study [118]. Some studies identified that the STRO-1 positive subpopulation of MSCs is more likely to be positive for CD106 [285,286], it may be that some donors contained more STRO-1 although this was not tested for in the MSCs. The most consistent explanation form the literature points to donor variations in MSCs [287].

The final objective of this chapter was to compare the growth, morphology, and surface marker characteristics of UCMSCs (n=4) to the BMMSC (n=1) control. The surface marker production and tri-lineage differentiation confirmed that BMMSCs were of a mesenchymal stem cell lineage. The BMMSCs had statistically slower population doubling times of 6.1 days (± 0.2 SD) in normoxia and 5.1 days (± 0.38 SD) in hypoxia compared to UCMSCs (**Figure *32***). This is not surprising as research shows that the growth of BMMSCs is variable with studies showing a PDT of 12.25 (± 4.49 SD) days [288] and another study reporting that PDTs of 2.17 to 7.96 days from passage 3 through to passage 8 [118]. Indeed, the slowed proliferation of BMMSCs after continuous passaging is commonly described in the literature with BMMSC proliferation plateauing after 14 days concurrent with telomere shortening of up to 2kb [118,289]. However, it is not clear if telomere shortening is the cause or result of slowed growth. Nevertheless, the UCMSCs showed a stronger proliferation *in vitro* compared to the BMMSCs, which is one indicator of a suitable growth environment for the UCMSC, although their morphology and surface marker expression were also analysed.

The normoxic and hypoxic UCMSCs showed similarities to the BMMSCs in normoxic and hypoxic conditions, respectively. The hypoxic BMMSC were spindle shaped whereas, in normoxia, the BMMSCs retracted from each other and formed small clusters over time. These findings are supported by research that found in hypoxic conditions, a higher proportion of BMMSCs displayed a spindle shape [261]. Research further highlights the importance of cell shape as this can often be indicative of functioning, with one study showing that thin, spindle shaped MSCs have a higher adipogenic differentiation ability and wider, spindle shaped MSCs have a higher chondrogenic differentiation ability [290]. However, the morphology of MSCs is highly donor dependent as one study comparing 10 BMMSCs donors, grown in hypoxic conditions, could not determine a consistent cell morphology with some donor's MSCs showing triangular clustered shapes and others appearing spindle-like [264]. Despite the variability of MSCs, only one BMMSCs donor was analysed. It would have been ideal to use more BM donors as comparative controls against which to measure the characterisation of UCMSCs in this study, however, the one donor used showed characteristics similar to those already studied in the literature and has therefore served as a good control for this part of the work. UCMSCs show all the characteristics of MSCs as defined by the ISCT, are easily obtained from waste tissue, retain modulatory properties, and proliferate faster in culture than the 'gold standard' BM derived MSCs, which is ideal for extracting larger volumes of EVs.

3.4 Conclusion

The characterisation of UCMSCs showed that they belong to a mesenchymal stem cell lineage as they were plastic adherent, capable of trilineage differentiation and expressed MSC surface markers in accordance with the ISCT criteria. Growth kinetic analysis showed that UCMSC in both conditions were highly proliferative. The morphology of UCMSCs in normoxia and hypoxia was also studied and showed that normoxic UCMSCs were larger than hypoxic UCMSCs.

Differences were identified between the UCMSCs grown in pro-inflammatory primed conditions compared to those grown in normoxia and hypoxia. Specifically, there was an increase in production of CD106 and HLA-DR in some donors. Two points can be taken away from these findings. First, the pro-inflammatory priming of UCMSCs is altering some of the UCMSC characteristics. This is an interesting finding going forward into their EVs analysis to see if pro-inflammatory priming will change the EVs too. Second, the UCMSC donors responded differentially to the pro-inflammatory priming, this shows that the four UCMSC donors did not have identical characteristics and will be interesting to see if this finding transpires into heterogeneity across EV samples too.

The overall goal of this thesis is to establish if UCMSC-EVs can dampen inflammation related to RA. From the characterisation applied in this chapter, the umbilical cord seems an appropriate source of MSCs to examine the immunomodulatory properties of EVs. This is because the UCMSCs displayed all the required MSC surface markers, had a spindle-like morphology and faster growth in culture compared to BMMSCs, making them a suitable choice for ongoing research into their EVs.

Chapter 4:

Characterisation of human UCMSC-EVs

4.1 Introduction

EV research is a new and growing field with recent publications detailing their potential use as therapeutic agents, disease biomarkers and drug delivery systems [291–293]. Hence, there has been a surge in research using different isolation and characterisation methods. The International Society of Extracellular Vesicles (ISEV) recognised the need to develop consistency within the field, therefore, they devised a set of guidelines aimed at researchers to fully characterise EVs before applying them to different treatment models or functional studies [155]. A consensus from experts in the field was drawn up and a set of EV characteristics identified in line with recent evidence. In order to comply with the ISEV guidelines, many different techniques must be employed to achieve a detailed characterisation. Failure to thoroughly characterise EVs hampers the credibility and reproducibility of the research. Therefore, characterisation in accordance with the ISEV guidelines is an important first step towards understanding EV functional properties. **Table 15** details many of the techniques used in EV research to characterise EVs, along with their advantages and disadvantages.

Another factor which must be considered prior to characterising EVs is the isolation method. The EV field contains a wide range of different isolation methods, all of which produce a different yield and purity of EVs. These methods come with their advantages and disadvantages, as detailed in **Section 1.3.10**. Historically, differential ultracentrifugation was the primary method of EV isolation and is still the most commonly used method in the field, despite some limitations [294]. Other methods such as ultrafiltration, sucrose cushion ultracentrifugation and immunoaffinity capture have emerged in recent years with a different set of advantages and disadvantages. Due to the diversity of isolation methods, it can be challenging to compare different methods and there is no single method that is profoundly

superior over the rest. Therefore, the ISEV recommends choosing an isolation method based on the downstream application of EVs [155].

With this considered, differential ultracentrifugation and sucrose cushion ultracentrifugation were employed in this study. Studies comparing EV isolation methods report that differential ultracentrifugation yields an intermediate recovery of EVs along with an intermediate specificity, however this method is also known to co-isolate impurities and damage EVs [155,295]. This study applied differential ultracentrifugation for immunoblotting experiments only, due to the considerable quantity of EVs required for immunodetection. In all other experiments, EVs were isolated using sucrose cushion ultracentrifugation. This isolation method is based on the principle that small EVs have a density 1.1 to 1.19 g/ml, and the sucrose cushion is made to have a density of 1.210 g/cm^3, so that the EVs float within the cushion [211]. This method can selectively enrich EVs of a specific flotation density but, overall, the EVs have a greater purity compared to differential ultracentrifugation [296]. Other methods for EV isolation were considered prior to the commencement of this study. These included size exclusion chromatography, immunoaffinity isolation and polymeric precipitation. Size exclusion chromatography separates EVs based on size by passing particles through filter pores which may cause damage and break up EVs [148]. Immunoaffinity uses antibodies attached to beads to target EVs with particular surface antigens [148]. However, there is some bias in this approach as only a specific population of EVs can be isolated based on the antibody chosen. Additionally, polymeric precipitation kits, such as ExoQuick (System Biosciences, CA, USA), are known to quickly precipitate EVs, but research has shown that these polymer based kits also co-isolate impurities, such as lipoproteins and non-EV material, which makes downstream protein analysis difficult [148]. In the end, differential and sucrose cushion ultracentrifugation were considered the most appropriate methods for the aims of this study.

Many research groups have also looked towards combining two different isolation methods to produce a population of EVs that suits their downstream analysis. However, adopting this two-method isolation approach further limits the EV yield and biases EV populations compared to methods used separately [297]. Therefore, there is scope in this field to create one method which yields a high quantity and purity of EVs, but this has not yet been achieved.

The **aim** of this chapter was to isolate and fully characterise EVs in accordance with the ISEV guidelines [155]. To do this, different techniques were applied. First, the growth conditions of UCMSCs in serum needed to be adjusted. FBS contains a rich source of EVs which is problematic as it contaminates the EV preparation and can skew results [202]. Thus, FBS requires depletion of EVs prior to its use in cell culture to limit the influence of bovine derived particulates. The decision to use EV depleted media over serum starving the EVs was based on research that shows that serum starvation alters the EV properties [298] and the EV depleted media was likely to better support the growth of UCMSCs *in vitro*, which were in limited supply. Second, the size, concentration, and morphology of EVs needed to be determined. Nanoparticle Tracking Analysis and Transmission Electron Microscopy were applied to achieve this goal. Third, it was important to identify characteristic EV surface markers, so the europium immunoassay and MACSPlex exosome detection kit were utilised for this purpose. Finally, the cytosolic content of EVs was analysed using immunoblotting with an aim to identify internal EV markers.

The application of these techniques to characterise EVs is essential to determine that the isolated particles are truly EVs and to be confident that any further functional, protein and miRNA analysis is from a genuine EV preparation. All these techniques were used with the

aim to garner as much information on EV characteristics as possible to fully understand their functional behaviour going forward. There are many studies characterising EVs from UCMSCs [158,235,299–305], but few that have looked at them as comprehensively as this study. Therefore, the data described henceforth will add to the growing research on UCMSC-EVs.

The second **aim** of this chapter is to establish if the culture of UCMSCs in normoxic, hypoxic and pro-inflammatory environments change the characteristics of their EVs. This aim will be achieved using the same characterisation techniques, but an extra layer of analysis will be added by comparing the different EV groups.

Some parts of this chapter as published in Hyland et al. [306]. This represents the first study comparing UCMSC-EVs derived from normal oxygen, low oxygen, and pro-inflammatory conditions together. Some studies have looked at one or two conditions [158], but none have looked at all four, so this data will add novelty to the field of UCMSC-EV research.

Table 15: Advantages and disadvantages of techniques used in EV research.

Technique	Advantage	Disadvantage
Transmission Electron Microscopy (TEM) [307]	• Powerful magnification • High quality images	• Potential artefacts from sample preparation • Images show low contrast
Atomic Force Microscopy [308]	• High resolution • Can produce 3D images	• Particles need to be absorbed onto surfaces, which can change their size and shape • The recurrent contact of the probing tip can move vesicles in a sample
Cryogenic Electron Microscopy [309]	• High magnification • Structure is preserved in a hydrated state • Specimen is not attached to surface, so its natural state is imaged • Specimen can be statistically analysed and reconstructed • No stain required	• Low contrast in images • Technique is very sensitive and can lead to the generation of low-quality images if cubic ice is formed.
Nanoparticle Tracking Analysis (NTA) [310]	• Accurately analyses size distribution • Analyses particle concentration • Requires optimisation of video capture and analysis • Enables visualisation of samples	• Cannot differentiate particles from EVs • Large particles can compromise results • Frequent blocking of tubes with air bubbles.
Tunable Resistive Pulse Sensing [311]	• Analyses a broad size range of particles • Can measure size and surface charge of individual particles simultaneously • Analyses particle aggregation and stability • High-resolution and large amount of data points • No data manipulation required	• Prone to pore blockages • Cannot discriminate between different types of particles
Dynamic Light Scattering [310]	• Fast and easy set-up; does not require much optimisation	• Cannot analyse submicron particle counts • Inaccurate for polydisperse samples

	• High accuracy in sizing	• Cannot visualise samples
Western Blotting/ Immunoblotting [312]	• High specificity - antibodies target specific proteins • Ability to detect low concentrations of protein	• Time consuming • Semi-quantitative results • Prone to false positives and false negatives • High cost • Requires optimisation and a skilled scientist • Small proteins may transfer poorly to membrane
Europium Immunoassay [313–315]	• Highly sensitive • Cost effective • No specialised equipment required • Low background fluorescence • Long fluorescent time • Minimal autofluorescence	• Fluorescence quenching of europium in the presence of water molecules • Potential for non-specific binding • Europium particles can aggregate
Flow Cytometry [316]	• High speed analysis • Can measure single cells and a large number of cells • Some flow cytometers can sort different cell populations • Fluorescent intensities can be quantified	• Standard flow cytometers not sensitive for nanoparticles - EVs too small and require conjugation to beads • Very expensive instrument • Requires trained operator • Prone to issues with microfluidics system
ELISA [314,317]	• Well known method • Absorbance is proportional to protein concentration • Easy to perform • High specificity and sensitivity • Cost effective	• Low detection limit • Non-specific interactions • Insufficient blocking can cause false results

4.2 Results

4.2.1 Partial depletion of EVs from FBS

In order to deplete FBS of EVs for use in cell culture media, it was subject to a long ultracentrifugation step (18 hours, 120,000xg at 4^{o}C). The supernatant was then collected, stopping 2cm before the bottom of the tube to avoid the cell pellet **(Figure 33A).** EVs (n=3) were isolated from the supernatant of the ultracentrifuged FBS and the untreated FBS and analysed for protein and RNA concentration. Protein concentration was analysed using the BCA protein assay and results showed that the average protein concentration of the ultracentrifuged FBS-EVs was 403µg/ml (± 84 SD) compared to 1851µg/ml (± 403 SD) for the untreated FBS-EVs. There was a statistically significant decrease in protein concentration of 76.3% (± 6.7 SD) in the EVs from ultracentrifuged FBS compared to EVs isolated from untreated FBS ($p<0.0001$) **(Figure 33B)**. This indicates that ultracentrifugation was effective in reducing the FBS-EV protein concentration. The RNA concentration of EVs from the untreated and ultracentrifuged FBS was analysed using the Agilent 4200 TapeStation (Agilent Technologies, Santa Clara, CA, USA). Results showed that the average concentration of the untreated FBS was 670pg/µl (± 277 SD) compared to 233pg/µl (± 210 SD) for the ultracentrifuged FBS. The data represents a statistically significant decrease of 65.2% in RNA concentration from the ultracentrifuged FBS compared to the untreated FBS ($p<0.05$) **(Figure 33C)**. The Dv200 score, which represents RNA fragments >200nt, found that 50.70% (± 25 SD) of RNA fragments were between 200-6000nt for the untreated FBS-EVs compared to 13.54% (± 20.6 SD) in the EV depleted FBS-EVs. A size profile of the RNA from the untreated FBS-EVs and the EV depleted FBS-EVs is represented in the electropherogram in **Figure 33D.**

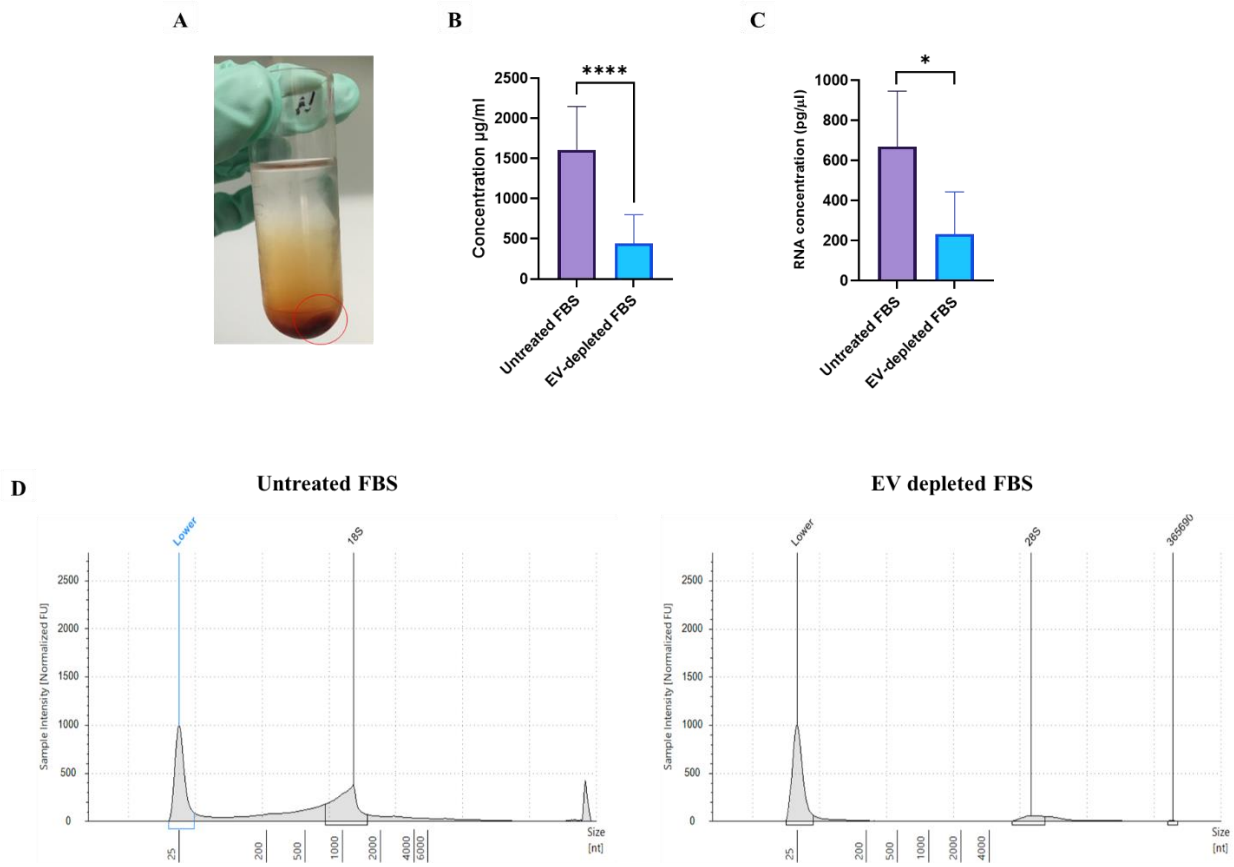

Figure 33: Depletion of EVs from FBS

A. *Image depicts a visible FBS pellet at the bottom of the tube (circled in red) after an 18-hour ultracentrifugation. The supernatant was collected, avoiding the pellet at the bottom which was likely to contain EVs.* ***B.*** *The protein concentration of the EVs (n=3) isolated from untreated FBS and from the supernatant of ultracentrifuged FBS was measured using a BCA protein assay. The bar chart displays the concentration in µg/ml (y-axis) and the EV depleted FBS and untreated FBS (x-axis). The protein concentration of the EV depleted FBS was statistically lower than the untreated FBS ($p<0.0001$)* ***C.*** *Bar chart displays the RNA concentration in pg/µl (y-axis) from EV depleted FBS-EVs (n=3) and the untreated FBS-EVs (n=3) (x-axis). The EVs isolated from EV depleted FBS had a statistically lower RNA concentration compared to the EVs from untreated FBS ($p<0.05$).* ***D.*** *Electropherograms displaying the RNA size profile from EVs derived from untreated FBS and EV depleted FBS. Sample intensity in Normalised Fluorescent Units is shown on the y-axis and nucleotide [nt] size is shown on the x-axis. Electropherograms were used to measure the Dv200 score.*

4.2.2 Analysis of isolated particles using NTA and TEM

The conditioned media and EVs from different culture conditions were analysed using Nanoparticle Tracking Analysis to gather data on their particle size and concentration. An image of particles in suspension passing through the chamber of the Nanosight NS300 instrument is displayed in **Figure 34A.** The average size of particles from the conditioned media was 169nm (± 58.9 SD) in normoxia, 164nm (± 37.5 SD) in normoxic/primed, 181nm (± 22.8 SD) in hypoxia and 168nm ± (19.1 SD) in hypoxic/primed. There were no statistical differences in size between the culture conditions when analysed using NTA. Donor 1 had the smallest size particles in all conditions as seen in **Figure 34B.** In a comparison of conditioned media and an EV suspension, there was a more diverse size range of particles from the conditioned media, shown by a higher standard deviation, compared to a more uniform size of particles from isolated EVs, shown by a lower standard deviation **(Figure 34C)**. The purified EVs had an average size of 167 nm (± 7 SD) compared to the un-purified conditioned media particles which had an average size of 171 nm (± 35 SD). Despite the range in standard deviation, there was little difference in the average size of particles between the purified EVs and un-purified conditioned media.

NTA cannot distinguish particles from EVs, so to further confirm that these particles were EVs, a CellMask™ Orange Plasma membrane Stain (Thermo Fisher, Warrington, UK) was added to an isolated hypoxic EV suspension. This dye binds to the plasma membrane and it detected the fluorescently labelled EVs to have a size of 110nm **(Figure 34D)**. This confirmed that the EV isolation protocol was isolating a population of particles with a plasma membrane that had the same size range of EVs.

The NTA also calculated the particle concentration of the conditioned media from different conditions. Samples were normalised to conditioned media from 7 x 10^4 cells as this represented the lowest cell number. There was an average of $1.98x10^{10}$ particles/ml for the normoxic conditions; $2.04x10^{10}$ for the normoxic/primed conditions; $9.21x10^9$ for the hypoxic conditions; and $1.08x10^{10}$ for the hypoxic/primed conditions. Normoxic conditions had a statistically higher concentration of particles compared to hypoxic conditions ($p=0.044$). There were no further statistical differences between the conditions **(Figure 34E).**

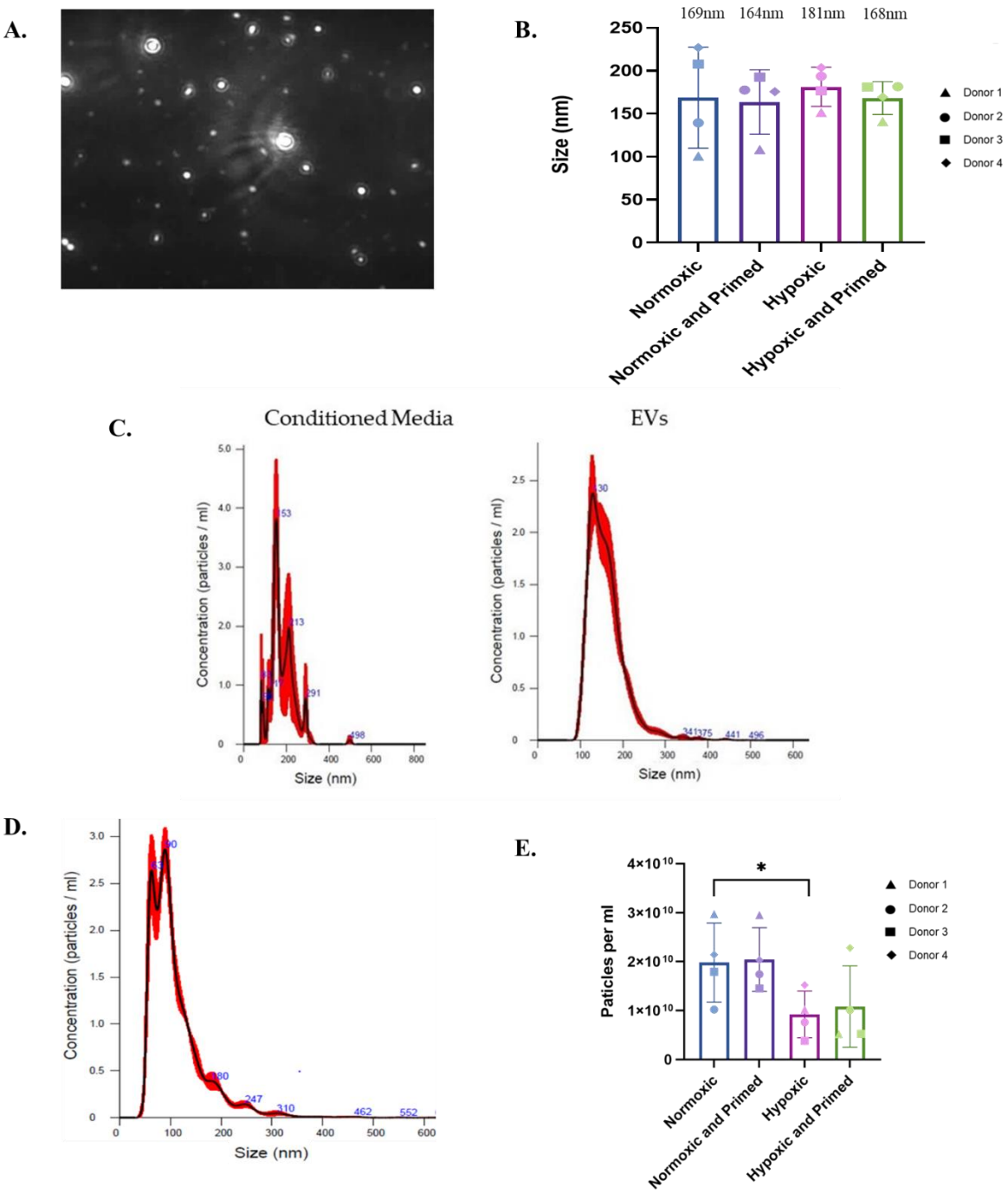

Figure 34: Analysis of EVs by NTA

A. *Image of particles in suspension from conditioned media passing thorough the chamber of the Nanosight NS300 instrument.* ***B.*** *Graph displaying the size of particles (nm) on the y-axis and the unprocessed conditioned media from four conditions on the x-axis. Each donor of UCMSCs is displayed with a different symbol. There was no statistical difference between the size of particles in the conditioned media from the four donors based on NTA data.* ***C.*** *Size profile of particles from conditioned media and particles from isolated EVs. The conditioned media has a more diverse size profile seen by*

many small peaks compared to the EVs which show a more uniform size profile, seen by one clear peak. ***D.*** *Particle distribution graph showing the size and concentration of EVs labelled with CellMask™ Orange, n=1. Concentration of EVs in particles/ml (y-axis) is plotted again size of EVs in nanometres (x-axis).* ***E.*** *Bar chart representing the particles/ml concentration of the conditioned media (y-axis) from cells grown in different conditions (x-axis). Statistical differences in concentration were found between normoxic and hypoxic conditions, n=4, p≤0.05. Data is shown as mean ± SD.*

To further confirm that the EV isolation protocol was recovering EVs, transmission electron microscopy (TEM) was applied to isolated EV preparations. TEM captures the image of EVs by passing a high voltage electron beam through EVs on a thin grid [318]. The subsequent scattering of electrons as they pass through the EVs are detected and an image can be generated [318]. TEM was carried out on EVs isolated from normoxic (n=2) and hypoxic conditions (n=2) **(Figure 35).** Results show that EVs had a characteristic round morphology and a visible bilayer membrane.

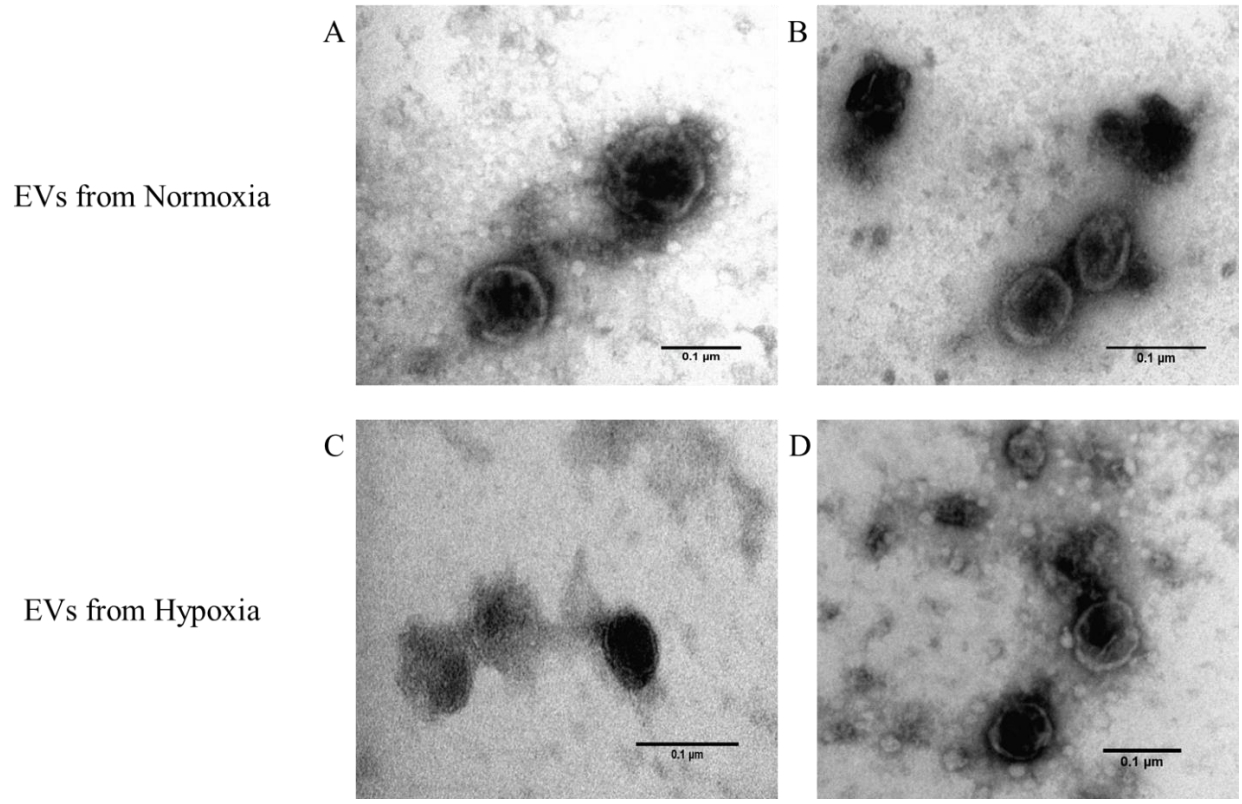

Figure 35: TEM images of EVs

Images of EVs in normoxia (A, B) and hypoxia (C, D) taken using TEM. EVs have a round morphology, size of ~100 nm and a visible bilayer membrane. Scale bars = 0.1 µm.

The size of EVs was analysed using ImageJ software as described in **Section 2.3.2.** Normoxic EVs had an average diameter of 91.4nm (± 41SD) compared to hypoxic EVs that had an average diameter of 71.4nm (± 28SD) **(Figure 36)**. There were no statistical differences between the conditions.

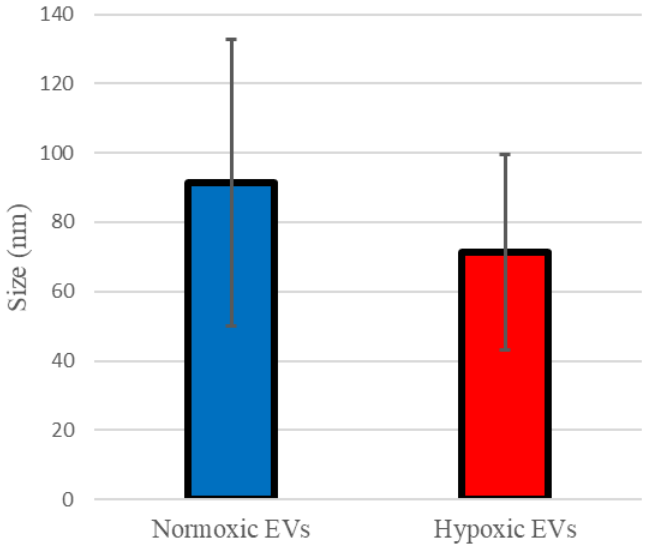

Figure 36: Comparison of EV size

Bar chart presents the average size of EVs from normoxia (n=2) and hypoxia (n=2). An average of 20 particles were analysed per condition. There were no statistical differences between the conditions. Data is shown as mean ±SD

4.2.3 EVs display tetraspanin surface markers and MSC lineage markers

The ISEV recommends detecting at least one tetraspanin surface marker when characterising EVs [155]. To do this, a europium immunoassay was chosen to detect the presence of common EV surface markers CD9 and CD81. An isotype control was also used to control for non-specific background signal. All EV samples were normalised to 3.87µg/ml, which was based on the protein concentration of the lowest EV sample. Results showed that CD9 and CD81 were detected in EV samples from all four conditions. The signal intensity of CD9 and CD81 was statistically higher in hypoxic compared to hypoxic/primed EVs ($p \leq 0.05$), indicating a higher presence of these surface markers **(Figure 37)**. In normoxic and normoxic/primed

conditions, Donor 3 had a considerably higher expression of CD9 and CD81 in comparison to the other donors which has contributed to the large error bars shown in **Figure 37.**

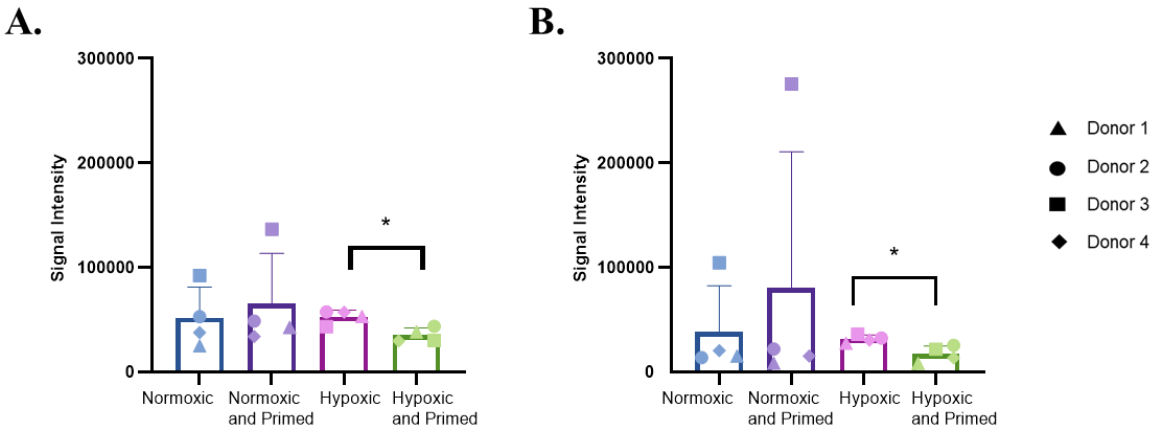

Figure 37: Tetraspanin expression on EVs

Bar chart showing the expression of tetraspanin markers CD9 ***(A)*** *and CD81* ***(B)****, in EVs (n=4) from four conditions detected using a europium-based immunoassay. Signal intensity is displayed on the y-axis and the EV conditions on the x-axis. Statistical differences in signal intensity were found between CD9 and CD81 in the hypoxic EVs compared to the hypoxic/primed EVs. All figures shown were calculated after subtracting the isotype control. Individual donors are depicted using different symbols. Data is shown as the mean ± SD. *p≤0.05.*

Further surface marker characterisation was carried out using the MACSPlex exosome detection kit to support the findings of the europium immunoassay and identify other EV surface proteins. The MACSPlex exosome detection kit, which probes for 37 exosomal protein epitopes and 2 isotype controls, showed that EVs contained the three tetraspanin surface markers CD9, CD63 and CD81. The EVs also contained the MSC marker CD105 and markers associated with cell adhesion and migration: CD29, CD44, and CD49e. There was a statistically higher signal intensity in melanoma chondroitin sulphate proteoglycan (MCSP), a protein that is associated with melanoma progression [319], in normoxic compared with normoxic/primed EVs (mean signal intensity: 15452 ± 2061 *vs* 6123 ± 3464) and in hypoxic

compared with hypoxic/primed EVs (mean signal intensity: 12482 ± 3322 *vs* 2018 ± 3197). Additionally, hypoxic EVs had a higher signal intensity compared to hypoxic/primed EVs for CD105 (mean signal intensity: 8692 ± 3052 *vs* 1795 ± 2153) and for CD146 (mean signal intensity: 4534 ± 1842 *vs* 871 ± 1313) indicating that there was a higher expression of these surface markers under non-primed conditions **(Figure 38).** With regards to CD9 and CD81, the hypoxic EVs had a higher expression of both markers compared to the hypoxic/primed EVs, similar to the europium assay **(Figure 37),** except the higher expression failed to reach statistical significance in this assay.

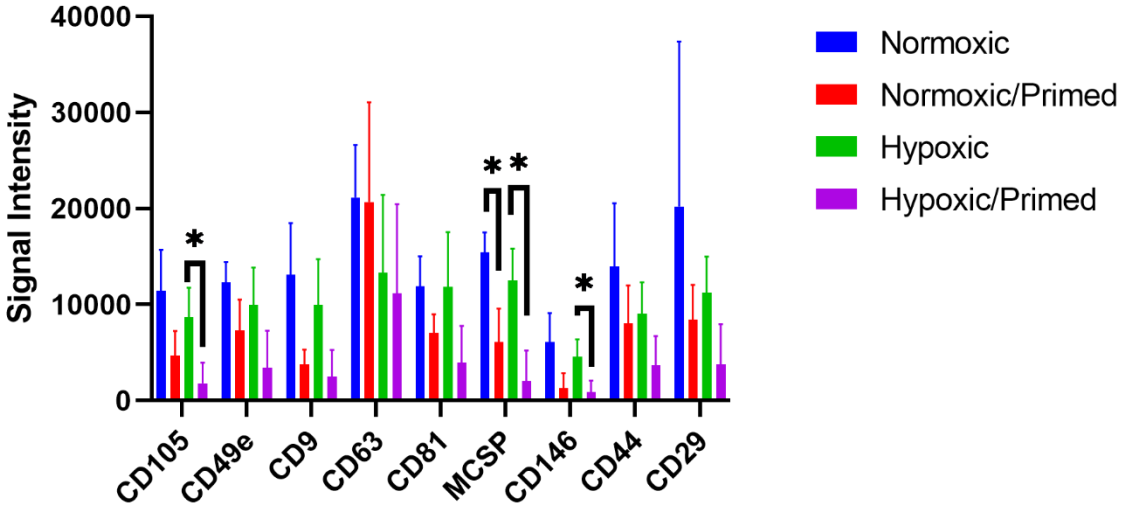

Figure 38: EV surface marker expression

*Bar chart shows a range of surface markers expressed on EVs (n=4) grown under normoxic, normoxic/primed, hypoxic, and hypoxic/primed conditions as detected using the MACSPlex exosome detection kit. Signal intensity is displayed on the y-axis and the surface markers on the x-axis. There was a statistically higher signal intensity in MSCP between normoxic and normoxic/primed EVs. Additionally, there was a statistically higher signal intensity in MCSP, CD105 and CD146 in the hypoxic EVs compared to the hypoxic/primed EVs. All figures shown were calculated after subtracting the isotype control. Data is shown as the mean ±SD . *p<0.05.*

4.2.4 Identification of cytosolic EV internal proteins Alix, Rab5a and Hsp70

The last experiment in the EV characterisation involved the detection of at least one cytosolic protein, as recommended by the ISEV guidelines [155]. Immunoblotting was carried out on one EV sample from normoxic, hypoxic, normoxic/primed, and hypoxic/primed conditions, and from one UCMSC sample. Four antibodies were chosen as positive cytosolic markers of EVs, namely Alix, Hsp70, Rab5a, and Tsg101. Additionally, Cytochrome C (12kDa), a mitochondrial marker, was chosen as a negative marker of EVs for this experiment.

Several protocol optimisation steps were carried out to clean the nitrocellulose membrane and produce the right signal intensity. Firstly, the washing and blocking steps were adjusted because the membrane was displaying a grainy picture after imaging **(Figure 39A).** The amount of washing steps increased from 3x5minute washes to 5x5minute washes in Tris-buffered saline with 0.05% Tween (TBST). Additionally, the membrane was blocked in a solution containing 5% semi-skimmed milk in TTBS for 2 hours instead of 5% semi-skimmed milk in PBS for 1 hour. Both these changes helped to produce 'cleaner' membranes as displayed in **Figure 41.** Other changes to the western blotting included the discontinuation of antibody GM130, a Golgi protein, which was intended to be used as a negative EV marker but showed unspecific binding on the membrane to many proteins at different molecular weights **Figure 39B)**. Lastly, Alix signal was absent from cell and EV samples **(Figure 39C)**. To adjust for this, a higher sensitivity chemiluminescent reagent, SuperSignal™ West Femto (Thermo Fisher Scientific, Waltham, MA, USA) was added, but this failed to improve the signal of Alix. Next the concentration of the primary antibody was increased from a 0.4µg/ml (1:500 dilution) to a 1µg/ml (1:200 dilution) which displayed a mildly positive signal for Alix shown in **Figure 41D.**

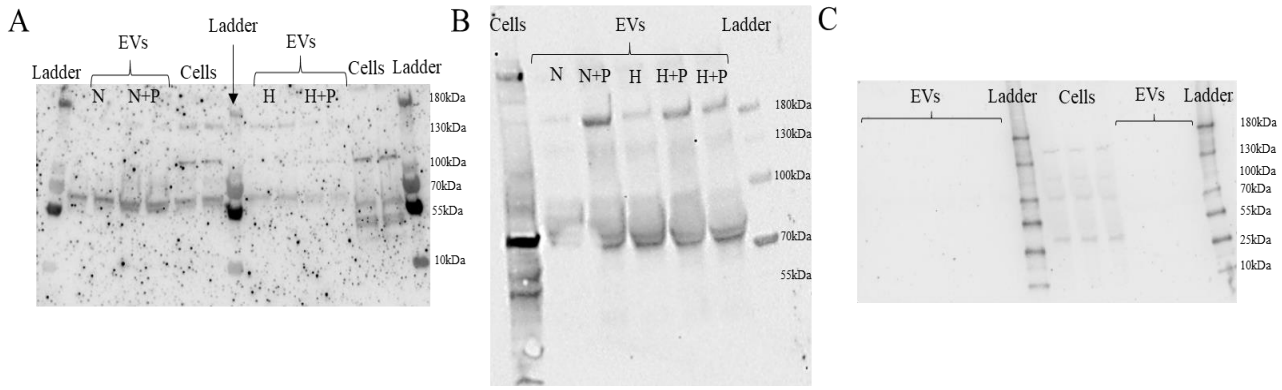

Figure 39: Optimisation of western blot

(A) *An example of the grainy image produced from nitrocellulose membranes after blocking, washing, and probing with antibodies prior to protocol optimisation.* ***(B)*** *GM130 displayed unspecific binding to many proteins on the nitrocellulose membrane. GM130 has a predicted molecular weight of 112 kDa and bands were expected to at 132-140 kDa using this antibody.* ***(C)*** *Absent signal for Alix when used at a 1:500 dilution. N= normoxic; N+P= normoxic/primed; H=hypoxic; H+P=hypoxic/primed.*

Before running protein samples on a gel, protein concentrations were measured using a BCA assay (Thermo Fisher, Warrington, UK) and the samples were normalised to 10µg of protein for EVs and UCMSCs. A TGX stain free gel was employed for the immunoblotting. This gel contains trihalo compounds which react with tryptophan in the protein to produce a fluorescence signal when UV activated [320]. The use of stain-free imaging eliminates the need to use loading controls and housekeeper genes as the protein bands can be seen on the gel after electrophoresis [320] and doesn't interfere with the subsequent western blotting. Results show relatively uniform loading of proteins onto the gel for Rab5a, Alix, Hsp70, Cytochrome C and Tsg101 **(Figure 40).**

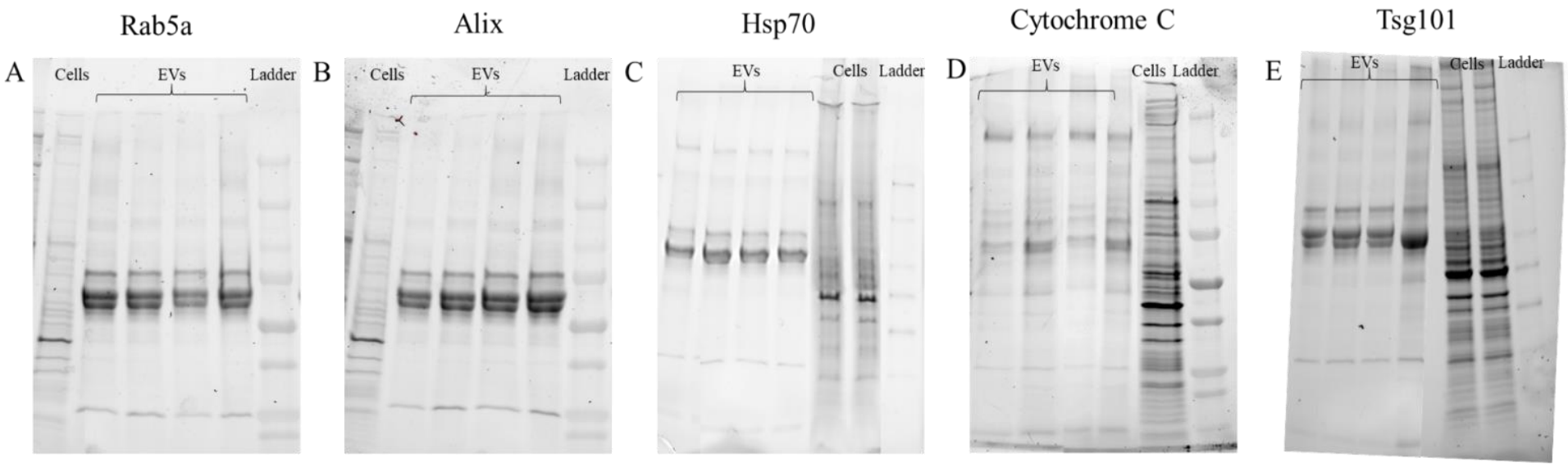

Figure 40: Gel image of proteins within EVs and cell samples after electrophoresis

Stain free gels were used to check for the equal loading of proteins. Image displays of stain free gels used to probe for ***(A)*** *Rab5a,* ***(B)*** *Alix,* ***(C)*** *Hsp70,* ***(D)*** *Cytochrome C, and* ***(E)*** *Tsg101. The lanes containing the cells show a much broader range of protein sizes compared to the EVs.*

Immunoblotting results show that the negative EV marker Cytochrome C was readily detected in UCMSC samples but absent from EV samples **(Figure 41A)**. There was a positive expression of Rab5a (25kDa), Hsp70 (70kDa) and Alix (96kDa) in EV and cell samples as detected by the presence of bands at the correct molecular weights **(Figure 41B-D).** To apply quantitative analysis to the results, protein bands were analysed using ImageJ software. Briefly, protein bands on the nitrocellulose membrane were transformed into peak graphs and the area under the peak was measured to obtain band intensity figures. The band intensity number is an arbitrary figure used to depict the relative change between samples. Rab5a, Alix and Hsp70 protein band peaks were compared in **Supplementary Figure 5,** but these figures could not be normalised to a loading control. Instead, a stain free gel was used to estimate differences in sample loading as previously described.

Hsp70 showed two bands for cell samples, one slightly above and one below the 70kDa mark. This was seen, to a lesser degree, by EV samples, shown in **Supplementary Figure 5.** There was some variability in expression of EV markers across different conditions. For example, there was a faint presence of Rab5a in normoxic EVs (band intensity 1969) compared to the other conditions (band range 4357-6000) **(Figure 41B, F)**. There was a weak detection of Hsp70 in hypoxic/primed EVs **(Figure 41C)** and Alix featured strongly in pro-inflammatory primed EVs compared to non-primed samples (**Figure 41D)**. In general, all EV conditions had a lower protein abundance of Alix and Rab5a compared to their parent cells (**Figure 41G)**. Tsg101, an ESCRT protein known to be involved in multivesicular body (MVB) biogenesis [321], was not identified in EVs but was present in UCMSCs (**Figure 41E)**. The recommended starting dilution for Tsg101 is 1:200 with a dilution range of 1:100 to 1:1000 according to the manufacturer's guidelines. Tsg101 was first probed at 1:200 and again at 1:100 but failed to produce signal in EVs.

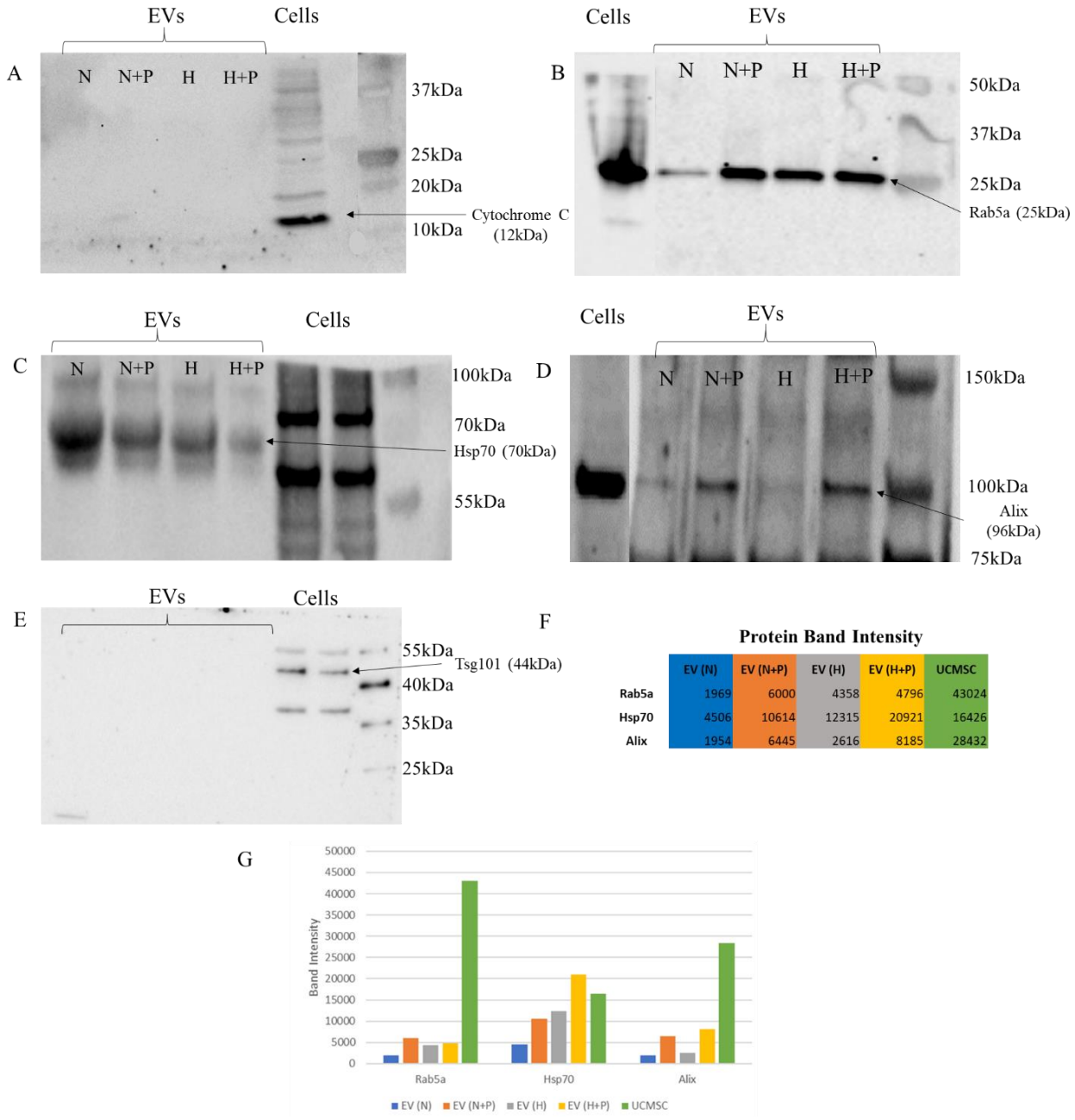

Figure 41: Immunoblotting analysis of intercellular EV markers

(A) *Immunoblotting images show the negative expression of Cytochrome C in EV samples and a positive expression in UCMSC cell lysates.* ***(B-D)*** *Positive expression of EV markers: Rab5a, Hsp70 and Alix in both EV and cell samples.* ***(E)*** *There was a negative expression of the EV marker Tsg101 in EV samples, but signal was detected in cell samples.* ***(F)*** *Band intensity figures for Rab5a, Alix and Hsp70 from different conditions. Band intensity figures were obtained from ImageJ software (v.1.53e).* ***(G)*** *Bar chart displaying the band intensity of Rab5a, Hsp70 and Alix from UCMSCs and EVs grown in different conditions (n=1). N= normoxic; N+P= normoxic/primed; H=hypoxic; H+P=hypoxic/primed.*

In all, the EVs from all conditions met the guidelines for the characterisation of EVs, established by the ISEV committee [155]. A detailed overview of requirements for characterisation and how these EVs met the criteria is shown in **Table 16.**

Table 16: Requirements for the characterisation of EVs

Table explains the ISEV 2018 and 2014 guidelines for the characterisation of EVs in the first column, including examples provided by the ISEV (column 2). The third column details the techniques and proteins identified in this study to meet the ISEV guidelines.

ISEV Requirement	Examples	Identified in study
At least three positive protein markers including at least one: • Transmembrane/lipid bound protein	• Tetraspanins (CD63, CD81, CD82) • MHC class I (HLA-A/B/C, H2-K/D/Q), • Integrins (ITGA*/ITGB*), transferrin receptor (TFR2) • TSPAN8 • CD37 • CD9 • CD90	• CD63 • CD81 • CD9
• Cytosolic protein	• TSG101 • ALIX (PDCD6IP) • Flotillins-1 and 2 • Caveolins (CAV*) • Annexins (ANXA*) • Heat shock proteins HSC70 (HSPA8), HSP84 (HSP90AB1)	• Alix • Hsp70
Lack of non-endocytic intracellular proteins, not part of EV biogenesis	• GM130 • Cytochrome C • Grp94	• Cytochrome C
Characterisation of single vesicles; use two different but complementary techniques, for example: • Electron or atomic force microscopy • Single particle analyses	• Electron microscopy (TEM) • Atomic-force microscopy • Tunable Resistive Pulse Sensing • Nanoparticle Tracking Analysis (NTA) • Flow Cytometry	• Sizing (NTA) • Concentration (NTA) • Morphology (TEM)

* Families of multiple proteins

4.3 Discussion

This chapter focused on the characterisation of EVs from UCMSCs grown in four conditions. The main aim was to confirm that the isolated preparations from the UCMSC conditioned media were of true EV origin and displayed characteristics in line with the ISEV guidelines. This chapter also had a second aim to identify differences in the EVs from normoxic, hypoxic, normoxic/primed, and hypoxic/primed conditions.

The first step was to establish the growth conditions for the UCMSCs. It was decided to use EV depleted FBS in the culture media to help support cellular growth. FBS was depleted of EVs using a long ultracentrifugation protocol and the efficiency of EV depletion was assessed. There was an approximate 76.3% decrease in EV protein and a 65.2% decrease in EV RNA from the FBS after 18-hour ultracentrifugation shown in **Figure 33**. However, this protocol comes with limitations. One of those limitations is the pelleting of larger FBS proteins during ultracentrifugation which are needed to support cell growth. Indeed, research shows that the use of EV depleted FBS has a reduced ability to support cell growth in culture, seen by the decreasing population doubling times and reduced cell viability after 48 hours [205]. However, these findings were not reproduced in this study, which showed strong growth of UCMSCs up to passage 8, shown in **Figure 26**. These figures are similar to other PDT analysis of the same cells by Mennan et al. [217] which showed an average PDT of 2-3 days up to P13. The maintained growth of UCMSCs up to P8 may be because the EV depleted media was only added for 48 hours for CM collection and then 'rescued' with normal complete media thereafter. Indeed, research has shown that serum depriving BMMSCs for a period of 2-4 weeks supports a subpopulation of MSCs with a small, spindle-like morphology [322]. These cells maintained their proliferation, had longer telomeres and expressed more OCT-4 in serum

deprived conditions compared to control cells [322]. As the EV depleted FBS is deprived of some serum components then this may be one theory as to why the UCMSCs in this study did not succumb to the EV depleted FBS conditions but rather maintained a strong proliferation through to P8.

In general, research is conflicted about the effectiveness of an ultracentrifugation protocol for the depletion of bovine EVs. Some studies have reported that this method is effective at removing 95% of RNA-containing FBS-EVs [202] and at reducing the particles/ml concentration of FBS [203–205]. However, there is also contradictory research showing that an abundant population of EVs are present after ultracentrifugation [323]. This study found a significant reduction in EV protein, but it was not a 100% depleted of bovine EVs, therefore, it is likely that there are some bovine EVs existing in the isolated EV suspension and this will need to be considered carefully in interpreting future analysis. This study would also have benefitted from utilising Nanoparticle Tracking Analysis to compare the concentration of particles in the untreated and EV depleted FBS. Additionally, an EV depleted media sample could have been analysed by western blotting and europium immunoassay to partially quantify the influence of FBS-EVs. At present, depleting FBS of 100% of its EVs has not been achieved and research is growing to develop affordable alternatives to serum to avoid this contamination issue.

The main aim of this chapter was to look at the size, morphological, and protein characteristics of EVs to confirm that the isolated particles were genuine EVs in line with the ISEV guidelines as detailed in **Table 16**. The NTA analysis provided insight into the biodistribution of particles in the conditioned media and in the EV suspension. It was clear from the size profiling graphs

that the CM had a more diverse range of particles compared to a more uniform profile seen in the analysed EV preparation **(Figure 34C).** This shows that the EVs had been purified during the isolation process and a specific size of EVs identified. The NTA analysis also showed that the CellMask™ Orange (CMO) plasma membrane stain successfully bound to the EVs and had an average size of 110nm, which is comparable to the size of small EVs [324]. This successful uptake of CMO shows that the EVs were plasma membrane enclosed particles as opposed to debris in the final preparation. This was further confirmed upon imaging of the EVs using TEM; they displayed a consistent, sphere-shaped morphology with a phospholipid bilayer indicative of EVs **(Figure 35).** The TEM analysis also showed that the particles were of a size profile similar to small EVs, with the normoxic EVs averaging 91nm in diameter and the hypoxic EVs averaging 71nm in diameter. There were no visible changes in the EV morphology between normoxic and hypoxic EVs.

The size of EVs did not statistically differ between conditions **(Figure 34B).** Previous research has also found similar results, showing no statistical differences in size, shape and electrodensity between EVs from normoxic and hypoxic conditions [82]. However, there have been changes seen with pro-inflammatory priming of MSC-EVs. Varkouhi et al. [325] found that IFN-γ primed UCMSC-EVs were approximately 1.5 times larger than their non-primed counterparts; however, this study used a higher concentration of IFN-γ and for a shorter time than the current study. Whether these differences cause functional changes or are completely negligible remains to be answered, as there is little research on whether subtle changes in EV size have a major bearing on their functional properties.

Interestingly, there was a statistically higher concentration of particles in normoxic conditions compared to hypoxic conditions, albeit there was a large range of particle concentrations detected from the four different donors. This may mean that normoxic cells are secreting more EVs compared to hypoxic cells, but it may also mean that there is more cellular 'debris' in the conditioned media as NTA does not discriminate between EVs and non-EV particulate. Findings differ in the literature with regards to particle concentration from MSCs grown in normoxia and hypoxia. Some groups have found no difference in particle concentration [326], while others have found the hypoxic MSCs have a higher particle concentration compared to normoxic MSCs [327]. This lack of consensus highlights the need for more research in this area.

The europium immunoassay and the MACSPlex exosome detection kit provided a thorough characterisation of EV surface markers. The europium immunoassay showed that all EVs expressed tetraspanin surface markers CD9 and CD81. There was an increased signal intensity of CD9/CD81 in hypoxic EVs compared to hypoxic/primed EVs which indicates a higher protein expression under non-primed conditions. This may mean that priming the UCMSCs in hypoxic conditions is altering the heterogeneity of the EV, as no differences in CD9/CD81 expression were found between normoxic and normoxic/primed conditions. Research shows that hypoxia triggers specific signalling pathways compared to growing cells in normoxic conditions [328–330], so low oxygen environments may play a role in changing EV surface marker expression. Further changes were also seen in the MACSplex exosome detection kit, which showed a downregulation of CD105 and CD146 in hypoxic/primed EVs. However, the connection between hypoxic-induced signalling pathways, pro-inflammatory priming and EV biogenesis remains largely elusive in the EV field. To further investigate a potential relationship, a larger sample size would be needed as there is a high variability amongst donors

as shown in **Figure 38**. Other groups have found differences in surface marker expression in EVs derived from different cell culture conditions. Lo Sicco et al. [82] found that CD63 was increased in hypoxic EVs compared to normoxic EVs, showing that this marker was altered by the culture environment. However, no differences were found between conditions in the levels of CD63 from the MACSPlex exosome detection kit in this study.

The most notable differences from the MACSPlex exosome detection kit were the downregulation of melanoma-associated chondroitin sulphate proteoglycan (MCSP) in pro-inflammatory primed conditions from both hypoxic and normoxic cell culture. These findings have also been shown in another study where pro-inflammatory priming of WJMSC-EVs reduced MCSP expression [327]. MCSP, also known as chondroitin sulphate proteoglycan 4 (CSPG4) or neuron-glial antigen 2 (NG2; rat homologue), is associated with melanoma cells [319], myofibres, blood vessels [331], and mesenchymal stromal cells [332]. Indeed it has a high expression in pericytes [333] (*in vivo* progenitors of MSCs [334]), and it's expression reduces significantly upon the terminal differentiation of MSCs [319,331,335]. This could mean that the primed UCMSCs were leading to terminal differentiation. To explore this further, a tri-lineage differentiation experiment of MSCs pre- and post- priming with pro-inflammatory cytokines would need to be conducted. It raises the question: does the pro-inflammatory priming of MSCs reduce their differentiation ability due to the loss of MSCP? It is interesting that the priming of UCMSCs reduced MCSP expression as stimulation with pro-inflammatory cytokines in a rat neuronal model of inflammation has been found to increase the levels of MCSP [336–338]. A study into the functional properties of MCSP on cord blood MSCs and their EVs found that MCSP-EVs promoted the proliferation and angiogenic properties of endothelial cells by increasing levels of basic fibroblast growth factor (bFGF) and platelet-derived growth factor (PDGF); and knockout of MCSP results in defects to blood vessel

formation [332]. Therefore, it may be possible that the downregulation of MCSP in primed EVs may make them less potent as angiogenic mediators.

EVs express many of the same markers as their cells of origin. This is due to either the microparticles blebbing from the plasma membrane or the intracellular uptake of proteins during exosome biogenesis when forming intraluminal vesicles. A paper by Witwer et al. [324] recommends identifying MSC surface markers on MSC-EVs to confirm that at least a subset of EVs are of genuine MSC origin. Therefore, it was a positive to see CD105 as a surface marker on the EVs in this study. However, CD105 was downregulated in hypoxic/primed EVs. CD105 is involved in cell proliferation, differentiation and migration [339] and the lack of expression of CD105 on UCMSCs and ATMSCs has been associated with stronger immunomodulatory properties [340]. This was shown in a study comparing CD105+ and CD105- UCMSCs and ATMSCs. When co-cultured with lymphocytes, CD105- MSCs showed a stronger ability to reduce pro-inflammatory cytokines (IFN-γ, TNF-α, IL-1β, IL-2) and increase the expression of TGF-β [340]. This is promising as the hypoxic/primed EVs may have a heightened ability to supress immune responses. Additionally, CD146 was downregulated in the hypoxic/primed EV group, and the downregulation of this surface marker is associated with senescence in umbilical cord blood MSCs [341]. Pro-inflammatory primed CD146- MSCs were associated with a higher release of IL-6, greater Th17 cell activation and an increased disease progression in CIA mice compared to CD146+ MSCs [342]. These findings question the anti-inflammatory potential of the hypoxic/primed EVs, however many other proteins and RNAs are involved and thus, need to be considered in determining anti-inflammatory potential.

Other noteworthy proteins identified on EVs from all conditions were CD29 and CD44, both considered to be mesenchymal stem cell markers [343]. The identified markers CD29, CD44 and CD49e are associated with cell-cell interactions and adhesion [344] and may explain how EVs are taken up by recipient cells during paracrine signalling.

Characterisation of cytosolic EV proteins was carried out using immunoblotting to identify the positive expression of Alix, Rab5a, Hsp70 and the negative expression of Cytochrome C. Blotting images show a negative expression of Cytochrome C in EVs and a positive expression in UCMSCs. The ISEV recommends that EVs be 'tested for the presence of non-vesicular, co-isolated components' (p.12), but it has updated its stance on the necessary identification of negative EV markers from the 2014 guidelines [155]. It is now understood that EVs can interact with any component of the cell given their size and approximation to different organelles, particularly in the case of larger EVs [155]. Therefore, the identification of a universal negative EV marker is elusive; instead the identification of proteins not commonly associated with the EV cargo (such as cytochrome C) can be used to assess the degree of EV purity [155]. It can therefore be deduced that the EVs isolated in this study were unlikely to have been associated with mitochondria during their biogenesis. Additionally, cytochrome C may be present in tiny apoptotic particles or cell debris, therefore, the absence of this protein indicates that the suspension containing EVs did not contain free floating cytochrome C.

A positive expression of Alix, Rab5a and Hsp70 was identified from the immunoblotting. Alix is a protein that is part of the endosomal sorting complex required for transport (ESCRT) pathway which is involved in EV biogenesis [142]. In a study of EVs from liver stem cells, Alix was found to play a crucial part in the packaging of miRNAs into EVs but not in the

secretion of EVs from cells [142]. Previously, Alix has shown a high affinity binding to Argonaute 2 (Ago2), a key protein involved in miRNA transport and processing [345]. When Alix was knocked down, the levels of miRNAs and Ago2 dropped significantly in EVs suggesting that it plays an important role in the loading of miRNAs into EVs via binding to Ago2 [142].

Another identified cytosolic protein was Rab5a, which is involved in endosome biogenesis and plays a role in the transport of materials from the cell membrane into early endosomes [346,347]. Hsp70, which is another EV marker known to stimulate TNF-α production by macrophages and promote NK cells [295,348], showed a positive expression in EVs although the molecular weight was different to the parent UCMSCs. The EVs contained bands at the expected 70kDa mark, but the UCMSCs contained two bands, one at 75kDa and one at 65kDa. The difference in molecular weight between cells and EVs is likely due to the presence of multiforms of Hsp70 created by different genes (isoforms) as the antibody used in this study recognised a range of Hsp70 isoforms [349]. It could also be due to post translational modification of Hsp70 particularly in the larger 75kDa protein band [349]. Another explanation could be the possibility of some non-specific binding to other Hsp forms especially in the smaller 65kDa size band. The Hsp70 detected in the EVs in this study was of the expected molecular weight so it can be deduced that the EVs were positive for Hsp70. As the characterisation of EVs was the main aim of this chapter, the double bands of Hsp70 in cellular samples were not investigated further, although is of interest to future work. In all, there was variability in the expression of cytosolic markers for EVs across the four different conditions: normoxic, normoxic/primed, hypoxic, and hypoxic/primed. This variable expression in cytosolic markers may be due to the cell culture conditions causing the differential expression of proteins or, likewise, it could also be due to the high degree of heterogeneity in EVs.

Tsg101 was not detected in the EVs from the UCMSCs and was detected in the parent UCMSCs. Other studies have shown that Tsg101 is detected in an inconsistent manner in EVs and the presence of it is highly dependent on the cell of origin [350]. Additionally, the lack of Tsg101 signal may be due to issues with the antibody. A higher than recommended concentration of antibody (1:100) was used and still failed to detect a signal in the EVs. No alternative antibody was available for this experiment, but a different antibody may still be worth trying in the future.

The characterisation of EVs in this chapter is detailed, but it could become more comprehensive by analysing the purity of EVs. This could have been done by comparing the protein concentration of the EVs from the BCA assay with the particles/ml concentration of the EVs from the Nanoparticle Tracking Analysis [296]. In hindsight this would have added an extra layer of analysis to the isolated EV preparations. Future work will aim to analyse the purity of all EV preparations as this is important for downstream functional studies, to be sure that any changes are EV mediated.

4.4 Conclusion

In summary, the characterisation data shows that the isolated EVs from the four conditions had 1) characteristic EV surface marker expression, 2) internal EV markers (Alix, Hsp70, Rab5a), 3) the correct size for EVs identified through NTA and TEM, and 4) the correct morphology for EVs, in line with ISEV guidelines. This evidence supports the conclusion that the isolated particles are EVs, and the EV isolation method employed in this chapter was successful. There were some differences between the surface marker expression and cytosolic protein expression

from the EVs derived from different conditions. This shows that the cell culture environment may be causing changes in the UCMSC secretome and this warrants further investigation to establish which source of EVs may be the most therapeutic. The next three chapters will cover in more depth how the cell culture environment can alter the UCMSC-EV protein expression, miRNA profile and functional abilities.

Chapter 5: Protein profile of human UCMSC-EVs

Part of this chapter have been published in:

Hyland, M., Mennan, C., Wilson, E., Clayton, A., & Kehoe, O. (2020). Pro-Inflammatory Priming of Umbilical Cord Mesenchymal Stromal Cells Alters the Protein Cargo of Their Extracellular Vesicles. *Cells*, *9*(3), 726. https://doi.org/10.3390/cells9030726

5.1 Introduction

Extracellular vesicles (EVs) are emerging as an alternative therapeutic option to MSCs [351], this is because they have a lower risk of transplant rejection, an inability to differentiate *in vivo* and a greater stability [351]. The EV cargo comprises of proteins, mRNAs, miRNAs, saccharides and lipids and the constituents of the cargo are unique to the cells that they originate from [129]. They are released by cells and travel to target cells where they EVs can interact with cells via receptor binding, direct fusion with the cell membrane, or endocytic internalization [352]. The EV cargo can then be transferred into the target cells where they can carry out a functional change [353]. EVs sourced from UCMSCs have shown promise as a potential immunosuppressive therapy both in *in vitro* and animal studies [160,302,303,305,325,354–356]. This is mainly due to their ability to inhibit T-cell proliferation [303,355,356] and reduce inflammation in animal models of type 2 diabetes mellitus [302], brain injury [305] and acute lung injury [325]. This evidence warrants further investigation into the therapeutic potential of UCMSC-EVs.

The immunosuppressive properties and functioning of EVs is changeable in response to different culture conditions that the parent cells are grown in [236]. This means the immunosuppressive content of EVs can potentially be upregulated when the UCMSCs are provided with the right stimulus. Some studies have shown the benefit of priming cells with pro-inflammatory cytokines and hypoxia, whereby the resulting primed EVs show enhanced

immunosuppressive abilities compared to their non-primed EV counterparts [243,252,325,357–360]. Specifically, research using EVs secreted from pro-inflammatory primed MSCs has shown positive immunosuppressive effects by polarising pro-inflammatory immune cells into anti-inflammatory immune cells *in vitro* [165,304,361–364]. One study showed that pro-inflammatory priming of ATMSC with TNF-α and IFN-γ caused an upregulation of HGF, TSG-6, PGE2 and TGF-β in EV cargo [357]. These EVs were then able to reduce inflammation in a mouse model of colitis [357]. Pro-inflammatory priming also caused an increase in RAB27B, A20 and TSG-6 in exosomes. These exosomes were then successful in inhibiting T-cell proliferation *in vitro* [365].

In addition to pro-inflammatory priming, hypoxic priming of UCMSCs has shown therapeutic effects. Culturing UCMSCs in hypoxia is associated with decreased apoptosis, lower levels of reactive oxygen species and an increases the angiogenic potential [243]. Hypoxic UCMSCs have been found to upregulate hepatocyte growth factor (HGF), brain-derived neurotrophic factor, and vascular endothelial growth factor (VEGF) leading to a reduction of inflammation and improved axonal growth in a rat spinal cord injury model [239]. The benefits of hypoxic priming also apply to the MSC-EVs which have shown enhanced therapeutic properties. ATMSC-EVs derived from cells grown at 5% O_2 had a more potent ability to polarise M1 macrophages into M2 macrophages in mice compared to the MSC-EVs derived from normal oxygen conditions [82]. This was seen by the enrichment of anti-inflammatory miRNAs (miR-223 and miR-146b) in the hypoxic EV cargo [82]. Hypoxic ATMSC-EVs have also been found to have a stronger angiogenic potential compared to normoxic EVs, seen by their ability to promote vascular tube formation *in vitro* [326].

These are just some examples of how EVs can function differently when their parent cells are exposed to different stimuli. However, despite the evidence of an increased therapeutic effect of priming MSCs with low oxygen and pro-inflammatory cytokines, there is variability in methods used across the literature and little research on the extent of alteration to the protein and miRNA cargo of EVs. Therefore, this chapter focuses on characterising the protein cargo of EV populations from MSCs (n=4) cultured in different conditions (normoxia, hypoxia ± pro-inflammatory conditions). In order to study the EV protein cargo, a proximity-based extension assay (PEA) was used, as described in **Section 2.8.1.** Using this PEA assay, the expression of internal proteins in the EV cargo could be measured. The EVs from different UCMSC growth conditions were compared to analyse how culture conditions were affecting the EV protein cargo.

The following groups were compared:

1. Normoxic EVs vs Hypoxic EVs: To investigate the effects of hypoxia on EV protein cargo.
2. Normoxic EVs vs Normoxic/Primed EVs: To investigate the effects of pro-inflammatory priming on EV protein cargo.
3. Hypoxic EVs vs Hypoxic/Primed EVs: To investigate the differences in protein expression of pro-inflammatory priming within the hypoxic milieu.
4. Normoxic/Primed EVs vs Hypoxic/Primed EVs: To investigate the effect of low vs normal oxygen concentration on protein expression when the EVs are primed with pro-inflammatory cytokines.

This study design was applied to give insight into which culture conditions resulted in the population of EVs with the most anti-inflammatory potential.

Aim

To compare the protein cargos of UCMSC-EVs from four different conditions using the proximity-based extension assay.

Hypothesis

1. UCMSC-EVs from cells that were primed with pro-inflammatory cytokines contain more anti-inflammatory proteins in their cargo.
2. UCMSC-EVs from cells that were primed with hypoxia contain more pro-angiogenic and anti-inflammatory proteins in their cargo.

Statistical Analysis

Before applying statistical analysis to the data, the Normalized Protein eXpression (NPX) value was generated. This was carried out by OLink (Uppsala, Sweden) and involved a number of data analysis steps. Firstly, the extension control Ct values were subtracted from the sample Ct values to control for technical variations; this generates the dCt. Next the internal control Ct values were subtracted from the dCt to adjust for normalisation between runs; this generates the ddCt. Finally, the sample ddCT was subtracted from the correction factor (a pre-determined value), to control for background noise and invert the scale. The formula for the generation of the NPX is shown in **Figure 42.**

The statistical analysis was carried out at RJAH using Graphpad Prism v.8 (GraphPad Software, San Diego, USA). A paired t-test was performed for the comparison of NPX values between conditions and multiple t-tests were used for the comparison of different proteins between conditions.

Extension Control:

$$Ct_{Analyte} - Ct_{Extension\ Control} = dCt_{Analyte}$$

Inter-plate Control:

$$dCt_{Analyte} - dCt_{Inter\text{-}plate\ Control} = ddCt_{Analyte}$$

Adjustment against a correction factor:

$$Correction\ factor - ddCt_{Analyte} = NPX_{Analyte}$$

Figure 42: Generation of NPX value

Equation used to generate the NPX value from the Ct read-out after PCR. It involves subtracting the extension and inter-plate control readings to account for technical variation and normalisation, respectively. Finally, the sample is subtracted from the correction factor to remove background noise and to invert the scale so that a high NPX corresponds to a high protein expression.

5.2 Results

5.2.1 Quality control check confirm intact EV protein

Four internal controls were added to the plate to monitor the plates performance and assess the quality of the EV samples. The whole plate passed the quality control as all the internal controls were within a standard deviation of 0.2 NPX of each other. Additionally, all the EVs samples passed the quality control as they deviated by less than 0.3 NPX from the median of the internal controls. Confirmation of this was received from the plate analysis certificate generated by OLink (Uppsala, Sweden) **(Figure 43)**.

Panel name	No. of samples that passed QC / Tot no. of samples	Passed samples (%)
Olink INFLAMMATION	19 / 19	100

Figure 43: Confirmation of EVs passing quality control

5.2.2 Changes in EV protein cargo after pro-inflammatory priming

The mean NPX values of all the 92 proteins were compared to see if one population of EVs contained a higher abundance of all the selected proteins as a group. The whole panel of 92 selected proteins, used for this analysis is shown in **Supplementary Table 1**.

Results showed that the primed EVs had statistically higher NPX values than the non-primed EVs, both in the normoxic/primed (p=0.001) and hypoxic/primed groups (p=0.0009) **(Figure 44)** suggesting that there were more proteins packaged into the primed EV cargo. There were no differences in NPX values identified between normoxic and hypoxic EVs (p=0.24).

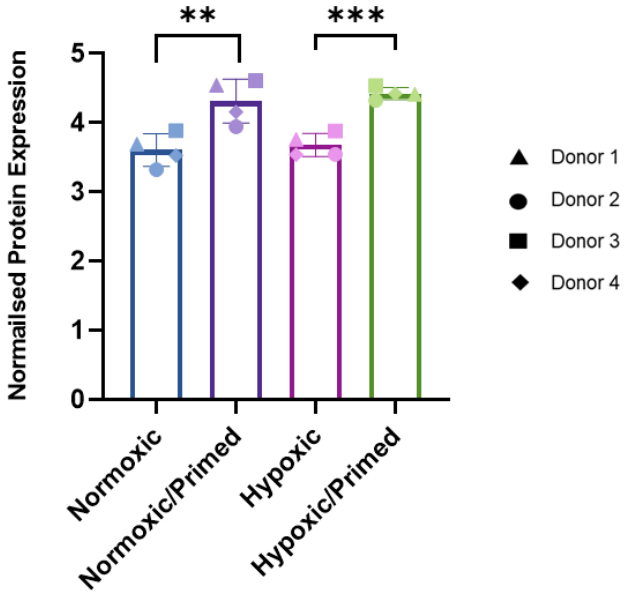

Figure 44: Normalised Protein Expression of EVs

*Bar chart represents the normalised protein expression of EVs (n=4) from four different conditions (normoxic, hypoxic, normoxic/primed, hypoxic/primed). There was a significantly higher NPX value for normoxic/primed and hypoxic/primed EVs compared to the normoxic and hypoxic EVs, respectively. **p<0.01 ***p<0.001.*

To explore possible changes in the protein-repertoire of EVs, a comparison of the NPX values from the different EV conditions was carried out. Of the 92 inflammatory-related proteins in the assay, 52 were detected in the EV samples. Statistical differences were identified in 16 proteins from the normoxic vs normoxic/primed group and 21 proteins from the hypoxic vs hypoxic/primed group, these can be found in **Table 17**, alongside the difference in Log2(fold change) showing the change in protein expression between primed/non-primed EVs. A comparative expression of all the proteins in the four EV conditions is shown in a heat map in **Figure 45.**

There were no statistical differences in EV protein cargo between the normoxic vs hypoxic group nor between normoxic/primed vs hypoxic/primed group. The only statistical differences were found between EVs with and without pro-inflammatory priming. In general, the EVs that were primed with pro-inflammatory cytokines had a higher abundance of proteins associated with chemotaxis and angiogenesis. IFN-γ showed the highest fold change in normoxic/primed and hypoxic/primed EVs compared to their non-primed counterparts, however, this protein was excluded from the data interpretation, because EVs were originally primed with this protein. There was also a considerable elevation in the proteins CSF-1, MCP2, MCP4 and CCL3, which showed at least a 10-fold higher change in primed compared to non-primed conditions. IL13 was only present in primed EVs, and CCL4, Beta-NGF and TGF-α was also only present in primed EVs, in all but one primed EV sample.

Table 17: List of detected and differentially expressed proteins

Table displays the 52 proteins detected in the EV cargo. Changes in the protein expression levels from primed and non-primed EVs grown in normoxia (left) and hypoxia (right). 16 proteins were differentially expressed between normoxic/primed and normoxic conditions and 21 proteins were differentially expressed between hypoxic/primed and hypoxic conditions. All differentially expressed proteins are listed above the black line and show a statistically significant q-value of ≤0.05. Data is presented with normalized protein expression (NPX) difference, p-values and adjusted p-values (q-values) using a false discovery rate method of 5%, as described by Storey [366].

Differences in Normoxic/Primed vs Normoxic				Differences in Hypoxic/Primed vs Hypoxic			
Protein	Difference	P-value	Q-value	Protein	Difference	P-value	Q-value
CSF1	3.724	0.000107	0.004274	CSF1	3.405	0.000002	0.000059
TGF-α	2.606	0.000652	0.006865	MCP3	3.204	0.000044	0.000617
CCL11	2.667	0.000493	0.006865	MCP2	5.55	0.000055	0.000617
CCL3	6.252	0.000688	0.006865	MCP4	4.188	0.000177	0.001487
IL13	2.564	0.00198	0.015802	CXCL5	3.353	0.00027	0.001818
MCP4	3.429	0.003354	0.017247	IL13	1.345	0.000533	0.002714
CXCL10	-0.9942	0.003387	0.017247	IFN-γ	8.305	0.000565	0.002714
MCP2	3.584	0.003458	0.017247	OPG	0.6904	0.001101	0.004624
CXCL5	2.708	0.004359	0.019325	TNF	5.416	0.002989	0.010316
TSLP	3	0.005407	0.021576	CCL3	6.477	0.00307	0.010316
CCL20	1.519	0.006182	0.022425	TGF-α	1.886	0.004504	0.012247
CCL4	1.752	0.009573	0.031829	BetaNGF	0.7525	0.004892	0.012247
IFN-γ	6.091	0.011497	0.035286	CXCL6	-1.14	0.005103	0.012247
MCP3	2.286	0.0125	0.035624	LIF	1.777	0.004892	0.012247
MMP10	2.437	0.015947	0.04242	CCL11	3.417	0.005601	0.012545
IL6	2.219	0.017416	0.04343	TSLP	1.681	0.006741	0.013323
LIF	1.677	0.021895	0.051389	Flt3L	1.537	0.0065	0.013323
Flt3L	1.438	0.028145	0.062389	CXCL10	-1.131	0.007153	0.013352
CXCL11	-0.8993	0.03173	0.065699	TRAIL	2.136	0.007908	0.013985
BetaNGF	0.8273	0.032932	0.065699	IL18R1	0.976	0.01305	0.021924
CXCL9	1.247	0.036151	0.068688	VEGFA	2.809	0.029564	0.047303
MMP1	3.377	0.044704	0.081077	IL1alpha	2.628	0.034249	0.050034
CXCL6	-0.7683	0.050333	0.084833	CCL4	1.336	0.033623	0.050034
TWEAK	-0.7422	0.051027	0.084833	GDNF	1.304	0.037223	0.050513
CASP8	0.4793	0.053369	0.085177	TWEAK	-1.316	0.037584	0.050513
TRAIL	1.451	0.058343	0.089534	IL6	1.581	0.058581	0.073036
VEGFA	2.791	0.061716	0.09083	CXCL11	-1.055	0.05869	0.073036
GDNF	0.9092	0.06374	0.09083	CCL20	1.526	0.069599	0.083519
TNF	3.588	0.06908	0.095045	MMP10	1.78	0.072603	0.084119
IL15RA	0.3619	0.107369	0.142801	STAMBP	-0.7282	0.097776	0.10951
IL1alpha	1.695	0.133531	0.171867	CASP8	0.5535	0.104303	0.113051
LAPTGFbeta1	0.3821	0.163333	0.1862	PDL1	0.8359	0.110889	0.116433
X.4eBP1	-1.504	0.152411	0.1862	ADA	-0.6468	0.136724	0.13921
STAMBP	-0.8797	0.160673	0.1862	HGF	-0.8479	0.193725	0.188803
ADA	-0.8529	0.154359	0.1862	CD40	0.8398	0.19667	0.188803
CST5	-0.2322	0.191432	0.21217	IL12B	-0.1342	0.248483	0.231918
IL18R1	1.121	0.251311	0.271008	MCP1	0.2859	0.447556	0.406429
CDCP1	-1.424	0.324902	0.341147	NT3	0.3725	0.47904	0.423572
TNFRSF9	0.9176	0.339618	0.347456	CST5	-0.1125	0.542072	0.467016
MCP1	0.38	0.377593	0.367463	LAPTGFbeta1	0.2458	0.598704	0.467825
CXCL1	0.4019	0.37241	0.367463	uPA	-0.7977	0.583845	0.467825
FGF5	-0.4146	0.396812	0.376971	CXCL1	0.2282	0.59355	0.467825
OPG	0.4844	0.413418	0.383613	DNER	-0.1554	0.598536	0.467825
uPA	-0.6801	0.489101	0.43367	CDCP1	-0.2375	0.615583	0.470081
FGF21	-0.2142	0.487206	0.43367	CXCL9	0.2274	0.649328	0.484832
IL8	-0.1714	0.552321	0.479079	TNFRSF9	0.1689	0.670158	0.489507
HGF	-0.3511	0.684531	0.572024	IL15RA	0.1402	0.753955	0.538998
IL12B	0.0644	0.688149	0.572024	FGF21	-0.09915	0.794852	0.556396
DNER	0.08519	0.736095	0.599392	IL8	-0.055	0.871955	0.596878
CD40	0.3371	0.842773	0.672533	X.4eBP1	-0.2175	0.888211	0.596878
PDL1	-0.1568	0.885785	0.692997	FGF5	-0.000475	0.999141	0.645599
NT3	-0.04924	0.94044	0.721607	MMP1	-0.01121	0.996219	0.645599

Beta-nerve growth factor (Beta-NGF); C-C motif chemokine 3 (CCL3); C-C motif chemokine 4 (CCL4); C-C motif chemokine 20 (CCL20); C-X-C motif chemokine 5 (CXCL5); C-X-C motif chemokine 6 (CXCL6); C-X-C motif chemokine 10 (CXCL10); Eotaxin (CCL11); FMS related tyrosine kinase 3 ligand (Flt3L); Interferon gamma (IFN-γ); Interleukin 6 (IL6); Interleukin-13 (IL13); Interleukin 18 receptor 1 (IL18R1); Leukemia inhibitory factor (LIF); Macrophage colony stimulating factor 1 (CSF1); Matrix metalloproteinase 10 (MMP10); Monocyte chemotactic protein 2 (MCP2); Monocyte chemotactic protein 3 (MCP3); Monocyte chemotactic protein 4 (MCP4); Osteoprotegerin (OPG); Thymic stromal lymphopoietin (TSLP); TNF related apoptosis inducing ligand (TRAIL); Transforming growth factor alpha (TGF-α); Tumor necrosis factor alpha (TNF-α); Vascular endothelial growth factor A (VEGFA)

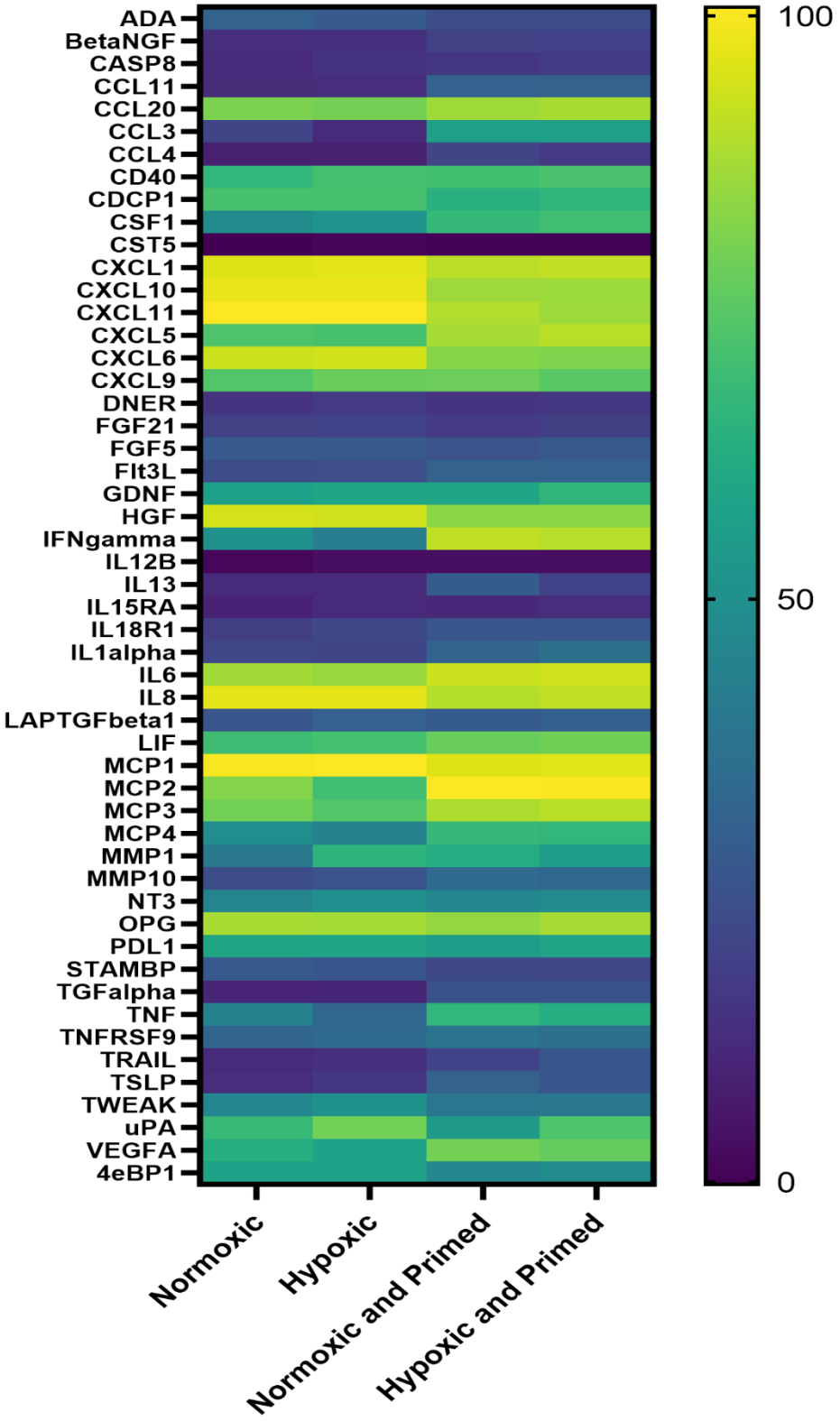

Figure 45: Hierarchical clustering and heatmap of the proteins in EVs

Heatmap displays the 52 detected proteins in the EV cargo (y-axis) and compares their expression in normoxic, hypoxic, normoxic/primed, and hypoxic/primed EVs (x-axis). NPX data was normalised to create a percentage and hierarchical clustering analysis was applied to the data set. The colour scale

bar on the right-hand side depicts the percentage expression of the protein, with '0' representing no expression of the protein to '100' representing the highest percentage expression of the protein. Proteins with a low expression are indicated in dark purple and proteins with a high expression are indicated in light yellow.

In total, there were 15 proteins with increased expression in the normoxic/primed EVs compared to the normoxic EVs **(Figure 46A)** and 19 proteins with increased expression in the hypoxic/primed EVs compared to the hypoxic EVs **(Figure 46B).** Of these differentially expressed proteins, there was an overlap of 12 proteins between both groups, shown in the Venn diagram in **Figure 47.** CXCL10 was the only protein that was decreased in response to priming in the normoxic EVs and it was also decreased alongside CXCL6 in response to priming in the hypoxic EVs.

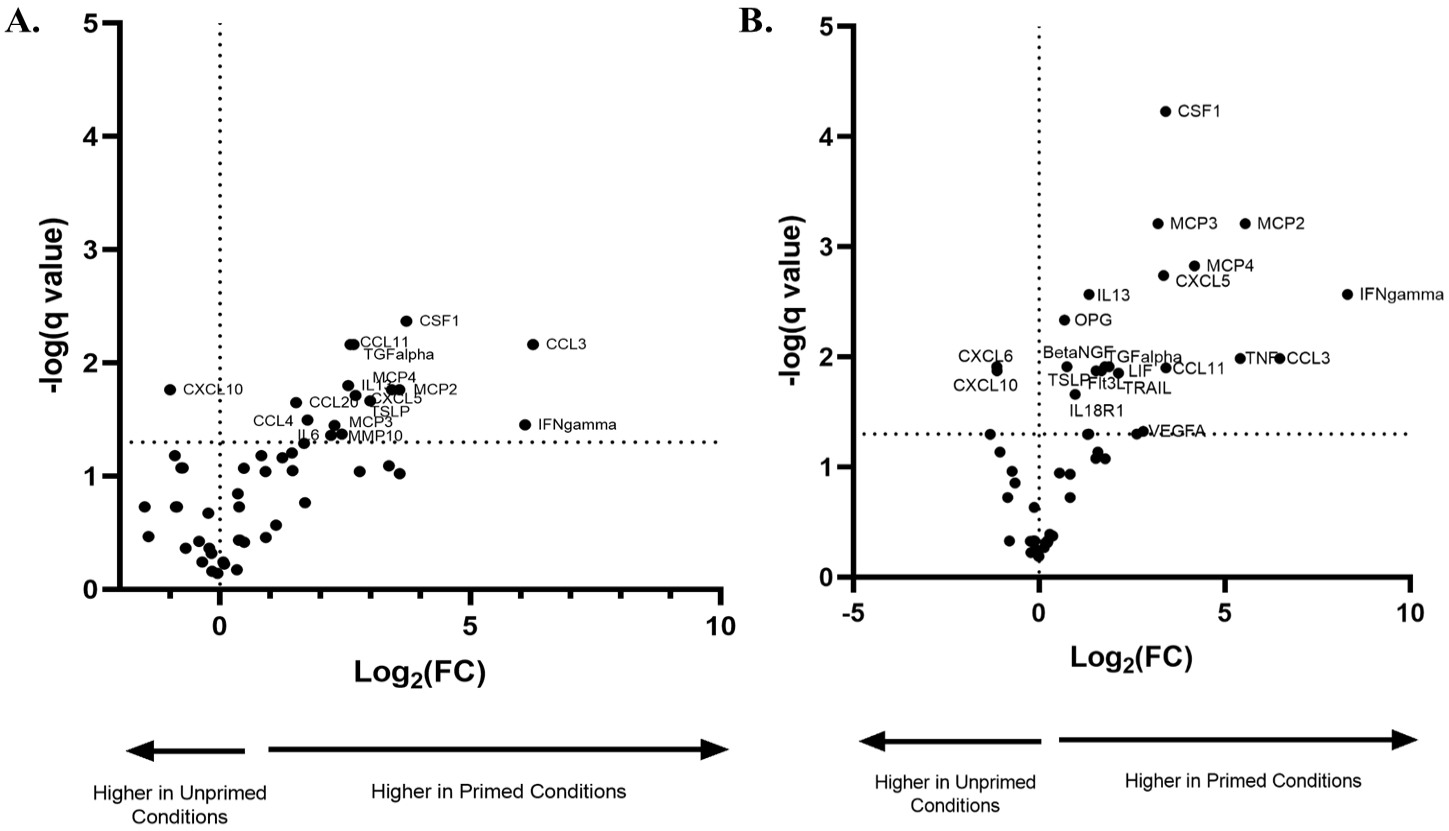

Figure 46: Volcano plot showing the differentially expressed proteins in primed and non-primed EVs

(A) *There was increased expression in 15 proteins from the normoxic/primed EVs compared to normoxic EVs and a decreased expression in 1 protein (CXCL10).* ***(B)*** *There was increased expression in 19 proteins from the hypoxic/primed EVs compared to hypoxic EVs and a decreased expression in 2 proteins (CXCL6, CXCL10). Values above the horizontal dotted line on the x-axis are statistically significant. Values to the left of the vertical dotted line on the y-axis have a decrease in NPX (Log_2(FC)); values to the right of this line have an increase in NPX (Log_2(FC)).*

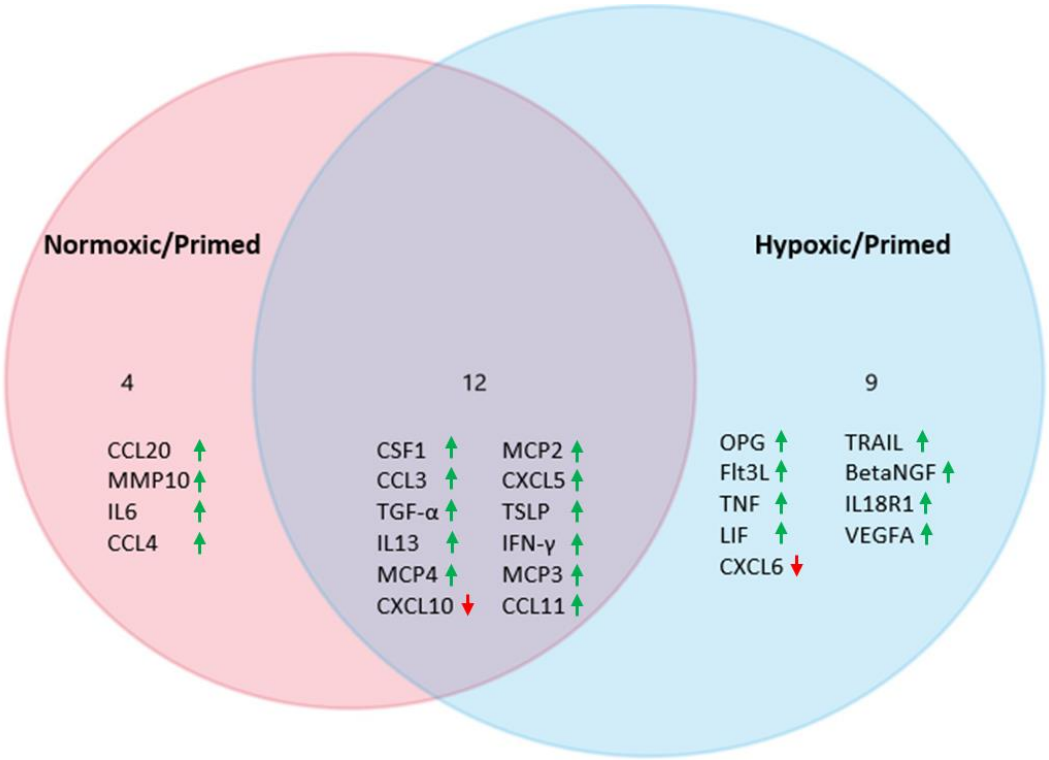

Figure 47: Venn diagram of differentially expressed proteins

There were 16 differentially expressed proteins in the normoxic/primed EVs compared to the normoxic EVs. There were 21 differentially expressed proteins in the hypoxic/primed EVs compared to the hypoxic EVs. The upregulated proteins in the primed EVs are shown by the green arrows. CXCL10 was downregulated in both primed EVs compared to non-primed EVs, and CXCL6 was downregulated in hypoxic/primed EVs compared to hypoxic EVs, shown by the red arrows. 12 differentially expressed proteins were common amongst both groups, seen by the overall in pink and blue circles.

As the differentially expressed proteins are associated with a wide range of immune responses, **Table 18** details some of their functions towards specific immune cells.

Table 18: List of proteins that were differentially expressed in UCMSC-EVs.

Table details the, the protein, the condition that they were differentially expressed in, and some of their roles in the immune system

Protein	Condition	Functions
CCL3	Upregulated in Normoxic/Primed and Hypoxic/Primed EVs	Promotes the infiltration of macrophages into the RA synovium [367].
CCL4	Upregulated in Normoxic/Primed EVs compared to Normoxic EVs	Chemoattractant for regulatory T-cells [368].
CCL11	Upregulated in Normoxic/Primed and Hypoxic/Primed EVs	Chemoattractant for eosinophils [369].
CCL20	Upregulated in Normoxic EVs compared to Normoxic/Primed EVs	Promote dendritic cell migration [369]. Recruits Th17 cells to site of injury [370]
CSF1	Upregulated in Normoxic/Primed and Hypoxic/Primed EVs	Regulates macrophage development [371]. Increases osteoclast like cells in bone marrow [372].
CXCL5	Upregulated in Normoxic/Primed and Hypoxic/Primed EVs	Aids neutrophil trafficking and homeostasis. Regulates IL17/G-CSF levels in the gut [369,373].
CXCL6	Downregulated in Hypoxic/Primed EVs compared to Hypoxic EVs	Chemoattractant for neutrophils [369].
CXCL10	Downregulated in Normoxic/Primed and Hypoxic/Primed EVs	Recruits activated T-cells to sites of inflammation [374]. Elevated levels in RA [375]. Inhibitor of angiogenesis [376].
Flt3L	Upregulated in Hypoxic/Primed EVs compared to Hypoxic EVs	Involved in the mobilization and differentiation of hematopoietic stem cells and in the development of dendritic cells [377,378].
IL6	Upregulated in Normoxic/Primed EVs compared to Normoxic EVs	Supports the production of antibodies by B-cells, activates T-cells, supports Th2 and Treg differentiation [379].
IL13	Upregulated in Normoxic/Primed and Hypoxic/Primed EVs	Mediator of allergic inflammation [380]. Inhibits IL-6 production by LPS-primed in human peripheral blood monocytes [381].
IL18R1	Upregulated in Hypoxic/Primed EVs compared to Hypoxic EVs	IL-18 is a pleiotropic pro-inflammatory cytokine. Enhances IFN-γ production from Th1 cells, stimulates NK cells, and Th1 cells, to produce IL-3, IL-9, and IL-13. In the presence of IL-3, IL-18 stimulates the release of IL-4 from basophils and mast cells [382].
LIF	Upregulated in Hypoxic/Primed EVs compared to Hypoxic EVs	Upregulates eosinophil migration, promotes mesenchymal cell proliferation [383]. Aids the production of regulatory T-cells [384]. Increases angiogenic potential of BMMSCs [385].
MCP2	Upregulated in Normoxic/Primed and Hypoxic/Primed EVs	Simulates basophils and eosinophils [386]. Inhibits HIV entry in CD4+ cells [387].
MCP3	Upregulated in Normoxic/Primed and Hypoxic/Primed EVs	Activates many immune cells such as lymphocytes, macrophages, dendritic cells, NK cells, eosinophils, basophils, and neutrophils [386].

MCP4	Upregulated in Normoxic/Primed and Hypoxic/Primed EVs	Chemoattractant for immune cells (eosinophils, basophils, monocytes, immature dendritic cells, T-cells) towards inflamed tissue [388].
MMP10	Upregulated in Normoxic/Primed EVs compared to Normoxic EVs	Polarises M1 macrophages into M2 macrophages [389]. Reduces pro-inflammatory response of macrophages [390].
OPG	Upregulated in Hypoxic/Primed EVs compared to Hypoxic EVs	Inhibits osteoclastogenesis. Regulates the interactions between T-cells and dendritic cells [391].
TGF-α	Upregulated in Normoxic/Primed and Hypoxic/Primed EVs	Promotes cell differentiation migration, stimulates gastrointestinal repair [392].
TRAIL	Upregulated in Hypoxic/Primed EVs compared to Hypoxic EVs	Induces apoptosis in malignant cells. Maintains immune tolerance by inducing the apoptosis of dendritic cells, preventing T-cell proliferation and promoting Treg cells [393].
TSLP	Upregulated in Normoxic/Primed and Hypoxic/Primed EVs	Maintains CD4+ T-cell homeostasis, promotes positive Treg selection in the thymus. In an inflammatory setting, TSLP stimulates dendritic cell maturation and promotes CD4+ T-cells to produce Th2 inflammatory cytokines [394].
VEGFA	Upregulated in Hypoxic/Primed EVs compared to Hypoxic EVs	Stimulates the migration of mesenchymal progenitor cells to promote vasculogenesis and osteogenesis [395]. Increases the survival of synovial fibroblasts in RA and protect against apoptosis death of synovial fibroblasts [396,397]
βNGF	Upregulated in Hypoxic/Primed EVs compared to Hypoxic EVs	Both pro- and anti-inflammatory functions. Promotes the survival of hematopoietic stem cells and immune cells (eosinophils, neutrophils, mast cells, B-cells, monocytes). Promotes proliferation of lymphocytes and B-cell differentiation. Reduces levels of pro-inflammatory cytokines. Promotes IL-10 [398].

*This table identified some of the roles of these proteins in the immune system. The author recognises that many other roles and functions exist for these proteins.

5.2.3 Proteins identified in all EV conditions

Analysis of the EV protein cargo identified some noteworthy proteins that have anti-inflammatory properties. These include TGF-β1, FGF5, FGF21, PDL1, HGF and STAMBP; which were detected in all EV conditions but were not differentially expressed between conditions **(Figure 48)**.

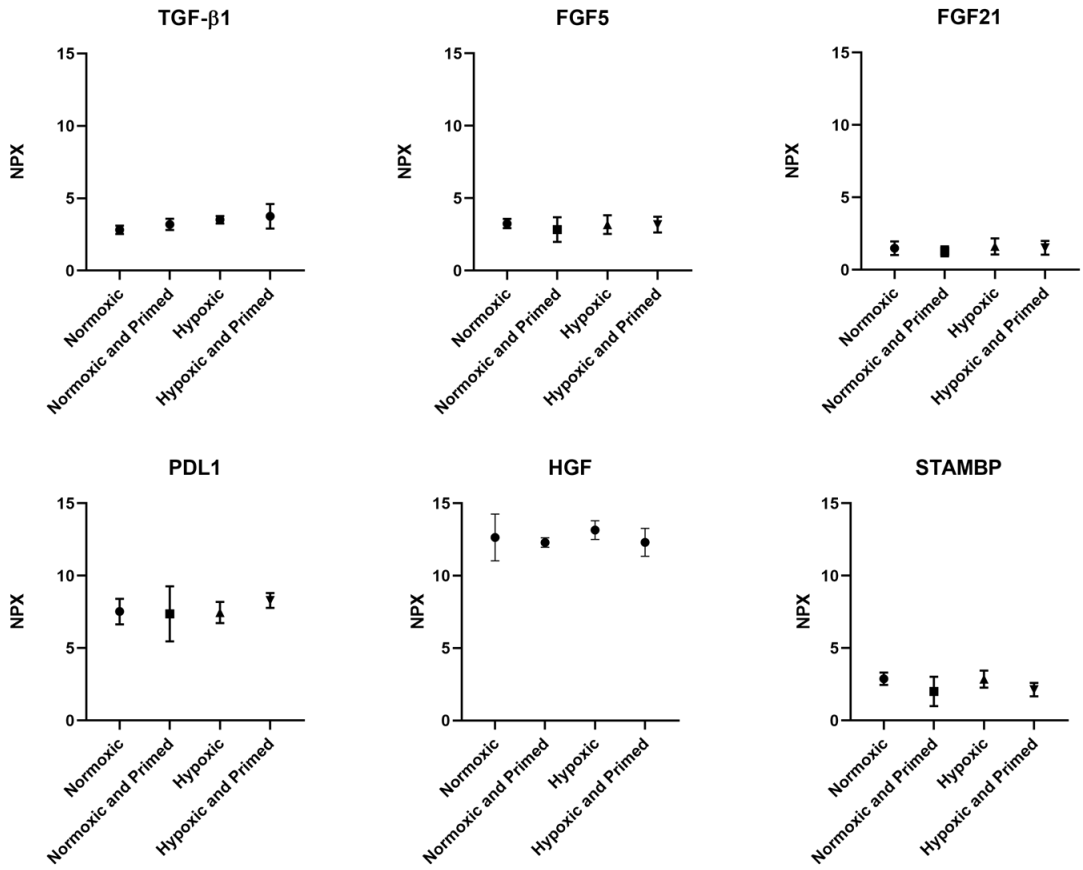

Figure 48: Anti-inflammatory proteins identified in EVs

The PEA assay probed for some proteins with an anti-inflammatory potential. TGF-β1, FGF5, FGF21, PDL1, HGF and STAMBP were identified in all EVs but were not differentially expressed between conditions. NPX values are presented on a Log_2 scale on the y-axis. The EV conditions are on the x-axis.

Similarly, proteins with pro-inflammatory properties, such as IL-8, MCP1, CXCL11, CXCL9, IL-1a, CXCL1, MMP1, CD40, were also found in all EVs but not differentially expressed between conditions (**Figure 49).**

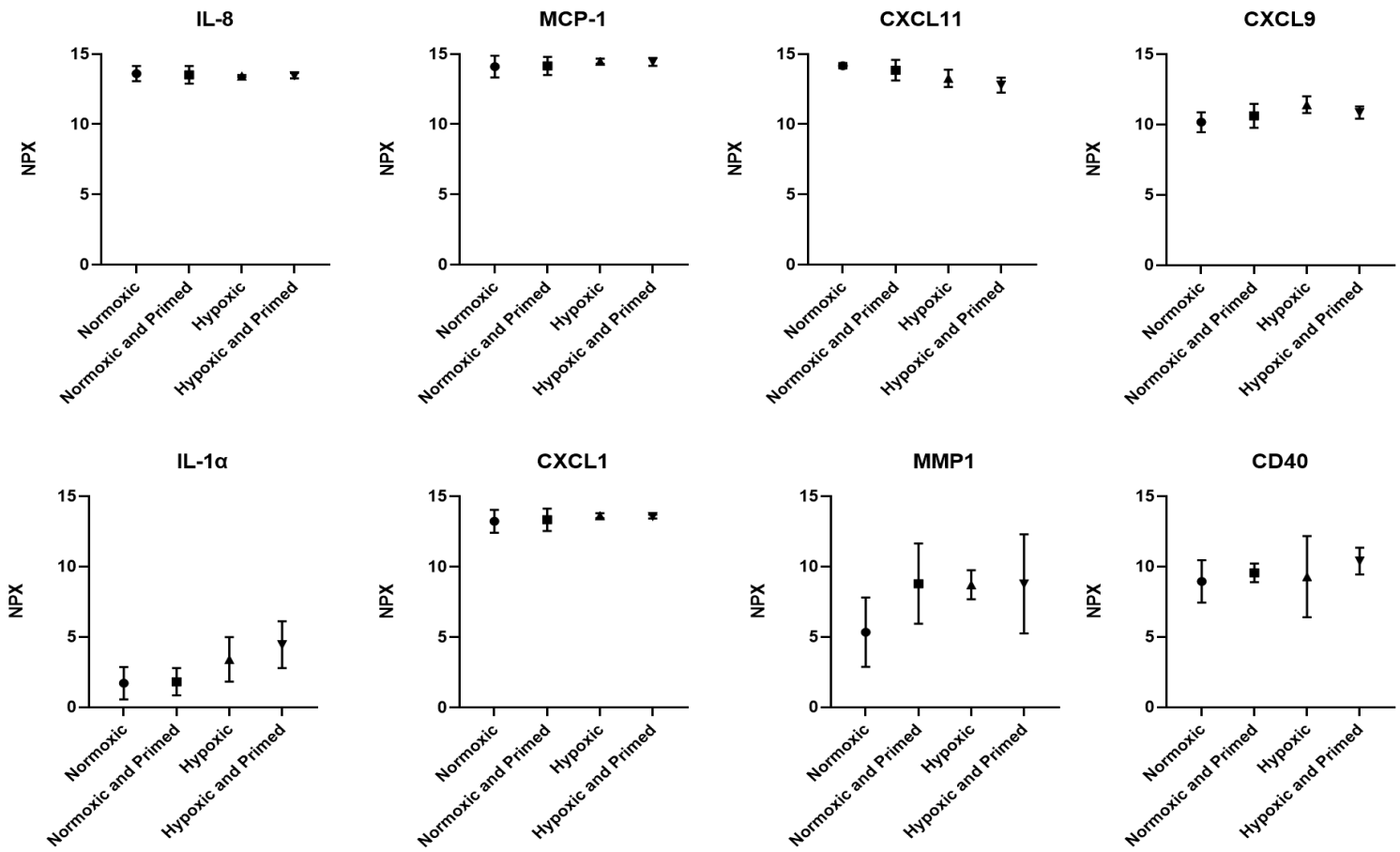

Figure 49: Pro-inflammatory proteins identified in EVs

The PEA assay identified the presence of IL-8, MCP-1, CXCL11, CXCL9, IL-1α, CXCL1, MMP1, and CD40 in all EV conditions. All proteins have a pro-inflammatory potential but were not differentially expressed between conditions. NPX values are presented on a Log_2 scale on the y-axis. The EV conditions are on the x-axis.

5.3 Discussion

This study aimed to compare the protein cargos of UCMSC-EVs from four different conditions to see if the hypoxic or pro-inflammatory priming of UCMSC is making their EVs more anti-inflammatory. The anti-inflammatory potential of the EVs was decided based upon the number of anti-inflammatory proteins that were increased and the number of pro-inflammatory proteins that were decreased.

The EV samples in this experiment passed all quality controls meaning that the data is valid and reliable. The cumulative NPX value was higher in the primed EVs compared to non-primed EVs which suggests that they contain a higher abundance of the 92 proteins probed for in the assay **(Figure 44).** A probable explanation for this is that the pro-inflammatory priming of UCMSCs triggered the selective packaging of immunomodulatory proteins into the EVs. Findings by Harting et al. [399] show differences in protein composition of BMMSC-EVs from TNF-α and IFN-γ primed conditions compared to naïve EVs. The primed EVs in this case showed an increase in expression of ICAM 1, CXCL12, and CCL5 and a decrease in IL-5, IL-6, IL-10, and IL-13, identified using a protein array [399]. Although these specific proteins do not match exactly with the results of the current study, it shows that the pro-inflammatory priming of MSCs is leading to the selective packaging of specific proteins.

The aim of this chapter was to compare the protein cargo of UCMSC-EVs from four different conditions. As there were many proteins differentially expressed in this study, with a range of different functions *in vivo,* only those with relevance to immune modulation or rheumatoid arthritis will be discussed.

Evidence from the PEA assay shows that the primed EVs contained an increase in proteins associated with chemotaxis (CCL3, CCL11, CCL20, MCP-2, MCP3, MCP-4), a pro-inflammatory response (IL-6, CSF-1, IL-18R1) and an anti-inflammatory response (IL-13, MMP10, LIF, TRAIL) compared to the non-primed EVs. MSCs are a heterogeneous group of cells, and they express both pro-inflammatory and anti-inflammatory proteins when primed [243,359]. Therefore, it was not unusual to see EVs from primed UCMSCs displaying both pro- and anti-inflammatory proteins. The increased production of IFN-γ in primed EVs is not surprising as the cells were primed with this pro-inflammatory cytokine and studies have shown that IFN-γ can become bound to interferon gamma receptor 1 on the membrane of EVs [400]. Therefore, IFN-γ was excluded from the discussion of EV protein cargo. This issue could have potentially could have been avoided by adding fluorescently tagged pro-inflammatory cytokines to the media so that they could be imaged to study their association with EVs.

The main finding in this chapter was that the primed EVs contained an increased expression of chemotactic proteins in their cargo. It is well described in the literature that MSCs contain many different chemokines that are responsible for MSC homing to the site of damage [401–404]. Specifically, research that has characterised the conditioned media of UCMSCs has found the presences of many (~40) chemokines [405]. They divided the chemokines up into homeostatic chemokines which are responsible for migration such as CCL20 which was upregulated in normoxic/primed EVs, and inflammatory chemokines which are created in pathological conditions and aid attracting immune cells to the affected site [405]. These include CCL3 and CCL11 which are upregulated in the primed EVs in this chapter. The normoxic/primed and hypoxic/primed EVs also had an increased amount of MCP-2, MCP-3, and MCP-4 which play a role in the homing of MSCs to sites of injury [406]. So, while MSCs promote the attraction of immune cells to sites of injury, the release of these chemokines also

facilitates the mobilisation of MSCs to these sites where they can modulate the immune environment. This may mean that the priming of MSCs is 'activating' them to induce a stronger signalling response seen through the upregulation of these proteins in the UCMSC-EVs. This also suggests that the primed MSCs have a greater motility compared to the normoxic or hypoxic UCMSCs.

However, it is recognised that the presence of some of these chemokines in the primed EV cargo have negative implications in RA, specifically, CCL3. CCL3 is found in the synovia and sera of RA patients and it stimulates T-cell, monocyte and NK cell activity [407]. It is also associated with the early onset of RA symptoms, shown by the early increase of CCL3 and neutrophils in a study of rats with AIA [408]. Research shows that MSCs secrete high levels of the CCR5 (C-C chemokine receptor type 5) and its chemokine ligand CCL3 which have been found to attract the homing of monocytes and macrophages to the site of injury [409] and support tumour growth [410]. Therefore, is unsurprising to see the elevated expression of this protein in their EVs. Furthermore, it is known to be augmented by the pro-inflammatory cytokines TNF-α and IL-1 [407]. However, due to the involvement of CCL3 with immune cells, the presence of this chemokine in UCMSC-EVs is slightly concerning for their potential use as a treatment for RA [407]. This is because many chemokine receptors such as CCR5 are abundantly expressed in the synovium in RA which can bind to CCL3 and stimulate an immune response. Indeed, this is why many drugs for RA target these chemokines. For example, Infliximab, an anti-TNF drug, reduces the expression of CCR3 and CCR5 on T-cells in RA [407], which may prevent an immune response associated with CCL3. This may mean that the EVs, which contain some anti-inflammatory proteins, would be most effective when used in combination with combination with DMARDs or anti-TNF drugs, to reduce the possible influence of chemotactic proteins attracting immune cells into the RA joint.

Other proteins, namely CXCL5, MCP4 and CSF-1, were consistently higher in primed conditions compared to non-primed conditions. CXCL5, also known as epithelial-neutrophil activating protein 78, is abundantly present in the sera and synovial fluid of patients with RA [407] and plays a role in attracting and activating neutrophils [411]. MCP-4 was also increased in EVs upon pro-inflammatory priming. This protein is highly expressed in the cartilage of patients with RA compared to healthy subjects and patients with OA. MCP-4 release from chondrocytes is known to be stimulated by IFN-γ, TNF-α and IL-1β, the same cytokine cocktail was used in the present study. MCP-4 promotes synovial hyperplasia in RA joints thus contributing to disease progression [412]. CSF-1 supports the survival and differentiation of monocytes and macrophages [413] and also increases inflammation by mobilizing myeloid cells into the blood [414,415].

When the data is considered as a whole, the presence of chemokines is positive for the migration of MSCs to the site of damage. However, if EVs are to be used as an alternative to MSCs, then the isolated expression of these chemokines in EVs alone may not trigger the same immunomodulatory effects as there will be no MSCs to mobilise, instead they may function to simply attract immune cells into the joint. However, this does not mean that the primed EVs are pro-inflammatory agents because they had an increase in anti-inflammatory proteins in their cargo, namely, leukaemia inhibitory factor (LIF), TRAIL, MMP10 and IL-13. The first two were increased in hypoxic/primed EVs, MMP10 in normoxic/primed EVs and IL-13 in both normoxic/primed and hypoxic/primed. All these proteins have anti-inflammatory potential.

LIF from MSCs plays a role in the modulation of T-cells [384]. Studies have shown that LIF from BMMSCs can suppress T-helper 17 cells in an experimental autoimmune encephalomyelitis mouse model [416] and promote Treg proliferation in an MSC mixed

lymphocyte co-culture [384]. The identification of LIF in UCMSC-EVs may also cause similar immunosuppressive effects, as studies have shown that WJMSCs express a higher level of LIF in comparison to BMMSCs and ATMSCs [417], and LIF expressed in WJMSCs is a more potent suppressor of T-cell proliferation *in vitro* compared to BMMSCs [418]. TRAIL was also increased in hypoxic/primed EVs. Evidence shows TRAIL can reduce self-antigens in RA by triggering the apoptosis of activated T-cells and synoviocytes [419]. Further evidence of its anti-inflammatory effect was seen in a mouse model of RA, where TRAIL reduced the expression of pro-inflammatory cytokines (TNF-α, IL-1β, IFN-γ, IL-6, IL-17) and macrophages [420]. It also shifted the Th17: Treg balance by reducing Th17 cells and increasing Tregs [420]. With regards to MMP10, research has found that MMP10 can polarise pro-inflammatory M1 macrophages into M2 macrophages in a murine model of acute infection [421]. As macrophages are highly activated in RA and release many pro-inflammatory cytokines that contribute to synovial inflammation [422], then the polarising of M1 macrophages towards a M2 phenotype is positive for disease amelioration. Lastly, IL-13 inhibits activated macrophages from secreting pro-inflammatory cytokines and research transfecting RA synovial tissue with IL-13 using gene therapy has identified it as a therapeutic candidate for immunosuppression in RA [423].

Other anti-inflammatory proteins, PD-L1 [424], HGF [425,426], FGF21 [427], were expressed in EVs, but their level did not vary between samples. Additionally, IL4 and IL10 were not detected. It could be possible that UCMSCs in this study also secreted more anti-inflammatory proteins in the form of soluble factors that were just not being packaged into EVs.

There were two outliers from the general trend of chemotactic proteins in the primed EV cargo, this included a higher expression of CXCL10 in normoxic and hypoxic EVs, and a higher

expression of CXCL6 in hypoxic EVs. Both CXCL10 and CXCL6 has chemotactic properties associated with MSCs [428], although similar to the chemotactic proteins in primed EVs, CXC10 and CXCL6 are also implicated in RA. CXCL10 binds with CXCR3 and can stimulate Th0-Th1 type inflammation in RA [407], therefore the lower production of it in the primed EVs reduces the likelihood of Th0-Th1 type inflammation in RA. Additionally, CXCL10 plays a role in CD4+ T-cell activation and NK cell migration [429]. The reason it showed a higher expression in the EVs that were not primed with an inflammatory stimulus is unknown, as this finding deviates from the expression of other chemotactic proteins identified in this study. However, the functional activity of CXCL10 is not completely pro-inflammatory. CXCL10 has been shown to attract Tregs in pancreatic cancer model [430] and a mouse model of vitiligo, an autoimmune condition of the skin [431]. As CXCL10 has chemoattractant properties towards NK cells and CD4+ T-cells, but also supports Treg activity, it is unclear which functions will prevail in RA. CXCL6, another outlier, was also increased in hypoxic EVs. It plays a role as a chemoattractant for neutrophils [369], so its lower expression in primed EVs may be reduce the likelihood of triggering an immune response.

The hypoxic/primed EVs displayed a more angiogenic profile identified through the expression of the pro-angiogenic protein VEGF-A [432–434], which was expressed in all conditions but increased in hypoxic/primed EV samples. It is interesting that the hypoxic EVs did not have a higher expression of VEGF compared to the normoxic EVs. Research shows that hypoxic MSC-EVs have a greater angiogenic potency compared to normoxic MSC-EVs [326]. This would suggest that hypoxic MSC-EVs would contain more pro-angiogenic proteins such as VEGF-α or Fibroblast Growth Factor (FGF-5, FGF-21) [168,435,436], but these proteins were not differentially expressed between hypoxic and normoxic EVs in this chapter. However, when considering the increased expression of VEGF in hypoxic/primed EVs compared to

hypoxic EVs, it may be worthwhile applying these EVs to a different disease model. The upregulation of VEGF-A is a well-documented hypoxic-induced response [437] and may be beneficial in treating ischaemic heart conditions or in wound healing [437]. The UCMSC-EVs in this chapter contain some valuable proteins that can ameliorate diseases, but whether an RA model is the right match for this cohort of EV proteins remains to be answered.

There were no statistical differences between normoxic and hypoxic EVs from the panel of probed proteins. This is surprising given that studies have shown that UCMSCs grown in hypoxia, have a higher angiogenic potential in the treatment of mouse hindlimb ischaemia [240,438] and rat spinal cord injury in comparison to UCMSCs grown in normoxia [239]. In general, hypoxia is advocated in the literature when growing MSCs in culture as it more closely mimics the oxygen levels that MSCs are exposed to *in vivo* [360]. Therefore, it could be hypothesised that growing UCMSCs in hypoxia would show some differences compared to normoxia. However, the lack of differences between normoxic and hypoxic UCMSC-EVs in this study are in line with other experiments carried out on the growth kinetics **(Chapter 3)**, size, morphology, and surface marker production **(Chapter 4)** in this cohort of UCMSCs and their EVs, which also found no statistical differences between normoxia and hypoxia. This lack of change may be due to the cells were first isolated under normal oxygen (21%) conditions, and then exposed to low oxygen (5%). Exposure to low oxygen from the start may be an influencing factor in UCMSC hypoxic-related characteristics. Additionally, there may be hypoxic related changes in the EVs that were not detected in this array; an array covering a broader repertoire of proteins might have identified more hypoxic-mediated changes.

There are limitations in this study, which should be considered when interpreting the data. Firstly, this study would have benefitted from analysing conditioned media samples from the

four conditions prior EV isolation. The addition of conditioned media samples to the PEA assay that have been normalised by protein concentration would have provided informative data on whether the proteins identified from the PEA assay originated from the EV cargo or had bound to the outside of EVs. The possibility of the proteins being extravesicular is low considering the established EV isolation method and extensive washing steps that were employed. Nevertheless, the possibility that some proteins may have co-isolated to the outside of EVs needs to be recognised and, in hindsight, the results would have been more robust on the addition of some conditioned media samples to act as a control. Secondly, this study had a sample size of four, and a larger sample size may have identified further differences between the conditions. Furthermore, the PEA assay only analysed proteins associated with inflammation and a wider repertoire of proteins would help develop a greater understanding of how different culture conditions alter EV cargo. For example, a study found that the priming MSCs with IFN-γ caused the differential expression of 210 cellular proteins [439]. Therefore, it is also likely that other potential anti-inflammatory proteins exist in EV cargo but were not included in the assay panel. Lastly further research is needed to optimise the priming of UCMSCs with pro-inflammatory cytokines. Studies using a stem cell neuronal model have shown that the expression of cytokines by cells primed with TNF-α, IL-6, and IL-1β is induced in a time and concentration dependent manner [440]. This may apply to some proteins within the EV cargo whereby a longer exposure time and different concentrations of a pro-inflammatory stimulus may lead to an increased packing of specific proteins into EVs. Therefore, further optimization of pro-inflammatory condition is another area to explore to understand the full influence of pro-inflammatory factors on EV protein expression.

Future work on the protein profile of EVs can take two approaches; the first approach would be to widen the search for proteins in EVs. It is recognised that the PEA assay employs a

targeted protein detection approach, and some proteins with immunomodulatory properties will not feature in the 92-panel assay. This adds bias to the data and hinders the discovery of new proteins. In comparison, mass spectrometry has an untargeted approach and enables the discovery of new proteins [441]. The second option is to adopt the opposite approach and focus specific proteins as a way to narrow down which differentially expressed proteins can generate a biologically therapeutic response. Cytokines possess a high affinity with their receptor target which means that only picomolar concentration are required to elicit a biologically significant response [442]. So, for the cytokines in the PEA assay that show a small increase in relative expression, this may be enough to trigger a pro- or anti-inflammatory response and is worth exploring.

The larger goal of therapeutic EV research is to identify the proteins, or a combination of proteins, that induce a therapeutic change and then try and recreate this therapeutic response in a more simplified way to treat diseases. One way to do this would be to focus research genetically manipulating the parent cells in order to change the EV cargo, so that specific anti-inflammatory proteins are packaged into EVs. Many studies have reprogrammed MSCs to secrete EVs with the desired EV cargo. For example, one study reprogrammed MSCs to overexpress GATA-4 which resulted in improved cardiac function in a model of rat cardiac injury [443]. Other researchers have manipulated dental pulp MSCs to overexpress HIF-1α, and the resulting HIF-1α positive EVs were effective at increasing angiogenic activity cardiac function in a mouse ischaemia model [444].

This study is essentially trying the manipulate the MSC secretome by mimicking environments that are normally experienced by MSCs *in vivo* such as hypoxia and inflammation. This approach is employed to promote the natural ability of MSCs to function as immune regulators.

However, the direct reprograming of MSCs and their EVs is a more targeted approach and perhaps may be more beneficial in controlling the MSC-EV functions. At present it is difficult to predict the immunomodulatory functions of MSCs for two reasons. First the MSCs contain both pro- and anti-inflammatory proteins therefore it is currently unknown which proteins will have a larger effect *in vivo.* Secondly, most research into MSCs, including this study, presents evidence of the heterogeneity of MSCs. This is a problem for clinical therapeutics as the product will need to be continually characterised from each donor. An immortalised MSCs line which overexpresses a specific EV profile many be more beneficial to achieve consistent results. Alternatively, if therapeutic factors in UCMSC-EVs, could be precisely identified then they could be recreated synthetically to establish batch-to-batch consistency.

5.4 Conclusion

This chapter looked at the basic characterisation of UCMSC-EV protein cargo from normoxic, hypoxic and pro-inflammatory environments. Research characterising EVs from UCMSCs grown in four different culture conditions represents the first of its kind. It aimed to identify how culture conditions could affect UCMSC-EV protein cargo. It is important to firstly explore the composition of EV cargo as a starting point towards understanding MSC-EV mediated immunosuppression.

The PEA assay did not show any differences in the expression of inflammatory proteins between the normoxic and hypoxic conditions. The main changes in EV protein cargo occurred between primed and non-primed EVs, which found an increase in proteins associated with chemotaxis in the primed EVs.

MSCs release chemotactic proteins as part of their paracrine signalling and research shows that this is enhanced when the MSCs are primed with pro-inflammatory cytokines. These chemotactic properties are widely beneficial in most studies for immunosuppression as it promotes MSC migration to the site of the disease where they can release their anti-inflammatory factors. But when considering the transplantation of EVs as an alternative product to MSCs, the presence of chemotactic proteins is unlikely to attract MSCs as they may be out of range of the signalling, but it may bolster a localised immune response, as many of the increased chemotactic proteins are also implicated in RA pathogenesis. This could be balanced by the presence of anti-inflammatory proteins in EVs, and these were present, namely a higher expression of MMP10, TRAIL and LIF. But whether these alone are sufficient to dampen an immune response in RA is unknown and functional studies are therefore needed to analyse their true effects in an activated immune environment.

In all, there are chemotactic proteins in the primed UCMSC-EVs cargo which are known to promote UCMSC migration, but it must also be considered that these chemotactic proteins may also promote immune cell activity. This study only looked at component of the EV cargo and further studies of the EVs miRNAome is needed to discover how they may have immunomodulatory functions. This information on EV protein cargo is a step towards understanding the biological characteristics of UCMSC-EVs.

Chapter 6: MicroRNA profile of human UCMSC-EVs

6.1 Introduction

Research shows that MSC-EVs contain anti-inflammatory miRNAs in their cargo that are capable of immune modulation [362,445–447]. **Chapter 5** explored the protein profile of UCMSC-EVs, this chapter now looks at their miRNA profile with an aim to uncover anti-inflammatory miRNAs responsible for EV mediated immune modulation.

MicroRNAs (miRNAs) are small noncoding RNA molecules measuring approximately 19-24 nucleotides in length that can control gene expression by cleaving mRNA which inhibits the translation of proteins [448,449]. Studies have shown that miRNAs can be selectively loaded into EVs within the cell and when the EV is released from the cell, the EV-miRNA can be transferred to recipient cells to carry out mRNA silencing [446,448,450]. The sorting of miRNAs into EVs in the cytoplasm has been investigated and it has been found that this process relies on specific binding motifs on the miRNA and the presence of specific proteins, such as Argonaute 2 (Ago2) and Alix [448]. Ago2 is regarded as a protein involved in miRNA sorting into EVs due to its facilitation in binding of miRNAs to the RNA-induced Silencing Complex (RISC). This complex can then be incorporated into multivesicular bodies, and subsequently EVs, highlighting the crucial role of Ago2 in miRNA sorting into EVs [450]. Alix, a protein involved in the biogenesis of EVs via the endosomal sorting complex required for transport (ESCRT), was also found to be associated with miRNA sorting in EVs. This was shown by the reduced number of miRNAs in EVs after Alix knockdown [142]. EVs containing the packaged miRNAs are released into the extracellular matrix and can enter recipient cells via endocytosis or direct fusion [448]. The route of entry into the cell depends on surface receptors on the EVs, such as tetraspanins, integrins and proteoglycans, all of which aid with binding of EVs with the plasma membrane of the target cell [133,451]. Once inside the cell, the miRNA can carry out gene silencing.

The functional transfer of miRNA from EVs has been shown in many studies. For example, Song et al. [361] showed that MSC-EVs were selectively packaged with miR-146a and this was transferred to macrophages upon co-culture, which resulted in M2 polarisation. This shows the functional transfer of miRNAs in EVs [361]. In all, miRNAs are estimated to control 30-80% of protein translation by targeting specific genes [452], which makes them important in gene regulation. Therefore, the study of the UCMSC-EV cargo to identify miRNAs capable of immune suppression was an aim of this chapter.

This chapter looks at the miRNAs in UCMSCs and their EVs, identified through Next Generation Sequencing (NGS) and validated using RT-qPCR. This chapter focuses on the miRNAs that are differentially expressed between normoxic, hypoxic, and pro-inflammatory primed EVs to see if these culture conditions make the miRNAome more anti-inflammatory. One caveat to the identification of miRNAs in EVs is the potential presence of FBS associated RNAs in the EV suspension. To control for the possibility of bovine EVs, one FBS-EV sample was sequenced, and three FBS-EV samples analysed via PCR to identify if they contained any highly expressed miRNAs that may lead to false positives for the target miRNAs. Additionally, EV samples underwent a proteinase and RNAase digestion to remove any extra-vesicular RNAs **(Section 2.9.2).** RNA contained within the EVs is protected from this treatment due to the presence of the EV's phospholipid bilayer.

Aim

The **aim** of this chapter is to identify the miRNA profile of UCMSCs and UCMSC EVs.

Objectives

1. Identify differences in miRNA expression of normoxic cells and their EVs through RNA sequencing.
2. Identify differences in miRNA expression between EVs from normoxic, hypoxic and normoxic/primed conditions through RNA sequencing.
3. Validate the RNA sequencing results through RT-qPCR.

6.2 Results

6.2.1 Preparation for RNA sequencing

6.2.1.1 Effective depletion of non-vesicular RNA

To reduce the possibility of extra-vesicular RNA being sequenced, and have greater certainty that the analysed RNA originated from the EV cargo, all EV samples were incubated with proteinase K and RNAase A prior to RNA extraction to digest any free floating or membrane bound RNAs [202,227] **(Section 2.9.2).** To test if the proteinase K/RNAase A treatment was reducing extra-vesicular RNA, an EV sample was analysed on the Agilent Bioanalyser before and after treatment. A comparison of the electropherograms showed that there was a decrease in the amount of RNA present in the EV-treated sample compared to the untreated sample indicating that the proteinase K/RNase A treatment was successful in digesting some extra-vesicular RNAs **(Figure 50).** The concentration of RNA from the EV-treated sample was 0.069 ng/µl compared to 0.562 ng/µl in the untreated sample. This equates to an 87.7% decrease of RNA, which indicated the removal of some non-vesicular RNA.

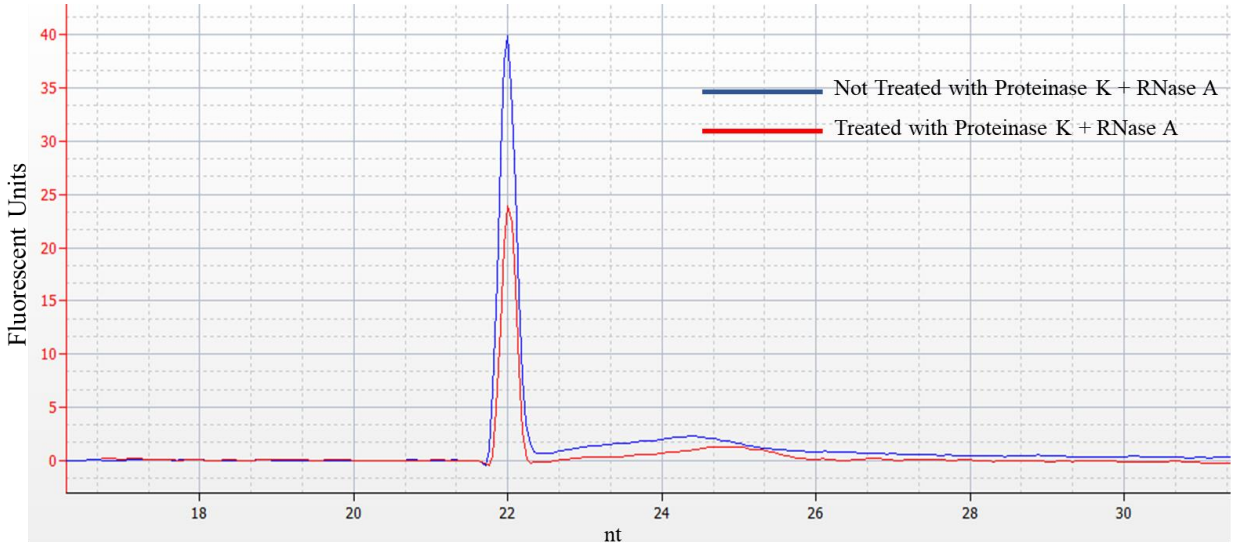

Figure 50: Comparison of EV before and after Proteinase K/RNase A treatment

Isolated EV suspensions were treated with Proteinase K and RNase A to remove any extra-vesicular RNA that may provide false reading of the EV RNA cargo. The same EV sample (n=1) was treated with

or without Proteinase K and RNase A and analysed on the Agilent Bioanalyzer using the RNA Pico chip. This generated an electrophoretic graph with Fluorescent Units (FU) on the y-axis and nucleotide length (nt) on the x-axis. Results show that the RNA concertation was 0.562ng/µl for the untreated sample (blue line) and 0.069ng/µl for the proteinase K/RNase A treated EV sample (red line).

6.2.1.2 Assessment of RNA quality and quantity

RNA was extracted from four donors UCMSCs and sequenced. The four UCMSC samples were grown in three different conditions (normoxic, hypoxic, normoxic/primed) to see how the EV miRNA content differed between these conditions. The EVs were isolated from the cells grown in these conditions and extracted for RNA. To control for the potential presence of FBS-EVs in the sample, EVs were isolated from FBS that had not been in contact with cells. A diagram of the samples taken forward for RNA sequencing is shown in **Figure 51.**

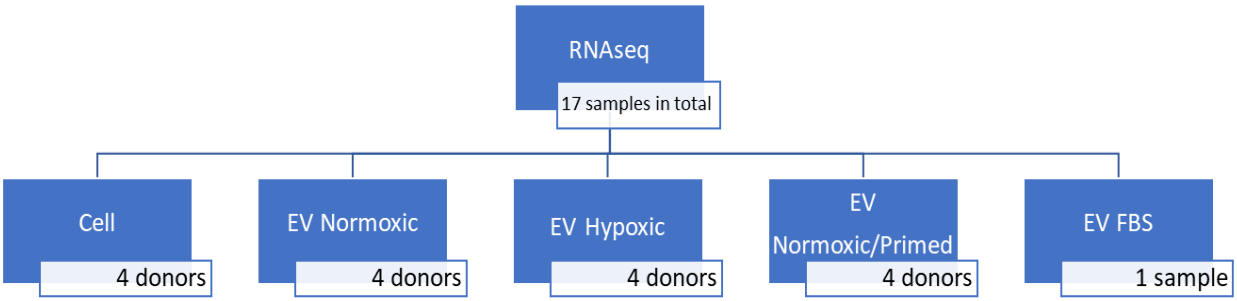

Figure 51: Diagram of study layout

17 samples were sequenced, these included normoxic cells and EVs from cells grown in normoxia, hypoxia, and normoxic/primed with pro-inflammatory cytokines, each containing 4 donors. As a control, 1 sample of EVs from FBS, which had not been in contact with cells, was sequenced.

Prior to library preparation and sequencing, the quality and concentration of the extracted RNA was identified. In this study, two methods were used to assess the quality and quantity of RNA, namely the Agilent Bioanalyser 2100 and the Qubit Fluorometer. The Agilent Bioanalyser 2100 provides valuable information on the RNA profile in the form of electrophoretic graphs

whereas the Qubit Fluorometer is a highly sensitive instrument that provides the most accurate quantification of low abundance RNAs [453]. There was a clear difference in electrophoretic gels between the cellular samples and the EV samples, with the cellular samples showing the characteristic 18s and 28s bands for rRNA, a distribution not seen in EV-RNA samples (**Figure 52A)**. The electropherograms showed that the cellular RNA had a size distribution ranging primarily from 200nt-4000nt whereas the EV-RNA samples mainly contained RNA traces <200nt indicative of small RNAs (**Figure 52B)**. This is consistent with previously published data on EV-RNA [202,228].

The presence of 18s and 28s peaks for the cellular RNA made it possible for a RIN score to be calculated. The RIN score is a measure of intact ribosomal RNA, and it is used to give an indication of the quality of RNA in a sample. The average RIN for the cell samples was 9.1 (± 0.55 SD), indicating that the majority of the RNA was intact and without degradation. Thus, this RIN indicates that RNA extraction procedures were of high quality. The mean RIN score for the EV samples was 1.3 (± 0.75 SD), however, this measurement was not suitable for EV samples due to their lack of rRNA.

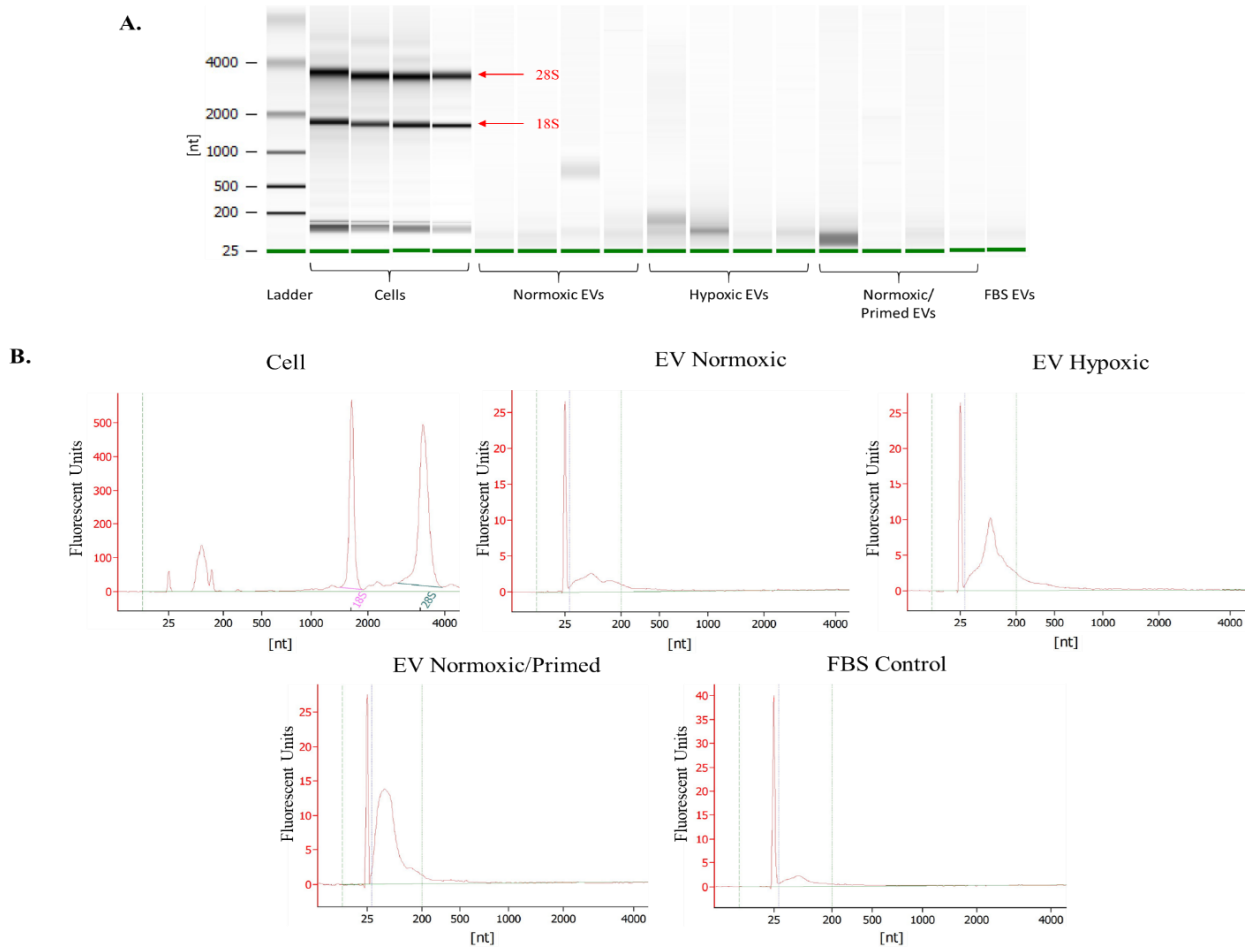

Figure 52: Gel and electropherogram graphs of cell and EV RNA

Gel and electropherogram graphs, obtained from the Agilent Bioanalyser 2100, show the size distribution of RNA in cell samples, normoxic EVs, hypoxic EVs, normoxia/primed EVs, and FBS-EVs. ***A.*** *Gel image depicts the RNA 6000 ladder standard (Lane 1) which is made up of six RNA fragments with size*

ranges from 0.2 to 6 kb. The cellular RNA (Lane 2-5) shows two clear bands for 18S (1900nt) and 28S (4700nt) rRNA indicated by the red arrows. No clear bands were detected at this level for EVs. Faint bands for EVs were seen in the small RNA area at 5S mark (120nt). ***B.*** *Electropherogram showing the size profile of samples. The x-axis displays the nucleotide length [nt] and the y-axis displays the fluorescent units. The cell sample shows strong peaks ~1800nt and ~3800nt while the EV samples show small peaks between ~25-200nt.*

The Qubit Fluorometer 2.0 was used to calculate the RNA concentration of the cells and EVs. The average concentration of the cells was 267ng/µl (± 172.5 SD) whereas EVs contained lower amounts of RNA with an average concentration of 0.15ng/µl (± 0.12 SD).

The DV_{200} score was used purely to gain additional insight into the nucleotide lengths of the isolated RNA. This DV_{200} metric calculates the percentage of RNA fragments >200nt [228]. The EV-RNA had an average DV_{200} of 28% (±17 SD) compared to 76% (±3 SD) in cell samples. This analysis shows that the EV-RNA contains short nucleotide sequences indicative of small RNAs. A full list of the quantity of RNA, RIN and DV_{200} is found in

Table 19. This is consistent with literature detailing the low yield of RNA from EV samples [454–456].

Table 19: List of samples and RNA concentrations for UCMSCs, EVs and FBS-EVs

Table shows UCMSC, EV and FBS-EV samples with their associated concentrations, RIN numbers and DV_{200} numbers. The RNA concentrations were measured through the Qubit Fluorometer 2.0 instrument with the Broad Range and High Sensitivity assay kits. The RIN and DV_{200} numbers were identified using the Agilent Bioanalyser 2100.

				Dv200	
Sample	**Concentration (ng/µl)**	**Total Quantity (ng)**	**RIN**	**40-200nt**	**200-8000nt**
Donor 1 Cell	75	825.00	8.4	25	74
Donor 2 Cell	442	4340.00	8.9	20	80
Donor 3 Cell	172	1720.00	9.3	23	76
Donor 4 Cell	380	3420.00	9.7	26	74
Donor 1 EV Normoxic	0.07	0.65	1	59	38
Donor 2 EV Normoxic	0.14	1.43	1	63	35
Donor 3 EV Normoxic	0.07	1.73	N/A	31	67
Donor 4 EV Normoxic	0.11	1.13	1.1	77	20
Donor 1 EV Hypoxic	0.34	4.03	2.3	64	36
Donor 2 EV Hypoxic	0.29	2.92	2.5	79	20
Donor 3 EV Hypoxic	0.08	0.82	1	77	21
Donor 4 EV Hypoxic	0.16	3.18	1.3	66	32
Donor 1 Normoxic/Primed	0.37	3.72	2.6	93	7
Donor 2 Normoxic/Primed	0.02	0.29	1	47	50
Donor 3 Normoxic/Primed	0.07	0.65	1	84	13
Donor 4 Normoxic/Primed	0.04	0.42	1.3	95	3
FBS EVs	0.13	1.43	2.2	79	17

6.2.2 Library preparation and sequencing

Preparation of the RNA sequencing libraries was performed at the University of Liverpool where all samples were successfully converted into cDNA **(Section 2.9.5).** The mean concentration of the cell samples was 7.24ng/µl (± 1.22 SD) compared to 0.74ng/µl (± 0.28 SD) in EV samples from all conditions. A list of the mean cDNA values for the cells and EVs in all conditions is provided in **Table 20**. Gel images show faint bands at 140-150bp **(Figure 53A)** and electrophoretic graphs showed peaks at 143-146bp (**Figure 53B)**, which is the size expected for miRNA.

Table 20: Cell and EV cDNA concentrations as measured by Qubit Fluorometer

	Mean cDNA concentration (ng/µl ±SD)
Cells (n=4)	7.24 (±1.22)
Normoxic EVs (n=4)	0.72 (±0.06)
Hypoxic EVs (n=4)	0.82 (±0.50)
Normoxic/Primed EVs (n=4)	0.69 (±0.13)
FBS EVs (n=1)	0.65

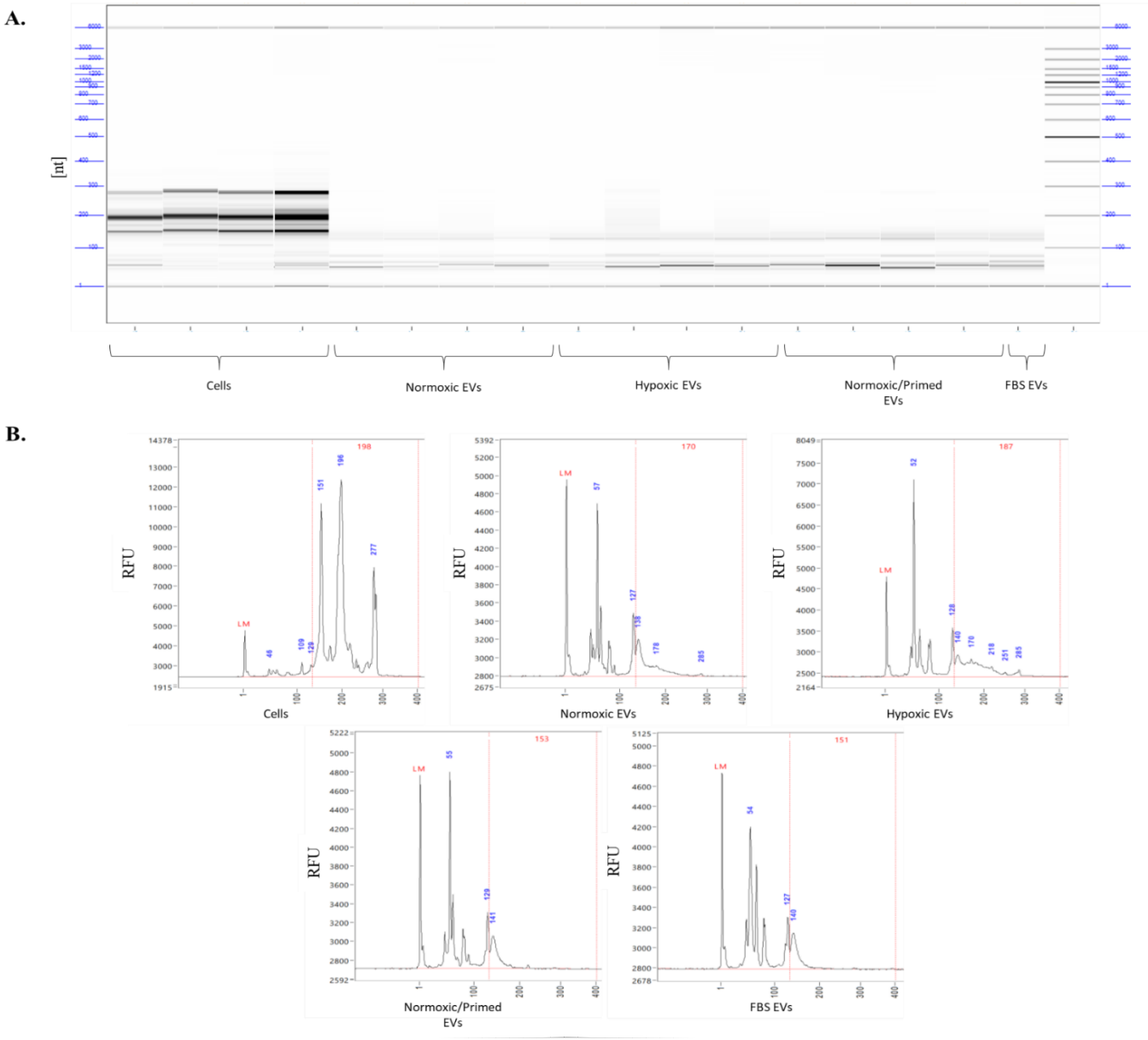
A.
[nt]
Cells
Normoxic EVs
Hypoxic EVs
Normoxic/Primed EVs
FBS EVs
B.
RFU
Cells
Normoxic EVs
Hypoxic EVs
Normoxic/Primed EVs
FBS EVs

Figure 53: Gel and Electrophoretogram Analysis of cDNA

A. *Fragment analysis of cell and EV samples ran through a gel. Nucleotide length (nt) is displayed on the y-axis and samples on the x-axis. The 140bp and 150bp bands correspond to miRNAs at 21nt.* ***B.*** *Electrophoretogram of RNA fragments. Each graph represents a different sample for one donor. MiRNA peaks exist between 143-146bp where the red line intersects the x-axis. Relative fluorescent units (RFU) are displayed on the y-axis.*

Prior to paired-end sequencing, the final pool of samples was Pippin size selected on the Agilent 2100 Bioanalyser which produced traces with an average size of 153bp. The gel and electropherogram size profiles are shown in **Figure 54.** Fastq file were prepared as previously mentioned in **Section 2.9.5.**

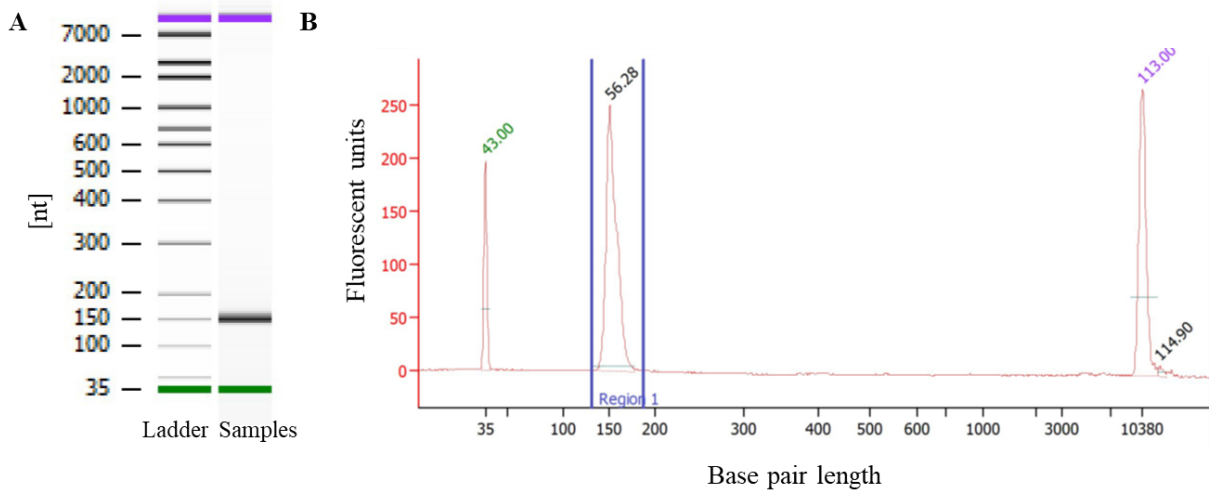

Figure 54: Final cDNA pool preparation.

*Gel image (**A**) and electropherogram **(B)** of RNA that was size selected for 130-160bp to include miRNAs. Gel image shows nucleotide length on the y-axis, electropherogram shows fluorescent units on the y-axis and base pair length on the x-axis.*

Paired-end sequencing was performed on the samples and R1 and R2 files were generated for the paired end sequencing reads. Samples had an estimated read length ~20 base pairs per sample shown in the boxplot containing the trimmed reads in **Figure 55A.** There were at least 40 million paired reads obtained per sample **(Figure 55B).** The FASTQC software analysed the quality of the Fastq files, it generated a Q score/Phred score of >30 for all files. This indicates that there is a high probability that a base call is at least 99.9% accurate by the sequencer [457], which shows that the sequencing run was successful and of a high quality.

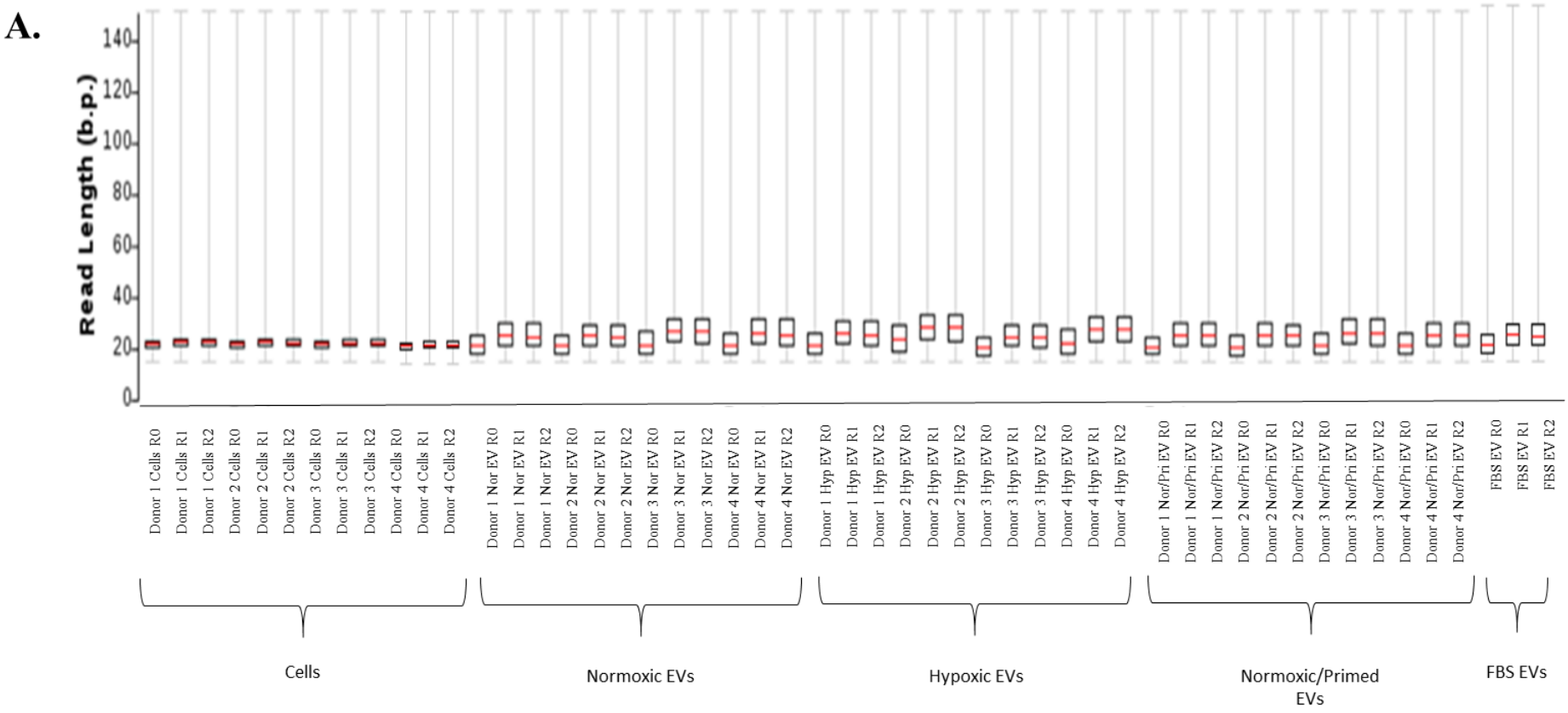
A.
Read Length (b.p.)
140
120
100
80
60
40
20
0
Donor 1 Cells R0
Donor 1 Cells R1
Donor 1 Cells R2
Donor 2 Cells R0
Donor 2 Cells R1
Donor 2 Cells R2
Donor 3 Cells R0
Donor 3 Cells R1
Donor 3 Cells R2
Donor 4 Cells R0
Donor 4 Cells R1
Donor 4 Cells R2
Donor 1 Nor EV R0
Donor 1 Nor EV R1
Donor 1 Nor EV R2
Donor 2 Nor EV R0
Donor 2 Nor EV R1
Donor 2 Nor EV R2
Donor 3 Nor EV R0
Donor 3 Nor EV R1
Donor 3 Nor EV R2
Donor 4 Nor EV R0
Donor 4 Nor EV R1
Donor 4 Nor EV R2
Donor 1 Hyp EV R0
Donor 1 Hyp EV R1
Donor 1 Hyp EV R2
Donor 2 Hyp EV R0
Donor 2 Hyp EV R1
Donor 2 Hyp EV R2
Donor 3 Hyp EV R0
Donor 3 Hyp EV R1
Donor 3 Hyp EV R2
Donor 4 Hyp EV R0
Donor 4 Hyp EV R1
Donor 4 Hyp EV R2
Donor 1 Nor/Pri EV R0
Donor 1 Nor/Pri EV R1
Donor 1 Nor/Pri EV R2
Donor 2 Nor/Pri EV R0
Donor 2 Nor/Pri EV R1
Donor 2 Nor/Pri EV R2
Donor 3 Nor/Pri EV R0
Donor 3 Nor/Pri EV R1
Donor 3 Nor/Pri EV R2
Donor 4 Nor/Pri EV R0
Donor 4 Nor/Pri EV R1
Donor 4 Nor/Pri EV R2
FBS EV R0
FBS EV R1
FBS EV R2
Cells
Normoxic EVs
Hypoxic EVs
Normoxic/Primed EVs
FBS EVs

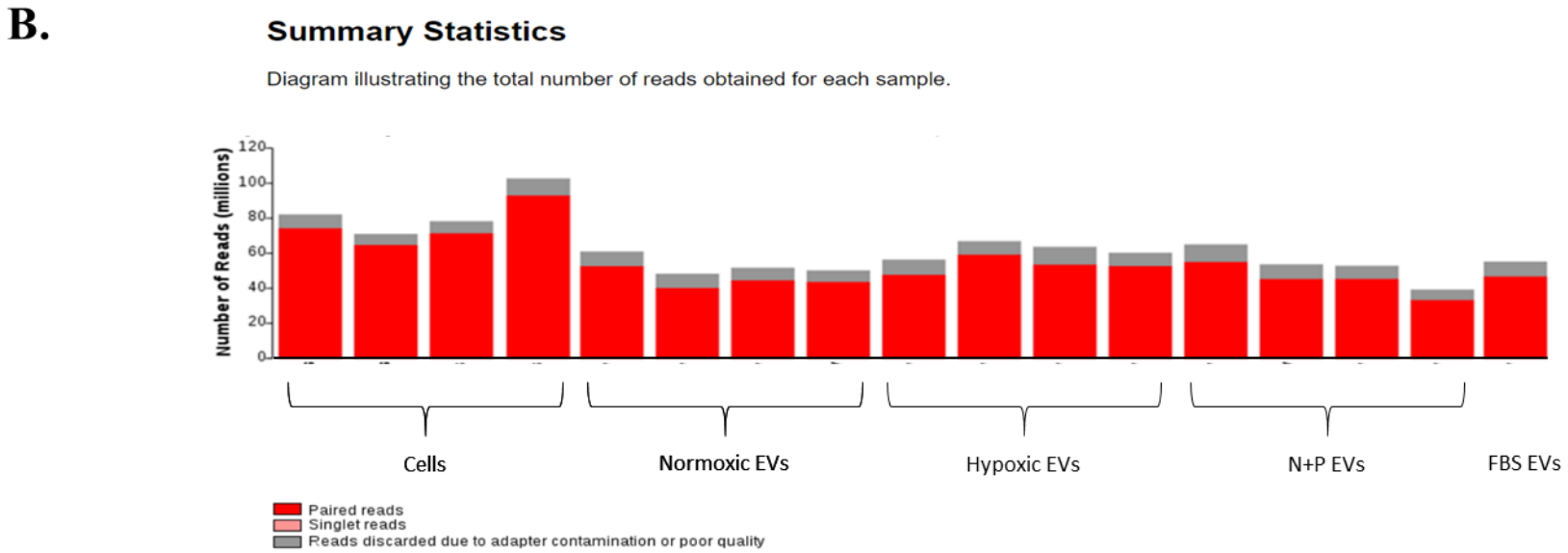

Figure 55: Summary profile of sequenced reads

A. *Box plot showing the distribution of trimmed reads for the forward (R1), reverse (R2) and singlet (R0) reads. Read length (b.p.) is presented on the y-axis and samples are presented on the x-axis. The box indicates the interquartile range, the red line in the box represents the median length, the whiskers indicate the minimum and maximum read lengths. A long tail can be seen on each sample. This distribution was expected as this is common for a small number of reads to consist of mostly adapter derived sequences.* ***B.*** *Bar chart illustrating the total number of reads obtained per sample. Number of reads (millions) is presented on the y-axis and samples on the x-axis.*

6.2.3 Analysis of cellular and EV RNA reads

To visually compare the similarity between samples, a heatmap was generated. This used hierarchical clustering to compare the Log_2 values on a colour scale, whereby the darker the colour indicated a higher similarity between samples (**Figure 56A)**. The heatmap showed that biologically, the cells were similar to one another, but there was a clear dissimilarity between the miRNA content of the cells versus the EVs, as was expected. However, within the EV samples, the miRNA content was varied. These findings were supported after carrying out a Principal Component Analysis (PCA) shown in **Figure 56B.** The cell samples clustered very closely together indicating robust reproducibility and low variation in miRNA signatures and this cluster was separate from any of the EV samples. The EV samples did not cluster by condition and there was no identifiable trend in clustering. This suggests that the priming approaches did not majorly alter the miRNA content. Similar to the heatmap, there was a clear difference between the miRNAome of the cells and EVs shown by 36% variance on the *x-axis* of the PCA plot. The sequenced FBS-EVs were considered as part of this analysis and they clustered closely with the EV samples which warranted further investigation as to which miRNAs were similar. As a result, all differentially expressed miRNAs between EV groups were compared to the FBS-EVs to check that these were of human origin and not from the FBS.

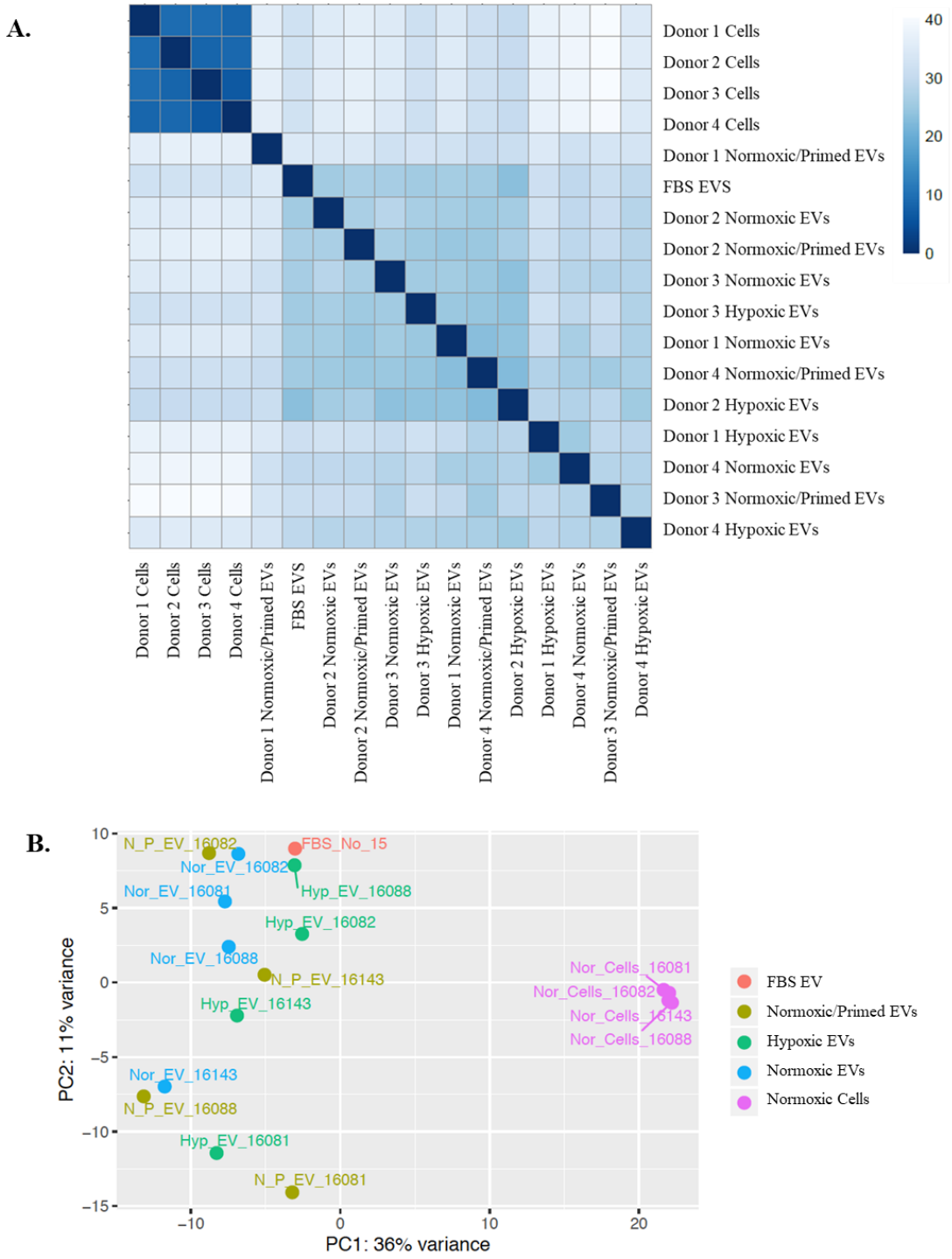

Figure 56: Similarity in miRNA profile between samples

A. *Heatmap displays the similarity between samples using the Log$_2$ data. Euclidean sample-to-sample distances are calculated, and measures are displayed on a scale of 0-40 where '0' is the darkest colour '40' is the lightest colour. Samples which overlap with dark blue squares are highly similar, whereas samples which overlap with light squares are dissimilar.* ***B.*** *Principal Component Analysis shows a 36% variance between cell and EV samples (PC1; x-axis) and a 11% variance within EV conditions (PC2; y-axis). Normoxic cell samples were highly similar seen by close clustering on the graph.*

6.2.4 Differential expression of miRNAs

To visualise the differential expression of miRNAs between two conditions, a Minus-Average (MA) plot was generated (**Figure 57A-C)**. This plot compared the average normalised count to the Log_2 fold change. Each miRNA is represented by a dot, with the significantly expressed miRNAs (i.e., $q<0.1$) shown in red. This plot shows that the miRNAs with a higher average normalised count required a lower Log_2 fold change to gain statistical significance as seen in **Figure 57A.**

To get an overview of the frequency of p-values between conditions, histograms were generated **(Figure 57D-F).** In the comparison between normoxic cells and normoxic EVs, there is a wide range on p-values <1, with a peak at the '0' mark representing the 61 miRNAs that were differentially expressed **(Figure 57D)**. In the comparison between normoxic EVs and the other two EV conditions (hypoxic EVs and normoxic/primed EVs), the highest peak is at '1' showing that most miRNAs did not reach a statistically significant adjusted p-value of <0.1, to be considered as differentially expressed.

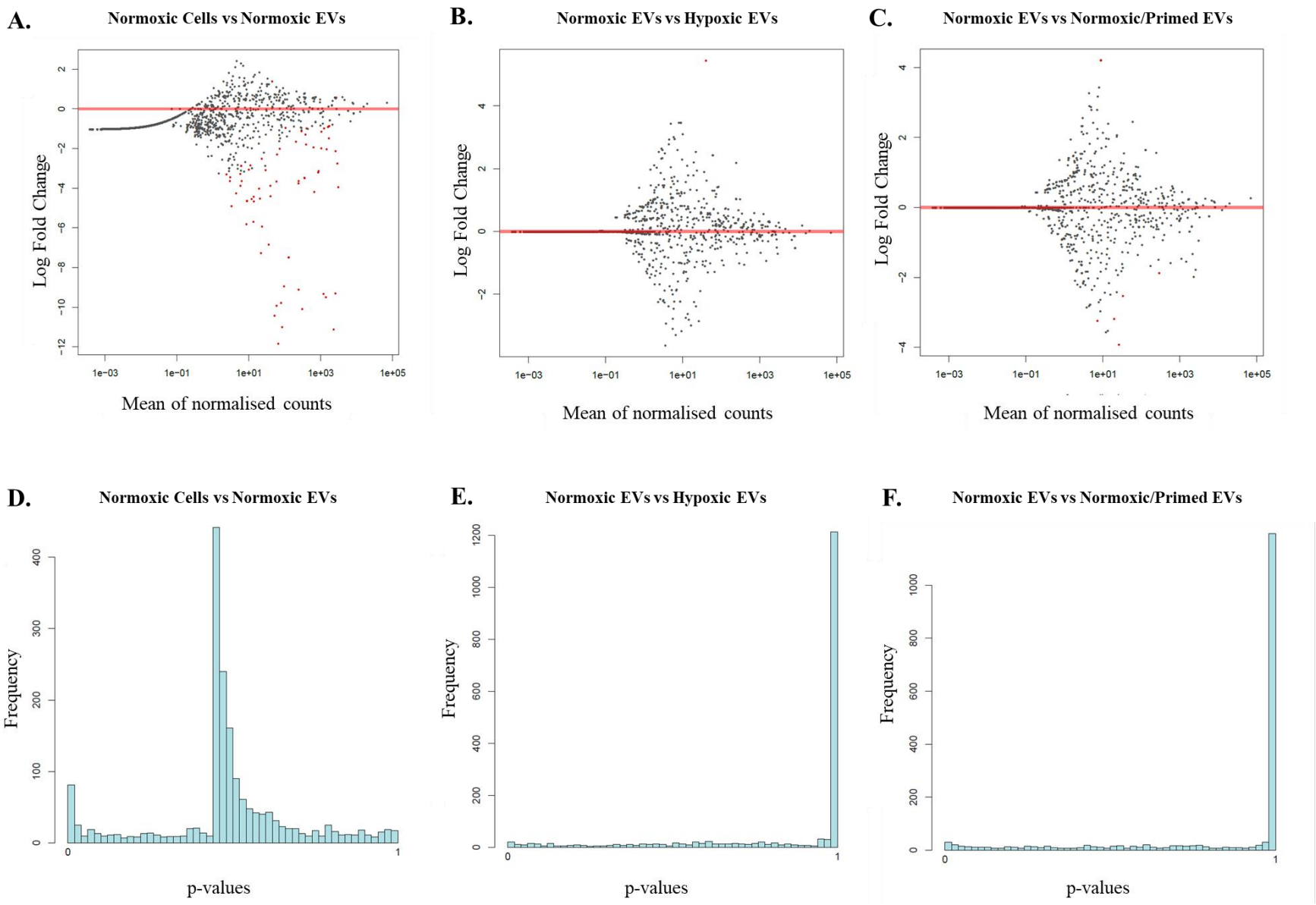
A.
Normoxic Cells vs Normoxic EVs
Log Fold Change
Mean of normalised counts
B.
Normoxic EVs vs Hypoxic EVs
Log Fold Change
Mean of normalised counts
C.
Normoxic EVs vs Normoxic/Primed EVs
Log Fold Change
Mean of normalised counts
D.
Normoxic Cells vs Normoxic EVs
Frequency
p-values
E.
Normoxic EVs vs Hypoxic EVs
Frequency
p-values
F.
Normoxic EVs vs Normoxic/Primed EVs
Frequency
p-values

Figure 57: Differential miRNA expression between samples and conditions

A-C: *MA plots comparing the average normalised count (x-axis) with the* Log_2*(Fold change) (y-axis) between two conditions. MiRNAs are represented by a black dot and the differentially expressed miRNAs with an adjusted p-value <0.1 are shown in red.* ***(A)*** *There were 61 differentially expressed miRNAs between normoxic cells and normoxic EVs after Benjamini-Hochberg correction.* ***(B)*** *2 differentially expressed miRNAs between normoxic EVs and hypoxic EVs.* ***(C)*** *6 differentially expressed miRNAs between normoxic EVs and normoxic/primed EVs.*
D-F: *Histograms comparing the relationship between p-values (x-axis) and their frequency of detection (y-axis).* ***(D)*** *Normoxic cells vs normoxic EVs showed the presence of miRNAs at ~p=0.* ***(E)*** *Normoxic EVs vs hypoxic EVs and* ***(F)*** *normoxic EVs vs normoxic/primed EVs showed a high frequency of miRNAs at ~p=1, indicating that most miRNAs did not reach statistical significance as being differentially expressed.*

The next stage was to identify which miRNAs were differentially expressed between the cell and EV samples and between the different EV conditions. In total, an average of 1,126 miRNAs were identified in cell samples, 377 in EVs and 241 in bovine samples. There were 12 miRNAs unique to only EVs, of which only one was also detected in FBS-EVs, shown in **Table 21**. In total, 44% of miRNAs expressed in cells were also found in the EVs.

Table 21: Uniquely expressed miRNAs in EVs

List of the 12 uniquely expressed miRNAs and their corresponding EV source.

Uniquely expressed miRNAs	EV Source
miR-4516	Normoxic EV
miR-7847	Normoxic EV; Normoxic/Primed EV
miR-5197	Normoxic EV
miR-1469	Normoxic EV
miR-7975	Normoxic EV; Hypoxic EV; Normoxic/Primed EV
miR-3168	Normoxic EV; Normoxic/Primed EV; FBS EV
miR-4716	Hypoxic EV
miR-4492	Normoxic/Primed EV
miR-4426	Normoxic/Primed EV
miR-4693	Normoxic/Primed EV
miR-1251	Normoxic/Primed EV
miR-6124	Normoxic/Primed EV

A total of 61 miRNAs were differentially expressed between normoxic cells and normoxic EVs (59 had a higher expression in EVs and 2 in cells). This compares to only 2 differentially expressed miRNAs between normoxic EVs and hypoxic EVs and 6 between normoxic EVs and normoxic/primed EVs, as shown in **Figure 58A-C**. The adjusted p-values were transformed using the negative log for visual representation on the volcano plot. A chart of the differentially expressed miRNAs and their corresponding adjusted p-value is shown in **Table 22.** The differentially expressed miRNAs were then cross-checked with miRNAs expressed in FBS-EVs to confirm that they were of human and not bovine origin. When all EV conditions are compared to the FBS control only one miRNA (miR-215-5p), has a statistically higher

expression in FBS-EVs compared to hypoxic EVs. Interestingly, miR-215-5p was also found to be downregulated in hypoxic EVs compared to normoxic EVs. With the exception of miR-193a-5p, which had an average normalised read count of 290, all other differentially expressed miRNAs between EV conditions had a low normalised read count from the RNA sequencing data (mean 21.4; SD ± 17.2).

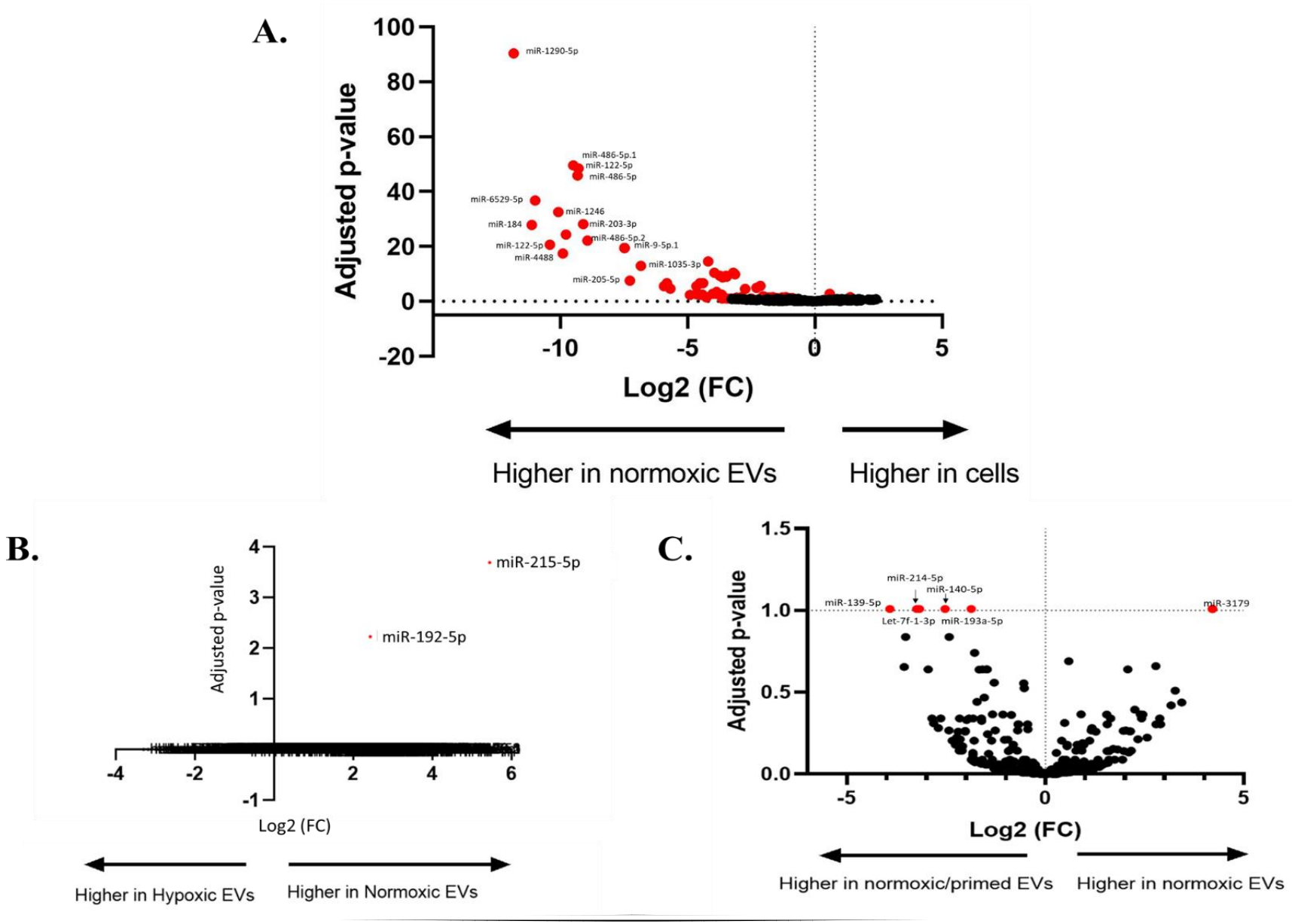
A.
Adjusted p-value
100
80
60
40
20
0
-20
-10
-5
0
5
Log2 (FC)
miR-1290-5p
miR-486-5p.1
miR-122-5p
miR-486-5p
miR-6529-5p
miR-1246
miR-184
miR-203-3p
miR-486-5p.2
miR-122-5p
miR-9-5p.1
miR-4488
miR-1035-3p
miR-205-5p
Higher in normoxic EVs
Higher in cells
B.
Adjusted p-value
4
3
2
1
-1
-4
-2
2
4
6
Log2 (FC)
miR-215-5p
miR-192-5p
Higher in Hypoxic EVs
Higher in Normoxic EVs
C.
Adjusted p-value
1.5
1.0
0.5
0.0
-5
0
5
Log2 (FC)
miR-214-5p
miR-140-5p
miR-139-5p
miR-3179
Let-7f-1-3p
miR-193a-5p
Higher in normoxic/primed EVs
Higher in normoxic EVs

Figure 58: Volcano plot of differentially expressed miRNAs

(A) *There was increased expression in 61 miRNAs (shown in red) from the normoxic EVs compared to normoxic cells. Two miRNAs had a higher expression in the normoxic cells (miR-127-3p, miR-340-5p)* ***(B)*** *There was an increased expression in 2 miRNAs (miR-192-5p, miR-215-5p) from the normoxic EVs compared to the hypoxic EVs.* ***(C)*** *There was an increased expression in 6 miRNAs from the normoxic/primed EVs compared to the normoxic EVs. Values above the horizontal dotted line on the y-axis are statistically significant. Values to the left of the vertical dotted line on the x-axis have a decrease in Log_2 (FC); values to the right of this line have an increase in Log_2 (FC). The red dots signify the miRNA's that reached statistical significance as being differentially expressed.*

Table 22: Differentially Expression miRNAs

List of differentially expressed miRNAs, their adjusted p-values, and their expression. There were 6 differentially expressed miRNAs between normoxic EVs and normoxic/primed EVs; 2 between normoxic EVs and hypoxic EVs, and 61 between normoxic cells and normoxic EVs, although only a snapshot of the first ten miRNAs with the lowest adjusted p-value, are shown in the table. A full list of the 61 differentially expressed miRNAs is shown in **Supplementary Table 2.**

	miRNA	Adjusted p-value	Expression
Normoxic EVs vs Normoxic/Primed EVs	let-7f-1-3p	0.0981	Higher in Normoxic/Primed EVs
	miR-139-5p	0.0981	Higher in Normoxic/Primed EVs
	miR-140-5p	0.0981	Higher in Normoxic/Primed EVs
	miR-193a-5p	0.0981	Higher in Normoxic/Primed EVs
	miR-214-5p	0.0981	Higher in Normoxic/Primed EVs
	miR-3179	0.0981	Higher in Normoxic EVs
Normoxic EVs vs Hypoxic EVs	miR-215-5p	0.0002	Higher in Normoxic EVs
	miR-192-5p	0.0060	Higher in Normoxic EVs
Normoxic Cells vs Normoxic EVs	miR-1290	4.19E-91	Higher in Normoxic EVs
	miR-486-5p	3.16E-50	Higher in Normoxic EVs
	miR-122-5p	3.89E-49	Higher in Normoxic EVs
	miR-6529-5p	1.71E-37	Higher in Normoxic EVs
	miR-1246	2.82E-33	Higher in Normoxic EVs
	miR-203a-3p	7.15E-29	Higher in Normoxic EVs
	miR-184	1.39E-28	Higher in Normoxic EVs
	miR-1291	4.55E-25	Higher in Normoxic EVs
	miR-122-5p	2.12E-21	Higher in Normoxic EVs
	miR-9-5p	3.62E-20	Higher in Normoxic EVs

6.2.5 Sequence conservation FBS-EV miRNA

The FBS-EV RNA (n=1) was mapped against both the human and bovine miRNAs databases to compare mapping rates/expression profiles between samples. The purpose of this was to give an indication of sequence conservation. Results show a high sequence conservation between human and bovine miRNAs. The similarity between mapping rates on the 20 most expressed miRNAs is shown in **Figure 59**. Statistical analysis was not carried out on samples as only one FBS-EV RNA sample was sequenced.

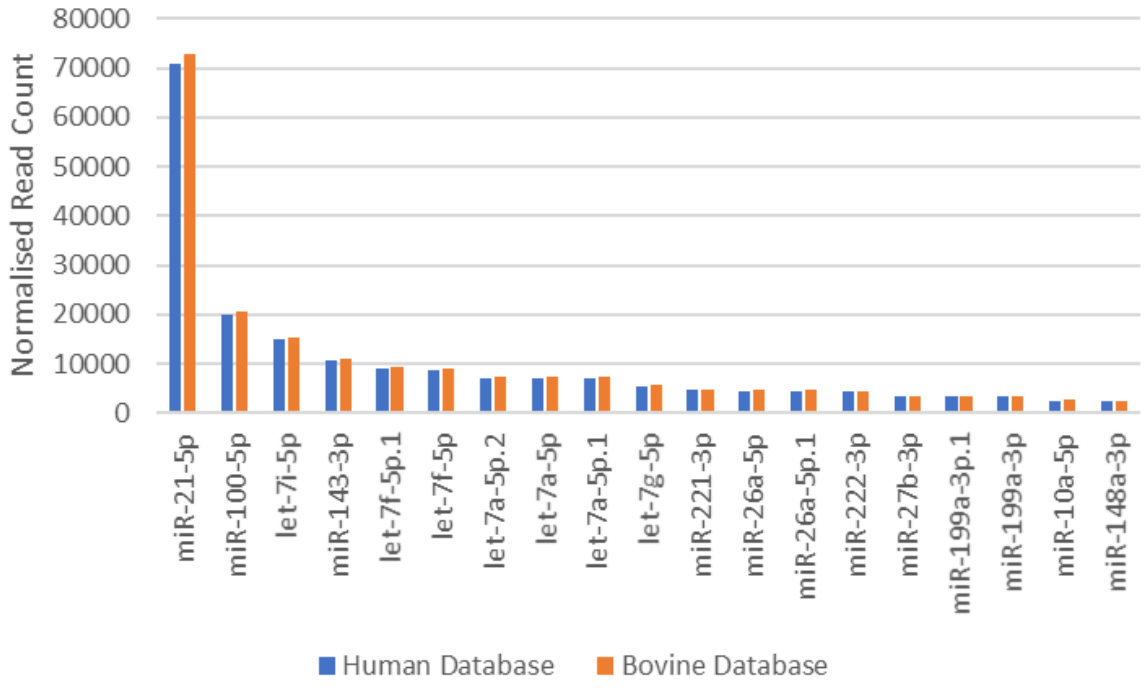

Figure 59: Sequence conservation between human and bovine miRNAs

FBS-EV RNA was sequenced and mapped to both the human and bovine miRNA databases to give an indication of sequence conservation. The mapping rate of FBS-EV samples was similar for both databases. The top 20 miRNAs are shown on the x-axis and the normalised read count shown on the y-axis.

MiR-21-5p was the most abundant miRNA expressed across all samples and conditions and accounts for 30.3% (±2.26 SD) of the normalised counts in cell samples, 21.7% (±2.6 SD) in EVs (across 3 conditions) and 26.2% FBS-EVs. In total, the top 10 miRNA readings, shown in **Figure 60A,** made of 64% of the total miRNA expression in cells, 54% (±4.8) in EVs (across 3 conditions), and 60% in FBS-EVs. A comparison of the normalised gene expression in the most commonly detected miRNAs is shown in **Figure 60B.** Across all samples and conditions, the top 100 miRNAs accounted for 95-97% of the detectable miRNA sequences, therefore, the remaining 3-5% accounted for low abundance miRNAs.

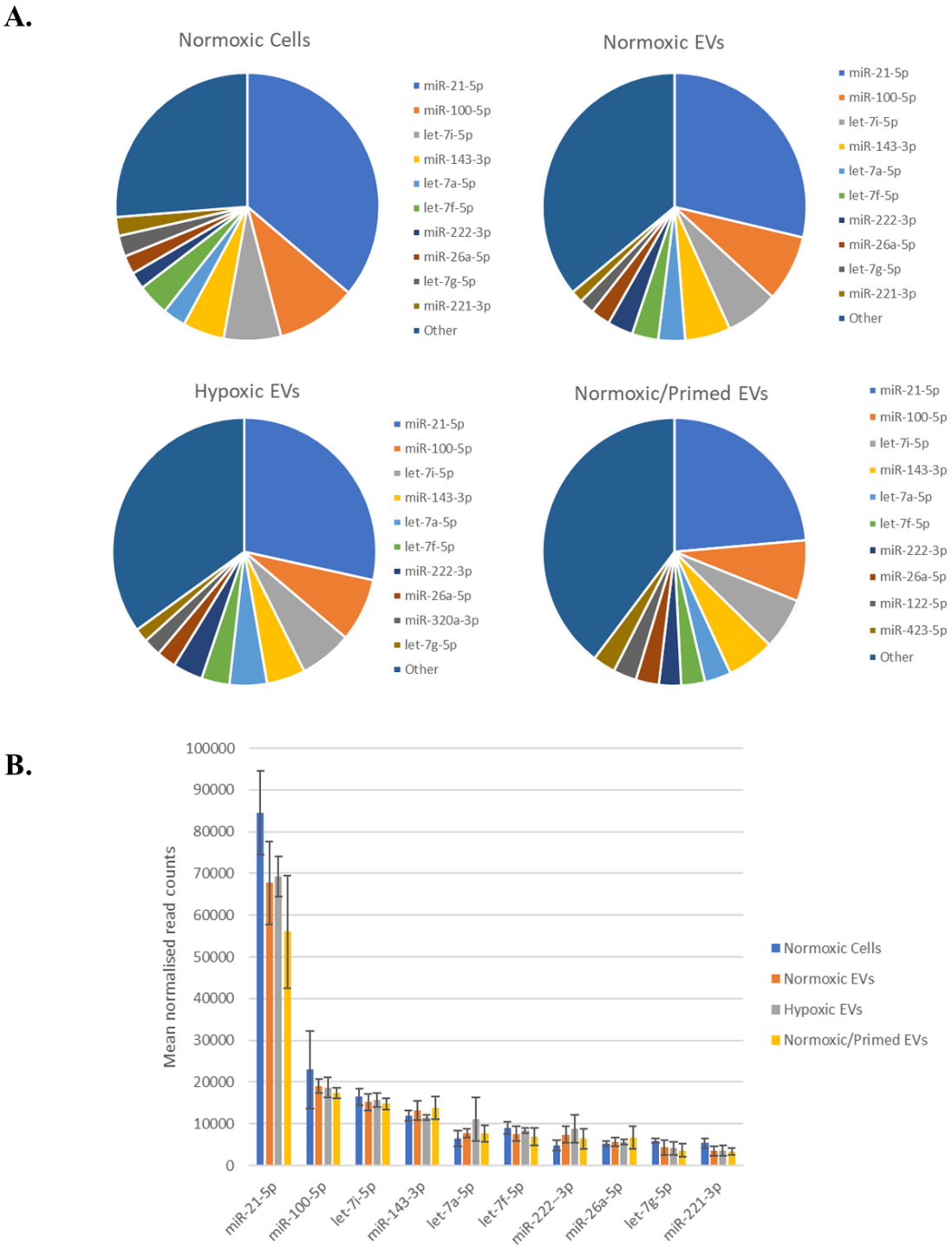

Figure 60: Profile of commonly expressed miRNAs in cells and EVs

A. *Venn diagrams displaying the 10 most expressed miRNAs in normoxic cells, normoxic EVs, hypoxic EVs, and normoxic/primed EVs.* ***B.*** *Bar chart comparing the expression of some of the most expressed miRNAs across samples and conditions. The miRNAs are presented on the x-axis and the mean normalised read count on the y-axis. There were no statistical differences between the samples for the miRNAs presented here.*

6.2.6 Target prediction of differentially expressed miRNAs

Pathway enrichment analysis was carried out on miRNet using the KEGG database. Analysis was carried out on the five upregulated miRNAs in the normoxic/primed EVs (let-7f-1-3p, miR-139-5p, mir-140-5p, miR-193a-5p, miR-214-5p) and the two downregulated miRNAs in hypoxic EVs compared to normoxic EVs (miR-215-5p and miR-192-5p). For the 5 upregulated miRNAs in normoxic/primed EVs, miRNet generated a network comprising of 555 nodes (genes: 550; miRNA: 5) and 565 edges, shown in **Figure 61A**. For the two downregulated miRNAs in hypoxic EVs, 1011 nodes were generated (genes: 1009; miRNA: 2) and 1749 edges, shown in **Figure 61B.**

For the upregulated miRNAs in the normoxic/primed EVs, miR-214-5p had the most potential gene targets at 188. In the normoxic EVs, miR-192-5p had 994 potential gene targets and miR-215-5p had 755. The analysis of the upregulated normoxic/primed EVs showed that cancer pathways contained the most hits and the most significance overall ($p=2x10^{-14}$). In all, the analysis generated many lists for cancer in the upregulated normoxic/primed EV-miRNAs, shown in the top 20 enriched pathways **(Table 23A).** For the two downregulated miRNAs in hypoxic EVs (miR-215-5p and miR-192-5p), the enriched pathways were associated with cell cycle genes and the Fanconi anaemia pathway. These were the only two pathways that had an adjusted p-value of <0.1 from the KEGG enrichment analysis **(Table 23B).**

To further examine the biological targets of the upregulated miRNAs, the GO: Biological Process database was applied to the dataset [458,459]. This database was used to support the data from the KEGG database and gain insight into what processes the miRNAs might engage in when inside their target cells. Analysis of the miRNAs on the GO: Molecular Function database would also have provided insight into the miRNA functions, and this will be explored

at a later stage. The most significantly enriched pathway from the upregulated normoxic/primed EV-miRNAs was the ‘negative regulation of cell proliferation’ pathway followed by ‘intracellular protein transport’. The downregulated miRNAs from the hypoxic EVs were found to be associated with cell cycle processes such as mitosis, with all the top 20 pathways connected to cell cycle regulation.

Further bioinformatic target prediction was performed on the five upregulated miRNAs in the normoxic/primed EVs (let-7f-1-3p, miR-139-5p, miR-140-5p, miR-193a-5p, miR-214-5p) to identify if they directly target secretome components. Three target prediction tools (miRNet [230,231], miRDB [232,233] and TargetScan (v.7.2) [234]) were chosen because they offered three different computational approaches to identify gene targets of miRNAs. The list of positively identified gene targets was then cross checked with the identified secretome components listed in **Table 17**. The normoxic/primed EVs were chosen for this analysis as they showed the most change from the protein and miRNA analysis.

All three web-based programmes identified miR-140-5p to directly target VEGFA. VEGFA protein was positively identified in the cargo of all EVs, but there was no statistical difference in VEGFA protein expression between the normoxic and normoxic/primed EVs. Other secretome components were directly targeted by the five upregulated miRNA but only identified in one out of three bioinformatic tools, therefore is a probability that these gene targets are inaccurate. These included:

- MiR-193a-5p targeted STAMBP and CSF-1
- MiR-140-5p targeted CSF-1
- Let-7f-1-3p targeted TSLP, HGF, IL6, CXCL11, VEGFA, IL15RA and CD40.

Many other gene targets were identified using these bioinformatic tools, but none included previously identified secretome components in the EV cargo. However, to further establish if the miRNAs in the EVs had targeted secretome components, gene prediction analysis was carried out on the top 5 miRNAs (miR-21-5p, miR-100-5p, let-7i-5p, miR-143-3p, let-7a-5p) expressed in the EVs, which were common across all conditions. Two out of three bioinformatic tools identified that miR-21-5p targeted CCL20 and let-7i-5p targeted IL-13. Both of these proteins had a higher expression in the normoxic/primed EVs.

Other gene targets which directly targeted secretome components in the EVs were identified but they were only present in one out of three bioinformatic tools. Therefore, there is a reduced confidence that this is a genuine connection. Other than the aforementioned gene targets, there was no further direct shared role between the proteins and the miRNAs in the EVs.

A.

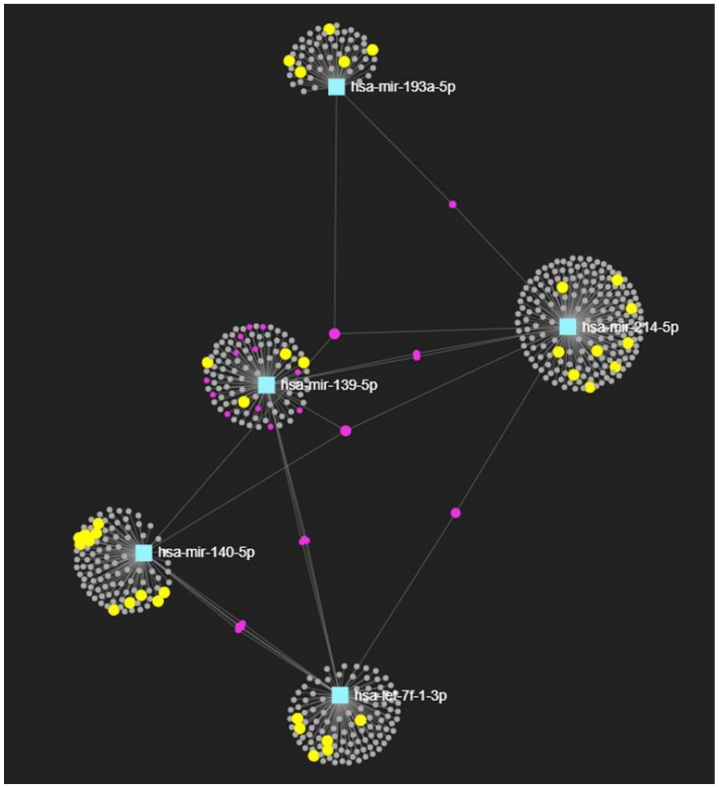

B.

miR-193a-5p

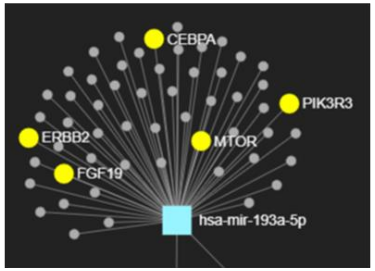

miR-214-5p

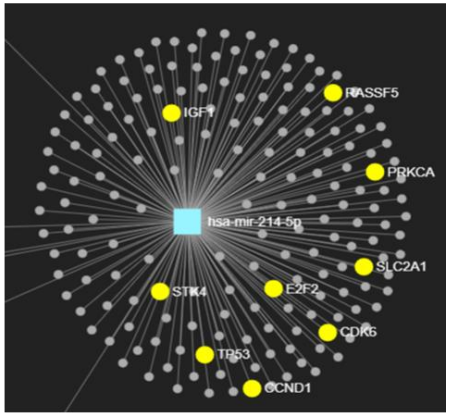

miR-139-5p

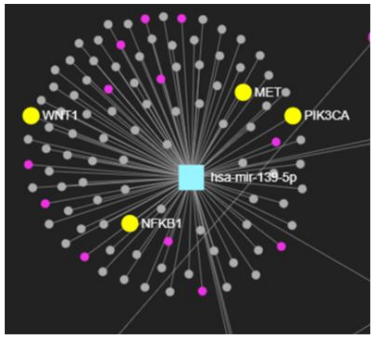

miR-140-5p

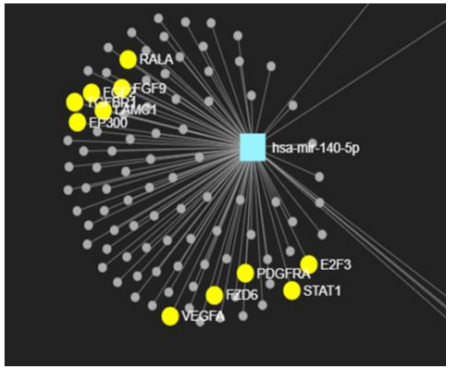

Let-7f-1-3p

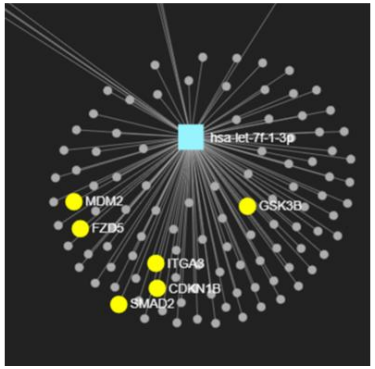

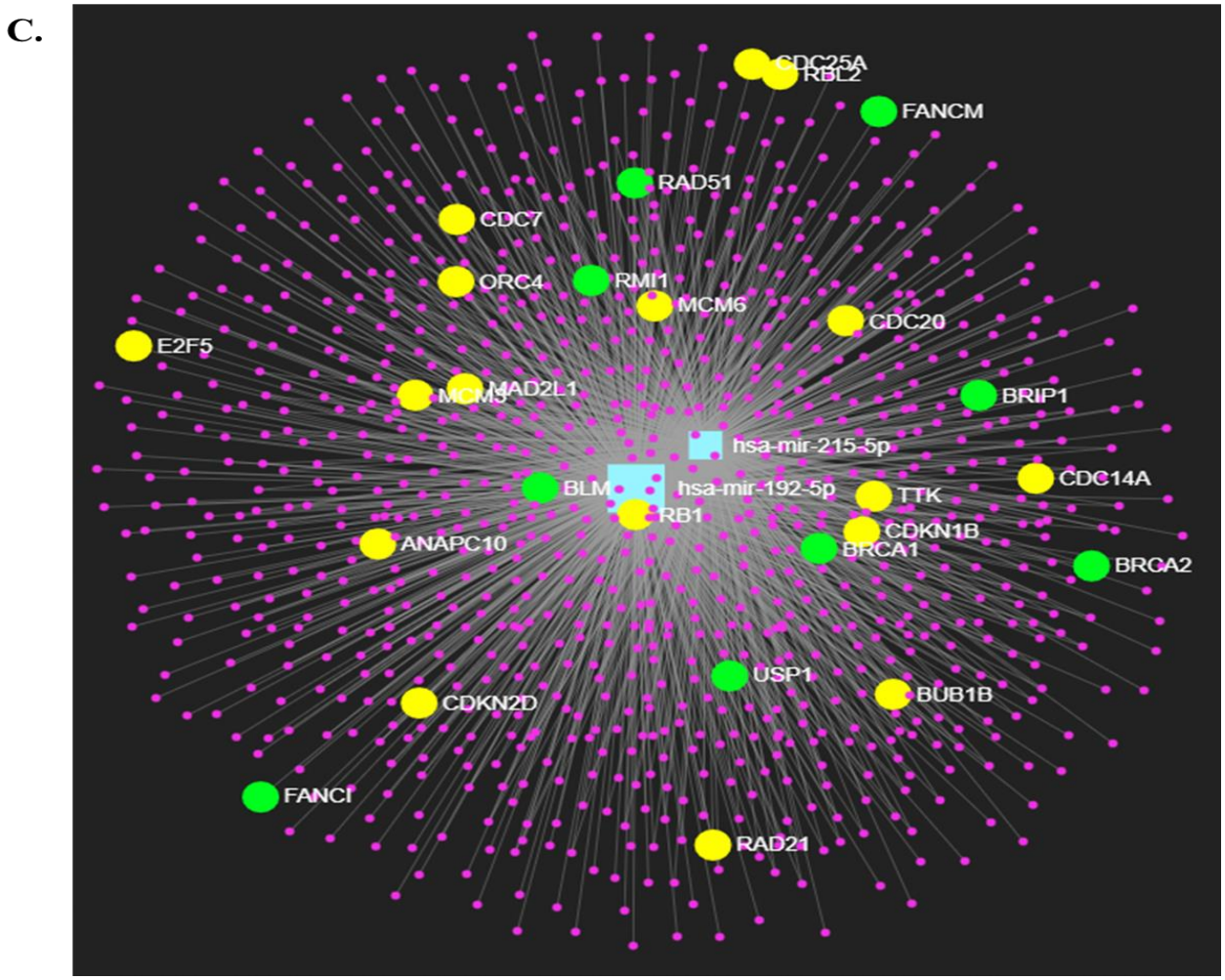

Figure 61: Predicted gene targets in differentially expressed miRNAs using the KEGG database

Visual representation of the gene targets from miRNet. The miRNAs are identified by a blue box and the gene targets by a pink dot. ***(A)*** *Image represents gene target from five upregulated miRNAs in normoxic/primed EVs vs normoxic EVs. Cancer pathways showed the most 'hits' in this analysis and these are*

highlighted in yellow. ***(B)*** *Close-up view of the gene targets associated with cancer pathways from the upregulated miRNAs.* ***(C).*** *Image of the gene targets from the two downregulated miRNAs in the hypoxic EVs vs the normoxic EVs. Cell cycle pathways and the Fanconi anaemia pathway contained the most statistically significant targets, and these have been highlighted yellow and green, respectively.*

Table 23: KEGG and GO: Biological Process enrichment analysis

List of predicted enriched pathways from the **(A)** KEGG database and the **(B)** GO: Biological Process database. Table shows the upregulated miRNAs in normoxic/primed EVs vs normoxic EVs and the downregulated miRNAs in the hypoxic EVs vs the normoxic EVs. The enriched pathway, hits, p-value, and adjusted p-value are shown in the columns.

A.

Normoxic /Primed EVs vs Normoxic EVs				Hypoxic EVs vs Normoxic EVs			
Name	**Hits**	**p-value**	**adj.p-value**	**Name**	**Hits**	**p-value**	**adj.p-value**
Pathways in cancer	41	2.00E-14	2.00E-12	Cell cycle	20	7.16E-06	7.16E-04
Prostate cancer	20	7.73E-12	3.87E-10	Fanconi anemia pathway	9	1.63E-04	8.15E-03
Melanoma	16	7.54E-10	2.51E-08	Pathways in cancer	28	3.99E-03	1.32E-01
Glioma	14	3.12E-08	7.80E-07	Folate biosynthesis	4	5.28E-03	1.32E-01
Pancreatic cancer	14	7.01E-08	1.40E-06	Apoptosis	10	1.26E-02	2.27E-01
Non-small cell lung cancer	11	1.22E-06	2.03E-05	Steroid biosynthesis	4	1.36E-02	2.27E-01
HTLV-I infection	21	4.39E-06	6.27E-05	Protein processing in endoplasmic reticulum	13	2.00E-02	2.66E-01
Chronic myeloid leukemia	12	6.58E-06	8.23E-05	Small cell lung cancer	9	2.63E-02	2.66E-01
Focal adhesion	20	1.71E-05	1.90E-04	Valine, leucine and isoleucine degradation	6	2.85E-02	2.66E-01
Colorectal cancer	9	3.94E-05	3.94E-04	Sphingolipid metabolism	6	3.46E-02	2.66E-01
Bladder cancer	7	4.64E-05	4.22E-04	TGF-beta signaling pathway	9	3.47E-02	2.66E-01
ErbB signaling pathway	11	1.95E-04	1.63E-03	HTLV-I infection	17	3.69E-02	2.66E-01
Cell cycle	13	3.47E-04	2.67E-03	Lysine degradation	6	3.80E-02	2.66E-01
Small cell lung cancer	10	4.20E-04	3.00E-03	ErbB signaling pathway	9	4.21E-02	2.66E-01
Renal cell carcinoma	8	1.04E-03	6.93E-03	Prostate cancer	9	4.21E-02	2.66E-01
Influenza A	11	1.17E-03	7.31E-03	Pyrimidine metabolism	10	4.30E-02	2.66E-01
Acute myeloid leukemia	7	3.45E-03	2.01E-02	Colorectal cancer	6	4.53E-02	2.66E-01
Endometrial cancer	6	3.95E-03	2.01E-02	Pertussis	6	5.78E-02	3.16E-01
Epstein-Barr virus infection	9	4.26E-03	2.01E-02	Thyroid cancer	4	6.01E-02	3.16E-01
Wnt signaling pathway	12	4.28E-03	2.01E-02	p53 signaling pathway	7	7.02E-02	3.51E-01

B.

Normoxic /Primed EVs vs Normoxic EVs				Hypoxic EVs vs Normoxic EVs			
Name	**Hits**	**p-value**	**adj.p-value**	**Name**	**Hits**	**p-value**	**adj.p-value**
negative regulation of cell proliferation	43	3.16E-07	3.2E-05	mitotic cell cycle	116	1.63E-15	1.63E-13
intracellular protein transport	50	3.25E-06	0.00016	cell division	75	6.31E-15	3.16E-13
sensory organ development	35	6.23E-06	0.00016	cell cycle phase	121	3.35E-14	1.12E-12
positive regulation of epithelial cell proliferation	15	0.0000065	0.00016	cell cycle process	146	7.71E-14	1.93E-12
epithelial cell differentiation	27	0.0000129	0.00026	mitosis	61	5.46E-12	1.09E-10
regulation of cell proliferation	73	0.0000342	0.0005	M phase of mitotic cell cycle	62	2.68E-11	4.47E-10
tube development	34	0.0000372	0.0005	cell cycle	168	6.78E-11	9.69E-10
positive regulation of transcription from RNA polymerase II promoter	47	0.00004	0.0005	M phase	77	1.12E-09	1.40E-08
tube morphogenesis	26	0.0000529	0.00059	chromosome segregation	32	2.13E-09	2.37E-08
protein targeting	35	0.0000718	0.00072	interphase of mitotic cell cycle	56	4.20E-09	4.20E-08
angiogenesis	29	0.000111	0.00089	interphase	56	8.15E-09	7.41E-08
negative regulation of signal transduction	45	0.000121	0.00089	cell cycle arrest	54	1.62E-08	1.35E-07
positive regulation of transcription, DNA-dependent	64	0.000128	0.00089	G1/S transition of mitotic cell cycle	34	1.76E-08	1.35E-07
positive regulation of nucleobase-containing compound metabolic process	64	0.000128	0.00089	regulation of cell cycle	90	1.90E-08	1.36E-07
MAPK cascade	73	0.000133	0.00089	negative regulation of cell cycle	58	3.69E-07	0.00000246
morphogenesis of an epithelium	39	0.000192	0.00114	cell cycle checkpoint	37	1.08E-06	0.00000675
positive regulation of RNA metabolic process	29	0.000193	0.00114	DNA replication initiation	10	3.09E-06	1.8176E-05
intracellular protein kinase cascade	66	0.000217	0.00115	microtubule cytoskeleton organization	40	5.58E-06	0.000031
embryonic morphogenesis	58	0.000248	0.00115	mitotic sister chromatid segregation	13	6.29E-06	0.00003235
vasculature development	35	0.000249	0.00115	microtubule-based process	54	6.47E-06	0.00003235

6.2.7 Validation of RNA sequencing data

PCR was carried out to validate the results of the RNA sequencing study. MiRNAs of interest (n=10) and reference miRNAs (n=4) were identified and are provided in

Table *12*, along with their target sequence. MiR-21-5p, let-7i-5p, miR-146a-5p, miR-181a-5p were chosen based on their reported immunosuppressive properties which may have relevance to RA. MiR-155-5p, miR-215-5p, let-7f-1-3p, miR-139-5p, miR-214-5p, miR-192-5p were chosen because these were differentially expressed between EV conditions from the RNA sequencing data. Reference genes/miRNAs were selected based on their high and consistent expression across all samples and conditions from the RNA sequencing data.

6.2.8 RNA concentration and size profile

Prior to carrying out RT-qPCR, all samples were analysed for their RNA concentration and quality using the Agilent 4200 (G2991AA) TapeStation (Agilent Technologies, Santa Clara, CA, USA) described in **Section 2.9.4.** RNA sample concentrations were obtained, shown in **Table 24.** Samples were then normalised to the lowest Ct value of 64.6 pg/µl and then carried forward for reverse transcription.

Table 24: Summary of RNA concentrations

The concentration of isolated RNA from the cell and EV samples was measured on the Agilent 4200 (G2991AA) TapeStation. Samples were normalised to the lowest concentration of 64.6pg/µl before being reverse transcribed.

	Condition	Sample	RNA Concentration (pg/ul)
Donor 1	Normoxic	Cells	640000
Donor 2	Normoxic	Cells	61000
Donor 3	Normoxic	Cells	174000
Donor 4	Normoxic	Cells	373000
Donor 1	Normoxic	EV	373
Donor 2	Normoxic	EV	122
Donor 3	Normoxic	EV	64.6
Donor 4	Normoxic	EV	421
Donor 1	Hypoxic	EV	368
Donor 2	Hypoxic	EV	445
Donor 3	Hypoxic	EV	451
Donor 4	Hypoxic	EV	1100
Donor 1	Normoxic/Primed	EV	298
Donor 2	Normoxic/Primed	EV	144
Donor 3	Normoxic/Primed	EV	87.3
Donor 4	Normoxic/Primed	EV	94.5
FBS EV		EV	386

The Agilent 4200 TapeStation also generated a size profile of the RNA length for cell and EV samples. All EV-RNA samples had a size distribution peak at 25nt with the exception of Donor 4 hypoxic EVs which deviated from this trend. A size profile peak around 25nt means that the isolated RNA comprises of short nucleotide structures, similar to the 21-25nt size profile of miRNAs. Donor 4 hypoxic EVs displayed a peak 200-500nt which indicates the presence of larger RNA structures in this sample **(Figure 62A).**

Cellular RNA samples showed two clear peaks at the 28S and 18S mark, shown in **Figure 62B.** RNA samples were run through a gel and a RIN was generated as an estimate of cellular RNA purity. The generated RIN represents the 28s:18s rRNA ratio and all cellular RNA samples had a RIN >9.3 indicating a high RNA quality **(Figure 62C)**.

A.

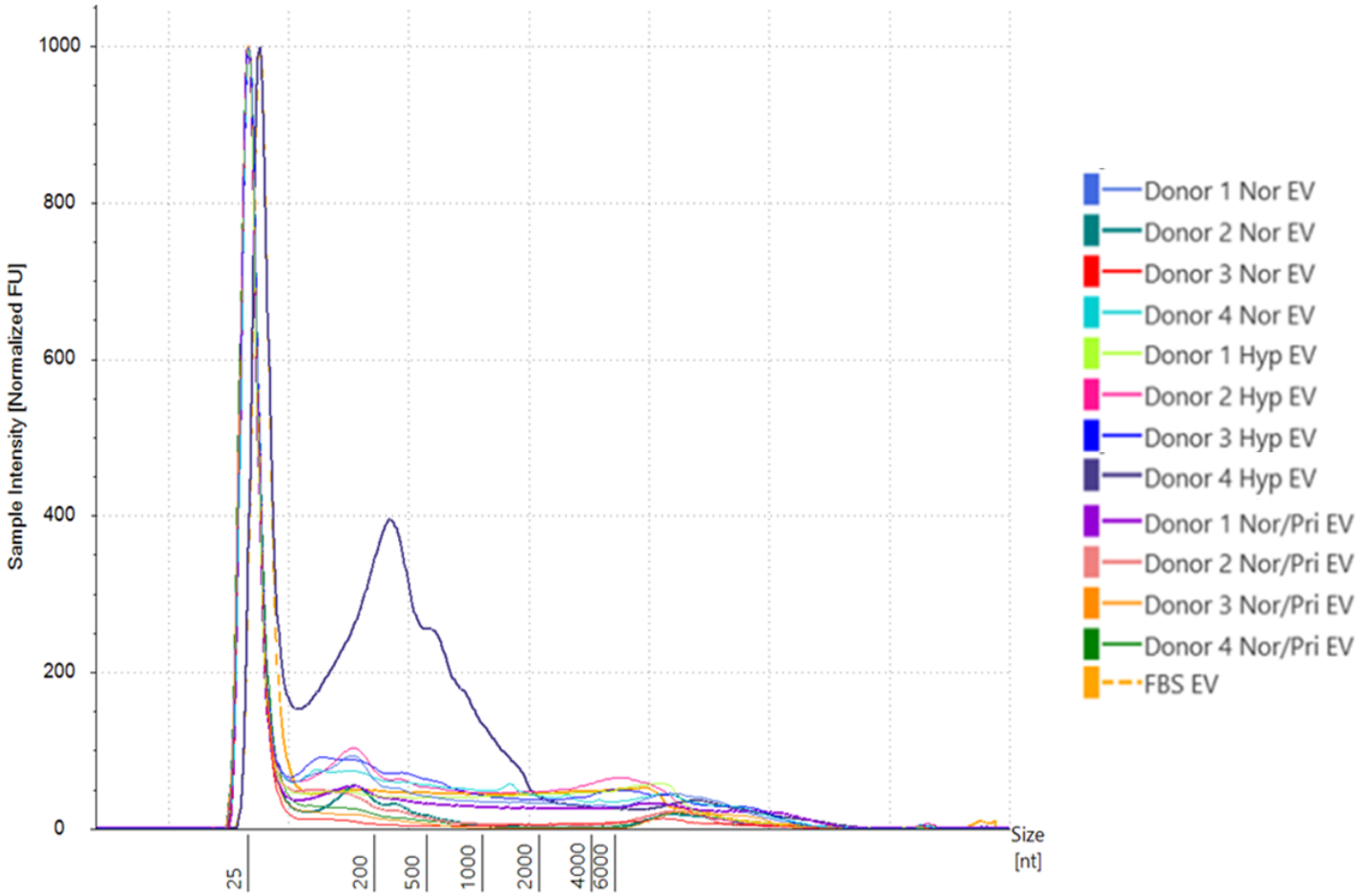
Sample Intensity [Normalized FU]
1000
800
600
400
200
0
25
200
500
1000
2000
4000
6000
Size [nt]
Donor 1 Nor EV
Donor 2 Nor EV
Donor 3 Nor EV
Donor 4 Nor EV
Donor 1 Hyp EV
Donor 2 Hyp EV
Donor 3 Hyp EV
Donor 4 Hyp EV
Donor 1 Nor/Pri EV
Donor 2 Nor/Pri EV
Donor 3 Nor/Pri EV
Donor 4 Nor/Pri EV
FBS EV

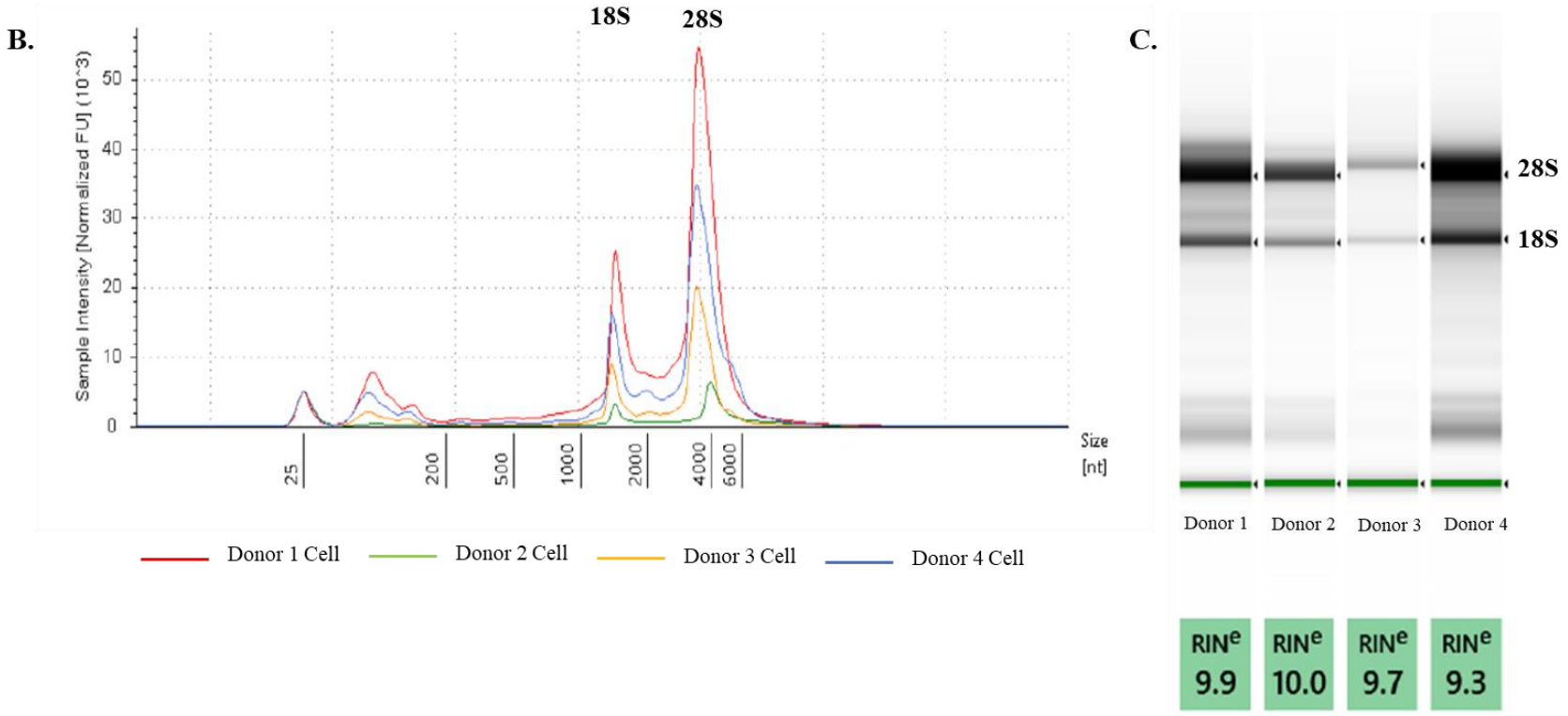

Figure 62: Comparison of cell and EV size distribution

A. *Electropherogram displaying the size distribution of EV samples. Sample Intensity in Normalised Fluorescent Units [FU] is shown on the y-axis and nucleotide size [nt] on the x-axis. All EV samples showed one strong peak around the 25nt mark except for Donor 4 hypoxic EVs which showed two peaks, one at 25nt and one ~200-500nt.* ***B.*** *Electrophoretogram displaying the size distribution of cellular RNA samples. Clear peaks were obtained at the 28S and 18S mark.* ***C.*** *Cellular RNA was run through a gel. Image displays two clear size bands at the 28S and 18S mark. All cellular RNA samples had a RIN value >9.3.*

6.2.9 Calibration of PCR data

RT-qPCR was carried out as described in **Section 2.9.9** and **2.9.10.** UniSp3 served as the inter-plate calibrator for the reactions. This was positively detected in each sample on the plate with an average Ct value of 18.8 (±0.15 SD). All samples were normalised to UniSp3 prior to data analysis of Ct values. UniSp6 was spiked into each sample before reverse transcription to monitor for cDNA synthesis and the presence of inhibitors in the reaction. The average Ct value for UniSp6 in all samples was 17.1 (±0.26 SD). There was a slight variation in hypoxic EV samples for UniSp6, with a Ct range of 16.9-17.5 but overall UniSp6 expression was consistent across samples **(Figure 63).**

Data from the multicomponent plots, provided in **Supplementary Figure *6***, show a consistent fluorescent signal in ROX, a passive fluorescent dye, indicating that there was little evaporation or bubbles affecting the reaction.

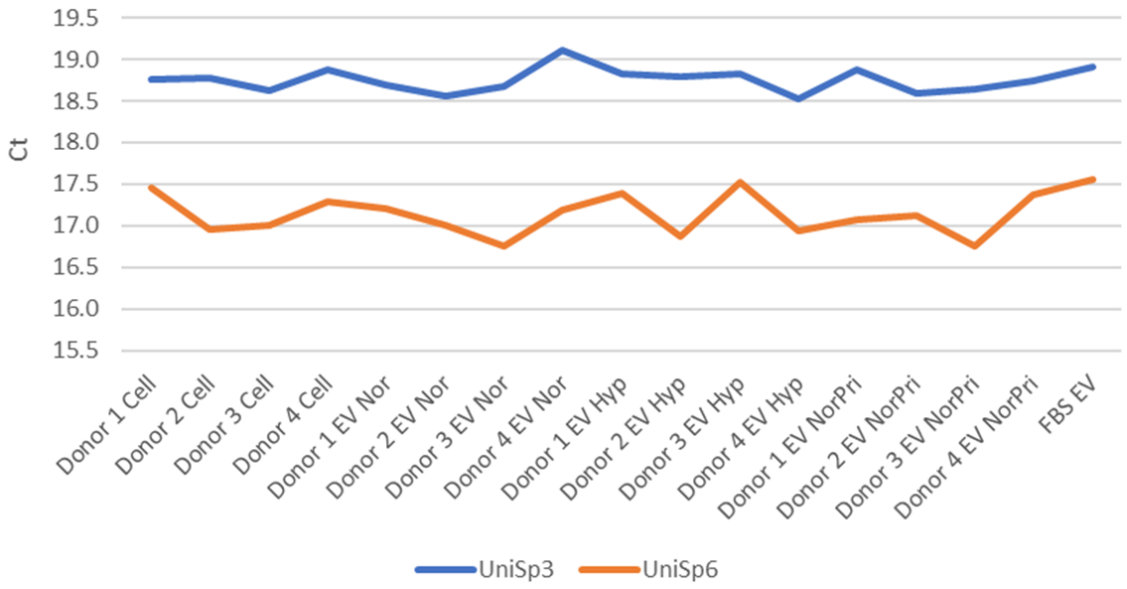

Figure 63: UniSp3 and UniSp6

UniSp3 was used as the inter-plate calibrator. Line graph displays Ct values on the y-axis and samples on the x-axis. UniSp3 (orange line) had an average Ct value of 18.8 (± 0.15 SD). UniSp6

(blue line) was spiked into the samples to assess for the quality of cDNA synthesis and presence of possible PCR inhibitors in the reaction. It had an average Ct of 17.1 (± 0.26 SD).

6.2.10 Reference gene selection

The reference/normaliser genes for PCR validation were chosen based on their high expression and similar read counts from the RNA sequencing data, which indicates stable gene expression. The resulting four miRNAs: miR-221-3p, miR-100-5p, miR-24-3p and miR-10a-5p, were chosen as reference genes and tested for in all samples via PCR.

miR-221-3p was selected as a single reference gene, as this was the only miRNA to be present in all samples and conditions from the RT-qPCR **(Figure 64A)**. MiR-10a-5p was under the detection limit of the instrument for all EV samples and therefore a Ct value was not generated, making it unistuiable for use as a reference gene. However, only one pair of primers was trialled for miR-10a-5p. Likewise, miR-100-5p and miR-24-3p were under the dectecion limit in Donor 1 Hypoxic EVs and a Ct value was not generated shown in **Figure 64B-C**, thereby also making these miRNAs unsuitable for use as a reference gene. As a result, miR-221-3p was the only reference miRNA that could be used for normalisation. All reference genes had variable Ct vales shown in the heatmaps in **Figure 64.** It is clear from the heat maps that there is a higher expresion of all reference genes in the cellular samples from each donor compared to the EV samples despite normalisation of RNA concentraiton before reverse transcription. This may indicate that there is a higher amount of miRNA per unit of total RNA in cells compared to EVs.

Figure 64D shows the amplification plot of miR-221-3p for all cell and EV samples. The resulting data shows that the FBS-EVs, which were run as a control for contamination, had the lowest amplification and therefore the highest Ct value of all samples tested (Ct 36.6) **(Figure 64D)**. The amplification plot displays the broad range of detected signals for the samples tested with the cell samples along with normoxic EVs from Donor 1 having the lowest Ct values.

A.

miR-221-3p

	Donor 1	Donor 2	Donor 3	Donor 4
Cell Normoxic	28.713	26.504	27.143	28.421
EV Normoxic	33.480	30.841	33.472	31.108
EV Hypoxic	33.837	35.393	32.606	32.182
EV Normoxic/Primed	31.524	32.425	30.870	31.964

B.

miR-100-5p

	Donor 1	Donor 2	Donor 3	Donor 4
Cell Normoxic	29.443	26.749	27.689	28.816
EV Normoxic	34.865	32.948	35.646	31.191
EV Hypoxic		33.248	31.883	33.579
EV Normoxic/Primed	33.500	32.756	32.073	32.039

C.

miR-24-3p

	Donor 1	Donor 2	Donor 3	Donor 4
Cell Normoxic	27.901	25.514	26.361	26.676
EV Normoxic	33.541	32.543	35.923	33.983
EV Hypoxic		33.270	32.844	33.954
EV Normoxic/Primed	31.701	33.067	29.386	31.851

D.

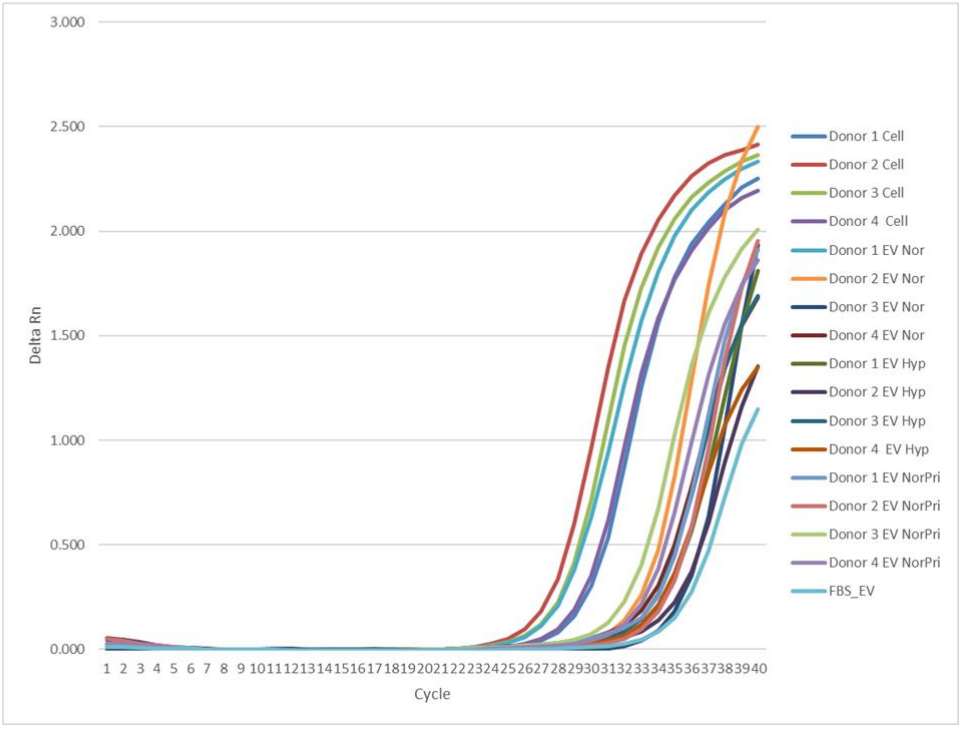

Figure 64: Heatmap and amplification efficiency of reference genes

Heatmaps displaying the Ct values of miR-221-3p ***(A)****, miR-100-3p* ***(B)*** *and miR-24-3p* ***(C)****. The lower Ct values are shown in red and the higher Ct values are shown in green. MiR-100-3p and miR-24-3p were undetected in Donor 1 hypoxic EVs, shown by missing values.* ***(D)*** *The amplification plot of miR-221-3p was compared between samples and conditions. Delta Rn values are shown on the y-axis and cycle number on the x-axis. There was a variable amplification of all samples with FBS-EVs showing the poorest amplification of miR-221-3p.*

6.2.11 MiR-21-5p and miR-24-3p statistically higher expression in UCMSCs

PCR was caried out on a selection of miRNAs listed in **Table 12.** After miRNAs were normalised to miR-221-3p, the relative miRNA expression was calculated, and compared between samples and conditions. The normoxic UCMSCs had a statistically higher expression of miR-21-5p (p=0.023) and miR-24-3p (p=0.014) compared to the normoxic EVs (**Figure 65A)**. There was no further statistical difference between the cells and EVs for the other miRNAs tested (**Figure 65B).** MiR-100-5p contains a numerical outlier for Donor 4 EV normoxia, where this sample is on average 3.4 times higher than the other three samples. On removal of this sample, the UCMSCs have a statistically higher expression of miR-100-5p compared to normoxic EVs (p=0.002), however, this sample was not removed from the final data analysis as it still may be a biologically genuine expression. MiR-139-5p was only detected in one of four cell donors compared to two of the four EV donors, therefore this miRNA did not generate enough data points for further statistical analysis. MiR-10a-5p was detected in normoxic cells (average Ct 34.6) but did not appear in EV samples showing that this miRNA either was not transferred from cells to EVs or had a very low expression, below the limit of detection of this assay.

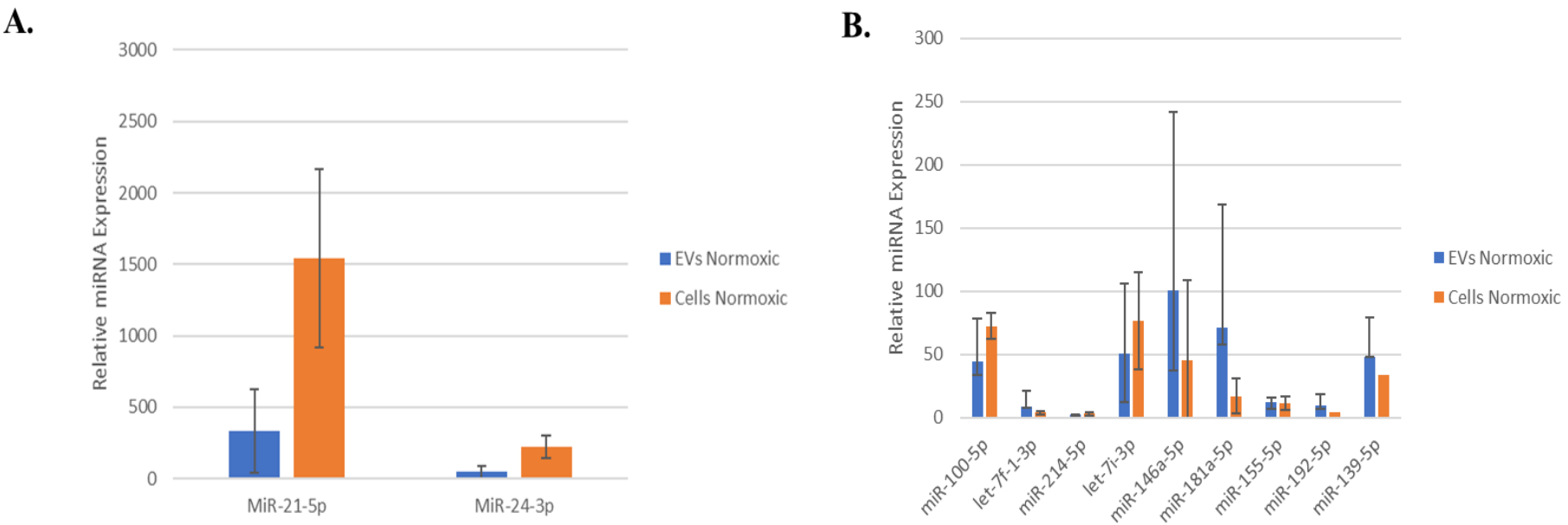

Figure 65: Comparison of relative miRNA expression between cells and EVs

A. *PCR analysis revealed that UCMSC (cell) samples had a statistically higher expression of miR-21-5p ($p<0.05$) and miR-24-5p ($p<0.05$) compared to EVs from the same condition.* ***B.*** *There were no statistical differences between cells and EVs with respect to the relative expression of miR-100-5p, let-7f-1-3p, miR-146a-5p, miR-181a-5p and miR-155-5p ($p>0.05$). Relative miRNA expression in shown on the y-axis and miRNAs on the x-axis.*

6.2.12 EV-miRNAs unchanged between conditions

The expression of miR-21-5p, miR-214-5p, let-7i-3p, miR-24-5p, miR-100-5p, let-7f-1-3p, miR-146a-5p, miR-181a-5p, miR-139-5p, miR-192-5p and miR-155-5p was analysed in the normoxic, hypoxic and normoxic/primed EVs. There were no statistical differences in the expression of any of the above miRNAs between normoxic and hypoxic EVs **Figure 66A)** and between normoxic and normoxic/primed EVs ($p>0.05$) **(Figure 66B).** MiR-155-5p was not detected in any hypoxic EV sample so this miRNA was excluded from further comparisons with this group. Likewise, Let-7f-1-5p was only detected in one hypoxic EV donor with a high Ct of 37.6, so this sample was also excluded from the analysis.

All cell and EV samples were highly heterogeneous seen by large error bars on the bar charts **(Figure 66).** The top 3 expressed miRNAs in the normoxic EV group included miR-21-5p, miR-146a-5p and miR-181a-5p. Hypoxic EVs also contained a high expression of miR-21-5p and miR-146a-5p, along with miR-100-5p. Within the normoxic/primed EV group, miR-21-5p, let-7i-5p and miR-24-5p showed the highest relative expression. There were no statistical differences between these groups.

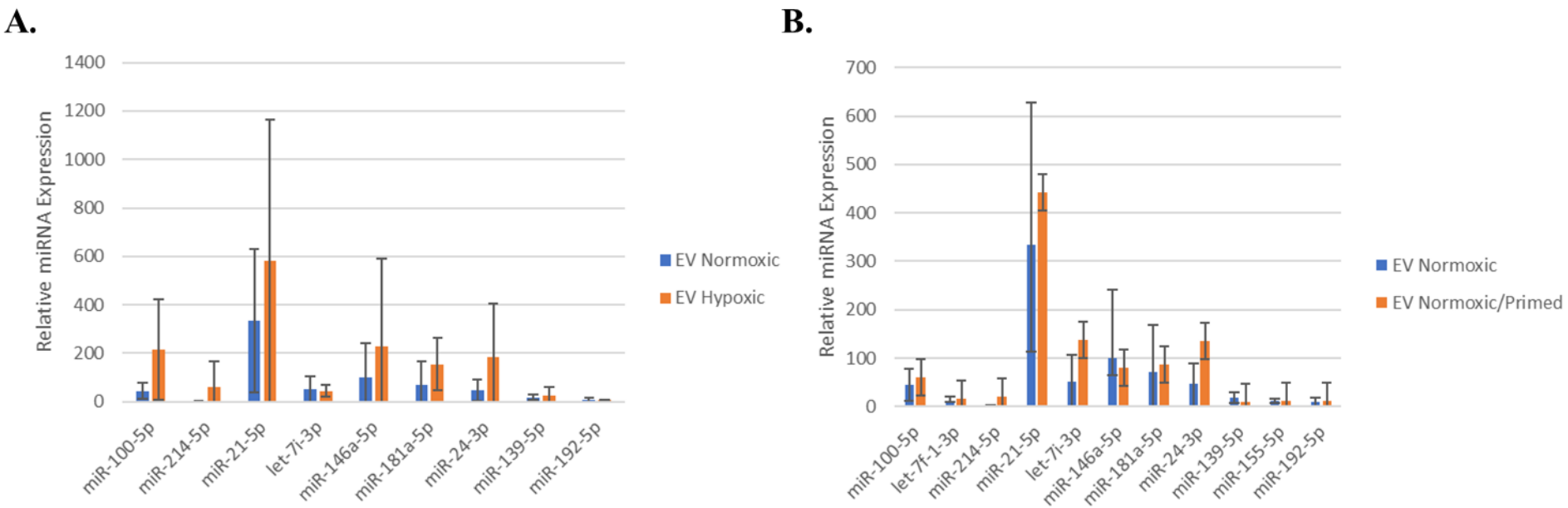

Figure 66: Comparison of miRNA expression in EVs from different conditions

There were no statistical differences in miRNA expression between ***(A)*** *normoxic and hypoxic EVs and between* ***(B)*** *normoxic and normoxic/primed EVs (p>0.05). Relative miRNA expression in shown on the y-axis and miRNAs on the x-axis.*

6.2.13 Identification of miR-21-5p in FBS-EVs

FBS-EVs (n=1) were run in triplicate on PCR to control for potential contamination in the reaction. The FBS-EVs were probed with the same miRNA profile as the cell and EV samples. Of the three repeated PCR runs, two out of three runs generated undetermined Ct values for the miRNA panel, indicating little presence of these miRNAs in the FBS-EVs. MiR-21-5p was the only miRNA to be detected in two FBS-EV samples. Its relative miRNA expression was statistically lower than the cell samples ($p<0.05$) but there was no statistical difference between the FBS-EVs and the normoxic, hypoxic and normoxic/primed EVs, indicating that the source of miR-21-5p could be of bovine nature in the EV samples **(Figure 67A).** There was some variability in the expression of miR-21-5p amongst the donors seen by the large error bars although this could not be linked to one specific donor.

The expression of miR-21-5p could be considered as a genuine expression in the FBS-EVs given the smooth, single peak seen on the melt curve analysis **(Figure 67B)**. The two peaks seen for miR-21-5p in the Donor 4 hypoxic EV sample indicate the SYBR green has bound non-specifically to some products in the reaction. As the second peak has a higher temperature melting point, it is possible that it contains genomic DNA contamination, and this sample Ct value must be considered with caution.

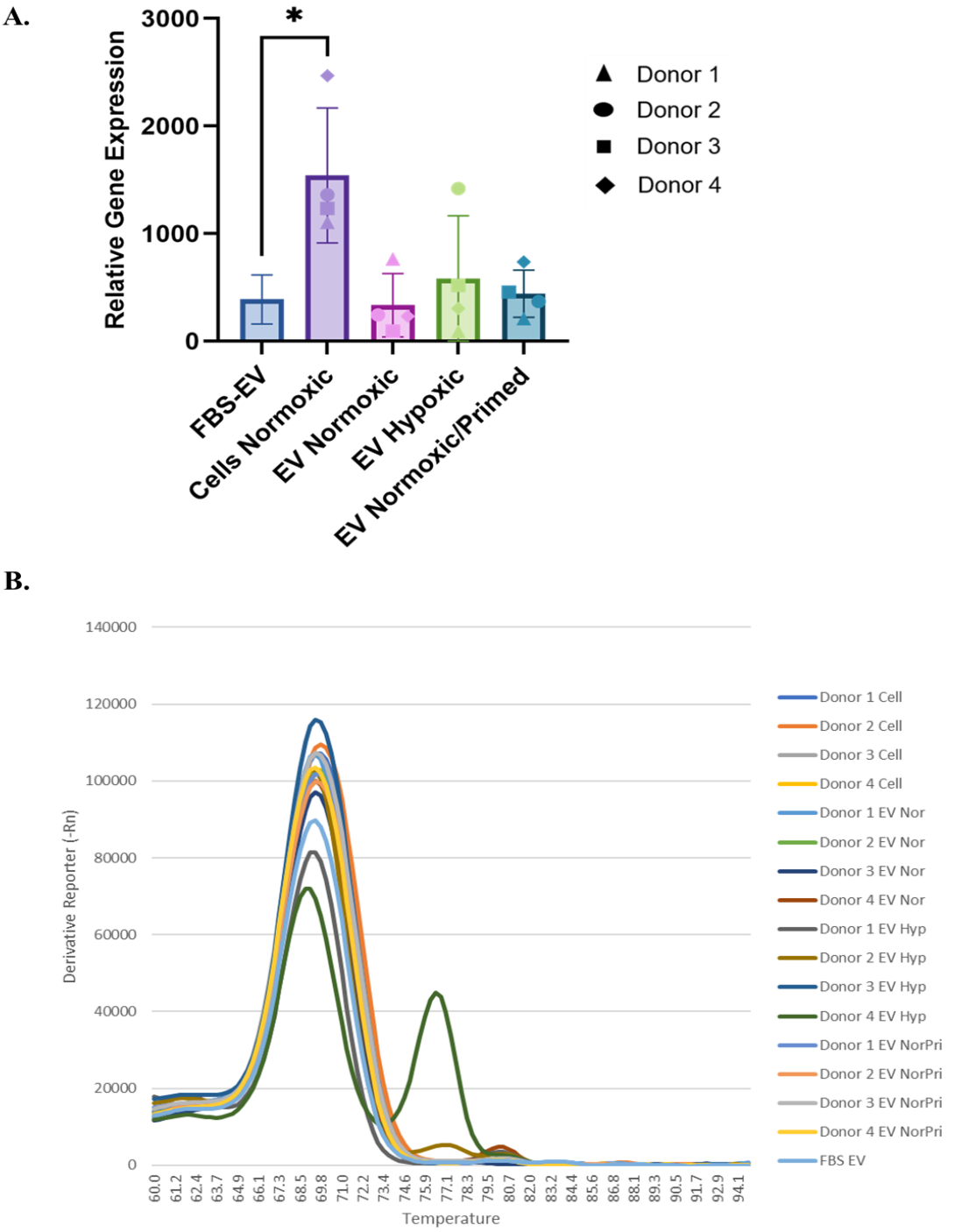

Figure 67: Expression of miR-21-5p

A. *Bar chart shows the relative miR-21-5p expression on the y-axis and samples on the x-axis. MiR-21-5p was positively expressed in FBS-EVs. There was a statistically higher relative expression of miR-21-5p in cell samples (p=0.03), but no statistical difference between FBS-EVs and other EV samples.* ***B.*** *Melt curve analysis revealed a single peak for miR-21-5p in FBS-EVs. A double peak was present for Donor 4 hypoxic EVs indicating potential contamination. Temperature is displayed on the x-axis and Derivative Reporter signal on the y-axis.*

6.3 Discussion

This chapter looked at the miRNA profile of EVs obtained through NGS and PCR. To our knowledge, the RNA from UCMSC-EVs has never been sequenced for small RNAs in hypoxia and pro-inflammatory primed conditions, so the data obtained in this chapter adds novelty to this research and a greater understanding of miRNAs in UCMSC-EVs.

This chapter firstly looked to control for the possibility of non-vesicular RNAs in the EV preparation. The EV suspensions were treated with proteinase K and RNase A to digest any protein complexes and degrade any non-vesicular RNAs. Results showed that there was an 87.7% decrease in RNA concentration after treatment of Proteinase K and RNAase which shows removal of non-vesicular miRNAs **(Section 6.2.1.1)**. This is consistent with another study that showed that 15% of miRNAs in plasma were associated with vesicle structures [226]. This proteinase K/RNase A digestion step was performed on all EV samples prior to RNA extraction to ensure a high confidence that the miRNAs are vesicle associated.

The first objective of this chapter was to identify differences in miRNA expression between normoxic cells and their EVs through RNA sequencing. An overview of the data was achieved through generating a PCA plot and this showed that there was separate grouping of EVs and cells, which indicates that the EVs have a different miRNA profile to their parent cells **(Figure 56B)**. Additionally, large shifts in miRNA expression were not identified as the different EV culture conditions did not cluster together on the PCA plot; this indicates that the different culture conditions did not have a large or unilateral impact. This polarised EV-miRNA profile has been found in other studies of MSC-EVs [460]. It

showed that the EVs were highly heterogeneous and had high donor-to-donor variation in terms of their miRNA profile. Additionally, the RNA content of EVs is dependent on their biogenesis pathway, and the condition of the cells upon EV isolation, which leads to further variability in the EV-RNA profile [227,461]. This heterogeneity is problematic for the potential of EVs to be used a clinical treatment. This is because variability in the miRNAome makes it difficult to predict their EV functions *in vivo,* and it may require all isolated EV preparations to be analysed using an omics approach before use, which is not feasible or cost-effective for most research groups. Despite this, there were some statistically significant differences between the cell and EV samples, and between the EV conditions.

There were 61 differentially expressed miRNAs between cells and EVs; 59 miRNAs were expressed at higher levels in EVs compared to cells, and two miRNAs were expressed at higher levels in cells compared to EVs. This indicates that specific miRNAs were selectively packaged into EVs, a finding commonly reported in the research [134,188,448,460]. Although, this could be the result of differences in miRNA enrichment in cells compared EVs. The low abundance miRNAs may be not as easily detectable in the cells because they have a large amount of high abundance miRNAs. Nevertheless, this study would have benefitted from pathway analysis to see if these 59 enriched miRNAs in EVs were associated. Identification of a shared pathway is important to predict the possible differences in functioning between cells and EVs. This pathway analysis was trialled on the 59 enriched miRNAs in EVs, but the input data generated too many ‘hits’ and required filtering, a process that introduces bias into the results, therefore, it was avoided for this study but should be considered for further investigation.

It has been reported that different culture environments such as hypoxia [462,463] and TNF-α priming [464] can alter the RNA content of EVs and equally their parent cells. Therefore, another objective of this chapter was to identify differences in miRNA expression between EVs from normoxic, hypoxic and normoxic/primed conditions through RNA sequencing. The identified miRNA profiles have been researched with an emphasis on anti-inflammatory properties for the treatment of RA.

Hypoxic EVs showed a downregulation of two miRNAs: miR-215-5p and miR-192-5p. Both miR-215 and miR-192 are located on the same chromosome and have the same seed sequence [465]. Likewise, both have been linked to a reduction in cell proliferation [466]. From reviewing the literature, miR-215-5p shows little immunosuppressive potential and most of the research centres on its increased expression in cancers [465,467], and its promotion of tumour progression [468]. Similarly, miR-192-5p has been linked to lung cancer [186] and hepatocellular carcinoma cancer stem cell development [469].

In terms of the immunoregulatory potential of miR-192, it was found in low levels in the blood of children with asthma but, when upregulated, it was able to block the activation of follicular helper T (Tfh) cells by targeting CXCR5 [470]. Tfh cells are present in many autoimmune diseases such as RA and they play a role in stimulating B-cells to produce antibodies [470]. Through blocking the actions of Tfh cells, miR-192 may be able to dampen a heightened immune response. Research also shows that transfection of miR-192 into airway smooth muscle cells decreased MMP-16, IL-4, IL-5, IL-13, iNOS and COX-2 expression is asthmatic mice [471]. MiR-192 also targets and silences macrophage inflammatory peptide (MIP)-2, where it has been identified as a possible therapy for active ulcerative colitis patients [472]. However, the anti-inflammatory role of miR-192 requires

further investigation as another research group found that hepatocyte-derived exosomal miR-192 activated M1 macrophages which also correlated with hepatic inflammation and an increase in IL-6 and TNF-α [473]. Furthermore, high levels of miR-192 are associated with unfavourable outcomes in stroke as it is positively correlated with systemic inflammatory response [474]. The discrepancies in the literature add doubt as to whether miR-192 is pro- or anti-inflammatory. In all, there is little difference between hypoxic and normoxic EVs, and neither show a significantly differing miRNA profile that would distinguish them as being more potent immunosuppressors.

In contrast, there were more differences identified between the normoxic and normoxic/primed EVs. Specifically, normoxic/primed EVs showed an upregulation of let-7f-1-3p, miR-139-5p, miR-140-5p, miR-193a-5p and miR-214-5p, and a downregulation of miR-3179 compared to normoxic EVs. One study compared IFN-γ primed UCMSCs with non-primed UCMSCs using an miRNA array and found 8 differentially expressed miRNAs, which is similar to the findings of this study [475].

When the differentially expressed miRNAs are considered individually, their functions *in vivo* are diverse, and many are understudied with regards to immune modulation. There is little research on the upregulated let-7f-1-3p but its forward strand let-7f-5p has some anti-inflammatory properties associated with the silencing of Nod-like receptor pyrin domain-containing protein 3 (NLRP3) inflammasome, which alleviated inflammation in a murine SLE model [476]. MiR-139-5p was also upregulated in normoxic/primed EVs compared to normoxic EVs, which is not surprising as other studies have shown that this miRNA can be upregulated and exclusively shuttled into EVs upon pro-inflammatory signalling

[477,478]. Many studies have focused on the anti-oncogenic properties of miR-139-5p in gastric cancer [479,480] or it role in osteogenesis [481,482] although findings are mixed with some research showing that is inhibits osteogenic differentiation [27] and some showing that it positively regulates osteogenic differentiation in BMMSCs [28]. In terms of miR-139-5p role in inflammation, overexpression of miR-139-5p was found to inhibit MMP9, MMP7, cell proliferation, and pro-inflammatory cytokines (IL-1β, IL-6, TNF-α) in colorectal cancer cell lines [483]. Its mechanism of action involved the suppression of the NF-κB pathway; a signalling pathway which is known to boost the production of pro-inflammatory cytokines [483,484]. Contrary to this, Katsumi et al. [485] showed that high expression of lymphocyte derived miR-139-5p inhibited cFOS, a proto-oncogene, which led to an increase in the production of TNF-α through the NF-κB pathway in hepatocyte-derived carcinoma cells. Again, its mechanism of action was targeting the NF-κB pathway, but the outcome was different to the aforementioned Zhu et al. [483] study.

Other upregulated miRNAs in normoxic/primed EVs were miR-193a-5p, miR-140-5p and miR-214-5p. MiR-193a-5p is a commonly detected miRNA in MSCs [486] but few studies have looked at its role in inflammation. One study found that miR-193a-3p improved intestinal inflammation through targeting the NF-κB pathway [487], but besides this, it's function in inflammation is relatively unknown. MiR-140-5p is commonly enriched in undifferentiated MSCs and has roles in suppressing osteogenesis [488] and promoting chondrogenesis [489,490]. One study, transfected miR-140-5p into synovial MSCs and their exosomes were applied to a rat model of osteoarthritis (OA) [490]. Those that received miR-140-5p transfected exosomes had milder OA symptoms and a thicker cartilage/collagen type II matrix than the exosome group without miR-140-5p [490]. This showed that miR-140-5p slowed down the progression of OA and prevented a severe OA

phenotype. Lastly, miR-214 is commonly secreted by cancer cells and is associated with cancer progression through targeting of the tumour suppresser gene PTEN [491,492]. Although, when delivered to CD4+ T-cells, miR-214 promoted Treg expansion and the production of IL-10, and through this immune suppressive role, it promoted tumour cell growth [492]. The downregulation of miR-214 in human umbilical vein endothelial cells (HUVECs) was associated with an increase in vascular endothelial cell apoptosis and inflammatory factors (TNF-α, IL-1β, IL-6, IL-18) suggesting that miR-214 may be a suppressor of vascular inflammation [493]. Similarly, its anti-inflammatory role was supported by a study of murine kidney disease which showed that the upregulation of miR-214 inhibited TLR4 expression and reduced inflammation [494]. However, few studies have looked at the immunosuppressive role of miR-214-5p in MSCs.

One area of concern when looking at the profile of miRNAs from different EV conditions is the range of different functions they have, and a lot are associated with different cancer pathways. Other studies that looked at miRNAs in UCMSCs have also a found connection to cancer and endocytosis, similar to the findings of this study [495]. This means the EVs may target other *in vivo* functions and not be specific to immune modulation. To get a clearer overview of the collective functions of the differentially expressed miRNAs, pathway enrichment analysis was trialled on the 5 upregulated miRNAs in the normoxic/primed EVs and the 2 downregulated miRNAs in the hypoxic EVs using the miRNet, a web-based tool designed to create network-based visualisations [230]. This analysis was done on an exploratory basis and input from a researcher with biostatistics experience is required for validation. Both KEGG and GO: Biological Process databases were used. Findings from this analysis support the role of the normoxic/primed miRNAs in cancer pathways, and as the upregulated miRNAs were also enriched in the ‘negative

regulation of cell proliferation' pathway, this suggest that the normoxic/primed EVs may be inhibiting cell growth more than the normoxic EVs. Interestingly, angiogenesis and vasculature development were associated with the normoxic/primed EVs, this was expected to be seen in the hypoxic EVs due to strong research connections between hypoxia and angiogenesis [437]. The two downregulated miRNAs (miR-215-5p, miR-192-5p) in hypoxic EVs were associated with cell cycle processes, suggesting the normoxic EVs may be stronger mediators of cell growth **(Figure 61** and **Table 23).**

In all, the data generated from the GO: Biological Process database strongly supports the analysis from the KEGG database and may suggest that the upregulated miRNAs in the normoxic EVs better support cell division and regeneration. Of relevance to this study was the potential identification of miRNAs with anti-inflammatory properties. Enrichment analysis from both databases did not find many 'hits' to immune modulatory functions from the differentially expressed miRNAs. This does not mean that they are not anti-inflammatory but rather that it is not their main function. Additionally, it is recognised that this is just a basic pathway analysis involving a few miRNAs and a more robust analysis of the whole RNA sequencing data set is required.

Further target prediction was carried out using three bioinformatic tools: miRNet [230,231], miRDB [232,233] and TargetScan (v.7.2) [234]. These three target prediction tools offer three different computational approaches to identify gene targets of miRNAs. MiRNet uses knowledge from 11 different databases to generate target predictions [230,231], miRDB is a bioinformatics tool that predicts miRNA targets using MiRTarget2 and PANTHER databases. The miRDB target prediction algorithm includes 3.5 million

predicted targets by 7000 miRNAs [233,496]. Lastly, TargetScan predicts miRNA gene targets by identifying 7-8nt sites complimentary to the seed region of the miRNAs [234]. All three web-based programmes identified miR-140-5p to directly target VEGFA, so there is a high probability that this prediction is accurate. VEGFA was found in the protein cargo of all EVs, but there was no statistical difference in VEGFA protein expression between the normoxic and normoxic/primed EVs. As miR-140-5p is upregulated in normoxic/primed EVs and targets VEGFA, this may mean that these EVs counteract the production of this protein in their target cell and are overall more anti-angiogenic compared to the normoxic EVs. Indeed, previous research shows that miR-140-5p is a genuine target of VEGFA and plays a role in inhibiting angiogenesis [497,498]. Additionally, from the analysis of the miRNAs with the highest expression in all EVs, it was identified that miR-21-5p targeted CCL20 and let-7i-5p targeted IL-13. This is further confirmed in the literature [499,500]. While miR-21-5p acts to silence the translation of CCL20, the higher protein expression of CCL20 in normoxic/primed EVs may promote chemotaxis more than the other EV conditions. Further analysis is required to establish if the expression of miR-21-5p is high enough to completely reduce the chemotactic properties of target cells through targeting CCL20. IL-13 gene was also a direct target of let-7i-5p. IL-13 has anti-inflammatory functions and the silencing of this gene by let-7i-5p would reduce the anti-inflammatory properties of target cells. However, IL-13 is present in higher amounts in the primed EVs, which may balance out the silencing effects.

Another area of concern is the relatively low read count of the differentially expressed miRNAs from the RNA sequencing data, with the exception of miR-193a-5p. This questions whether the expression of these miRNAs is high enough to be biologically significant *in vivo*. Even if small changes are statistically significant they may not be worth

investigating due to their low expression [501]. For this reason, it is worthwhile looking into the functions of the three most expressed miRNAs (miR-21-5p, miR-100-5p and let-7i-5p) which were common across all samples and conditions.

MiR-21-5p has a strong association with cancer and immune cells, but it has also been found in UCMSCs and UCMSC-EVs [445], although its exact functions have yet to be discovered. Most of the studies into miR-21-5p involve its overexpression in cancer by counteracting tumour suppression genes [502,503]. It is also associated with neovascularisation, angiogenesis, cell survival and osteogenic differentiation [188,504–507]. But, miR-21-5p's role in inflammation is more complex [508]. Some studies show that it can stimulate the immune system. For example, miR-21-5p was found to enhance GM-CSF, a cytokine which supports eosinophil survival [509]. It was also found to promote T-cell activation and proliferation by targeting APK/ERK and MAPK/JNK signalling pathways and by promoting activator protein 1 and IL-2 expression [510].

Other studies show that miR-21-5p may have anti-inflammatory properties by inhibiting IL-12 which reduces Th1 cells and promotes Th2 cells, which are strong contributors in autoimmune disease [508]. It can also positively regulate FoxP3 expression in Tregs cells [511] and MSC-EV derived miR-21-5p reduces CCR7 expression on dendritic cells [460]. CCR7 is increased in the synovial tissue in RA and contributes towards the pro-inflammatory environment [512], therefore the downregulation of CCR7 by MSC-EVs is a positive step towards identifying MSC-EV immunosuppressive abilities. MiR-21-5p was found to be downregulated in RA patients compared to healthy controls, which may explain why there was a low level of Tregs and a high level of Th17 in RA patients, this suggests

that miR-21-5p may be contributing to Th17/Treg imbalance, a common feature of RA pathogenesis [513]. However, a separate study on the role of miR-21-5p in RA showed that when it was upregulated by IL-34 and Stat3 activation, it promoted the survival of fibroblast like synoviocytes which infiltrate the joint and cause inflammation [514]. Therefore, there is some disparity over the role of miR-21-5p in RA disease progression. This diversity in functions of miR-21-5p could be due to its involvement in multiple signalling pathways making it difficult to evaluate if it has a potential immunosuppressive involvement in UCMSC-EVs.

The second most expressed miRNA in cells and EVs was miR-100-5p. This miRNA is enriched in endothelial cells and was found to reduce vascular inflammation by suppressing endothelial cell adhesion molecules which improves leukocyte–endothelial interactions [515]. Its expression is also associated with reduced inflammatory cell count in patients with cardiovascular disease [515] and the suppression of pro-inflammatory cytokines (IL-6, IL-8, MMP1, MMP3, MMP9, MMP13) in temporomandibular joint OA [516].

The third most expressed miRNA in cells and EVs was let-7i-5p, which is cited as having anti-inflammatory properties in many studies. Xiang et al. [185] showed that Let-7i could reduce inflammation and protect human brain microvascular endothelial cells in an oxygen-glucose deprivation model. Let-7i carried out it's anti-inflammatory effects by silencing the expression of TLR4 mRNA, MMP9 and iNOS [185]. Let-7i was found to be downregulated in leukocytes of patients with ischaemic stroke and the lower level of let-7i was correlated with stroke severity and an increase in MMP9 levels [517]. Pathway analysis revealed that Let 7i targeted CD86, HMGB1b and CXCL8 genes, all three of which have a role in inflammation [517]. Let-7i, found in cardiac fibroblasts was also found to reduce

cardiac inflammation and fibrosis in mice by inhibiting the expression of IL-6 and collagens (Col1a2, Col3a1, Col4a1, Col5a2) [518]. In all, these studies shown that let-7i-5p has the potential to modulate immune responses.

When considering the miRNA profile of normoxic/primed EVs and especially the upregulated miRNAs, many connections can be made to anti-inflammatory functions, but the role of these miRNAs in MSCs and MSC-EVs is largely understudied. Therefore, knowledge on their functioning must be drawn from the function of these miRNAs in other cell types. Additionally, the roles of the 12 uniquely expressed miRNAs in EVs are understudied and thereby difficult to make any functional connections.

An objective of this chapter was to validate the RNA sequencing results through RT-qPCR to ensure that the data gathered was valid and reliable. In order to analyse the PCR data, the miRNA of interest must be analysed against an endogenous reference miRNA, also known as a 'reference gene'. This reference gene must be active, abundant and stably expressed across all samples and conditions [519,520]. As reference genes are an essential part of RT-qPCR validation, it is recommended to choose at least three [227]. This experiment initially chose four reference genes (miR-221-3p, miR-24-3p, miR-100-5p, miR-10a-5p) for the purpose of validation data to make the study more robust. However, miR-10a-5p failed to amplify in EVs and, miR-100-5p and miR-24-3p failed to show amplification in hypoxic EVs from Donor 1, making them unsuitable for use as reference miRNAs **(Figure 64).** It unlikely that the hypoxic conditions were negatively regulating the expression of this miRNA in this donor, as the presence of this miRNA was found in other donors from hypoxic conditions. Furthermore, it is unlikely that there were inhibitors

in the reaction as UniSp6 amplified normally across plates. Therefore, the lack of expression of miR-100-5p and miR-24-3p in hypoxic EVs Donor 1 could be attributed to donor specific differences, but overall, the lack of consistent miRNA expression in the chosen reference genes questions the validity of the RNA sequencing data.

The chosen reference gene, miR-221-3p, did not show a stable expression across all donors and conditions which made the analysis of the relative miRNA expression challenging. It is difficult to identify stably expressed reference genes in EV research as genes are often differentially sorted into EVs introducing an inconsistent gene expression in different EV samples [227]. It could be argued that a reference gene selection tool would have employed a more stringent reference gene selection process. Tools such as NormFinder, GeNorm, and BestKeeper have been reported in the literature as reliable resources to achieve this goal [520]. All these tools use different types of statistical modelling to identify the most stably expressed reference genes. Instead, the reference gene selection for PCR was chosen based on the existing data generated from the RNA sequencing experiment. In hindsight, the use of a gene selection tool would have added an extra layer of certainty to the selection. However, due to the highly heterogenous nature of EVs, it is likely that expression levels will vary regardless of the method chosen.

To ensure consistency between PCR plates, UniSp3 was chosen as the inter plate calibrator for the PCR reactions. All samples were normalised against UniSp3 prior to data analysis to ensure a fair comparison. Overall, UniSp3 showed a consistent expression across plates shown by a small standard deviation of ±0.15 Ct. Additionally, UniSp6 was added to the samples before reverse transcription. The UniSp6 spike-in was added to identify potential

issues associated with cDNA synthesis and inhibition during PCR [227]. The consistent expression of UniSp6 from the amplification plot indicates that reverse transcription was successful and there was little presence of inhibitors in the reaction [521–523] **(Figure 63).**

The RNA sequencing data showed that let-7f-1-3p, miR-139-5p, miR-214-5p and miR-155-5p were all higher in normoxic/primed EVs and miR-192-5p was higher in normoxic EVs compared to hypoxic EVs. The PCR data failed to support this, showing no difference in relative miRNA expression between these conditions. The PCR results found that miR-21-5p and miR-24-3p had a higher relative expression in cell samples compared to normoxic EVs; the RNA sequencing data failed to corroborate these findings as no differences in miRNA expression were found between the samples. Interestingly, from the PCR data, normoxic EVs had a high relative expression miR-146a-5p and miR-181a-5p, and hypoxic EVs also expressed a high level miR-146a-5p compared to other miRNAs probed for in the assay. This is promising as these miRNAs from MSCs have been shown to suppress TNF-α, IL-6, IL-1β and pro-inflammatory gene targets [524–526]. Overall, the data from the PCR experiments provided a differing expression of the miRNAs in the cells and the EVs compared to the RNA sequencing results.

The final consideration of this study was to establish if there was contamination of FBS derived RNA in the EV samples. This step was carried out for two reasons; firstly research show that no supplemented media is free of EVs and an FBS control is strongly advised [527]. Secondly, previous experiments, described in **Section 4.2.1,** found that the depletion of EVs from FBS was not 100% successful therefore, there may be some bovine RNA present in the EV samples. To control for this, an FBS-EV sample was sequenced, and its expression compared with the EV samples. Results from this show that only one

differentially expressed miRNA (miR-215-5p) was higher in the sequenced FBS-EVs compared to hypoxic EVs. This miRNA was also downregulated in the hypoxic EVs when compared to the normoxic EVs. From the PCR experiment, only one miRNA, miR-21-5p, was detected in the FBS-EVs and showed a similar expression to the EVs. With the exception of miR-215-5p and miR-21-5p, all other miRNAs detected in FBS-EVs do not show a higher expression. Therefore, the degree of FBS contamination was determined to be minimal. However, it must be noted that it is difficult to gauge FBS RNA contamination due to sequence similarity between human and bovine sources. Therefore, FBS contamination cannot be ruled out.

This situation raises some interesting questions. Are they bovine miRNAs entering cells and being packaged into EVs? If so, what is the biological reason for the cells to package them? If the bovine miRNAs are not in the EVs, and are therefore extra-vesicular, is there the possibility that some miRNAs are resistant to the RNAase treatment? These are all some important questions for EV biology and discovering how EVs function.

This project has some limitations which hampered the analysis of the results. It was clear that there were few similarities in the EV profiles seen on the PCA plot, therefore this study would have benefitted from analysing just the EV conditions together and excluding the cellular group to see if more differences could be identified. Additionally, the PCA plot identified the EVs as being highly heterogeneous and showing donor-to-donor variation. This heterogeneity is problematic for EV research and for the potential to make concrete conclusions on the therapeutic potential of EVs. Thus, a higher sample size would have been advantageous to see trends in clustering. Therefore, a combination of factors could

explain the lack of differences in miRNAs between the EVs from different conditions. Namely, a low sample size, the heterogenic nature of EVs and the layout of the study design to include cellular samples in the analysis.

Secondly, in the PCR experiment, there was a lack of stable expression from the reference genes. This made normalising the miRNA expression challenging and more reference miRNAs could have been chosen based on the use of reference gene selection tools.

Finally, this study would have benefitted from pathway analysis of the whole RNA sequencing dataset and of the differentially expressed miRNAs in normoxic EVs versus cells. This is because miRNAs have multiple gene targets [495,528], and it would be more advantageous to review the miRNAs as a collective. This would give a stronger overview of their *in vivo* functions.

6.4 Conclusion

This chapter focused on identifying differences in miRNA expression between normoxic cells and normoxic EVs. 59 miRNAs were upregulated in EVs compared to cells indicating that the miRNAs were selectively being packaged into EVs. RNA sequencing also identified differences in the miRNA profile of EVs from normoxia, hypoxia and normoxia/primed, although these differences were few and not confirmed by PCR validation.

To answer the question, do the EVs and cells have anti-inflammatory miRNA? There is a degree of certainty that they contain miRNAs with anti-inflammatory properties, but the issue is that these miRNAs target many genes and may carry out other *in vivo* functions, thereby it is not possible to say that they will elicit a purely anti-inflammatory response.

It is equally challenging to identify an EV condition that has the most anti-inflammatory potential. The obvious frontrunner is the normoxic/primed EVs because they contained the most upregulated miRNAs and research supports findings that pro-inflammatory primed EVs are more immunosuppressive. However, the differentially expressed miRNAs had a low normalised read count which questions their ability to make a significant biological change *in vivo.* Even if these miRNAs had a higher expression, this does not necessarily mean these EVs are anti-inflammatory, as a combination of different factors are involved in generating an anti-inflammatory response.

Overall, it is promising to see some miRNAs with anti-inflammatory functions present in the EVs but there are doubts raised as to whether their expression is enough to be biologically significant, therefore functional studies are required.

Chapter 7: Functional analysis of UCMSCs and UCMSC-EVs

7.1 Introduction

Autoimmune diseases are often defined by a breakdown in immune tolerance whereby the immune system targets self-antigens [529]. In RA, this leads to an infiltration of immune cells (lymphocytes, dendritic cells, mast cells) into joints which causes pain, swelling and eventually joint destruction [34]. There is an imbalance of adaptive immune cells, in particular T-cells, which are one of the primarily contributors to an activated immune response [37,38]. In general, there is an abundance of Th1 cells over Th2 cells and Th17 cells over Treg cells [530,531]. Th1 cells release IFN-γ, and Th17 cells release IL-17, both of which are enriched in RA and contribute to a pro-inflammatory environment [532,533]. To counteract this pro-inflammatory response, IL-4 is secreted by mast cells, Th2 cells, eosinophils, and basophils. IL-4 is known to inhibit the maturation of Th1 cells and promote Th2 cells, this cytokine can help towards reducing the IFN-γ pro-inflammatory response [534,535]. IL-4 is also known to reduce the potency of dendritic cells and the levels of TNF-α [536]. However, despite the anti-inflammatory effects of IL-4, there is an imbalance of pro- to anti-inflammatory immune cells in RA. This can be seen by the abundance Th17 cells and the low levels of Treg cells which are often defective, thus contributing to RA disease pathogenesis [1,537].

The autoreactive immune response in RA often escalates in an uncontrollable fashion, therefore, identifying an immunosuppressive therapy is a high priority. This priority is heightened by the fact that many patients with RA do not respond well to pharmaceuticals which opens up a new opportunity for a more effective therapy for RA [10].

To tackle this problem and reduce the inflammatory immune environment, this chapter looks at the ability of MSCs and MSC-EVs to modulate the cytokine and surface marker profile of T-cells. The increased interest surrounding MSCs and their EVs is due to studies showing that they can suppress B- and NK- cells [184], polarise Th1 cells towards a Th2 phenotype and shift the Th17/Treg ratio in favour of Tregs [157,165]. Specifically, UCMSCs have been shown to increase Treg cells in a PBMC co-culture [86] and likewise, BMMSC-EVs were found to increase the number of FoxP3+ Tregs in a co-culture with PBMCs [538]. All this research has led to the emergence of MSC-EVs as a promising immunosuppressive treatment. Therefore, this chapter will also look at the percentage of Tregs in the PBMCs and see if these levels vary after co-culture with UCMSCs and UCMSC-EVs. For MSCs and EVs to be truly therapeutic agents for RA they will be able to shift the Treg: Th17 environment and reduce the level of pro-inflammatory cytokines. MSC-EVs have also been found to change the cytokine profiles of PBMCs/T-cells, particularly reducing TNF-α, IFN-γ and IL-1β, and increasing TGF-β in *in vitro* co-cultures [157,399]. This chapter will analyse if MSCs and EVs could increase IL-4 levels in the PBMC co-culture and decrease IFN-γ and IL-17A, as this would aid in the suppression of immune cells which exacerbate inflammation in RA.

Evidence points towards an immunosuppressive role of MSC-EVs, and their attraction as therapeutic agents over MSCs is heightened by the fact that they avoid some issues associated with injecting cells *in vivo* such as the potential for cell differentiation and tumour formation [66]. For this reason, research into EVs and their therapeutic properties is gaining momentum. However, no study has yet looked at the effect of normoxic and normoxic/primed UCMSC-EVs on PBMCs. It is important to see if UCMSC-EVs are a viable alternative to immune cell suppression as their parent cells, as they may present a

more suitable therapeutic option for RA. Furthermore, as research has shown that pro-inflammatory priming can improve MSC-mediated immunosuppression, it is important that this is analysed in the EV population [243].

The practice of pro-inflammatory priming MSCs is common in regenerative medicine as it mimics the inflammatory *in vivo* environment and 'activates' MSCs [243]. Similarly activating MSCs before EV generation is likely to be effective in promoting a potentially therapeutic 'anti-inflammatory' EV, so it was decided to look at both primed and non-primed MSCs and EVs in this chapter in normoxic conditions only. Results in previous chapters showed that there were more protein and miRNA differences identified between primed and non-primed in normoxia compared to those cultured in hypoxic conditions and, therefore, hypoxic conditions were not used.

Due to delays imposed by the Covid pandemic, there was not enough time to isolate CD4+ T-cells from the PBMCs so it was decided to use the whole PBMC population for the co-culture experiments and gate the lymphocytes as part of the flow cytometry analysis. This did not negatively affect the analysis of the immunomodulatory properties of MSCs and EVs as their co-culture with whole population PBMCs is studying the interaction of T-cells in their natural environment. However, the mixed population of PBMCs makes discovering the EV- and MSC- mediated effects on T-cells more challenging, as different interactions are happening between immune cells in the co-culture. Therefore, recognising the benefit of using an isolated population of T-cells, Jurkat cells were sourced as a readily available source of T-cells. Jurkat cells are an immortalised T-cell leukaemia line [539] that are utilised extensively in *in vitro* studies to simulate the function of primary T-cells and these

cells provided another means of studying MSC and EV interactions with T-cells. They also add novelty to this chapter as no study has looked at the immunomodulatory ability of MSC-EVs on Jurkat cells, there has only been one study by Matula et al. [540] that studied the uptake of MSC-exosomes by Jurkat cells.

This chapter looks at the functional properties of UCMSCs and their EVs and, specifically, if they can polarise PBMCs and Jurkat cells towards a more anti- inflammatory phenotype. Previous chapters have analysed the protein and RNA cargo of UCMSC-EVs, and findings revealed the presence of anti-inflammatory proteins and miRNAs. However, there were also some pro-inflammatory proteins and miRNAs contained within the EV cargo therefore, it is hoped that this chapter will shed light on whether UCMSC-EVs function as pro- or anti- inflammatory agents.

Aim

The aim of this chapter is to assess the immunosuppressive ability of UCMSCs and UCMSC-EVs on PBMCs and Jurkat cells.

Objectives

1. Assess the effect of CD3/CD28 activation on PBMCs and Jurkat cells by analysing cell morphology, surface markers and cytokine production before and after activation.
2. Establish the optimal concentration of EVs to co-culture with PBMCs. This will be achieved by co-culturing PBMCs with three concentrations of EVs and analysing the subsequent protein production of PBMCs.

3. Analyse the protein markers on PBMCs from different co-culture conditions using a combination of cell surface markers and intracellular markers via flow cytometry.
4. Identify the percentage of CD3+CD4+ cells, the IL-4: IFN-γ ratio and the percentage CD4+CD25+CD127- Tregs in PBMCs/Jurkat cells co-cultured with EVs and MSCs.

An outline of the co-culture experiments is provided in **Figure 68.**

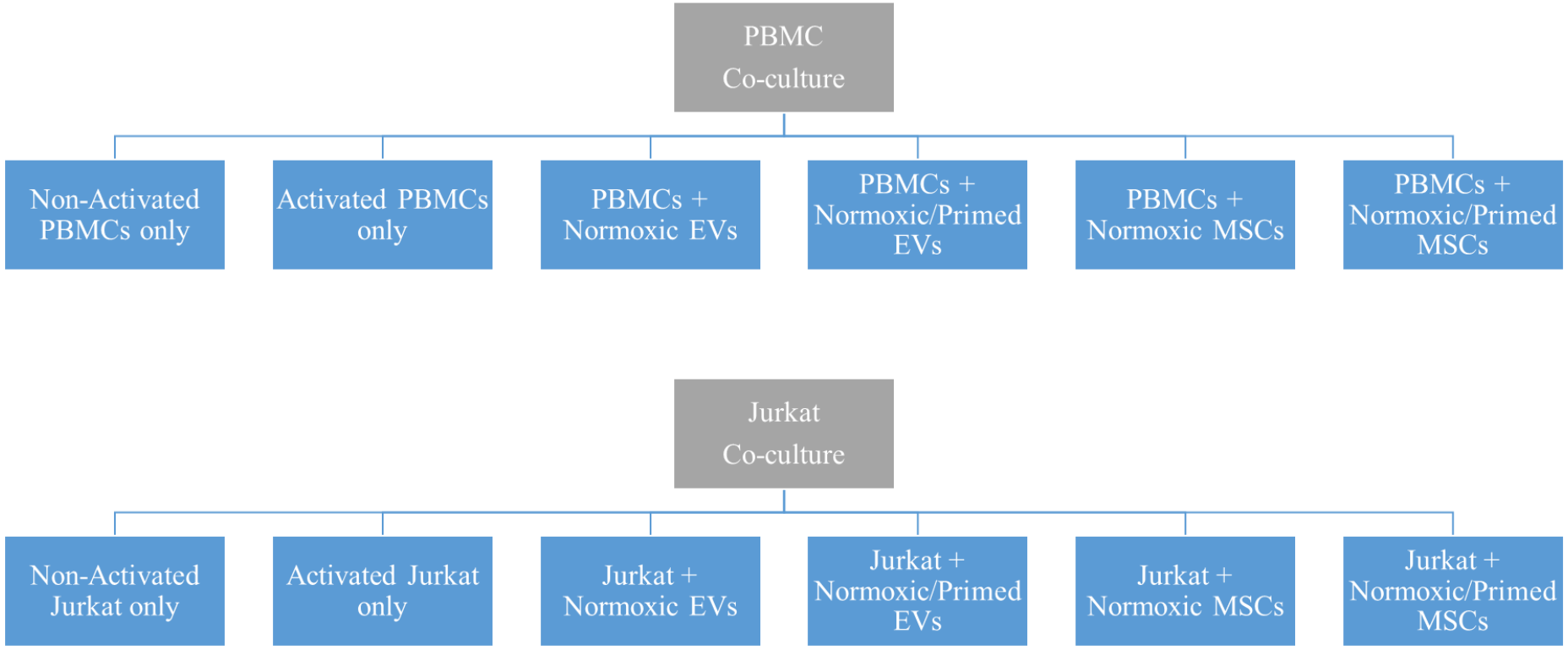

Figure 68: Design of co-culture experiments

7.2 Results

7.2.1 Yield of PBMCs from whole blood

PBMCs were isolated from the whole blood of healthy volunteers (n=6) as described in **Section 2.10.1.** The median age of the volunteers was 36.5 years (interquartile range 22.75). The average yield of PBMCs was 1.25 x 10^6 cells/ml (± 6.02 x 10^5), which was inside the expected yield of 0.5–2 × 10^6 cells/ml from the blood of healthy individuals [541]. One donor had a slightly lower yield of 0.42 × 10^6 cells/ml, and one donor had a slightly higher yield of 2.11 × 10^6 cells/ml **(Figure 69A).** A linear regression analysis was carried out to determine if age was an influencing factor in the yield of PBMCs. Results show that there was no clear relationship between the age of the donor and the yield of PBMCs, shown by a flat line in **Figure 69B.**

A.

	PBMCs (cells/ml)	Age
Donor 1	1.57 x 10^6	64
Donor 2	1.51 x 10^6	29
Donor 3	1.05 x 10^6	30
Donor 4	0.42 x 10^6	55
Donor 5	0.86 x 10^6	26
Donor 6	2.11 x 10^6	43

B.

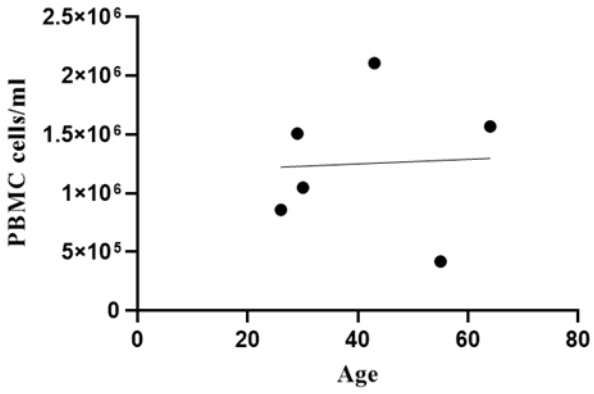

Figure 69: Patient characteristics and PBMC yield

(A) *List of the PBMC yield in cells/ml and ages of the blood donors (n=6).* ***(B)*** *Linear regression analysis of the PBMCs (cells/ml) on the y-axis and age on the x-axis. There was no clear relationship between the PBMC yield and the age of the donors.*

There was a limited number of PBMCs available for the co-culture experiments. This is mainly because PBMCs were used for experiment optimisation and some were lost due to

a flow cytometer breakdown. For this reason, the same PBMC donor was not used for each experiment. A breakdown of the PBMCs that were used for each experiment is shown in **Figure 70.** The first set of experiments involved comparing the activated vs non-activated PBMCs. The objective of this experiment was to establish that the CD3/CD28 activation worked and to establish how it changed the protein profile and morphology of PBMCs. PBMC Donors 1, 2 and 3 were used for this purpose. The same 3 donors were used for the dose response experiments and the co-culture experiments with normoxic EVs and normoxic MSCs. Due to sample availability, three different donors (Donor 4, 5, 6) were used for co-culture experiments with normoxic/primed EVs and normoxic/primed MSCs.

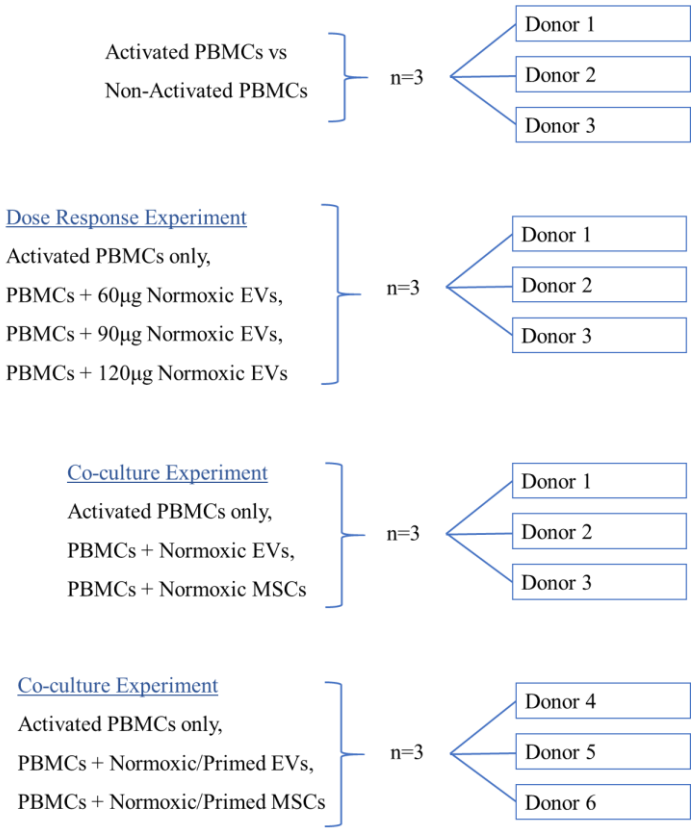

Figure 70: PBMCs used in co-culture experiments

Flow diagram details the donor PBMCs that were used in activation, dose response, and co-culture experiments. PBMC donor 1,2 and 3 were used to compare activated vs non-activated PBMCs, to compare different doses of EVs, and in co-culture experiments with normoxic EVs and MSCs. PBMC donor 4,5 and 6 were used in co-culture experiments with normoxic/primed EVs and MSCs.

7.2.2 Morphology of activated vs non-activated Jurkat and PBMCs

PBMCs (n=3) and Jurkat cells (n=1) were activated with a CD3/CD28 agonist (TransAct™, Miltenyi Biotec, Woking, UK) for 48 hours before their addition to co-cultures for 3 days. Non-activated PBMCs (n=3) and Jurkat cells (n=1) only acted as a negative control for the co-culture experiments. To determine the influence of the CD3/CD28 agonist on the cells, their morphology and surface marker profile was analysed. Experiments on Jurkat cells were carried out in triplicate.

The PBMCs and Jurkat cells were imaged before CD3/CD28 activation and 48 hours after activation to see if their morphology changed. Non-activated PBMCs were polydisperse in suspension **(Figure 71A)** compared to activated PBMCs which tended to cluster together (**Figure 71B).** Both activated and non-activated Jurkat cells clumped together which is typical for this cell line [542]. The only obvious change in morphology between the conditions was the larger cell clusters identified in activated Jurkat cells **(Figure 71C-D)**.

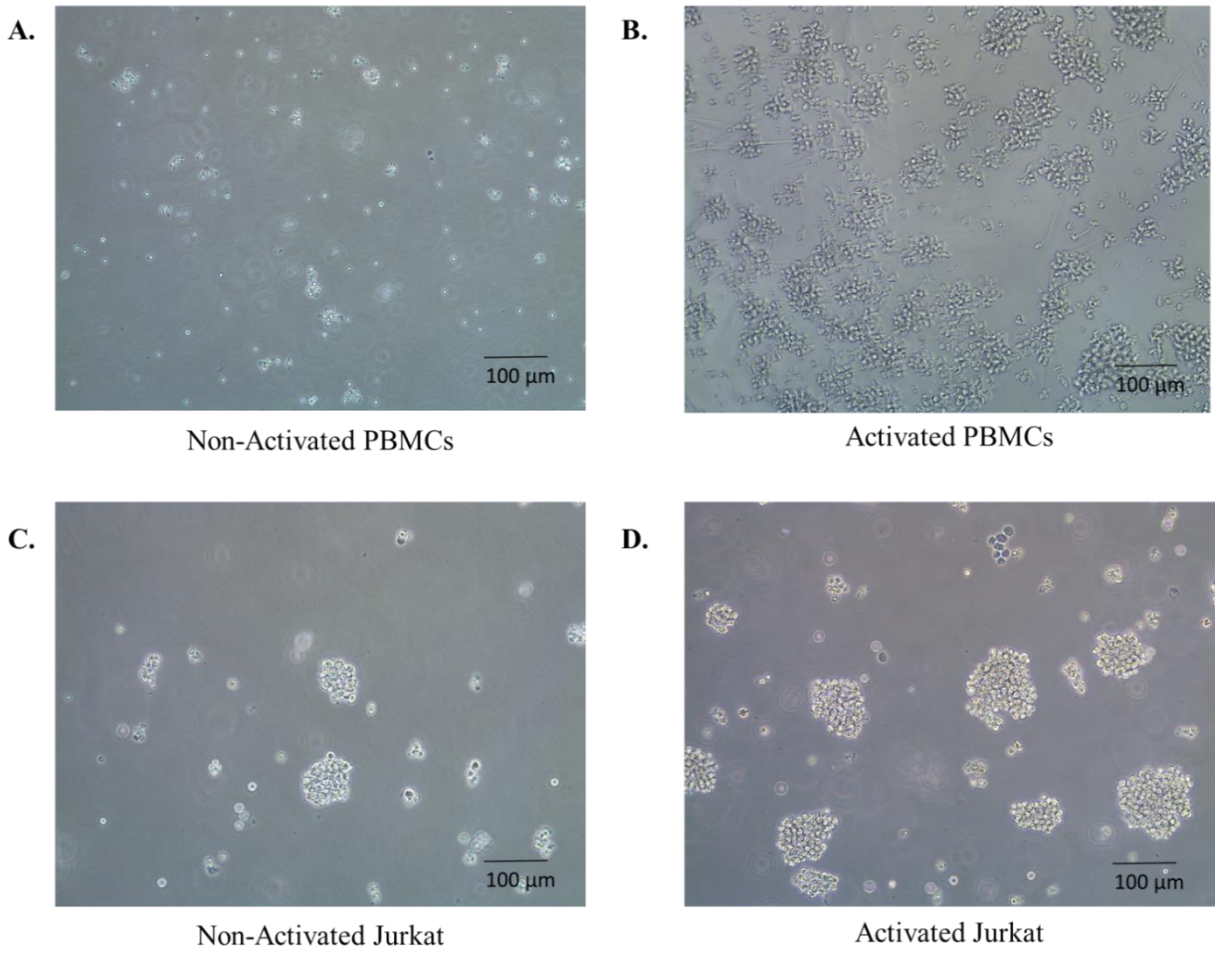

Figure 71: Activated vs non-activated PBMCs and Jurkat cells

*Image of non-activated **(A)** and activated **(B)** PBMCs. Non-activated PBMCs appear polydisperse in suspension whereas activated PBMCs show small cell cluster formations. Images of non-activated **(C)** and activated **(D)** Jurkat cells. Jurkat cells form clusters in both activated and non-activated suspensions. Scale bars represent 100µm. All images taken at 10x objective on a Nikon TS100 microscope.*

7.2.3 Immunophenotyping of activated vs non-activated PBMCs and Jurkat cells

Flow cytometry analysis was carried out on PBMCs (n=3) and Jurkat cells (n=1) to determine the effect of activation on these populations. All Jurkat cell experiments were carried out in triplicate. The first task of flow cytometry was to gate the target population.

Gating was carried out according to the images in **Supplementary Figure *7*.** In brief, the cell debris was first removed by gating out this population, the lymphocytes were selected, and gates drawn based on the forward scatter, clustering and CD3 positivity. This population was then gated further to remove doublet cells, as the presence of doublets would skew the analysis. The immune profile of this population was then analysed based on gating of <2% of the relevant fluorochrome-conjugated isotype control. All flow cytometry analysis gathered 10,000 events from each cell population. Initial analysis of the flow cytometry dot plots shows a diverse cell profile between the activated and non-activated PBMCs **(Figure 72A-B),** which was expected. There is an obvious difference between the activated and non-activated PBMCs in the bottom left-hand corner where the *x-axis* intersects the *y-axis*. There is a higher density of particles in the non-activated PBMCs, which could signify apoptotic debris. There are also changes in the forward scatter area (FSC-A), with activated PBMCs having an increase FSC-A, indicating that CD3/CD28 activation may be increasing the size of activated cells. There are also slight changes in the side scatter area (SSC-A), although not as obvious as FSC-A, between the activated and non-activated PBMCs, with the activated PBMCs appearing more polydisperse. This change in SSC-A indicates a difference the internal complexity of the cell, i.e., in the nucleus or via the presence of granules.

Jurkat cells contained a uniform cell population with no visible differences between the activated and non-activated cells **(Figure 72C-D).**

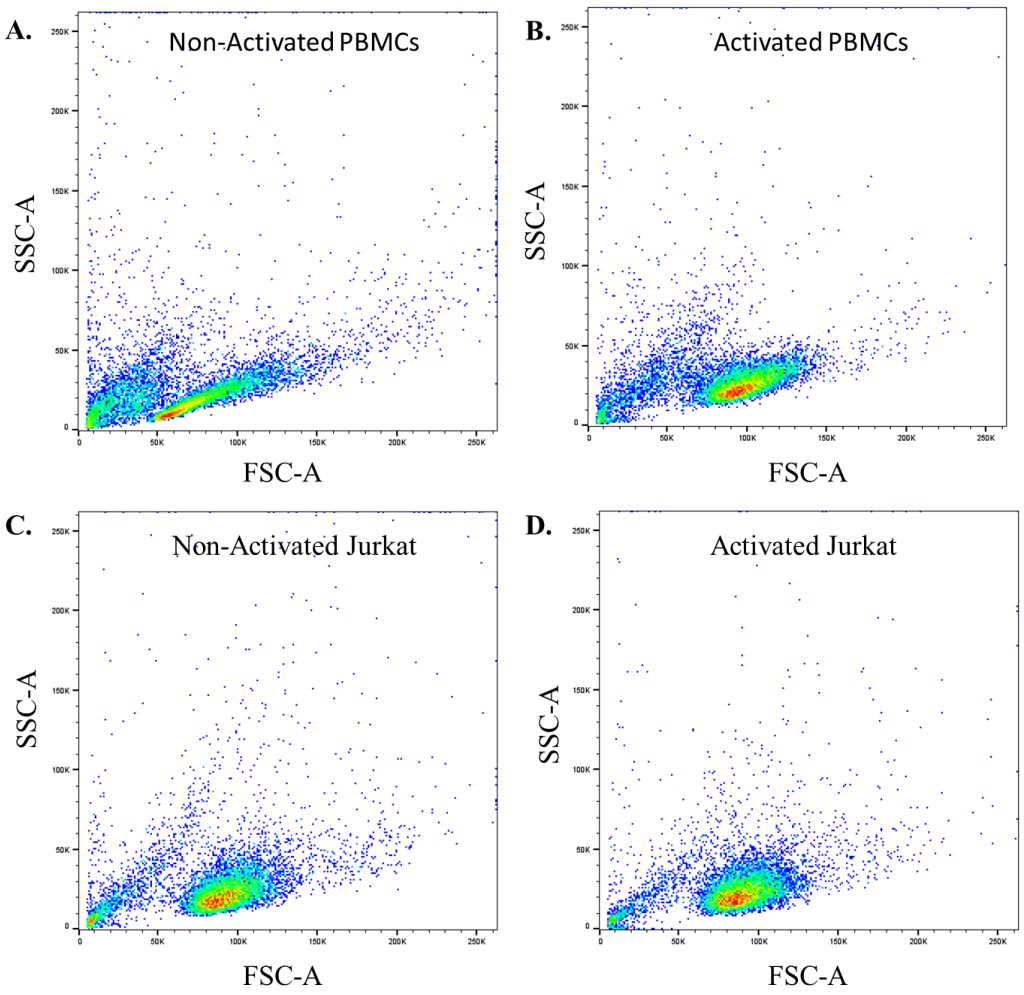

Figure 72: Dot plot of activated and non-activated PBMCs and Jurkat cells

Flow cytometry generated dot plots of 10,000 events for non-activated and activated PBMCs ***(A-B)*** *and for non-activated and activated Jurkat cells* ***(C-D).*** *Dot plots show the Side Scatter Area (SSC-A) on the y-axis and the Forward Scatter Area (FSC-A) on the x-axis. On comparison, non-activated PBMCs have a different cell clustering pattern compared to the activated PBMCs. The non-activated and activated Jurkat cells have highly similar clustering patterns.*

A protein marker panel was created to incorporate characteristic immune markers, and pro- and anti-inflammatory markers. It included CD3, CD4, CD25, CD127, HLA-DR, CD19, CD45, FoxP3, IL-4, IL-17A and IFN-γ. There were numerous differences identified

between activated and non-activated PBMCs from the flow cytometry experiment. Analysis of the protein profile of activated and non-activated PBMCs revealed that non-activated PBMCs contained a 58.85% (± 18.74 SD) production of CD4 and activated PBMCs had a statistically higher production at 79.9% (± 13.42 SD) ($p<0.05$). Activated PBMCs contained a statistically higher level of CD25 (99.47% ± 0.29 SD) compared to non-activated PBMCs (18.83% ± 3.76 SD) ($p<0.0001$). As CD25 is a marker of T-cell activation [543], this shows that the activation protocol was successful in inducing activation of PBMCs, making them suitable for use in further experiments. Further differences were found in the percentage of cells expressing IFN-γ and FoxP3, which was also statistically higher in the activated PBMC group (40.50% ± 25.97 SD) compared to the non-activated PBMC group (6.92% ± 3.29 SD) ($p<0.05$). There was a lower percentage of cells with CD127 in the activated PBMCs compared to non-activated PBMCs (7.39% ± 3.37 SD versus 31.33% ± 12.45 SD), which is a marker for Treg cells when negatively expressed with CD4+ and CD25+ markers ($p<0.05$) **(Figure 73A)** [544]**.**

There were no statistical differences between the protein marker profile of activated and non-activated Jurkat cells **(Figure 73B).** They expressed high levels of CD3 (>86%) and low levels of CD4 (<13.4%). The mean production of protein markers in PBMCs and Jurkat cells is included in **Table 25.**

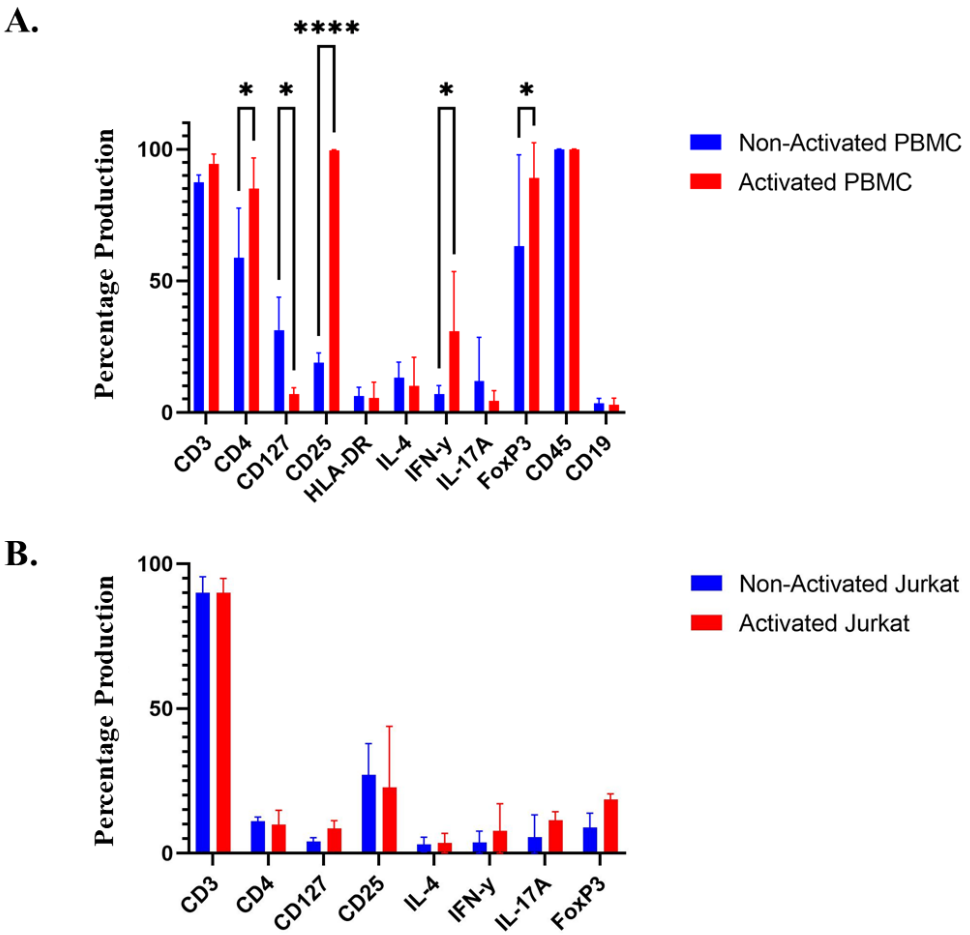

Figure 73: Activation of PBMCs and Jurkat Cells

PBMCs and Jurkat cells were activated with CD3/CD28 beads, 48 hours before being added to co-cultures for 3 days. Bar chart shows the protein profile of PBMCs (n=3) ***(A)*** *and Jurkat cells (n=1)* ***(B)*** *before and after activation. PDTs for Jurkat cells were calculated using three technical replicated. Activated PBMCs (shown in red) had a statistically higher production of CD4 ($p<0.05$), CD25 ($p<0.0001$), IFN-γ ($p<0.05$) and FoxP3 ($p<0.05$), and a lower production of CD127 ($p<0.05$) compared to non-activated PBMCs (shown in blue). No statistical differences were found between the activated and non-activated Jurkat cells. Data is shown as the mean ± SD.*

Table 25: Average production of proteins in PBMCs and Jurkat cells

Table displays the mean production and standard deviation (SD) of proteins in activated and non-activated PBMCs (n=3) and Jurkat cells (n=1). Jurkat cell experiments were performed in triplicate.

	Non-Activated PBMCs		Activated PBMCs		Non-Activated Jurkat		Activated Jurkat	
	Mean	SD	Mean	SD	Mean	SD	Mean	SD
CD3	87.30	2.86	95.90	4.42	89.95	5.59	89.95	5.02
CD4	58.83	18.74	79.90	13.42	11.01	1.55	9.86	5.01
CD127	31.33	12.45	7.39	3.37	4.07	1.35	8.52	2.80
CD25	18.83	3.76	99.47	0.29	27.05	10.82	22.81	21.06
HLA-DR	6.15	3.40	7.70	7.28				
IL-4	13.19	5.91	13.12	14.12	3.04	2.50	3.51	3.39
IFN-y	6.92	3.29	40.50	25.97	3.69	3.97	7.83	9.30
IL-17A	11.88	16.64	1.69	1.06	5.56	7.70	11.35	3.04
FoxP3	63.13	34.74	87.87	18.78	8.90	4.96	18.60	1.98
CD45	99.93	0.12	100.00	0.00				
CD19	3.57	1.79	1.32	0.94				

As activated cells were used in the co-culture experiments, a representative immune profile from one PBMC donor and the Jurkat cells is shown in **Figure 74A & B.** In total, activated PBMCs from Donor 1 had a positive production (>90%) of CD3, CD25, CD45 and a negative production of CD19, HLA-DR, IL-4 and IL-17A (<5%). There was an average of 72.1% production of CD4, 9.95% production of CD127, 66.3% production of IFN-γ and a 66.2% production of FoxP3.

Jurkat cells showed a positive production of CD3, CD45 and a <15% production of CD4, CD127, CD25, CD19, IL-4, IFN-γ. Jurkat cells had a 16.3% and 21.8% production of IL-17A and FoxP3, respectively.

A.

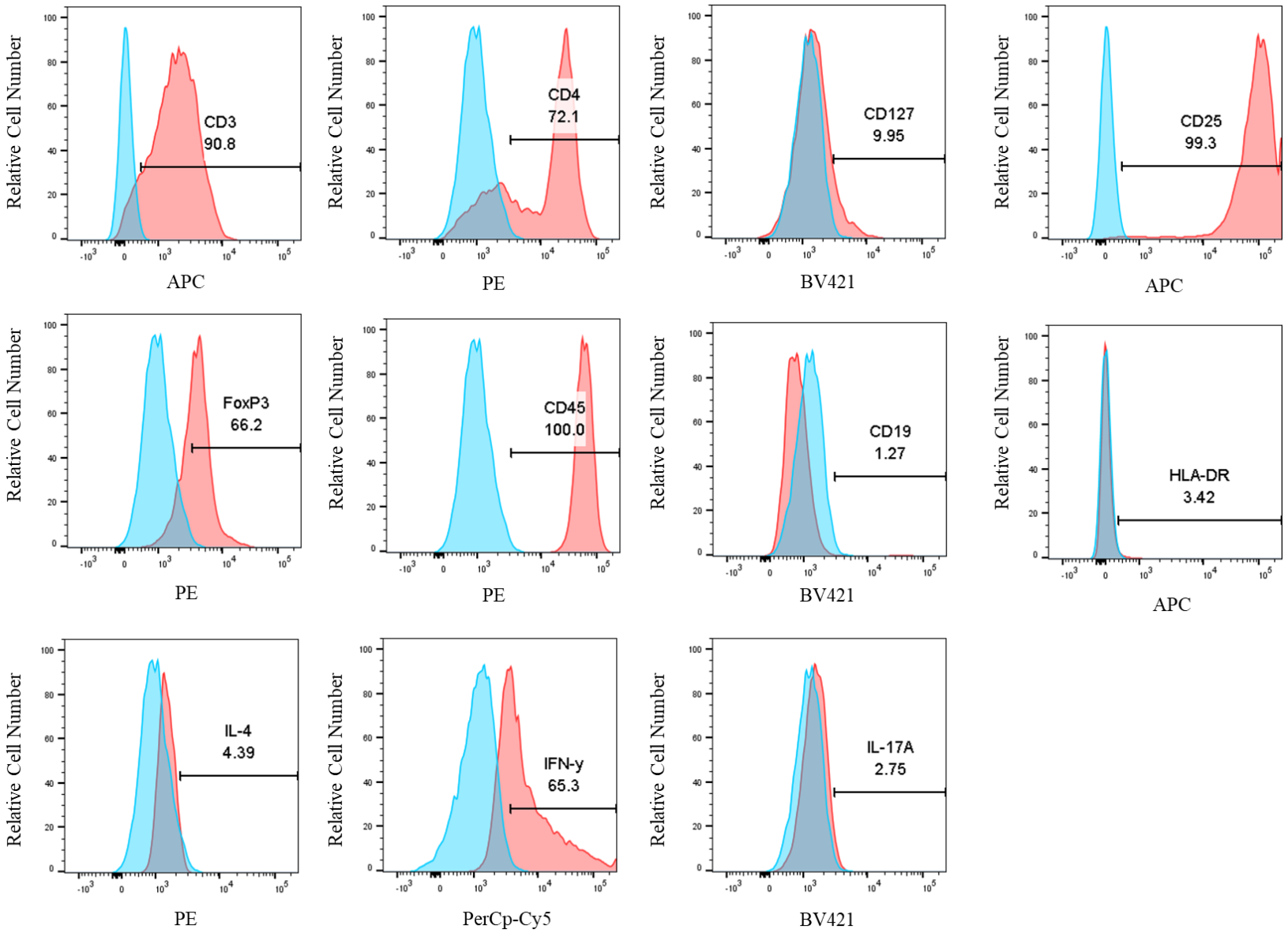
Relative Cell Number
CD3
90.8
APC
Relative Cell Number
CD4
72.1
PE
Relative Cell Number
CD127
9.95
BV421
Relative Cell Number
CD25
99.3
APC
Relative Cell Number
FoxP3
66.2
PE
Relative Cell Number
CD45
100.0
PE
Relative Cell Number
CD19
1.27
BV421
Relative Cell Number
HLA-DR
3.42
APC
Relative Cell Number
IL-4
4.39
PE
Relative Cell Number
IFN-γ
65.3
PerCp-Cy5
Relative Cell Number
IL-17A
2.75
BV421

B.

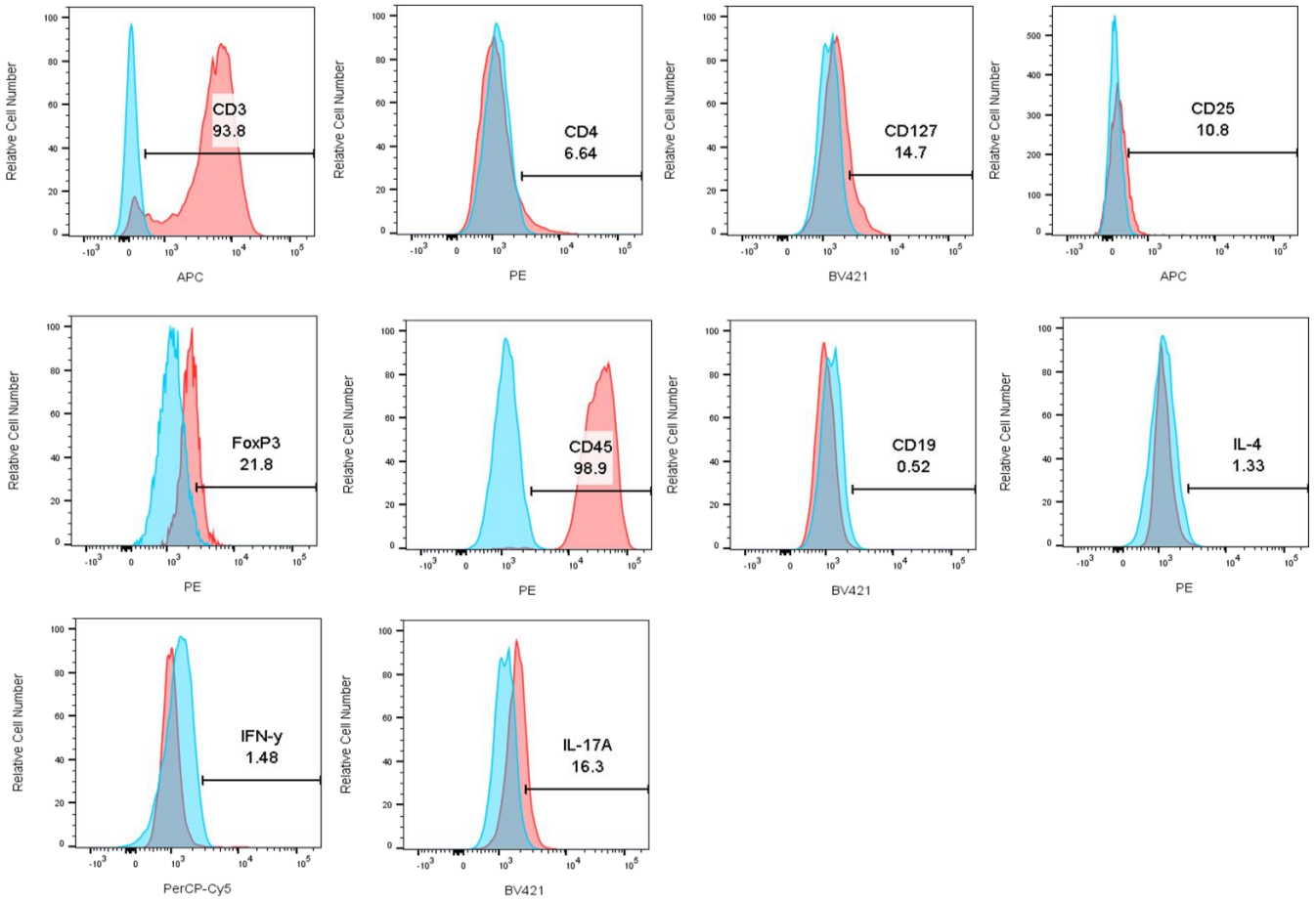

Figure 74: Immune profile of activated PBMCs and Jurkat cells

*Single parameter histograms of immune marker production of activated PBMCs from one donor **(A)** and activated Jurkat cells **(B)**. Relative Cell Number is displayed on the y-axis and the fluorochrome is displayed on the x-axis. Numbers provided above the gating line are the percentage production of that antibody. Expression of proteins on cells is shown by the red histograms and isotype controls are shown in blue.*

7.2.4 EV dose response experiment

Prior to setting up co-culture experiments with EVs and PBMCs, a dose response experiment was carried out to determine the optimal concentration of EVs to have an anti-inflammatory effect on PBMCs. Three different concentrations of normoxic EVs: 60µg, 90µg and 120µg were added to $2x10^6$ PBMCs (n=3), following research by Ma et al. [235]. The concentrations of 60µg, 90µg and 120µg refer to the vesicular protein concentration of the EVs, calculated using a BCA protein assay as described in **Section 2.5.1.** PBMCs were then analysed for their protein marker profile, specifically the production of IFN-γ, IL-17A, IL-4 and FoxP3 using ICCS described in **Section 2.10.5.**

The PBMCs were characterised based on their surface marker profile and cytokine production to identify differences between the groups. All PBMCs had a high production (>90%) of CD3, CD25 and CD45 **(Figure 75A).** The PBMCs that were co-cultured with 60µg EVs showed the largest range of production in CD4 (69.7-96.9%) averaging 81.3% (±11.4 SD) across all three donors. The 60µg EV co-culture led to a statistically higher production of IL-4 (31.6% ± 23 SD) in PBMCs compared to the 120µg EV group (7.73% ± 4.3 SD) ($p<0.05$) (**Figure 75B).** Additionally, in the PBMC donors that were co-cultured with 60µg EVs, there was a wide range of production in IL-4 (5.13%-46.4%). There was a statistically lower amount of IFN-γ in PBMCs from the 120µg EV co-culture compared to the 60µg EV co-culture (18.5% ± 8.5 SD vs 46% ± 41 SD) ($p<0.01$) **(Figure 75C).** The production of FoxP3 and IL-17A was consistent in PBMCs across EV concentrations. In all, the PBMCs from the 60µg EV co-culture showed more inconsistencies in cytokine production, seen by large error bars for most markers (IL-4, IFN-γ, FoxP3), in comparison to the PBMCs from the other EV concentrations. The

120µg EV concentration was chosen for upcoming co-cultures due to its ability to reduce IFN-γ levels in PBMCs.

A representative profile of the PBMCs that were co-cultured with 120µg EVs is shown in the histograms in **Figure 76.**

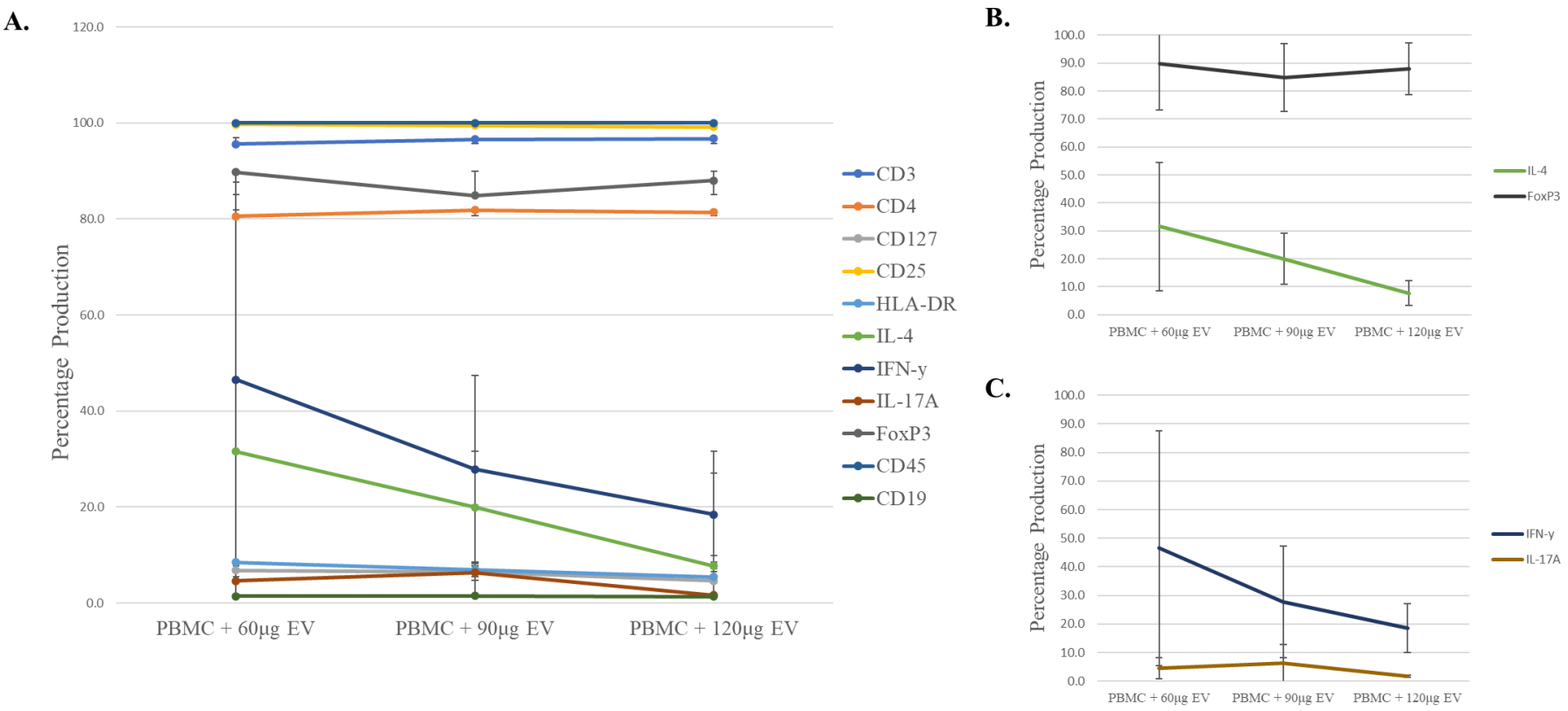

Figure 75: Dose response curve of PBMC co-culture with EVs

PBMC (n=3) were co-cultured with EVs of 3 different concentrations: 60µg, 90µg and 120µg (x-axis) and their percentage production of different markers was measured (y-axis). ***(A)*** *Line graph shows the production of all proteins in the PBMC flow cytometry panel.* ***(B)*** *Line graph shows a closer view of the IL-4 and FoxP3 production. There was a statistically lower production of IL-4 in the PBMCs that were co-cultured with 120µg EVs compared to the PBMCs co-cultured with 60µg EVs ($p<0.05$).* ***(C)*** *Line graph shows the production of IFN-γ and IL-17A in PBMCs after co-culturing with EVs. IFN-γ had a statistically lower production in the 120µg EV co-culture compared to the 60µg EV co-culture ($p<0.01$). There was no statistical difference in IL-17A.*

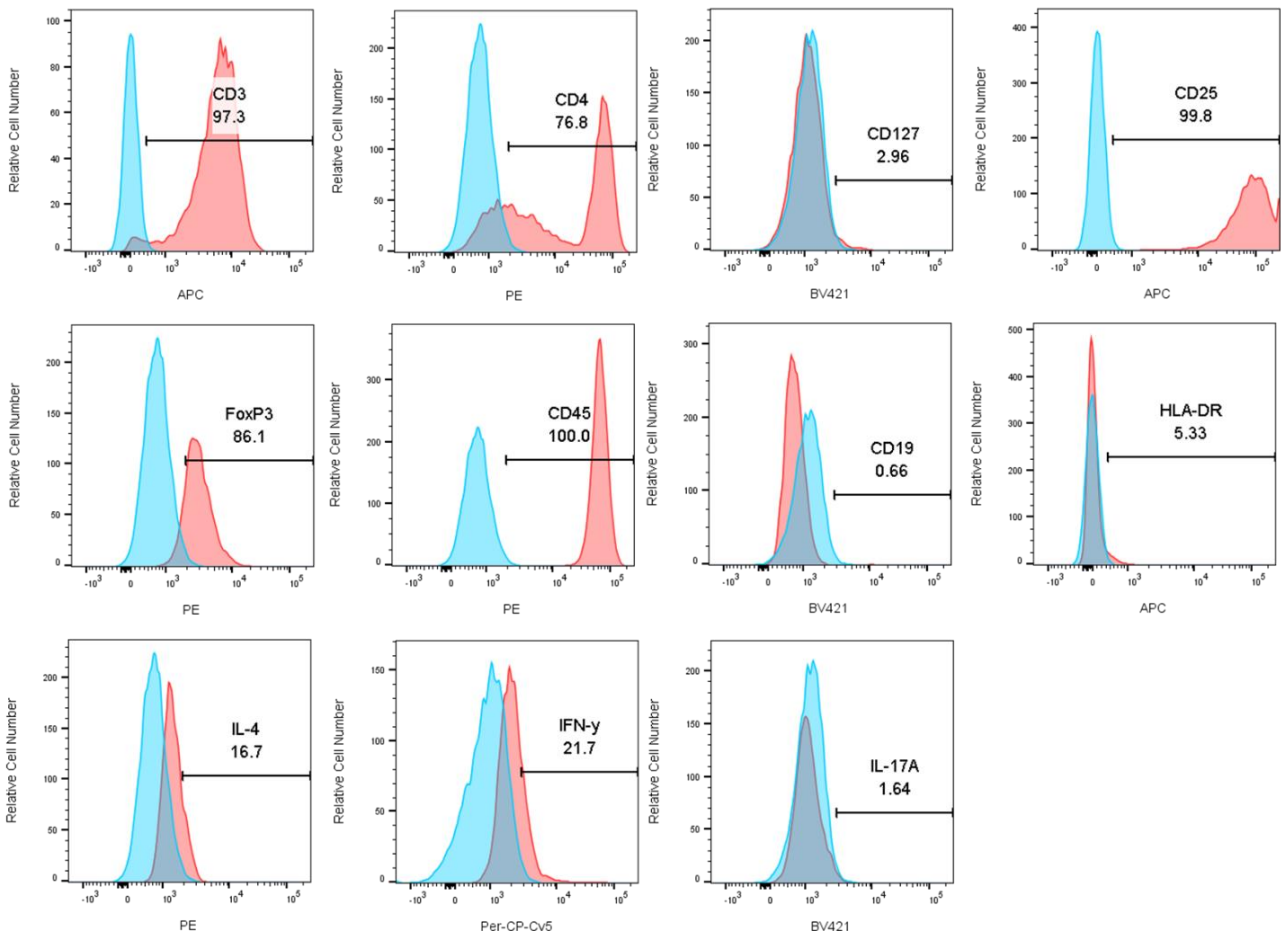

Figure 76: Immune profile of PBMCs after co-culture with 120µg EVs

Single parameter histograms displaying the immune profile of one PBMC donor that was co-cultured with 120µg normoxic EVs. Relative Cell Number is displayed on the y-axis and the fluorochrome is displayed on the x-axis. Numbers provided above the gating line are the percentage production of that antibody. Expression of proteins on cells is shown by the red histograms and isotype controls are shown in blue.

7.2.5 Morphology of PBMCs and Jurkat cells

PBMCs and Jurkat cells were co-cultured in the following conditions:

1. Non-activated only
2. Activated
3. Activated with normoxic EVs
4. Activated with normoxic/primed EVs
5. Activated with normoxic MSCs
6. Activated with normoxic/primed MSCs

Flow cytometry generated dot plot profiles of PBMCs and Jurkat cells from the different co-culture conditions. These profiles were compared and it is clear that the PBMCs had a varied cell clustering profile after co-culturing and activation, shown in **Figure 77.** This may be indicative of changes in cell size, shape, and granularity. Photos of PBMC co-cultures with EVs and MSCs is provided in **Figure 78.** Jurkat cells, on the other hand had a very similar cell clustering and no obvious differences could be seen **(Figure 79).**

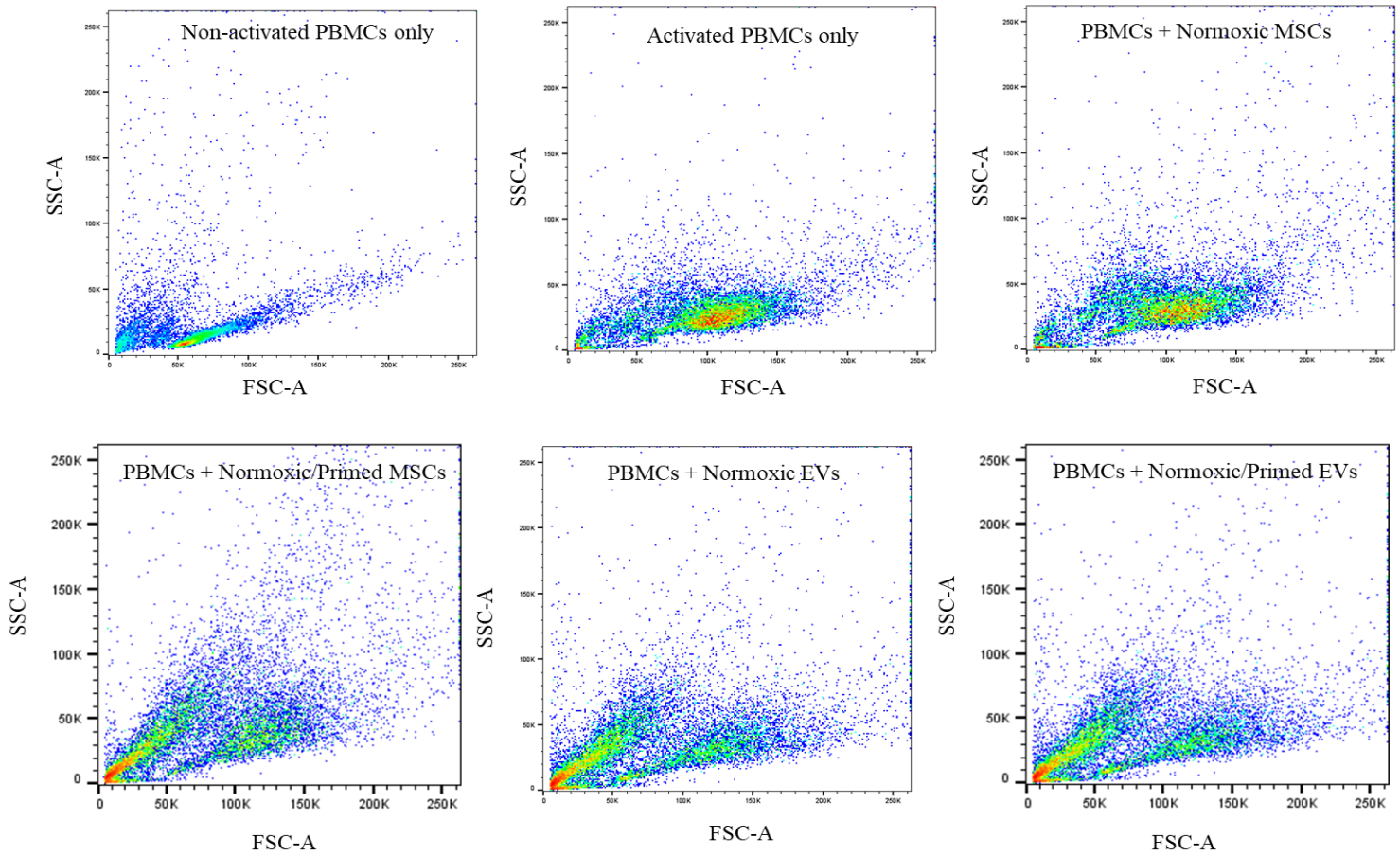

Figure 77: Dot plots comparing the different co-cultures with PBMCs

Dot plot comparing PBMCs that were activated, non-activated, and co-cultured with normoxic and normoxic/primed EVs and MSCs. There was a varied clustering profile across all conditions seen by different cell clustering patterns and heat intensity profiles. Dot plots display Side Scatter Area (SSC-A) on the y-axis and the Forward Scatter Area (FSC-A) on the x-axis.

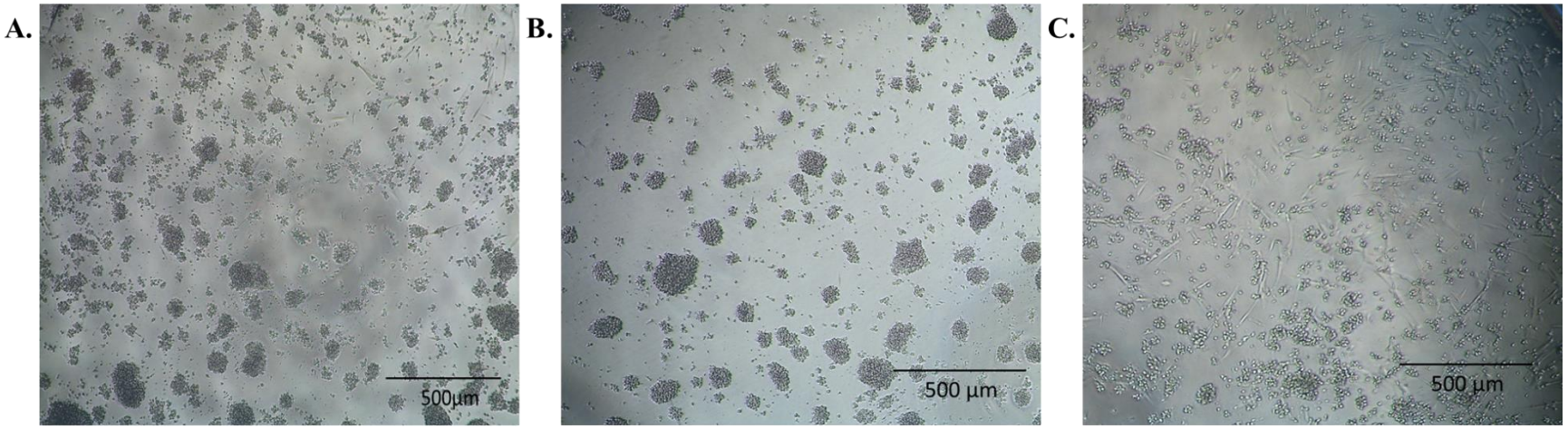

Figure 78: Images of PBMC co-culture with EVs and MSCs

(A) *Image displays activated PBMCs only, there is a mix of cell clusters and single cells in the well.* ***(B)*** *Image displays PBMCs that were co-cultured with normoxic EVs. PBMCs show visible cell clustering in the well, although they were easily dispersed through gentle pipetting.* ***(C)*** *Image of PBMC + normoxic MSC co-culture. MSCs can be seen by long spindle like cells in the well. Scale bars represent 500µm. All images taken at 4x objective on a Nikon TS100 microscope.*

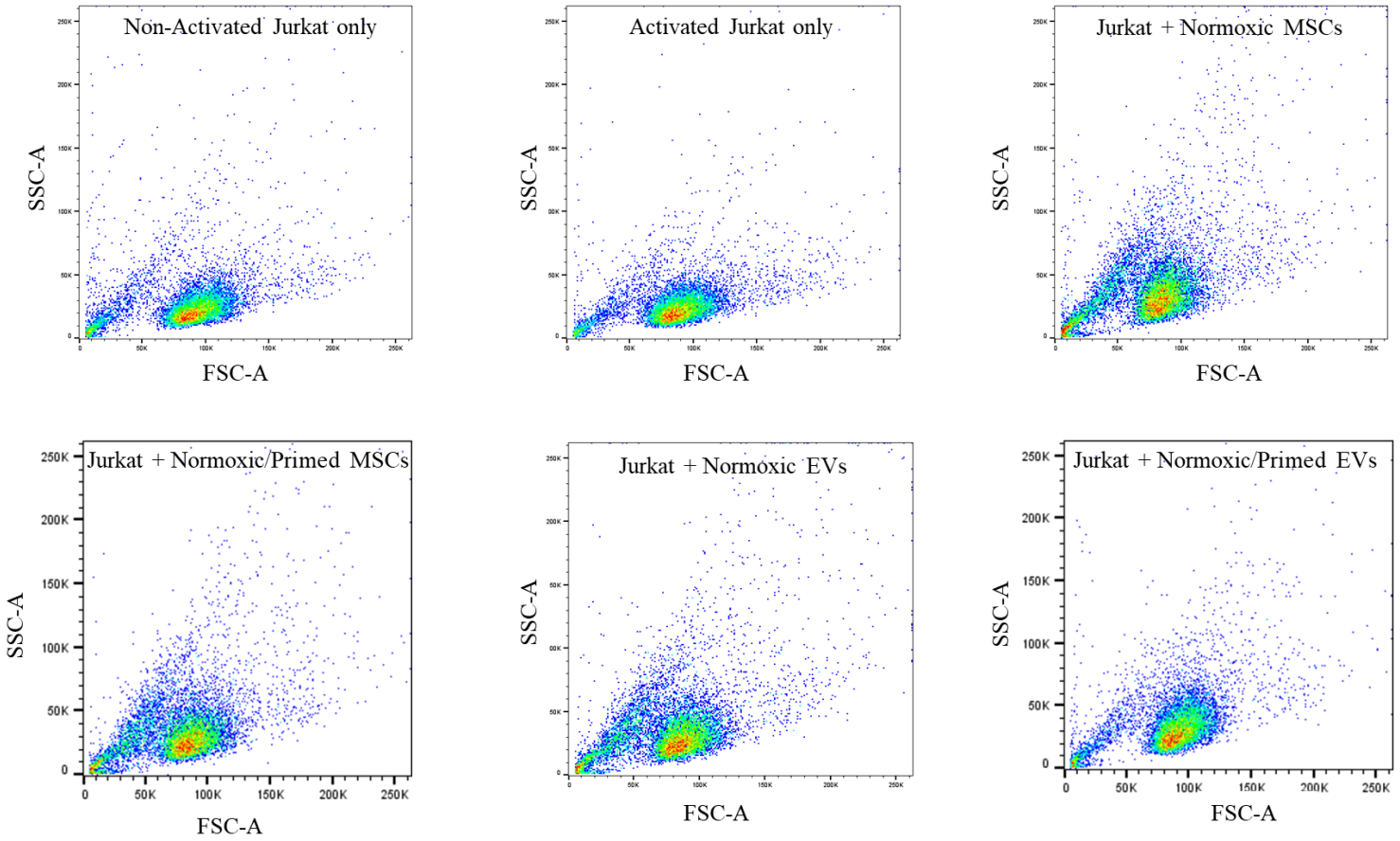

Figure 79: Dot plots comparing the different co-cultures with Jurkat cells.

Dot plot comparing Jurkat cells that were activated, non-activated, and co-cultured with normoxic and normoxic/primed EVs and MSCs. There was a similar cell profile obtained under all conditions. Dot plots display Side Scatter Area (SSC-A) on the y-axis and the Forward Scatter Area (FSC-A) on the x-axis.

7.2.6 Immunophenotyping of PBMCs from co-cultures

The immune profile of PBMCs was analysed by flow cytometry after PBMCs were co-cultured with normoxic EVs and MSCs (n=3) and normoxic/primed EVs and MSCs (n=3); experimental set-up shown in **Figure 70**. PBMCs from the co-cultures were compared to activated PBMCs alone. With the exception of non-activated PBMCs, PBMCs in all other conditions had a >90.8% production of CD3, >95.3% production of CD25 and a >98.6% production of CD45. PBMCs in all conditions were largely negative for CD19 (<2.7%). As CD19, is a marker of B-cells, this indicates that there are few B-cells in the gated lymphocyte population and the cells are primarily of CD3+ origin [545].

There was a reduction in the production of IFN-γ in the PBMCs that were co-cultured with normoxic EVs compared to normoxic MSCs ($p<0.05$) **(Figure 80A).** There were no further differences between the activated PBMCs, PBMCs + normoxic EVs, and PBMCs + normoxic MSCs. In relation to the PBMCs that were co-cultured with normoxic/primed EVs and normoxic/primed MSCs, there was a significantly increased production of FoxP3 in the PBMCs compared to the activated PBMCs alone ($p<0.05$, $p<0.0001$). Furthermore, the normoxic/primed MSCs had a statistically higher production of FoxP3 compared to the normoxic/primed EVs ($p<0.01$) **(Figure 80B).** There were no further statistical differences between the conditions. IFN-γ was not probed for the in PBMC + normoxic /primed EVs/MSC due to issues with antibody availability.

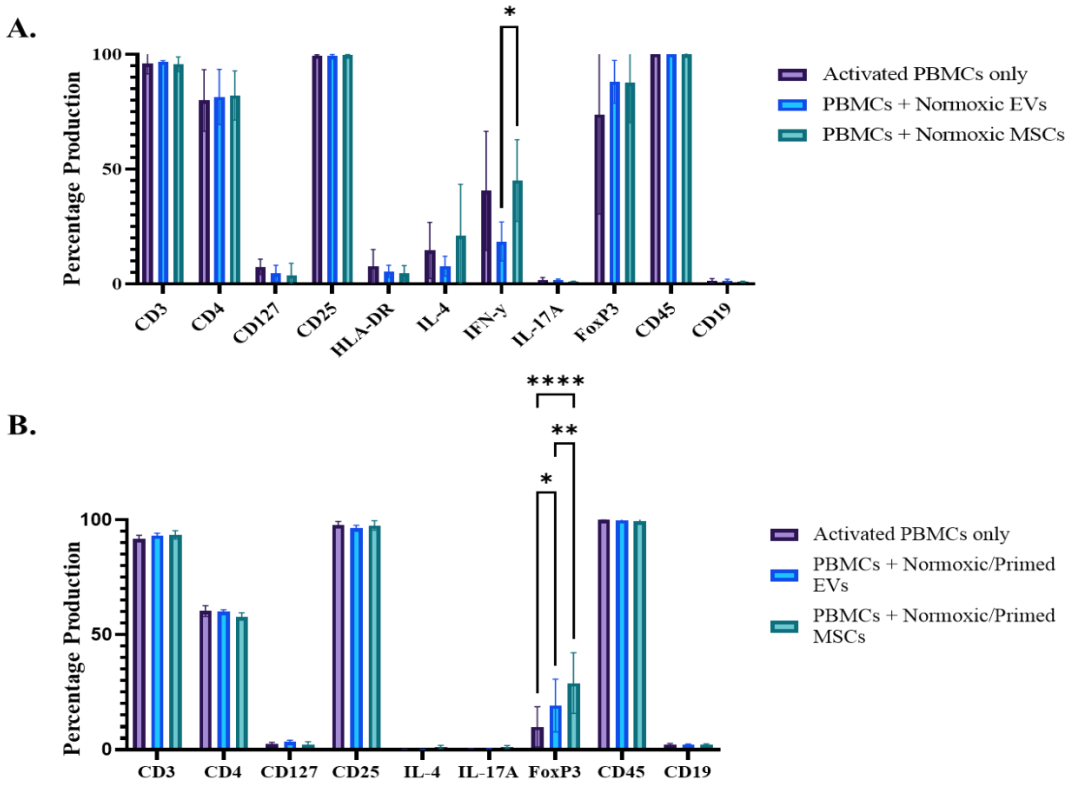

Figure 80: Protein production of PBMCs after co-culture with EVs and MSCs

*PBMCs were co-cultured with EVs and MSCs and their protein markers were analysed by flow cytometry. Bar chart displays percentage production on the y-axis and protein markers on the x-axis. **(A)** PBMCs (n=3) that were co-cultured with normoxic EVs had a statistically lower production of IFN-γ compared PBMCs + normoxic MSCs (p<0.05). **(B)** In the PBMC (n=3) co-culture with normoxic/primed EVs and MSCs, there was a statistically higher production of FoxP3 between normoxic/primed EVs and MSCs compared to activated PBMCs only (*p<0.05, ****p<0.0001). Additionally, PBMCs co-cultured with normoxic/primed MSCs had a statistically higher production of FoxP3 compared to PBMCs from the normoxic/primed EV co-culture (**p<0.01).*

7.2.7 Immunophenotyping of Jurkat cells from co-cultures

Similar to the PBMCs, flow cytometry was carried out on Jurkat cells (n=1) after co-culture with EVs and MSCs, in normoxic and normoxic/primed conditions. All experiments were carried out in triplicate. Jurkat cells, in all conditions, had a >86.4% production of CD3. All other protein markers had a low production (<22.3%) in Jurkat cells **(Figure 81).**

The production of CD25, IL-17A, and FoxP3 was significantly lower in Jurkat cells that were co-cultured with normoxic EVs compared to activated Jurkat cells alone ($p<0.05$; $p<0.001$) **(Figure 81).** Additionally, normoxic/primed EVs had a reduced production of both IL-17A and FoxP3 in Jurkat cells ($p<0.05$; $p<0.001$) **(Figure 81).**

For the MSCs, both normoxic and normoxic/primed MSCs reduced the production of IL-17A in Jurkat cells. Jurkat cells that were co-cultured with normoxic MSCs also had a statistically higher production of FoxP3 compared to the Jurkat cells from the normoxic EV co-culture ($p<0.01$), however, its production did not differ from the Jurkat-only control. There were no further statistical differences between activated Jurkat cells only, Jurkat cells co-cultured with normoxic MSCs, and Jurkat cells co-cultured with normoxic/primed MSCs.

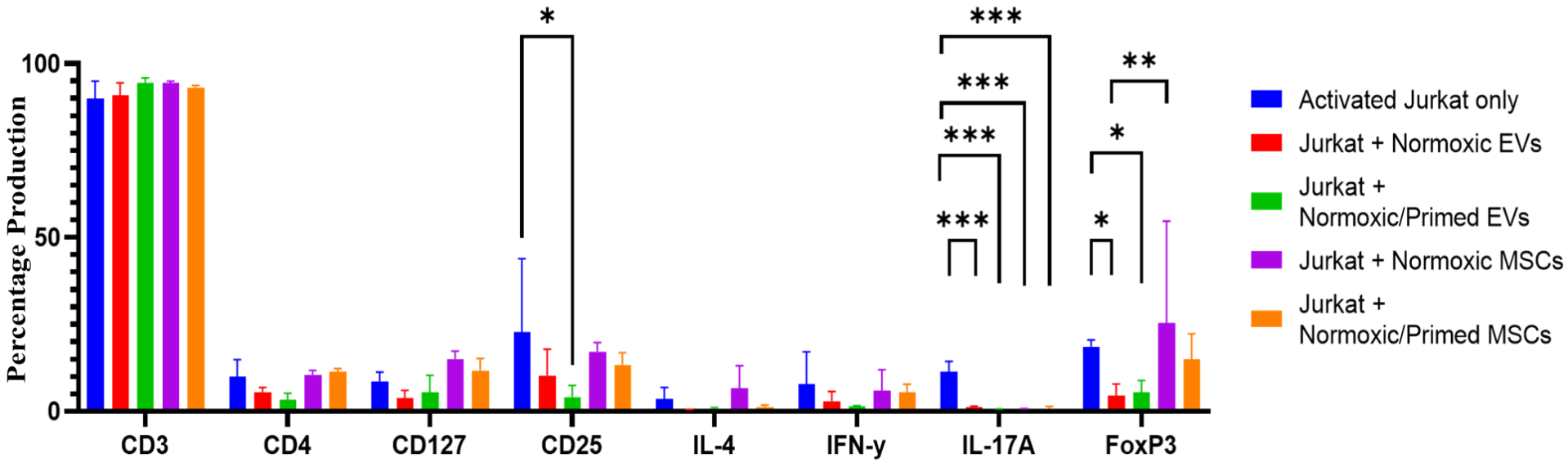

Figure 81: Protein production in Jurkat cells after co-culture with EVs and MSCs

Jurkat cells (n=1) were cultured with normoxic EVs, normoxic/primed EVs, normoxic MSCs and normoxic/primed MSCs. Flow cytometry was carried out to calculate the percentage production (y-axis) of different immune markers (x-axis). CD25 was statistically lower in Jurkat + normoxic/primed EVs compared to activated Jurkat cells alone ($p<0.05$). IL-17A was lower in all co-cultures compared to activated Jurkat cells alone, and FoxP3 was significantly reduced in normoxic and normoxic/primed EVs compared to activated Jurkat cells ($p<0.05$). There was also a higher production of FoxP3 from Jurkats that were co-cultured with normoxic MSCs compared to normoxic EVs (**$p<0.01$). All experiments were carried out in triplicate.*

7.2.8 Percentage CD3+CD4+ in PBMCs and Jurkat cells

There is a higher prevalence of CD3+CD4+ T-cells in RA which contribute to the pathophysiology of the disease, particularly IFN-γ producing Th1 cells. Other CD4+ T-cells, such as IL-4 secreting Th2 cells and Treg cells, act to suppress immune responses. As the balance of CD4+ Th1, Th2 and Treg cells influence disease activity in RA, the percentage of CD3+CD4+ cells were analysed in the PBMCs and Jurkat cells from the different co-cultures to see if MSCs and EVs alter their levels. This was followed by analysis of the IL-4: IFN-γ ratio, and analysis of the percentage of CD4+CD25+CD127- Tregs in PBMCs. Firstly, PBMCs and Jurkat cells were gated for their CD3+CD4+ populations, as shown in the contour plots in **Figure 82** ***&*** **Figure 83.** The average percentage of CD3+CD4+ cells in activated PBMCs and Jurkat cells is shown in **Table 26.**

There was a statistically lower amount of CD3+CD4+ PBMCs (n=3) in the normoxic/primed MSC group compared to activated PBMCs alone ($p<0.05$) **(Figure 82D).** No further differences in the percentage CD3+CD4+ cells were identified between the groups. There is a large standard deviation in the PBMCs that were co-cultured with normoxic EVs and normoxic MSCs. This is due to PBMC Donor 1 having a 1.5 times higher amount of CD3+CD4+ cells compared to the other donors. A comparison of the CD3+CD4+ population from the three donors used in this experiment is shown in **Supplementary Figure *8*.**

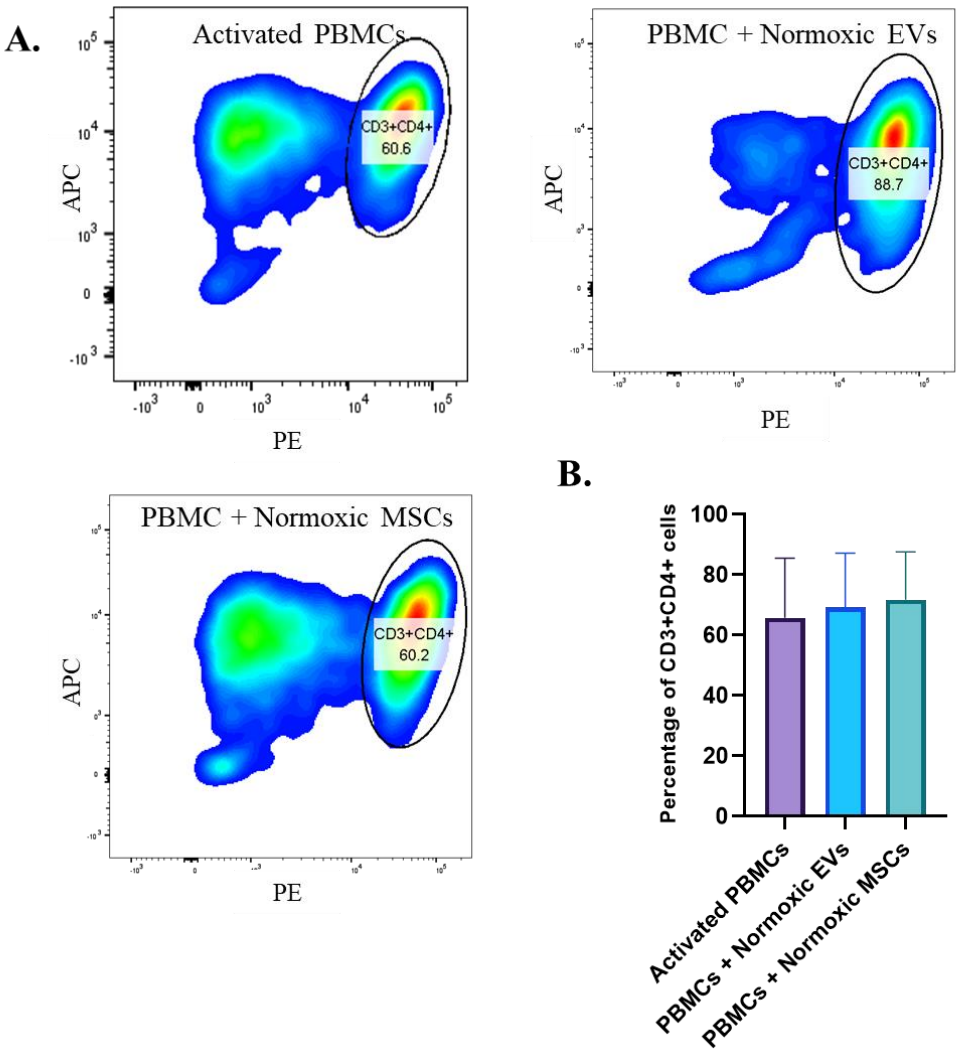
A.
Activated PBMCs
CD3+CD4+
60.6
APC
PE
PBMC + Normoxic EVs
CD3+CD4+
88.7
APC
PE
PBMC + Normoxic MSCs
CD3+CD4+
60.2
APC
PE
B.
Percentage of CD3+CD4+ cells
100
80
60
40
20
0
Activated PBMCs
PBMCs + Normoxic EVs
PBMCs + Normoxic MSCs

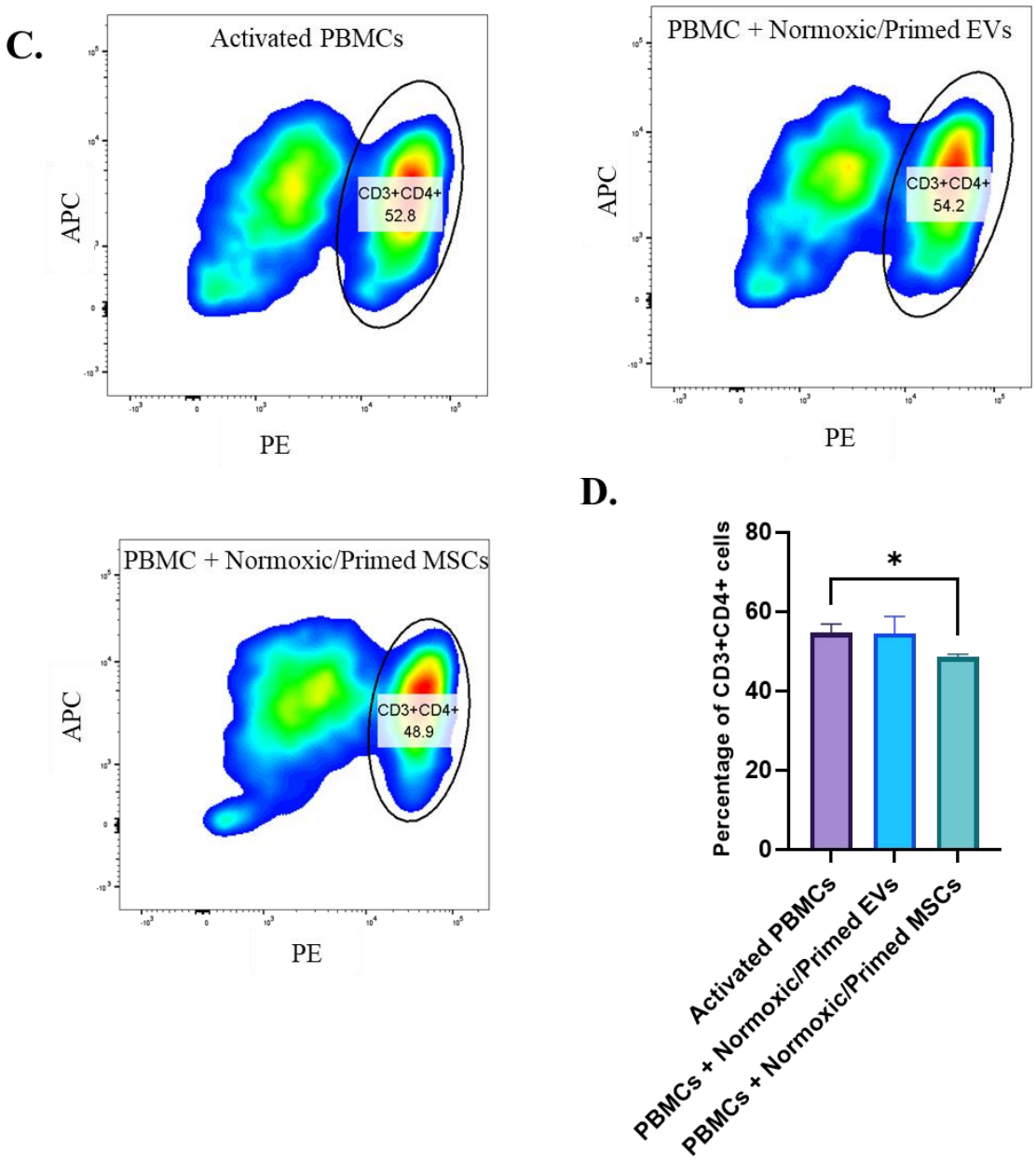

Figure 82: Percentage of CD3+CD4+ cells in PBMCs

*PBMCs were gated for CD3 and CD4 positivity by plotting CD3 (APC; y-axis) against CD4 (PE; x-axis). (**A**) Density plots show the percentage of CD3+CD4+ in activated PBMCs and PBMCs co-cultured with normoxic EVs and normoxic MSCs. (**B**) The bar chart shows the percentage of CD3+CD4+ cells (y-axis) in PBMCs (n=3) in activated, normoxic EV and normoxic MSC groups (x-axis). There was no statistical difference between the conditions. (**C**) Density plots show the production of CD3+CD4+ in activated PBMCs and PBMCs co-cultured with normoxic/primed EVs and normoxic/primed MSCs. (**D**) Bar chart shows the percentage of CD3+CD4+ (y-axis) in PBMCs (n=3) in activated, normoxic/primed EV and normoxic/primed MSC groups (x-axis). There was a statistical*

higher percentage of CD3+CD4+ cells in the activated PBMCs compared to PBMCs cultured with normoxic/primed MSCs ($p \leq 0.05$).

Table 26: Mean percentage of CD3+CD4+ T-cells in PBMCs and Jurkat cells

	Mean	SD
Activated PBMC	65.80	19.72
PBMC + Normoxic EV	69.17	18.05
PBMC + Normoxic MSC	71.80	15.80
Activated PBMC	54.70	2.13
PBMC + Normoxic/Primed EV	54.50	4.26
PBMC + Normoxic/Primed MSC	48.47	0.75
Activated Jurkat	2.43	0.69
Jukat + Normoxic EV	3.99	1.34
Jurkat + Normoxic/Primed EV	3.50	0.45
Jurkat + Normoxic MSC	2.53	0.94
Jurkat + Normoxic/Primed MSC	2.60	1.42

For the Jurkat cells (n=1), all conditions contained a low level of CD3+CD4+ cells (<4%) **(Figure 83A).** There was no statistical difference between groups **(Figure 83B).**

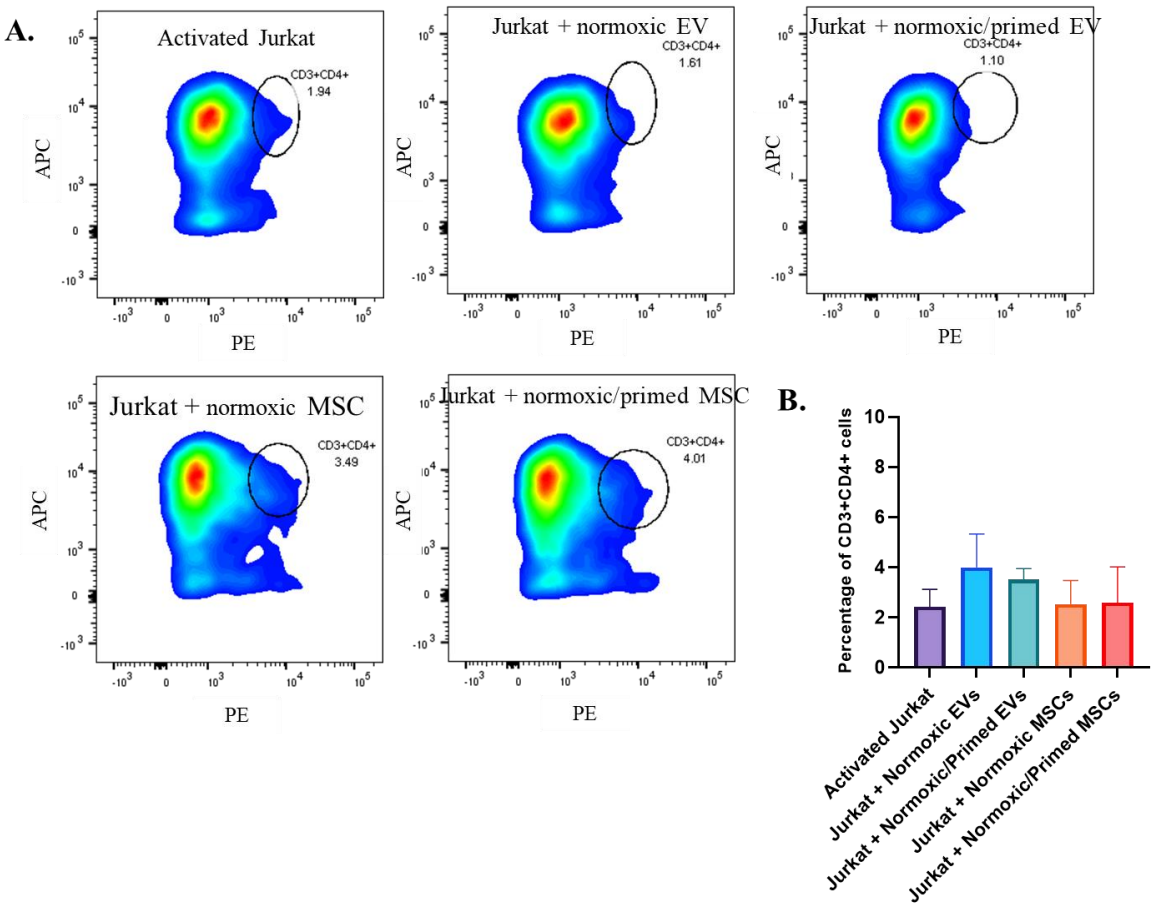

Figure 83: Percentage of CD3+CD4+ cells in Jurkat cells

*Jurkat cells were gated for CD3 and CD4 positivity by plotting CD3 (APC; y-axis) against CD4 (PE; x-axis). **(A)** Density plots show the production of CD3+CD4+ in Jurkat cells from different co-culture conditions. **(B)** The bar chart shows the percentage production of CD3+CD4+ (y-axis) in Jurkat cells (n=1) across all groups (x-axis). There was no statistical difference between conditions. All experiments were performed in triplicate.*

7.2.9 Ratio of IL-4: IFN-γ in PBMCs

In RA, Th1 cells produce large amount of IFN-γ and a decreased amount of IL-4 which contributes to synovial inflammation [546]. To understand if MSCs and EVs are capable of supressing immune responses, the production of IFN-γ and IL-4 was assessed in activated PBMCs. IFN-γ was gated against IL-4 and the percentage production was analysed for non-activated PBMCs, activated PBMCs, PBMCs + normoxic EVs, PBMCs + normoxic MSCs, shown in **Figure 84A**. Due to lack of IFN-γ antibody available, this cytokine was not assessed in the normoxic/primed EV and MSC groups. In the non-activated PBMCs, there was a higher ratio of IL-4 compared to IFN-γ (3.62:1). All other conditions had a higher ratio of IFN-γ compared to IL-4. Activated PBMCs had a IL4: IFN-γ ratio of 0.5:1, PBMCs + normoxic EVs had a ratio of 0.64:1, and PBMC + normoxic/MSCs had a ratio of 0.52:1. While the normoxic EVs and MSCs increased the IL-4 levels relative to IFN-γ compared to the activated PBMCs, there was no statistical difference in the conditions **(Figure 84B).**

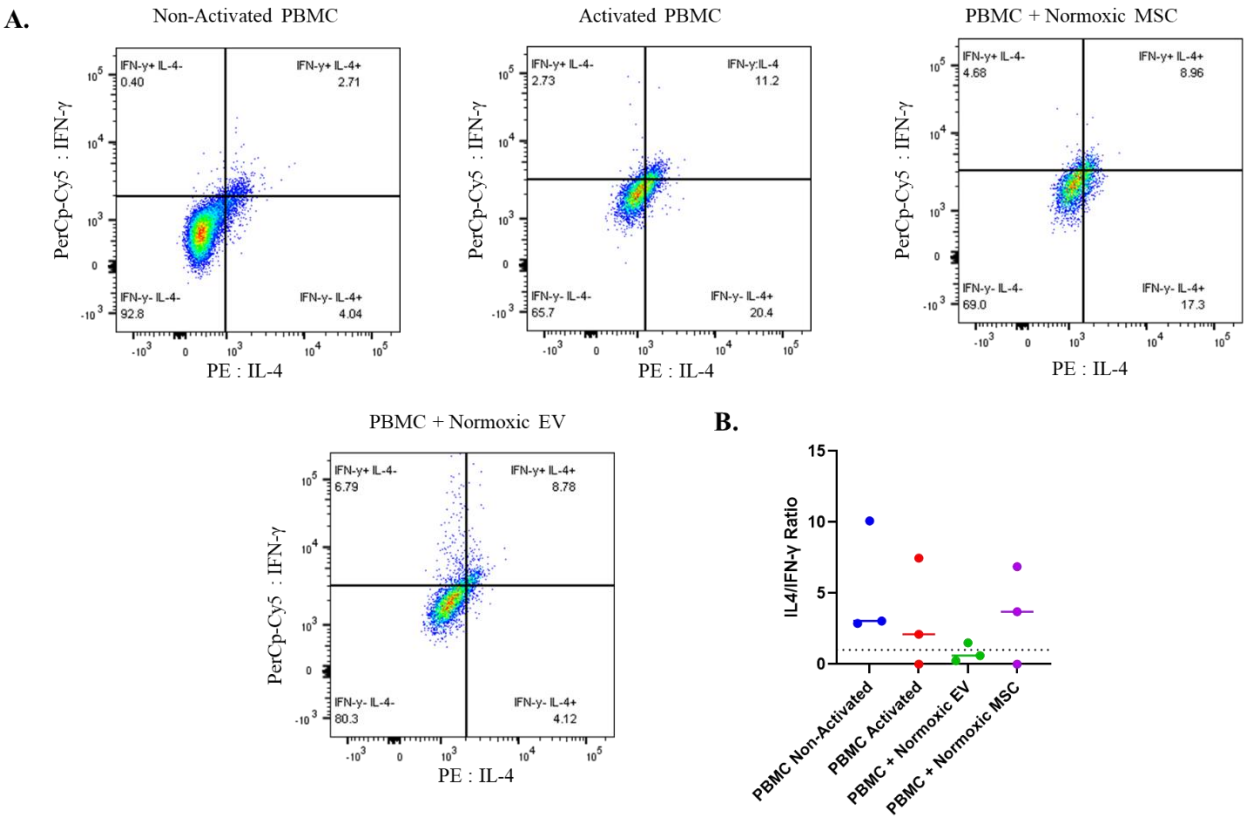

Figure 84: Ratio of IL-4: IFN-γ in PBMCs

(*A) Dot plot displays a representative flow cytometry analysis from one donor of PBMCs. Analysis was carried out on PBMC (n=3) donors in activated, non-activated and co-cultured with normoxic EVs/MSCs. Cells were gated based on their production of IFN-γ (PerCp-Cy5 fluorochrome; y-axis) and IL-4 (PE fluorochrome; x-axis). IFN-γ positive/IL-4 negative cells are displayed in the top left quadrant. IFN-γ negative/IL-4 positive cells are displayed in the bottom right quadrant. The percentage production of IL-4: IFN-γ were compared to give a ratio value for PBMCs in each condition.* ***(B)*** *Bar chart represents the IL-4/IFN-γ ratio on the y-axis and the different culture conditions on the x-axis. Points below the dotted line at y=1 represent a higher amount of IFN-γ to IL-4, points above the dotted represent a higher amount of IL-4 to IFN-γ. There were no statistical differences between conditions.*

PBMC Donor 2 showed a different IFN-γ and IL-4 production to Donors 1 and 3, shown in **Figure 85.** There was a high production of IFN-γ (>50%) in the activated and normoxic MSC groups and this coincided with a low production of IL-4 (<1%). This level of production of IFN-γ was not seen in other donors and could be considered as skewing the results.

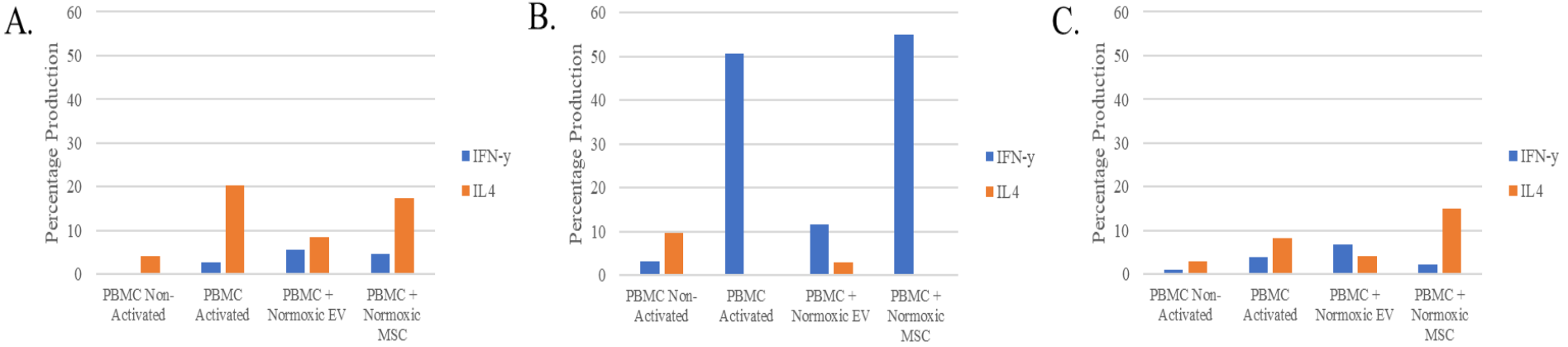

Figure 85: IFN-γ and IL-4 production in individual PBMC donors

Bar charts represent a comparison of IFN-γ and IL-4 in PBMC Donor 1 ***(A),*** *Donor 2* ***(B),*** *and Donor 3* ***(C).*** *The percentage production of IFN-γ and IL-4 is presented on the y-axis and the culture conditions on the x-axis. PBMC Donors 1 and 3 are highly similar, showing a higher amount of IL-4 compared to IFN-γ in non-activated, activated and normoxic MSC conditions. Donor 2 does not follow the same profile, showing a >50% production of IFN-γ in activated and normoxic MSC conditions.*

Jurkat cells were also gated based on their production of IL-4 and IFN-γ in all conditions, shown in **Figure 86A.** In all conditions, except Jurkat + normoxic MSCs, there is on average a higher percentage of IFN-γ over IL-4. The higher production of IL-4 in Jurkat + normoxic MSCs is due to the higher production of IL-4 in one donor which is skewing the ratio, shown in **Figure 86B.** However, biologically, this production was considered to be legitimate, despite it differing from other samples, so it was included in the analysis. The ratio of IL-4: IFN-γ was 0.45:1 in activated Jurkat, 0.14:1 in Jurkat + normoxic EV, 0.59:1 in Jurkat + normoxic/primed EV, 1.13:1 in Jurkat + normoxic MSC, and 0.25:1 in Jurkat + normoxic/primed MSC.

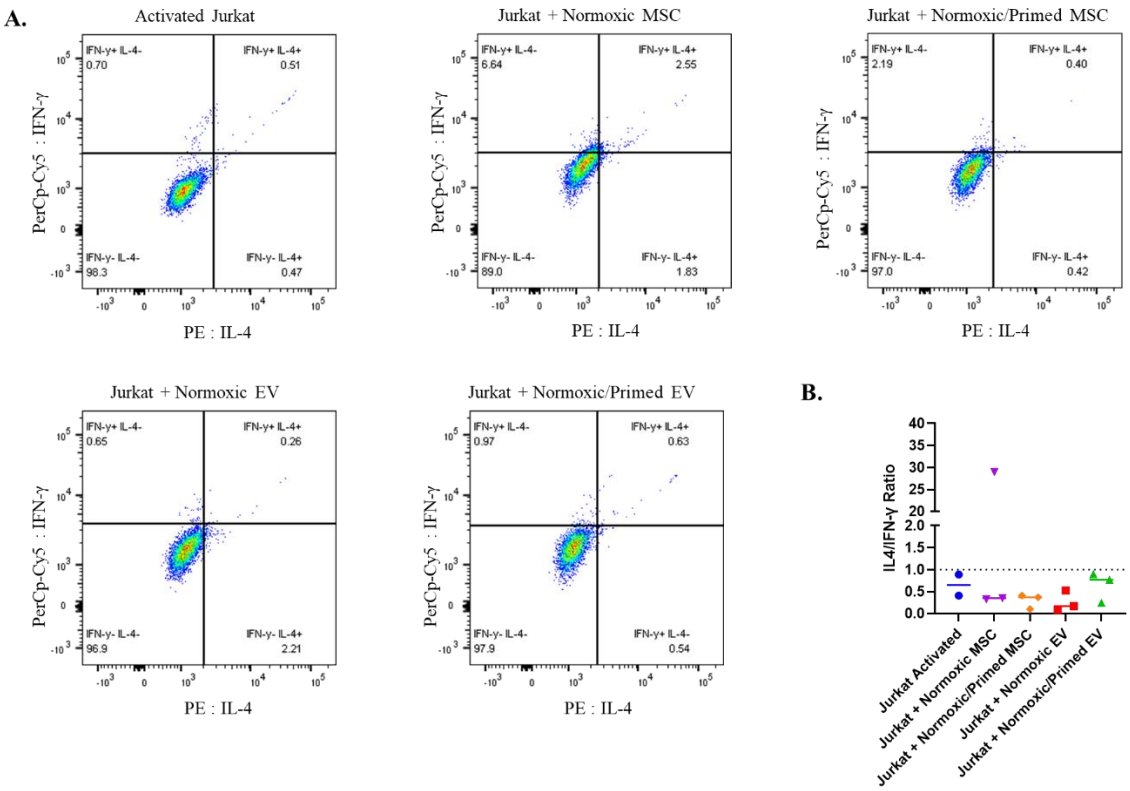

Figure 86: Production of IL-4 and IFN-γ in Jurkat cells

(A) *Dot plot displays the flow cytometry analysis of Jurkat cells in activated, non-activated and co-culture conditions (normoxic EVs, normoxic/primed EVs, normoxic MSCs and normoxic/primed MSCs). Cells were gated based on their production of IFN-γ (PerCp-Cy5 fluorochrome; y-axis) and IL-*

4 (PE fluorochrome; x-axis). IFN-γ positive/IL-4 negative cells are displayed in the top left quadrant. IFN-γ negative/IL-4 positive cells are displayed in the bottom right quadrant. The percentage production of IL-4: IFN-γ were compared to give a ratio value for Jurkats in each condition. ***(B)*** *Bar chart represents the IL-4/IFN-γ ratio on the y-axis and the different culture conditions on the x-axis. Points below the dotted line at y=1 represent a higher amount of IFN-γ to IL-4, points above the dotted represent a higher amount of IL-4 to IFN-γ. There was one outlier from the Jurkat + normoxic MSC co-culture that had a substantially increased ratio of IL-4: IFN-γ. There were no statistical differences between conditions.*

7.2.10 Tregs identification

Tregs are a subset of CD4+ T-cells capable of suppressing Th1 cells and pro-inflammatory signalling [547,548]. There are many different subsets of Tregs, including CD4+CD25+CD127- Treg cells and CD4+CD25+FoxP3+ Tregs [549]. FoxP3+ was upregulated by normoxic/primed EVs and MSCs **(Figure 80),** but as the FoxP3 antibody was conjugated to the same flourochrome as CD4, the percentage of CD4+CD25+FoxP3+ Tregs could not be measured. Instead, CD4+CD25+CD127- Tregs were analysed. Researchers have found a correlation between CD4+CD25+CD127- Treg cells and CD4+CD25+FoxP3 Tregs [550–552]. So, it was of interest to see if the increased production of FoxP3 in normoxic/primed EVs and MSCs correlated with an increase in CD4+CD25+CD127- Treg cells.

All PBMCs used in the co-culture experiments had an average CD25 production of 97.6% (±1.6 SD) so the PBMCs were gated on CD4 (PE) and CD127 (BV421) to identify this Tregs subset. CD4+CD25+CD127- Treg cells were compared between the activated PBMCs, PBMCs + normoxic EVs, and PBMCs + normoxic MSCs but failed to show any statistical differences **(Figure 87A, B).** There was a high standard deviation in the activated PBMCs, PBMCs + normoxic EVs, and PBMCs + normoxic MSCs in this experiment and, like the experiment that analysed CD3+CD4+ cells **(Section 7.2.8),** this was due to PBMC Donor 1 having a 1.54 times

higher amount of Tregs **(Supplementary Figure *8*B).** CD4+CD25+CD127- Treg cells were also compared between the activated PBMCs, PBMCs + normoxic/primed EVs, and PBMCs + normoxic/primed MSCs **(Figure 87C).** Normoxic/primed MSCs decreased the percentage of CD4+CD25+CD127- Tregs compared to activated PBMCs alone ($p<0.05$) **(Figure 87D),** which means that this result failed to correlate with the increased FoxP3 production identified in **Figure 80.** The average percentage of CD4+CD25+CD127- in PBMCs from the co-cultures is shown in **Table 27.**

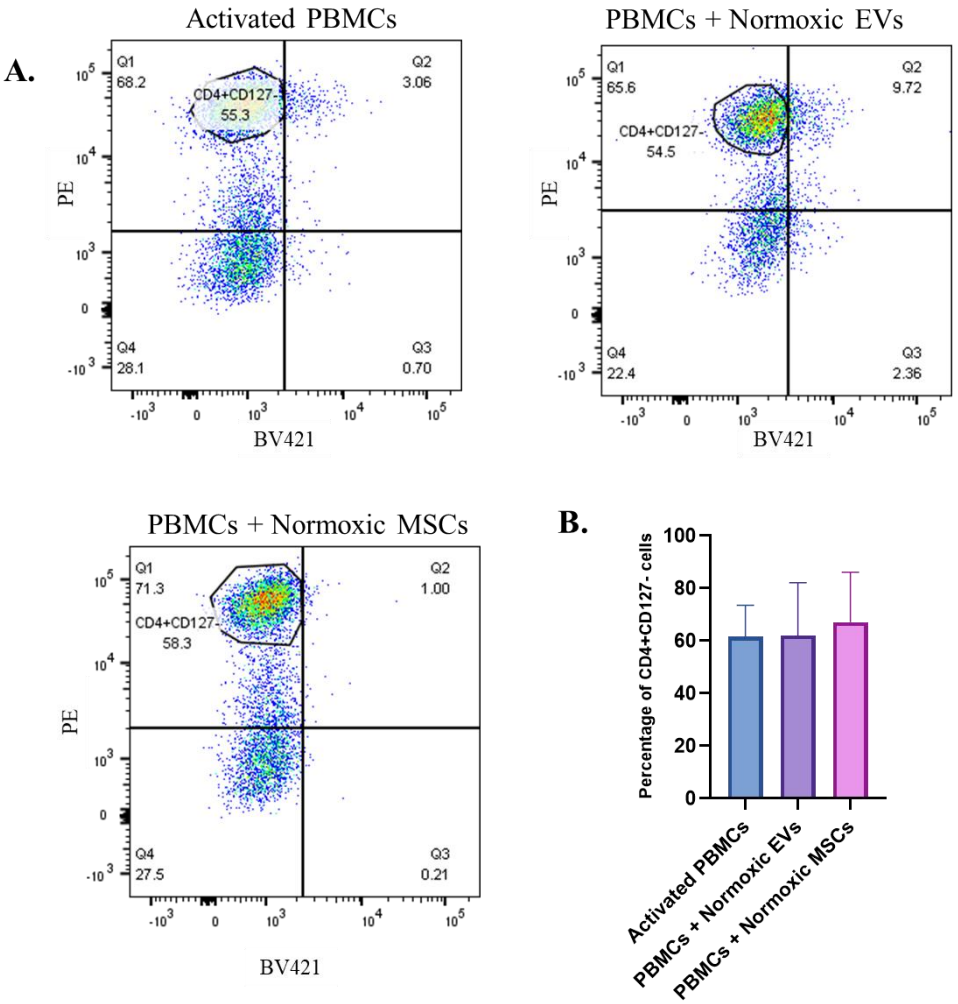

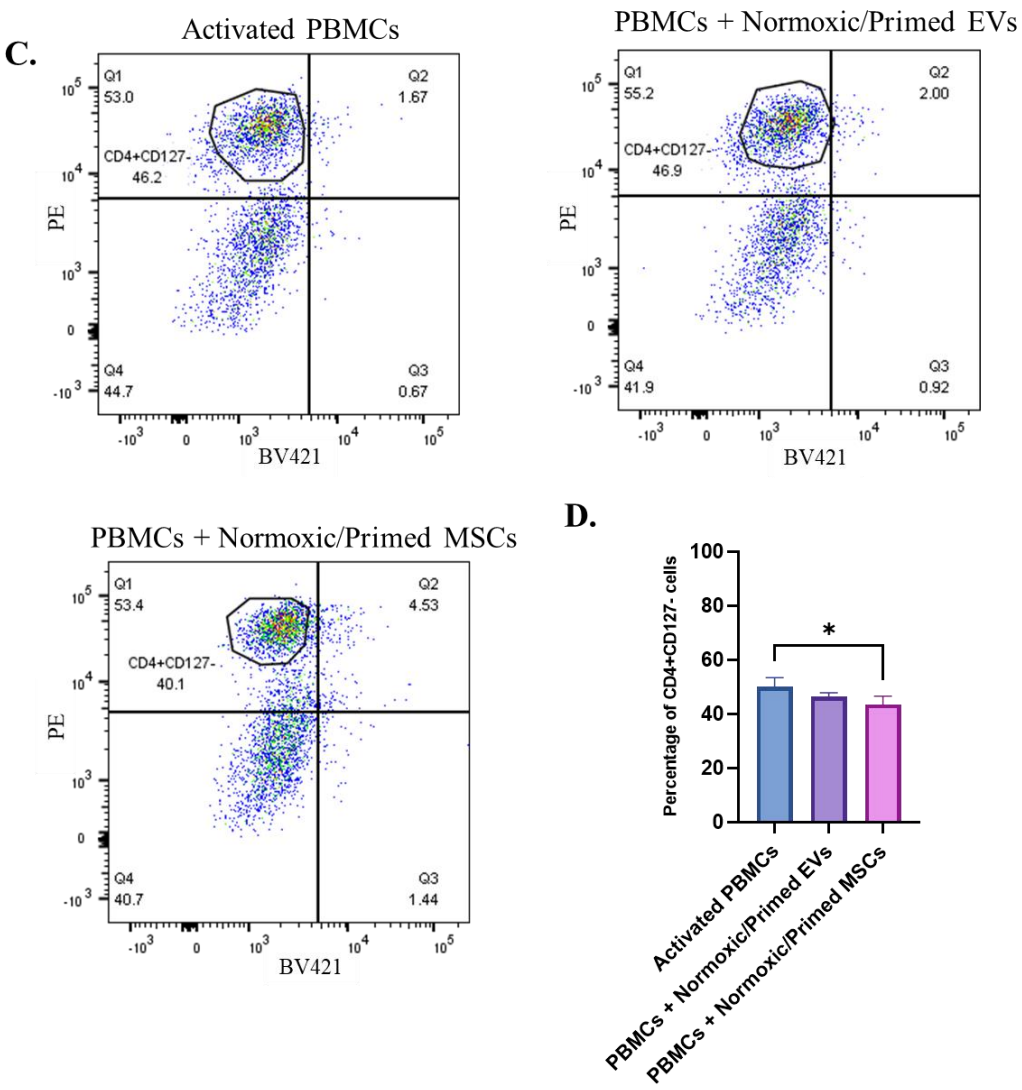

Figure 87: Percentage CD4+CD25+CD127- cells in PBMCs

*Dot plot showing the percentage of CD4+CD25+CD127- Tregs in PBMCs from co-culture conditions. PE (CD4) is shown on the y-axis and BV421 (CD127) on the x-axis. Gates are drawn for the subset of cells that are CD4 positive and CD127 negative. (**A**) Representative dot plot from activated PBMCs, PBMCs + normoxic EVs, PBMCs + normoxic MSCs. (**B**) Bar chart comparing the percentage (y-axis) of Tregs from PBMCs in different co-culture conditions (x-axis). There were no significant differences. (**C**) Representative dot plot from activated PBMCs, PBMCs + normoxic/primed EVs, PBMCs + normoxic/primed MSCs. (**D**) Bar chart shows that the activated PBMCs had a statistically higher percentage of CD4+CD127- Tregs compared to PBMCs + normoxic/primed MSCs ($p<0.05$).*

Table 27: Mean percentage of CD4+CD25+CD127- in PBMCs

	Mean	SD
Activated PBMCs	61.57	12.00
PBMCs + Normoxic EVs	62.00	20.13
PBMCs + Normoxic MSCs	67.13	18.96
Activated PBMCs	50.07	3.36
PBMCs + Normoxic/Primed EVs	46.43	1.46
PBMCs + Normoxic/Primed MSCs	43.53	3.09

7.3 Discussion

This chapter used *in vitro* co-culturing to study the effect of MSCs and EVs on PBMCs and Jurkat cells. The aim was to see if MSCs and EVs were anti-inflammatory and able to supress immune cell activity. Identifying cells and vesicles that can suppress the immune system is important for autoimmune conditions such as RA, where there is an abundance of pro-inflammatory cells. Therefore, it was initially planned to study the effect of MSCs and MSC-EVs on PBMCs/T-cells from the blood of people with rheumatoid arthritis. However, due to the coronavirus pandemic, it was not possible to access these patients at the Robert Jones and Agnes Hunt Orthopaedic Hospital. Ethical approval and consent had been obtained, and in the future, it would be beneficial to go back and analyse how EVs interact with PBMCs from patients with RA. This would provide a better understanding of the therapeutic potential of EVs as a therapy for RA.

There was a limited number of PBMCs available for the co-culture experiments. This was due to a few factors such as a variable cell yield, using PBMCs to optimise experiments and some PBMCs were lost due to the flow cytometer breaking down. This meant that three different PBMC donors had to be used for the co-culture experiments with normoxic/primed EVs and normoxic/primed MSCs. Pooling of all PBMC donors was considered prior to plating them for co-culturing, but this would have involved thawing every PBMC donor at once and carrying out all the co-culture experiments at the same time. Due to the large scale of the experiments, this was not possible. In hindsight, it may have been better to pool all donors immediately after PBMC isolation and prior to storage in liquid nitrogen.

The first objective of this chapter was to see how the CD3/CD28 activation was affecting PBMC and Jurkat morphology and protein production. CD3/CD28 stimulation has been found to influence the morphology of lymphocytes, particularly increase the size of T-cells [553] and increase clumping in activated T-cells [554]. The findings in this chapter show an increase in cell clumping of PBMCs and Jurkat cells, showing that CD3/CD28 activation is changing the cell morphology. In terms of PBMC protein production, the activated PBMCs had an increase in the production of CD4, CD25, IFN-γ and FoxP3, and a lower production of CD127 in the activated PBMCs. The increase in CD25 is positive because this is a marker of T-cell activation [543], which shows that activation was successful in this group. Furthermore, an increase in CD4, IFN-γ and FoxP3 in the activated PBMCs has previously been found in the literature after activation with CD3/CD28 [543,555,556]. This activation links closely to the immunology of RA as CD4+ T-cells are dominant (although CD8+ T-cells are present too) and these cells release a high amount of IFN-γ [532]. Therefore, the activation of PBMCs is sending them towards an RA immune cell phenotype. However, there is one deviation from this trend, and that is the increase in FoxP3 which is typically decreased in RA [1]. CD127 which inversely correlates with Foxp3 in Treg cells, [551], was lower in activated PBMCs, thereby activation may be directing the PBMCs down a Treg cell lineage. Research into CD3/CD28 activation of PBMCs also shows that IL-4 and HLA-DR levels should increase [556–558], but this was not seen between the activated and non-activated PBMCs. In all, it is clear that activation changed the phenotype of PBMCs as this was seen in changes in PBMC protein production, morphology and in their dot plot profile, as shown in **Figure 71**, **Figure 72** and **Figure 73**.

Jurkat cells were sourced as a readily available source of T-cells. They expressed CD3 but were largely negative for CD4 (<13.4%). This is in line with other studies that have shown Jurkat cells express low levels of CD4 [21]. There was no change in the production of CD4, CD25,

IFN-γ, IL-4, or FoxP3 in Jurkat cells showing that the activation of these cells was not effective in altering these specific proteins. It could be that the dose of CD3/CD28 was not strong enough to induce activation in these cells. CD3/CD28 activation works by conjugating CD3/CD28 agonists to synthetic microbeads which mimic antigen presenting cells to physiologically activate T-cells [559]. Another method for activating T-cells involves the use of phorbol 12-myristate 13-acetate (PMA) which activates protein kinase C and bypasses the TCR complex [560]. PMA causes a wide range of effects on cells as it activates many intracellular signalling pathways [561]. Indeed, Smeets et al. [562] found that PMA/CD3 and PMA/CD28 induce a stronger activation of Jurkat cells compared to CD3/CD28 activation. This was seen by the regulation of more genes and the higher production of IL-2 [562]. PMA was not employed in this study as the PBMCs were activated with CD3/CD28 and the addition of a new type of activator would add another variable, making the interpretation of results challenging. In all, CD3/CD28 activation did not have a significant effect on the Jurkat cells as there were no changes in the tested proteins, the cell morphology, or the dot plot profile.

Additionally, the limitations of Jurkat cells, must be taken into consideration as research has shown that Jurkat cells have a different actin organisation compared to primary T-cells [563]. The actin cytoskeleton plays an important part of T-cell functioning particularly the activation of T-cells at the immunological synapse [563]. Therefore, despite Jurkat cells and primary T-cells having comparable T-cell receptor signalling pathways, a different organisation of actin on the cell surface may lead to different results compared to primary T-cells [563] and this may further explain the non-response of CD3/CD28 activation by Jurkat cells.

Prior to commencing the co-culture experiments, a dose response experiment was conducted. This experiment was the second objective in this chapter, and it aimed to establish the optimal concentration of EVs to co-culture with PBMCs. EVs were added at 60µg, 90µg and 120µg to 2×10^6 PBMCs. This is based on a study by Ma et al. [564] who carried out a dose response experiment analysing the ability of UCMSC-EVs to downregulate Th17 cells and upregulate Treg cells. They dosed 2×10^6 PBMCs with 30µg, 60µg and 90µg EVs and found that the highest dose of 90µg EVs were effective at downregulating Th17 cells, inhibiting, IL-17, and upregulating Tregs and TGF-β production. Based on this evidence, a dose response experiment was set up using 60µg, 90µg and 120µg EVs.

Flow cytometry analysis of PBMC protein production, found that IFN-γ had a statistically lower production in the 120µg EV co-culture compared to the 60µg EV co-culture as shown in **Figure 75C**. IFN-γ is produced by Th1 cells and is the main contributor toward inflammation and activated macrophages/monocytes [565], therefore the lower production of this cytokine in PBMCs points towards an anti-inflammatory effect. However, the levels of IL-4 were reduced in the 120µg EV co-culture compared to the 60µg EV co-culture. This cytokine is expressed on Th2 cells and plays a role in regulating pro-inflammatory cytokine production by T-cells [566], thereby its reduced production is not indicative of an anti-inflammatory shift. However, there was a highly variable cytokine production in PBMCs that were co-cultured with 60µg EVs, and this could be explained by less EV availability, thus decreasing the likelihood of an EV-mediated change. The variable production could be caused by the uptake of EVs in some PBMCs but not in others, thereby only some PBMCs meet the threshold for a functional change, creating this variability in culture. This variable cytokine production adds doubt to the efficacy of the 60µg EV co-culture.

In general, the dose response curve did not show a linear increase in IL-4 or FoxP3, or a decrease in IL-17A with increasing EV concentrations. The only exception was a reduced IFN-γ production in PBMCs from the 120µg EV co-culture. This evidence, along with previous research showing that lower EVs concentrations aren't as effective as high concentrations in suppressing pro-inflammatory T-cells [564], led to the decision to use the higher concentration of 120µg EVs in the co-culture experiments. Despite the 60µg EV co-culture causing a statistically higher production of IL-4 in PBMCs, there was a large variation in this group when questions the reproducibility of these results. Therefore, EVs were used at the higher dose of 120µg EV to 2×10^6 PBMCs/Jurkat cells in upcoming experiments. The ratio of MSCs to PBMCs/Jurkat cells was 1:10. This is based on evidence from Kay et al. [121] and del Fattore et al. [165] who all used the same ratio and found that MSCs were effective in increasing FoxP3, decreasing IL-17A, and shifting the Treg/T-effector cell ratio in favour of Tregs, thereby causing an anti-inflammatory shift in the PBMCs.

PBMCs/Jurkat cells were co-cultured with normoxic MSCs, normoxic/primed MSCs, normoxic EVs and normoxic/primed EVs. **(Figure 68).** A comparison was made between MSCs and EVs, to see which one showed the most immunosuppressive potential, and between normoxic and normoxic/primed conditions, to see if the culture environments were generating a population of MSCs or EVs that were more anti-inflammatory. The PBMCs/Jurkat cells were assessed based on their production of protein markers after co-cultures.

Interestingly, normoxic EVs and MSCs were unable to reduce the production of IFN-γ in activated PBMCs compared to PBMCs alone. However, the PBMCs that were co-cultured with normoxic EVs did have a statistically lower production of IFN-γ when compared to the PBMCs

co-cultured with normoxic MSCs, which means that the EVs may be modulating the production of this pro-inflammatory cytokine to a greater extent than the MSCs. This is the different to other studies which have found UCMSCs to be a more potent suppressor of IFN-γ in PBMCs compared to their EVs [540].

IL-4 is another anti-inflammatory cytokine of interest. IL-4 has been found to support Treg functioning and it can polarise naïve Th cells into Th2 effector cells which inhibit Th1 activity via IL-12 signalling [567–569]. However, its production was unchanged in PBMCs. The lack of change in IL-4 is not uncommon and has been found when another group co-cultured placenta, bone marrow and umbilical cord blood MSCs with activated T-cells [570].

When comparing the primed to non-primed MSCs and EVs, FoxP3 was statistically higher in the PBMCs co-cultured with primed EVs and MSCs, but no changes were identified in the PBMCs co-cultured with normoxic EVs and MSCs. This may mean that the pro-inflammatory priming of MSCs/EVs is improving their immunomodulatory abilities by causing them to upregulate FoxP3, a marker of Tregs cells which are reduced in RA patients [571]. Indeed, canine MSC-EV were able to upregulate FoxP3 in PBMCs and the effect of this upregulation was stronger in pro-inflammatory primed EVs compared to non-primed EVs [357].

The protein profile of Jurkat cells (n=1) was affected by all conditions, but mostly by normoxic/primed EVs which reduced the production of CD25, IL-17A and FoxP3 in Jurkat cells compared to Jurkat cells alone. A decrease in CD25 may suggest that these EVs are reducing their activated state. There was a reduction in the pro-inflammatory cytokine, IL-17A

in all conditions showing that the normoxic and normoxic/primed MSCs and EVs are targeting this cytokine. The decrease production of IL-17A is a positive immunosuppressive move as it is produced by Th17 cells which are upregulated in RA and contribute to chronic inflammation [533]. Previous research has shown that high glucose media upregulates the production of IL-17A gene in Jurkat cells [572], as the Jurkat cells were grown in a DMEM containing high glucose this would explain the presence of IL-17A in Jurkat cells, nevertheless, the MSCs and EVs were able to decrease the amount of IL-17A in the co-cultures. This is in clear contrast to the PBMCs, in which the production of IL-17A was unchanged after co-culture with MSCs and EVs, albeit there was a low production of IL-17A to begin with.

Despite these anti-inflammatory changes, the production of FoxP3 was reduced in Jurkat cells co-cultured with normoxic and normoxic/primed EVs. FoxP3 is a key regulator of pro-inflammatory responses, and this data shows that EVs are modulating the production of FoxP3 in Jurkat cells. Additionally, FoxP3 has a statistically lower production in Jurkat cells that were co-cultured with normoxic EVs compared to normoxic MSCs, further showing that these EVs are targeting FoxP3 in Jurkat cells. This is in clear contrast to the effects of normoxic/primed EVs on PBMCs which statistically increased the production of FoxP3. It shows that the EVs may have different mechanisms of action to their parent MSCs, which has also been found in other studies [165,184,190].

There were no identified changes in the production of IL-4, IFN-γ or CD127 in Jurkat cells. Indeed, previous studies have found little uptake of ATMSC-EVs in Jurkat cells and no changes to IFN-γ production [540]. However, when considering the change in production of CD25, IL-17A and FoxP3, the evidence shows that MSCs and EVs are altering the Jurkat cell protein production.

The next objective was to look at the percentage of CD3+CD4+ cells, the IL-4: IFN-γ ratio and the percentage CD4+CD25+CD127- Tregs in PBMCs/Jurkat cells that were co-cultured with EVs and MSCs. This was carried out because the interpretation of functional performance is limited when analysing single marker changes, as it does not give a true insight into the relationship between different proteins in the cell population. The percentage of CD4+CD25+CD127- Tregs were also assessed to see if they correlated with the increased production of FoxP3 by normoxic/primed MSCs and EVs.

CD3+CD4+ T-cells in RA directly contribute to a chronic inflammatory response. Specifically, two types of CD4+ T-cells, Th1 and Th17, are highly activated in RA [530]. Th1 cells secrete IFN-γ, IL-12, IL-2 and TNF-α, and Th17 cells secrete IL-17, all of which promote a pro-inflammatory immune response [530]. Flow cytometry analysis revealed that normoxic/primed MSCs were able to statistically lower the percentage of CD3+CD4+ T-cells in PBMCs. This shows that normoxic/primed MSCs are reducing this population which could lead to a suppressed immune response. The percentage of CD3+CD4+ cells in all other PBMC co-cultures and in Jurkat cells remained unchanged.

The analysis of CD3+CD4+ T-cells in PBMCs does not detail if they are belonging to a Th1 and Th2 lineage. This is important as there is an imbalance in Th1/Th2 cells in RA, which is characterised mainly by the production levels of IFN-γ and IL-4 [556]. In particular, Th1 cells are major contributors towards RA pathogenesis, whereas Th2 cells have immunosuppressive properties [546]. This is mainly due to the fact the Th1 cells secrete IFN-γ, a pro-inflammatory cytokine and Th2 cells secrete IL-4, IL-5, and IL-13 which are cytokines with anti-inflammatory properties [546,573]. IL-4 levels are reduced in RA which directly correlates with disease severity. For this reason, the relationship between IFN-γ and IL-4 was assessed

with the hypothesis that MSCs or EVs could shift the IL-4: IFN-γ balance in favour of IL-4, thus favouring anti-inflammatory signalling. Results showed that the ratio of IL-4: IFN-γ was unchanged in PBMCs that were co-cultured with normoxic EVs and MSCs. So, despite PBMCs having a statistically lower production of IFN-γ when co-cultured with normoxic EVs compared to normoxic MSCs (**Figure 80**), this change did not translate into a difference in the IL-4: IFN-γ ratio. The lack of change shown here shows that the normoxic EVs/MSCs did not target Th1 or Th2 specifically. However, other cytokines such as IL-5 and IL-13 are released from Th2 cells [573], so an exploration of these cytokines and their ratio to IFN-γ would provide a stronger conclusion to the immunomodulatory ability of MSCs and EVs.

This study would have benefitted from the analysis of IFN-γ in the PBMC + normoxic/primed MSC/EV co-culture. This is a key pro-inflammatory cytokine in RA and insight into its expression would have been valuable in determining MSC immunosuppression. However, due to unforeseen antibody shortage this wasn't carried out.

There were no differences identified in IL-4: IFN-γ ratio in the Jurkat cells from all co-cultures **(Figure 86)**. This was expected as no considerable increase in either protein markers were identified from the single protein analysis, shown in **Figure 81.**

Another type of CD3+CD4+ T-cell are Tregs which have strong anti-inflammatory properties through suppressing T-cell proliferation and pro-inflammatory cytokine release [547,548]. In patients with autoimmune disease, Treg cells are either less abundant or defective, or both, which leads to the expansion of autoreactive T-cells [548,550,574,575]. Therefore, this

population of cells was assessed in the PBMCs to see if EVs or MSCs could increase their numbers, as this would represent an immunosuppressive ability. Jurkat cells were not analysed for their expression of Tregs as these cells had a very low number of CD4+ T-cells.

Two of the mostly commonly researched Tregs include CD4+CD25+CD127- Tregs and CD4+CD25+FoxP3+ Tregs. FoxP3 is a marker for natural Tregs but is also expressed to a lower extent in CD8+ T-cells [548]. When FoxP3 is stably expressed and present on CD4+CD25+ cells, this population of cells is capable of inhibiting the expression of pro-inflammatory cytokines [550]. In this study, there was an increase of FoxP3 by primed MSCs and EVs so it would have been beneficial to analyse the amount of CD4+CD25+FoxP3+ cells from the co-cultures, but a technical issue arising from the conjugation of both FoxP3 and CD4 to the same fluorochrome meant that this could not be carried out. Therefore, CD4+CD25+CD127- cells were used to characterise Tregs, and to see if their expression correlated with the identified increase in FoxP3 from the normoxic/primed EV and MSC co-culture with PBMCs [549]. This comparison was carried out because studies found that CD4+CD25+CD127- Tregs express high levels FoxP3, have a strong correlation with CD4+CD25+FoxP3+ Tregs, and functionally, they are equally as effective in suppressing CD4+ T-cell responses [550–552].

Results found that there was a significant decrease in CD4+CD25+CD127- Tregs in normoxic/primed MSCs compared to activated PBMCs **(Figure 87D).** This shows that the levels of FoxP3 and CD4+CD25+CD127- Tregs did not correlate in this experiment, because normoxic/primed MSCs increased the production of FoxP3 in PBMCs but did not increase the percentage of CD4+CD25+CD127- Tregs. Likewise, a correlation was not identified for the normoxic/primed EVs, as they increased FoxP3 in PBMCs but the percentage of

CD4+CD25+CD127- Tregs was unchanged. So, despite research showing a strong correlation, this was not found in these experiments.

All other MSCs and EV co-cultures with PBMCs were unable to change the percentage of CD4+CD25+CD127- Tregs compared to the control. This finding is surprising as MSCs are known to downregulate CD127, to maintain the Treg phenotype [576], and MSC-EVs can increase the proliferation of CD4+CD25+CD127- cells [165]. Nevertheless, the use of CD127 as a negative marker of Tregs is debated with many researchers arguing that the negative expression of CD127 is unreliable and not as accurate as FoxP3 [577,578]. Researchers also advocate for FoxP3 as the best indicator of Tregs, specifically the demethylation of the Treg cell-specific demethylated region (TSDR) which is associated with stable Tregs [579]. Therefore, in this chapter, the regulation of FoxP3 is regarded as being more influential to MSC and EV mediated immune modulation than the percentage of CD4+CD25+CD127- Tregs.

Additionally, many studies state that the ratio of Treg:Th17 is more important, as Tregs are capable of suppressing their pro-inflammatory counterparts [580–582]. Therefore, analysis of the Treg: Th17 ratio may have been more beneficial, as it is widely accepted that this Treg:Th17 imbalance contributes to autoimmunity and a loss of immune tolerance [583]. This is a limitation of the study and the the flow cytometry panel could be improved to include all Treg and Th17 cell markers in the one tube. An example of an improved flow cytometry panel along with the functions of the markers is provided in **Supplementary Table 3.**

Despite MSCs and EVs not increasing CD4+CD25+CD127- Tregs or the IL-4: IFN-γ ratio in the PBMCs, it must be recognised that they may be influencing other cell populations within the PBMCs. For example, research shows that EVs can polarise macrophages towards the M2

phenotype [584] and they're also known to have an immunomodulatory effect on B-cells [585,586]. Indeed, research studying the uptake of EVs by different subpopulations of PBMCs found that the majority of BMMSC-derived exosomes were found in monocyte and B-cell populations as opposed to T-cells [585]. A different study also reported that EVs were taken up by monocytes and rarely taken up by lymphocytes [184], so this evidence suggests that EVs may primarily act on other PBMC subsets and not directly target T-cells.

Overall, the main aim of this chapter is to assess the immunosuppressive ability of UCMSCs and UCMSC-EVs on PBMCs and Jurkat cells. So, the most important question to ask is: are MSCs and EVs immunosuppressive?

For the normoxic EVs, they were unable to change the protein profile of PBMCs and there was no change in CD3+CD4+ cells, IL-4: IFN-γ ratio or Treg cells indicating that they did not make a significant anti-inflammatory change. In the Jurkat cells, they reduced both IL-17A and FoxP3. As IL-17 is pro-inflammatory and FoxP3 is anti-inflammatory, and both contribute to the Th17: Treg ratio, then these finding could be considered to balance each other out.

For the normoxic/primed EVs, they were able to increase FoxP3 production in PBMCs, but no further differences were found in the percentage CD3+CD4+ cells, IL-4: IFN-γ ratio or Treg cells. In the Jurkat cells, they reduced their activated state by decreasing CD25 and similar to the normoxic EVs, they reduced both IL-17A and FoxP3. Due to their increase in FoxP3 in PBMCs and decrease of CD25 and IL-17A in Jurkat cells, normoxic/primed EVs are moderately immunosuppressive. The reason they are not considered to be strong immunosuppressors is because they were unable to increase Treg numbers in PBMCs or the

IL-4: IFN-γ ratio in Jurkat cells. The Treg: Th17 and Th1: Th2 balance is often used to determine the immunosuppressive properties of MSCs and EVs [587] and it is this balance that is polarised in RA [1,37,38,537,556]. So, for the EVs to change the immune profile of RA they would need to change the ratio of these cells.

The normoxic MSCs showed no effect on the PBMC immune profile in any experiment, they were only able to decrease the pro-inflammatory cytokine IL-17A in Jurkat cells. It is therefore doubtful if this change alone would be able to trigger a biologically significant anti-inflammatory effect.

The normoxic/primed MSCs displayed the most changes in the PBMC profile. They were able to upregulate FoxP3, decrease the percentage of CD3+CD4+ cells and CD4+CD25+CD127- Tregs. Out of these changes, FoxP3 is regarded as having the most impact of MSC immune modulation and as it is one marker of Tregs, its increase would improve immune tolerance. In the Jurkat cells, normoxic/primed MSCs reduced the production of IL-17A, which is considered and immunosuppressive effect.

The next question to ask is: Is the pro-inflammatory priming making EVs and MSCs more immunosuppressive?

It is clear that pro-inflammatory priming is better at increasing Foxp3 in PBMCs, so based on this evidence, it could be considered to be more beneficial. There was no evidence to suggest the pro-inflammatory priming was more affective in changing the Jurkat phenotype. The priming of MSCs does not always ensure that MSCs travel down an immunosuppressive path. Djouad et al. [105] found that MSCs had a reduced ability to suppress T-cell proliferation when

exposed to increasing concentrations of TNF-α. Additionally, Cosenza et al. [190] found that pro-inflammatory priming didn't affect the anti-inflammatory ability of MSCs and EVs when co-cultured with CD4+ and CD8+ T lymphocytes. So, while research heavily cites the immunosuppressive abilities of MSCs post pro-inflammatory priming, it is not a flawless or straightforward process approach.

One limitation to this study was the lack of analysis of PBMC/Jurkat proliferation and viability. Cell stains such as Violet Proliferation Dye, CSFE or a luminescence based assay provide a sensitive means to measure cell proliferation [588]. For cell viability, fluorescent-tagged annexin V staining is a commonly used method to measure cell apoptosis [589]. However, due to unforeseen set backs to the experimental plan, these experiments could not be carried out at the time of writing. Another limitation was the low number of PBMC donors. The addtion of more donors would have made the data more robust and possibly would have increased the likehood of identifiying more statistical differences.

7.4 Conclusion

This chapter looked at the immunosuppressive effect of MSCs and MSC-EVs on PBMCs and Jurkat cells. Specifically, it looked at the protein profile of the PBMCs/Jurkat after a 3-day co-culture. There is an imbalance of pro- to anti- inflammatory immune cells and cytokines in RA, so this chapter explored the ability of MSCs and EVs to shift the PBMCs/Jurkats to an anti-inflammatory phenotype.

Results showed that normoxic/primed EVs had the most potential to suppress immune responses as they were able to upregulate FoxP3 in PBMCs. Their parent normoxic/primed MSCs were also upregulated FoxP3. No changes were identified in PBMCs that were co-cultured with normoxic MSCs/EVs, therefore, the primed MSC/EVs are most likely to be able to carry out a functional change in PBMCs, although it is not clear if it will be a biologically significant change in RA. This is because there was lack of change seen in IL-4: IFN-γ ratio and the largely unchanged level of Tregs, and as the ratio of pro- to anti- inflammatory immune cells is important in RA, this questions the ability of MSCs and EVs to shift the balance of immune cells.

The normoxic/primed EVs reduced the production of IL-17A and CD25 in Jurkat cells and increased the production of FoxP3, which overall is considered to be an immunosuppressive move. MSCs in both conditions reduced the production of IL-17A showing that they too have anti-inflammatory properties. Overall, this study sheds light on the influence of MSCs and EVs towards PBMCs and Jurkat cells. It shows that their influence involves the increase of FoxP3 in PBMCs from primed MSCs/EVs and a decrease in the production of IL-17A in Jurkat cells.

Chapter 8: Discussion

8.1 Overview of Thesis

Rheumatoid arthritis is an inflammatory autoimmune disease where there is a breakdown of immune tolerance causing an activation of immune cells [4,36]. CD4+ T-cells, specifically, Th1 and Th17 cells [37,38], continually secrete pro-inflammatory cytokines (IL-2, IFN-γ, IL-17A) that are responsible for the sustainment of inflammation in RA [39]. Current pharmaceutical treatments for RA come with serious side effects and are not effective in all patients with RA [45–47]. Alternative treatments have explored the use of UCMSCs and results have found positive therapeutic effects in reducing RA symptoms [115,116]. However, these cells bring some safety risks such as cell differentiation *in vivo* and tumorigenicity [590]. Therefore, to exploit the therapeutic properties of UCMSCs without the cell-associated risks, their EVs were explored in this thesis to uncover their anti-inflammatory potential for the treatment of RA. This aim was created from evidence that MSC-EVs can inhibit the proliferation of CD4+ T-cells, suppress pro-inflammatory cytokine production and promote the expansion of Tregs [184,538,591–593], thereby making them a possible therapeutic option for RA patients. Additionally, the cell culture environment has been found to influence the immunosuppressive properties of MSCs and MSC-EVs, so it was decided to culture the UCMSCs in normoxia, hypoxia and with pro-inflammatory cytokines. It was thereby the hypothesis that the hypoxic and pro-inflammatory priming would bolster the immunosuppressive properties of UCMSCs and their EVs and make them more anti-inflammatory.

To achieve this aim and to understand the properties of UCMSC-EVs, they needed to be thoroughly characterised and analysed in functional tests. **Chapter 3** focused on the characterisation of their parent UCMSCs as a starting point towards understanding EV

characteristics. This chapter aimed to confirm that the cells were of a mesenchymal stem cell lineage while following the MSC characterisation criteria set out by the International Society for Cellular Therapy [51]. This chapter provided insight into the growth, morphology, and surface marker expression of UCMSCs. They were compared to a BMMSC control, and overall, they had a similar surface marker expression and faster *in vitro* growth. In all, the UCMSCs displayed all the required MSC markers, they had a spindle-like morphology and proliferated faster than BMMSCs making them a promising cell source for EV research.

As one of the aims of this thesis was to see how culture conditions alter EV properties, the MSCs were characterised under four different conditions (normoxia ± pro-inflammatory priming, hypoxia ± pro-inflammatory priming). When comparing the different culture conditions of UCMSCs, the pro-inflammatory priming caused an increase in CD106 and HLA-DR in some donors. These findings have relevance to immune modulation as CD106+ MSCs can suppress immune responses [277] and HLA-DR is known trigger immune responses, although on MSCs this is unlikely without the presence of co-stimulatory markers CD80 and CD86 [119,272]. These findings showed the heterogenic nature of the four umbilical cord donors as some responded differentially to pro-inflammatory priming. On the other hand, there were no differences in proliferation or surface marker expression between normoxic and hypoxic UCMSCs. While hypoxia supported the growth of UCMSCs, it didn't significantly increase its proliferation as was found with other studies of UCMSCs in hypoxia [266]. The lack of change in surface marker expression of UCMSCs in hypoxia is similar to findings in the research [267,268].

Chapter 4 details the numerous techniques employed to discover the properties of UCMSC-EVs. The main finding was that, in all four culture conditions, the EVs contained the characteristic EV protein markers, and they displayed the correct size and morphology of EVs, in line with the ISEV guidelines. This chapter also found some changes in EV characteristics between conditions. Some noteworthy differences include a higher concentration of particles in normoxic conditions compared to the hypoxic conditions, and a higher production of tetraspanins CD9, CD81, MSC marker CD105 and cell adhesion molecule CD146 in hypoxic EVs compared to hypoxic/primed EVs. Additionally, MCSP was lower in pro-inflammatory primed EVs compared to non-primed EVs. This protein has been found to functionally improve MSCs angiogenic properties and its decreased production may mean that the pro-inflammatory primed EVs were less angiogenic. In all, **Chapter 4** mainly focused on establishing that the isolated EV preparation were true EVs, and the following chapter delved further into the characterisation of EVs by looking at their protein cargo.

Chapter 5 employed the use of a proximity-based extension assay to study how hypoxic and pro-inflammatory culture conditions were affecting the EV protein cargo. Some commonly cited anti-inflammatory proteins (TGF-β1, PDL1, HGF, FGF21 [78,594]) were present in all EVs, but not differentially expressed between conditions. Indeed, there were no identified differences in the protein cargo of normoxic and hypoxic EVs. All the changes occurred in the expression of proteins between primed and non-primed EVs. In general, there was an increase in proteins associated with chemotaxis (CCL3, CCL11, CCL20, CXCL5) in the pro-inflammatory primed EVs. The expression of some anti-inflammatory proteins was also increased in pro-inflammatory primed EVs, such as MMP10 in normoxic/primed EVs, and LIF and TRAIL in hypoxic/primed EVs. MMP10 has been found to polarise M1 macrophages into an M2 phenotype [421] and both LIF and TRAIL protein are known to shift the Th17: Treg

balance [416,420]. This shows that the pro-inflammatory primed EVs contained both anti-inflammatory and chemotactic proteins. It remains to be answered whether the anti-inflammatory proteins will prevail and suppress immune responses or whether the chemotactic proteins will promote immune cell activity. However, before any solid conclusions could be formed, it was important to look at the other constituents of the EV cargo.

Chapter 6 looked at the miRNA cargo of EVs. MiRNAs are gaining increasing popularity after the discovery that EVs can transfer functional miRNAs into target cells whereby they can carry out gene silencing [445,595–597]. This study represents the first of its kind to sequence RNA for UCMSC-EVs in hypoxic and pro-inflammatory conditions. It aimed to identify miRNAs in UCMSC-EVs capable of suppressing immune responses, and to see if the culture conditions were influencing specific miRNAs to be packaged into EVs. A principal component analysis found that the cells clustered closely together indicating a high similarity, but the EVs in the different conditions showed no clear trends in clustering indicating that their miRNA profile is dissimilar in comparison. In all, there were 59 upregulated miRNAs in EVs compared to cells, showing that miRNAs were being selectively packaged into EVs. On comparison of the different types of EVs, there were 5 miRNAs upregulated in normoxic/primed EVs compared to normoxic EVs, and two downregulated in hypoxic EVs compared to normoxic EVs. The differentially expressed miRNAs, some contained anti-inflammatory properties, namely miR-139-5p, miR-140-5p, miR-214-5p but, in general, the miRNAs were either understudied, lowly expressed, or had multiple gene targets. This makes it very difficult to establish the *in vivo* functioning of the miRNAs. Furthermore, the RT-qPCR failed to validate the RNA sequencing findings, but this experiment ran into difficulties with data normalisation. It did positively identify miR-146a-5p and miR-181a-5p in all EVs, and these two miRNAs are reported to have anti-inflammatory functions on immune cells [445,524].

Up to this point, the information on EV characterisation **(Chapter 4),** protein cargo **(Chapter 5)** and miRNA cargo **(Chapter 6)** is all very valuable information about how EVs may function a specific way when encountering immune cells. Specifically, the characterisation of the EVs showed that they contained anti-inflammatory molecules, but it also showed that they contained pro-inflammatory proteins, and miRNAs with multiple gene targets. Therefore, at this point, it was not possible to ascertain how they would function against T-cells. It was then necessary to conduct functional experiments *in vitro* to see if the EVs were truly anti-inflammatory agents.

Chapter 7 detailed the co-culture of UCMSCs and their EVs with PBMCs and Jurkat cells. Initially the aim was to analyse the impact of MSCs and MSC-EVs on PBMCs from patients with RA, as this would be the most direct *in vitro* link towards determining the potential of EVs to be a therapeutic agent for RA. However, access to these patients was not possible at the time of the experiments so the analysis of EV immunosuppressive functioning was carried out on PBMCs from healthy volunteers and Jurkat cells. The findings of the co-culture experiments were mixed with neither normoxic EVs nor MSCs showing any effect on PBMCs, however, both normoxic/primed EVs and MSCs increased the production of FoxP3 in the PBMCs, which is considered a positive immunomodulatory change. Normoxic/primed MSCs decreased the percentage CD3+CD4+ T-cells. To get a clearer picture of which subset of T-cells they were targeting (i.e., Th1 or Th2), the ratio of IL4: IFN-γ was compared, although results show that the ratios were unchanged compared to the control. This shows that the normoxic/primed MSCs were not targeting IFN-γ-producing Th1 cells or IL-4-producing Th2 cells specifically. CD4+CD25+CD127- Tregs were downregulated in normoxic/primed MSCs only, which does not correlate with the increased expression of FoxP3, although there are doubts over the reliability of CD127 as a negative marker of Tregs [577,578,598]. All this evidence points

towards anti-inflammatory properties of the normoxic/primed MSCs and EVs based on their ability to increase FoxP3 production.

In terms of Jurkat cells, all EVs and MSCs reduced the production of IL-17A. The normoxic and normoxic/primed EVs also reduced FoxP3, therefore when deciphering the pro- and anti-inflammatory properties of these EVs, the reduction of IL-17A and FoxP3 balance each other out, as IL-17A is a pro-inflammatory cytokine secreted by Th17 cells, and FoxP3 is a marker associated with immunomodulatory Tregs. Normoxic/primed EVs also reduced the production of CD25 which is a marker of T-cell activation. When all changes in protein molecules are considered, the normoxic/primed EVs and both groups of MSCs elicit anti-inflammatory changes through the reduction of pro-inflammatory proteins in Jurkat cells, although their functional change is limited to IL-17A and CD25, as no differences were identified in CD3+CD4+ cells or the IL4: IFN-γ ratio.

Whether the increase in FoxP3 in PBMCs, and the reduction of IL17A/CD25 in Jurkat cells is enough to shift a pro-inflammatory response into an anti-inflammatory one is unknown and cannot be fully known without investigating these EVs in an animal model of RA. Overall, the findings from **Chapter 7** show that UCMSC-EVs have some anti-inflammatory effects on PBMCs and Jurkat cells and these anti-inflammatory properties are enhanced after MSCs priming with pro-inflammatory cytokines.

8.1.1 Outcome of hypoxic and pro-inflammatory priming

When considering all the chapters as a collective, this thesis identified the presence of some anti-inflammatory agents in EVs. But this project also proposed the hypothesis that pro-inflammatory priming and cell culture in hypoxia would improve the EV anti-inflammatory potential. However, many of the anti-inflammatory proteins and miRNAs (TGF-β1, PDL1, HGF, let-7i-5p, miR-100-5p) identified in the EV cargo did not show any changes in hypoxic or pro-inflammatory primed environments. There was an increased production of a few anti-inflammatory factors in the pro-inflammatory primed conditions, namely CD106 and LIF from the protein analysis, and an increased expression of miR-139-5p, miR-140-5p and miR-214-5p from the RNA sequencing analysis. But these findings are balanced by evidence that the miRNAs with multiple gene targets and there were many chemotactic proteins in the pro-inflammatory/primed EV cargo. Some alarm was raised by the presence of these chemotactic proteins (e.g. CCL3, MCP-4), as they are known to stimulate T-cells [407] and are associated with the early onset of RA symptoms [408]. But it must also be recognised that these proteins are widely cited to be key components of MSC immunomodulation [401–404] and it is unsurprising that these proteins are increased in the primed EV samples as it may indicate that the pro-inflammatory priming is ‘activating’ MSCs to seek out immune cells where they can carry out their anti-inflammatory effects. The concern presented in this **Chapter 5** is whether the RA disease model is the right choice due to the connections between these chemotactic proteins and RA.

Another concern was the association between many of the differentially expressed miRNAs and cancer pathways, many of which supported tumour progression, although this may be because cancer is a heavily researched field and studies on miRNAs relating to the immune

response is largely understudied [509,599]. Nevertheless, the association with cancer cannot be discredited. In all EVs, there was a high expression of miRNAs that were pleiotropic in nature, such as miR-21-5p and miR-139-5p. There is an uncertainty as to which gene these miRNAs will target *in vivo*, or they may target multiple pathways. It is clear that the culture conditions alter EVs, particularly between normoxic and normoxic/primed EVs as changes were found in the surface marker expression, protein cargo, miRNA profiles and in immune cell cytokine secretion. These changes are not necessarily anti-inflammatory, instead they are rather pleotropic and have targets in many different diseases. It shows that the pro-inflammatory priming conditions require further study as the findings from this study do not yield a large anti-inflammatory response despite what the research says.

However, despite the findings on EV miRNA and protein characterisation, the functional experiments did not promote a pro-inflammatory response, but rather caused a mild anti-inflammatory shift. This was seen in the ability of the normoxic/primed EVs and MSCs to increase FoxP3 production in PBMCs. It can be appreciated that in the EV cargo there is a diverse range of biological material and the PEA protein assay cherry-picked some specific proteins. It is likely that many other components of the EV cargo interacted with PBMCs.

Hypoxic EVs, showed a lack of change in terms of size, surface marker production, protein cargo and only had two downregulated miRNAs in comparison to normoxic EVs. Instead, evidence from the protein analysis suggest that EVs may have a role in other pathways such an angiogenesis. Specifically, VEGF-A was increased in the hypoxic/primed EVs cargo and this protein has strong connections to angiogenesis and vascular permeability [600]. The progression of inflammation in RA joints is often associated with increased blood vessel

formation which provides extra routes for immune cell access the joints and thereby help facilitate the progression of inflammation [601]. Additionally, research has shown that high serum levels of VEGF-A in RA is associated with increased joint damage [600], therefore, considering the aim of this thesis was to establish if UCMSC-EVs could be a potential therapy for RA-related inflammation, then the presence of angiogenic proteins is not desired. However, VEGF-A in the EV cargo may be more suited towards the treatment of myocardial infarction, ischaemic heart disease, skin burns and wound healing by which UCMSCs have already shown positive therapeutic outcomes [602–607]. Therefore, the hypoxic EVs in this study may have a therapeutic potential when applied to the right disease model.

Going back to the original hypothesis that hypoxic and pro-inflammatory priming bolsters the EVs anti-inflammatory properties, the evidence tends to point towards an unsuccessful priming approach for hypoxia but a mildly successful pro-inflammatory priming approach in normoxia.

8.1.2 Challenges faced in thesis

One main theme emerging throughout all chapters is the heterogeneity of UCMSCs and their EVs. Many research groups have reported MSC heterogeneity [608–611] and this rather expectantly has resulted in EV heterogeneity both in terms of characterisation and functioning [612]. Indeed Kordelas et al. [199] found huge variability in MSC-EV protein cargo from four donors of the same MSC source and using the same isolation method which is similar to the variability identified in this study. Other researchers found high variations between MSC-EV batches from the same donor in terms of immunomodulatory abilities [612]. This makes the function of MSC-EVs somewhat stochastic and unless this marker of ‘functionality’ can be found, this poses a problem for the application of MSC-EVs in research. To gain a greater

understanding if the variability in samples was the result of one donor skewing the results, the data was analysed for each donor and compared. However, there were no obvious trends identified. Different donors responded differently to the conditions, for example, Donor 2 had higher levels of HLA-DR/CD106 in response to priming in normoxia and hypoxia; Donor 4 only had an increase of HLA-DR/CD106 in normoxic/primed conditions, and Donor 1 only had an increase of HLA-DR/CD106 in hypoxic/primed conditions (**Figure 31**). When examining the size of particles, Donor 1 had the smallest size particles in all conditions (**Figure 34**), and when the tetraspanin profile of the EVs was examined, Donor 3 had a considerably higher expression of CD9 and CD81 in normoxic and normoxic/primed conditions, compared to the other donors (**Figure 37**). Other analysis of normalised protein expression and miR-21-5p expression did not show donor variability. In all, this heterogeneity complicates the therapeutic development of an EV product as its function *in vivo* will be unpredictable. Therefore, to combat this variability in EV profiles, they would need to be analysed using an omics approach before use in the clinic, which is not feasible due to time and cost. Thus, an approach that uses a cell line that overexpresses specific anti-inflammatory miRNAs would establish consistency and reproducibility each time [447,613]. Other groups have tried this by altering MSCs to overexpress c-myc and found that the process was scalable under GMP conditions [447,614]. Another growing area of EV research is their potential to be used as carrier vehicles whereby desired miRNAs or anti-inflammatory drugs are transfected into an isolated EV population, this targeted approach would thereby establish a consistent therapeutic product [613,615]. EVs contain a phospholipid bilayer membrane structure which makes them suitable for this purpose. Thereby MSC-EVs are still therapeutic candidates for RA, just in a different capacity.

Finally, a reocurring challenge throughout this thesis was generating the required amount of EVs for characterisation and functional assessment. The process of obtaining enough conditioned media when cells are grown on tissue culture plastic is very time consuming and labour itensive, and is likely to be a challenge facing many research groups. Therefore, the large-scale growth of cells in bioreactors is a quicker way and more effeicient way to obtain conditioned media enriched in EVs. The emergence of bioreactors and bioreactor flasks to grow cells has been noticed by the EV field and is growing in popularity [616–619]. The UCMSCs in this study were initially expanded by Mennan et al. [63] in the Quantum® cell proliferation system, however the use of this system could not be continued for this poject due to the high costs involved. However, it would be a solution to the challenge of obtaining enough EVs.

8.1.3 Impact of thesis

This thesis achieved a number of goals which will aid UCMSC-EV research going forward. One of the benefits of this work was the detailed characterisation of EVs from normoxic, hypoxic, and pro-inflammatory conditions. The analysis of EVs from these conditions has not been done before on Quantum® expanded UCMSCs. Similarly, this thesis analysed the EV protein cargo by means of a PEA assay. This assay has been used by other research groups for EV protein analysis, but none have applied it to UCMSC-EVs. Furthermore, no studies have been carried out on UCMSC-EVs from normoxic, hypoxic and pro-inflammatory conditions using the PEA assay. So, there is further novelty in the range of inflammatory proteins tested for in the UCMSC-EV cargo from different conditions.

This thesis also provided the first insight into the miRNA cargo of hypoxic and pro-inflammatory primed UCMSC-EVs, obtained through NGS. Few studies have looked at sequencing the miRNA content of EVs, and even less at comparing EVs derived from different culture conditions. This thesis describes the successful sequencing of the UCMSC-EV small RNA cargo and provides valuable data to the understanding of EVs and their miRNA composition.

The impact of this thesis is extended by the functional studies carried out on PBMCs and Jurkat cells. To our knowledge, there has only been one study that looks at the immunomodulatory effect of MSC-EVs on Jurkat cells [540] and this study used adipose tissue as the source of MSCs. So, this thesis adds extra novelty to the EV field and pushes the boundary towards discovery new interactions between EVs and T-cells.

Finally, this thesis has applied the findings of EV properties and functioning to RA. Most EV research looks at chronic kidney disease, graft vs host disease, sepsis, ischaemia and respiratory diseases [620,621] and very few EV studies have looked at inflammatory arthritic conditions [190]. Although this research was not able to access RA blood, it still provided very useful functional studies of UCMSCs and EVs interactions with activated T-cells and it related the findings to RA as a disease. In all, this thesis used a variety of different techniques to achieve an overview of UCMSC-EVs.

8.2 Future Work

There are some interesting areas left to explore. One of these is trying to establish a standardised EV isolation method. All current methods yield a different range and purity of EVs, and for this reason there is no preferred EV isolation method. The resulting lack of consensus on isolation methods has impacted EV research greatly. It has hampered the ability of different research groups to obtain reproducible results especially in terms of functional studies where the properties and functions of EVs vary depending on their isolation method. This study used differential ultracentrifugation combined with a 30% sucrose cushion as it is based on the EV floating density which research recommends as an extra purification step for EVs [209,622], albeit it has been found to decrease the protein concentration of up to 1000-fold [623]. It would be useful to identify one EV isolation method for cell conditioned media so that future work with UCMSC-EVs would be performed under consistent and optimal conditions.

A reoccurring challenge in this project was controlling for the potential of FBS-EV contamination throughout. EV depletion of FBS was carried out in this study but it was ineffective at removing all FBS-EVs. An alternative to using EV depleted FBS is to purchase different media supplements to replace the growth factors present in the FBS. However, Auber et al. [624] found that the alternative media supplementation also contained contaminating miRNAs, so despite the serum alternative chosen, experiment adaptation would still be required to control for contamination. For this reason, future work would look at substituting FBS to serum free media for short periods during conditioned media collecting and to see if this alters the EVs compared to EVs from cells grown in normal FBS. However, a thorough

analysis of the cells response to short term serum free conditions will need to be evaluated as serum free conditions are known to ‘stress’ cells [625].

The anti-inflammatory protein profile of the EVs could be explored further. Ideally, mass spectrometry is the ideal technique to provide information on the whole proteome, but this was not available for this study. In the future, it’d be beneficial to look at specific anti-inflammatory proteins such as IDO and PGE2 which have known immunomodulatory functions [626–628] in a europium-based immunoassay as this is a highly sensitive and cost-effective method. This would provide information on whether the UCMSCs are packaging their anti-inflammatory factors into EVs.

A priority for future work is the deeper analysis of the RNA sequencing data. The RNA sequencing experiment sequenced all small RNAs and not just miRNAs. Therefore there is data available to look at transfer RNAs (tRNAs) which have been reported to be highly enriched in MSC-EVs compared to their cells [188]. They are also found to have similar properties to miRNAs although their functioning is largely unknown [188]. Therefore, this could be designed as an explorative study to discover the tRNA repertoire in MSC-EVs. It would also be useful to compare just the EV groups, without the cells, to see if more differentially expressed miRNAs could be identified. The RNA sequencing experiment generated a large amount of data and the analysis of this data has just skimmed the surface. Issues arose around accessing university facilities and staff support during the Covid pandemic which affected the study design of the RNA sequencing analysis. However, the further analysis of the RNA sequencing data is a priority for future work.

Finally, future work would look at co-culturing hypoxic EVs and MSCs with activated PBMCs as these EVs were not used in **Chapter 7.** Normoxic/primed EVs were chosen over hypoxic EVs for the co-culture experiments, due to time constraints and because they had more differentially expressed proteins and miRNAs in their cargo, thereby it was more likely that differences would be observed in this group. However, it would be premature to exclude the EVs just based on their characterisation and not look at their functioning *in vivo.* Many research groups have identified immunomodulatory properties in hypoxic ATMSC-EVs and BMMSC-EVs [82,629,630] so therefore to make any strong conclusions about the hypoxic UCMSC-EVs, functional studies need to be carried out.

8.3 Conclusion

This thesis describes the isolation and characterisation of EVs from UCMSCs. It characterises EVs from four different culture conditions and an aimed to discover a population of EVs with the most anti-inflammatory potential. The normoxic/primed EVs contained the most differentially expressed proteins and miRNAs in response to pro-inflammatory priming. The increased proteins had chemotactic and immunomodulatory properties, and the upregulated miRNAs were pleotropic in nature with the most connections associated with cancer pathways and immune suppression. This diverse protein and miRNA profile means that the EVs may have wide ranging effects if applied to an RA model. When these EVs were carried forward into functional studies with activated PBMCs from healthy donors and Jurkat cells, the normoxic/primed EVs showed stronger anti-inflammatory potential compared to normoxic EVs as they were able to increase FoxP3 in PBMCs and decrease IL-17A in Jurkat cells. Therefore, out of the range of proteins and miRNAs that were increased in the normoxic/primed EVs, it was those with anti-inflammatory properties that caused a mild anti-inflammatory shift in the PBMCs and Jurkat cells. When considering if EVs from UCMSCs can be therapeutic agents in RA, the normoxic/primed EVs are most likely to be anti-inflammatory.

Supplementary Information

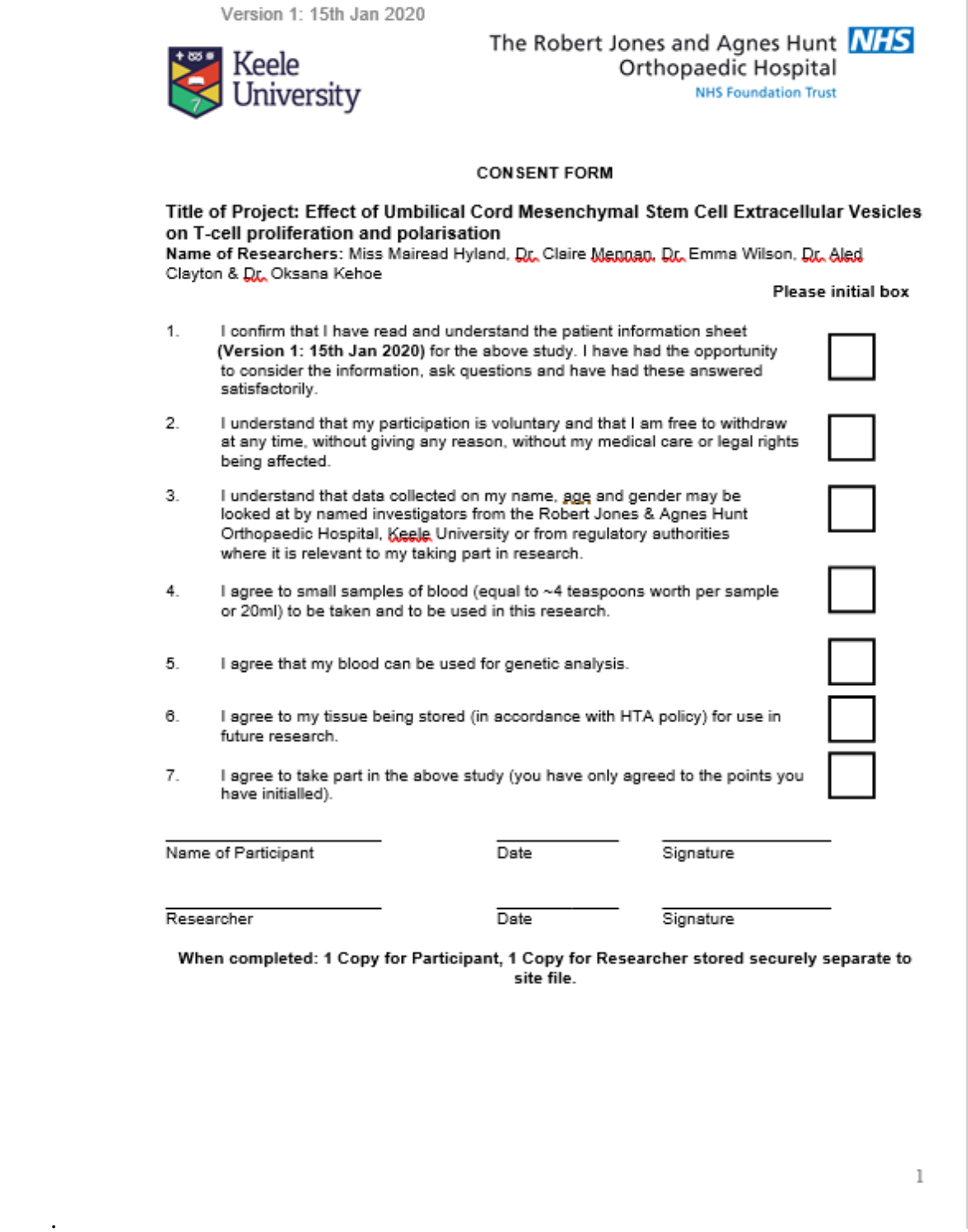

Version 1: 15th Jan 2020

Keele University

The Robert Jones and Agnes Hunt Orthopaedic Hospital NHS Foundation Trust

CONSENT FORM

Title of Project: Effect of Umbilical Cord Mesenchymal Stem Cell Extracellular Vesicles on T-cell proliferation and polarisation

Name of Researchers: Miss Mairead Hyland, Dr. Claire Mennan, Dr. Emma Wilson, Dr. Aled Clayton & Dr. Oksana Kehoe

Please initial box

1. I confirm that I have read and understand the patient information sheet **(Version 1: 15th Jan 2020)** for the above study. I have had the opportunity to consider the information, ask questions and have had these answered satisfactorily. ☐
2. I understand that my participation is voluntary and that I am free to withdraw at any time, without giving any reason, without my medical care or legal rights being affected. ☐
3. I understand that data collected on my name, age and gender may be looked at by named investigators from the Robert Jones & Agnes Hunt Orthopaedic Hospital, Keele University or from regulatory authorities where it is relevant to my taking part in research. ☐
4. I agree to small samples of blood (equal to ~4 teaspoons worth per sample or 20ml) to be taken and to be used in this research. ☐
5. I agree that my blood can be used for genetic analysis. ☐
6. I agree to my tissue being stored (in accordance with HTA policy) for use in future research. ☐
7. I agree to take part in the above study (you have only agreed to the points you have initialled). ☐

Name of Participant	Date	Signature
Researcher	Date	Signature

When completed: 1 Copy for Participant, 1 Copy for Researcher stored securely separate to site file.

1

.

Supplementary Figure 1:Consent for given to patients prior to blood donation

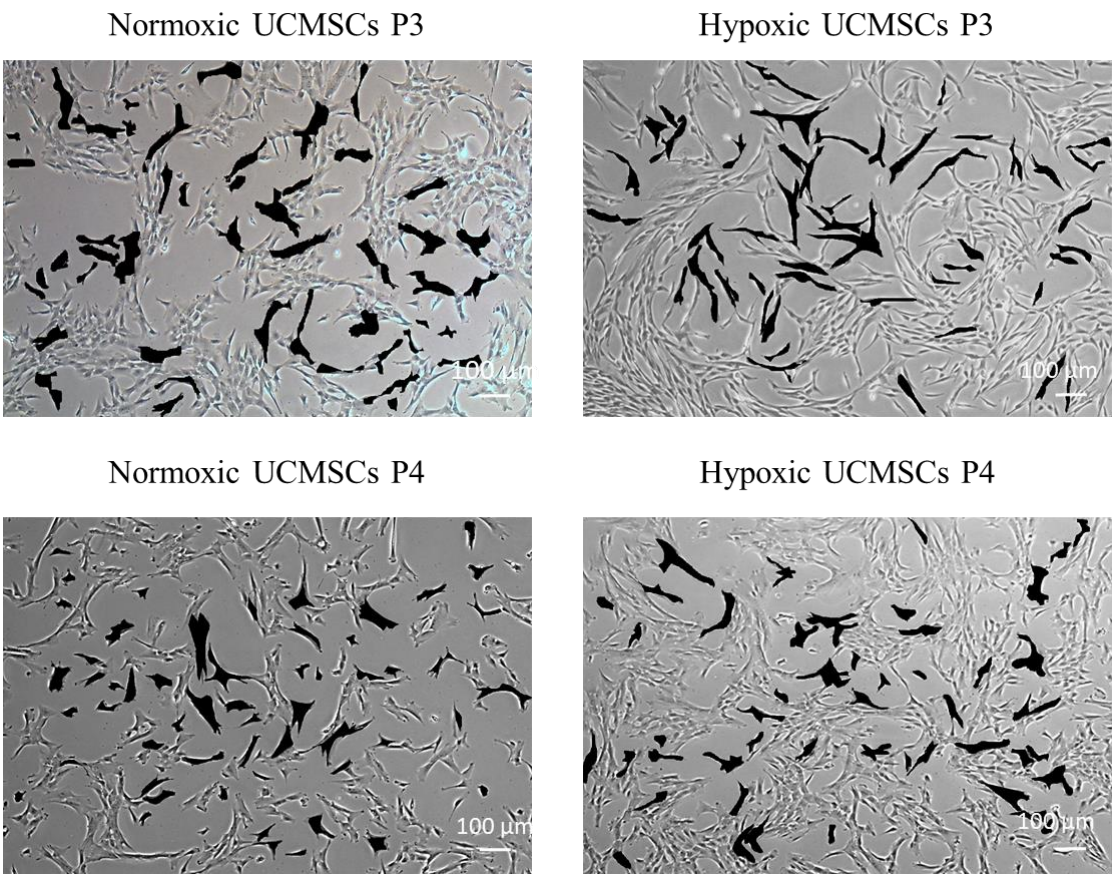

Supplementary Figure 2: ImageJ analysis of cells

Representative photos of ImageJ analysis carried out on UCMSCs in normoxia and hypoxia at P3 and P4, taken using the 4x objective. A line was drawn around the boundary of the cells and the surface area mapped out (shown in black). The pixel density of the cell was calculated on the software. This figure was converted into surface area using the scale bar as a reference point.

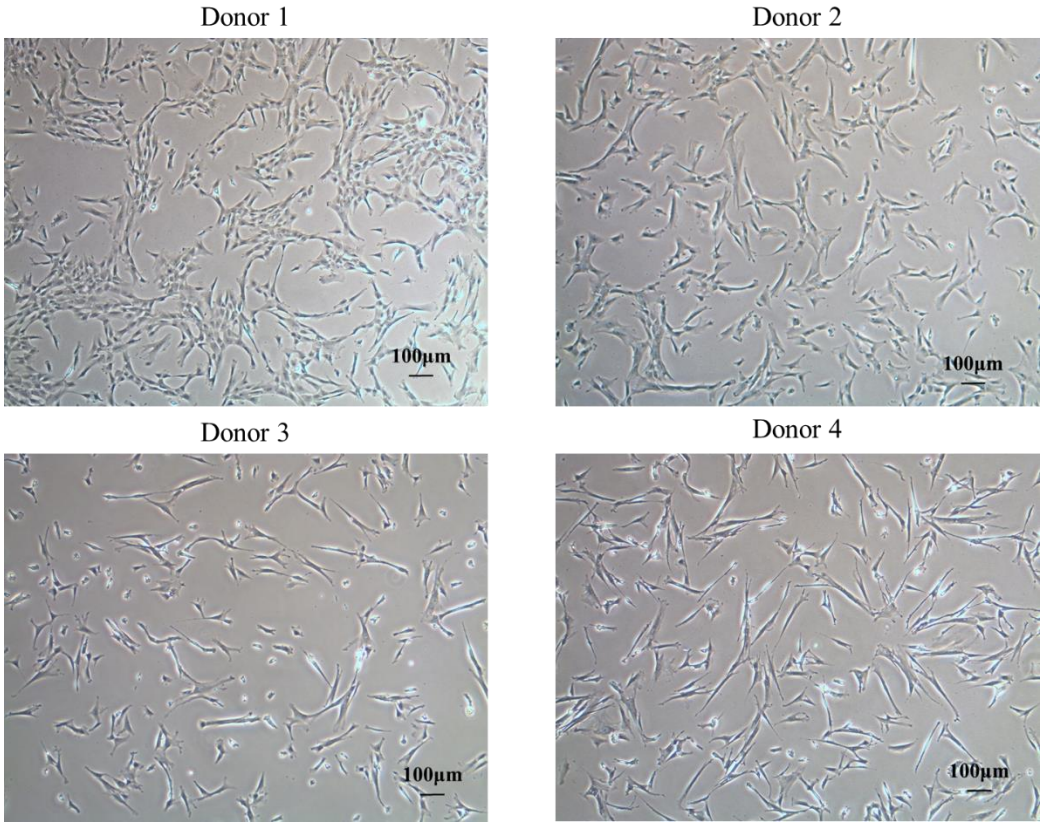

Supplementary Figure 3: Variability in donor morphology

UCMSCs showed variability in cell morphology across the four donors. MSCs from donor 1 appeared to cluster more and were similar to Donor 2. Donor 3 MSCs contained a more heterogeneous population with a mix of round and spindle-like cells. Donor 4 MSCs displayed more properties of inactive fibroblasts as they were more elongated. Images taken of Donor 1-4 from P3-6 of cells in normoxic conditions.

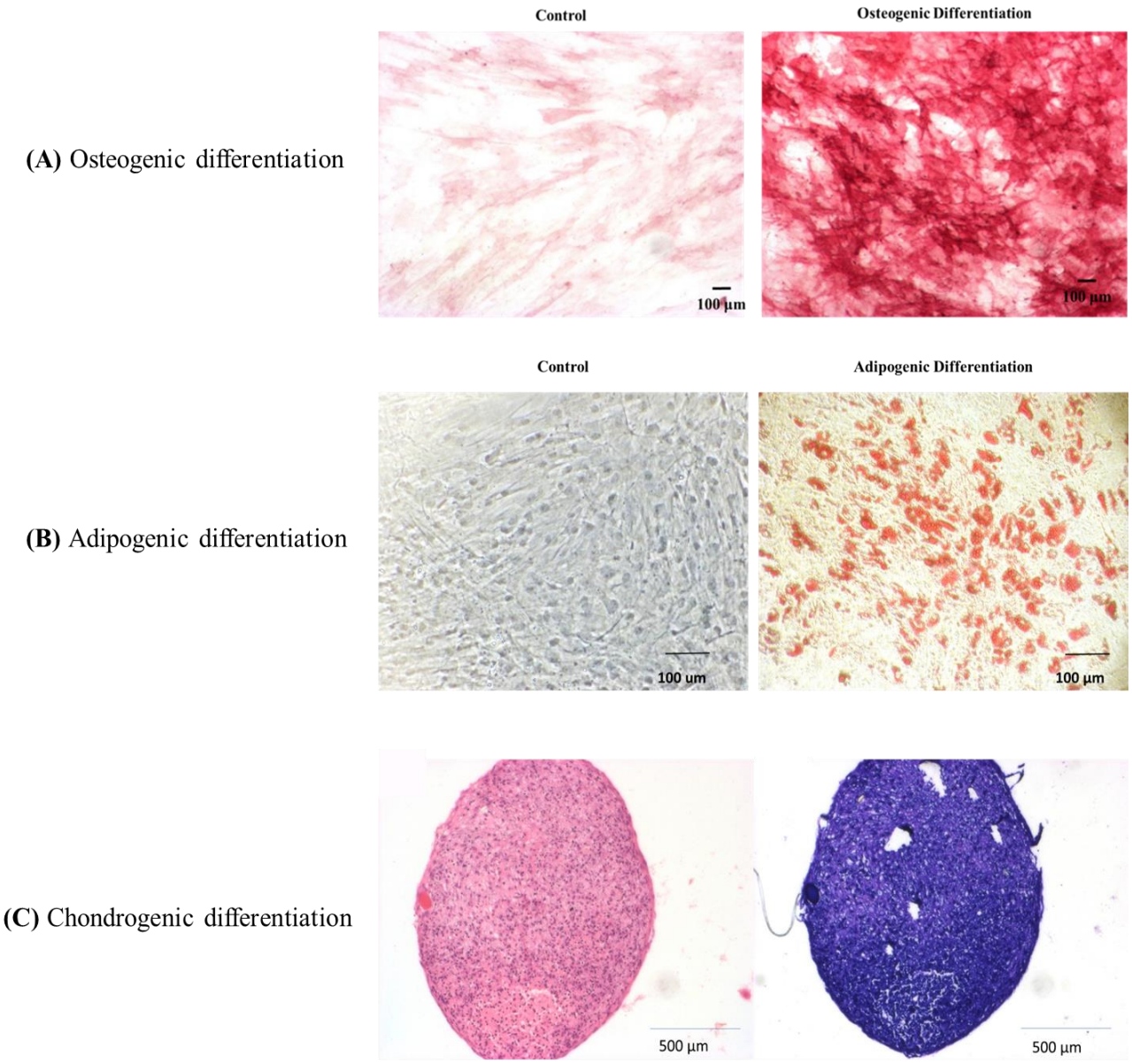

Supplementary Figure 4: Tri-lineage differentiation of BMMSCs

BMMSCs (n=1) at passage 2 underwent trilineage differentiation. ***(A)*** *Images display the osteogenic differentiation of BMMSCs stained with alkaline phosphatase stain. The darker red deposits indicate ALP activity and an early indicator of osteogenesis. Images taken at 4x objective on an Eclipse TS100 microscope.* ***(B)*** *Images display the adipogenic differentiation of BMMSCs. Lipid droplets from BMMSC monolayer appear red after Oil Red O staining. Images taken at x20 objective on an Eclipse TS100 microscope.* ***(C)*** *Images display a H&E stain (pink) showing the presence of a densely packed pellet of BMMSCs and a toluidine blue stain showing dark blue/purple deposits of glycosaminoglycans on the pellet sections which indicate positive staining for chondroblasts. Images taken on a Leica Diaplan microscope and show a scale bar of 500µm.*

Supplementary Table 1: List of 92 proteins included in the Inflammation Panel Assay (Olink Bioscience, Uppsala, Sweden).

1.	**Adenosine Deaminase (ADA)**	**24.**	**Fibroblast growth factor 5 (FGF-5)**	**47.**	**Interleukin-17A (IL-17A)**	**70.**	**Oncostatin-M (OSM)**
2.	**Artemin (ARTN)**	**25.**	Fibroblast growth factor 19 (FGF-19)	**48.**	Interleukin-17C (IL-17C)	**71.**	Osteoprotegerin (OPG)
3.	**Axin-1 (AXIN1)**	**26.**	Fibroblast growth factor 21 (FGF-21)	**49.**	Interleukin-18 (IL-18)	**72.**	Programmed cell death 1 ligand 1 (PD-L1)
4.	**Beta-nerve growth factor (Beta-NGF)**	**27.**	Fibroblast growth factor 23 (FGF-23)	**50.**	Interleukin-18 receptor 1 (IL-18R1)	**73.**	Protein S100-A12 (EN-RAGE)
5.	**Caspase 8 (CASP-8)**	**28.**	Fms-related tyrosine kinase 3 ligand (Flt3L)	**51.**	Interleukin-20 (IL-20)	**74.**	Signalling lymphocytic activation molecule (SLAMF1)
6.	**C-C motif chemokine 4 (CCL4)**	**29.**	Fractalkine (CX3CL1)	**52.**	Interleukin-20 receptor subunit alpha (IL-20RA)	**75.**	SIR2-like protein 2 (SIRT2)
7.	**C-C motif chemokine 19 (CCL19)**	**30.**	Glial cell line-derived neurotrophic factor (GDNF)	**53.**	Interleukin-22 receptor subunit alpha-1 (IL-22 RA1)	**76.**	STAM-binding protein (STAMPB)
8.	**C-C motif chemokine 20 (CCL20)**	**31.**	Hepatocyte growth factor (HGF)	**54.**	Interleukin-24 (IL-24)	**77.**	Stem cell factor (SCF)
9.	**C-C motif chemokine 23 (CCL23)**	**32.**	Interferon gamma (IFN-gamma)	**55.**	Interleukin-33 (IL-33)	**78.**	Sulfotransferase 1A1 (ST1A1)
10.	**C-C motif chemokine 25 (CCL25)**	**33.**	Interleukin-1 alpha (IL-1 alpha)	**56.**	Latency-associated peptide transforming growth factor beta 1 (LAP TGF-beta-1)	**79.**	T-cell surface glycoprotein CD5 (CD5)
11.	**C-C motif chemokine 28 (CCL28)**	**34.**	Interleukin-2 (IL-2)	**57.**	Leukemia inhibitory factor (LIF)	**80.**	T-cell surface glycoprotein CD6 isoform (CD6)
12.	**CD40L receptor (CD40)**	**35.**	Interleukin-2 receptor subunit beta (IL-2RB)	**58.**	Leukemia inhibitory factor receptor (LIF-R)	**81.**	T-cell surface glycoprotein CD8 alpha chain (CD8A)
13.	**CUB domain-containing protein 1 (CDCP1)**	**36.**	Interleukin-4 (IL-4)	**59.**	Macrophage colony-stimulating factor 1 (CSF-1)	**82.**	Thymic stromal lymphopoietin (TSLP)
14.	**C-X-C motif chemokine 1 (CXCL1)**	**37.**	Interleukin-5 (IL-5)	**60.**	Macrophage inflammatory protein 1-alpha (CCL3)	**83.**	TNF-beta (TNFB)
15.	**C-X-C motif chemokine 5 (CXCL5)**	**38.**	Interleukin-6 (IL-6)	**61.**	Matrix metalloproteinase-1 (MMP-1)	**84.**	TNF-related activation-induced cytokine (TRANCE)
16.	**C-X-C motif chemokine 6 (CXCL6)**	**39.**	Interleukin-7 (IL-7)	**62.**	Matrix metalloproteinase-10 (MMP-10)	**85.**	TNF-related apoptosis-inducing ligand (TRAIL)
17.	**C-X-C motif chemokine 9 (CXCL9)**	**40.**	Interleukin-8 (IL-8)	**63.**	Monocyte chemotactic protein 1 (MCP-1)	**86.**	Transforming growth factor alpha (TGF-alpha)
18.	**C-X-C motif chemokine 10 (CXCL10)**	**41.**	Interleukin-10 (IL-10)	**64.**	Monocyte chemotactic protein 2 (MCP-2)	**87.**	Tumor necrosis factor (Ligand) superfamily, member 12 (TWEAK)
19.	**C-X-C motif chemokine 11 (CXCL11)**	**42.**	Interleukin-10 receptor subunit alpha (IL-10RA)	**65.**	Monocyte chemotactic protein 3 (MCP-3)	**88.**	Tumor necrosis factor alpha (TNF-α)
20.	**Cystatin D (CST5)**	**43.**	Interleukin-10 receptor subunit beta (IL-10RB)	**66.**	Monocyte chemotactic protein 4 (MCP-4)	**89.**	Tumor necrosis factor ligand superfamily

			member 14 (TNFSF14)
21. Delta and Notch-like epidermal growth factor related receptor (DNER)	**44.** Interleukin-12 subunit beta (IL-12B)	**67.** Natural killer cell receptor 2B4 (CD244)	**90.** Tumor necrosis factor receptor superfamily member 9 (TNFRSF9)
22. Eotaxin-1 (CCL11)	**45.** Interleukin-13 (IL-13)	**68.** Neurotrophin-3 (NT-3)	**91.** Urokinase-type plasminogen activator (uPA)
23. Eukaryotic translation initiation factor 4E-binding protein 1 (4E-BP1)	**46.** Interleukin-15 receptor subunit alpha (IL-15RA)	**69.** Neurturin (NRTN)	**92.** Vascular endothelial growth factor A (VEGF-A)

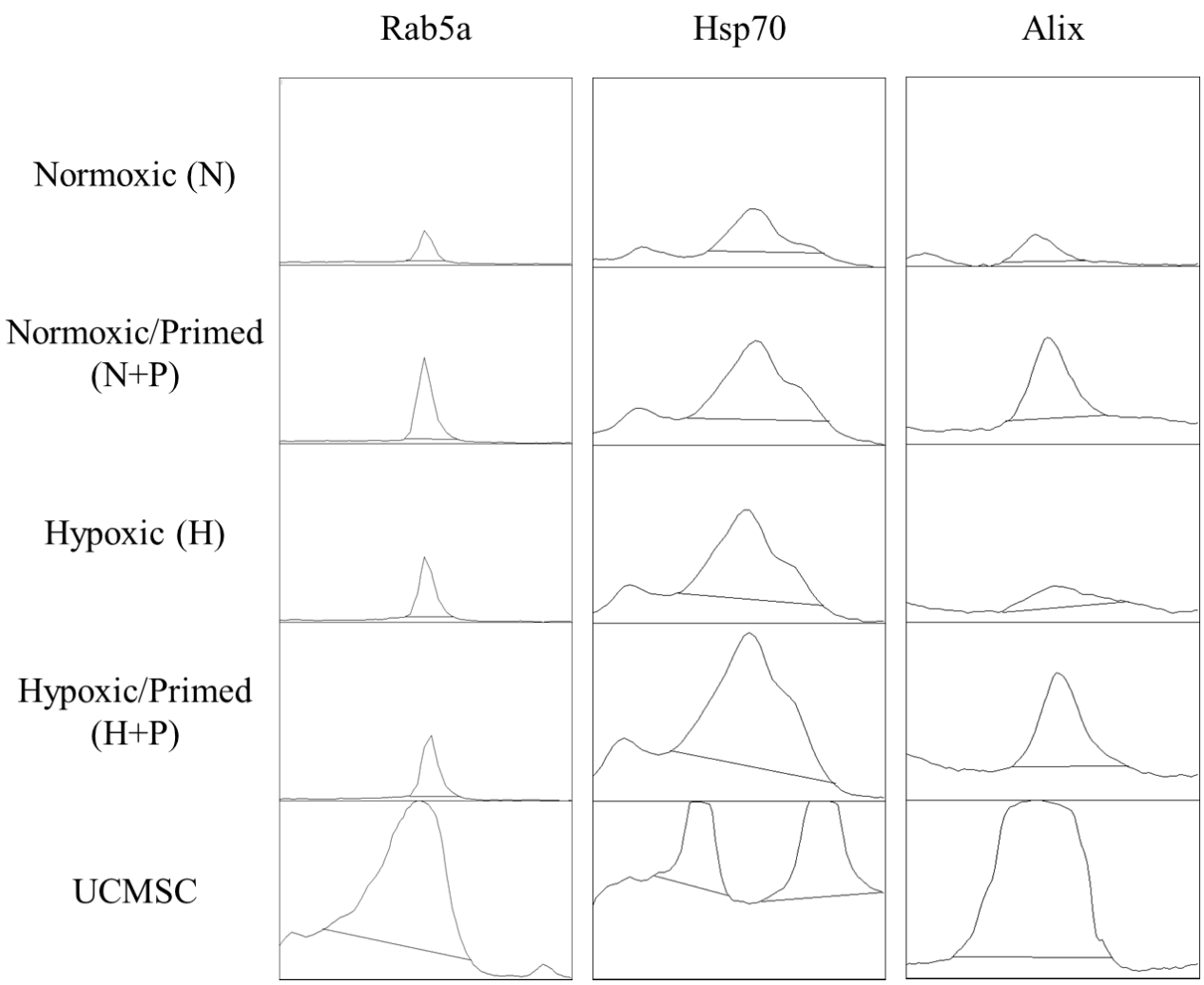

Supplementary Figure 5: Protein band peaks for Rab5a, Alix and Hsp70

ImageJ software was used to quantify the protein expression from the western blot bands. Protein bands on the nitrocellulose membrane were gated and a pixel density generated. This pixel density was transformed into a peak graph shown in the figure above. A line was drawn at the baseline, and the surface area above this line was calculated. The band intensity number is an arbitrary figure used to depict the relative change between samples. Figure shows images of band peaks for Rab5a, Hsp70 and Alix show at the top of the figure and the conditions are represented on the left of the figure.

Supplementary Table 2: List of differentially expressed miRNAs between cells and EVs

Table displays a full list of the 61 differentially expressed miRNAs between normoxic cells and normoxic EVs along with the Log2(FC) and the adjusted p-value. 59 miRNAs had a higher expression in EVs, and 2 miRNAs (miR-127-3p and miR340-5p) had a higher expression in cells.

	Log2 (FC)	Adjusted p-value		Log2 (FC)	Adjusted p-value
hsa-miR-1290	-11.83	4.19E-91	hsa-miR-142-3p	-4.41	0.003162
hsa-miR-486-5p	-9.50	3.16E-50	hsa-miR-200b-3p	-3.67	0.003303
hsa-miR-122-5p	-9.29	3.89E-49	hsa-miR-6131	-4.90	0.004151
hsa-miR-6529-5p	-10.99	1.71E-37	hsa-miR-323a-5p	-4.53	0.004944
hsa-miR-1246	-10.09	2.82E-33	hsa-let-7c-5p	-2.04	0.015102
hsa-miR-203a-3p	-9.11	7.15E-29	hsa-miR-543	-1.99	0.01641
hsa-miR-184	-11.13	1.39E-28	hsa-miR-92b-3p	-1.65	0.025211
hsa-miR-1291	-9.78	4.55E-25	hsa-miR-3158-3p	-2.87	0.029505
hsa-miR-122-5p	-10.41	2.12E-21	hsa-miR-5100	-3.64	0.029505
hsa-miR-9-5p	-7.48	3.62E-20	hsa-miR-340-5p	1.39	0.031254
hsa-miR-4488	-9.91	3.40E-18	hsa-miR-6826-3p	-4.26	0.033039
hsa-miR-126-3p	-4.19	2.82E-15	hsa-miR-1307-3p	-1.28	0.034358
hsa-miR-10395-3p	-6.84	1.13E-13	hsa-miR-432-5p	-1.80	0.034705
hsa-miR-423-5p	-3.95	3.33E-11	hsa-miR-760	-3.07	0.045366
hsa-miR-320b	-3.14	1.37E-10	hsa-miR-148b-5p	-3.07	0.046511
hsa-miR-1-3p	-3.74	4.16E-10	hsa-miR-485-5p	-2.02	0.046511
hsa-miR-320c	-3.48	1.01E-09	hsa-miR-151a-3p	-0.90	0.050443
hsa-miR-205-5p	-7.27	3.12E-08	hsa-miR-409-3p	-1.49	0.055556
hsa-miR-320d	-4.52	2.17E-07	hsa-miR-615-3p	-1.95	0.0588
hsa-miR-215-5p	-4.39	2.31E-07	hsa-miR-423-3p	-0.99	0.063741
hsa-miR-4448	-5.82	2.31E-07	hsa-miR-128-3p	-0.99	0.070354
hsa-let-7b-5p	-2.14	2.00E-06	hsa-miR-200c-3p	-2.85	0.07534
hsa-miR-142-5p	-5.92	2.97E-06	hsa-miR-92a-3p	-0.85	0.084618
hsa-miR-192-5p	-2.29	1.17E-05	hsa-miR-3605-5p	-3.29	0.095663
hsa-miR-4671-5p	-5.68	2.21E-05	hsa-miR-363-3p	-3.64	0.095663
hsa-miR-320a-3p	-2.74	2.75E-05	hsa-miR-92b-5p	-2.50	0.095663
hsa-miR-193b-5p	-3.87	0.000365	hsa-miR-99a-5p	-1.16	0.095663
hsa-miR-320e	-3.86	0.001598	hsa-miR-4680-3p	-3.45	0.096476
hsa-miR-127-3p	0.58	0.001676	hsa-miR-744-5p	-0.96	0.097327
hsa-miR-342-5p	-4.01	0.001676	hsa-miR-1228-5p	-3.29	0.097544
hsa-miR-3179	-4.65	0.002396			

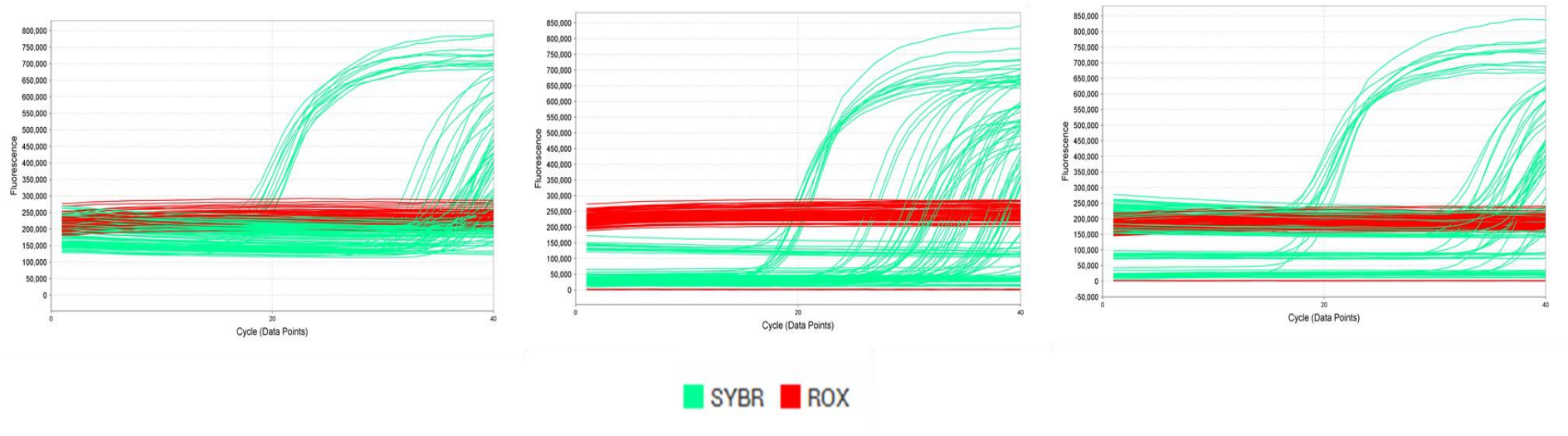

Supplementary Figure 6: Multicomponent PCR plot

Multicomponent plot displaying SYBR Green fluorescent and ROX fluorescence. Fluorescent intensity is depicted on the y-axis and the cycle number is on the x-axis. ROX fluorescence was consistent from cycles 1-40 in all plates analysed.

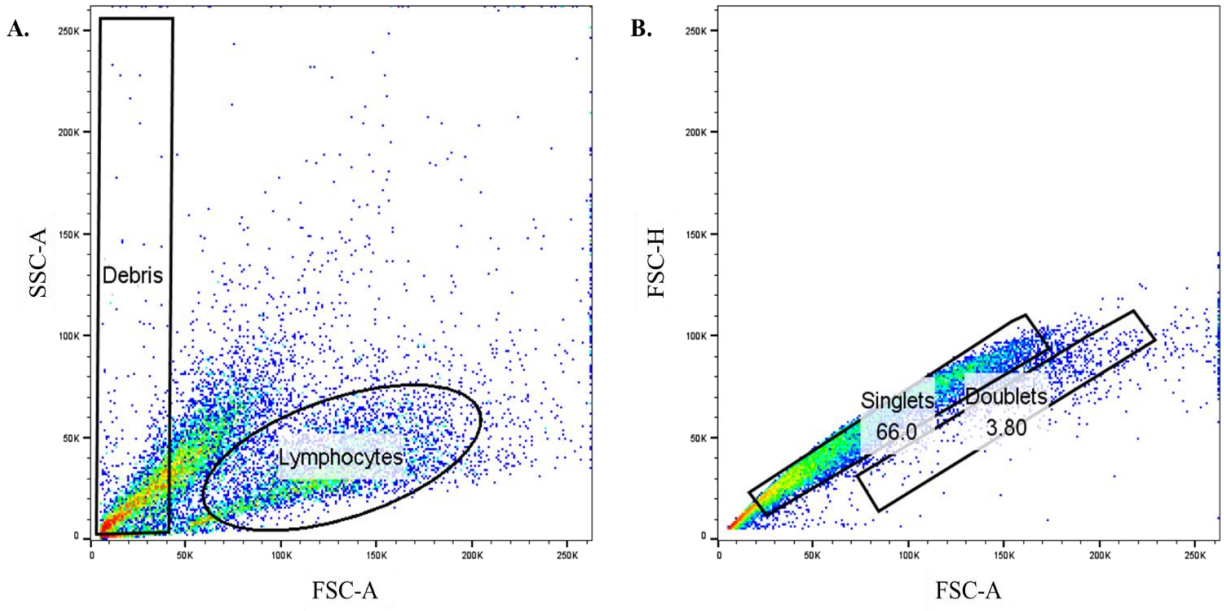

Supplementary Figure 7: Gating of Lymphocytes on Flow Cytometry

(A) *Flow cytometry generated a dot plot of the PBMCs, with the Side Scatter Area (SSC-A) shown on the y-axis and the Forward Scatter Area (FSC-A) shown on the x-axis. Dead cells and debris were gated and excluded from analysis of this population. A gate was drawn around the lymphocyte subtype, based on its high forward scatter and clustering, and this population was used for further analysis. (**B)** Using the gated lymphocyte population, another scatter plot was created based on the Forward Scatter Height (FSC-H; y-axis) and Forward Scatter Area (FSC-A; x-axis). The lymphocytes were gated a second time to remove doublet cells which may provide false readings in the analysis.*

Supplementary Table 3: Proposed flow cytometry panel for PBMCs and Jurkat cells

Antibody	Fluorochrome	Function
CD3	APC	T-cell marker
CD4	PE	Helper T-cell marker
CD8	BV421	Cytotoxic T-cell marker
HLA-DR	FITC	Marker of activated T-cells
TNF-α	APC	Pro-inflammatory cytokine secreted by macrophages
IFN-γ	PerCp-Cy5.5	Pro-inflammatory cytokine secreted by activated T-cells
TGF-β	FITC	Anti-inflammatory cytokine secreted by macrophages
CD45	PE	Lymphocyte marker
CD28	FITC	T-cell activation marker
FoxP3	PerCp-Cy5.5	Treg Marker
CD25	APC	Treg marker and T-cell activation marker
CD127	FITC	Treg marker
CD19	BV421	B-cell marker
IL-4	FITC	Anti-inflammatory cytokine secreted by Th2 cells
IL-17a	BV421	Pro-inflammatory cytokine secreted by Th17 cells

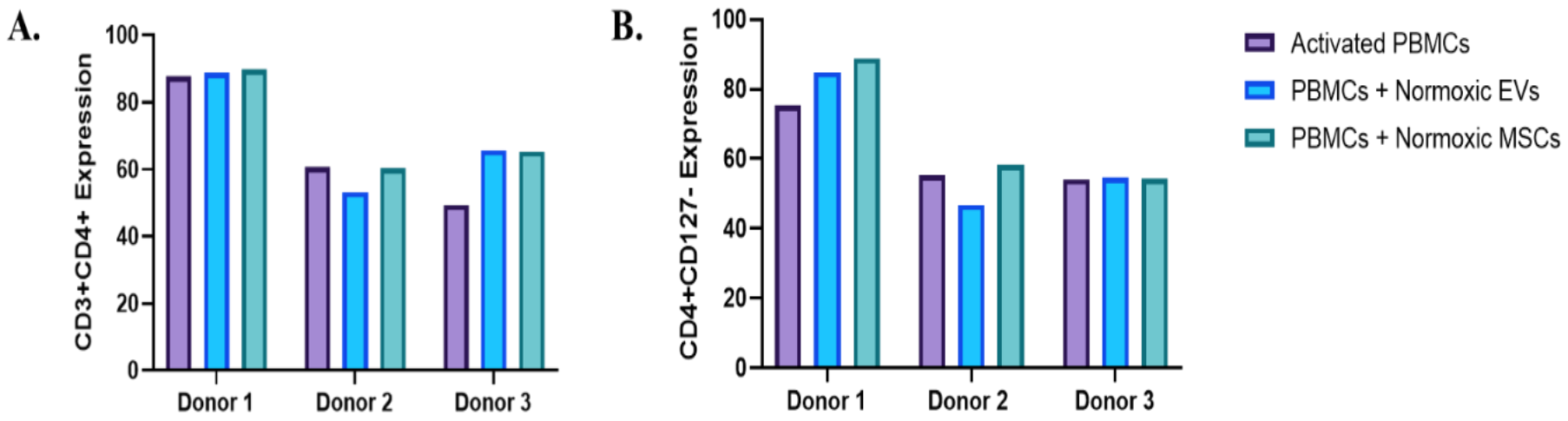

Supplementary Figure 8: CD3+CD4+ and CD4+CD127- expression on PBMCs

(A) *Bar chart shows the percentage expression of CD3+CD4+ (y-axis) on the three PBMC donors (x-axis). Donor 1 had on average a 1.5 times higher expression of CD3/CD4 compared to Donor 2 and Donor 3 in all conditions.* ***(B)*** *Bar chart shows the percentage expression of CD4+CD127- (y-axis) on the three PBMC donors (x-axis). Donor 1 had on average a 1.54 times higher expression of CD4+CD127- compared to Donor 2 and Donor 3 in all conditions.*

Bibliography

[1] Al-Zifzaf DS, El Bakry SA, Mamdouh R, Shawarby LA, Ghaffar AYA, Amer HA, et al. FoxP3+T regulatory cells in Rheumatoid arthritis and the imbalance of the Treg/TH17 cytokine axis. *Egypt Rheumatol* . 2015;37(1):7–15. DOI:10.1016/j.ejr.2014.06.004

[2] Smolen JS, Aletaha D, Barton A, Burmester GR, Emery P, Firestein GS, et al. Rheumatoid arthritis. *Nat Rev Dis Prim* . 2018;4:1–23. DOI:10.1038/nrdp.2018.1

[3] Firestein GS. Evolving concepts of rheumatoid arthritis. *Nature*. 2003;423(6937):356–61. DOI:10.1038/nature01661

[4] Doan T, Massarotti E. Rheumatoid arthritis: An overview of new and emerging therapies. *J Clin Pharmacol*. 2005;45(7):751–62. DOI:10.1177/0091270005277938

[5] Kevin D. Deane, M. Kristen Demoruelle, Lindsay B. Kelmenson, Kristine A. Kuhn, Jill M. Norris and VMH. Genetic and environmental risk factors for rheumatoid arthritis. *Best Pr Res Clin Rheumatol*. 2017;31(1):3–18.

[6] Jeremy Sokolove, Dannette S. Johnson, Lauren J. Lahey, Catriona A. Wagner, Danye Cheng, Geoffrey M. Thiele, Kaleb Michaud, Harlan Sayles, Andreas M. Reimold L, Caplan, Grant W. Cannon, Gail Kerr, Ted R. Mikuls and WHR. Rheumatoid factor as a potentiator of anti-citrullinated protein antibody mediated inflammation in rheumatoid arthritis. *Arthritis Rheumatol* . 2014;66(4):813–21.

[7] Versus Arthritis. The State of Musculoskeletal Health. 2019;17.

[8] Cross M, Smith E, Hoy D, Carmona L, Wolfe F, Vos T, et al. The global burden of rheumatoid arthritis: Estimates from the Global Burden of Disease 2010 study. *Ann Rheum Dis*. 2014;73(7):1316–22. DOI:10.1136/annrheumdis-2013-204627

[9] Kerlan-Candon S, Combe B, Vincent R, Clot J, Pinet V, Eliaou JF. HLA-DRB1 gene transcripts in rheumatoid arthritis. *Clin Exp Immunol*. 2001;124(1):142–9. DOI:10.1046/j.1365-2249.2001.01498.x

[10] Chimenti MS, Triggianese P, Conigliaro P, Candi E, Melino G, Perricone R. The interplay between inflammation and metabolism in rheumatoid arthritis. *Cell Death Dis*. 2015;6. DOI:10.1038/cddis.2015.246

[11] Finckh A, Turesson C. The impact of obesity on the development and progression of rheumatoid arthritis. *Ann Rheum Dis*. 2014;73(11):1911–3. DOI:10.1136/annrheumdis-2014-205741

[12] Feng X, Xu X, Shi Y, Liu X, Liu H, Hou H, et al. Body Mass Index and the Risk of Rheumatoid Arthritis: An Updated Dose-Response Meta-Analysis. Bogdanos DP, editor. *Biomed Res Int* . 2019;2019:3579081. DOI:10.1155/2019/3579081

[13] Sugiyama D, Nishimura K, Tamaki K, Tsuji G, Nakazawa T, Morinobu A, et al.

Impact of smoking as a risk factor for developing rheumatoid arthritis: A meta-analysis of observational studies. *Ann Rheum Dis*. 2010;69(1):70–81. DOI:10.1136/ard.2008.096487

[14] Sokolove J, Wagner CA, Lahey LJ, Sayles H, Duryee MJ, Reimold AM, et al. Increased inflammation and disease activity among current cigarette smokers with rheumatoid arthritis: A cross-sectional analysis of US veterans. *Rheumatol (United Kingdom)*. 2016;55(11):1969–77. DOI:10.1093/rheumatology/kew285

[15] Stolt P, Yahya A, Bengtsson C, Källberg H, Rönnelid J, Lundberg I, et al. Silica exposure among male current smokers is associated with a high risk of developing ACPA-positive rheumatoid arthritis. *Ann Rheum Dis*. 2010;69(6):1072–6. DOI:10.1136/ard.2009.114694

[16] Stolt P, Källberg H, Lundberg I, Sjögren B, Klareskog L, Alfredsson L. Silica exposure is associated with increased risk of developing rheumatoid arthritis: Results from the Swedish EIRA study. *Ann Rheum Dis*. 2005;64(4):582–6. DOI:10.1136/ard.2004.022053

[17] Sigaux J, Biton J, André E, Semerano L, Boissier MC. Air pollution as a determinant of rheumatoid arthritis. *Jt Bone Spine*. 2019;86(1):37–42. DOI:10.1016/j.jbspin.2018.03.001

[18] Bengtsson C, Malspeis S, Orellana C, Sparks JA, Costenbader KH, Karlson EW. Menopausal factors are associated with seronegative RA in large prospective cohorts: results from the Nurses' Health Studies. *Arthritis Care Res (Hoboken)* . 2017;69(11):1676–84. DOI:10.1002/acr.23194

[19] Merlino LA, Cerhan JR, Criswell LA, Mikuls TR, Saag KG. Estrogen and Other Female Reproductive Risk Factors Are Not Strongly Associated With the Development of Rheumatoid Arthritis in Elderly Women. *Semin Arthritis Rheum*. 2003;33(2):72–82. DOI:10.1016/S0049-0172(03)00084-2

[20] Johannes Wollbold, Rene Huber, Raimund Kinne and KE. Conceptual Representation of Gene Expression Processes. *Knowl Process Data Anal*. 2011;6581:79–100.

[21] Kurkó, Júlia, Besenyei, Timea, Laki, Judit, Glant, Tibor T., Katalin Mikecz, Szekanecz Z. Genetics of Rheumatoid Arthritis — A Comprehensive Review. *Clin Rev Allergy Immunol*. 2013;45(2):170–9. DOI:10.1038/jid.2014.371

[22] Rieck M, Arechiga A, Onengut-Gumuscu S, Greenbaum C, Concannon P, Buckner JH. Genetic Variation in PTPN22 Corresponds to Altered Function of T and B Lymphocytes. *J Immunol*. 2007;179(7):4704–10. DOI:10.4049/jimmunol.179.7.4704

[23] Faragó B, Magyari L, Sáfrány E, Csöngei V, Járomi L, Horvatovich K, et al. Functional variants of interleukin-23 receptor gene confer risk for rheumatoid arthritis but not for systemic sclerosis. *Ann Rheum Dis*. 2008;67(2):248–50. DOI:10.1136/ard.2007.072819

[24] Plenge RM, Padyukov L, Remmers EF, Purcell S, Lee AT, Karlson EW, et al. Replication of putative candidate-gene associations with rheumatoid arthritis in >4,000 samples from North America and Sweden: Association of susceptibility with PTPN22, CTLA4, and PADI4. *Am J Hum Genet*. 2005;77(6):1044–60. DOI:10.1086/498651

[25] Remmers EF, Plenge RM, Lee AT, Graham RR, Hom G, Behrens TW, et al. STAT4

and the risk of rheumatoid arthritis and systemic lupus erythematosus. *N Engl J Med*. 2007;357(10):977–86. DOI:10.1056/NEJMoa073003

[26] Ferreira RC, Freitag DF, Cutler AJ, Howson JMM, Rainbow DB, Smyth DJ, et al. Functional IL6R 358Ala Allele Impairs Classical IL-6 Receptor Signaling and Influences Risk of Diverse Inflammatory Diseases. *PLoS Genet*. 2013;9(4). DOI:10.1371/journal.pgen.1003444

[27] Ruyssen-Witrand A, Rouanet S, Combe B, Dougados M, Le Loët X, Sibilia J, et al. Fcγ receptor type IIIA polymorphism influences treatment outcomes in patients with rheumatoid arthritis treated with rituximab. *Ann Rheum Dis*. 2012;71(6):875–7. DOI:10.1136/annrheumdis-2011-200337

[28] Tolusso B, Pietrapertosa D, Morelli A, De Santis M, Gremese E, Farina G, et al. IL-1B and IL-1RN gene polymorphisms in rheumatoid arthritis: Relationship with protein plasma levels and response to therapy. *Pharmacogenomics*. 2006;7(5):683–95. DOI:10.2217/14622416.7.5.683

[29] Picchianti-Diamanti A, Rosado MM, D'Amelio R. Infectious agents and inflammation: The role of microbiota in autoimmune arthritis. *Front Microbiol*. 2018;8(JAN):1–9. DOI:10.3389/fmicb.2017.02696

[30] Klareskog L, Gregersen PK, Huizinga TWJ. Prevention of autoimmune rheumatic disease: State of the art and future perspectives. *Ann Rheum Dis*. 2010;69(12):2062–6. DOI:10.1136/ard.2010.142109

[31] Orellana C, Saevarsdottir S, Klareskog L, Karlson EW, Alfredsson L, Bengtsson C. Postmenopausal hormone therapy and the risk of rheumatoid arthritis: results from the Swedish EIRA population-based case-control study. *Eur J Epidemiol*. 2015;30(5):449–57. DOI:10.1007/s10654-015-0004-y

[32] Heidari B. Rheumatoid arthritis: Early diagnosis and treatment outcomes. *Casp J Intern Med*. 2011;2(1):161–70.

[33] Haque M, Fino K, Lei F, Xiong X, Song J. Utilizing regulatory T cells against rheumatoid arthritis. *Front Oncol*. 2014;4 JUL(August):1–9. DOI:10.3389/fonc.2014.00209

[34] Gierut A, Perlman H, Pope RM. Innate immunity and rheumatoid arthritis. *Rheum Dis Clin North Am*. 2010;36(2):271–96. DOI:10.1016/j.rdc.2010.03.004

[35] Merlo LMF, Mandik-Nayak L. Adaptive Immunity: B Cells and Antibodies . Second Edi. Cancer Immunotherapy: Immune Suppression and Tumor Growth: Second Edition. Elsevier; 2013. 25–40 p. DOI:10.1016/B978-0-12-394296-8.00003-8

[36] Firestein GS, McInnes IB. Immunopathogenesis of Rheumatoid Arthritis. *Immunity*. 2017;46(2):183–96. DOI:10.1016/j.immuni.2017.02.006

[37] Luque-Campos N, Contreras-López RA, Paredes-Martínez MJ, Torres MJ, Bahraoui S, Wei M, et al. Mesenchymal stem cells improve rheumatoid arthritis progression by controlling memory T cell response. *Front Immunol*. 2019;10(MAR). DOI:10.3389/fimmu.2019.00798

[38] Zhen Yang, Yi Shen, Hisashi Oishi, Eric L. Matteson, Lu Tian, Jörg J. Goronzy and CMW. Restoring oxidant signaling suppresses pro-arthritogenic T-cell effector

functions in rheumatoid arthritis. *Sci Transl Med*. 2016;8(331):1–24. DOI:Doi:10.1126/scitranslmed.aad7151.

[39] Choy E. Understanding the dynamics: Pathways involved in the pathogenesis of rheumatoid arthritis. *Rheumatology*. 2012;51(5):3–11. DOI:10.1093/rheumatology/kes113

[40] Deng GM, Lenardo M. The role of immune cells and cytokines in the pathogenesis of rheumatoid arthritis. *Drug Discov Today Dis Mech*. 2006;3(2):163–8. DOI:10.1016/j.ddmec.2006.06.009

[41] Bartok B, Firestein GS. Fibroblast-like synoviocytes: Key effector cells in rheumatoid arthritis. *Immunol Rev*. 2010;233(1):233–55. DOI:10.1111/j.0105-2896.2009.00859.x

[42] Wilsdon TD, Hill CL. Managing the drug treatment of rheumatoid arthritis. *Aust Prescr*. 2017;40(2):51–8. DOI:10.18773/austprescr.2017.012

[43] Kesharwani D, Paliwal R, Satapathy T, Das Paul S. Rheumatiod Arthritis: An Updated Overview of Latest Therapy and Drug Delivery. *J pharmacopuncture* . 2019;22(4):210–24. DOI:10.3831/KPI.2019.22.029

[44] Quan LD, Thiele GM, Tian J, Wang D. The development of novel therapies for rheumatoid arthritis. *Expert Opin Ther Pat*. 2008;18(7):723–38. DOI:10.1517/13543776.18.7.723

[45] Kroesen S, Widmer AF, Tyndall A, Hasler P. Serious bacterial infections in patients with rheumatoid arthritis under anti-TNF-α therapy. *Rheumatology*. 2003;42(5):617–21. DOI:10.1093/rheumatology/keg263

[46] Lee JH, Slifman NR, Gershon SK, Edwards ET, Schwieterman WD, Siegel JN, et al. Life-threatening histoplasmosis complicating immunotherapy with tumor necrosis factor α antagonists infliximab and etanercept. *Arthritis Rheum*. 2002;46(10):2565–70. DOI:10.1002/art.10583

[47] Brown SL, Greene MH, Gershon SK, Edwards ET, Braun MM. Tumor necrosis factor antagonist therapy and lymphoma development: Twenty-six cases reported to the Food and Drug Administration. *Arthritis Rheum*. 2002;46(12):3151–8. DOI:10.1002/art.10679

[48] Yamaoka K. Janus kinase inhibitors for rheumatoid arthritis. *Curr Opin Chem Biol* . 2016;32:29–33. DOI:10.1016/j.cbpa.2016.03.006

[49] Harrington R, Al Nokhatha SA, Conway R. JAK Inhibitors in Rheumatoid Arthritis: An Evidence-Based Review on the Emerging Clinical Data. *J Inflamm Res* . 2020;13:519–31. DOI:10.2147/JIR.S219586

[50] Kirwan JR, Bijlsma JWJ, Boers M, Shea BJ. Effects of glucocorticoids on radiological progression in rheumatoid arthritis. *Cochrane Database Syst Rev*. 2007;(1). DOI:10.1002/14651858.CD006356

[51] Dominici M, Le Blanc K, Mueller I, Slaper-Cortenbach I, Marini FC, Krause DS, et al. Minimal criteria for defining multipotent mesenchymal stromal cells. The International Society for Cellular Therapy position statement. *Cytotherapy*. 2006;8(4):315–7. DOI:10.1080/14653240600855905

[52] Chamberlain G, Fox J, Ashton B, Middleton J. Concise Review: Mesenchymal Stem

Cells: Their Phenotype, Differentiation Capacity, Immunological Features, and Potential for Homing. *Stem Cells*. 2007;25(11):2739–49. DOI:10.1634/stemcells.2007-0197

[53] Mizukami A, Swiech K. Mesenchymal stromal cells: From discovery to manufacturing and commercialization. *Stem Cells Int*. 2018;2018:1–13. DOI:10.1155/2018/4083921

[54] Nombela-Arrieta, C., Ritz, J., Silberestein LE. The elusive nature and function of mesenchymal stem cells. *Nat Rev Mol Cell Biol* . 2011;12(2):126–31. DOI:10.1038/jid.2014.371

[55] Caplan, A I. Mesenchymal stem cells. *J Orthop Res*. 1991;9:641–50. DOI:10.1201/b13978

[56] Swart JF, Wulffraat NM. Mesenchymal stromal cells for treatment of arthritis. *Best Pract Res Clin Rheumatol*. 2014;28(4):589–603. DOI:10.1016/j.berh.2014.10.023

[57] Schwab KE, Hutchinson P, Gargett CE. Identification of surface markers for prospective isolation of human endometrial stromal colony-forming cells. *Hum Reprod*. 2008;23(4):934–43. DOI:10.1093/humrep/den051

[58] Huang GTJ, Gronthos S, Shi S. Critical reviews in oral biology & medicine: Mesenchymal stem cells derived from dental tissues vs. those from other sources: Their biology and role in Regenerative Medicine. *J Dent Res*. 2009;88(9):792–806. DOI:10.1177/0022034509340867

[59] De Bari C, Dell'Accio F, Tylzanowski P, Luyten FP. Multipotent mesenchymal stem cells from adult human synovial membrane. *Arthritis Rheum*. 2001;44(8):1928–42. DOI:10.1002/1529-0131(200108)44:8<1928::AID-ART331>3.0.CO;2-P

[60] Macdonald GIA, Augello A, Bari C De. Arthritis & Rheumatism Role of Mesenchymal Stem Cells in Reestablishing. 2011;63(9):2547–57. DOI:10.1002/art.30474

[61] El-Jawhari JJ, El-Sherbiny YM, Jones EA, McGonagle D. Mesenchymal stem cells, autoimmunity and rheumatoid arthritis. *Qjm*. 2014;107(7):505–14. DOI:10.1093/qjmed/hcu033

[62] Ding D-C, Chang Y-H, Shyu W-C, Lin S-Z. Human Umbilical Cord Mesenchymal Stem Cells: A New Era for Stem Cell Therapy. *Cell Transplant*. 2015;24(3):339–47. DOI:10.3727/096368915X686841

[63] Mennan C, Wright K, Bhattacharjee A, Balain B, Richardson J, Roberts S. Isolation and characterisation of mesenchymal stem cells from different regions of the human umbilical cord. *Biomed Res Int*. 2013;2013. DOI:10.1155/2013/916136

[64] Li G, Zhang XA, Wang H, Wang X, Meng CL, Chan CY, et al. Comparative proteomic analysis of mesenchymal stem cells derived from human bone marrow, umbilical cord, and placenta: Implication in the migration. *Proteomics*. 2009;9(1):20–30. DOI:10.1002/pmic.200701195

[65] Cheng H, Qiu L, Ma J, Zhang H, Cheng M, Li W, et al. Replicative senescence of human bone marrow and umbilical cord derived mesenchymal stem cells and their differentiation to adipocytes and osteoblasts. *Mol Biol Rep*. 2011;38(8):5161–8. DOI:10.1007/s11033-010-0665-2

[66] Rawat S, Gupta S, Mohanty S. Mesenchymal Stem Cells Modulate the Immune System in Developing Therapeutic Interventions. *Immune Response Act Immunomodulation*. 2019; DOI:10.5772/intechopen.80772

[67] Weiss ARR, Dahlke MH. Immunomodulation by Mesenchymal Stem Cells (MSCs): Mechanisms of action of living, apoptotic, and dead MSCs. *Front Immunol*. 2019;10(JUN):1–10. DOI:10.3389/fimmu.2019.01191

[68] Luk F, Carreras-Planella L, Korevaar SS, de Witte SFH, Borràs FE, Betjes MGH, et al. Inflammatory conditions dictate the effect of mesenchymal stem or stromal cells on B cell function. *Front Immunol*. 2017;8(AUG):1–13. DOI:10.3389/fimmu.2017.01042

[69] Luz-Crawford P, Noël D, Fernandez X, Khoury M, Figueroa F, Carrión F, et al. Mesenchymal Stem Cells Repress Th17 Molecular Program through the PD-1 Pathway. *PLoS One*. 2012;7(9). DOI:10.1371/journal.pone.0045272

[70] Li Y, Zhang D, Xu L, Dong L, Zheng J, Lin Y, et al. Cell–cell contact with proinflammatory macrophages enhances the immunotherapeutic effect of mesenchymal stem cells in two abortion models. *Cell Mol Immunol* . 2019;16(12):908–20. DOI:10.1038/s41423-019-0204-6

[71] Zhang B, Liu R, Shi D, Liu X, Chen Y, Dou X, et al. Mesenchymal stem cells induce mature dendritic cells into a novel Jagged-2 dependent regulatory dendritic cell population. *Blood*. 2009;113(1):46–57. DOI:10.1182/blood-2008-04-154138

[72] Fan XL, Zhang Z, Ma CY, Fu QL. Mesenchymal stem cells for inflammatory airway disorders: Promises and challenges. *Biosci Rep*. 2019;39(1):1–13. DOI:10.1042/BSR20182160

[73] English K, Ryan JM, Tobin L, Murphy MJ, Barry FP, Mahon BP. Cell contact, prostaglandin E2 and transforming growth factor beta 1 play non-redundant roles in human mesenchymal stem cell induction of CD4+CD25Highforkhead box P3+ regulatory T cells. *Clin Exp Immunol*. 2009;156(1):149–60. DOI:10.1111/j.1365-2249.2009.03874.x

[74] De Luca L, Trino S, Laurenzana I, Lamorte D, Caivano A, Del Vecchio L, et al. Mesenchymal stem cell derived extracellular vesicles: A role in hematopoietic transplantation? *Int J Mol Sci*. 2017;18(5):1–17. DOI:10.3390/ijms18051022

[75] Nicola M Di, Carlo-Stella C, Magni M, Milanesi M, Longoni PD, Matteucci P, et al. Human bone marrow stromal cells suppress T-lymphocyte proliferation induced by cellular or nonspecific mitogenic stimuli. *Blood*. 2002;99(10):3838–43. DOI:10.1182/blood.V99.10.3838

[76] DiNicola M Di, Carlo-Stella C, Magni M, Milanesi M, Longoni PD, Grisanti S, et al. induced by cellular or nonspecific mitogenic stimuli Human bone marrow stromal cells suppress T-lymphocyte proliferation induced by cellular or nonspecific mitogenic stimuli. *Blood*. 2013;99(10):3838–43. DOI:10.1182/blood.V99.10.3838

[77] Németh K, Leelahavanichkul A, Yuen PST, Mayer B, Parmelee A, Doi K, et al. Bone marrow stromal cells attenuate sepsis via prostaglandin E 2-dependent reprogramming of host macrophages to increase their interleukin-10 production. *Nat Med*. 2009;15(1):42–9. DOI:10.1038/nm.1905

[78] Shi Y, Su J, Roberts AI, Shou P, Rabson AB, Ren G. How mesenchymal stem cells

interact with tissue immune responses. Trends in Immunology. 2012. DOI:10.1016/j.it.2011.11.004

[79] Aggarwal S, Pittenger MF. Human mesenchymal stem cells modulate allogeneic immune cell responses. *Transplantation*. 2009;105(4):1815–22. DOI:10.1182/blood-2004-04-1559.Supported

[80] Kyurkchiev D. Secretion of immunoregulatory cytokines by mesenchymal stem cells. *World J Stem Cells*. 2014;6(5):552. DOI:10.4252/wjsc.v6.i5.552

[81] Chen K, Wang D, Du WT, Han ZB, Ren H, Chi Y, et al. Human umbilical cord mesenchymal stem cells hUC-MSCs exert immunosuppressive activities through a PGE2-dependent mechanism. *Clin Immunol* . 2010;135(3):448–58. DOI:10.1016/j.clim.2010.01.015

[82] Lo Sicco, Cluadia E; Reverberi, Daniele; Balbi, Carolina; Ulivi, Valentina; Principi, Elisa; Pascucci, Rincipi Luisa; Becherini, Pamela; Bosco, Maria Carla; Varesio, Luigi; Franzin, Aresio Chiara; Pozzobon, G Michela, Cancedda, Ranieri; Tasso R. Mesenchymal Stem Cell-Derived Extracellular Vesicles as Mediators of Anti-Inflammatory Effects : Endorsement of Macrophage Polarization. *Stem Cells Transl Med*. 2017;6:1018–28.

[83] Arutyunyan I, Elchaninov A, Makarov A, Fatkhudinov T. Umbilical Cord as Prospective Source for Mesenchymal Stem Cell-Based Therapy. *Stem Cells Int*. 2016;2016. DOI:10.1155/2016/6901286

[84] Melief SM, Geutskens SB, Fibbe WE, Roelofs H. Multipotent stromal cells skew monocytes towards an anti-inflammatory interleukin-10-producing phenotype by production of interleukin-6. *Haematologica*. 2013;98(6):888–95. DOI:10.3324/haematol.2012.078055

[85] Newman RE, Yoo D, LeRoux MA, Danilkovitch-Miagkova A. Treatment of inflammatory diseases with mesenchymal stem cells. *Inflamm Allergy - Drug Targets*. 2009;8(2):110–23. DOI:10.2174/187152809788462635

[86] Yang H, Sun J, Li Y, Duan WM, Bi J, Qu T. Human umbilical cord-derived mesenchymal stem cells suppress proliferation of PHA-activated lymphocytes in vitro by inducing CD4+CD25highCD45RA+ regulatory T cell production and modulating cytokine secretion. *Cell Immunol*. 2016;302:26–31. DOI:10.1016/j.cellimm.2016.01.002

[87] Liu X, Feng T, Gong T, Shen C, Zhu T, Wu Q, et al. Human umbilical cord mesenchymal stem cells inhibit the function of allogeneic activated Vγ9Vδ2 T lymphocytes in vitro. *Biomed Res Int*. 2015;2015. DOI:10.1155/2015/317801

[88] Castella B, Melaccio A, Foglietta M, Riganti C, Massaia M. Vγ9Vδ2 T cells as strategic weapons to improve the potency of immune checkpoint blockade and immune interventions in human myeloma. *Front Oncol*. 2018;8(NOV):1–8. DOI:10.3389/fonc.2018.00508

[89] Hu C, Qian L, Miao Y, Huang Q, Miao P, Wang P, et al. Antigen-presenting effects of effector memory Vγ9VδT cells in rheumatoid arthritis. *Cell Mol Immunol*. 2012;9(3):245–54. DOI:10.1038/cmi.2011.50

[90] Cutler AJ, Limbani V, Girdlestone J, Navarrete C V. Umbilical Cord-Derived

Mesenchymal Stromal Cells Modulate Monocyte Function to Suppress T Cell Proliferation. *J Immunol*. 2010;185(11):6617–23. DOI:10.4049/jimmunol.1002239

[91] Liu R, Li X, Zhang Z, Zhou M, Sun Y, Su D, et al. Allogeneic mesenchymal stem cells inhibited T follicular helper cell generation in rheumatoid arthritis. *Sci Rep*. 2015;5(August):1–11. DOI:10.1038/srep12777

[92] Yu M, Cavero V, Lu Q, Li H. Follicular helper T cells in rheumatoid arthritis. *Clin Rheumatol*. 2015;34(9):1489–93. DOI:10.1007/s10067-015-3028-5

[93] Liu Y, Mu R, Wang S, Long L, Liu X, Li R, et al. Therapeutic potential of human umbilical cord mesenchymal stem cells in the treatment of rheumatoid arthritis. *Arthritis Res Ther*. 2010;12(6):1–13. DOI:10.1186/ar3187

[94] Bernardo ME, Fibbe WE. Mesenchymal stromal cells: Sensors and switchers of inflammation. *Cell Stem Cell*. 2013;13(4):392–402. DOI:10.1016/j.stem.2013.09.006

[95] Krampera M. Mesenchymal stromal cell 'licensing': a multistep process. *Leukemia*. 2011;25(9):1408–14. DOI:10.1038/leu.2011.108

[96] Ren G, Zhang L, Zhao X, Xu G, Zhang Y, Roberts AI, et al. Mesenchymal Stem Cell-Mediated Immunosuppression Occurs via Concerted Action of Chemokines and Nitric Oxide. *Cell Stem Cell*. 2008;2(2):141–50. DOI:10.1016/j.stem.2007.11.014

[97] Sabapathy V, Sundaram B, Vm S, Mankuzhy P, Kumar S. Human wharton's jelly mesenchymal stem cells plasticity augments scar-free skin wound healing with hair growth. *PLoS One*. 2014;9(4):1–10. DOI:10.1371/journal.pone.0093726

[98] Duijvestein M, Wildenberg ME, Welling MM, Hennink S, Molendijk I, Van Zuylen VL, et al. REGENERATIVE MEDICINE Pretreatment with Interferon-c Enhances the Therapeutic Activity of Mesenchymal Stromal Cells in Animal Models of Colitis. *Stem Cells*. 2011;29:1549–58.

[99] Herrmann JL, Wang Y, Abarbanell AM, Weil BR, Tan J, Meldrum DR. Preconditioning mesenchymal stem cells with transforming growth factor alpha improves mesenchymal stem cell mediated cardioprotection. *SHOCK*. 2010;33(1):24–30. DOI:10.1097/SHK.0b013e3181b7d137

[100] Kadle RL, Abdou SA, Villarreal-Ponce AP, Soares MA, Sultan DL, David JA, et al. Microenvironmental cues enhance mesenchymal stem cell-mediated immunomodulation and regulatory T-cell expansion. *PLoS One* . 2018;13(3):1–18. DOI:10.1371/journal.pone.0193178

[101] Fehrer C, Brunauer R, Laschober G, Unterluggauer H, Reitinger S, Kloss F, et al. Reduced oxygen tension attenuates differentiation capacity of human mesenchymal stem cells and prolongs their lifespan. *Aging Cell*. 2007;6(6):745–57. DOI:10.1111/j.1474-9726.2007.00336.x

[102] Li C, Ju H, Zhou X, Zeng X, He Y. Human Umbilical Cord Mesenchymal Stem Cells Suppress Systemic Lupus Erythematosus Lesions by Rebalancing CD4+/CD8+ Cell Population. *Stud Stem Cells Res Ther*. 2015;1(1):004–11. DOI:10.17352/sscrt.000003

[103] Luz-Crawford P, Kurte M, Bravo-Alegría J, Contreras R, Nova-Lamperti E, Tejedor G, et al. Mesenchymal stem cells generate a CD4+CD25+Foxp3 + regulatory T cell population during the differentiation process of Th1 and Th17 cells. *Stem Cell Res*

Ther. 2013;4(3). DOI:10.1186/scrt216

[104] Kehoe O, Cartwright A, Askari A, El Haj AJ, Middleton J. Intra-articular injection of mesenchymal stem cells leads to reduced inflammation and cartilage damage in murine antigen-induced arthritis. *J Transl Med*. 2014;12(1):1–10. DOI:10.1186/1479-5876-12-157

[105] Djouad F, Fritz V, Apparailly F, Louis-Plence P, Bony C, Sany J, et al. Reversal of the immunosuppressive properties of mesenchymal stem cells by tumor necrosis factor α in collagen-induced arthritis. *Arthritis Rheum*. 2005;52(5):1595–603. DOI:10.1002/art.21012

[106] Rasmusson I, Le Blanc K, Sundberg B, Ringdén O. Mesenchymal stem cells stimulate antibody secretion in human B cells. *Scand J Immunol*. 2007;65(4):336–43. DOI:10.1111/j.1365-3083.2007.01905.x

[107] Bouffi C, Bony C, Courties G, Jorgensen C, Noël D. IL-6-dependent PGE2 secretion by mesenchymal stem cells inhibits local inflammation in experimental arthritis. *PLoS One*. 2010;5(12). DOI:10.1371/journal.pone.0014247

[108] Augello A, Tasso R, Negrini SM, Cancedda R, Pennesi G. Cell therapy using allogeneic bone marrow mesenchymal stem cells prevents tissue damage in collagen-induced arthritis. *Arthritis Rheum*. 2007;56(4):1175–86. DOI:10.1002/art.22511

[109] Squillaro T, Peluso G, Galderisi U. Clinical trials with mesenchymal stem cells: An update. *Cell Transplant*. 2016;25(5):829–48. DOI:10.3727/096368915X689622

[110] Chang J-W, Hung S-P, Wu H-H, Wu W-M, Yang A-H, Tsai H-L, et al. Therapeutic Effects of Umbilical Cord Blood-Derived Mesenchymal Stem Cell Transplantation in Experimental Lupus Nephritis. *Cell Transplant*. 2011;20(2):245–58. DOI:10.3727/096368910X520056

[111] Zhang J, Lv S, Liu X, Song B, Shi L. Umbilical cord mesenchymal stem cell treatment for Crohn's disease: A randomized controlled clinical trial. *Gut Liver*. 2018;12(1):73–8. DOI:10.5009/gnl17035

[112] Riordan NH, Morales I, Fernández G, Allen N, Fearnot NE, Leckrone ME, et al. Clinical feasibility of umbilical cord tissue-derived mesenchymal stem cells in the treatment of multiple sclerosis. *J Transl Med*. 2018;16(1):1–12. DOI:10.1186/s12967-018-1433-7

[113] De Bari C. Are mesenchymal stem cells in rheumatoid arthritis the good or bad guys? *Arthritis Res Ther* . 2015;17(1):1–9. DOI:10.1186/s13075-015-0634-1

[114] Liang J, Li X, Zhang H, Wang D. Allogeneic mesenchymal stem cells transplantation in patients with refractory RA. 2012;157–61. DOI:10.1007/s10067-011-1816-0

[115] Wang L, Wang L, Cong X, Liu G, Zhou J, Bai B, Li Y, Bai W, Li M, Ji H, Zhu D, Wu M LY. Human umbilical cord mesenchymal stem cell therapy for patients with active rheumatoid arthritis: safety and efficacy. *Stem Cells Dev*. 2013;Dec 15(22(24)):3192-202.

[116] Wang L, Huang S, Li S, Li M, Shi J, Bai W, et al. Efficacy and safety of umbilical cord mesenchymal stem cell therapy for rheumatoid arthritis patients: A prospective phase I/II study. *Drug Des Devel Ther*. 2019;13:4331–40.

DOI:10.2147/DDDT.S225613

[117] Bonab MM, Alimoghaddam K, Talebian F, Ghaffari SH, Ghavamzadeh A, Nikbin B. Aging of mesenchymal stem cell in vitro. *BMC Cell Biol*. 2006;7:1–7. DOI:10.1186/1471-2121-7-14

[118] Yang YHK, Ogando CR, Wang See C, Chang TY, Barabino GA. Changes in phenotype and differentiation potential of human mesenchymal stem cells aging in vitro. *Stem Cell Res Ther*. 2018;9(1):1–14. DOI:10.1186/s13287-018-0876-3

[119] Le Blanc K, Tammik L, Sundberg B, Haynesworth SE, Ringdén O. Mesenchymal Stem Cells Inhibit and Stimulate Mixed Lymphocyte Cultures and Mitogenic Responses Independently of the Major Histocompatibility Complex. *Scand J Immunol*. 2003;57(1):11–20. DOI:10.1046/j.1365-3083.2003.01176.x

[120] Bernardo ME, Fibbe WE. Safety and efficacy of mesenchymal stromal cell therapy in autoimmune disorders. *Ann N Y Acad Sci*. 2012;1266(1):107–17. DOI:10.1111/j.1749-6632.2012.06667.x

[121] Kay AG, Long G, Tyler G, Stefan A, Broadfoot SJ, Piccinini AM, et al. Mesenchymal Stem Cell-Conditioned Medium Reduces Disease Severity and Immune Responses in Inflammatory Arthritis. *Sci Rep* . 2017;7(1):1–11. DOI:10.1038/s41598-017-18144-w

[122] Kim YH, Cho KA, Park M, Kim HS, Park JW, Woo SY, et al. Conditioned Medium from Tonsil-Derived Mesenchymal Stem Cells Relieves CCl 4 -Induced Liver Fibrosis in Mice. *Tissue Eng Regen Med* . 2019;16(1):51–8. DOI:10.1007/s13770-018-0160-8

[123] Elshaer SL, Evans W, Pentecost M, Lenin R, Periasamy R, Jha KA, et al. Adipose stem cells and their paracrine factors are therapeutic for early retinal complications of diabetes in the Ins2Akita mouse. *Stem Cell Res Ther*. 2018;9(1):1–18. DOI:10.1186/s13287-018-1059-y

[124] Pati S, Gerber MH, Menge TD, Wataha KA, Zhao Y, Baumgartner JA, et al. Bone marrow derived mesenchymal stem cells inhibit inflammation and preserve vascular endothelial integrity in the lungs after hemorrhagic shock. *PLoS One*. 2011;6(9). DOI:10.1371/journal.pone.0025171

[125] Yim HE, Kim DS, Chung HC, Shing B, Moon KH, George SK, et al. Controlled Delivery of Stem Cell-Derived Trophic Factors Accelerates Kidney Repair After Renal Ischemia-Reperfusion Injury in Rats. *Stem Cells Transl Med*. 2019;8(9):959–70. DOI:10.1002/sctm.18-0222

[126] Hashemi SM, Hassan ZM, Hossein-Khannazer N, Pourfathollah AA, Soudi S. Investigating the route of administration and efficacy of adipose tissue-derived mesenchymal stem cells and conditioned medium in type 1 diabetic mice. *Inflammopharmacology* . 2020;28(2):585–601. DOI:10.1007/s10787-019-00661-x

[127] Chen W, Sun Y, Gu X, Hao Y, Liu X, Lin J, et al. Conditioned medium of mesenchymal stem cells delays osteoarthritis progression in a rat model by protecting subchondral bone, maintaining matrix homeostasis, and enhancing autophagy. *J Tissue Eng Regen Med*. 2019;13(9):1618–28. DOI:10.1002/term.2916

[128] Aryan A, Bayat M, Bonakdar S, Taheri S, Haghparast N, Bagheri M, et al. Human Bone Marrow Mesenchymal Stem Cell Conditioned Medium Promotes Wound Healing in Deep Second-Degree Burns in Male Rats. *Cells Tissues Organs*.

2019;206(6):317–29. DOI:10.1159/000501651

[129] Zaborowski MP, Balaj L, Breakefield XO, Lai CP. Extracellular Vesicles: Composition, Biological Relevance, and Methods of Study. *Bioscience*. 2015;65(8):783–97. DOI:10.1093/biosci/biv084

[130] Burrello J, Monticone S, Gai C, Gomez Y, Kholia S, Camussi G. Stem cell-derived extracellular vesicles and immune-modulation. *Front Cell Dev Biol*. 2016;4(AUG):1–10. DOI:10.3389/fcell.2016.00083

[131] Robbins PD, Morelli AE. Regulation of immune responses by extracellular vesicles. Nature Reviews Immunology. 2014. DOI:10.1038/nri3622

[132] Burke J, Kolhe R, Hunter M, Isales C, Hamrick M, Fulzele S. Stem cell-derived exosomes: A potential alternative therapeutic agent in orthopaedics. *Stem Cells Int*. 2016;2016:5–8. DOI:10.1155/2016/5802529

[133] Mulcahy LA, Pink RC, Carter DRF. Routes and mechanisms of extracellular vesicle uptake. *J Extracell Vesicles*. 2014;3(1):1–14. DOI:10.3402/jev.v3.24641

[134] Valadi H, Ekström K, Bossios A, Sjöstrand M, Lee JJ, Lötvall JO. Exosome-mediated transfer of mRNAs and microRNAs is a novel mechanism of genetic exchange between cells. *Nat Cell Biol*. 2007;9(6):654–9. DOI:10.1038/ncb1596

[135] Bruno S, Deregibus MC, Camussi G. The secretome of mesenchymal stromal cells: Role of extracellular vesicles in immunomodulation. *Immunol Lett*. 2015;168(2):154–8. DOI:10.1016/j.imlet.2015.06.007

[136] Rani S, Ryan AE, Griffin MD, Ritter T. Mesenchymal stem cell-derived extracellular vesicles: Toward cell-free therapeutic applications. *Mol Ther*. 2015;23(5):812–23. DOI:10.1038/mt.2015.44

[137] Thery C, Boussac M, Veron P, Ricciardi-Castagnoli P, Raposo G, Garin J, et al. Proteomic Analysis of Dendritic Cell-Derived Exosomes: A Secreted Subcellular Compartment Distinct from Apoptotic Vesicles. *J Immunol*. 2001; DOI:10.4049/jimmunol.166.12.7309

[138] Rak J. Extracellular vesicles - biomarkers and effectors of the cellular interactome in cancer. Frontiers in Pharmacology. 2013. DOI:10.3389/fphar.2013.00021

[139] Bobrie A, Colombo M, Krumeich S, Raposo G, Théry C. Diverse subpopulations of vesicles secreted by different intracellular mechanisms are present in exosome preparations obtained by differential ultracentrifugation. *J Extracell Vesicles*. 2012; DOI:10.3402/jev.v1i0.18397

[140] Hessvik NP, Llorente A. Current knowledge on exosome biogenesis and release. *Cell Mol Life Sci*. 2018;75(2):193–208. DOI:10.1007/s00018-017-2595-9

[141] Tu C, Ahmad G, Mohapatra B, Bhattacharyya S, Ortega-Cava CF, Chung BM, et al. ESCRT proteins: Double-edged regulators of cellular signaling. *Bioarchitecture*. 2011;1(1):45–8. DOI:10.4161/bioa.1.1.15173

[142] Iavello A, Frech VSL, Gai C, Deregibus MC, Quesenberry PJ, Camussi G. Role of Alix in miRNA packaging during extracellular vesicle biogenesis. *Int J Mol Med*. 2016;37(4):958–66. DOI:10.3892/ijmm.2016.2488

[143] Anand PK. Exosomal membrane molecules are potent immune response modulators. *Commun Integr Biol*. 2010;3(5):405–8. DOI:10.4161/cib.3.5.12474

[144] Oshima K, Aoki N, Kato T, Kitajima K, Matsuda T. Secretion of a peripheral membrane protein, MFG-E8, as a complex with membrane vesicles: A possible role in membrane secretion. *Eur J Biochem*. 2002;269(4):1209–18. DOI:10.1046/j.1432-1033.2002.02758.x

[145] Buzás EI, Tóth E, Sódar BW, Szabó-Taylor K. Molecular interactions at the surface of extracellular vesicles. *Semin Immunopathol*. 2018;40(5):453–64. DOI:10.1007/s00281-018-0682-0

[146] Laulagnier, Karine., Motta, Claude., Hamdi, Safouane., Roy, Sébastien., Fauvelle, Florence., Pageaux, Jean-François., Kobayashi, Toshihide., Salles, Jean-Pierre., Perret, Bertrand., Bonnerot, Christian., Record M. Mast cell- and dendritic cell-derived exosomes display a specific lipid composition and an unusual membrane organization. *Biochem J*. 2004;380(1):161–71.

[147] Baglio SR, Pegtel DM, Baldini N. Mesenchymal stem cell secreted vesicles provide novel opportunities in (stem) cell-free therapy. *Front Physiol*. 2012;3 SEP(September):1–11. DOI:10.3389/fphys.2012.00359

[148] Witwer KW, Buzás EI, Bemis LT, Bora A, Lässer C, Lötvall J, et al. Standardization of sample collection, isolation and analysis methods in extracellular vesicle research. *J Extracell Vesicles*. 2013;2(1). DOI:10.3402/jev.v2i0.20360

[149] Bruno S, Grange C, Deregibus MC, Calogero RA, Saviozzi S, Collino F, et al. Mesenchymal stem cell-derived microvesicles protect against acute tubular injury. *J Am Soc Nephrol*. 2009;20(5):1053–67. DOI:10.1681/ASN.2008070798

[150] Atkin-Smith GK, Paone S, Zanker DJ, Duan M, Phan TK, Chen W, et al. Isolation of cell type-specific apoptotic bodies by fluorescence-activated cell sorting. *Sci Rep* . 2017;7(August 2016):1–7. DOI:10.1038/srep39846

[151] György B, Szabó TG, Pásztói M, Pál Z, Misják P, Aradi B, et al. Membrane vesicles, current state-of-the-art: Emerging role of extracellular vesicles. *Cell Mol Life Sci*. 2011;68(16):2667–88. DOI:10.1007/s00018-011-0689-3

[152] Naito Y, Yoshioka Y, Yamamoto Y, Ochiya T. How cancer cells dictate their microenvironment: present roles of extracellular vesicles. *Cell Mol Life Sci*. 2017;74(4):697–713. DOI:10.1007/s00018-016-2346-3

[153] Minciacchi VR, Freeman MR, Vizio D Di, Sciences B, Angeles L, Diseases U, et al. Extracellular Vesicles in Cancer: Exosomes, Microvesicles and the Emerging Role of Large Oncosomes. *Semin Cell Dev Biol*. 2015;40:41–51. DOI:10.1016/j.semcdb.2015.02.010.Extracellular

[154] Buzas EI, György B, Nagy G, Falus A, Gay S. Emerging role of extracellular vesicles in inflammatory diseases. *Nat Rev Rheumatol* . 2014;10(6):356–64. DOI:10.1038/nrrheum.2014.19

[155] Théry C, Witwer KW, Aikawa E, Alcaraz MJ, Anderson JD, Andriantsitohaina R, et al. Minimal information for studies of extracellular vesicles 2018 (MISEV2018): a position statement of the International Society for Extracellular Vesicles and update of the MISEV2014 guidelines. *J Extracell Vesicles*. 2018;7(1).

DOI:10.1080/20013078.2018.1535750

[156] Cocucci E, Meldolesi J. Ectosomes and exosomes: Shedding the confusion between extracellular vesicles. *Trends Cell Biol* . 2015;25(6):364–72. DOI:10.1016/j.tcb.2015.01.004

[157] Chen W, Huang Y, Han J, Yu L, Li Y, Lu Z, et al. Immunomodulatory effects of mesenchymal stromal cells-derived exosome. *Immunol Res*. 2016;64(4):831–40. DOI:10.1007/s12026-016-8798-6

[158] Ti D, Hao H, Tong C, Liu J, Dong L, Zheng J, et al. LPS-preconditioned mesenchymal stromal cells modify macrophage polarization for resolution of chronic inflammation via exosome-shuttled let-7b. *J Transl Med*. 2015;13(1):1–14. DOI:10.1186/s12967-015-0642-6

[159] Teng G gen, Wang W hong, Dai Y, Wang S jun, Chu Y xiang, Li J. Let-7b Is Involved in the Inflammation and Immune Responses Associated with Helicobacter pylori Infection by Targeting Toll-Like Receptor 4. *PLoS One*. 2013;8(2). DOI:10.1371/journal.pone.0056709

[160] Monguió-Tortajada M, Roura S, Gálvez-Montón C, Pujal JM, Aran G, Sanjurjo L, et al. Nanosized UCMSC-derived extracellular vesicles but not conditioned medium exclusively inhibit the inflammatory response of stimulated T cells: Implications for nanomedicine. *Theranostics*. 2017;7(2):270–84. DOI:10.7150/thno.16154

[161] Blazquez R, Sanchez-Margallo FM, de la Rosa O, Dalemans W, Álvarez V, Tarazona R, et al. Immunomodulatory potential of human adipose mesenchymal stem cells derived exosomes on in vitro stimulated T cells. *Front Immunol*. 2014;5(NOV):1–9. DOI:10.3389/fimmu.2014.00556

[162] Pachler K, Ketterl N, Desgeorges A, Dunai ZA, Laner-Plamberger S, Streif D, et al. An in vitro potency assay for monitoring the immunomodulatory potential of stromal cell-derived extracellular vesicles. *Int J Mol Sci*. 2017;18(7):1–11. DOI:10.3390/ijms18071413

[163] Conforti A, Scarsella M, Starc N, Giorda E, Biagini S, Proia A, et al. Microvescicles derived from mesenchymal stromal cells are not as effective as their cellular counterpart in the ability to modulate immune responses in vitro. *Stem Cells Dev*. 2014;23(21):2591–9. DOI:10.1089/scd.2014.0091

[164] Mokarizadeh A, Delirezh N, Morshedi A, Mosayebi G, Farshid AA, Mardani K. Microvesicles derived from mesenchymal stem cells: Potent organelles for induction of tolerogenic signaling. *Immunol Lett* . 2012;147(1–2):47–54. DOI:10.1016/j.imlet.2012.06.001

[165] Del Fattore A, Luciano R, Pascucci L, Goffredo BM, Giorda E, Scapaticci M, et al. Immunoregulatory effects of mesenchymal stem cell-derived extracellular vesicles on T lymphocytes. *Cell Transplant*. 2015;24(12):2615–27. DOI:10.3727/096368915X687543

[166] Yin K, Wang S, Zhao RC. Exosomes from mesenchymal stem/stromal cells: A new therapeutic paradigm. *Biomark Res*. 2019;7(1):1–8. DOI:10.1186/s40364-019-0159-x

[167] Turchinovich A, Drapkina O, Tonevitsky A. Transcriptome of extracellular vesicles: State-of-the-art. *Front Immunol*. 2019;10(FEB). DOI:10.3389/fimmu.2019.00202

[168] Qiu G, Zheng G, Ge M, Wang J, Huang R, Shu Q, et al. Functional proteins of mesenchymal stem cell-derived extracellular vesicles. *Stem Cell Res Ther*. 2019;10(1):1–11. DOI:10.1186/s13287-019-1484-6

[169] Kim HS, Choi DY, Yun SJ, Choi SM, Kang JW, Jung JW, et al. Proteomic analysis of microvesicles derived from human mesenchymal stem cells. *J Proteome Res*. 2012;11(2):839–49. DOI:10.1021/pr200682z

[170] Anderson, D. J., Johansson, H. J., Graham, C. S., Vesterlund, M., Pham, M. T., Bramlett, C. S., Montgomery, E. N., Mellema, M. S., Bardini, R. L., Contreras, Z., Hoon, M., Bauer, G., Fink, K. D., Fury, B., Hendrix, K. J., Chedin, F., El-Andaloussi, S., Hw JA. Comprehensive Proteomic Analysis of Mesenchymal Stem Cell Exosomes Reveals Modulation of Angiogenesis via Nuclear Factor-KappaB Signaling. *Stem Cells*. 2016;34(3):601–13. DOI:10.1016/j.physbeh.2017.03.040

[171] La Greca A, Solari C, Furmento V, Lombardi A, Biani MC, Aban C, et al. Extracellular vesicles from pluripotent stem cell-derived mesenchymal stem cells acquire a stromal modulatory proteomic pattern during differentiation. *Exp Mol Med* . 2018;50(9). DOI:10.1038/s12276-018-0142-x

[172] Álvarez V, Sánchez-Margallo FM, Macías-García B, Gómez-Serrano M, Jorge I, Vázquez J, et al. The immunomodulatory activity of extracellular vesicles derived from endometrial mesenchymal stem cells on CD4+ T cells is partially mediated by TGFbeta. *J Tissue Eng Regen Med*. 2018;12(10):2088–98. DOI:10.1002/term.2743

[173] Crain SK, Robinson SR, Thane KE, Davis AM, Meola DM, Barton BA, et al. Extracellular Vesicles from Wharton's Jelly Mesenchymal Stem Cells Suppress CD4 Expressing T Cells Through Transforming Growth Factor Beta and Adenosine Signaling in a Canine Model. *Stem Cells Dev*. 2019;28(3):212–26. DOI:10.1089/scd.2018.0097

[174] Garı MI, Chu C, Golshayan D, Cernuda-morollo E, Wait R, Lechler RI. Galectin-1 : a key effector of regulation mediated by CD4 ♀ CD25 ♀ T cells. 2018;109(5):2058–66. DOI:10.1182/blood-2006-04-016451.The

[175] Francisco LM, Salinas VH, Brown KE, Vanguri VK, Freeman GJ, Kuchroo VK, et al. PD-L1 regulates the development, maintenance, and function of induced regulatory T cells. *J Exp Med*. 2009;206(13):3015–29. DOI:10.1084/jem.20090847

[176] Tran DQ. TGF-beta: the sword, the wand, and the shield of FOXP3(+) regulatory T cells. *J Mol Cell Biol*. 2012;4(1):29–37. DOI:10.1093/jmcb/mjr033

[177] Garín MI, Chu NC, Golshayan D, Cernuda-Morollón E, Wait R, Lechler RI. Galectin-1: A key effector of regulation mediated by CD4 +CD25+ T cells. *Blood*. 2007;109(5):2058–65. DOI:10.1182/blood-2006-04-016451

[178] Patel SA, Meyer JR, Greco SJ, Corcoran KE, Bryan M, Rameshwar P. Mesenchymal Stem Cells Protect Breast Cancer Cells through Regulatory T Cells: Role of Mesenchymal Stem Cell-Derived TGF-β. *J Immunol*. 2010;184(10):5885–94. DOI:10.4049/jimmunol.0903143

[179] Mardpour S, Hamidieh AA, Taleahmad S, Sharifzad F, Taghikhani A, Baharvand H. Interaction between mesenchymal stromal cell-derived extracellular vesicles and immune cells by distinct protein content. *J Cell Physiol*. 2018;234(6):8249–58.

DOI:10.1002/jcp.27669

[180] Lee H, Han S, Kwon CS, Lee D. Biogenesis and regulation of the let-7 miRNAs and their functional implications. *Protein Cell*. 2016;7(2):100–13. DOI:10.1007/s13238-015-0212-y

[181] Su J-L, Chen P-S, Johansson G, Kuo M-L. Function and Regulation of Let-7 Family microRNAs. *MicroRNA e*. 2012;1(1):34–9. DOI:10.2174/2211536611201010034

[182] Viswanathan, S. R., Daley, D. Q., Gregory R 1. Selective blockade of microRNA processing by Lin-28. *Science (80-)*. 2013;320(5872):97–100. DOI:10.1126/science.1154040.Selective

[183] Peng Y, Li H, Li X, Yu S, Xiang H, Peng J, et al. MicroRNA-215 impairs adipocyte differentiation and co-represses FNDC3B and CTNNBIP1. *Int J Biochem Cell Biol* . 2016;79:104–12. DOI:10.1016/j.biocel.2016.08.014

[184] Di Trapani M, Bassi G, Midolo M, Gatti A, Kamga PT, Cassaro A, et al. Differential and transferable modulatory effects of mesenchymal stromal cell-derived extracellular vesicles on T, B and NK cell functions. *Sci Rep*. 2016;6(March):1–13. DOI:10.1038/srep24120

[185] Xiang W, Tian C, Peng S, Zhou L, Deng Z, Pan S. Let-7i attenuates human brain microvascular endothelial cell damage in oxygen glucose deprivation model by decreasing toll-like receptor 4 expression. *Biochem Biophys Res Commun*. 2017;493(1):788–93. DOI:10.1016/j.bbrc.2017.08.093

[186] Zou P, Zhu M, Lian C, Wang J, Chen Z, Zhang X, et al. miR-192-5p suppresses the progression of lung cancer bone metastasis by targeting TRIM44. *Sci Rep*. 2019;9(1):1–9. DOI:10.1038/s41598-019-56018-5

[187] Ono M, Kosaka N, Tominaga N, Yoshioka Y, Takeshita F, Takahashi RU, et al. Exosomes from bone marrow mesenchymal stem cells contain a microRNA that promotes dormancy in metastatic breast cancer cells. *Sci Signal*. 2014;7(332). DOI:10.1126/scisignal.2005231

[188] Baglio SR, Rooijers K, Koppers-Lalic D, Verweij FJ, Pérez Lanzón M, Zini N, et al. Human bone marrow- and adipose-mesenchymal stem cells secrete exosomes enriched in distinctive miRNA and tRNA species. *Stem Cell Res Ther* . 2015;6:127. DOI:10.1186/s13287-015-0116-z

[189] Annunziato F, Cosmi L, Liotta F, Maggi E, Romagnani S. The phenotype of human Th17 cells and their precursors, the cytokines that mediate their differentiation and the role of Th17 cells in inflammation. *Int Immunol*. 2008;20(11):1361–8. DOI:10.1093/intimm/dxn106

[190] Cosenza S, Toupet K, Maumus M, Luz-Crawford P, Blanc-Brude O, Jorgensen C, et al. Mesenchymal stem cells-derived exosomes are more immunosuppressive than microparticles in inflammatory arthritis. *Theranostics*. 2018;8(5):1399–410. DOI:10.7150/thno.21072

[191] Budoni M, Fierabracci A, Luciano R, Petrini S, Di Ciommo V, Muraca M. The immunosuppressive effect of mesenchymal stromal cells on B lymphocytes is mediated by membrane vesicles. *Cell Transplant*. 2013;22(2):369–79. DOI:10.3727/096368911X582769

[192] Zhao Y, Sun X, Cao W, Ma J, Sun L, Qian H, et al. Exosomes Derived from Human Umbilical Cord Mesenchymal Stem Cells Relieve Acute Myocardial Ischemic Injury. *Stem Cells Int*. 2015;2015. DOI:10.1155/2015/761643

[193] Li T, Yan Y, Wang B, Qian H, Zhang X, Shen L, et al. Exosomes derived from human umbilical cord mesenchymal stem cells alleviate liver fibrosis. *Stem Cells Dev*. 2013;22(6):845–54. DOI:10.1089/scd.2012.0395

[194] Wu S, Ju GQ, Du T, Zhu YJ, Liu GH. Microvesicles Derived from Human Umbilical Cord Wharton's Jelly Mesenchymal Stem Cells Attenuate Bladder Tumor Cell Growth In Vitro and In Vivo. *PLoS One*. 2013;8(4):1–12. DOI:10.1371/journal.pone.0061366

[195] Park JH, Hwang I, Hwang SH, Han H, Ha H. Human umbilical cord blood-derived mesenchymal stem cells prevent diabetic renal injury through paracrine action. *Diabetes Res Clin Pract* . 2012;98(3):465–73. DOI:10.1016/j.diabres.2012.09.034

[196] Shigemoto-Kuroda T, Oh JY, Kim D ki, Jeong HJ, Park SY, Lee HJ, et al. MSC-derived Extracellular Vesicles Attenuate Immune Responses in Two Autoimmune Murine Models: Type 1 Diabetes and Uveoretinitis. *Stem Cell Reports* . 2017;8(5):1214–25. DOI:10.1016/j.stemcr.2017.04.008

[197] Kannan K, Ortmann RA, Kimpel D. Animal models of rheumatoid arthritis and their relevance to human disease. *Pathophysiology*. 2005;12(3):167–81. DOI:10.1016/j.pathophys.2005.07.011

[198] Atkinson SM, Usher PA, Kvist PH, Markholst H, Haase C, Nansen A. Establishment and characterization of a sustained delayed-type hypersensitivity model with arthritic manifestations in C57BL/6J mice. *Arthritis Res Ther* . 2012;14(3):R134. DOI:10.1186/ar3867

[199] Kordelas L, Rebmann V, Ludwig AK, Radtke S, Ruesing J, Doeppner TR, et al. MSC-derived exosomes: A novel tool to treat therapy-refractory graft-versus-host disease. *Leukemia*. 2014;28(4):970–3. DOI:10.1038/leu.2014.41

[200] Nassar W, El-Ansary M, Sabry D, Mostafa MA, Fayad T, Kotb E, et al. Umbilical cord mesenchymal stem cells derived extracellular vesicles can safely ameliorate the progression of chronic kidney diseases. *Biomater Res* . 2016;20(1):1–11. DOI:10.1186/s40824-016-0068-0

[201] Vader P, Mol EA, Pasterkamp G, Schiffelers RM. Extracellular vesicles for drug delivery. *Adv Drug Deliv Rev* . 2016;106:148–56. DOI:10.1016/j.addr.2016.02.006

[202] Shelke GV, Lässer C, Gho YS, Lötvall J. Importance of exosome depletion protocols to eliminate functional and RNA-containing extracellular vesicles from fetal bovine serum. *J Extracell Vesicles*. 2014;3(1). DOI:10.3402/jev.v3.24783

[203] Kornilov R, Puhka M, Mannerström B, Hiidenmaa H, Peltoniemi H, Siljander P, et al. Efficient ultrafiltration-based protocol to deplete extracellular vesicles from fetal bovine serum. *J Extracell Vesicles* . 2018;7(1). DOI:10.1080/20013078.2017.1422674

[204] Liao Z, Muth DC, Eitan E, Travers M, Learman LN, Lehrmann E, et al. Serum extracellular vesicle depletion processes affect release and infectivity of HIV-1 in culture. *Sci Rep*. 2017;7(1):1–13. DOI:10.1038/s41598-017-02908-5

[205] Eitan E, Zhang S, Witwer KW, Mattson MP. Extracellular vesicle-depleted fetal

bovine and human sera have reduced capacity to support cell growth. *J Extracell Vesicles*. 2015;4(2015):1–10. DOI:10.3402/jev.v4.26373

[206] Willms E, Johansson HJ, Mäger I, Lee Y, Blomberg KEM, Sadik M, et al. Cells release subpopulations of exosomes with distinct molecular and biological properties. *Sci Rep* . 2016;6(March):1–12. DOI:10.1038/srep22519

[207] Greening DW, Xu R, Ji H, Tauro BJ, Simpson RJ. Proteomic Profiling . Vol. 1295. 2015. 6 p. DOI:10.1007/978-1-4939-2550-6

[208] Aswad H, Jalabert A, Rome S. Depleting extracellular vesicles from fetal bovine serum alters proliferation and differentiation of skeletal muscle cells in vitro. *BMC Biotechnol* . 2016;16(1):1–12. DOI:10.1186/s12896-016-0262-0

[209] Théry C, Clayton A, Amigorena S, Raposo and G. Isolation and Characterization of Exosomes from Cell Culture Supernatants. *Curr Protoc Cell Biol*. 2006;30:3.22:3.22.1–3.22.29.

[210] Jeppesen DK, Hvam ML, Primdahl-Bengtson B, Boysen AT, Whitehead B, Dyrskjøt L, et al. Comparative analysis of discrete exosome fractions obtained by differential centrifugation. *J Extracell Vesicles*. 2014;3(1):1–16. DOI:10.3402/jev.v3.25011

[211] Taylor DD, Shah S. Methods of isolating extracellular vesicles impact down-stream analyses of their cargoes. *Methods* . 2015;87:3–10. DOI:10.1016/j.ymeth.2015.02.019

[212] Lobb RJ, Becker M, Wen SW, Wong CSF, Wiegmans AP, Leimgruber A, et al. Optimized exosome isolation protocol for cell culture supernatant and human plasma. *J Extracell Vesicles*. 2015;4(1):1–11. DOI:10.3402/jev.v4.27031

[213] Fricke, Fabia; Buschmann, Dominik; Pfaffl MW. Isolation and characterization of extracellular vesicles. *Trillium Extracell Vesicles*. 2019;1(1):1–52.

[214] Wu D, Yotnda P. Induction and testing of hypoxia in cell culture. *J Vis Exp*. 2011;(54). DOI:10.3791/2899

[215] Mennan C, Garcia J, Roberts S, Hulme C, Wright K. A comprehensive characterisation of large-scale expanded human bone marrow and umbilical cord mesenchymal stem cells. *Stem Cell Res Ther*. 2019;10(1):1–15. DOI:10.1186/s13287-019-1202-4

[216] Lechanteur C. Large-Scale Clinical Expansion of Mesenchymal Stem Cells in the GMP-Compliant, Closed Automated Quantum® Cell Expansion System: Comparison with Expansion in Traditional T-Flasks. *J Stem Cell Res Ther*. 2014;04(08):1–11. DOI:10.4172/2157-7633.1000222

[217] Mennan C, Brown S, McCarthy H, Mavrogonatou E, Kletsas D, Garcia J, et al. Mesenchymal stromal cells derived from whole human umbilical cord exhibit similar properties to those derived from Wharton's jelly and bone marrow. *FEBS Open Bio*. 2016;6(11):1054–66. DOI:10.1002/2211-5463.12104

[218] Agrawal R, Dale TP, Al-Zubaidi MA, Malgulwar PB, Forsyth NR, Kulshreshtha R. Pluripotent and multipotent stem cells display distinct hypoxic miRNA expression profiles. *PLoS One*. 2016;11(10):1–20. DOI:10.1371/journal.pone.0164976

[219] Khalilifar MA, Eslaminejad MB, Ghasemzadeh M, Hosseini S, Baharvand H. In vitro and in vivo comparison of different types of rabbit mesenchymal stem cells for

cartilage repair. *Cell J*. 2018;21(2):150–60. DOI:10.22074/cellj.2019.6149

[220] Esteves CL, Sheldrake TA, Mesquita SP, Pesántez JJ, Menghini T, Dawson L, et al. Isolation and characterization of equine native MSC populations. *Stem Cell Res Ther*. 2017;8(1). DOI:10.1186/s13287-017-0525-2

[221] Gardiner C, Ferreira YJ, Dragovic RA, Redman CWG, Sargent IL. Extracellular vesicle sizing and enumeration by nanoparticle tracking analysis. *J Extracell Vesicles*. 2013;2(1):1–11. DOI:10.3402/jev.v2i0.19671

[222] Samuel Eguasi Inkabi*, Kristianna Marie Fredenburg MR. Western Blot Comparison of Wet Transfer and Semi-Dry Transfer Methods. *Int J Sci Res Methodol*. 2019;13(4):54–64.

[223] Sztefko K. Interferences in immunoassay. *Przegląd Lek*. 2002;59(6):477–80. DOI:10.5772/35797

[224] Huang DW, Sherman BT, Lempicki RA. Bioinformatics enrichment tools: paths toward the comprehensive functional analysis of large gene lists. *Nucleic Acids Res*. 2009;37(1):1–13. DOI:10.1093/nar/gkn923

[225] Huang DW, Sherman BT, Lempicki RA. Systematic and integrative analysis of large gene lists using DAVID bioinformatics resources. *Nat Protoc*. 2009;4(1):44–57. DOI:10.1038/nprot.2008.211

[226] Arroyo JD, Chevillet JR, Kroh EM, Ruf IK, Pritchard CC, Gibson DF, et al. Argonaute2 complexes carry a population of circulating microRNAs independent of vesicles in human plasma. *Proc Natl Acad Sci U S A*. 2011;108(12):5003–8. DOI:10.1073/pnas.1019055108

[227] Mateescu B, Kowal EJK, van Balkom BWM, Bartel S, Bhattacharyya SN, Buzás EI, et al. Obstacles and opportunities in the functional analysis of extracellular vesicle RNA - An ISEV position paper. *J Extracell Vesicles* . 2017;6(1). DOI:10.1080/20013078.2017.1286095

[228] Eikrem O, Beisland C, Hjelle K, Flatberg A, Scherer A, Landolt L, et al. Transcriptome sequencing (RNAseq) enables utilization of formalin-fixed, paraffin-embedded biopsies with clear cell renal cell carcinoma for exploration of disease biology and biomarker development. *PLoS One*. 2016;11(2):1–19. DOI:10.1371/journal.pone.0149743

[229] Spornraft M, Kirchner B, Haase B, Benes V, Pfaffl MW, Riedmaier I. Optimization of extraction of circulating RNAs from plasma - Enabling small RNA sequencing. *PLoS One*. 2014;9(9). DOI:10.1371/journal.pone.0107259

[230] Fan Y, Siklenka K, Arora SK, Ribeiro P, Kimmins S, Xia J. miRNet - dissecting miRNA-target interactions and functional associations through network-based visual analysis. *Nucleic Acids Res*. 2016;44(W1):W135–41. DOI:10.1093/nar/gkw288

[231] Fan Y, Xia J. miRNet—Functional analysis and visual exploration of miRNA–target interactions in a network context. *Methods Mol Biol*. 2018;1819:215–33. DOI:10.1007/978-1-4939-8618-7_10

[232] Liu W, Wang X. Prediction of functional microRNA targets by integrative modeling of microRNA binding and target expression data. *Genome Biol* . 2019;20(1):18.

DOI:10.1186/s13059-019-1629-z

[233] Chen Y, Wang X. miRDB: an online database for prediction of functional microRNA targets. *Nucleic Acids Res* . 2020;48(D1):D127–31. DOI:10.1093/nar/gkz757

[234] Agarwal V, Bell GW, Nam JW, Bartel DP. Predicting effective microRNA target sites in mammalian mRNAs. *Elife*. 2015;4(AUGUST2015):1–38. DOI:10.7554/eLife.05005

[235] Ma Y, Dong L, Zhou D, Li L, Zhang W, Zhen Y, et al. Extracellular vesicles from human umbilical cord mesenchymal stem cells improve nerve regeneration after sciatic nerve transection in rats. *J Cell Mol Med*. 2019;23(4):2822–35. DOI:10.1111/jcmm.14190

[236] Ferreira JR, Teixeira GQ, Santos SG, Barbosa MA, Almeida-Porada G, Gonçalves RM. Mesenchymal Stromal Cell Secretome: Influencing Therapeutic Potential by Cellular Pre-conditioning. *Front Immunol*. 2018;9(December):2837. DOI:10.3389/fimmu.2018.02837

[237] Pavlacky J, Polak J. Technical Feasibility and Physiological Relevance of Hypoxic Cell Culture Models. *Front Endocrinol (Lausanne)*. 2020;11(February):1–15. DOI:10.3389/fendo.2020.00057

[238] Mark L. Weiss, Troyer DL. Stem Cells in the Umbilical Cord. *Stem Cells Rev* . 2006;2(2):155–62. DOI:10.1007/s12015-006-0022-y.Stem

[239] Zhilai Z, Biling M, Sujun Q, Chao D, Benchao S, Shuai H, et al. Preconditioning in lowered oxygen enhances the therapeutic potential of human umbilical mesenchymal stem cells in a rat model of spinal cord injury. *Brain Res*. 2016;1642:426–35. DOI:10.1016/j.brainres.2016.04.025

[240] Leroux L, Descamps B, Tojais NF, Séguy B, Oses P, Moreau C, et al. Hypoxia preconditioned mesenchymal stem cells improve vascular and skeletal muscle fiber regeneration after ischemia through a wnt4-dependent pathway. *Mol Ther* . 2010;18(8):1545–52. DOI:10.1038/mt.2010.108

[241] Haque N, Rahman MT, Abu Kasim NH, Alabsi AM. Hypoxic culture conditions as a solution for mesenchymal stem cell based regenerative therapy. *Sci World J*. 2013;2013. DOI:10.1155/2013/632972

[242] Antebi B, Rodriguez LA, Walker KP, Asher AM, Kamucheka RM, Alvarado L, et al. Short-term physiological hypoxia potentiates the therapeutic function of mesenchymal stem cells. *Stem Cell Res Ther*. 2018;9(1):1–15. DOI:10.1186/s13287-018-1007-x

[243] Noronha Nc NDC, Mizukami A, Caliári-Oliveira C, Cominal JG, Rocha JLM, Covas DT, et al. Priming approaches to improve the efficacy of mesenchymal stromal cell-based therapies. *Stem Cell Res Ther*. 2019;10(1):1–21. DOI:10.1186/s13287-019-1224-y

[244] Kay AG, Dale TP, Akram KM, Mohan P, Hampson K, Maffulli N, et al. BMP2 repression and optimized culture conditions promote human bone marrow-derived mesenchymal stem cell isolation. *Regen Med*. 2015;10(2):109–25. DOI:10.2217/rme.14.67

[245] Fan L, Liu R, Li J, Shi Z, Dang X, Wang K. Low Oxygen Tension Enhances Osteogenic Potential of Bone Marrow-Derived Mesenchymal Stem Cells with

Osteonecrosis-Related Functional Impairment. *Stem Cells Int*. 2015;1–8. DOI:10.1155/2015/950312

[246] Krampera M, Cosmi L, Angeli R, Pasini A, Liotta F, Andreini A, et al. Role for Interferon-γ in the Immunomodulatory Activity of Human Bone Marrow Mesenchymal Stem Cells. *Stem Cells* . 2006;24(2):386–98. DOI:Https://doi.org/10.1634/stemcells.2005-0008

[247] Antebi B, Rodriguez LA, Walker KP, Asher AM, Kamucheka RM, Alvarado L, et al. Short-term physiological hypoxia potentiates the therapeutic function of mesenchymal stem cells. *Stem Cell Res Ther* . 2018;9(1):265. DOI:10.1186/s13287-018-1007-x

[248] Balgi-Agarwal S, Winter C, Corral A, Mustafa SB, Hornsby P, Moreira A. Comparison of Preterm and Term Wharton's Jelly-Derived Mesenchymal Stem Cell Properties in Different Oxygen Tensions. *Cells Tissues Organs*. 2018;205(3):137–50. DOI:10.1159/000489256

[249] Lavrentieva A, Majore I, Kasper C, Hass R. Effects of hypoxic culture conditions on umbilical cord-derived human mesenchymal stem cells. *Cell Commun Signal*. 2010;8:1–9. DOI:10.1186/1478-811X-8-18

[250] Lönne M, Lavrentieva A, Walter JG, Kasper C. Analysis of oxygen-dependent cytokine expression in human mesenchymal stem cells derived from umbilical cord. *Cell Tissue Res*. 2013;353(1):117–22. DOI:10.1007/s00441-013-1597-7

[251] Deuse T, Stubbendorff M, Tang-Quan K, Phillips N, Kay MA, Eiermann T, et al. Immunogenicity and immunomodulatory properties of umbilical cord lining mesenchymal stem cells. *Cell Transplant*. 2011;20(5):655–67. DOI:10.3727/096368910X536473

[252] Fan H, Zhao G, Liu L, Liu F, Gong W, Liu X, et al. Pre-treatment with IL-1β enhances the efficacy of MSC transplantation in DSS-induced colitis. *Cell Mol Immunol*. 2012;9(6):473–81. DOI:10.1038/cmi.2012.40

[253] Prasanna SJ, Gopalakrishnan D, Shankar SR, Vasandan AB. Pro-inflammatory cytokines, IFNγ and TNFα, influence immune properties of human bone marrow and Wharton jelly mesenchymal stem cells differentially. *PLoS One*. 2010;5(2). DOI:10.1371/journal.pone.0009016

[254] Rodriguez LA, Mohammadipoor A, Alvarado L, Kamucheka RM, Asher AM, Cancio LC, et al. Preconditioning in an Inflammatory Milieu Augments the Immunotherapeutic Function of Mesenchymal Stromal Cells. *Cells*. 2019;8(5):462. DOI:10.3390/cells8050462

[255] Wobma HM, Kanai M, Ma SP, Shih Y, Li HW, Duran-Struuck R, et al. Dual IFN-γ/hypoxia priming enhances immunosuppression of mesenchymal stromal cells through regulatory proteins and metabolic mechanisms. *J Immunol Regen Med* . 2018/04/25. 2018;1:45–56. DOI:10.1016/j.regen.2018.01.001

[256] Rodríguez-Fuentes DE, Fernández-Garza LE, Samia-Meza JA, Barrera-Barrera SA, Caplan AI, Barrera-Saldaña HA. Mesenchymal Stem Cells Current Clinical Applications: A Systematic Review. *Arch Med Res* . 2021;52(1):93–101. DOI:Https://doi.org/10.1016/j.arcmed.2020.08.006

[257] Garcia J, Mennan C, McCarthy HS, Roberts S, Richardson JB, Wright KT.

Chondrogenic Potency Analyses of Donor-Matched Chondrocytes and Mesenchymal Stem Cells Derived from Bone Marrow, Infrapatellar Fat Pad, and Subcutaneous Fat. *Stem Cells Int*. 2016;2016. DOI:10.1155/2016/6969726

[258] Li X, Bai J, Ji X, Li R, Xuan Y, Wang Y. Comprehensive characterization of four different populations of human mesenchymal stem cells as regards their immune properties, proliferation and differentiation. *Int J Mol Med*. 2014;34(3):695–704. DOI:10.3892/ijmm.2014.1821

[259] Silva-Cote I, Cruz-Barrera M, Cañas-Arboleda M, Correa-Araujo L, Méndez L, Jagielska J, et al. Strategy for the Generation of Engineered Bone Constructs Based on Umbilical Cord Mesenchymal Stromal Cells Expanded with Human Platelet Lysate. *Stem Cells Int*. 2019;2019. DOI:10.1155/2019/7198215

[260] Zhan XS, El-Ashram S, Luo DZ, Luo HN, Wang BY, Chen SF, et al. A comparative study of biological characteristics and transcriptome profiles of mesenchymal stem cells from different canine tissues. *Int J Mol Sci*. 2019;20(6). DOI:10.3390/ijms20061485

[261] Grayson WL, Zhao F, Bunnell B, Ma T. Hypoxia enhances proliferation and tissue formation of human mesenchymal stem cells. *Biochem Biophys Res Commun*. 2007;358(3):948–53. DOI:10.1016/j.bbrc.2007.05.054

[262] D'Ippolito G, Diabira S, Howard GA, Menei P, Roos BA, Schiller PC. Marrow-isolated adult multilineage inducible (MIAMI) cells, a unique population of postnatal young and old human cells with extensive expansion and differentiation potential. *J Cell Sci*. 2004;117(14):2971–81. DOI:10.1242/jcs.01103

[263] Estrada JC, Albo C, Benguría A, Dopazo A, López-Romero P, Carrera-Quintanar L, et al. Culture of human mesenchymal stem cells at low oxygen tension improves growth and genetic stability by activating glycolysis. *Cell Death Differ*. 2012;19(5):743–55. DOI:10.1038/cdd.2011.172

[264] Holzwarth C, Vaegler M, Gieseke F, Pfister SM, Handgretinger R, Kerst G, et al. Low physiologic oxygen tensions reduce proliferation and differentiation of human multipotent mesenchymal stromal cells. *BMC Cell Biol*. 2010;11. DOI:10.1186/1471-2121-11-11

[265] Elabd C, Ichim TE, Miller K, Anneling A, Grinstein V, Vargas V, et al. Comparing atmospheric and hypoxic cultured mesenchymal stem cell transcriptome: Implication for stem cell therapies targeting intervertebral discs. *J Transl Med* . 2018;16(1):1–14. DOI:10.1186/s12967-018-1601-9

[266] Lavrentieva A, Majore I, Kasper C, Hass R. Effects of hypoxic culture conditions on umbilical cord-derived human mesenchymal stem cells. *Cell Commun Signal* . 2010;8(1):18. DOI:10.1186/1478-811X-8-18

[267] Nekanti U, Dastidar S, Venugopal P, Totey S, Ta M. Increased proliferation and analysis of differential gene expression in human Wharton's jelly-derived mesenchymal stromal cells under hypoxia. *Int J Biol Sci*. 2010;6(5):499–512. DOI:10.7150/ijbs.6.499

[268] Widowati W, Wijaya L, Murti H, Widyastuti H, Agustina D, Laksmitawati DR, et al. Conditioned medium from normoxia (WJMSCs-norCM) and hypoxia-treated

WJMSCs (WJMSCs-hypoCM) in inhibiting cancer cell proliferation. *Biomarkers Genomic Med*. 2015;7(1):8–17. DOI:10.1016/j.bgm.2014.08.008

[269] Kot M, Baj-Krzyworzeka M, Szatanek R, Musiał-Wysocka A, Suda-Szczurek M, Majka M. The importance of hla assessment in "off-the-shelf" allogeneic mesenchymal stem cells based-therapies. *Int J Mol Sci*. 2019;20(22). DOI:10.3390/ijms20225680

[270] Buyl K, Merimi M, Rodrigues RM, Moussa Agha D, Melki R, Vanhaecke T, et al. The Impact of Cell-Expansion and Inflammation on The Immune-Biology of Human Adipose Tissue-Derived Mesenchymal Stromal Cells. *J Clin Med*. 2020;9(3):696. DOI:10.3390/jcm9030696

[271] Chan JL, Tang KC, Patel AP, Bonilla LM, Pierobon N, Ponzio NM, et al. Antigen-presenting property of mesenchymal stem cells occurs during a narrow window at low levels of interferon-γ. *Blood*. 2006;107(12):4817–24. DOI:10.1182/blood-2006-01-0057

[272] Van Megen KM, Van 't Wout EJT, Motta JL, Dekker B, Nikolic T, Roep BO. Activated mesenchymal stromal cells process and present antigens regulating adaptive immunity. *Front Immunol*. 2019;10(APR):1–10. DOI:10.3389/fimmu.2019.00694

[273] Fu X, Chen Y, Xie FN, Dong P, Liu WB, Cao Y, et al. Comparison of immunological characteristics of mesenchymal stem cells derived from human embryonic stem cells and bone marrow. *Tissue Eng - Part A*. 2015;21(3–4):616–26. DOI:10.1089/ten.tea.2013.0651

[274] Romieu-Mourez R, François M, Boivin M-N, Stagg J, Galipeau J. Regulation of MHC Class II Expression and Antigen Processing in Murine and Human Mesenchymal Stromal Cells by IFN-γ, TGF-β, and Cell Density. *J Immunol*. 2007;179(3):1549–58. DOI:10.4049/jimmunol.179.3.1549

[275] Grau-Vorster M, Laitinen A, Nystedt J, Vives J. HLA-DR expression in clinical-grade bone marrow-derived multipotent mesenchymal stromal cells: a two-site study. *Stem Cell Res Ther* . 2019;10(1):164. DOI:10.1186/s13287-019-1279-9

[276] Nagamura-Inoue T. Umbilical cord-derived mesenchymal stem cells: Their advantages and potential clinical utility. *World J Stem Cells*. 2014;6(2):195. DOI:10.4252/wjsc.v6.i2.195

[277] Yang ZX, Han ZB, Ji YR, Wang YW, Liang L, Chi Y, et al. CD106 Identifies a Subpopulation of Mesenchymal Stem Cells with Unique Immunomodulatory Properties. *PLoS One*. 2013;8(3):1–12. DOI:10.1371/journal.pone.0059354

[278] Lu S, Ge M, Zheng Y, Li J, Feng X, Feng S, et al. CD106 is a novel mediator of bone marrow mesenchymal stem cells via NF-κB in the bone marrow failure of acquired aplastic anemia. *Stem Cell Res Ther*. 2017;8(1):1–14. DOI:10.1186/s13287-017-0620-4

[279] Wang Q, Yang Q, Wang Z, Tong H, Ma L, Zhang Y, et al. Comparative analysis of human mesenchymal stem cells from fetal-bone marrow, adipose tissue, and Warton's jelly as sources of cell immunomodulatory therapy. *Hum Vaccines Immunother*. 2016;12(1):85–96. DOI:10.1080/21645515.2015.1030549

[280] Ren G, Zhao X, Zhang L, Zhang J, L'Huillier A, Ling W, et al. Inflammatory

Cytokine-Induced Intercellular Adhesion Molecule-1 and Vascular Cell Adhesion Molecule-1 in Mesenchymal Stem Cells Are Critical for Immunosuppression. *J Immunol*. 2010;184(5):2321–8. DOI:10.4049/jimmunol.0902023

[281] Perry J, McCarthy HS, Bou-Gharios G, van 't Hof R, Milner PI, Mennan C, et al. Injected human umbilical cord-derived mesenchymal stromal cells do not appear to elicit an inflammatory response in a murine model of osteoarthritis. *Osteoarthr Cartil Open*. 2020;2(2):100044. DOI:10.1016/j.ocarto.2020.100044

[282] Halfon S, Abramov N, Grinblat B, Ginis I. Markers distinguishing mesenchymal stem cells from fibroblasts are downregulated with passaging. *Stem Cells Dev*. 2011;20(1):53–66. DOI:10.1089/scd.2010.0040

[283] Yang C, Chen Y, Li F, You M, Zhong L, Li W, et al. The biological changes of umbilical cord mesenchymal stem cells in inflammatory environment induced by different cytokines. *Mol Cell Biochem* . 2018;446(1–2):171–84. DOI:10.1007/s11010-018-3284-1

[284] Jones EA, English A, Kinsey SE, Straszynski L, Emery P, Ponchel F, et al. Optimization of a flow cytometry-based protocol for detection and phenotypic characterization of multipotent mesenchymal stromal cells from human bone marrow. *Cytom Part B - Clin Cytom*. 2006;70(6):391–9. DOI:10.1002/cyto.b.20118

[285] Gronthos S, Zannettino ACW. A Method to Isolate and Purify Human Bone Marrow Stromal Stem Cells. In: Prockop DJ, Bunnell BA, Phinney DG, editors. Mesenchymal Stem Cells: Methods and Protocols . Totowa, NJ: Humana Press; 2008. p. 45–57. DOI:10.1007/978-1-60327-169-1_3

[286] Gronthos S, Zannettino ACW, Hay SJ, Shi S, Graves SE, Kortesidis A, et al. Molecular and cellular characterisation of highly purified stromal stem cells derived from human bone marrow. *J Cell Sci*. 2003;116(9):1827–35. DOI:10.1242/jcs.00369

[287] Bara JJ, Richards RG, Alini M, Stoddart MJ. Concise review: Bone marrow-derived mesenchymal stem cells change phenotype following in vitro culture: Implications for basic research and the clinic. *Stem Cells*. 2014;32(7):1713–23. DOI:10.1002/stem.1649

[288] Liu R, Chang W, Wei H, Zhang K. Comparison of the Biological Characteristics of Mesenchymal Stem Cells Derived from Bone Marrow and Skin. *Stem Cells Int*. 2016;2016. DOI:10.1155/2016/3658798

[289] Mohamed-Ahmed S, Fristad I, Lie SA, Suliman S, Mustafa K, Vindenes H, et al. Adipose-derived and bone marrow mesenchymal stem cells: A donor-matched comparison. *Stem Cell Res Ther*. 2018;9(1):1–15. DOI:10.1186/s13287-018-0914-1

[290] Sekiya, I., Larson, B. L., Smith, J. R., Pochampally, R., Cui, J. G., Prockop DJ. Expansion of Human Adult Stem Cells from Bone Marrow Stroma: Conditions that Maximize the Yields of Early Progenitors and Evaluate Their Quality. *Stem Cells*. 2002;(20):530–41.

[291] György B, Hung ME, Breakefield XO, Leonard JN. Therapeutic Applications of Extracellular Vesicles: Clinical Promise and Open Questions. *Annu Rev Pharmacol Toxicol*. 2014;55(1):439–64. DOI:10.1146/annurev-pharmtox-010814-124630

[292] Whiteside TL. Extracellular vesicles isolation and their biomarker potential: Are we

ready for testing? *Ann Transl Med*. 2017;5(3):3–6. DOI:10.21037/atm.2017.01.62

[293] Meng W, He C, Hao Y, Wang L, Li L, Zhu G. Prospects and challenges of extracellular vesicle-based drug delivery system: considering cell source. *Drug Deliv* . 2020;27(1):585–98. DOI:10.1080/10717544.2020.1748758

[294] Gardiner C, Vizio D Di, Sahoo S, Théry C, Witwer KW, Wauben M, et al. Techniques used for the isolation and characterization of extracellular vesicles: Results of a worldwide survey. *J Extracell Vesicles*. 2016;5(1):1–6. DOI:10.3402/jev.v5.32945

[295] Konoshenko MY, Lekchnov EA, Vlassov A V., Laktionov PP. Isolation of Extracellular Vesicles: General Methodologies and Latest Trends. *Biomed Res Int*. 2018;2018. DOI:10.1155/2018/8545347

[296] Webber J, Clayton A. How pure are your vesicles? *J Extracell Vesicles*. 2013;2(1):1–6. DOI:10.3402/jev.v2i0.19861

[297] Brennan K, Martin K, FitzGerald SP, O'Sullivan J, Wu Y, Blanco A, et al. A comparison of methods for the isolation and separation of extracellular vesicles from protein and lipid particles in human serum. *Sci Rep*. 2020;10(1):1–13. DOI:10.1038/s41598-020-57497-7

[298] Li J, Lee Y, Johansson HJ, Mäger I, Vader P, Nordin JZ, et al. Serum-free culture alters the quantity and protein composition of neuroblastoma-derived extracellular vesicles. *J Extracell Vesicles*. 2015;4(2015):1–12. DOI:10.3402/jev.v4.26883

[299] Bobis-Wozowicz S, Kmiotek K, Kania K, Karnas E, Labedz-Maslowska A, Sekula M, et al. Diverse impact of xeno-free conditions on biological and regenerative properties of hUC-MSCs and their extracellular vesicles. *J Mol Med*. 2017;95(2):205–20. DOI:10.1007/s00109-016-1471-7

[300] Li X, Liu LL, Yao JL, Wang K, Ai H. Human umbilical cord mesenchymal stem cell-derived extracellular vesicles inhibit endometrial cancer cell proliferation and migration through delivery of exogenous miR-302a. *Stem Cells Int*. 2019;2019. DOI:10.1155/2019/8108576

[301] Rohde E, Pachler K, Gimona M. Manufacturing and characterization of extracellular vesicles from umbilical cord–derived mesenchymal stromal cells for clinical testing. *Cytotherapy*. 2019;21(6):581–92. DOI:10.1016/j.jcyt.2018.12.006

[302] Sun Y, Shi H, Yin S, Ji C, Zhang X, Zhang B, et al. Human mesenchymal stem cell derived exosomes alleviate type 2 diabetes mellitus by reversing peripheral insulin resistance and relieving β-cell destruction. *ACS Nano*. 2018;12(8):7613–28. DOI:10.1021/acsnano.7b07643

[303] Wang L, Gu Z, Zhao X, Yang N, Wang F, Deng A, et al. Extracellular Vesicles Released from Human Umbilical Cord-Derived Mesenchymal Stromal Cells Prevent Life-Threatening Acute Graft-Versus-Host Disease in a Mouse Model of Allogeneic Hematopoietic Stem Cell Transplantation. *Stem Cells Dev*. 2016;25(24):1874–83. DOI:10.1089/scd.2016.0107

[304] Zhang B, Yin Y, Lai RC, Tan SS, Choo ABH, Lim SK. Mesenchymal stem cells secrete immunologically active exosomes. *Stem Cells Dev*. 2014;23(11):1233–44. DOI:10.1089/scd.2013.0479

[305] Thomi G, Surbek D, Haesler V, Joerger-Messerli M, Schoeberlein A. Exosomes derived from umbilical cord mesenchymal stem cells reduce microglia-mediated neuroinflammation in perinatal brain injury. *Stem Cell Res Ther*. 2019;10(1):1–16. DOI:10.1186/s13287-019-1207-z

[306] Hyland M, Mennan C, Wilson E, Clayton A, Kehoe O. Pro-Inflammatory Priming of Umbilical Cord Mesenchymal Stromal Cells Alters the Protein Cargo of Their Extracellular Vesicles. *Cells*. 2020;9(3):726. DOI:10.3390/cells9030726

[307] Choudhary, P. & Choudhary OP. Uses of Transmission Electron Microscope in Microscopy and its Advantages and Disadvantages. *Int J Curr Microbiol Appl Sci*. 2018;7(05):743–7. DOI:10.20546/ijcmas.2018.705.090

[308] Robson AL, Dastoor PC, Flynn J, Palmer W, Martin A, Smith DW, et al. Advantages and limitations of current imaging techniques for characterizing liposome morphology. *Front Pharmacol*. 2018;9(FEB):1–8. DOI:10.3389/fphar.2018.00080

[309] Lyumkis D. Challenges and opportunities in cryo-EM single-particle analysis. *J Biol Chem*. 2019;294(13):5181–97. DOI:10.1074/jbc.REV118.005602

[310] Filipe V, Hawe A, Jiskoot W. Critical evaluation of nanoparticle tracking analysis (NTA) by NanoSight for the measurement of nanoparticles and protein aggregates. *Pharm Res*. 2010;27(5):796–810. DOI:10.1007/s11095-010-0073-2

[311] Sivakumaran M, Platt M. Tunable resistive pulse sensing: Potential applications in nanomedicine. *Nanomedicine*. 2016;11(16):2197–214. DOI:10.2217/nnm-2016-0097

[312] Ghosh R, Gilda JE, Gomes A V. The necessity of and strategies for improving confidence in the accuracy of western blots. *Expert Rev Proteomics*. 2014;11(5):549–60. DOI:10.1586/14789450.2014.939635.The

[313] Xia X, Xu Y, Ke R, Zhang H, Zou M, Yang W, et al. A highly sensitive europium nanoparticle-based lateral flow immunoassay for detection of chloramphenicol residue. *Anal Bioanal Chem*. 2013;405(23):7541–4. DOI:10.1007/s00216-013-7210-9

[314] Nimse SB, Sonawane MD, Song KS, Kim T. Biomarker detection technologies and future directions. *Analyst*. 2016;141(3):740–55. DOI:10.1039/c5an01790d

[315] Hartjes TA, Mytnyk S, Jenster GW, van Steijn V, van Royen ME. Extracellular vesicle quantification and characterization: Common methods and emerging approaches. *Bioengineering*. 2019;6(1). DOI:10.3390/bioengineering6010007

[316] Davey HM, Kell DB. Flow cytometry and cell sorting of heterogeneous microbial populations: The importance of single-cell analyses. *Microbiol Rev*. 1996;60(4):641–96. DOI:10.1128/mmbr.60.4.641-696.1996

[317] Sakamoto S, Putalun W, Vimolmangkang S, Phoolcharoen W, Shoyama Y, Tanaka H, et al. Enzyme-linked immunosorbent assay for the quantitative/qualitative analysis of plant secondary metabolites. *J Nat Med* . 2018;72(1):32–42. DOI:10.1007/s11418-017-1144-z

[318] Ebnesajjad S. Surface and Material Characterization Techniques. Surface Treatment of Materials for Adhesive Bonding. 2014. 39–75 p. DOI:10.1016/b978-0-323-26435-8.00004-6

[319] Ilieva KM, Cheung A, Mele S, Chiaruttini G, Crescioli S, Griffin M, et al. Chondroitin

sulfate proteoglycan 4 and its potential as an antibody immunotherapy target across different tumor types. *Front Immunol*. 2018;8(JAN). DOI:10.3389/fimmu.2017.01911

[320] Rivero-Gutiérrez B, Anzola A, Martínez-Augustin O, De Medina FS. Stain-free detection as loading control alternative to Ponceau and housekeeping protein immunodetection in Western blotting. *Anal Biochem*. 2014;467:1–3. DOI:10.1016/j.ab.2014.08.027

[321] Katzmann DJ, Odorizzi G, Emr SD. Receptor downregulation and multivesicular-body sorting. *Nat Rev Mol Cell Biol*. 2002;3(12):893–905. DOI:10.1038/nrm973

[322] Pochampally RR, Smith JR, Ylostalo J, Prockop DJ. Serum deprivation of human marrow stromal cells (hMSCs) selects for a subpopulation of early progenitor cells with enhanced expression of OCT-4 and other embryonic genes. *Blood* . 2004;103(5):1647–52. DOI:10.1182/blood-2003-06-1967.Supported

[323] Lehrich BM, Liang Y, Khosravi P, Federoff HJ, Fiandaca MS. Fetal bovine serum-derived extracellular vesicles persist within vesicle-depleted culture media. *Int J Mol Sci*. 2018;19(11):1–11. DOI:10.3390/ijms19113538

[324] Witwer KW, Van Balkom BWM, Bruno S, Choo A, Dominici M, Gimona M, et al. Defining mesenchymal stromal cell (MSC)-derived small extracellular vesicles for therapeutic applications. *J Extracell Vesicles* . 2019;8(1). DOI:10.1080/20013078.2019.1609206

[325] Varkouhi, Amir K; Jerkic, Mirjana; Ormesher, Lindsay; Gagnon, Stéphane; Goyal, Sakshi; Rabani, Razieh; Masterson, Claire; Spring, Chris; Chen, Paul Z; Gu, Frank X; dos Santos, Claudia C; Curley, Gerard F; Laffey JG. Extracellular Vesicles Human Umbilical Cord coli – induced Acute Lung Injury in Rats. 2019;(5):778–90.

[326] Almeria C, Weiss R, Roy M, Tripisciano C, Kasper C, Weber V, et al. Hypoxia Conditioned Mesenchymal Stem Cell-Derived Extracellular Vesicles Induce Increased Vascular Tube Formation in vitro. *Front Bioeng Biotechnol*. 2019;7(October):1–12. DOI:10.3389/fbioe.2019.00292

[327] Andrews S, Maughon T, Marklein R, Stice S. Priming of MSCs with inflammation-relevant signals affects extracellular vesicle biogenesis , surface markers , and modulation of T cell subsets. *bioRxiv*. 2020;1–29.

[328] Xu W, Xu R, Li Z, Wang Y, Hu R. Hypoxia changes chemotaxis behaviour of mesenchymal stem cells via HIF-1α signalling. *J Cell Mol Med*. 2018;23(3):1899–907. DOI:10.1111/jcmm.14091

[329] Yu X, Wan Q, Ye X, Cheng Y, Pathak JL, Li Z. Cellular hypoxia promotes osteogenic differentiation of mesenchymal stem cells and bone defect healing via STAT3 signaling. *Cell Mol Biol Lett*. 2019;24(1):1–17. DOI:10.1186/s11658-019-0191-8

[330] Alijani N, Johari B, Moradi M, Kadivar M. A review on transcriptional regulation responses to hypoxia in mesenchymal stem cells. *Cell Biol Int*. 2020;44(1):14–26. DOI:10.1002/cbin.11211

[331] Petrini S, Tessa A, Carrozzo R, Verardo M, Pierini R, Rizza T, et al. Human melanoma/NG2 chondroitin sulfate proteoglycan is expressed in the sarcolemma of postnatal human skeletal myofibers: Abnormal expression in merosin-negative and Duchenne muscular dystrophies. *Mol Cell Neurosci*. 2003;23(2):219–31.

DOI:10.1016/S1044-7431(03)00033-2

[332] Barilani M, Peli V, Cherubini A, Dossena M, Dolo V, Lazzari L. NG2 as an Identity and Quality Marker of Mesenchymal Stem Cell Extracellular Vesicles. *Cells*. 2019;8(12):1524. DOI:10.3390/cells8121524

[333] Stallcup WB. The NG2 Proteoglycan in Pericyte Biology. *Adv Exp Med Biol*. 2018;1109:5–19. DOI:10.1007/978-3-030-02601-1

[334] Crisan M, Yap S, Casteilla L, Chen CW, Corselli M, Park TS, et al. A Perivascular Origin for Mesenchymal Stem Cells in Multiple Human Organs. *Cell Stem Cell*. 2008;3(3):301–13. DOI:10.1016/j.stem.2008.07.003

[335] Kozanoglu I, Boga C, Ozdogu H, Sozer O, Maytalman E, Yazici AC, et al. Human bone marrow mesenchymal cells express NG2: Possible increase in discriminative ability of flow cytometry during mesenchymal stromal cell identification. *Cytotherapy* . 2009;11(5):527–33. DOI:10.1080/14653240902923153

[336] Rhodes KE, Raivich G, Fawcett JW. The injury response of oligodendrocyte precursor cells is induced by platelets, macrophages and inflammation-associated cytokines. *Neuroscience*. 2006;140(1):87–100. DOI:10.1016/j.neuroscience.2006.01.055

[337] Gao Q, Lu J, Huo Y, Baby N, Ling EA, Dheen ST. NG2, a member of chondroitin sulfate proteoglycans family mediates the inflammatory response of activated microglia. *Neuroscience* . 2010;165(2):386–94. DOI:10.1016/j.neuroscience.2009.10.022

[338] Ampofo E, Schmitt BM, Menger MD, Laschke MW. The regulatory mechanisms of NG2/CSPG4 expression. *Cell Mol Biol Lett*. 2017;22:4. DOI:10.1186/s11658-017-0035-3

[339] Maleki M, Ghanbarvand F, Behvarz MR, Ejtemaei M, Ghadirkhomi E. Comparison of mesenchymal stem cell markers in multiple human adult stem cells. *Int J Stem Cells*. 2014;7(2):118–26. DOI:10.15283/ijsc.2014.7.2.118

[340] Pham LH, Vu NB, Van Pham P. The subpopulation of CD105 negative mesenchymal stem cells show strong immunomodulation capacity compared to CD105 positive mesenchymal stem cells. *Biomed Res Ther*. 2019;6(4):3131–40. DOI:10.15419/bmrat.v6i4.538

[341] Jin HJ, Kwon JH, Kim M, Bae YK, Choi SJ, Oh W, et al. Downregulation of Melanoma Cell Adhesion Molecule (MCAM/CD146) Accelerates Cellular Senescence in Human Umbilical Cord Blood-Derived Mesenchymal Stem Cells. *Stem Cells Transl Med*. 2016;5(4):427–39. DOI:10.5966/sctm.2015-0109

[342] Wu CC, Liu FL, Sytwu HK, Tsai CY, Chang DM. CD146+ mesenchymal stem cells display greater therapeutic potential than CD146- cells for treating collagen-induced arthritis in mice. *Stem Cell Res Ther* . 2016;7(1):1–13. DOI:10.1186/s13287-016-0285-4

[343] Lv, F.J, Tuan, R. S, Cheung, K.M.C, Leung VY. Concise Review : The Surface Markers and Identity of Human Mesenchymal Stem Cells. *Stem Cells*. 2014;32:1408–19. DOI:10.1002/stem.1499

[344] Rojewski MT, Weber BM, Schrezenmeier H. Phenotypic characterization of

mesenchymal stem cells from various tissues. *Transfus Med Hemotherapy*. 2008;35(3):168–84. DOI:10.1159/000129013

[345] Peters L, Meister G. Argonaute Proteins: Mediators of RNA Silencing. *Mol Cell*. 2007;26(5):611–23. DOI:10.1016/j.molcel.2007.05.001

[346] McLauchlan H, Newell J, Morrice N, Osborne A, West M, Smythe E. A novel role for Rab5-GDI in ligand sequestration into clathrin-coated pits. *Curr Biol*. 1998;8(1):34–45. DOI:10.1016/S0960-9822(98)70018-1

[347] Sönnichsen B, De Renzis S, Nielsen E, Rietdorf J, Zerial M. Distinct membrane domains on endosomes in the recycling pathway visualized by multicolor imaging of Rab4, Rab5, and Rab11. *J Cell Biol*. 2000;149(4):901–13. DOI:10.1083/jcb.149.4.901

[348] Xie F, Zhou X, Fang M, Li H, Su P, Tu Y, et al. Extracellular Vesicles in Cancer Immune Microenvironment and Cancer Immunotherapy. *Adv Sci*. 2019;6(24). DOI:10.1002/advs.201901779

[349] Dutta A, Girotra M, Merchant N, Nair P, Dutta SK. Evidence of multimeric forms of HSP70 with phosphorylation on serine and tyrosine residues - implications for roles of HSP70 in detection of gi cancers. *Asian Pacific J Cancer Prev*. 2013;14(10):5741–5. DOI:10.7314/APJCP.2013.14.10.5741

[350] Yoshioka Y, Konishi Y, Kosaka N, Katsuda T, Kato T, Ochiya T. Comparative marker analysis of extracellular vesicles in different human cancer types. *J Extracell Vesicles*. 2013;2(1):1–9. DOI:10.3402/jev.v2i0.20424

[351] Cai J, Wu J, Wang J, Li Y, Hu X, Luo S, et al. Extracellular vesicles derived from different sources of mesenchymal stem cells: Therapeutic effects and translational potential. *Cell Biosci*. 2020;10(1):1–14. DOI:10.1186/s13578-020-00427-x

[352] Théry C, Ostrowski M, Segura E. Membrane vesicles as conveyors of immune responses. *Nat Rev Immunol*. 2009;9(8):581–93. DOI:10.1038/nri2567

[353] Rackov G, Garcia-Romero N, Esteban-Rubio S, Carrión-Navarro J, Belda-Iniesta C, Ayuso-Sacido A. Vesicle-mediated control of cell function: The role of extracellular matrix and microenvironment. *Front Physiol*. 2018;9(JUN):1–12. DOI:10.3389/fphys.2018.00651

[354] Farinazzo A, Angiari S, Turano E, Bistaffa E, Dusi S, Ruggieri S, et al. Nanovesicles from adipose-derived mesenchymal stem cells inhibit T lymphocyte trafficking and ameliorate chronic experimental autoimmune encephalomyelitis. *Sci Rep*. 2018;8(1):1–11. DOI:10.1038/s41598-018-25676-2

[355] Nojehdehi S, Soudi S, Hesampour A, Rasouli S, Soleimani M, Hashemi SM. Immunomodulatory effects of mesenchymal stem cell–derived exosomes on experimental type-1 autoimmune diabetes. *J Cell Biochem*. 2018;119(11):9433–43. DOI:10.1002/jcb.27260

[356] Guo L, Lai P, Wang Y, Huang T, Chen X, Luo C, et al. Extracellular vesicles from mesenchymal stem cells prevent contact hypersensitivity through the suppression of Tc1 and Th1 cells and expansion of regulatory T cells. *Int Immunopharmacol*. 2019;74(March). DOI:10.1016/j.intimp.2019.05.048

[357] An JH, Li Q, Bhang DH, Song WJ, Youn HY. TNF-α and INF-γ primed canine stem

cell-derived extracellular vesicles alleviate experimental murine colitis. *Sci Rep*. 2020;10(1):1–14. DOI:10.1038/s41598-020-63115-3

[358] Yang R, Huang H, Cui S, Zhou Y, Zhang T, Zhou Y. IFN-γ promoted exosomes from mesenchymal stem cells to attenuate colitis via miR-125a and miR-125b. *Cell Death Dis* . 2020;11(7). DOI:10.1038/s41419-020-02788-0

[359] Jin P, Zhao Y, Liu H, Chen J, Ren J, Jin J, et al. Interferon-γ and Tumor Necrosis Factor-α Polarize Bone Marrow Stromal Cells Uniformly to a Th1 Phenotype. *Sci Rep* . 2016;6(May):1–11. DOI:10.1038/srep26345

[360] Saparov A, Ogay V, Nurgozhin T, Jumabay M, Chen WCW. Preconditioning of human mesenchymal stem cells to enhance their regulation of the immune response. *Stem Cells Int*. 2016;2016. DOI:10.1155/2016/3924858

[361] Song Y, Dou H, Li X, Zhao X, Li Y, Liu D, et al. Exosomal miR-146a Contributes to the Enhanced Therapeutic Efficacy of Interleukin-1β-Primed Mesenchymal Stem Cells Against Sepsis. *Stem Cells*. 2017;35(5):1208–21. DOI:10.1002/stem.2564

[362] Zhao H, Shang Q, Pan Z, Bai Y, Li Z, Zhang H, et al. Exosomes from adipose-derived stem cells attenuate adipose inflammation and obesity through polarizing M2 macrophages and beiging in white adipose tissue. *Diabetes*. 2018;67(2):235–47. DOI:10.2337/db17-0356

[363] Favaro E, Carpanetto A, Caorsi C, Giovarelli M, Angelini C, Cavallo-Perin P, et al. Human mesenchymal stem cells and derived extracellular vesicles induce regulatory dendritic cells in type 1 diabetic patients. *Diabetologia*. 2016;59(2):325–33. DOI:10.1007/s00125-015-3808-0

[364] Willis GR, Fernandez-Gonzalez A, Anastas J, Vitali SH, Liu X, Ericsson M, et al. Mesenchymal stromal cell exosomes ameliorate experimental bronchopulmonary dysplasia and restore lung function through macrophage immunomodulation. *Am J Respir Crit Care Med*. 2018;197(1):104–16. DOI:10.1164/rccm.201705-0925OC

[365] Cheng A, Choi D, Lora M, Shum-Tim D, Rak J, Colmegna I. Human multipotent mesenchymal stromal cells cytokine priming promotes RAB27B-regulated secretion of small extracellular vesicles with immunomodulatory cargo. *Stem Cell Res Ther* . 2020;11(1):539. DOI:10.1186/s13287-020-02050-6

[366] Storey JD. The positive false discovery rate: A Bayesian interpretation and the q-value. *Ann Stat*. 2003;31(6):2013–35. DOI:10.1214/aos/1074290335

[367] Hanaoka R, Kasama T, Muramatsu M, Yajima N, Shiozawa F, Miwa Y, et al. A novel mechanism for the regulation of IFN-γ inducible protein-10 expression in rheumatoid arthritis. *Arthritis Res Ther* . 2003;5(2):R74. DOI:10.1186/ar616

[368] Bystry RS, Aluvihare V, Welch KA, Kallikourdis M, Betz AG. B cells and professional APCs recruit regulatory T cells via CCL4. *Nat Immunol* . 2001;2(12):1126–32. DOI:10.1038/ni735

[369] Sokol CL, Luster AD. The chemokine system in innate immunity. *Cold Spring Harb Perspect Biol* . 2015;7(5):a016303. DOI:10.1101/cshperspect.a016303

[370] Hu J, Yang Z, Li X, Lu H. C-C motif chemokine ligand 20 regulates neuroinflammation following spinal cord injury via Th17 cell recruitment. *J*

Neuroinflammation . 2016;13(1):162. DOI:10.1186/s12974-016-0630-7

[371] Stanley ER, Berg KL, Einstein DB, Lee PSW, Pixley FJ, Wang Y, et al. Biology and action of colony-stimulating factor-1. *Mol Reprod Dev* . 1997;46(1):4–10. DOI:Https://doi.org/10.1002/(SICI)1098-2795(199701)46:1<4::AID-MRD2>3.0.CO;2-V

[372] MacDonald BR, Mundy GR, Clark S, Wang EA, Kuehl TJ, Stanley ER, et al. Effects of human recombinant CSF-GM and highly purified CSF-1 on the formation of multinucleated cells with osteoclast characteristics in long-term bone marrow cultures. *J bone Miner Res Off J Am Soc Bone Miner Res*. 1986;1(2):227–33. DOI:10.1002/jbmr.5650010210

[373] Mei J, Liu Y, Dai N, Hoffmann C, Hudock KM, Zhang P, et al. Cxcr2 and Cxcl5 regulate the IL-17/G-CSF axis and neutrophil homeostasis in mice. *J Clin Invest* . 2012/02/13. 2012;122(3):974–86. DOI:10.1172/JCI60588

[374] Dufour JH, Dziejman M, Liu MT, Leung JH, Lane TE, Luster AD. IFN-γ-Inducible Protein 10 (IP-10; CXCL10)-Deficient Mice Reveal a Role for IP-10 in Effector T Cell Generation and Trafficking. *J Immunol* . 2002;168(7):3195 LP – 3204. DOI:10.4049/jimmunol.168.7.3195

[375] Patel DD, Zachariah JP, Whichard LP. CXCR3 and CCR5 ligands in rheumatoid arthritis synovium. *Clin Immunol*. 2001;98(1):39–45. DOI:10.1006/clim.2000.4957

[376] Angiolillo AL, Sgadari C, Taub DD, Liao F, Farber JM, Maheshwari S, et al. Human interferon-inducible protein 10 is a potent inhibitor of angiogenesis in vivo. *J Exp Med*. 1995;182(1):155–62. DOI:10.1084/jem.182.1.155

[377] Lyman SD, James L, Johnson L, Brasel K, de Vries P, Escobar SS, et al. Cloning of the human homologue of the murine flt3 ligand: a growth factor for early hematopoietic progenitor cells. *Blood*. 1994;83(10):2795–801.

[378] Hannum C, Culpepper J, Campbell D, McClanahan T, Zurawski S, Bazan JF, et al. Ligand for FLT3/FLK2 receptor tyrosine kinase regulates growth of haematopoietic stem cells and is encoded by variant RNAs. *Nature*. 1994;368(6472):643–8. DOI:10.1038/368643a0

[379] Turner MD, Nedjai B, Hurst T, Pennington DJ. Cytokines and chemokines: At the crossroads of cell signalling and inflammatory disease. *Biochim Biophys Acta - Mol Cell Res*. 2014;1843(11):2563–82. DOI:10.1016/j.bbamcr.2014.05.014

[380] Rael EL, Lockey RF. Interleukin-13 Signaling and Its Role in Asthma. *World Allergy Organ J* . 2011;4(3):54–64. DOI:10.1097/WOX.0b013e31821188e0

[381] Minty A, Chalon P, Derocq J-M, Dumont X, Guillemot J-C, Kaghad M, et al. lnterleukin-13 is a new human lymphokine regulating inflammatory and immune responses. *Nature* . 1993;362(6417):248–50. DOI:10.1038/362248a0

[382] Yasuda K, Nakanishi K, Tsutsui H. Interleukin-18 in Health and Disease. Vol. 20, International Journal of Molecular Sciences . 2019. DOI:10.3390/ijms20030649

[383] Fayon M, Rebola M, Berger P, Daburon S, Ousova O, Lavrand F, et al. Increased secretion of leukemia inhibitory factor by immature airway smooth muscle cells enhances intracellular signaling and airway contractility. *Am J Physiol Cell Mol*

Physiol . 2006;291(2):L244–51. DOI:10.1152/ajplung.00474.2005

[384] Nasef A, Mazurier C, Bouchet S, François S, Chapel A, Thierry D, et al. Leukemia inhibitory factor: Role in human mesenchymal stem cells mediated immunosuppression. *Cell Immunol*. 2008;253(1–2):16–22. DOI:10.1016/j.cellimm.2008.06.002

[385] Santos GC, Silva DN, Fortuna V, Silveira BM, Orge ID, de Santana TA, et al. Leukemia Inhibitory Factor (LIF) Overexpression Increases the Angiogenic Potential of Bone Marrow Mesenchymal Stem/Stromal Cells . Vol. 8, Frontiers in Cell and Developmental Biology . 2020. p. 778.

[386] Proost P, Wuyts A, Van Damme J. Human monocyte chemotactic proteins-2 and -3: structural and functional comparison with MCP-1. *J Leukoc Biol*. 1996;59(1):67–74. DOI:10.1002/jlb.59.1.67

[387] Gong W, Howard OMZ, Turpin JA, Grimm MC, Ueda H, Gray PW, et al. Monocyte Chemotactic Protein-2 Activates CCR5 and Blocks CD4/CCR5-mediated HIV-1 Entry/Replication. *J Biol Chem* . 1998;273(8):4289–92. DOI:10.1074/jbc.273.8.4289

[388] Mendez-Enriquez E, García-Zepeda EA. The multiple faces of CCL13 in immunity and inflammation. *Inflammopharmacology*. 2013;21(6):397–406. DOI:10.1007/s10787-013-0177-5

[389] Rohani MG, Dimitrova E, Beppu A, Wang Y, Jefferies CA, Parks WC. Macrophage MMP10 Regulates TLR7-Mediated Tolerance. *Front Immunol* . 2018;9:2817. DOI:10.3389/fimmu.2018.02817

[390] McMahan RS, Birkland TP, Smigiel KS, Vandivort TC, Rohani MG, Manicone AM, et al. Stromelysin-2 (MMP10) Moderates Inflammation by Controlling Macrophage Activation. *J Immunol*. 2016;197(3):899–909. DOI:10.4049/jimmunol.1600502

[391] Bengtsson AK, Ryan EJ. Immune function of the decoy receptor osteoprotegerin. *Crit Rev Immunol*. 2002;22(3):201–15.

[392] Playford RJ. Growth Factors. In: Johnson LRBT-E of G, editor. Encyclopedia of Gastroenterology . New York: Elsevier; 2004. p. 249–56. DOI:Https://doi.org/10.1016/B0-12-386860-2/00341-5

[393] Bossi F, Bernardi S, Zauli G, Secchiero P, Fabris B. TRAIL Modulates the Immune System and Protects against the Development of Diabetes. Blaser K, editor. *J Immunol Res* . 2015;2015:680749. DOI:10.1155/2015/680749

[394] Liu Y-J, Soumelis V, Watanabe N, Ito T, Wang Y-H, Malefyt R de W, et al. TSLP: an epithelial cell cytokine that regulates T cell differentiation by conditioning dendritic cell maturation. *Annu Rev Immunol*. 2007;25:193–219. DOI:10.1146/annurev.immunol.25.022106.141718

[395] Fiedler J, Leucht F, Waltenberger J, Dehio C, Brenner RE. VEGF-A and PlGF-1 stimulate chemotactic migration of human mesenchymal progenitor cells. *Biochem Biophys Res Commun* . 2005;334(2):561–8. DOI:Https://doi.org/10.1016/j.bbrc.2005.06.116

[396] Kim H-R, Kim K-W, Kim B-M, Cho M-L, Lee S-H. The effect of vascular endothelial growth factor on osteoclastogenesis in rheumatoid arthritis. *PLoS One* .

2015;10(4):e0124909–e0124909. DOI:10.1371/journal.pone.0124909

[397] Kim W-U, Kang SS, Yoo S-A, Hong K-H, Bae D-G, Lee M-S, et al. Interaction of vascular endothelial growth factor 165 with neuropilin-1 protects rheumatoid synoviocytes from apoptotic death by regulating Bcl-2 expression and Bax translocation. *J Immunol*. 2006;177(8):5727–35. DOI:10.4049/jimmunol.177.8.5727

[398] Minnone G, De Benedetti F, Bracci-Laudiero L. NGF and Its Receptors in the Regulation of Inflammatory Response. *Int J Mol Sci* . 2017;18(5):1028. DOI:10.3390/ijms18051028

[399] Harting MT, Srivastava AK, Zhaorigetu S, Bair H, Prabhakara KS, Toledano Furman NE, et al. Inflammation-Stimulated Mesenchymal Stromal Cell-Derived Extracellular Vesicles Attenuate Inflammation. *Stem Cells*. 2018;36(1):79–90. DOI:10.1002/stem.2730

[400] Cossetti C, Iraci N, Mercer TR, Leonardi T, Alpi E, Drago D, et al. Extracellular Vesicles from Neural Stem Cells Transfer IFN-γ via Ifngr1 to activate Stat1 signaling in target cells. *Mol Cell*. 2014;56(4):609. DOI:10.1016/j.molcel.2014.11.009

[401] Honczarenko M, Le Y, Swierkowski M, Ghiran I, Glodek AM, Silberstein LE. Human Bone Marrow Stromal Cells Express a Distinct Set of Biologically Functional Chemokine Receptors. *Stem Cells*. 2006;24(4):1030–41. DOI:10.1634/stemcells.2005-0319

[402] Fu, Liu, Halim, Ju, Luo, Song. Mesenchymal Stem Cell Migration and Tissue Repair. *Cells*. 2019;8(8):784. DOI:10.3390/cells8080784

[403] Wu Y, Zhao RCH. The Role of Chemokines in Mesenchymal Stem Cell Homing to Myocardium. *Stem Cell Rev Reports*. 2012;8(1):243–50. DOI:10.1007/s12015-011-9293-z

[404] Smith H, Whittall C, Weksler B, Middleton J. Chemokines stimulate bidirectional migration of human mesenchymal stem cells across bone marrow endothelial cells. *Stem Cells Dev*. 2012;21(3):476–86. DOI:10.1089/scd.2011.0025

[405] Brian M Mehling, Manvelyan, Marine, Gabrielle Benesh DCW. Characterization of Human Umbilical Cord Mesenchymal Stem Cells-Derived Conditioned Medium. *J Stem Cell Res Ther*. 2016;1(6):218–20. DOI:10.15406/jsrt.2016.01.00038

[406] Belema-Bedada F, Uchida S, Martire A, Kostin S, Braun T. Efficient Homing of Multipotent Adult Mesenchymal Stem Cells Depends on FROUNT-Mediated Clustering of CCR2. *Cell Stem Cell* . 2008;2(6):566–75. DOI:Https://doi.org/10.1016/j.stem.2008.03.003

[407] Szekanecz, Z., Vegvari, A., Szabo, Z. & Koch AE. Chemokines and chemokine receptors in arthritis. *Front Biosci (Schol Ed)* . 2010;2:153–67. DOI:10.1038/jid.2014.371

[408] Szekanecz Z, Halloran MM, Volin M V., Woods JM, Strieter RM, Haines GK, et al. Temporal expression of inflammatory cytokines and chemokines in rat adjuvant-induced arthritis. *Arthritis Rheum*. 2000;43(6):1266–77. DOI:10.1002/1529-0131(200006)43:6<1266::AID-ANR9>3.0.CO;2-P

[409] Le Blanc K, Davies LC. Mesenchymal stromal cells and the innate immune response.

Immunol Lett. 2015;168(2):140–6. DOI:10.1016/j.imlet.2015.05.004

[410] Nishikawa G, Kawada K, Nakagawa J, Toda K, Ogawa R, Inamoto S, et al. Bone marrow-derived mesenchymal stem cells promote colorectal cancer progression via CCR5. *Cell Death Dis* . 2019;10(4). DOI:10.1038/s41419-019-1508-2

[411] Zineh I, Beitelshees AL, Welder GJ, Hou W, Chegini N, Wu J, et al. Epithelial neutrophil-activating peptide (ENA-78), acute coronary syndrome prognosis, and Modulatory effect of statins. *PLoS One*. 2008;3(9). DOI:10.1371/journal.pone.0003117

[412] Iwamoto T, Okamoto H, Kobayashi S, Ikari K, Toyama Y, Tomatsu T, et al. A role of monocyte chemoattractant protein-4 (MCP-4)/CCL13 from chondrocytes in rheumatoid arthritis. *FEBS J*. 2007;274(18):4904–12. DOI:10.1111/j.1742-4658.2007.06013.x

[413] Sordet O, Hermine O, Vainchenker W, Garrido C, Solary E, Dubrez-daloz L. Specific involvement of caspases in the differentiation of monocytes into macrophages. *Blood*. 2002;100(13):4446–53. DOI:10.1182/blood-2002-06-1778.Supported

[414] Hamilton JA. Colony-stimulating factors in inflammation and autoimmunity. *Nat Rev Immunol*. 2008;8(7):533–44. DOI:10.1038/nri2356

[415] Ragni E, Orfei CP, Luca P De, Mondadori C, Viganò M, Colombini A, et al. Inflammatory priming enhances mesenchymal stromal cell secretome potential as a clinical product for regenerative medicine approaches through secreted factors and EV-miRNAs : the example of joint disease. *Stem Cell Res Ther*. 2020;11(165):1–19.

[416] Cao W, Yang Y, Wang Z, Liu A, Fang L, Wu F, et al. Leukemia Inhibitory Factor Inhibits T Helper 17 Cell Differentiation and Confers Treatment Effects of Neural Progenitor Cell Therapy in Autoimmune Disease. *Immunity*. 2011;35(2):273–84. DOI:10.1016/j.immuni.2011.06.011

[417] Bárcia RN, Santos JM, Filipe M, Teixeira M, Martins JP, Almeida J, et al. What makes umbilical cord tissue-derived mesenchymal stromal cells superior immunomodulators when compared to bone marrow derived mesenchymal stromal cells? *Stem Cells Int*. 2015;5(2):1–16. DOI:10.1155/2015/583984

[418] Najar M, Raicevic G, Boufker HI, Fayyad-Kazan H, De Bruyn C, Meuleman N, et al. Adipose-Tissue-Derived and Wharton's jelly-derived mesenchymal stromal cells suppress lymphocyte responses by secreting leukemia inhibitory factor. *Tissue Eng - Part A*. 2010;16(11):3537–46. DOI:10.1089/ten.tea.2010.0159

[419] Neve A, Corrado A, Cantatore FP. TNF-related apoptosis-inducing ligand (TRAIL) in rheumatoid arthritis: what's new? *Clin Exp Med* . 2014;14(2):115–20. DOI:10.1007/s10238-012-0226-1

[420] Park J-S, Oh Y, Park O, Foss CA, Lim SM, Jo D-G, et al. PEGylated TRAIL ameliorates experimental inflammatory arthritis by regulation of Th17 cells and regulatory T cells. *J Control Release* . 2017;267:163–71. DOI:Https://doi.org/10.1016/j.jconrel.2017.10.004

[421] McMahan RS, Birkland TP, Smigiel KS, Vandivort TC, Rohani MG, Manicone AM, et al. Stromelysin-2 (MMP10) Moderates Inflammation by Controlling Macrophage Activation. *J Immunol* . 2016;197(3):899 LP – 909. DOI:10.4049/jimmunol.1600502

[422] Kinne RW, Bräuer R, Stuhlmüller B, Palombo-Kinne E, Burmester GR. Macrophages in rheumatoid arthritis. *Arthritis Res* . 2000/04/12. 2000;2(3):189–202. DOI:10.1186/ar86

[423] Woods JM, Katschke KJ, Tokuhira M, Kurata H, Arai K-I, Campbell PL, et al. Reduction of Inflammatory Cytokines and Prostaglandin E 2 by IL-13 Gene Therapy in Rheumatoid Arthritis Synovium . *J Immunol*. 2000;165(5):2755–63. DOI:10.4049/jimmunol.165.5.2755

[424] Davies LC, Heldring N, Kadri N, Le Blanc K. Mesenchymal Stromal Cell Secretion of Programmed Death-1 Ligands Regulates T Cell Mediated Immunosuppression. *Stem Cells*. 2017;35(3):766–76. DOI:10.1002/stem.2509

[425] Molnarfi N, Benkhoucha M, Funakoshi H, Nakamura T, Lalive PH. Hepatocyte growth factor: A regulator of inflammation and autoimmunity. *Autoimmun Rev*. 2015;14(4):293–303. DOI:10.1016/j.autrev.2014.11.013

[426] Okunishi K, Dohi M, Fujio K, Nakagome K, Tabata Y, Okasora T, et al. Hepatocyte Growth Factor Significantly Suppresses Collagen-Induced Arthritis in Mice. *J Immunol*. 2007;179(8):5504–13. DOI:10.4049/jimmunol.179.8.5504

[427] Yu Y, He J, Li S, Song L, Guo X, Yao W, et al. Fibroblast growth factor 21 (FGF21) inhibits macrophage-mediated inflammation by activating Nrf2 and suppressing the NF-κB signaling pathway. *Int Immunopharmacol* . 2016;38:144–52. DOI:10.1016/j.intimp.2016.05.026

[428] Anton K, Banerjee D, Glod J. Macrophage-associated mesenchymal stem cells assume an activated, migratory, pro-inflammatory phenotype with increased IL-6 and CXCL10 secretion. *PLoS One* . 2012/04/04. 2012;7(4):e35036–e35036. DOI:10.1371/journal.pone.0035036

[429] Sokol CL, Luster AD. The chemokine system in innate immunity. *Cold Spring Harb Perspect Biol*. 2015;7(5):1–20. DOI:10.1101/cshperspect.a016303

[430] Lunardi S, Lim SY, Muschel RJ, Brunner TB. IP-10/CXCL10 attracts regulatory T cells: Implication for pancreatic cancer. *Oncoimmunology*. 2015;4(9):1–3. DOI:10.1080/2162402X.2015.1027473

[431] Essien KI, Richmond JM, Strassner JP, Harris JE. T regulatory cells follow CXCL10 to suppress T effector cells through a contact-dependent mechanism in the skin during vitiligo. *J Immunol* . 2017;198(1 Supplement):156.7 LP-156.7.

[432] Eleuteri S, Fierabracci A. Insights into the secretome of mesenchymal stem cells and its potential applications. *Int J Mol Sci*. 2019;20(18). DOI:10.3390/ijms20184597

[433] Kehl D, Generali M, Mallone A, Heller M, Uldry A-C, Cheng P, et al. Proteomic analysis of human mesenchymal stromal cell secretomes: a systematic comparison of the angiogenic potential. *npj Regen Med*. 2019;4(1). DOI:10.1038/s41536-019-0070-y

[434] Han Y, Ren J, Bai Y, Pei X, Han Y. Exosomes from hypoxia-treated human adipose-derived mesenchymal stem cells enhance angiogenesis through VEGF/VEGF-R. *Int J Biochem Cell Biol* . 2019;109(28):59–68. DOI:10.1016/j.biocel.2019.01.017

[435] Seo HR, Jeong HE, Joo HJ, Choi SC, Park CY, Kim JH, et al. Intrinsic FGF2 and FGF5 promotes angiogenesis of human aortic endothelial cells in 3D microfluidic

angiogenesis system. *Sci Rep* . 2016;6(June):1–11. DOI:10.1038/srep28832

[436] Huang W, Shao M, Liu H, Chen J, Hu J, Zhu L, et al. Fibroblast growth factor 21 enhances angiogenesis and wound healing of human brain microvascular endothelial cells by activating PPARγ. *J Pharmacol Sci* . 2019;140(2):120–7. DOI:10.1016/j.jphs.2019.03.010

[437] Krock BL, Skuli N, Simon MC. Hypoxia-Induced Angiogenesis: Good and Evil. *Genes and Cancer*. 2011;2(12):1117–33. DOI:10.1177/1947601911423654

[438] Zhang HC, Liu X Bin, Huang S, Bi XY, Wang HX, Xie LX, et al. Microvesicles derived from human umbilical cord mesenchymal stem cells stimulated by hypoxia promote angiogenesis both in vitro and in vivo. *Stem Cells Dev*. 2012;21(18):3289–97. DOI:10.1089/scd.2012.0095

[439] Guan Q, Ezzati P, Spicer V, Krokhin O, Wall D, Wilkins JA. Interferon γ induced compositional changes in human bone marrow derived mesenchymal stem/stromal cells. *Clin Proteomics*. 2017;14(1):1–14. DOI:10.1186/s12014-017-9161-1

[440] Thelin EP, Hall CE, Gupta K, Carpenter KLH, Chandran S, Hutchinson PJ, et al. Elucidating Pro-Inflammatory Cytokine Responses after Traumatic Brain Injury in a Human Stem Cell Model. *J Neurotrauma*. 2018;35(2):341–52. DOI:10.1089/neu.2017.5155

[441] Petrera A, Von Toerne C, Behler J, Huth C, Thorand B, Hilgendorff A, et al. Multiplatform Approach for Plasma Proteomics: Complementarity of Olink Proximity Extension Assay Technology to Mass Spectrometry-Based Protein Profiling. *J Proteome Res*. 2021;20(1):751–62. DOI:10.1021/acs.jproteome.0c00641

[442] Barnes BJ, Somerville CC. Modulating Cytokine Production via Select Packaging and Secretion From Extracellular Vesicles. *Front Immunol*. 2020;11(May):1–11. DOI:10.3389/fimmu.2020.01040

[443] Yu B, Kim HW, Gong M, Wang J, Millard RW, Wang Y, et al. Exosomes secreted from GATA-4 overexpressing mesenchymal stem cells serve as a reservoir of anti-apoptotic microRNAs for cardioprotection. *Int J Cardiol*. 2015;182:349–60. DOI:10.1016/j.ijcard.2014.12.043

[444] Gonzalez-King H, García NA, Ontoria-Oviedo I, Ciria M, Montero JA, Sepúlveda P. Hypoxia Inducible Factor-1α Potentiates Jagged 1-Mediated Angiogenesis by Mesenchymal Stem Cell-Derived Exosomes. *Stem Cells* . 2017;35(7):1747–59. DOI:Https://doi.org/10.1002/stem.2618

[445] Ti D, Hao H, Fu X, Han W. Mesenchymal stem cells-derived exosomal microRNAs contribute to wound inflammation. *Sci China Life Sci*. 2016;59(12):1305–12. DOI:10.1007/s11427-016-0240-4

[446] Giunti D, Marini C, Parodi B, Usai C, Milanese M, Bonanno G, et al. Role of miRNAs shuttled by mesenchymal stem cell-derived small extracellular vesicles in modulating neuroinflammation. *Sci Rep* . 2021;11(1):1740. DOI:10.1038/s41598-021-81039-4

[447] Park KS, Bandeira E, Shelke G V., Lässer C, Lötvall J. Enhancement of therapeutic potential of mesenchymal stem cell-derived extracellular vesicles. *Stem Cell Res Ther*. 2019;10(1):1–15. DOI:10.1186/s13287-019-1398-3

[448] Qiu G, Zheng G, Ge M, Wang J, Huang R, Shu Q, et al. Mesenchymal stem cell-derived extracellular vesicles affect disease outcomes via transfer of microRNAs. *Stem Cell Res Ther*. 2018;9(1):1–9. DOI:10.1186/s13287-018-1069-9

[449] David PB. MicroRNA Target Recognition and Regulatory Functions. *Cell*. 2009;136(2):215–33.

[450] Gibbings DJ, Ciaudo C, Erhardt M, Voinnet O. Multivesicular bodies associate with components of miRNA effector complexes and modulate miRNA activity. *Nat Cell Biol*. 2009;11(9):1143–9. DOI:10.1038/ncb1929

[451] Kinsley C. French, Marc A. Antonyak and RAC. Extracellular Vesicle Docking at the Cellular Port: Extracellular Vesicle Binding and Uptake. *Semin Cell Dev Biol*. 2017;67:48–55. DOI:10.1016/j.physbeh.2017.03.040

[452] Jia Y, Wei Y. Modulators of microrna function in the immune system. *Int J Mol Sci*. 2020;21(7). DOI:10.3390/ijms21072357

[453] Schipor S, Vladoiu S, Baciu AE, Niculescu AM, Caragheorgheopol A, Iancu I, et al. A comparative analysis of three methods used for RNA quantitation. *Rom Reports Phys*. 2016;68(3):1078–88.

[454] Kaur S, Abu-Shahba AG, Paananen RO, Hongisto H, Hiidenmaa H, Skottman H, et al. Small non-coding RNA landscape of extracellular vesicles from human stem cells. *Sci Rep*. 2018;8(1):1–18. DOI:10.1038/s41598-018-33899-6

[455] Tosar JP, Cayota A, Eitan E, Halushka MK, Witwer KW. Ribonucleic artefacts: are some extracellular RNA discoveries driven by cell culture medium components? *J Extracell Vesicles* . 2017;6(1):1–10. DOI:10.1080/20013078.2016.1272832

[456] Sork H, Corso G, Krjutskov K, Johansson HJ, Nordin JZ, Wiklander OPB, et al. Heterogeneity and interplay of the extracellular vesicle small RNA transcriptome and proteome. *Sci Rep*. 2018;8(1):1–12. DOI:10.1038/s41598-018-28485-9

[457] Illumina®. Understanding Illumina Quality Scores. Quality scores for next-generations sequencing. 2011.

[458] Consortium GO. The Gene Ontology resource: enriching a GOld mine. *Nucleic Acids Res*. 2021;49(D1):D325–34. DOI:10.1093/nar/gkaa1113

[459] Ashburner M, Ball CA, Blake JA, Botstein D, Butler H, Cherry JM, et al. Gene ontology: tool for the unification of biology. The Gene Ontology Consortium. *Nat Genet*. 2000;25(1):25–9. DOI:10.1038/75556

[460] Reis M, Mavin E, Nicholson L, Green K, Dickinson AM, Wang XN. Mesenchymal stromal cell-derived extracellular vesicles attenuate dendritic cell maturation and function. *Front Immunol*. 2018;9(NOV):1–14. DOI:10.3389/fimmu.2018.02538

[461] Willms E, Johansson HJ, Mäger I, Lee Y, Blomberg KEM, Sadik M, et al. Cells release subpopulations of exosomes with distinct molecular and biological properties. *Sci Rep* . 2016;6(February):1–12. DOI:10.1038/srep22519

[462] Li L, Li C, Wang S, Wang Z, Jiang J, Wang W, et al. Exosomes derived from hypoxic oral squamous cell carcinoma cells deliver miR-21 to normoxic cells to elicit a prometastatic phenotype. *Cancer Res*. 2016;76(7):1770–80. DOI:10.1158/0008-5472.CAN-15-1625

[463] Gray WD, French KM, Ghosh-Choudhary S, Maxwell JT, Brown ME, Platt MO, et al. Identification of therapeutic covariant microRNA clusters in hypoxia-treated cardiac progenitor cell exosomes using systems biology. *Circ Res*. 2015;116(2):255–63. DOI:10.1161/CIRCRESAHA.116.304360

[464] de Jong OG, Verhaar MC, Chen Y, Vader P, Gremmels H, Posthuma G, et al. Cellular stress conditions are reflected in the protein and RNA content of endothelial cell-derived exosomes. *J Extracell Vesicles*. 2012;1(1):1–12. DOI:10.3402/jev.v1i0.18396

[465] Jia Y, Guan M, Zheng Z, Zhang Q, Tang C, Xu W, et al. MiRNAs in Urine Extracellular Vesicles as Predictors of Early-Stage Diabetic Nephropathy. *J Diabetes Res*. 2016;2016. DOI:10.1155/2016/7932765

[466] Boni V, Bitarte N, Cristobal I, Zarate R, Rodriguez J, Maiello E, et al. miR-192/miR-215 influence 5-fluorouracil resistance through cell cycle-mediated mechanisms complementary to its post-transcriptional thymidilate synthase regulation. *Mol Cancer Ther*. 2010;9(8):2265–75. DOI:10.1158/1535-7163.MCT-10-0061

[467] Z Jin, FM Selaru, Y Cheng, T Kan, R Agarwal, Y Mori, AV Olaru, J Yang, S David, JP Hamilton, JM Abraham, J Harmon, M Duncan, EA Montgomery and SM. MicroRNA-192 and -215 are upregulated in human gastric cancer in vivo and suppress ALCAM expression in vitro. *Oncogene*. 2011;30(13):1577–85. DOI:10.1016/j.physbeh.2017.03.040

[468] Hu J, Sun T, Wang H, Chen Z, Wang S, Yuan L, et al. MiR-215 is induced post-transcriptionally via HIF-Drosha complex and mediates glioma-initiating cell adaptation to hypoxia by targeting KDM1B. 2016;29(1):49–60. DOI:10.1016/j.ccell.2015.12.005.MiR-215

[469] Gu Y, Wei X, Sun Y, Gao H, Zheng X, Wong LL, et al. MiR-192-5p silencing by genetic aberrations is a key event in hepatocellular carcinomas with cancer stem cell features. *Cancer Res*. 2019;79(5):941–53. DOI:10.1158/0008-5472.CAN-18-1675

[470] Zhang D, Wu Y, Sun G. miR-192 suppresses T follicular helper cell differentiation by targeting CXCR5 in childhood asthma. *Scand J Clin Lab Invest*. 2018;78(3):236–42. DOI:10.1080/00365513.2018.1440628

[471] Lou L, Tian M, Chang J, Li F, Zhang G. MiRNA-192-5p attenuates airway remodeling and autophagy in asthma by targeting MMP-16 and ATG7. *Biomed Pharmacother* . 2020;122(November 2019):109692. DOI:10.1016/j.biopha.2019.109692

[472] Wu F, Zikusoka M, Trindade A, Dassopoulos T, Harris ML, Bayless TM, et al. MicroRNAs Are Differentially Expressed in Ulcerative Colitis and Alter Expression of Macrophage Inflammatory Peptide-2α. *Gastroenterology*. 2008;135(5):1624–35. DOI:10.1053/j.gastro.2008.07.068

[473] Liu X, Pan Q, Cao H, Xin F, Zhao Z, Yang R, et al. Lipotoxic Hepatocyte-Derived Exosomal miR-192-5p Activates Macrophages via Rictor/Akt/FoxO1 Signaling in NAFLD . *Hepatology*. 2019; DOI:10.1002/hep.31050

[474] He XW, Shi YH, Liu YS, Li GF, Zhao R, Hu Y, et al. Increased plasma levels of miR-124-3p, miR-125b-5p and miR-192-5p are associated with outcomes in acute ischaemic stroke patients receiving thrombolysis. *Atherosclerosis* . 2019;289(November 2018):36–43. DOI:10.1016/j.atherosclerosis.2019.08.002

[475] Chi Y, Cui J, Wang Y, Du W, Chen F, Li Z, et al. Interferon alters the microRNA profile of umbilical cord derived mesenchymal stem cells. *Mol Med Rep*. 2016;14(5):4187–97. DOI:10.3892/mmr.2016.5748

[476] Tan W, Gu Z, Leng J, Chen H, Min F. Biomedicine & Pharmacotherapy Let-7f-5p ameliorates in fl ammation by targeting NLRP3 in bone marrow- derived mesenchymal stem cells in patients with systemic lupus erythematosus. *Biomed Pharmacother* . 2019;118(368):109313. DOI:10.1016/j.biopha.2019.109313

[477] Groot M, Lee H. Sorting Mechanisms for MicroRNAs into Extracellular Vesicles and Their Associated Diseases. *Cells* . 2020;9(4):1–16. DOI:10.3390/cells9041044

[478] Gayen M, Bhomia M, Balakathiresan N, Knollmann-Ritschel B. Exosomal microRNAs released by activated astrocytes as potential neuroinflammatory biomarkers. *Int J Mol Sci*. 2020;21(7). DOI:10.3390/ijms21072312

[479] Zhang Y, Shen WL, Shi ML, Zhang LZ, Zhang Z, Li P, et al. Involvement of aberrant miR-139/Jun feedback loop in human gastric cancer. *Biochim Biophys Acta - Mol Cell Res* . 2015;1853(2):481–8. DOI:10.1016/j.bbamcr.2014.12.002

[480] Zhang Y, Bai J, Si W, Yuan S, Li Y, Chen X. SLC39A7, regulated by miR-139-5p, induces cell proliferation, migration and inhibits apoptosis in gastric cancer via Akt/mTOR signaling pathway. *Biosci Rep*. 2020;40(2):1–9. DOI:10.1042/BSR20200041

[481] Long H, Sun B, Cheng L, Zhao S, Zhu Y, Zhao R, et al. MiR-139-5p Represses BMSC Osteogenesis via Targeting Wnt/β-Catenin Signaling Pathway. *DNA Cell Biol*. 2017;36(8):715–24. DOI:10.1089/dna.2017.3657

[482] Xu S, Yang F, Liu R, Li X, Fan H, Liu J, et al. Serum microRNA-139-5p is downregulated in lung cancer patients with lytic bone metastasis. *Oncol Rep*. 2018;39(5):2376–84. DOI:10.3892/or.2018.6316

[483] Zhu M, Zhang W, Ma J, Dai Y, Zhang Q, Liu Q, et al. MicroRNA-139-5p regulates chronic inflammation by suppressing nuclear factor-κB activity to inhibit cell proliferation and invasion in colorectal cancer. *Exp Ther Med*. 2019;4049–57. DOI:10.3892/etm.2019.8032

[484] Liu T, Zhang L, Joo D, Sun SC. NF-κB signaling in inflammation. *Signal Transduct Target Ther*. 2017;2(March). DOI:10.1038/sigtrans.2017.23

[485] Katsumi T, Ninomiya M, Nishina T, Mizuno K, Tomita K, Haga H, et al. MiR-139-5p is associated with inflammatory regulation through c-FOS suppression, and contributes to the progression of primary biliary cholangitis. *Lab Investig* . 2016;96(11):1165–77. DOI:10.1038/labinvest.2016.95

[486] Clark EA, Kalomoiris S, Nolta JA, Fierro FA. Concise review: MicroRNA function in multipotent mesenchymal stromal cells. *Stem Cells*. 2014;32(5):1074–82. DOI:10.1002/stem.1623

[487] Dai X, Chen X, Chen Q, Shi L, Liang H, Zhou Z, et al. MicroRNA-193a-3p Reduces Intestinal Inflammation in Response to Microbiota via Down-regulation of Colonic. 2015;290(26):16099–115. DOI:10.1074/jbc.M115.659318

[488] Hwang S, Park S, Lee HY, Kim SW, Lee JS, Choi EK, et al. miR-140-5p suppresses

BMP2-mediated osteogenesis in undifferentiated human mesenchymal stem cells. *FEBS Lett* . 2014; DOI:10.1016/j.febslet.2014.05.048

[489] Nakamura Y, Miyaki S, Ishitobi H, Matsuyama S, Nakasa T, Kamei N, et al. Mesenchymal-stem-cell-derived exosomes accelerate skeletal muscle regeneration. *FEBS Lett* . 2015;589(11):1257–65. DOI:10.1016/j.febslet.2015.03.031

[490] Tao SC, Yuan T, Zhang YL, Yin WJ, Guo SC, Zhang CQ. Exosomes derived from miR-140-5p-overexpressing human synovial mesenchymal stem cells enhance cartilage tissue regeneration and prevent osteoarthritis of the knee in a rat model. *Theranostics*. 2017;7(1):180–95. DOI:10.7150/thno.17133

[491] Yang H, Kong W, He L, Zhao JJ, O'Donnell JD, Wang J, et al. MicroRNA expression profiling in human ovarian cancer: miR-214 induces cell survival and cisplatin resistance by targeting PTEN. *Cancer Res*. 2008;68(2):425–33. DOI:10.1158/0008-5472.CAN-07-2488

[492] Yin Y, Cai X, Chen X, Liang H, Zhang Y, Li J, et al. Tumor-secreted miR-214 induces regulatory T cells: A major link between immune evasion and tumor growth. *Cell Res* . 2014;24(10):1164–80. DOI:10.1038/cr.2014.121

[493] Wang M, Liu M, Ni T, Liu Q. miR-214 mediates vascular inflammation and apoptosis via PTEN expression. *Mol Med Rep*. 2018;18(2):2229–36. DOI:10.3892/mmr.2018.9185

[494] Lakhia R, Yheskel M, Flaten A, Ramalingam H, Aboudehen K, Ferrè S, et al. Interstitial microRNA miR-214 attenuates inflammation and polycystic kidney disease progression. *JCI Insight*. 2020;5(7):1–14. DOI:10.1172/jci.insight.133785

[495] Meng X, Sun B, Xue M, Xu P, Hu F, Xiao Z. Comparative analysis of microRNA expression in human mesenchymal stem cells from umbilical cord and cord blood. *Genomics* . 2016;107(4):124–31. DOI:10.1016/j.ygeno.2016.02.006

[496] Shaker F, Nikravesh A, Arezumand R, Aghaee-Bakhtiari SH. Web-based tools for miRNA studies analysis. *Comput Biol Med* . 2020;127:104060. DOI:Https://doi.org/10.1016/j.compbiomed.2020.104060

[497] Sun J, Tao S, Liu L, Guo D, Xia Z, Huang M. miR-140-5p regulates angiogenesis following ischemic stroke by targeting VEGFA. *Mol Med Rep* . 2016;13(5):4499–505. DOI:10.3892/mmr.2016.5066

[498] Lu Y, Qin T, Li J, Wang L, Zhang Q, Jiang Z, et al. MicroRNA-140-5p inhibits invasion and angiogenesis through targeting VEGF-A in breast cancer. *Cancer Gene Ther*. 2017;24(9):386–92. DOI:10.1038/cgt.2017.30

[499] Vicinus B, Rubie C, Faust SK, Frick VO, Ghadjar P, Wagner M, et al. miR-21 functionally interacts with the 3'UTR of chemokine CCL20 and down-regulates CCL20 expression in miR-21 transfected colorectal cancer cells. *Cancer Lett*. 2012;316(1):105–12. DOI:10.1016/j.canlet.2011.10.031

[500] Kumar M, Ahmad T, Sharma A, Mabalirajan U, Kulshreshtha A, Agrawal A, et al. Let-7 microRNA–mediated regulation of IL-13 and allergic airway inflammation. *J Allergy Clin Immunol* . 2011;128(5):1077-1085.e10. DOI:10.1016/j.jaci.2011.04.034

[501] Love MI, Huber W, Anders S. Moderated estimation of fold change and dispersion for RNA-seq data with DESeq2. *Genome Biol*. 2014;15(12). DOI:10.1186/s13059-014-0550-8

[502] Pan X, Wang ZX, Wang R. MicroRNA-21: A novel therapeutic target in human cancer. *Cancer Biol Ther*. 2010;10(12):1224–32. DOI:10.4161/cbt.10.12.14252

[503] Trohatou O, Zagoura D, Bitsika V, Pappa KI, Antsaklis A, Anagnou NP, et al. Sox2 Suppression by miR-21 Governs Human Mesenchymal Stem Cell Properties. *Stem Cells Transl Med*. 2014;3(1):54–68. DOI:10.5966/sctm.2013-0081

[504] Urbich C, Kuehbacher A, Dimmeler S. Role of microRNAs in vascular diseases, inflammation, and angiogenesis. *Cardiovasc Res*. 2008;79(4):581–8. DOI:10.1093/cvr/cvn156

[505] Zhou Y, Zhu Y, Zhang L, Wu T, Wu T, Zhang W, et al. Human Stem Cells Overexpressing MIR-21 Promote Angiogenesis in Critical Limb Ischemia by Targeting CHIP to Enhance HIF-1α Activity. *Stem Cells*. 2016;34(4):924–34. DOI:10.1002/stem.2321

[506] Yang C, Liu X, Zhao K, Zhu Y, Hu B, Zhou Y, et al. MiRNA-21 promotes osteogenesis via the PTEN/PI3K/Akt/HIF-1α pathway and enhances bone regeneration in critical size defects. *Stem Cell Res Ther*. 2019;10(1):1–11. DOI:10.1186/s13287-019-1168-2

[507] Xue X, Xia W, Wenzhong H. A modeled dynamic regulatory network of NF-κB and IL-6 mediated by miRNA. *BioSystems* . 2013;114(3):214–8. DOI:10.1016/j.biosystems.2013.09.001

[508] Garo LP, Murugaiyan G. Contribution of MicroRNAs to autoimmune diseases. *Cell Mol Life Sci*. 2016;73(10):2041–51. DOI:10.1007/s00018-016-2167-4

[509] Wong CK, Lau KM, Chan IHS, Hu S, Lam YYO, Choi AOK, et al. MicroRNA-21 * regulates the prosurvival effect of GM-CSF on human eosinophils. *Immunobiology* . 2013;218(2):255–62. DOI:10.1016/j.imbio.2012.05.019

[510] Wang L, He L, Zhang R, Liu X, Ren Y, Liu Z, et al. Regulation of T lymphocyte activation by microRNA-21. *Mol Immunol* . 2014;59(2):163–71. DOI:10.1016/j.molimm.2014.02.004

[511] Rouas R, Fayyad-Kazan H, El Zien N, Lewalle P, Rothé F, Simion A, et al. Human natural Treg microRNA signature: Role of microRNA-31 and microRNA-21 in FOXP3 expression. *Eur J Immunol*. 2009;39(6):1608–18. DOI:10.1002/eji.200838509

[512] Pickens SR, Chamberlain ND, Volin M V, Pope RM, Talarico NE, Mandelin 2nd AM, et al. Role of the CCL21 and CCR7 pathways in rheumatoid arthritis angiogenesis. *Arthritis Rheum* . 2012;64(8):2471–81. DOI:10.1002/art.34452

[513] Dong L, Wang X, Tan J, Li H, Qian W, Chen J, et al. Decreased expression of microRNA-21 correlates with the imbalance of Th17 and Treg cells in patients with rheumatoid arthritis. *J Cell Mol Med*. 2014;18(11):2213–24. DOI:10.1111/jcmm.12353

[514] Yang S, Jiang S, Wang Y, Tu S, Wang Z, Chen Z. Interleukin 34 upregulation contributes to the increment of MicroRNA 21 expression through STAT3 activation

associated with disease activity in rheumatoid arthritis. *J Rheumatol*. 2016;43(7):1312–9. DOI:10.3899/jrheum.151253

[515] Pankratz F, Hohnloser C, Bemtgen X, Jaenich C, Kreuzaler S, Hoefer I, et al. MicroRNA-100 suppresses chronic vascular inflammation by stimulation of endothelial autophagy. *Circ Res*. 2018;122(3):417–32. DOI:10.1161/CIRCRESAHA.117.311428

[516] Luo P, Jiang C, Ji P, Wang M, Xu J. Exosomes of stem cells from human exfoliated deciduous teeth as an anti-inflammatory agent in temporomandibular joint chondrocytes via miR-100-5p/mTOR. *Stem Cell Res Ther*. 2019;10(1):1–12. DOI:10.1186/s13287-019-1341-7

[517] Jickling GC, Ander BP, Shroff N, Orantia M, Stamova B, Dykstra-Aiello C, et al. Leukocyte response is regulated by microRNA let7i in patients with acute ischemic stroke. *Neurology*. 2016;87(21):2198–205. DOI:10.1212/WNL.0000000000003354

[518] Wang X, Wang HX, Li YL, Zhang CC, Zhou CY, Wang L, et al. MicroRNA Let-7i negatively regulates cardiac inflammation and fibrosis. *Hypertension*. 2015;66(4):776–85. DOI:10.1161/HYPERTENSIONAHA.115.05548

[519] Bustin SA, Benes V, Garson JA, Hellemans J, Huggett J, Kubista M, et al. The MIQE guidelines: Minimum information for publication of quantitative real-time PCR experiments. *Clin Chem*. 2009;55(4):611–22. DOI:10.1373/clinchem.2008.112797

[520] Gouin K, Peck K, Antes T, Johnson JL, Li C, Vaturi SD, et al. A comprehensive method for identification of suitable reference genes in extracellular vesicles. *J Extracell Vesicles* . 2017;6(1). DOI:10.1080/20013078.2017.1347019

[521] Blondal T, Jensby Nielsen S, Baker A, Andreasen D, Mouritzen P, Wrang Teilum M, et al. Assessing sample and miRNA profile quality in serum and plasma or other biofluids. *Methods* . 2013;59(1):S1–6. DOI:10.1016/j.ymeth.2012.09.015

[522] Nordén J. Assessment of methods for microRNA isolation , microRNA amplification , and development of a normalization strategy for sepsis biomarker research . 2020;1–26.

[523] Cirillo PDR, Margiotti K, Mesoraca A, Giorlandino C. Quantification of circulating microRNAs by droplet digital PCR for cancer detection. *BMC Res Notes* . 2020;13(1):1–6. DOI:10.1186/s13104-020-05190-3

[524] Wu H, Fan H, Shou Z, Xu M, Chen Q, Ai C, et al. Extracellular vesicles containing miR-146a attenuate experimental colitis by targeting TRAF6 and IRAK1. *Int Immunopharmacol* . 2019;68:204–12. DOI:Https://doi.org/10.1016/j.intimp.2018.12.043

[525] Xu J, Wu W, Zhang L, Dorset-Martin W, Morris MW, Mitchell ME, et al. The role of microRNA-146a in the pathogenesis of the diabetic wound-healing impairment: correction with mesenchymal stem cell treatment. *Diabetes* . 2012/07/30. 2012;61(11):2906–12. DOI:10.2337/db12-0145

[526] Qu Y, Zhang Q, Cai X, Li F, Ma Z, Xu M, et al. Exosomes derived from miR-181-5p-modified adipose-derived mesenchymal stem cells prevent liver fibrosis via autophagy activation. *J Cell Mol Med* . 2017;21(10):2491–502. DOI:Https://doi.org/10.1111/jcmm.13170

[527] Mannerström B, Paananen RO, Abu-Shahba AG, Moilanen J, Seppänen-Kaijansinkko R, Kaur S. Extracellular small non-coding RNA contaminants in fetal bovine serum and serum-free media. *Sci Rep* . 2019;9(1):5538. DOI:10.1038/s41598-019-41772-3

[528] Ferguson SW, Wang J, Lee CJ, Liu M, Neelamegham S, Canty JM, et al. The microRNA regulatory landscape of MSC-derived exosomes: A systems view. *Sci Rep* . 2018;8(1):1–12. DOI:10.1038/s41598-018-19581-x

[529] Smith DA, Germolec DR. Introduction to immunology and autoimmunity. *Environ Health Perspect* . 1999;107 Suppl(Suppl 5):661–5. DOI:10.1289/ehp.99107s5661

[530] Yap H-Y, Tee SZ-Y, Wong MM-T, Chow S-K, Peh S-C, Teow S-Y. Pathogenic Role of Immune Cells in Rheumatoid Arthritis: Implications in Clinical Treatment and Biomarker Development. *Cells* . 2018;7(10):161. DOI:10.3390/cells7100161

[531] Gaafar T, Farid R. The TH17/Treg Imbalance in Rheumatoid Arthritis and Relation to Disease Activity. *J Clin Cell Immunol*. 2015;06(06). DOI:10.4172/2155-9899.1000381

[532] Weyand CM, Goronzy JJ. The immunology of rheumatoid arthritis. *Nat Immunol*. 2021;22(1):10–8. DOI:10.1038/s41590-020-00816-x

[533] Leipe J, Grunke M, Dechant C, Reindl C, Kerzendorf U, Schulze-Koops H, et al. Role of Th17 cells in human autoimmune arthritis. *Arthritis Rheum*. 2010;62(10):2876–85. DOI:10.1002/art.27622

[534] Lazarski CA, Ford J, Katzman SD, Rosenberg AF, Fowell DJ. IL-4 attenuates Th1-associated chemokine expression and Th1 trafficking to inflamed tissues and limits pathogen clearance. *PLoS One* . 2013;8(8):e71949–e71949. DOI:10.1371/journal.pone.0071949

[535] Gadani SP, Cronk JC, Norris GT, Kipnis J. IL-4 in the brain: a cytokine to remember. *J Immunol* . 2012;189(9):4213–9. DOI:10.4049/jimmunol.1202246

[536] Chabot V, Martin L, Meley D, Sensebé L, Baron C, Lebranchu Y, et al. Unexpected impairment of TNF-α-induced maturation of human dendritic cells in vitro by IL-4. *J Transl Med* . 2016;14(1):93. DOI:10.1186/s12967-016-0848-2

[537] Al-Saadany HM, Hussein MS, Gaber RA, Zaytoun HA. Th-17 cells and serum IL-17 in rheumatoid arthritis patients: Correlation with disease activity and severity. *Egypt Rheumatol* . 2016;38(1):1–7. DOI:Https://doi.org/10.1016/j.ejr.2015.01.001

[538] Fattore A Del, Luciano R, Pascucci L, Goffredo BM, Giorda E, Scapaticci M, et al. Immunoregulatory effects of mesenchymal stem cell-derived extracellular vesicles on T lymphocytes. *Cell Transplant*. 2015;24(12):2615–27. DOI:10.3727/096368915X687543

[539] Inoue T, Swain A, Nakanishi Y, Sugiyama D. Multicolor analysis of cell surface marker of human leukemia cell lines using flow cytometry. *Anticancer Res*. 2014;34(8):4539–50.

[540] Matula Z, Németh A, Lorincz P, Szepesi Á, Brózik A, Buzás EI, et al. The Role of Extracellular Vesicle and Tunneling Nanotube-Mediated Intercellular Cross-Talk Between Mesenchymal Stem Cells and Human Peripheral T Cells. *Stem Cells Dev*. 2016;25(23):1818–32. DOI:10.1089/scd.2016.0086

[541] Bittersohl H, Steimer W. Intracellular Concentrations of Immunosuppressants .

Personalized Immunosuppression in Transplantation: Role of Biomarker Monitoring and Therapeutic Drug Monitoring. Elsevier Inc.; 2016. 199–226 p. DOI:10.1016/B978-0-12-800885-0.00009-6

[542] Snow K, Judd W. Heterogeneity of a Human T-Lymphoblastoid. *Exp Cell Res*. 1987;171:389–403.

[543] Kmieciak M, Gowda M, Graham L, Godder K, Bear HD, Marincola FM, et al. Human T cells express CD25 and Foxp3 upon activation and exhibit effector/memory phenotypes without any regulatory/suppressor function. *J Transl Med*. 2009;7:1–7. DOI:10.1186/1479-5876-7-89

[544] Vidal JG, Boyce CS, Hingorani R, Li L. CD127 is a robust surface marker for the enumeration of natural Treg cells. *FASEB J* . 2008;22(S1):848.29-848.29. DOI:Https://doi.org/10.1096/fasebj.22.1_supplement.848.29

[545] Wang K, Wei G, Liu D. CD19: a biomarker for B cell development, lymphoma diagnosis and therapy. *Exp Hematol Oncol* . 2012;1(1):36. DOI:10.1186/2162-3619-1-36

[546] Skapenko A, Leipe J, Lipsky PE, Schulze-Koops H. The role of the T cell in autoimmune inflammation. *Arthritis Res Ther* . 2005;7(2):S4. DOI:10.1186/ar1703

[547] Liu W, Putnam AL, Xu-Yu Z, Szot GL, Lee MR, Zhu S, et al. CD127 expression inversely correlates with FoxP3 and suppressive function of human CD4+ T reg cells. *J Exp Med* . 2006/07/03. 2006;203(7):1701–11. DOI:10.1084/jem.20060772

[548] Otero M, Favero M, Dragomir C, Hachem K El, Hashimoto K, Plumb DA, et al. Human Cell Culture Protocols. *Methods Mol Biol* . 2012;806:301–36. DOI:10.1007/978-1-61779-367-7

[549] Romano M, Fanelli G, Albany CJ, Giganti G, Lombardi G. Past, present, and future of regulatory T cell therapy in transplantation and autoimmunity. *Front Immunol*. 2019;10(JAN). DOI:10.3389/fimmu.2019.00043

[550] Yu N, Li X, Song W, Li D, Yu D, Zeng X, et al. CD4+CD25+CD127low/- T cells: A more specific treg population in human peripheral blood. *Inflammation*. 2012;35(6):1773–80. DOI:10.1007/s10753-012-9496-8

[551] Liu W, Putnam AL, Xu-yu Z, Szot GL, Lee MR, Zhu S, et al. CD127 expression inversely correlates with FoxP3 and suppressive function of human CD4+ T reg cells. *J Exp Med*. 2006;203(7):1701–11. DOI:10.1084/jem.20060772

[552] Seddiki N, Santner-Nanan B, Martinson J, Zaunders J, Sasson S, Landay A, et al. Expression of interleukin (IL)-2 and IL-7 receptors discriminates between human regulatory and activated T cells. *J Exp Med* . 2006/07/03. 2006;203(7):1693–700. DOI:10.1084/jem.20060468

[553] Heylmann D, Badura J, Becker H, Fahrer J, Kaina B. Sensitivity of CD3/CD28-stimulated versus non-stimulated lymphocytes to ionizing radiation and genotoxic anticancer drugs: key role of ATM in the differential radiation response. *Cell Death Dis* . 2018;9(11):1053. DOI:10.1038/s41419-018-1095-7

[554] Munisvaradass R, Suet Lee SD, Koh AEH, Kumar S, Nian LM, Vellasamy S, et al. Overcoming the challenge of transduction of human T-cells with chimeric antigen

receptor (CAR) specific for ERBB2 antigen. *Sains Malaysiana*. 2017;46(10):1831–8. DOI:10.17576/jsm-2017-4610-21

[555] Li Y, Kurlander RJ. Comparison of anti-CD3 and anti-CD28-coated beads with soluble anti-CD3 for expanding human T cells: Differing impact on CD8 T cell phenotype and responsiveness to restimulation. *J Transl Med* . 2010;8(1):104. DOI:10.1186/1479-5876-8-104

[556] Verhoef CM, Van Roon JA, Vianen ME, Glaudemans CA, Lafeber FP, Bijlsma JW. Lymphocyte stimulation by CD3-CD28 enables detection of low T cell interferon-gamma and interleukin-4 production in rheumatoid arthritis. *Scand J Immunol*. 1999;50(4):427–32. DOI:10.1046/j.1365-3083.1999.00617.x

[557] Arruvito L, Payaslián F, Baz P, Podhorzer A, Billordo A, Pandolfi J, et al. Identification and Clinical Relevance of Naturally Occurring Human CD8 + HLA-DR + Regulatory T Cells . *J Immunol*. 2014;193(9):4469–76. DOI:10.4049/jimmunol.1401490

[558] Revenfeld ALS, Bæk R, Jørgensen MM, Varming K, Stensballe A. Induction of a regulatory phenotype in CD3+ CD4+ HLA-DR+ T cells after allogeneic mixed lymphocyte culture; indications of both contact-dependent and -independent activation. *Int J Mol Sci*. 2017;18(7). DOI:10.3390/ijms18071603

[559] Kyung-Ho Roh. Artificial Methods for T Cell Activation: Critical Tools in T Cell Biology and T Cell Immunotherapy. *Biomim Med Mater*. 2018;1064:207–19.

[560] Ai W, Li H, Song N, Li L, Chen H. Optimal method to stimulate cytokine production and its use in immunotoxicity assessment. *Int J Environ Res Public Health* . 2013;10(9):3834–42. DOI:10.3390/ijerph10093834

[561] Olsen I, Sollid LM. Pitfalls in determining the cytokine profile of human T cells. *J Immunol Methods* . 2013;390(1):106–12. DOI:Https://doi.org/10.1016/j.jim.2013.01.015

[562] Smeets RL, Fleuren WWM, He X, Vink PM, Wijnands F, Gorecka M, et al. Molecular pathway profiling of T lymphocyte signal transduction pathways; Th1 and Th2 genomic fingerprints are defined by TCR and CD28-mediated signaling. *BMC Immunol* . 2012;13(1):12. DOI:10.1186/1471-2172-13-12

[563] Colin-York H, Kumari S, Barbieri L, Cords L, Fritzsche M. Distinct actin cytoskeleton behaviour in primary and immortalised T-cells. Lennon-Duménil A-M, editor. *J Cell Sci* . 2019;133(5). DOI:10.1242/jcs.232322

[564] Ma D, Xu K, Zhang G, Liu Y, Gao J, Tian M, et al. Immunomodulatory effect of human umbilical cord mesenchymal stem cells on T lymphocytes in rheumatoid arthritis. *Int Immunopharmacol*. 2019;74(May). DOI:10.1016/j.intimp.2019.105687

[565] Kato M. New insights into IFN-γ in rheumatoid arthritis: role in the era of JAK inhibitors. *Immunol Med* . 2020;43(2):72–8. DOI:10.1080/25785826.2020.1751908

[566] Cuneo AA, Autieri M V. Expression and function of anti-inflammatory interleukins: the other side of the vascular response to injury. *Curr Vasc Pharmacol* . 2009;7(3):267–76. DOI:10.2174/157016109788340721

[567] Chatterjee P, Chiasson VL, Bounds KR, Mitchell BM. Regulation of the Anti-

Inflammatory Cytokines Interleukin-4 and Interleukin-10 during Pregnancy . Vol. 5, Frontiers in Immunology . 2014. p. 253.

[568] Skapenko A, Kalden JR, Lipsky PE, Schulze-Koops H. The IL-4 Receptor α-Chain-Binding Cytokines, IL-4 and IL-13, Induce Forkhead Box P3-Expressing CD25⁺CD4⁺ Regulatory T Cells from CD25[−]CD4⁺ Precursors. *J Immunol* . 2005;175(9):6107 LP – 6116. DOI:10.4049/jimmunol.175.9.6107

[569] Luzina IG, Keegan AD, Heller NM, Rook GAW, Shea-Donohue T, Atamas SP. Regulation of inflammation by interleukin-4: a review of "alternatives." *J Leukoc Biol* . 2012/07/10. 2012;92(4):753–64. DOI:10.1189/jlb.0412214

[570] Castro-Manrreza ME, Mayani H, Monroy-García A, Flores-Figueroa E, Chávez-Rueda K, Legorreta-Haquet V, et al. Human mesenchymal stromal cells from adult and neonatal sources: A comparative in vitro analysis of their immunosuppressive properties against t cells. *Stem Cells Dev*. 2014;23(11):1217–32. DOI:10.1089/scd.2013.0363

[571] Avdeeva A, Rubtsov Y, Dyikanov D, Popkova T, Nasonov E. Regulatory T cells in patients with early untreated rheumatoid arthritis: Phenotypic changes in the course of methotrexate treatment. *Biochimie* . 2020;174:9–17. DOI:Https://doi.org/10.1016/j.biochi.2020.03.014

[572] Kumar P, Natarajan K, Shanmugam N. High glucose driven expression of pro-inflammatory cytokine and chemokine genes in lymphocytes: molecular mechanisms of IL-17 family gene expression. *Cell Signal*. 2014;26(3):528–39. DOI:10.1016/j.cellsig.2013.11.031

[573] van Roon JAG, Bijlsma JWJ. Th2 mediated regulation in RA and the spondyloarthropathies. *Ann Rheum Dis* . 2002;61(11):951 LP – 954. DOI:10.1136/ard.61.11.951

[574] Dominguez-Villar M, Hafler DA. Regulatory T cells in autoimmune disease. *Nat Immunol* . 2018;19(7):665–73. DOI:10.1038/s41590-018-0120-4

[575] Danke NA, Koelle DM, Yee C, Beheray S, Kwok WW. Autoreactive T Cells in Healthy Individuals. *J Immunol* . 2004;172(10):5967 LP – 5972. DOI:10.4049/jimmunol.172.10.5967

[576] Di Ianni M, Del Papa B, De Ioanni M, Moretti L, Bonifacio E, Cecchini D, et al. Mesenchymal cells recruit and regulate T regulatory cells. *Exp Hematol*. 2008;36(3):309–18. DOI:10.1016/j.exphem.2007.11.007

[577] Klein S, Kretz CC, Krammer PH, Kuhn A. $CD127^{low/-}$ and $FoxP3^{+}$ Expression Levels Characterize Different Regulatory T-Cell Populations in Human Peripheral Blood. *J Invest Dermatol* . 2010;130(2):492–9. DOI:10.1038/jid.2009.313

[578] Żabińska M, Krajewska M, Kościelska-Kasprzak K, Jakuszko K, Bartoszek D, Myszka M, et al. CD4+CD25+CD127− and CD4+CD25+Foxp3+ Regulatory T Cell Subsets in Mediating Autoimmune Reactivity in Systemic Lupus Erythematosus Patients. *Arch Immunol Ther Exp (Warsz)*. 2016;64(5):399–407. DOI:10.1007/s00005-016-0399-5

[579] Ferreira LMR, Muller YD, Bluestone JA, Tang Q. Next-generation regulatory T cell

therapy. *Nat Rev Drug Discov* . 2019;18(10):749–69. DOI:10.1038/s41573-019-0041-4

[580] Liu Q, Zheng H, Chen X, Peng Y, Huang W, Li X, et al. Human mesenchymal stromal cells enhance the immunomodulatory function of CD8+ CD28- regulatory T cells. *Cell Mol Immunol*. 2015;12(6):708–18. DOI:10.1038/cmi.2014.118

[581] Fletcher JM, Lonergan R, Costelloe L, Kinsella K, Moran B, O'Farrelly C, et al. CD39 + Foxp3 + Regulatory T Cells Suppress Pathogenic Th17 Cells and Are Impaired in Multiple Sclerosis . *J Immunol*. 2009;183(11):7602–10. DOI:10.4049/jimmunol.0901881

[582] Othy S, Jairaman A, Dynes JL, Dong TX, Tune C, Yeromin A V, et al. Regulatory T cells suppress Th17 cell Ca²⁺ signaling in the spinal cord during murine autoimmune neuroinflammation. *Proc Natl Acad Sci* . 2020;117(33):20088 LP – 20099. DOI:10.1073/pnas.2006895117

[583] Lee GR. The Balance of Th17 versus Treg Cells in Autoimmunity. *Int J Mol Sci* . 2018;19(3):730. DOI:10.3390/ijms19030730

[584] Lo Sicco C, Reverberi D, Balbi C, Ulivi V, Principi E, Pascucci L, et al. Mesenchymal Stem Cell-Derived Extracellular Vesicles as Mediators of Anti-Inflammatory Effects: Endorsement of Macrophage Polarization. *Stem Cells Transl Med*. 2017;6(3):1018–28. DOI:10.1002/sctm.16-0363

[585] Khare D, Or R, Resnick I, Barkatz C, Almogi-Hazan O, Avni B. Mesenchymal Stromal Cell-Derived Exosomes Affect mRNA Expression and Function of B-Lymphocytes . Vol. 9, Frontiers in Immunology . 2018. p. 3053.

[586] Adamo A, Brandi J, Caligola S, Delfino P, Bazzoni R, Carusone R, et al. Extracellular vesicles mediate mesenchymal stromal cell-dependent regulation of B cell PI3K-Akt signaling pathway and actin cytoskeleton. *Front Immunol*. 2019;10(MAR):1–22. DOI:10.3389/fimmu.2019.00446

[587] Bazzoni R, Takam Kamga P, Tanasi I, Krampera M. Extracellular Vesicle-Dependent Communication Between Mesenchymal Stromal Cells and Immune Effector Cells . Vol. 8, Frontiers in Cell and Developmental Biology . 2020. p. 1291.

[588] Morten BC, Scott RJ, Avery-Kiejda KA. Comparison of Three Different Methods for Determining Cell Proliferation in Breast Cancer Cell Lines. *J Vis Exp* . 2016;(115):54350. DOI:10.3791/54350

[589] Cummings BS, Schnellmann RG. Measurement of cell death in mammalian cells. *Curr Protoc Pharmacol* . 2004;Chapter 12:10.1002/0471141755.ph1208s25-12.8. DOI:10.1002/0471141755.ph1208s25

[590] Neri S. Genetic Stability of Mesenchymal Stromal Cells for Regenerative Medicine Applications: A Fundamental Biosafety Aspect. *Int J Mol Sci* . 2019;20(10):2406. DOI:10.3390/ijms20102406

[591] Jin P, Zhao Y, Liu H, Chen J, Ren J, Jin J, et al. Interferon-γ and Tumor Necrosis Factor-α Polarize Bone Marrow Stromal Cells Uniformly to a Th1 Phenotype. *Sci Rep* . 2016;6(April):1–11. DOI:10.1038/srep26345

[592] Zheng J, Lu T, Zhou C, Cai J, Zhang X, Liang J, et al. Extracellular Vesicles Derived

from Human Umbilical Cord Mesenchymal Stem Cells Protect Liver Ischemia/Reperfusion Injury by Reducing CD154 Expression on CD4+ T Cells via CCT2. *Adv Sci* . 2020;7(18):1903746. DOI:Https://doi.org/10.1002/advs.201903746

[593] Massa M, Croce S, Campanelli R, Abbà C, Lenta E, Valsecchi C, et al. Clinical Applications of Mesenchymal Stem/Stromal Cell Derived Extracellular Vesicles: Therapeutic Potential of an Acellular Product. *Diagnostics*. 2020;10(12):999. DOI:10.3390/diagnostics10120999

[594] Davies LC, Heldring N, Kadri N, Le Blanc K. Mesenchymal Stromal Cell Secretion of Programmed Death-1 Ligands Regulates T Cell Mediated Immunosuppression. *Stem Cells*. 2017;35(3):766–76. DOI:10.1002/stem.2509

[595] Kosaka N, Iguchi H, Yoshioka Y, Takeshita F, Matsuki Y, Ochiya T. Secretory mechanisms and intercellular transfer of microRNAs in living cells. *J Biol Chem*. 2010;285(23):17442–52. DOI:10.1074/jbc.M110.107821

[596] Pegtel DM, Cosmopoulos K, Thorley-Lawson DA, van Eijndhoven MAJ, Hopmans ES, Lindenberg JL, et al. Functional delivery of viral miRNAs via exosomes. *Proc Natl Acad Sci* . 2010;107(14):6328 LP – 6333. DOI:10.1073/pnas.0914843107

[597] Zhang Y, Liu D, Chen X, Li J, Li L, Bian Z, et al. Secreted monocytic miR-150 enhances targeted endothelial cell migration. *Mol Cell*. 2010;39(1):133–44. DOI:10.1016/j.molcel.2010.06.010

[598] Aerts NE, Dombrecht EJ, Ebo DG, Bridts CH, Stevens WJ, De Clerck LS. Activated T cells complicate the identification of regulatory T cells in rheumatoid arthritis. *Cell Immunol* . 2008;251(2):109–15. DOI:Https://doi.org/10.1016/j.cellimm.2008.04.008

[599] Gaudet AD, Fonken LK, Watkins LR, Nelson RJ, Popovich PG. MicroRNAs: Roles in Regulating Neuroinflammation. *Neurosci* . 2017;24(3):221–45. DOI:10.1177/1073858417721150

[600] N. Maruotti, F.P. Cantatore, E. Crivellato AV and DR. Angiogenesis in rheumatoid arthritis. *Histol Histopathol*. 2006;21:557–66. DOI:10.1080/08916930903143083

[601] Taylor PC. VEGF and imaging of vessels in rheumatoid arthritis. *Arthritis Res* . 2002/05/09. 2002;4 Suppl 3(Suppl 3):S99–107. DOI:10.1186/ar582

[602] Liu L, Yu Y, Hou Y, Chai J, Duan H, Chu W, et al. Human Umbilical Cord Mesenchymal Stem Cells Transplantation Promotes Cutaneous Wound Healing of Severe Burned Rats. *PLoS One* . 2014;9(2):e88348.

[603] Zhang S, Chen L, Zhang G, Zhang B. Umbilical cord-matrix stem cells induce the functional restoration of vascular endothelial cells and enhance skin wound healing in diabetic mice via the polarized macrophages. *Stem Cell Res Ther* . 2020;11(1):39. DOI:10.1186/s13287-020-1561-x

[604] Jorge B, J. VF, L. GP, E. LR, Ema A, Carlos G, et al. Safety and Efficacy of the Intravenous Infusion of Umbilical Cord Mesenchymal Stem Cells in Patients With Heart Failure. *Circ Res* . 2017;121(10):1192–204. DOI:10.1161/CIRCRESAHA.117.310712

[605] Lim M, Wang W, Liang L, Han Z, Li Z, Geng J, et al. Intravenous injection of allogeneic umbilical cord-derived multipotent mesenchymal stromal cells reduces the

infarct area and ameliorates cardiac function in a porcine model of acute myocardial infarction. *Stem Cell Res Ther* . 2018;9(1):129. DOI:10.1186/s13287-018-0888-z

[606] Jeschke MG, Rehou S, McCann MR, Shahrokhi S. Allogeneic mesenchymal stem cells for treatment of severe burn injury. *Stem Cell Res Ther* . 2019;10(1):337. DOI:10.1186/s13287-019-1465-9

[607] Suzdaltseva Y, Zhidkih S, Kiselev SL, Stupin V. Locally Delivered Umbilical Cord Mesenchymal Stromal Cells Reduce Chronic Inflammation in Long-Term Nonhealing Wounds: A Randomized Study. *Stem Cells Int* . 2020;2020:5308609. DOI:10.1155/2020/5308609

[608] Phinney DG. Functional heterogeneity of mesenchymal stem cells: implications for cell therapy. *J Cell Biochem*. 2012;113(9):2806–12. DOI:10.1002/jcb.24166

[609] Phinney DG, Kopen G, Righter W, Webster S, Tremain N, Prockop DJ. Donor variation in the growth properties and osteogenic potential of human marrow stromal cells. *J Cell Biochem* . 1999;75(3):424–36. DOI:Https://doi.org/10.1002/(SICI)1097-4644(19991201)75:3<424::AID-JCB8>3.0.CO;2-8

[610] Vogel W, Grünebach F, Messam CA, Kanz L, Brugger W, Bühring H-J. Heterogeneity among human bone marrow-derived mesenchymal stem cells and neural progenitor cells. *Haematologica*. 2003;88(2):126–33.

[611] Maslova OO, Shuvalova NS, Sukhorada OM, Zhukova SM, Deryabina OG, Makarenko M V, et al. Heterogeneity of Umbilical Cords as a Source for Mesenchymal Stem Cells. Pacherník J, Marcinkiewicz C, Boulaiz H, Trajkovic V, editors. *Dataset Pap Biol* . 2013;2013:370103. DOI:10.7167/2013/370103

[612] Madel RJ, Börger V, Dittrich R, Bremer M, Tertel T, Thi Phuong NN, et al. Independent human mesenchymal stromal cell-derived extracellular vesicle preparations differentially affect symptoms in an advanced murine Graft-versus-Host-Disease model. *bioRxiv*. 2020; DOI:10.1101/2020.12.21.423658

[613] Munir J, Yoon JK, Ryu S. Therapeutic miRNA-Enriched Extracellular Vesicles : 2020;1–18.

[614] Lai RC, Yeo RWY, Padmanabhan J, Choo A, de Kleijn DP V, Lim SK. Isolation and Characterization of Exosome from Human Embryonic Stem Cell-Derived C-Myc-Immortalized Mesenchymal Stem Cells. *Methods Mol Biol*. 2016;1416:477–94. DOI:10.1007/978-1-4939-3584-0_29

[615] Lener T, Gimona M, Aigner L, Börger V, Buzas E, Camussi G, et al. Applying extracellular vesicles based therapeutics in clinical trials - An ISEV position paper. *J Extracell Vesicles*. 2015;4(1):1–31. DOI:10.3402/jev.v4.30087

[616] Yan IK, Shukla N, Borrelli DA, Patel T. Use of a Hollow Fiber Bioreactor to Collect Extracellular Vesicles from Cells in Culture. *Methods Mol Biol*. 2018;1740:35–41. DOI:10.1007/978-1-4939-7652-2_4

[617] Mitchell JP, Court J, Mason MD, Tabi Z, Clayton A. Increased exosome production from tumour cell cultures using the Integra CELLine Culture System. *J Immunol Methods* . 2008;335(1):98–105. DOI:Https://doi.org/10.1016/j.jim.2008.03.001

[618] Guerreiro EM, Vestad B, Steffensen LA, Aass HCD, Saeed M, Øvstebø R, et al.

Efficient extracellular vesicle isolation by combining cell media modifications, ultrafiltration, and size-exclusion chromatography. *PLoS One* . 2018;13(9):e0204276–e0204276. DOI:10.1371/journal.pone.0204276

[619] Palviainen M, Saari H, Kärkkäinen O, Pekkinen J, Auriola S, Yliperttula M, et al. Metabolic signature of extracellular vesicles depends on the cell culture conditions. *J Extracell Vesicles* . 2019;8(1). DOI:10.1080/20013078.2019.1596669

[620] Gowen A, Shahjin F, Chand S, Odegaard KE, Yelamanchili S V. Mesenchymal Stem Cell-Derived Extracellular Vesicles: Challenges in Clinical Applications . Vol. 8, Frontiers in Cell and Developmental Biology . 2020. p. 149.

[621] Gomzikova MO, James V, Rizvanov AA. Therapeutic Application of Mesenchymal Stem Cells Derived Extracellular Vesicles for Immunomodulation. *Front Immunol*. 2019;10(November):1–9. DOI:10.3389/fimmu.2019.02663

[622] Gupta S, Rawat S, Arora V, Kottarath SK, Dinda AK, Vaishnav PK, et al. An improvised one-step sucrose cushion ultracentrifugation method for exosome isolation from culture supernatants of mesenchymal stem cells. *Stem Cell Res Ther*. 2018;9(1):1–11. DOI:10.1186/s13287-018-0923-0

[623] Lamparski HG, Metha-Damani A, Yao J-Y, Patel S, Hsu D-H, Ruegg C, et al. Production and characterization of clinical grade exosomes derived from dendritic cells. *J Immunol Methods* . 2002;270(2):211–26. DOI:Https://doi.org/10.1016/S0022-1759(02)00330-7

[624] Auber M, Fröhlich D, Drechsel O, Karaulanov E, Krämer-Albers EM. Serum-free media supplements carry miRNAs that co-purify with extracellular vesicles. *J Extracell Vesicles* . 2019;8(1). DOI:10.1080/20013078.2019.1656042

[625] Parker AM, Shang H, Khurgel M, Katz AJ. Low serum and serum-free culture of multipotential human adipose stem cells. *Cytotherapy* . 2007;9(7):637–46. DOI:10.1080/14653240701508452

[626] Cagliani J, Grande D, Molmenti EP, Miller EJ, Rilo HLR. Immunomodulation by Mesenchymal Stromal Cells and Their Clinical Applications. *J stem cell Regen Biol* . 2017/04/10. 2017;3(2):10.15436/2471-0598.17.022. DOI:10.15436/2471-0598.17.022

[627] Spaggiari GM, Capobianco A, Abdelrazik H, Becchetti F, Mingari MC, Moretta L. Mesenchymal stem cells inhibit natural killer-cell proliferation, cytotoxicity, and cytokine production: role of indoleamine 2,3-dioxygenase and prostaglandin E2. *Blood*. 2008;111(3):1327–33. DOI:10.1182/blood-2007-02-074997

[628] Munn DH, Mellor AL. Indoleamine 2,3 dioxygenase and metabolic control of immune responses. *Trends Immunol*. 2013;34(3):137–43. DOI:10.1016/j.it.2012.10.001

[629] Dong L, Wang Y, Zheng T, Pu Y, Ma Y, Qi X, et al. Hypoxic hUCMSC-derived extracellular vesicles attenuate allergic airway inflammation and airway remodeling in chronic asthma mice. *Stem Cell Res Ther* . 2021;12(1):4. DOI:10.1186/s13287-020-02072-0

[630] Ren W, Hou J, Yang C, Wang H, Wu S, Wu Y, et al. Extracellular vesicles secreted by hypoxia pre-challenged mesenchymal stem cells promote non-small cell lung cancer cell growth and mobility as well as macrophage M2 polarization via miR-21-5p delivery. *J Exp Clin Cancer Res* . 2019;38(1):62. DOI:10.1186/s13046-019-1027-0